NUREG/CP–0149
Vol. 2

Proceedings of the U.S. Nuclear Regulatory Commission

Twenty-Third Water Reactor Safety Information Meeting

Volume 2
- Human Factors Research
- Advanced I&C Hardware and Software
- Severe Accident Research
- Probabilistic Risk Assessment Topics
- Individual Plant Examination

Held at
Bethesda Marriott Hotel
Bethesda, Maryland
October 23–25, 1995

U.S. Nuclear Regulatory Commission

Office of Nuclear Regulatory Research

Proceedings prepared by
Brookhaven National Laboratory

AVAILABILITY NOTICE

Availability of Reference Materials Cited in NRC Publications

Most documents cited in NRC publications will be available from one of the following sources:

1. The NRC Public Document Room, 2120 L Street, NW., Lower Level, Washington, DC 20555-0001

2. The Superintendent of Documents, U.S. Government Printing Office, P. O. Box 37082, Washington, DC 20402-9328

3. The National Technical Information Service, Springfield, VA 22161-0002

Although the listing that follows represents the majority of documents cited in NRC publications, it is not intended to be exhaustive.

Referenced documents available for inspection and copying for a fee from the NRC Public Document Room include NRC correspondence and internal NRC memoranda; NRC bulletins, circulars, information notices, inspection and investigation notices; licensee event reports; vendor reports and correspondence; Commission papers; and applicant and licensee documents and correspondence.

The following documents in the NUREG series are available for purchase from the Government Printing Office: formal NRC staff and contractor reports, NRC-sponsored conference proceedings, international agreement reports, grantee reports, and NRC booklets and brochures. Also available are regulatory guides, NRC regulations in the *Code of Federal Regulations*, and *Nuclear Regulatory Commission Issuances*.

Documents available from the National Technical Information Service include NUREG-series reports and technical reports prepared by other Federal agencies and reports prepared by the Atomic Energy Commission, forerunner agency to the Nuclear Regulatory Commission.

Documents available from public and special technical libraries include all open literature items, such as books, journal articles, and transactions. *Federal Register* notices, Federal and State legislation, and congressional reports can usually be obtained from these libraries.

Documents such as theses, dissertations, foreign reports and translations, and non-NRC conference proceedings are available for purchase from the organization sponsoring the publication cited.

Single copies of NRC draft reports are available free, to the extent of supply, upon written request to the Office of Administration, Distribution and Mail Services Section, U.S. Nuclear Regulatory Commission, Washington, DC 20555-0001.

Copies of industry codes and standards used in a substantive manner in the NRC regulatory process are maintained at the NRC Library, Two White Flint North, 11545 Rockville Pike, Rockville, MD 20852-2738, for use by the public. Codes and standards are usually copyrighted and may be purchased from the originating organization or, if they are American National Standards, from the American National Standards Institute, 1430 Broadway, New York, NY 10018-3308.

DISCLAIMER NOTICE

NUREG/CP–0149
Vol. 2

Proceedings of the U.S. Nuclear Regulatory Commission

Twenty-Third Water Reactor Safety Information Meeting

Volume 2

- Human Factors Research
- Advanced I&C Hardware and Software
- Severe Accident Research
- Probabilistic Risk Assessment Topics
- Individual Plant Examination

Held at
Bethesda Marriott Hotel
Bethesda, Maryland
October 23–25, 1995

Manuscript Completed: February 1996
Date Published: March 1996

Compiled by: Susan Monteleone

C. Bonsby, NRC Project Manager

Office of Nuclear Regulatory Research
U.S. Nuclear Regulatory Commission
Washington, DC 20555–0001

Proceedings prepared by
Brookhaven National Laboratory

PROCEEDINGS OF THE
23rd WATER REACTOR SAFETY INFORMATION MEETING

October 23-25, 1995

Published in Three Volumes

GENERAL INDEX

VOLUME 1

VOLUME 2

VOLUME 3

REGISTERED ATTENDEES (NON-NRC)
23RD WATER REACTOR SAFETY INFORMATION MEETING

D. AGARWAL
U.S. DEPARTMENT OF ENERGY
NE-50/GTN-E478
WASHINGTON, DC 20585 USA

M. AHMED
WESTINGHOUSE ELECTRIC CORP.
4350 NORTHERN PIKE
MONROEVILLE, PA 15146-2886 USA

T. AL-HUSSAINI
DUKE POWER CO.
1010 SHORELINE CO.
STANLEY, NC 28164 USA

M. ALLEN
SANDIA NATIONAL LABORATORY
PO BOX 5800
ALBUQUERQUE, NM 87185-1137 USA

C. ALLISON
IDAHO NATIONAL ENGINEERING LAB
PO BOX 1625, MS 3840
IDAHO FALLS, ID 83415 USA

A. ALONSO
SONSEJO DE SEGURIDAD NUCLEAR
JUSTO DORADO, 11
MADRID, 28040 SPAIN

R. ANDERSON
NORTHERN STATES POWER CO.
414 NICOLLET MALL
MINNEAPOLIS, MN 55401 USA

A. ANKRUM
PACIFIC NORTHWEST LAB
PO BOX 999, MS K828
RICHLAND, WA 99352 USA

K. ARAI
TOSHIBA NUCLEAR ENGINEERING LAB
4-1, UKISHIMA-CHI, KAWASAKI-KU
KAWASAKI, 210 JAPAN

P. ARNOLD
PJA ENGINEERING
FORCHHEIMERSTR. 31
ERLANGEN, 91056 GERMANY

V. ASMOLOV
RRC "KURCHATOV INSTITUTE"
KURCHATOV SQUARE 1
MOSCOW, 123182 RUSSIA

S. AZUMI
KANSAI ELECTRIC POWER CO., INC.
2001 L ST., N.W., SUITE 801
WASHINGTON, DC 20036 USA

M. BALE
B&W FUEL COMPANY
3315 OLD FOREST RD
LYNCHBURG, VA 24506-0935 USA

A. BARATTA
PENN STATE UNIVERSITY
231 SACKETT
UNIVERSITY PARK, PA 16803 USA

J. BARDELAY
IIPSN/CEA
60-68 AV. DU GEN. LECLERC PG6
FONTENAY AUX ROSES, 92265 FRANCE

R. BARI
BROOKHAVEN NATIONAL LABORATORY
BLDG. 197C, PO BOX 5000
UPTON, NY 11973-5000 USA

M. BEAUMONT
WESTINGHOUSE ELECTRIC CORPORATION
11921 ROCKVILLE PIKE - SUITE 450
ROCKVILLE, MD 20852 USA

J. BECKHAM
SOUTHERN NUCLEAR-GEORGIA POWER CO.
PO BOX 1295
BIRMINGHAM, AL 35201 USA

L. BELBLIDIA
SCANDPOWR, INC.
101 LAKE FOREST BLVD, #340
GAITHERSBURG, MD 20877 USA

D. BERRY
SANDIA NATIONAL LABORATORY
P.O. BOX 5800
ALBUQUERQUE, NM 87185-0744 USA

C. BEYER
BATTELLE PNL
11300 W. COURT
PASCO, WA 99302 USA

D. BHARGAVA
VIRGINIA POWER
5000 DOMINION BLVD.
GLEN ALLEN, VA 23060 USA

N. BIXLER
SANDIA NATIONAL LABORATORY
P.O. BOX 5800
ALBUQUERQUE, NM 87185-0739 USA

T. BJORLO
OECD HALDEN REACTOR PROJECT
P.O. BOX 173, OS ALLE 4
N-1751 HALDEN, NORWAY

J. BLASS
OAK RIDGE NATIONAL LABORATORY
236 GUM HOLLOW ROAD
OAK RIDGE, TN 37830 USA

J. BOCCIO
BROOKHAVEN NATIONAL LABORATORY
BLDG. 130, PO BOX 5000
UPTON, NY 11973-5000 USA

L. BOLSHOV
RUSSIAN ACADEMY OF SCIENCES
B. TULSKAYA, 52
MOSCOW, 113191 RUSSIA

M. BONNER
BROOKHAVEN NATIONAL LABORATORY
BLDG. 197C, PO BOX 5000
UPTON, NY 11973-5000 USA

B. BOYACK
LOS ALAMOS NATIONAL LABORATORY
P.O. BOX 1663
LOS ALAMOS, NM 87575 USA

U. BREDOLT
ABB ATOM
ABB ATOM AKTIEBOLAG
VASTERAS S72163 SWEDEN

G. BROWN
AEA TECHNOLOGY
TH5C8, RISLEY WARRINGTON
CHESHIRE, WA36A5 ENGLAND

T. BROWN
SANDIA NATIONAL LABORATORY
PO BOX 5800
ALBUQUERQUE, NM 87185-0748 USA

R. BUDNITZ
FUTURE RESOURCES ASSOCIATES INC.
2039 SHATTUCK AVENUE, SUITE 402
BERKELEY, CA 94704 USA

S. CALPENA
DIR. FOR SAFETY OF NUCLEAR INSTALLATIONS
60-64 AV. DE LA DIVISION LECLERC
FONTENAY AUX ROSES, 92265 FRANCE

A. CAMP
SANDIA LABS.
P.O. BOX 5800, MS 0747
ALBUQUERQUE, NM 87185 USA

G. CAPPONI
ANPA
VIA VITALIANO BRANCATI, 48
ROME, 00144 ITALY

R. CARLSON
LAWRENCE LIVERMORE NATIONAL LAB.
PO BOX 808, L634
LIVERMORE, CA 94551 USA

M. CARLSSON
STUDSVIK NUCLEAR AB
S-611 82 NYKOPING
NYKOPING, S-611 82 SWEDEN

D. CASADA
OAK RIDGE NATIONAL LABORATORY
P.O. BOX 2009
OAK RIDGE, TN 37831-8065 USA

N. CAVLINA
U. OF ZAGREB, ELECT. ENG'G & COMPUTING
UNSKA 3
ZAGREB, 10000 CROATIA

S. CHAKRABORTY
SWISS FEDERAL NUCLEAR SAFETY
INSPECTORATE
VILLIGEN, CH-5232 SWITZERLAND

W. CHEN
ENERGY TECHNOLOGY ENGIN. CENTER
6633 CANOGA AVENUE
CANOGA PARK, CA 91304 USA

F.-B. CHEUNG
PENNSYLVANIA STATE UNIVERSITY
304 REBER BLDG.
UNIVERSITY PARK, PA 16802 USA

D. CHO
ARGONNE NATIONAL LABORATORY
9700 CO. CASS AVE., BLDG. 208
ARGONNE, IL 60439 USA

J-S. CHOI
KOREA INSTITUTE OF NUCLEAR SAFETY
PO BOX 114
YUSUNG, TAEJON, 305-600 KOREA

T. CHU
SANDIA NATIONAL LABORATORY
PO BOX 5800
ALBUQUERQUE, NM 87185-1137 USA

H. CHUNG
ARGONNE NATIONAL LAB
9700 S. CASS AVE
ARGONNE, IL 60439 USA

G. CICCARELLI
BROOKHAVEN NATIONAL LABORATORY
BLDG. 130, PO BOX 5000
UPTON, NY 11973-5000 USA

J. CLAUSS
SANDIA NATIONAL LABORATORY
PO BOX 5800, MS-0741
ALBUQUERQUE, NM 87185-0741 USA

P. COLAIANNI
DUKE POWER CO.
MAIL STOP EC12R P.O. BOX 1006
CHARLOTTE, NC 28201-1006 USA

R. COLE
SANDIA NATIONAL LABORATORY
SANDIA NATIONAL LAB, DEPT. 6421
ALBUQUERQUE, NM 87185-0739 USA

L. CONNOR
STS, INC.
3 METRO CENTER - SUITE 610
BETHESDA, MD 20814 USA

S. COOPER
SCIENCE APPLICATIONS INTERNATIONAL CORP.
11251 ROGER BACON D, M/S R-3-1
RESTON, VA 22090 USA

B. CORWIN
OAK RIDGE NATIONAL LABORATORY
P.O. BOX 2008
OAK RIDGE, TN 37831-6151 USA

M. COURTAUD
COMMISSARIAT A L'ENERGIE ATOMIQUE
CEA/GRENOBLE - 17, RUE DES MARTYRS
GRENOBLE CEDEX 9, 38054 FRANCE

M. CUNNINGHAM
PACIFIC NORTHWEST LAB.
PO BOX 999
RICHLAND, WA 99352 USA

C. CZAJKOWSKI
BROOKHAVEN NATIONAL LABORATORY
BLDG. 130, PO BOX 5000
UPTON, NY 11973-5000 USA

J. DAVIS
BROOKHAVEN NATIONAL LABORATORY
BLDG. 130, PO BOX 5000
UPTON, NY 11973-5000 USA

J. DAVIS
NEI
1776 I ST NW
WASHINGTON, DC 20002 USA

D. DIAMOND
BROOKHAVEN NATIONAL LABORATORY
BLDG. 130, PO BOX 5000
UPTON, NY 11973-5000 USA

S. DINGMAN
SANDIA NATIONAL LABORATORY
PO BOX 5800, MS 0747
ALBUQUERQUE, NM 87185-0747 USA

S. DOROFEEV
RRC "KURCHATOV INSTITUTE"
KURCHATOV SQUARE 1
MOSCOW, 123182 RUSSIA

A. DRAKE
WESTINGHOUSE ELECTRIC CORP.
P.O. BOX 350
PITTSBURGH, PA 15239 USA

J-L. DROULAS
ELECTRICITE DE FRANCE-SEPTEN
12-14, AVENUE DUTRIEVOZ
VILLEURBANNE CEDEX, 69628 FRANCE

J. DUCO
IPSN/DPEI CEA-FAR
BP6
FONTENAY-AUX-ROSES, 92265 FRANCE

M. EL-HAWARY
ATOMIC ENERGY CONTROL BOARD, CANADA
280 SLATER STREET
OTTAWA, ONT K1P 5S9 CANADA

Z. ELAWAR
PALO VERDE NUCLEAR PLANT
PO BOX 52034
PHOENIX, AZ 85072-2034 USA

R. ENNIS
TENERA
1901 RESEARCH BLVD.
ROCKVILLE, MD 20850 USA

P. EWING
OAK RIDGE NATIONAL LABORATORY
PO BOX 2008, MS 6006
OAK RIDGE, TN 37831 USA

R. FENECH
NUCLEAR OPERATIONS, PALISADES PLANT
27780 BLUE STAR MENORIAL HWY.
COVERT, MI 49043 USA

D. FERETIC
U. OF ZAGREB, ELECT. ENG'G & COMPUTING
UNSKA 3
ZAGREB, 10000 CROATIA

R. FIELDHACK
WISCONSIN ELECTRIC POWER CO.
231 W. MICHIGAN
MILWAUKEE, WI 53201 USA

I. FIERO
ABB COMBUSTION ENGINEERING
1000 PROSPECT HILL RD
WINDSOR, CT 06095 USA

L. FISCHER
LAWRENCE LIVERMORE NATIONAL LAB.
PO BOX 808, L631
LIVERMORE, CA 94551 USA

M. FLETCHER
AECL TECHNOLOGIES
19041 RAINES DRIVE
DERWOOD, MD 20855 USA

K. FOLK
SOUTHER NUCLEAR
P.O. BOX 1295
BINMINGHAM, AL 35201 USA

J. FORESTER
SANDIA NATIONAL LABORATORY
PO BOX 5800, MS 0747
ALBUQUERQUE, NM 87185-0747 USA

E. FOX
OAK RIDGE NATIONAL LABORATORY
P.O. BOX 2009
OAK RIDGE, TN 37832-8063 USA

W. FRID
SWEDISH NUCLEAR POWER INSPECTORATE
UTLANDSGIRO 7, UT/S/
STOCKHOLM, S-10658 SWEDEN

T. FUKETA
JAPAN ATOMIC ENERGY RESEARCH INSTITUTE
TOKAI, IBARAKI 319-11
TOKAI, 319-11 JAPAN

W. GALYEAN
IDAHO NATIONAL ENGINEERING LAB
PO BOX 1625
IDAHO FALLS, ID 83415-3850 USA

R. GAMBLE
GE NUCLEAR ENERGY
75 CURTNER AVE., MC 781
SAN JOSE, CA 95125 USA

P. GANGO
IVO INTERNATIONAL LTD.
RAJATORPANTLE 8, VANTAA
IVO, 01019 FINLAND

R. GAUNTT
SANDIA NATIONAL LABORATORY
PO BOX 5800, MS 1139
ALBUQUERQUE, NM 87185 USA

G. GAUTHIER
INST. OF PROTECTION & NUCLEAR SAFETY
DES/SAMS BP 6F
FONTENAY-AUX-ROSES, 92265 FRANCE

R. GAZDZINSKI
OGDEN ENVIRONMENTAL & ENERGY SVCS.
1777 SENTRY PKWY W., STE 300
BLUE BELL, PA 19422 USA

N. GHADIALI
BATTELLE COLUMBUS LABORATORIES
505 KING AVE
COLUMBUS, OH 43201 USA

G. GIGGER
WESTINGHOUSE ELECTRIC
PO BOX 79
WEST MIFFLIN, PA 15122 USA

K. GILLEN
SANDIA NATIONAL LABORATORY
PO BOX 5800, MS 1407
ALBUQUERQUE, NM 87185-1407 USA

R. GILLILAND
OAK RIDGE NATIONAL LABORATORY
PO BOX 2009, MS 8063
OAK RIDGE, TN 37830-8063 USA

J. GLEASON
CONSULTANT TO BNL
1819 CROSS CREEK RD.
HUNTSVILLE, AL 35802 USA

L. GOLDSTEIN
S.M. STOLLER CORP.
485 WASHINTON AVENUE
PLEASANTVILLE, NY 10570 USA

M. GOMOLINSKI
IPSN - FRANCE
BP 6
FONTENAY AUX ROSES, 92265 FRANCE

S. GRAHAM
NAVAL SURFACE WARFARE CENTER
CODE 614, 3A LEGGETT CIR.
ANNAPOLIS, MD 21402 USA

D. GRAND
CEA DRN/DTP/STR
STR CEA-GRENOBLE 17, RUE DES MARTYRS
GRENOBLE-CEDEX 9, 38054 FRANCE

W. GRANT
ATOMIC ENERGY CONTROL BOARD - CANADA
P.O. BOX 1046, STN. B, 280 SLATER STREET
OTTAWA, ONT K1P 5S9 CANADA

M. GREGORIC
SLOVENIAN NUCLEAR SAFETY ADMIN.
VOJKOVA 59
LJUBLJANA, 61113 SLOVENIA

F. GRIFFIN
OAK RIDGE NATIONAL LABORATORY
PO BOX 2009
OAK RIDGE, TN 37831-8057 USA

M. GROUNES
STUDSVIK NUCLEAR AB
S-611 82 NYKOPING
NYKOPING, S-611 82 SWEDEN

K. HADDAD
PENNSYLVANIA STATE UNIVERSITY
215 REBER BLDG.
UNIVERSITY PARK, PA 16802 USA

L. HANES
EPRI
3412 HILLVIEW AVENUE
PALO ALTO, CA 94304 USA

A. HANEVIK
OECD HALDEN PROJECT
OS ALLE 13
1750 HALDEN, NORWAY

D. HARRISON
U.S. DEPT. OF ENERGY
NE-50
WASHINGTON, DC 20545 USA

G. HART
PERFORMANCE CONTRACTING INC.
4025 BONNE INDUSTRIAL
SHAWNEE, KS 66226 USA

H. HASHEMIAN
ANALYSIS & MEASUREMENT SERVICES CORP.
AMS 9111 CROSS PARK DR.
KNOXVILLE, TN 37923 USA

K. HASHIMOTO
JAPAN ATOMIC ENERGY RESEARCH INSTITUTE
TOKAI-MURA
IBARAKI-KEN, 319-11 JAPAN

G. HECKER
ALDEN RESEARCH LABORATORY, INC.
30 SHREWSBURY STREET
HOLDEN, MA 01520 USA

G. HEUSENER
FORSCHUNGSZENTRUM KARLSRUHE
POSTFACH 3640
KARLSRUHE, 76021 GERMANY

J. HIGGINS
BROOKHAVEN NATIONAL LABORATORY
BLDG. 130, PO BOX 5000
UPTON, NY 11973-5000 USA

L. HOCHREITER
WESTINGHOUSE ELECTRIC CORP.
P.O. BOX 355
PITTSBURGH, PA 15230 USA

P. HOFMANN
FORSCHUNGSZENTRUM KARLSRUHE
POSTFACH 3640
KARLSRUHE, 76021 GERMANY

S.W. HONG
SANDIA NATIONAL LABORATORY
PO BOX 5800, MS 1139
ALBUQUERQUE, NM 87185 USA

E. HONTANON
C.I.E.M.A.T. RESEARCH CENTER
AVDA. COMPLUTENSE, 22
MADRID, 28040 SPAIN

W. HORIN
WINSTON & STRAWN
1400 I ST. N.W.
WASHINGTON, DC 20005 USA

L. HORVATH
BROOKHAVEN NATIONAL LABORATORY
BLDG. 130, P.O. BOX 5000
UPTON, NY 11973 USA

R. HOUSER
WESTINGHOUSE BETTIS ATOMIC POWER LAB.
PO BOX 79
WEST MIFFLIN, PA 15122 USA

T. HSU
VIRGINIA POWER
5000 DOMINION BLVD.
GLEN ALLEN, VA 23060 USA

A. HUERTA
CNSNS
DR. BARRAGAN 779; COL. NARVARIC
MEXICO D.F., MEXICO 03020 MEXICO

J. HUTCHINSON
EPRI PLANT SUPPORT ENGINEERING
1300 W. HARRIS BLVD
CHARLOTTE, NC 28262 USA

Y.D. HWANG
KOREA ATOMIC ENERGY RESEARCH INSTITUTE
POWER REACTOR DEVELOPMENT TEAM
YUSUNG-GU, TAEJUN KOREA

T. HYRSKY
IVO INTERNATIONAL LTD.
RAJATORPANTLE 8, VANTAA
IVO, 01019 FINLAND

J. HYVARINEN
FINNISH CENTRE FOR RAD. & NUC. SAFETY
PO BOX 14
HELSINKI, FIN-00881 FINLAND

K. IDO
SHIKOKU ELECTRIC POWER CO., INC.
6-1-2 MINATOMACHI
MATSUYAMA, 790 JAPAN

J. IRELAND
LOS ALAMOS NATIONAL LABORATORY
PO BOX 1663, MS F606
LOS ALAMOS, NM 87545 USA

M. ISHII
PURDUE UNIVERSITY
1290 NUCLEAR ENGINEERING BLDG.
WEST LAFAYETTE, IN 47907-1290 USA

K. ISHIJIMA
JAPAN ATOMIC ENERGY RESEARCH INSTITUTE
TOKAI, IBARAKI 319-11
TOKAI, 319-11 JAPAN

R. ISLAMOV
RUSSIAN ACADEMY OF SCIENCES
B. TULSKAYA, 52
MOSCOW, 113191 RUSSIA

T. ITO
JAPAN INSTITUTE OF NUCLEAR SAFETY
FUJITA KANKO TORANOMON BLDG. 4F
MINATO-KU, TOKYO 105 JAPAN

R. JAMES
ELECTRIC POWER RESEARCH INSTITUTE
3412 HILLVIEW AVENUE
PALO ALTO, CA 94304 USA

F. JANSKY
BTB-JANSKY GMBH
GERLIUGER STR. 151
LEONBERG, 71229 GERMANY

M. JIMINEZ
FLORIDA POWER & LIGHT
700 UNIVERSE BLVD.
JUNO BEACH, FL 33408 USA

R. JOHNSON
PACIFIC GAS & ELECTRIC CO.
PO BOX 770000, MC A10A
SAN FRANCISCO, CA 94177 USA

W. JOHNSON
UNIVERSITY OF VIRGINIA
REACTOR BUILDING, UNIVERSITY OF VIRGINIA
CHARLOTTESVILLE, VA 22903 USA

S. KARIMIAN
PSE&G
PO BOX 236
HANCOCK'S BRIDGE, NJ 08038 USA

T. KASSNER
ARGONNE NATIONAL LAB
9700 S. CASS AVE
ARGONNE, IL 60439 USA

S. KERCEL
OAK RIDGE NATIONAL LABORATORY
PO BOX 2008, MS 6318
OAK RIDGE, TN 37831 USA

S. KIKKAWA
NUCLEAR POWER ENGINEERING CORP.
3-CHOME TORANOMON, 8F, 17-1
MINATO-KU, TOKYO 105 JAPAN

K. KILPI
VTT ENERGY
PO BOX 1604, FIN-02044 VTT
ESPOO 15, 02150 FINLAND

B. KIM
KOREA INSTITUTE OF NUCLEAR SAFETY
PO BOX 114
YUSUNG, TAEJON, 305-600 KOREA

H. KIM
KOREA INSTITUTE OF NUCLEAR SAFETY
PO BOX 114
YUSUNG, TAEJON, 305-600 KOREA

H.C. KIM
KOREA INSTITUTE OF NUCLEAR SAFETY
PO BOX 114
YUSUNG, TAEJON, 305-600 KOREA

H.Y. KIM
KOREA INSTITUTE OF NUCLEAR SAFETY
PO BOX 114
YUSUNG, TAEJON, 305-600 KOREA

S.B. KIM
KOREA ATOMIC ENERGY RESEARCH INSTITUTE
P.O. BOX 105, YUSEONG
TAEJON, KOREA

S. KINNERSLY
AEA TECHNOLOGY
UK WINFRITH
DORCITESTER, DORSET U.K.

A. KISSELEV
RUSSIAN ACADEMY OF SCIENCES
B. TULSKAYA, 52
MOSCOW, 113191 RUSSIA

M. KITAMURA
NUCLEAR POWER ENGINEERING CORP.
3-13, 4-CHOME TORANOMON, MINATO-KU
TOKYO, 105 JAPAN

J. KLAPPROTH
GENERAL ELECTRIC
PO BOX 780, MC J26
WILMINGTON, NC 28409 USA

L. KLEIN
ATOMIC ENERGY CONTROL BOARD CANADA
PO BOX 1046, STA. B, 280 SLATER ST.
OTTAWA, ONT K1P 5S9 CANADA

J. KLUGEL
SWISS FEDERAL NUC. SAFETY INSPECTORAT
VILLIGEN, CH-5232 SWITZERLAND

N. KOJIMA
MITSUBISHI HEAVY INDUSTRIES, LTD.
1-1, WADAMISAKI-CHO, 1-CHOME
HYOGO-KU, KOBW JAPAN

K. KORSAH
OAK RIDGE NATIONAL LABORATORY
PO BOX 2008, MS 6010
OAK RIDGE, TN 37831 USA

D. KOSS
PENNSYLVANIA STATE UNIVERSITY
202A STEIDLE BLDG.
UNIVERSITY PARK, PA 16802 USA

F. KRAMER
CONSULTANT TO MITSUBISHI HEAVY IND.
5427 FAIR OAKS ST.
PITTSBURGH, PA 15217 USA

B. KUJAL
NUCLEAR RESEARCH INSTITUTE
NUCLEAR POWER & SAFETY DIV.
REZ, 25068 CZECH REPUBLIC

Y. KUKITA
JAPAN ATOMIC ENERGY RESEARCH INSTITUTE
TOKAI, IBARAKI 319-11
TOKAI, 319-11 JAPAN

K. KURODA
NUCLEAR POWER ENGINEERING CORP.
3-CHOME TORANOMON, 8F, 17-1
MINATO-KU, TOKYO 105 JAPAN

K. KUSSMAUL
MPA, UNIVERSITY OF STUTTGART
PFAFFENWALDRING 32
STUTTGART, 70569 GERMANY

J. LA CHANCE
SCIENCE APPLICATIONS INTERNATIONAL CORP.
2109 AIR PARK RD SE
ALBUQUERQUE, NM 87106 USA

P. LACY
UTILITY RESOURCE ASSOCIATES CORP.
51 MONROE ST., STE 1600
ROCKVILLE, MD 20850 USA

J. LAKE
IDAHO NATIONAL ENGINEERING LABORATORY
BOX 1625, MS 3860
IDAHO FALLS, ID 83415-3860 USA

S. LANGENBUCH
GRS - GERMANY
FORSCHUNGSGELANDE
GARCHING, 85748 GERMANY

H-K. LEE
NUCLEAR TECH DEPT.
ATOMIC ENERGY COUNCIL
TAIPEI, TAIWAN ROC

J. LEE
KOREA INSTITUTE OF NUC. SAFETY
P.O. BOX 114 YUSUNG
TAEJON, KOREA

S. LEE
ONTARIO HYDRO
700 UNIVERSITY AVENUE
TORONTO, ONTARIO M5G 1X6 CANADA

Y-W. LEE
KOREA INSTITUTE OF NUCLEAR SAFETY
PO BOX 114
YUSUNG, TAEJON, 305-600 KOREA

J. LEHNER
BROOKHAVEN NATIONAL LABORATORY
BLDG. 130, PO BOX 5000
UPTON, NY 11973-5000 USA

S. LEVINSON
B&W NUCLEAR TECHNOLOGIES
3315 OLD FOREST RD.
LYNCHBURG, VA 24501 USA

R. LICCIARDO
PROFESSIONAL ENGINEER & ECONOMIST
11801 ROCKVILLE PIKE, SUITE 1405
NO. BETHESDA, MD 20852 USA

M. LIVOLANT
IPSN
CE/FAR BP6
FONTENAY-AUX-ROSES CEDEX, 92265 FRANCE

K. LOCKWOOD
KNOLLS ATOMIC POWER LABORATORY
PO BOX 1072 (P3-172)
SCHENECTADY, NY 12301-1072 USA

R. LOFARO
BROOKHAVEN NATIONAL LABORATORY
BLDG. 130, PO BOX 5000
UPTON, NY 11973-5000 USA

J.-L. LUC
DIR. FOR SAFETY OF NUCLEAR INSTALLATIONS
4 IMPASSE MATHIEU
PARIS, 75015 FRANCE

W. LUCKAS
BROOKHAVEN NATIONAL LABORATORY
BLDG. 130, PO BOX 5000
UPTON, NY 11973-5000 USA

D. MAGALLON
CEC-JRC-ISPRA
JRC-EURATOM ISPRA
ISPRA, 20120 ITALY

H. MAGLEBY
IDAHO NATIONAL ENGINEERING LAB
PO BOX 1625, MS 3870
IDAHO FALLS, ID 83415 USA

B. MAGONDEAUX
ELECTRICITE DE FRANCE-SEPTEN
12-14, AVENUE DUTRIEVOZ
VILLEURBANNE CEDEX, 69628 FRANCE

J. MARN
U. OF MARIBOR, FAC. OF MECHANICAL ENG'G.
PO BOX 224
MARIBOR, SI62000 SLOVENIA

R. MARTINEZ, JR.
JUPITER CORPORATION
STE 900, 2730 UNIVERSITY BLVD. W.
WHEATON, MD 20902 USA

T. MATSUMOTO
NUCLEAR POWER ENGINEERING CORP.
5F 17-1, TORANOMON, MINATO-KU
TOKYO, 105 JAPAN

G. MEYER
B&W FUEL COMPANY
3315 OLD FOREST RD
LYNCHBURG, VA 24506-0935 USA

P. MEYER
SWISS FEDERAL NUC. SAFETY INSPECTORATE
(HSK)
VILLIGEN, AG CH-5232 SWITZERLAND

T. MIEDA
ISHIKAWAJIMA-HARIMA HEAVY INDUSTRIES
1, SHIN-NAKAHARA-CHO, ISOGO-KU
YOKOHAMA, 235 JAPAN

P. MILELLA
ANPA
VIA VITALIANO BRANCATI 68
ROME, 00144 ITALY

J. MILLER
SCIENTECH
11140 ROCKVILLE PIKE, SUITE 500
ROCKVILLE, MD 20874 USA

R. MILLER
WESTINGHOUSE ELECTRIC CORP.
PO BOX 355
PITTSBURGH, PA 15230 USA

S. MIRSKY
SCIENCE APPLICATIONS INTERNATIONAL CORP.
20201 CENTURY BLVD.
GERMANTOWN, MD 20770 USA

S. MODRO
IDAHO NATIONAL ENGINEERING LABORATORY
P.O. BOX 1625, MS 3895
IDAHO FALLS, ID 83415 USA

S. MONTELEONE
BROOKHAVEN NATIONAL LABORATORY
BLDG. 130, PO BOX 5000
UPTON, NY 11973-5000 USA

M. MONTGOMERY
NUCLEAR FUEL INDUSTRIES, LTD.
3845 NORWOOD CT.
BOULDER, CO 80304 USA

D. MOON
WASHINGTON PUBLIC PWR SUPPLY SYS
PO BOX 968 (MD PE21)
RICHLAND, WA 99352 USA

E. MOREL
FRAMATOME
TOUR FIAT
PARIS LA DEFENSE, 92084 FRANCE

A. MOTTA
PENNSYLVANIA STATE UNIVERSITY
231 SACKETT BLDG.
UNIVERSITY PARK, PA 16802 USA

M. MUHLHEIM
OAK RIDGE NATIONAL LABORATORY
P.O. BOX 2009
OAK RIDGE, TN 37831-8065 USA

M. MUNTZING
MORGAN LEWIS & BOCKIUS LLP
1800 M ST., NW
WASHINGTON, DC 20036 USA

Y.W. NA
KOREA ATOMIC ENERGY RESEARCH INSTITUTE
PO BOX 105, YUSONG
TAEJON, 305-600 KOREA

A. NAKAMURA
NUCLEAR POWER ENGINEERING CORP.
3-13. 4-CHOME, TORANOMON.MINATO-KU
TOKYO, 105 JAPAN

Y. NARUSE
TOSHIBA CORP.
8, SHINSUGITA-CHO, ISOGO-KU
YOKOHAMA, 235 JAPAN

D. NAUS
OAK RIDGE NATIONAL LABORATORY
P.O. BOX 2009
OAK RIDGE, TN 37831-8065 USA

U. NAYAK
WESTINGHOUSE ELECTRIC CORP.
PO BOX 355
PITTSBURGH, PA 15230 USA

G. NIEDERAUER
LOS ALAMOS NATIONAL LABORATORY
MS K575 LANL
LOS ALAMOS, NM 87545 USA

A. NUNEZ
CNSNS
DR. BARRAGAN 779; COL. NARVARIC
MEXICO D.F., MEXICO 03020 MEXICO

S. ONO
HITACHI WORKS, HITACHI LTD.
1-1 SAIWAI-CHO 3-CHOME, HIMCHI-SHI
IBARAKI-KEN, 317 JAPAN

N. ORTIZ
SANDIA NATIONAL LABORATORY
PO BOX 5800, MS 0736
ALBUQUERQUE, NM 87185-0736 USA

D. OSETEK
LOS ALAMOS TECHNICAL ASSOCIATES
BLDG. 1 SUITE 400, 2400 LOUISIANA BLVD. NE
ALBUQUERQUE, NM 87110 USA

F. OWRE
OECD HALDEN REACTOR PROJECT
OS ALLE 13
N 1751 HALDEN, NORWAY

O. OZER
EPRI
PO BOX 10412
PALO ALTO, CA 94303-0813 USA

J. PAPIN
IPSN
CE CADARACHE
ST PAUL LEZ DURANCE, 13108 FRANCE

K-B. PARK
KOREA ATOMIC ENERGY RESEARCH INST.
PO BOX 105, YUSONG
TAEJON, 305-600 KOREA

M. PARKER
IL DEPT. OF NUCLEAR SAFETY
1035 OUTER PARK DRIVE
SPRINGFIELD, IL 62704 USA

J. PELTIER
IPSN
C.E. FONTENAY - AUX - ROSES BP6
FONTENAY-AUX-ROSES, 92965 FRANCE

W. PENNELL
OAK RIDGE NATIONAL LABORATORY
PO BOX 2009, MS-8056
OAK RIDGE, TN 37830-8056 USA

A. PEREZ-NAVARRO
UNIV. ALFONSO X EL SABIO
AVDA D E LA UNIVERSIDAD, 1
MADRID, 28691 SPAIN

V. PETENYI
NUC. REG. AUTHORITY OF SLOVAK REPUBLIC
BAJKALSKA 27, PO BOX 24
BRATISLAVA, 820 07 SLOVAKIA

M. PILCH
SANDIA NATIONAL LABORATORY
PO BOX 5800
ALBUQUERQUE, NM 87185-1137 USA

A. POOLE
OAK RIDGE NATIONAL LABORATORY
Y12 PLANT, BLDG. 9102-1 BEAR CREEK RD.
OAK RIDGE, TN 37831-8038 USA

V. PROKLOV
RRC "KURCHATOV INSTITUTE"
KURCHATOV SQUARE 1
MOSCOW, 123182 RUSSIA

J. PUGA
UNESA
FRANCISCO GERVAS 3
MADRID, 28020 SPAIN

C. PUGH
OAK RIDGE NATIONAL LABORATORY
PO BOX 2009, MS 8063
OAK RIDGE, TN 37831 USA

E. PURVIS
10105 CLEAR SPRING ROAD
DAMASCUS, MD 20872 USA

L. RANEY
COMMONWEALTH EDISON CO.
1400 OPUS PL.
DOWNERS GROVE, IL 60515 USA

V. RANSOM
PURDUE UNIVERSITY
SCHOOL OF NUCLEAR ENGINEERING - NUCL 140
WEST LAFAYETTE, IN 47907 USA

D. RAPP
WESTINGHOUSE BETTIS ATOMIC POWER LAB.
PO BOX 79
WEST MIFFLIN, PA 15122 USA

J. RASHID
ANATECH RESEARCH CORP.
5435 OBERLIN DR.
SAN DIEGO, CA 92121 USA

S. RAY
WESTINGHOUSE ELECTRIC CORP.
PO BOX 355
PITTSBURGH, PA 15230 USA

P. REGNIER
INST. OF PROTECTION & NUCLEAR SAFETY
DES/SAMS BP 6F
FONTENAY-AUX-ROSES, 92265 FRANCE

K. REIL
SANDIA NATIONAL LABORATORY
PO BOX 5800, MS 1139
ALBUQUERQUE, NM 87185-1139 USA

M. REOCREUX
IPSN
CE CADARACHE
ST PAUL LEZ DURANCE, 13108 FRANCE

W. RETTIG
DEPARTMENT OF ENERGY
1574 LOLA STREET
IDAHO FALLS, ID 83402 USA

J. REYES, JR.
OREGON STATE UNIVERSITY
RADIATION CENTER C116
CORVALLIS, OR 97331-5902 USA

M. RHATIB-RAHBAR
ENERGY RESEARCH INC.
P.O. BOX 2034
ROCKVILLE, MD 20854 USA

U. ROHATGI
BROOKHAVEN NATIONAL LABORATORY
BLDG. 475B, PO BOX 5000
UPTON, NY 11973-5000 USA

P. ROTHWELL
HM NUCLEAR INSTALLATIONS INSPECTORATE
ST. PETER'S HOUSE, BALLIOL RD., BOOTLE
LIVERPOOL, L20 3LZ UNITED KINGDOM

J. ROYEN
OECD NUCLEAR ENERGY AGENCY
12 BLVD. DES ILES
ISSY-LES-MOULINEAUX, F-92130 FRANCE

K. RUSSELL
IDAHO NATIONAL ENGINEERING LABORATORY
PO BOX 1625, MS 3779
IDAHO FALLS, ID 83415 USA

O. SANDERVAG
SWEDISH NUCLEAR POWER INSPECTORATE
KLARABERGSVIADUKTEN 90
STOCKHOLM, 10658 SWEDEN

H. SASAJIMA
TOSHIBA CORP.
8, SHINSUGITA-CHO, ISOGO-KU
YOKOHAMA, 235 JAPAN

M. SATTISON
LOCKHEED IDAHO TECHNOLOGIES CO.
PO BOX 1625, MS 3850
IDAHO FALLS, ID 83415-3850 USA

N. SCHAUKI
SIEMENS/WYLE
445 UPSHIRE CIRC.
GAITHERSBURG, MD 20878 USA

P. SCHEINERT
WESTINGHOUSE BETTIS ATOMIC POWER LAB.
PO BOX 79
WEST MIFFLIN, PA 15122 USA

E. SCHMIDT
NUS CORP.
910 CLOPPER ROAD
GAITHERSBURG, MD 20878 USA

F. SCHMITZ
IPSN
CE CADARACHE
ST PAUL LEZ DURANCE, 13108 FRANCE

W. SCHOLTYSSEK
FORSCHUNGSZENTRUM KARLSRUHE
POSTFACH 3640
KARLSRUHE, 76021 GERMANY

M. SCHWARZ
IPSN
CE CADARACHE
ST PAUL LEZ DURANCE, 13108 FRANCE

M. SEITO
JAPAN INSTITUTE OF NUCLEAR SAFETY
FUJITA KANKO TORANOMON BLDG. 7F
MINATO-KU, TOKYO 105 JAPAN

P. SEONG
KOREA ADVANCED INST. OF SCIENCE & TECH.
373-1 GUSONG-DONG YUSONG-KU
TAEJON, 305-701 KOREA

S. SETH
THE MITRE CORPORATION
MS:W779, 7525 COLSHIRE DRIVE
MC LEAN, VA 22102 USA

W. SHA
ARGONNE NATIONAL LABORATORY
9700 S. CASS AVENUE
ARGONNE, IL 60439 USA

W. SHACK
ARGONNE NATIONAL LAB
BLDG. 212
ARGONNE, IL 60439 USA

J. SHEFFIELD
OAK RIDGE NATIONAL LABORATORY
PO BOX 2008
OAK RIDGE, TN 37831-6248 USA

S. SIM
KOREA ATOMIC ENERGY RESEARCH INSTITUTE
DUKJIN-DONG 150, KAERI
TAEJON, KOREA

L. SIMPSON
ATOMIC ENERGY OF CANADA LTD.
WHITESHELL LABORATORIES
PINAWA, MANITOBA ROE 1L0 CANADA

W. SLAGLE
WESTINGHOUSE ELECTRIC CORP.
PO BOX 355
PITTSBURGH, PA 15230 USA

L. SLEGERS
SIEMENS-KWU
P.O. BOX 101063, BERLINER STR. 295
OFFENBACH, D63067 GERMANY

S. SLOAN
IDAHO NATIONAL ENGINEERING LABORATORY
PO BOX 1625
IDAHO FALLS, ID 83415-3895 USA

V. SMIRNOV
RRC "KURCHATOV INSTITUTE"
KURCHATOV SQUARE 1
MOSCOW, 123182 RUSSIA

F. SOUTO
SCIENCE & ENGINEERING ASSOCIATES, INC.
6100 UPTOWN BLVD. NE, STE 700
ALBUQUERQUE, NM 87110 USA

K. ST. JOHN
YANKEE ATOMIC ELECTRIC CO.
580 MAIN ST.
BOLTON, MA 01741 USA

R. STEELE, JR.
IDAHO NATIONAL ENGINEERING LAB
PO BOX 1625
IDAHO FALLS, ID 83415-3870 USA

P. STOOP
NETHERLANDS ENERGY RES. FOUNDATION
PO BOX 1, 1755 ZG PETTEN
WESTERDUINWEG 3, PETTEN,
THE NETHERLANDS

M. STRAND
SCIENTECH, INC.
11140 ROCKVILLE PIKE, SUITE 500
ROCKVILLE, MD 20852 USA

V. STRIZHOV
RUSSIAN ACADEMY OF SCIENCES
B. TULSKAYA, 52
MOSCOW, 113191 RUSSIA

E. STUBBE
TRACTEBEL ENERGY ENGINEERING
AVENUE ARIANE 7
BRUSSELS, 1200 BELGIUM

W. STUBLER
BROOKHAVEN NATIONAL LABORATORY
BLDG. 130, PO BOX 5000
UPTON, NY 11973-5000 USA

S. SUNG
KOREAN NUCLEAR FUEL CO.
HYUPSIN-MEMSION #101,
177-9 YONGDUZ-DONG JUNG-GU,
TAEJON, SOUTH KOREA

H. TAGAWA
NUPEC
BROOKHAVEN NAT. LAB., APT. 4C
UPTON, NY 11973 USA

M. TAKAYASU
NUCLEAR FUEL INDUSTRIES, LTD.
950, OHAZA NODA KUMATORI-CHO
SENNAN-GUN, OSAKA 590-04 JAPAN

T. TANAKA
SANDIA NATIONAL LABORATORY
PO BOX 5800, MS 0737
ALBUQUERQUE, NM 87185-0737 USA

J. TAYLOR
BROOKHAVEN NATIONAL LABORATORY
BLDG. 130, PO BOX 5000
UPTON, NY 11973-5000 USA

C. THIBAULT
WYLE LABORATORIES
7800 HIGHWAY 20 WEST
HUNTSVILLE, AL 35807-7777 USA

H. THORNBURG
CONSULTANT
901 S. WARFIELD DR.
MT. AIRY, MD 21771 USA

E. TITLAND
MATERIALS & ENERGY ASSOCIATES, INC.
512 IDLEWILD RD., PO BOX 1107
BEL AIR, MD 21014 USA

J. TONG
ATOMIC ENERGY CONTROL BOARD, CANADA
280 SLATER STREET
OTTAWA, ONT KIP 5S9 CANADA

I. TOTH
KFKI ATOMIC ENERGY RESEARCH INST.
PO BOX 49
BUDAPEST, H-1525 HUNGARY

R. TREGONING
NAVAL SURFACE WARFARE CENTER
CODE 614, 3A LEGGETT CIR.
ANNAPOLIS, MD 21402 USA

R. VALENTIN
ARGONNE NATIONAL LABORATORY
9700 S. CASS AVENUE - BLDG. 308
ARGONNE, IL 60439 USA

K. VALTONEN
FINNISH CENTRE FOR RAD. & NUC. SAFETY
PO BOX 14
HELSINKI, FIN-00881 FINLAND

T. VAN ETTEN
KNOLLS ATOMIC POWER LABORATORY
PO BOX 1072 (P3-172)
SCHENECTADY, NY 12301-1072 USA

M. VESCHUNOV
RUSSIAN ACADEMY OF SCIENCES
B. TULSKAYA, 52
MOSCOW, 113191 RUSSIA

Y. WAARANPERA
ABB ATOM
NUCLEAR SYSTEMS DIV.
VASTERAS, S-72163 SWEDEN

N. WAECKEL
EDF SEPTEN
12-14 AVENUE DUTRIEVOZ
VILLEURBANNE, 69628 FRANCE

J. WATKINS
IDAHO NATIONAL ENGINEERING LAB
PO BOX 1625
IDAHO FALLS, ID 83415-3870 USA

M. WETZEL
BECHTEL CORP.
9801 WASHINGTONIAN BLVD.
GAITHERSBURG, MD 20878 USA

K. WHITT
SOUTHERN NUCLEAR
40 INVERNESS CENTER PKWY.
BIRMINGHAM, AL 35201 USA

W. WIESENACK
OECD HALDEN REACTOR PROJECT
P.O. BOX 171
HALDEN, NORWAY

G. WILKOWSKI
BATTELLE COLUMBUS
505 KING AVENUE
COLUMBUS, OH 43201 USA

S. WILLIAMS
DOMINION ENGINEERING, INC.
6862 ELM ST.
MC LEAN, VA 22101 USA

R. WOOD
OAK RIDGE NATIONAL LABORATORY
PO BOX 2008, MS 6010
OAK RIDGE, TN 37831 USA

J. WREATHALL
WREATHWOOD GROUP
4157 MACDUFF WAY
DUBLIN, OH 43016 USA

J. WRIGHT
MODELING & COMPUTING SERVICES
6400 LOOKOUT ROAD
BOULDER, CO 80301 USA

G. WROBEL
ROCHESTER GAS & ELECTRIC CORP.
89 EAST AVENUE
ROCHESTER, NY 14649 USA

L. WUNDERLICH
KNOLLS ATOMIC POWER LABORATORY
PO BOX 1072 (D2-221)
SCHENECTADY, NY 12301-1072 USA

G. YADIGAROGLU
SWISS FED. INST. OF TECH. &
PAUL SCHERRER INST.
ETH-ZENTRUM, CLT
ZURICH, CH-8092 SWITZERLAND

L. YEGOROVA
RRC "KURCHATOV INSTITUTE"
KURCHATOV SQUARE 1
MOSCOW, 123182 RUSSIA

K-J. YOO
KOREA ATOMIC ENERGY RESEARCH INST.
PO BOX 105, YUSONG
TAEJON, 305-600 KOREA

M. YOUNG
SANDIA NATIONAL LABORATORY
PO BOX 5800
ALBUQUERQUE, NM 87185-0748 USA

T. ZAMA
TOKYO ELECTRIC POWER CO., INC.
1901 L ST., NW, SUITE 720
WASHINGTON, DC 20036 USA

G. ZIGLER
SCIENCE & ENGINEERING ASSOCIATES, INC.
6100 UPTOWN BLVD. NE, STE 700
ALBUQUERQUE, NM 87110 USA

PROCEEDINGS OF THE
23rd WATER REACTOR SAFETY INFORMATION MEETING
October 23-25, 1995

CONTENTS - VOLUME 2

SEVERE ACCIDENT RESEARCH I
C. Tinkler, Chair

SEVERE ACCIDENT RESEARCH II
A. Rubin, Chair

Review of EPRI Nuclear Human Factors Program

Lewis F. Hanes and John F. O'Brien
Electric Power Research Institute
Palo Alto, CA

The Electric Power Research Institute (EPRI) Human Factors Program, which is part of the EPRI Nuclear Power Group, was established in 1975. Over the years, the Program has changed emphasis based on the shifting priorities and needs of the commercial nuclear power industry. The Program has produced many important products that provide significant safety and economic benefits for EPRI member utilities. This presentation will provide a brief history of the Program and products. Current projects and products that have been released recently will be mentioned.

Introduction

The EPRI human factors program, which is formally named the Human Performance Technology (HPT) Product Group (PG), was initiated in 1975. Since then, 67 products have been produced by 23 contractors. In addition, EPRI HPT PG staff personnel have worked closely with and supported other EPRI PGs on projects in which human performance was important. Examples include support provided in developing the Man-Machine Interface Systems chapters of the Advanced Light Water Reactor Utility Requirements Documents, and in planning an experiment on the effects of respirator use on worker performance.

The 67 products reviewed in this report include only those that have been the prime responsibility of the HPT PG. The products consist of reports, guidelines, functional specifications, videotapes, authoring software, decision-aiding software, training material, tests, hardware and complete systems (e.g., heat stress personal monitor).

Utility Need and EPRI Response

The utility need for HPT is to maintain safety while reducing Operations & Maintenance (O&M) costs by increasing worker productivity and reducing consequential human error. The EPRI HPT activity has responded to this need by developing and providing products to improve:

- the process and to reduce costs of assessing personnel qualifications and proficiency, and preparing personnel to perform jobs.
- performance of control room operators in managing and craft personnel in maintaining the plant.

The HPT PG has developed an approach to create products that responds to high priority industry needs. The approach involves very close coordination with the HPT PG utility subcommittee that provides direction to the choice of projects and reviews and approves plans, budgets and progress. In addition, in almost every project at least one utility with high interest participates actively in all phases of the effort. The approach first involves identification of a major problem (e.g., high costs associated with training maintenance craft workers who already possess the knowledge and skills to perform a job, but are given training because no satisfactory method exists to provide a basis for training exemption). The typical approach in creating a product that solves such a problem involves the following phases:

1. Survey industry to determine seriousness, nature, underlying causes, etc., of the problem and need for a solution.

2. Develop prototype interventions/solutions to the problem.

3. Working with at least one utility, implement and evaluate the intervention / solution, and perform a cost-benefit analysis.

4. Modify and finalize the intervention/solution as a product based on phase 3 results.

5. Distribute the product and assist utilities during implementation.

Product Description

The 67 products developed by the HPT PG may be classified as shown in Figure 1. An example

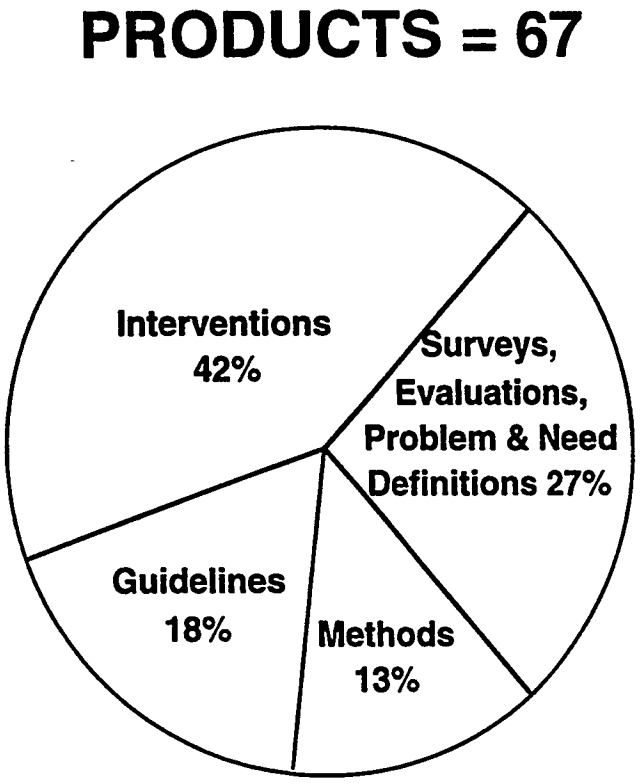

Figure 1. Classification of HPT Products by Type of Product.

of a product in the Surveys, Evaluations, and Problem & Need Definitions category was a 1988 report entitled, "Control Room Deficiencies, Remedial Options, and Human Factors Research Needs" (EPRI NP-5795). A 1993 report (EPRI TR-101981) entitled, "Workbook for Maintenance Proficiency Testing," is an example of a Methods product. One example of a Guidelines product is a 1994 report (EPRI TR-102872) entitled, "Functional Specification Requirements for a Microprocessor-Based Replacement Annunciator System." A recent Intervention that utilities have accepted widely is Maintenance Job Cards (EPRI TR-104602). Several thousand Job Cards have been distributed and are in use. Job Cards are pocket size

card packets containing accurate reference information that can be used directly on the job (e.g., torquing conversion formulas). Another example of a successful intervention is a commercially available Heat Stress Personal Monitor described in a 1991 report (EPRI NP-4453-L) entitled, "Heat-Stress Management Program for Power Plants." (The Heat-Stress Management Program is another example of a very successful product.)

Figure 2 classifies the 67 HPT products into three categories. The types of products in the

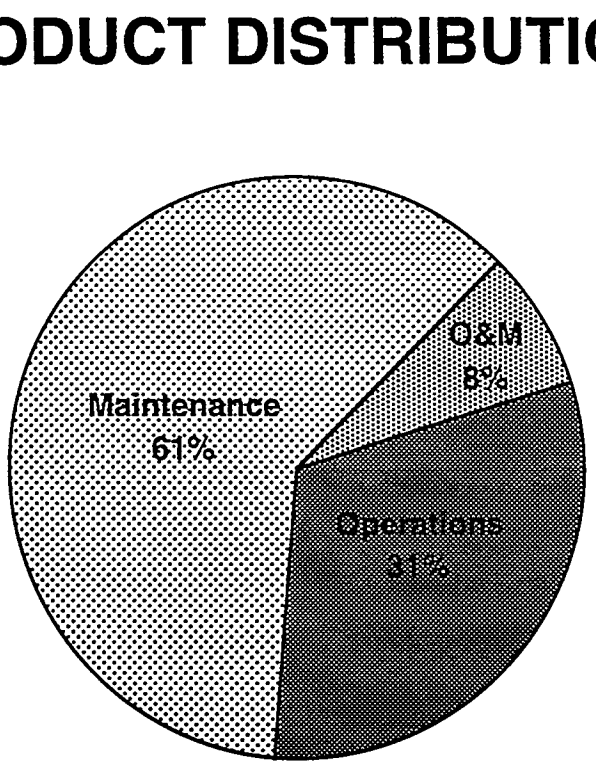

Figure 2. Classification of HPT Products by Application.

Operations and the Maintenance categories are obvious. An example of a product in the O&M category is a 1988 report (EPRI NP-6209) entitled, "Effective Plant Labeling and Coding." This document provides recommendations applicable both to the control room and to the remainder of the plant.

The HPT PG thrust has changed over the years with shifting utility needs (Figure 3). Products in pre-TMI years were concerned with control room reviews and methods for correcting human factors deficiencies. Following TMI, products addressing control room human factors issues were expanded. Products were delivered dealing with control room enhancements, displays, and alarm systems. A Human Factors Primer was published to make nuclear plant management more aware of the need for and value of human factors. During the immediate post-TMI period, human factors products addressing maintenance issues were completed, also. The interest in maintenance resulted from recognition that the majority of consequential human errors occur during maintenance tasks, that high costs are associated with such errors, and that worker training is expensive. In recent years, the EPRI HPT program has shifted mainly to products solving maintenance problems. This has occurred because of recommendations by the EPRI utility advisors who provide direction to the HPT PG.

Current Projects

The HPT PG is currently involved in three major projects: Maintenance Proficiency Assessment Tools (MPAT), Tools for Procedure Preparation, and Tools to Improve Qualification of Nondestructive Evaluation (NDE) Personnel.

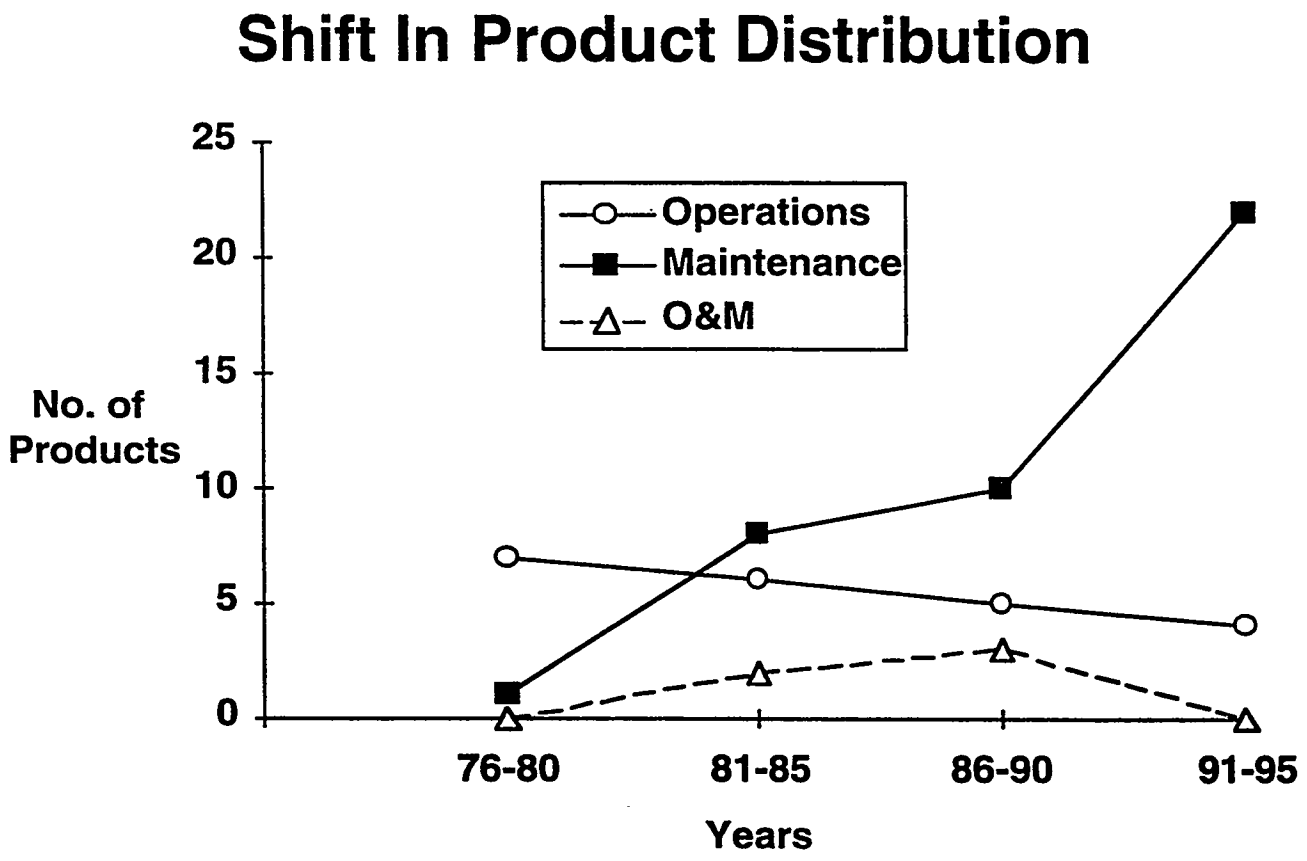

Figure 3. Shift in Product Applications with Changing Utility Needs.

The industry need for MPAT is to reduce the costs of unnecessary training and to ensure the assignment of qualified and proficient workers to perform important plant tasks. MPAT consists of a set of written and performance tests to assess the knowledge and skill level of personnel to accomplish specific plant tasks, and a methodology by which additional reliable and valid tests may be developed by utilities. Demonstrating competency of plant and contractor personnel through knowledge and skills testing ensures that only those needing training are required to attend a plant's training program. The methodology and validated tests have been applied in selected crafts (primarily for mechanical, electrical and I&C tasks) by a number of utilities, resulting in significant utility documented cost savings and other benefits. INPO has accepted that successfully passing a test developed by this methodology provides a basis for exempting a worker from training.

MPAT has been identified by several utilities as an effective way to reduce O&M costs. For example, one utility uses MPAT tests to assess the knowledge and skills of its contracted outage support workers. Personnel successful on both the written and performance tests are allowed to complete the pre-outage processing. Significant cost savings are being realized by the utility.

EPRI's MPA Test Bank, now containing 106 tests, became operational in 1994. The Test Bank is designed to provide a data base of task-specific written and performance evaluation tests for use by participating member utilities. This minimizes the need for each utility to develop its own tests, thus reducing duplication of effort. This saves time, reduces costs, and provides high quality validated tests. Utilities have found that the task-specific tests developed by one utility and entered into the Test Bank are suitable to be used by other utilities either as-developed or with only minor, usually plant-specific, modifications.

In addition to the Test Bank, EPRI is creating an on-line Contractor Qualification Registry. This Registry will contain all the data necessary for participating members to identify contract workers who have successfully completed MPA tests and the necessary details to determine if additional training is needed by these workers prior to performing site tasks.

The Tools for Maintenance Procedures Preparation project was initiated in 1995. The utility need for this project revolves around the question of whether procedures should be written with a high level of detail, so that craft workers are expected to follow instructions verbatim in the performance of their work, or written with less detail, assuming that the workers will apply common knowledge that constitutes the "skill of the craft." In interviews conducted by an EPRI contractor (1994 report EPRI TR-103247 entitled, "Procedures Software Tool (PST) Requirements Analysis and Functional Description") plant personnel cited cases where procedures with insufficient detail resulted in a maintenance error, which subsequently resulted in equipment malfunction. Insufficiently detailed instructions were also cited as a frequent reason for delaying maintenance work while the necessary instructions were obtained by craft workers. Craft workers, however, also identified problems related to maintenance and testing instructions that were too detailed. Such procedures were cited as contributing to reduced attention to the job and limiting the craft workers' use of their best judgment. Procedures that were too detailed were also cited as being too difficult to follow, due to the excessive amounts of text. Thus, both maintenance errors and maintenance inefficiencies were identified as resulting from procedures that were written at an inappropriate detail level.

The objectives of the EPRI project are as follows:

- develop a method to measure the level of detail in plant maintenance procedures and determine if the level of detail is at an appropriate level for workers at a given plant.

- develop guidelines for use of the method so that utilities may measure level of detail in their procedures, and may determine if procedures should be modified, training provided to facilitate procedure use, etc.

This project is expected to produce a product that is tested and available to utilities in 1996.

The Tools to Improve Qualification of NDE Personnel project has been on-going for several years. The industry need for this effort is based on observations that NDE inspectors may be the weakest link in the NDE process, and that reliable NDE is essential as plants age. Research conducted as part of this project revealed relatively large individual differences in performance among NDE personnel, even among those who have received extensive training and have extensive experience. These differences, combined with the high failure rates that have been associated with ultrasonic operator training programs, suggested the potential value of improved training and screening candidates for these jobs prior to their entering the training and qualification process. In fact, revised training emphasizing decision strategies has improved course completion rate by 55%. A recent cost analysis indicated that even a moderately successful screening program would provide a substantial return on investment because per-candidate screening costs are very small relative to per-candidate training and qualification costs. In 1995 a computer-based screening test usable by utilities was completed and is being

validated for early identification of personnel most likely to succeed on NDE jobs.

The 1996 plan is to continue product development in NDE inspector qualification and training. Even though the project has created useful and cost effective products that are in wide use, the need exists for additional improvements. The major remaining problems in NDE qualification and training will be evaluated and prioritized. Recent technological developments, such as multi-media and virtual reality, will be screened against the problems, and a product developed and tested.

Concluding Remarks

The EPRI HPT program is completing its twentieth year in 1995. Review of the program reveals that it has produced many useful products that are currently being applied by utilities. Net cost savings realized by utilities for a few of the more recent HPT products are presented below.

	Plant Upgrade Savings
Alarm System Upgrade	$4.13M
	Annual Cost Savings per Plant
Heat Stress Management Program	$811K
Maintenance Proficiency Assessment Tools	$240K
Job Cards Information Support	$106K
Video Technology	$30K
	Program Setup Cost Savings per Plant
Shift Work Program	$65K

An important role that the EPRI HPT program fulfills is to maintain close coordination with other industry (e.g., INPO and NEI), government (e.g., the NRC and DOE), and international (e.g., OECD Halden Reactor Project and the Central Research Institute of Electric Power Industry of Japan) groups. It is important utilities be aware of relevant human factors and related activities that could have impact (positive or negative).

The HPT program emphasis has shifted over the years in response to utility needs. Currently, maintenance products that can be demonstrated to produce major cost savings in the near-term are of high priority. One senior EPRI utility advisor, however, cautions that HPT should be on the leading edge "bubble," and should not be doing things others can do. In addition, utility advisors are recommending that HPT work closely with other EPRI PGs on joint projects where human performance is an important element (e.g., on-line maintenance), and respond to emerging industry issues.

Recent data clearly show that human performance deficiencies account for a large proportion of plant O&M non-fuel costs. Even though the EPRI HPT program products have been one of the important contributors in the reduction of significant events and O&M costs, the need for even more dramatic reduction is needed. The challenge to the EPRI HPT activity, and for that matter, all technical activities, is to demonstrate that investment in the activity will produce results of great value to the industry.

Interim Results of the Study of Control Room Crew Staffing for Advanced Passive Reactor Plants

Bruce P. Hallbert, Angelia Sebok, & Kjell Haugset
OECD Halden Reactor Project
P.O. Box 173, N-1751, Halden NORWAY

Dolores S. Morisseau & Julius J. Persensky
U.S. Nuclear Regulatory Commission

ABSTRACT

Differences in the ways in which vendors expect the operations staff to interact with advanced passive plants by vendors have led to a need for reconsideration of the minimum shift staffing requirements of licensed Reactor Operators and Senior Reactor Operators contained in current federal regulations (i.e., 10 CFR 50.54(m)). A research project is being carried out to evaluate the impact(s) of advanced passive plant design and staffing of control room crews on operator and team performance. The purpose of the project is to contribute to the understanding of potential safety issues and provide data to support the development of design review guidance. Two factors are being evaluated across a range of plant operating conditions: control room crew staffing; and characteristics of the operating facility itself, whether it employs conventional or advanced, passive features.

This paper presents the results of the first phase of the study conducted at the Loviisa nuclear power station earlier this year. Loviisa served as the conventional plant in this study. Data collection from four crews were collected from a series of design basis scenarios, each crew serving in either a normal or minimum staffing configuration. Results of data analyses show that crews participating in the minimum shift staffing configuration experienced significantly higher workload, had lower situation awareness, demonstrated significantly less effective team performance, and performed more poorly as a crew than the crews participating in the normal shift staffing configuration. The baseline data on crew configurations from the conventional plant setting will be compared with similar data to be collected from the advanced plant setting, and a report prepared providing the results of the entire study.

INTRODUCTION

Staffing Requirements for Operating Nuclear Power Units

The operation and management of a nuclear power plant require a sustained, coordinated effort to achieve both economic goals and compliance with established safety requirements. During much of the time, the focal point of these efforts is the main control room, where power operations are conducted by licensed personnel. This control room staff has the responsibility for oversight and decisions about the operation of the plant, except during unusual events in which the command and control of the plant may be temporarily exercised from another centralized location (e.g., the technical support center). Because of the dependence on these personnel, qualification requirements and minimum staffing of nuclear power plants are specified by federal regulation. These requirements are found in 10CFR 50.54(m).

In addition to these requirements, licensees are required to provide engineering expertise on shift (50 FR 53621). This has resulted in the creation of the Shift Technical Advisor (STA) position, which can be filled either by the addition of a staff member, or by combining the STA job requirements with those of one of the existing senior reactor operator (SRO) positions. By complying with the federal regulations, an operating single unit nuclear power plant would, at a minimum, have either four or five licensed Reactor

Operators (ROs) and SROs per shift, depending upon whether or not a dual role SRO/STA is used to fulfill the STA requirement.

Review of New Reactor Designs

In addition to ensuring compliance of existing nuclear units with regulatory requirements, the U.S. Nuclear Regulatory Commission also conducts Design Certification reviews of proposed reactor designs to ensure the compliance of a vendor's proposed design with regulatory requirements. New plant designs have been produced by a number of vendors for which Design Certification is underway. Some of these advanced plant designs rely on new design or application approaches using passive systems to achieve increased redundancy and/or diversity of methods to achieve safety objectives. Although they use proven technologies to a large extent, these advanced passive plant designs also differ in many respects from conventional plant design.

By improvements in ease of plant operation gained through such features as passive design and digital instrumentation and control systems, vendors expect differences in the ways in which the operations staff will interact with passive plants to fulfill their responsibility in achieving plant safety objectives for foreseeable, credible events. These differences have led to a need for reconsideration of the requirements for minimum shift staffing of licensed Reactor Operators and Senior Reactor Operators contained in current federal regulations (i.e., 10 CFR 50.54(m)). For example, performance-based regulation could be potentially more desirable than numerical requirements, given the features of passive plant design.

Since the advanced passive plants under consideration are not yet built there is no opportunity to observe the operation of the plant and the demands placed on the operating staff. Operating experience with these plants and systems is limited to similar systems in other plants (e.g., BWR isolation condenser designs, PWR N_2 injection accumulators, etc.) and designs incorporating similar features (e.g., backfit of digital control systems into existing analog-based control rooms, etc.). Although the basic principles of operating these new plants are similar to existing plants, the range of operating conditions and response requirements may be quite different. Hence, the demands placed on the operating crew itself may be different and this would have significant implications in the design certification process for the advanced passive plants.

Purpose and Objectives

The purpose of this research project is to evaluate the impact(s) of advanced passive plant design and staffing of control room crews on operator and team performance. Such an evaluation will contribute to the understanding of potential safety issues and provide data to support the development of design review guidance in these areas. Two factors are being evaluated across a range of plant operating conditions: 1) control room crew staffing configuration; and, 2) characteristics of the operating facility itself, whether employing conventional or advanced, passive features.

This research is being carried out by conducting a study of control room crew performance. The first phase of this study was carried out at the Loviisa nuclear power station, in Loviisa, Finland. The second phase of this study will be carried out at the Halden Human-Machine Laboratory (HAMMLAB) at the OECD Halden Reactor Project in Halden, Norway. In the first phase, the Loviisa plant served as the conventional reference plant for this study; HAMMLAB will serve as the advanced reference plant in the second phase. Both facilities run a simulated plant model of the Loviisa nuclear power plant. The control room systems at Loviisa used in this study are representative of those in conventional control rooms, as are the time constants of the plant's thermal-hydraulic performance. The control room systems used in HAMMLAB will consist of video display unit-based information and control systems, similar in form and function to those of advanced plant control rooms. In addition, some of the time constants of the thermal-hydraulic model in HAMMLAB will be longer than at Loviisa to emulate longer thermal-hydraulic time

constants in advanced plants. These longer time constants are due to the performance of passive systems or other design features different from conventional plants.

Two different control room crew staffing configurations are used: a normal control room crew staffing configuration level, and a minimum control room crew staffing configuration. The normal staffing configuration is based on current federal regulation for staffing of a single operating unit at a single unit site, which is similar to the current staffing practice at the Loviisa plant. The minimum staffing configuration is based on the minimum crew size considered by an advanced passive plant vendor, or the minimum crew composition which would typically occur at Loviisa.

A final objective of this research is to evaluate the utility of simulation techniques for studying operator and crew performance. Task network simulations were constructed for the scenarios in this research prior to collecting data on crew performance. Following data collection, the actual performance of the crew will be compared with that predicted by the simulation. The results of these comparisons will be used to evaluate the fidelity of the models developed. These results will be used to identify strengths and limitations in the methods and current techniques available for modeling crew performance, the relationships between the quality of information provided by such techniques relative to others (e.g., ranging from static task analyses to full scale simulator studies, etc.), and their utility in planning large scale studies, such as the present research, for predicting beforehand the types of possible outcomes and data collection requirements.

APPROACH

Scenarios

Five design-basis scenarios were developed for this study. They are:

- Steam Generator Tube Rupture (SGTR)with a Fire in the Turbine Building and stuck open steam generator safety relief valve;
- Total Loss of Feedwater (LOFW);
- Loss of Offsite Power (LOOP) with stuck open steam generator safety relief valve;
- Interfacing Systems Loss of Coolant Accident (ISLOCA), and;
- Steam Generator Overfill (SGOF).

The scenarios were chosen to cover a range of design basis conditions including overheating of the primary coolant system, overcooling of the primary coolant system, and loss of coolant from the primary system. These conditions correspond to those which are analyzed both in conventional plant safety analyses, and in the safety analysis reports produced by the nuclear steam supply system (NSSS) vendors for the plant designs considered in this study.

The first three scenarios, above, are rule-based. The crews at Loviisa are well-trained on the procedures for these scenarios and have experienced them during training. These three scenarios are not difficult to diagnose, each having a number of very salient symptoms. The last two scenarios may be considered knowledge-based scenarios. The ISLOCA includes a number of secondary failures that are produced by the initiating event and that complicate the determination of the source of the leak. In the SGOF scenario, the failures of the feedwater flow control valves and ensuing steam generator level increase occur in quick succession, interfering with the crew's resources to identify and select the correct system procedure for responding to this event.

Each of the scenarios requires significant mobilization and coordination of crew activities to minimize challenges to the safety of the plant, personnel, and environment. All scenarios require coordination with personnel outside the control room, such as maintenance, instrumentation, radiation protection personnel, and field operators. In addition, offsite notification of plant management, local safety and national safety

authorities were included as part of the scope of these scenarios. The intent of including these features was to simulate all of the control room and outside control room activities that would take place if similar events were to actually occur, to determine whether or how these activities interact with the crew's ability to conduct necessary procedurally-governed control room tasks, and to identify whether the mobilization of onsite and offsite personnel could be affected by a reduced shift staff.

Simulator Performance Characteristics Used to Emulate Reference Plants

In specifying performance characteristics of the two simulators used for this research, the aim was to produce performance representative of characteristics of the reference plants identified for the study. The Loviisa nuclear power plant model is used in the simulations both at Loviisa and in Halden. Since this nuclear power plant is a Russian light-water VVER design, it was important to ensure the performance of the simulators could produce performance representative of both conventional and advanced plants. For the phase of the study that occurred at Loviisa, U.S. conventional plant performance characteristics were identified from published information. For the phase of the study planned to occur at Halden, advanced passive plant performance characteristics were identified from the safety analysis reports for the advanced plants used in this research.

For the conventional plant, key event and time constants for specific thermal-hydraulic behavior of conventional plants were identified from Wheatley et al. (1987). The reference study provides information on three design basis scenarios, similar to or having features in common with, three of the scenarios used in this study. Wheatley *et al.* include modeling of plant response to a total loss of feedwater, steam generator overfill, and small-break loss of coolant accident for a Babcock & Wilcox, Combustion Engineering, and Westinghouse plant. Using key events or thermal hydraulic time constants from the reference study meant that for the overheating and overcooling scenarios, the steam generator models in the Loviisa Training Simulator (LOTS) were reduced to about 1/3 of their actual capacity. This ensured that dryout of the steam generators and heatup of the primary coolant system in the loss of feedwater scenario, for example, occurred at about the same rate and in the same range of time as were predicted to occur in the conventional plants in the reference study.

For the advanced plant, the safety analysis report (SAR) provided to the NRC by the vendors were reviewed to find time constant, key events (e.g., passive system actuations, etc.) and a description of thermal-hydraulic performance for scenarios similar to those used in this study. The advanced plant reference plant designs used include the Westinghouse AP600, ABB Atom PIUS Plant, General Electric Simplified Boiling Water Reactor, and the Atomic Energy of Canada Limited CANDU 3 plant designs. Of the four safety analyses used, only two describe design basis or accident analyses to a level of detail that allowed extrapolation of key events or thermal hydraulic time constants to the level of detail required. Of these two safety analyses, only one is a PWR. However, the accident analyses in the SAR for the particular scenarios include different assumptions about equipment availability and recovery than the designed scenarios. As a result, best estimates, based on the advanced plant SAR were used to determine the significant characteristics to be used in emulating advanced plant performance. This means, for example, that dryout of the steam generators and heatup of the primary coolant system in the loss of feedwater scenario will take approximately twice as long to occur in HAMMLAB than at LOTS. In addition, some safety system actuations have been programmed to occur automatically (e.g., HPSI, etc.) when certain conditions exist in the plant (e.g., inventory loss, etc.) to emulate passive system actuations.

In addition to simulator thermal-hydraulic performance characteristics, the instrumentation and control (I&C) systems at Loviisa and in the Halden Man-Machine Laboratory (HAMMLAB) were reviewed and adjusted accordingly to make them representative of both conventional and advanced plants.

Training

Prior to participating in the study, operators received training on the changes in the plant model that had been made to the simulation and were briefed on the overall purpose of the study. They also discussed the types of results that would be produced together with the simulator training personnel from Loviisa, who assisted in this study. The data collection materials were presented to the operators for familiarization, and they received instructions on the data collection materials used in this study. Following the training and familiarization period, each crew had a short break prior to participating in the scenarios and data collection.

Data Collection

Four crews participated in the collection of data at the Loviisa training simulator. Each crew was presented with the five study scenarios over a period of two days. The sequence of scenario presentation was randomized for each crew, in order to minimize order and practice effects. Two of the crews participated in the normal shift staffing configuration, having one control room supervisor (CRS), one reactor operator (RO), one balance of plant operator - or turbine operator - (TO), and one control room technician (CRT). The remaining two crews participated in the minimum shift staffing configuration, which included the CRS, RO, and TO but did not have the control room technician in the crew. All of these control room crew members are licensed operators, having either the equivalent of an RO or SRO license. Control room supervisors at this station are also degreed technical personnel (e.g., engineers, etc.).

During each scenario, the crew was given a normal operating task involving, for example, load following, monitoring at full power, etc., during the outset of the scenario. Typically during this non-disturbed portion of the scenario the simulator would be paused for the first time, the crew informed, and measures of each crew member's situation awareness and subjective workload obtained. The ratings of team interaction for this period of the scenario were also obtained from the two trained observers participating in the study. These observers sat in the simulator area behind and to the side of the shift crew in an area which would not interfere with the crew's activities, and observed the crew's team performance (e.g., procedures accessed, communication between members, discussions and decisions, etc.).

The pauses lasted an average of approximately 5-7 minutes. The simulated initiating event was typically introduced after the first pause, though this differed from scenario to scenario. Some time after the crew had noticed a malfunction in the plant and had mobilized to respond, the next pause occurred and the same performance measures were obtained. Three of the scenarios contain five data collection intervals during the scenario for obtaining subjective workload, situation awareness, and team performance data, while two scenarios contain four data collection intervals.

The intent in collecting performance measures throughout each scenario is to establish a baseline of operator performance data during normal operation, and then to obtain several sets of measures following the onset and peak of the disturbance, and during the resolution phase of the scenario when mitigation efforts should be mostly complete and stabilization of the plant is achieved. Comparisons can then be made of crew performance to determine the effect of these types of design basis scenarios on baseline measures. Comparisons can also be made between crew staffing configurations to determine if differences between crews can be observed, and whether these differences increase as a function of scenario length, demands of specific scenarios, etc. The baselines also provide a measure that can be used to evaluate the comparability of crews, to ensure that any potential pre-study differences between crews do not affect the outcomes and inferences drawn from the study of performance data.

In addition to these measures, data on crews' management of the scenarios were collected. Task completion times were obtained for important tasks (e.g., manual reactor trip, pressurizer cooldown, etc.) identified prior to the simulator portion of the study via task analyses of each scenario. Data on a number of plant parameters were logged from the simulator and stored for later analysis. Event logs produced at

the simulator facility provide a listing of key system events (e.g., reactor protection system signals, pressurizer heater bank actuations, etc.) indicating automatic and manual system actions, and alarms (e.g., accumulator level low level or gradient alarm, critical function alarms, etc.). In addition, audio-video recordings of each crew's performance was recorded on video cassette at the simulator for later use.

Performance Measures

Situation Awareness

SA is a necessary but not sufficient requirement for optimal performance (Endsley, 1990). A primary reason for measuring SA is that some of the factors influencing SA are likely to be different between the conventional plant and advanced plant. Some features of the advanced plant should tend to increase SA by integrating information from various sources, such as the integrated process overview display, while others should minimize the amount of information an operator should need to attend to in processing disturbance information (e.g., alarm filtering features). However, some aspects of the advanced plant control room could interfere with SA. Automation of operations which is more easily accomplished in the advanced plant control systems emulated in this study, reduces overall workload, but may also leave the operator out of the loop or unaware of system functioning. Overall, one of the advantages of advanced control room design is expected to be enhanced operator SA (O'Hara, 1990). However, no studies have been conducted to assess this expectation.

As Endsley (1993) demonstrated in a series of experiments, SA differs from workload. These experiments showed that workload influences SA in a variety of ways. With low workload, operators may have low SA due to boredom, lack of attention, vigilance problems, etc. However, if an operator with low workload pays attention to information in his/her environment and if the information is presented in an efficient or well-understood manner, the operator may have high SA. In high workload situations, the operator may have such low SA due to being so overburdened with tasks, the pace of incoming information, etc., that s/he is unable to formulate an accurate assessment of what is occurring in the plant. In the scenarios selected for this study, one of the workload parameters to be affected will be the number of crew members available in the two shift staffing configurations. If the remaining crew members must work harder to accomplish the same goals or suffer information loss due to the loss of the other crew member, then systematic differences might occur in situation awareness between the normal and minimum shift staffing configurations.

SA assessment methodologies have been applied in the aviation industry and serve as basic evaluation and a major design criteria for the design of new pilot support systems (Selcon and Taylor, 1989). SA is measured to assess whether or not pilot support systems do in fact provide the pilot with an enhanced understanding of the state of the aircraft. The human factors community has realized the relevance of SA to the nuclear process control industry and has identified the need to evaluate new complex system designs in terms of how well they support operator SA (AIAA, 1992). Research in the nuclear and process control industry (Hogg et al, 1994) has shown SA measurement to be applicable to this domain. It is this latter adaptation of the SA measurement technique to the nuclear power plant process control domain which was used to obtain measures of operator SA in this study.

Subjective Workload

Workload is of particular importance in complex systems, especially in nuclear power plant control rooms, because of its effect on human error and performance. In general, a certain amount of workload is considered optimal. If the workload is much below this level, operators become under-stimulated and may become inattentive, lose SA, and suffer degraded performance when the situation demands increased effort. Also, overloaded operators generally suffer performance degradation as they are simply unable to keep up with the demands of the task. Some expert operators may be able to perform satisfactorily, at least temporarily in an over-loaded condition, but over time their performance degrades. Between these

two extremes is the optimal workload which provides sufficient challenge to keep operators stimulated without excessively taxing their capabilities (Huey and Wickens, 1993).

A further consideration on workload and performance is that sudden changes in workload, specifically a sudden transition from low to high workload results in the most pronounced decrements in performance (Kantowitz and Casper, 1988). This aspect of the relationship between workload and performance is especially significant for advanced NPP control room evaluation. In the advanced plants reviewed for this study, many routine operations of the plant will be automated. Sudden increases in workload when the crew is called upon by the system to respond to an unanticipated situation may be a potential source of performance problems. In this study, there may also be some additional workload placed on the members of the 3-person crew who will not have the extra licensed operator at their disposal to assist during peak activity periods, and to assist in EOP tracking, etc. A further research issue in the present study is whether the degree of workload produced by this staffing configuration change will produce any marked differences in the workload experienced by the remaining members of the minimum control room crew configurations.

One of the subjective workload measurement techniques that has been validated in several studies and widely applied is the NASA TLX (Wierwille and Eggemeier, 1993; Hill, Iavecchia, Byers, Bittner, Zaklad, and Christ, 1992; and Moroney, Biers, Eggemeier, and Mitchell, 1992). This technique offers several advantages over other subjective measurement techniques. NASA TLX is particularly suited for use in complex systems (Weirwille and Eggemeier, 1993) and applied settings (Nygren, 1991). The NASA TLX is a globally sensitive measure and the sensitivity of the technique has been demonstrated (Moroney et al, 1992). As Weirwille and Eggemeier (1993) recommend, TLX should be given strong consideration in test and evaluation applications. Hill et al (1992) found TLX to be one of the best subjective workload assessment techniques in terms of operator acceptance and validity. For the measurement of subjective workload in this study, NASA TLX was used.

Team Performance

All of the activities performed in the control room of a nuclear power plant are done so by teams of operators. However, few studies have considered the performance of teams in complex, dynamic systems (Coury and Terranova, 1991). In those that have looked at team performance, teams have been shown to perform better than individuals in controlling a dynamic system. Teams are better able to control a complex, dynamic system and diagnose failures than individuals, control deviations better, may require fewer control actions to achieve control, and are more efficient in information gathering than individuals (Hooper, Coury, and Terranova, 1991; Montgomery and Hauth, 1991).

However, teams do not always work to the advantage of a situation. In a team situation, individual members may become complacent, relying on other members to do certain tasks without necessarily verifying that the tasks have actually been performed. Teams may also develop overly cohesive or dependent thinking in which members are hesitant to introduce or entertain discrepant information, for fear of creating conflict or disturbing group cohesion. Pooling the abilities of a number of highly skilled individuals should result in a better product, but this is sometimes not the case. Group processes can be slow, cumbersome, inefficient, and lead to individual member frustration. This process loss inherent in the way a group functions must be considered in determining the correct balance between crew tasks and system dependence on humans (Foushee and Helmreich, 1983; Cooper, White, and Lauber, 1979).

Several measurement techniques have been developed to assess teamwork. These measure the communication and other aspects of teams. One particularly relevant technique is the Behaviorally Anchored Rating Scale (BARS). This is a technique or a type of test used to assess team performance; it is not an actual test (Meister, 1985). Using the BARS technique, six (Montgomery, Gaddy, and Toquam, 1991) or seven dimensions (Baker and Salas, 1992; Montgomery and Hauth, 1992) of team interaction are assessed. The actual crew interaction dimensions assessed varied in different studies, but in general they

are dimensions relevant for team behavior. Some common examples include: communication, openness, task coordination, team spirit, maintaining task focus, and adaptability (Montgomery et al, 1991); adaptability, coordination, acceptance of criticism, giving criticism, team sprit and morale, cooperation, and communication (Glickman et al, 1987; Glickman et al, 1986).

The present study assessed team performance using a BARS developed with experienced plant personnel. Five behavioral categories were used to assess team performance, based upon input and refinement from an initial group of six. These include communication, openness, coordination as a crew, team spirit, and task focus and decision making. Specific behaviors for each of the dimensions were obtained from previous studies which used similar categories (Glickman et al, 1987; Morgan et al, 1986).

Crew performance

An additional crew performance rating technique was taken from a prior study which focused on the performance of nuclear power plant control room crews (Hanson et al, 1987). Similar to BARS, this technique uses the observations of knowledgeable or trained observers to provide an evaluation of how well the crew performs on a variety of dimensions. These dimensions are intuitively linked to the types of behavior required to achieve and maintain control of plant performance. These crew performance measures include selection of the proper mitigation path, control of the plant, crew communications, and confidence in their own performance and decision making. These measures were created through evaluation of crew performance in a previous study of crew performance by licensed operator examiner personnel.

RESULTS

Analysis of Data

Analyses of data are required for subjective measures, objective measures, and plant performance measures to determine whether overall the performance of crews, and which specific aspects of crew performance, are affected by crew staffing levels (e.g., normal vs. minimum crew configurations). Analyses are also required to determine whether crew performance varies as a function of scenario and whether any such differences occur in specific scenarios (e.g., SGTR, etc.) or in different types of scenarios (e.g., rule-based, knowledge-based). At present, analyses have been performed for subjective crew measures. The experimental design of the study comprises a between-within design, having both between groups factors (e.g., crew size) and within-subjects factors (e.g., repeated measurement of situation awareness, etc., during each scenario).

The data analyses from this study were performed using the Statistica software package. Applying statistical tests to experimental data introduces the risk of two fundamental errors. A Type I error occurs when the researcher concludes that there are main experimental effects where there actually are none present, as opposed to Type II errors in which the researcher concludes that there are no experimental effects when such effects actually are present. In dynamic simulator studies like these, the likelihood of committing a Type II error is larger than committing a Type I error. According to Wiener (1971), far too much emphasis has been put on the significance level convention of 0.05 and 0.01:

> "When the power of tests is likely to be low under these levels of significance (0.05 and 0.01), and when type I and type II errors are of approximately the same importance, then .30 and .20 levels of significance may be more appropriate than the .05 and .01 levels" (Wiener, 1971 page 14)

In this study, to avoid erroneously concluding that the performance of the different-sized crews are equal when they in fact are different, is equally important as to avoid concluding that they are different when they, in fact, are equal. To avoid type II errors, results approaching the 0.20 level are also taken into account and discussed.

Subjective Workload, Situation Awareness,, and Team Performance

A repeated measures Multivariate Analysis of Variance (MANOVA) was performed on the situation awareness, subjective workload, and team performance data. As mentioned earlier, data on each of these measures was obtained a number of times during each scenario, and these are the repeated measures in this analysis. The independent variables in the analysis are: crew size (3- or 4-person crew), scenario, and scenario period (e.g., period in the scenario in which measures were obtained). Table 1 summarizes the results of this analysis.

Table 1. Results of repeated measures MANOVA on subjective measures.

	Summary of Effects:			
Effect	**Rao's R**	**df (effect)**	**df (error)**	**p-level (α)**
Scenario	1.14	12	21	not significant
Crew size	5.39	3	8	< 0.025
Period	68.94	9	2	< 0.014
Scenario X period	3.84	36	9	< 0.02

The results of the analysis demonstrate a significant effect of crew size, scenario period, and a significant interaction between scenarios and the data collection interval (Scenario X Period interaction). This means that the two shift staffing complements differed on the dependent measures, but does not indicate how (e.g., for which measures or which crew size configuration had higher/lower scores). The results also show a significant main effect for scenario period, indicating that somehow the performance of all crews differed on the subjective measures during different periods of the scenarios. The significant interaction effect of scenario and scenario period indicates that although the performance measures do not differ significantly across scenarios alone, differences in performance are observed between performance during some portion(s) across scenarios. This means that aggregating performance data across scenarios may not be warranted for some measures. In subsequent univariate analyses of individual performance measures, the effect of scenario is tested separately, prior to aggregating scenario data.

Subjective Workload

Subjective workload measures obtained from individual crew members during the data collection intervals from all scenarios were analyzed. The independent variables used in the analysis are: scenario, crew size, crew member position (e.g., control room supervisor, reactor operator, turbine operator), and scenario period. A 4-way repeated measures Analysis of Variance (ANOVA) was conducted on the subjective workload data. Table 2 summarizes the results of this analysis.

Table 2. Table of effects of scenario, crew size, position, and scenario period on subjective workload.

	Summary of Effects:			
Effect	**F**	**df (effect)**	**df (error)**	**p-level (α)**
Scenario	1.32	4	30	not significant
Crew size	8.54	1	30	< 0.01
Position	9.73	2	30	< 0.01
Period	78.44	3	90	< 0.0001
Scenario X position	2.41	8	30	< 0.05
Crew size X position	3.89	2	30	< 0.05
Scenario X period	4.70	12	90	< 0.01
Crew size X period	2.14	3	90	< 0.10

Scenario and Scenario Period Effects

The results of the analysis show that the scenarios used in this study, in general, do not produce significantly different levels of workload on crews. All of the scenarios used in this study are design basis events, and appear to create roughly equivalent amounts of workload. Some of the crew members experienced more demand on some scenarios than other crew members (e.g., the significant Scenario X Position interaction). This makes intuitive sense, since some scenarios result in challenges to the primary systems, while others are initiated in the balance of the plant. Thus, specific crew members should experience some difference in the amount of workload placed upon them by the demands of the scenario. In addition, subjective workload differs across scenarios and scenario periods. This simply means that although there are no differences in subjective workload produced by the different scenarios on the whole, there are periods in some scenarios in which the workload of crew members is higher than in other scenarios.

In summary, the results indicate that the scenarios produced roughly the same amount of physical, mental, temporal demand, etc., on the crews. As these are all design basis scenarios which require significant crew efforts to contain their effects, this result is not surprising. The two additional findings related to scenario effects indicate that the specific measurement technique used for measuring subjective workload in this study is sensitive to differences in the amount of workload produced by the scenarios on different crew members, and during different periods of the scenarios.

The effect of scenario period was found to be highly significant. Figure 1 shows the development of workload over scenario periods. We refer to this as the workload effect. The subjective workload scale has a range from 0 (total absence of workload) to 100 (extremely high workload). As can be seen, workload increases dramatically following the onset of the disturbance. The amount of subjective workload experienced by the operator following a major disturbance is approximately double the amount experienced during non-disturbed (e.g., normal) operations. After reaching a peak during the middle of the scenario, workload subsides somewhat, but does not fall to pre-disturbance levels.

Crew Size and Position Effects

The results show significant effects of workload produced by crew size, position, and the interaction of crew size and position (Crew size X Position). In addition, the two crew sizes experienced different amounts of workload over scenario periods. The 4 person crew experienced significantly less workload than the 3-person crew.

Figure 2 is a graph of the crew member workload in the 3-person and 4-person crews. An examination of the differences among crew members shows that it is the control room supervisor in the 3-person crew who experiences the greatest amount of workload. The additional crew member in the 4-person crew may account for this difference as it is his/her presence in the crew that differs between the two crew configurations. Differences in the subjective workload of the RO in the two crew configurations is much smaller, and the TOs in the different crew configurations experience the same amount of workload

Figure 3 is a graph of the 3-person and 4-person crew subjective workload across scenario periods. As can be seen in the graph, the 3-person crew experiences higher workload across all scenario periods.

Figure 1. Subjective Workload by Scenario Period

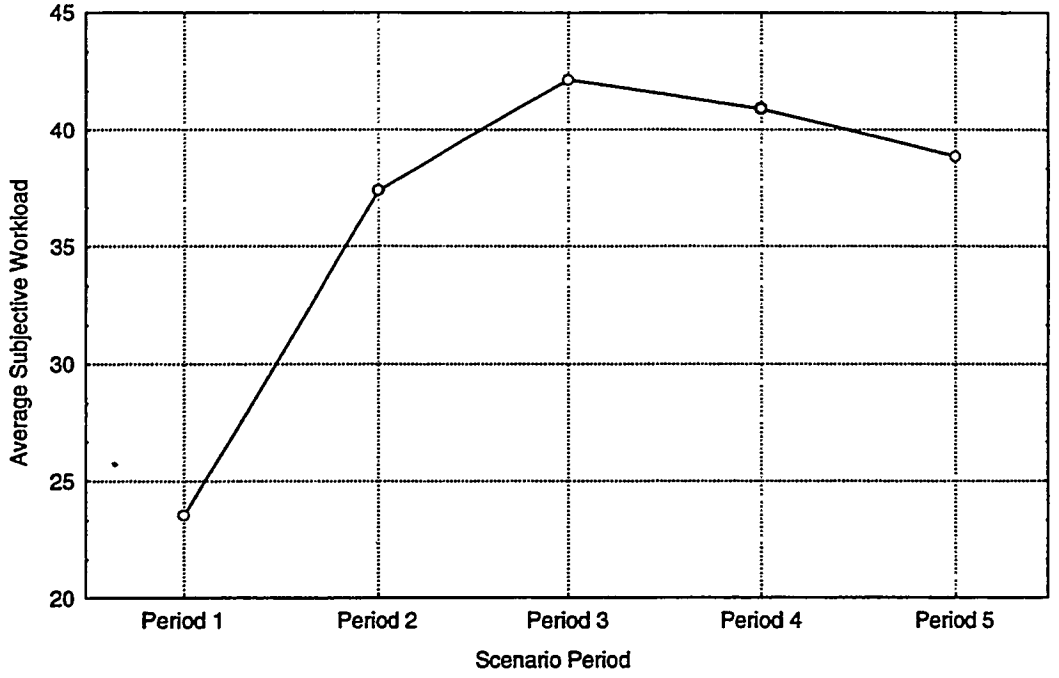

Figure 2. Plot of Subjective Workload by Position and Crew Size
2-Way Interaction

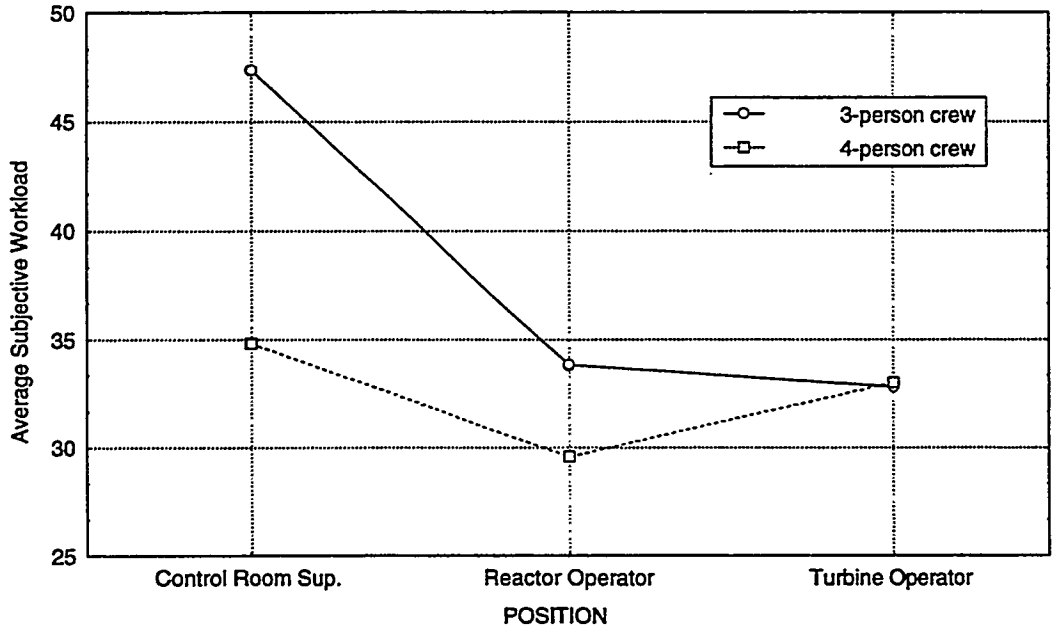

Figure 3. Plot of Subjective Workload by Crew Size and Scenario Period
2-Way Interaction

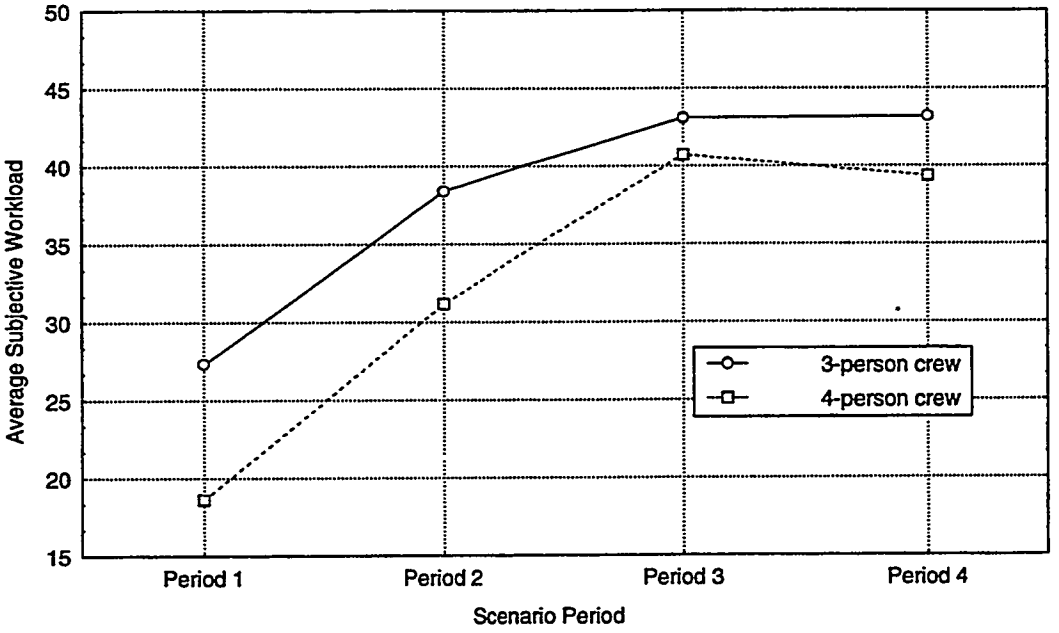

Situation Awareness

Situation Awareness measures obtained from individual crew members during the data collection intervals from all scenarios were analyzed. The independent variables used in the analysis are: scenario, crew size, crew member position (e.g., control room supervisor, reactor operator, turbine operator), and scenario period. A 4-way repeated measures Analysis of Variance (ANOVA) was conducted on situation awareness data. Table 3 summarizes the results of this analysis.

Table 3. Table of effects of scenario, crew size, position, and scenario period on situation awareness.

	Summary of Effects:			
Effect	**F**	**df (effect)**	**df (error)**	**p-level (α)**
Scenario	2.71	4	50	< 0.05
Crew size	11.64	1	50	< 0.005
Position	1.49	2	30	not significant
Period	8.87	3	150	< 0.01
Scenario X period	5.38	12	150	< 0.001
Crew size X period	1.6	3	150	< 0.20
Scenario X crew size X period	1.53	12	150	< 0.15

Scenario and Period Effects

The analyses show that the situation awareness of crews, in general, differed across scenarios. Table 4 shows the Average SA scores of crew members on all scenarios. As discussed in the scenario descriptions, three of the scenarios were rule-based and two were knowledge based. To evaluate whether this grouping of scenarios could account for the differences in situation awareness observed across scenarios, a planned comparison was conducted in which the SA of crews in the rule-based scenarios was contrasted with SA in knowledge-based scenarios. An analysis of variance was conducted and showed a significant difference between SA in rule-based and knowledge-based scenarios ($F\ 1,50 = 9.87, p < 0.01$); crews having significantly higher SA in rule-based than in knowledge-based scenarios.

Table 4. Average situation awareness across study scenarios.

Scenario	Average SA	Standard Deviation
Steam generator tube rupture	0.78	0.10
Loss of feedwater	0.76	0.07
Loss of offsite power	0.75	0.06
Interfacing systems loss of coolant	0.7	0.11
Steam generator overfill	0.68	0.12

Similar to the workload effect identified earlier, analysis of SA across scenario periods reveals a similar Situation Awareness effect. This is shown in Figure 4. The situation awareness score ranges from a low of 0 (poor SA) to 1.0 (complete SA). Following disturbance onset, situation awareness experiences a marked reduction. The loss of SA from baseline conditions to it's trough represents a loss of approximately 20% of the baseline SA. Following a sharp decline in SA, crew members gradually regain their SA later in the scenario after they have determined the causes of the disturbance, have implemented the necessary mitigation actions, and have regained control of plant parameters. However, post-accident SA levels (i.e. Period 5 measurement) are still lower than pre-accident SA levels.

Crew Size Effects

The analysis results show that 3-person and 4-person crews differ significantly from each other in terms of their Situation Awareness. Three-person crews have significantly lower SA than four-person crews. In addition, this effect occurs consistently across scenario administration period. Figure 5 is a graph of situation awareness of the 3-person and 4-person crews across scenario periods. The graph shows a similar initial drop in SA for both the minimum and normal crew staffing configurations. However, by the third and fourth interrupts across all scenarios in general, the 4-person crew made substantial progress in regaining SA to pre-disturbance levels. On the other hand, the 3-person crews SA continues to decrease. This difference is quite marked: whereas the 4-person crew is able to regain it's SA, the 3-person crews' SA continue to decline over the course of the scenarios.

Figure 4. Average Situation Awareness across Scenario Periods

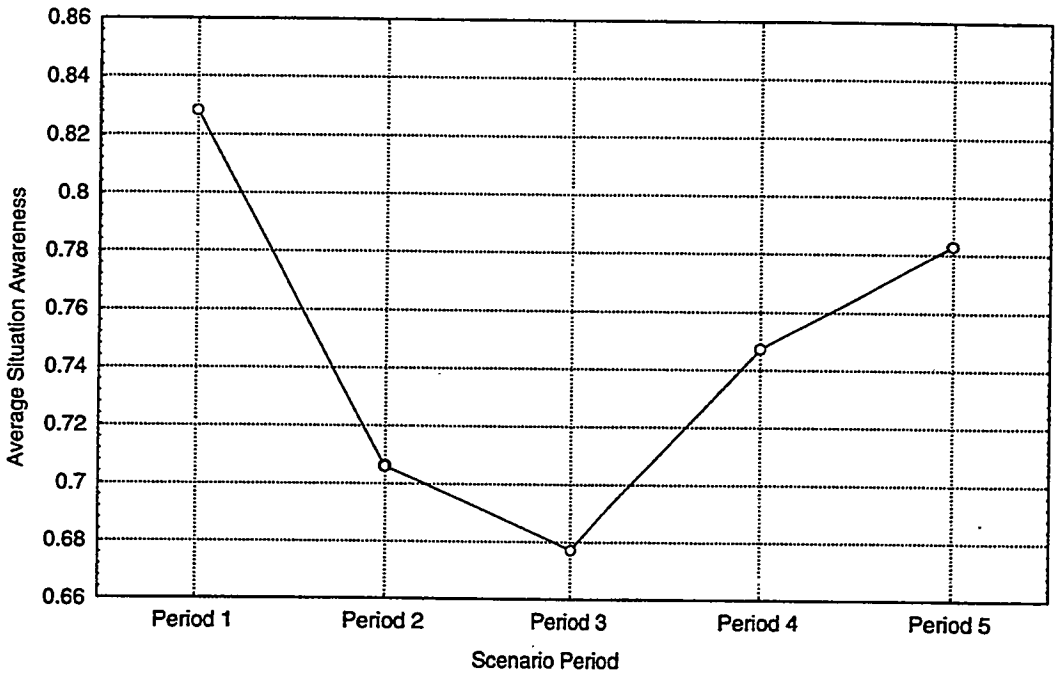

Figure 5. Plot of Situation Awareness by Crew Size and Scenario Period
2-Way Interaction

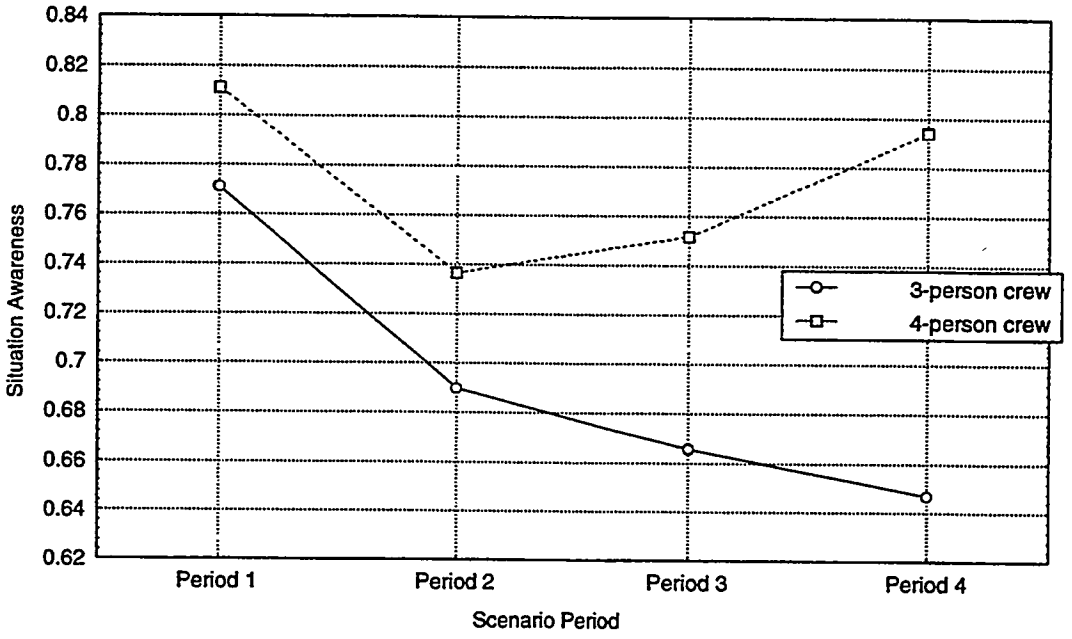

Team Performance

Team performance measures obtained from the trained observers during the data collection intervals from all scenarios were analyzed. The independent variables used in the analysis are: scenario, crew size, and scenario period. A 3-way repeated measures Analysis of Variance (ANOVA) was conducted on the team performance data. Table 5 summarizes the results of this analysis.

Table 5. Table of Effects of scenario, crew size, and scenario period on team performance.

	Summary of Effects:			
Effect	**F**	**df (effect)**	**df (error)**	**p-level (α)**
Scenario	0.81	4	10	not significant
Crew size	2.55	1	10	< 0.15
Period	2.90	3	30	< 0.05
Scenario X period	2.17	12	30	< 0.05
Crew size X period	2.44	3	30	< 0.10

Scenario and Scenario Period Effects

The results show that team performance did not differ significantly across scenarios, but as is the case with the other subjective measures, team performance was significantly different across scenario periods. The results show a strong scenario period effect, indicating that there is some systematic variation in teamwork over the course of the scenarios. Figure 6 provides a plot of team performance scores across scenario periods. The team performance scale is from 1 (poor teamwork) to 7 (optimum teamwork). The figure shows that during non-disturbed conditions, crews show an average level (e.g., a score of ~4.5 on a scale from 1 to 7) of crew performance. Following the initiating event, crews mobilize, and team performance increases. This is probably because during normal operating activities, there is not always a demand for a close coupling of activities. During an abnormal event, however, and especially during a design basis event, the challenges to the plant require much closer and sustained coordination of activities. Following this initial mobilization, team performance gradually declines. Between the third and fourth data collection period, team performance has fallen to pre-disturbance levels. By the end of the scenario, team performance has declined substantially.

Crew Size Effects

The results of the analysis also show crew size and crew size by scenario period effects. In general, 3-member crews had lower levels of team performance than did 4-person crews. The results also indicate that this effect interacts with scenario period. Figure 7 shows a plot of team performance across scenario periods for 3-member and 4-member crews. Following the initial mobilization which both crews experience, the 3-person crews' team performance declines rapidly, and stabilizes at a lower level. The team performance of the 4-person crew continues to increase beyond the mobilization period though it, too, declines towards the end of the scenario. However, the team performance of the 4-person crews are markedly better in the disturbance portion of the scenarios than that of the 3-person crews.

Figure 6. Average Team Performance across Scenario Periods

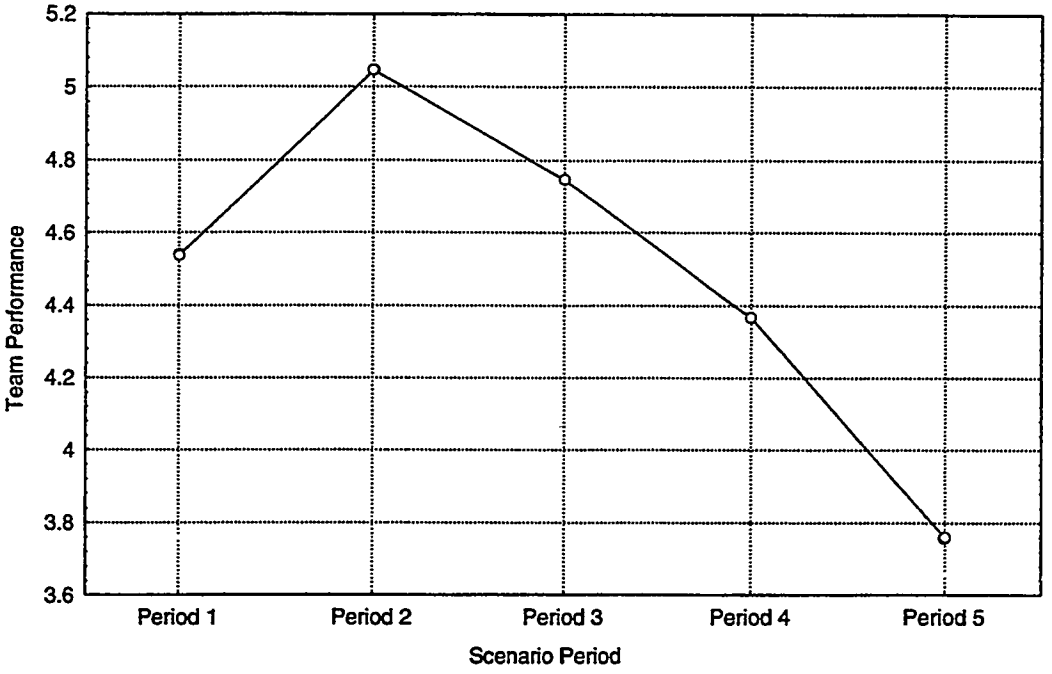

Figure 7. Team Performance by Crew Size and Scenario Period
2-Way Interaction

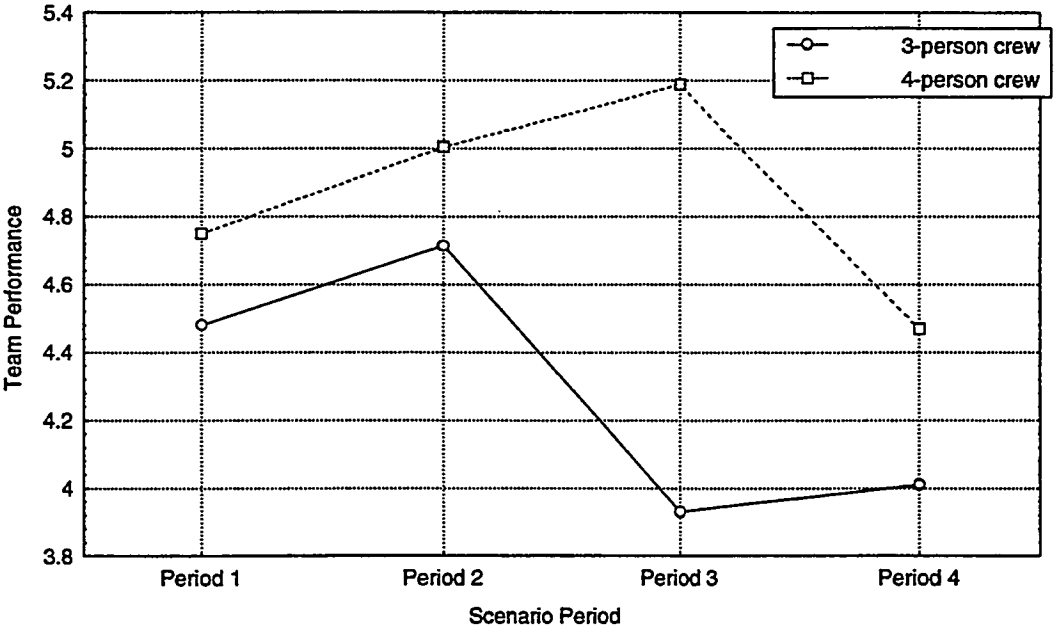

Rated Crew Performance

Ratings of crew performance obtained from the trained observers following each scenario were analyzed. The independent variables used in the analysis are: scenario and crew size. A 2-way Analysis of Variance (ANOVA) was conducted on the data, and the results are summarized in Table 6.

Table 6. Table of Effects of scenario and crew size on rated crew performance.

	Summary of Effects:			
Effect	**F**	**df (effect)**	**df (error)**	**p-level (α)**
Scenario	1.29	4	10	not significant
Crew size	22.10	1	10	< 0.001
Crew size X scenario	4.15	4	10	< 0.05

Figure 8 is a plot of the ratings obtained on crew performance measures for the 3-person and 4-person crews. Ratings on the measures of crew performance range from 1 (poor performance) to 10 (excellent performance). The figure shows that 4-person crews obtained higher ratings than the 3-person crews on all of the crew performance measures. Crews participating in the normal crew size staffing configuration exhibited better control of the plant, adopted consistently better solution paths in mitigating the disturbance, communicated better, and displayed more confidence in their performance and decisions than did 3-member crews.

Figure 8. Crew Performance Ratings for Minimum and Normal Crew Configurations

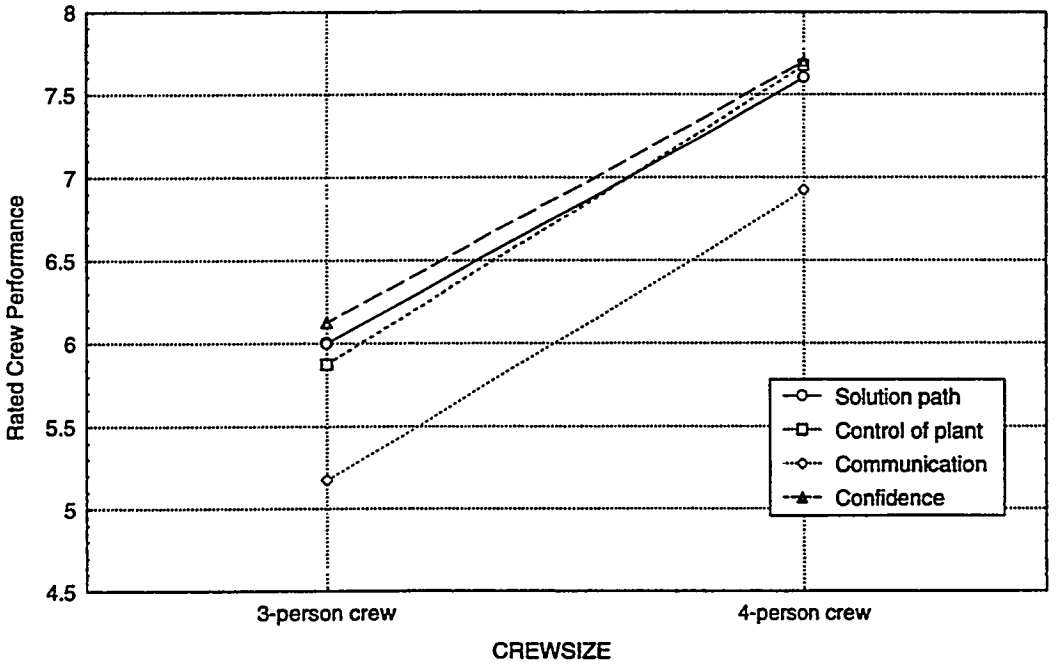

CONCLUSIONS

The conclusions that are drawn reflect the first phase of the study, and the results of the analysis of a portion of the data from this study phase. Not all of the relevant performance measures obtained in the study have been analyzed, nor will they be until the data collection from the advanced plant condition in this study is completed. Thus, the conclusions reached are tentative, and await the results of analysis of other measures.

The trends in crew performance measures collected at the Loviisa nuclear power plant are very consistent, and merit consideration. This phase of the study dealt with studying a normal and minimum crew staffing configuration in a conventional plant. To ensure that the Loviisa plant would produce thermal-hydraulic performance (e.g., key events, etc.) similar to U.S. plants, modifications were made to the plant model at the simulator prior to crew participation. Some striking results were obtained on all of the subjective measures used in this study relating to crew size.

Before discussing the effects of crew size on performance measures, however, it is important to consider some of the aspects contributing to the validity of the study itself. Simulator studies are often criticized because they take place outside of the real control room, involve scenarios that crews are or may be highly trained on, don't include offsite notifications and communications with outside control room staff, or performance of activities outside the control room. Simulator studies, however, represent the best approximation of the actual control room environment, and are, after all, the environment in which crews performance is tested as part of licensing and requalification. The scenarios used in this study represent a broad range of design basis events, involving scenarios for which crews are well-trained , and some for which they have much less training. The analysis of situation awareness of these rule-based and knowledge-based scenarios also demonstrates these differences. Finally, all necessary notification and communication tasks with external personnel, whether on-site or offsite, were included in the scope of these scenarios to maintain a high degree of realism in the scenarios.

Based on the analysis of the subjective workload, situation awareness, and team interaction and crew performance measures, it is apparent that these scenarios challenged the resources of the crews in mobilizing to respond to and mitigating the disturbances. Subjective workload nearly doubled from baseline conditions during the most disturbed phase of the scenario, and situation awareness dropped significantly from baseline conditions. Team interaction degraded over the course of these lengthy scenarios. Feedback from crew members and training personnel who are experienced with observing crews also supports the conclusion that the scenarios contained a high degree of realism and challenge. The difference between the minimum and normal staffing configurations used in this phase of the study is only one crew member. However, significant differences were observed on all subjective performance measures and ratings of crew performance between 3-person and 4-person crews.

The 3-person shift staffing crews experienced significantly higher workload than the normal configuration shift staffing crews. Moreover, the control room supervisor appears to be most directly affected by this difference. The control room supervisor has the overall responsibility for decision making, selection, and prioritization of crew mitigation efforts. Although it is not desirable for any other crew member to receive the additional workload caused by one less crew member, increasing the workload of the CRS in the manner observed in this study may have some serious implications for crew performance. If the CRS becomes over-burdened beyond a level of optimal performance, degradation in the quality of interaction with external staff, notification and mobilization of off-site organizations, and even decision-making within the crew may suffer. Although other crew members' workload do not appear to be affected, the coordination of the crew and communication, for which the CRS often takes the lead or initiative, may be impaired in situations in which the CRS becomes burdened beyond capacity. This may account for some of the reason(s) why crew performance measures (e.g., solution path, control of plant, confidence in actions, etc.) in the 3-person crews were lower than those of the 4-person crews.

The situation awareness of the 3-person crews was found to be significantly lower than the that of the 4-person crews. Whereas all crews experienced an initial SA decrease in response to the onset of the transient, the 4-person crew members were able to recover SA faster and maintain a positive trend following recovery. The 3-person crews, in contrast, tended to lose SA over the course of the scenario. In some situations, late in a disturbance, a crew may be called upon to make an important decision or take an important action. Accurately understanding the development of process events and being able to predict the development of trends in the plant are especially important at such times. The results from SA measurements obtained from both the minimum and normal crew staffing configurations indicate that a normal shift staffing complement may be in a better position to understand the course and direction of events in the plant later in a long disturbance, and make better-informed decisions than a minimum shift staffing complement.

Team interaction also suffers as a consequence of reducing control room crew members. Although all crews mobilized in response to the scenarios used in this study, the crews with a normal shift staffing did so more effectively. Overall, team interaction of crews in the a minimum staffing configuration degrades following mobilization, and does not recover significantly. During the most disturbed portion of the scenarios, the largest difference in team interaction is observed between the minimum and normal-sized crews. Effective team performance is required during design basis events, in which the activities and decisions of the crew affect the utilization of resources and systems at the plant. In addition, since most significant events occur over a protracted period of time, demands will be placed on the operating crew to sustain its performance as a team during stressful circumstances. The results from this phase of the study indicate that a minimum staffing configuration is much more challenged to maintain effective teamwork skills of communication, task focus and decision making, coordination, openness, and team spirit than a normal shift staffing complement.

The effects of workload, situation awareness, and performance as a team also appear to influence how well the crew carries out control room tasks. Both the trained observers and training personnel rated performance of 4-member crews as significantly better than 3-member crews. The differences between the two groups were observed on all rated performance measures. These performance measures are significant, and reflect some of the criteria which an operator examiner might also consider when evaluating crew performance. These results demonstrate both the effect of degraded subjective performance measures that possess a high degree of face validity for predicting behavior, and some of the effects of a reduced shift staffing complement on crew performance. Crews having the minimum shift staffing configuration, as a whole, exhibited more difficulty in establishing relevant mitigation strategies, maintaining control of important plant parameters during disturbance situations and communicating. They also did not demonstrate as much confidence in their activities as the crews having the normal shift staffing configuration.

The results of this phase of the study demonstrate a significant effect on crew performance from a reduction of one crew member. The role of this crew member is not as well defined as those of the reactor operator, balance of plant operator, and control room supervisor. S/he carries out a variety of tasks such as procedure and critical function monitoring, notifications and communication with outside control room and off-site personnel, and assisting as needed in the control room. However, this member's absence appears to exert a more negative effect on the performance, workload, situation awareness, and team performance of the remaining crew members. These results underscore the sensitivity of important crew performance measures to even minor changes in crew composition (e.g., a reduction of only one crew member). They also identify some of the measures that are or may be sensitive to these differences.

STATUS AND PLANS

A baseline set of data has been collected about performance of a minimum and normal shift staffing complement from a setting representative of a conventional nuclear power plant. Further analyses are planned on the objective performance data collected, including study of plant parameter data, task performance data, notifications and coordination with necessary external agencies, etc. In addition, validation of the task network simulations will be performed. The validations will check the accuracy of both the task analysis techniques employed and the simulation results.

The next phase of this study will involve collecting data from crews in the Halden Man-Machine Laboratory at the OECD Halden Reactor Project, which is serving as the advanced plant for this study. Four different crews will come from the Loviisa plant and experience the same design basis scenarios, in a simulated advanced control room. The model used will be that of their own plant and will include additional automatics or passive system features. Two of the crews will serve in the minimum and two in the normal shift staffing configurations. The collection of this data will permit comparison of crew performance between a conventional plant setting and advanced plant setting. It will also help to further evaluate the impact of reduced shift staffing configurations. A report which describes the full study in detail and presents the findings and conclusions will be issued later.

REFERENCES

10 CFR 50.54(m), "Energy: Conditions of Licensees," *Code of Federal Regulations*, Washington, D.C., January 1, 1992.

ABB Atom Preliminary Safety Information Document (PSID). *PIUS: The PIUS Arrangement Principle for a Simplified Passive Advanced Light Water Reactor Plant.*, December, 1989.

American Institute of Aeronautics and Astronautics (1992). *Guide to Human Performance Measurement.* American National Standards Institute. BSR/AIAA G-035-1992.

Atomic Energy of Canada Limited, CANDU Operations. *The CANDU 3 Technical Description.* Technical Report 74-01371-TED-001, Rev. 3, September 15, 1989.

Atomic Energy of Canada Limited, CANDU Operations. *The CANDU 3 Technical Outline.* Technical Report 74-01010-TED-001, Rev. 9, September 15, 1989.

Baker, D.P., and Salas, E. *Principles for Measuring Teamwork Skills.* Human Factors, 34(4), pp. 469-475, 1992.

Cooper, G.E., White, M.D. & Lauber, J.K. (Eds.). *Resource Management on the flight deck.* NASA Conference Publication 2120, Moffet Field, CA: NASA-Ames Research Center, 1979.

Coury, B. G., & Terranova, M. *Collaborative Decision Making in Dynamic Systems.* In *Proceedings of the Human Factors Society 35th Annual Meeting*, September 2-6, San Francisco, CA, 1991.

Endsley, M.R. *Towards a Theory of Situation Awareness in Dynamic Systems.* TTU-IE-94-04. Texas Tech University, Department of Industrial Engineering internal report, Lubbock, TX, 1993.

Endsley, M.R. *Predictive Utility of an Objective Measure of Situation Awareness.* In *Proceedings of the Human Factors Society 34th Annual Meeting*, pp. 41-45, 1992.

Foushee, H.C., & Helmreich, R.L. *Group Interaction and Flight Crew Performance.* in *Human Factors in Aviation*, E. Wiener & D. Nagel (eds.), New York, NY: Academic Press, 1988.

GE Nuclear Energy. *SBWR Standard Safety Analysis Report.* Report 25A5113 Rev. A, August 1992.

Glickman, A.S., Zimmer, S., Montero, R.C., Guerette, P.J., Campbell, W.J., Morgan, B.B. Jr., & Salas, E. *The Evolution of Teamwork Skills: An Empirical Assessment with Implications for Training.* Technical Report 87-016. Prepared for the Office of Naval Research and Human Factors Division (Naval Training Systems Center), Orlando, FL, 1987.

Hanson, D.J., Meyer, O.R., Blackman, H.S., Nelson, W.R., & Hallbert, B.P. *Evaluation of Operation Safety at Babcock and Wilcox Plants Volume 1 - Results Overview.* NUREG/CR-4966, Volume 1, U.S. Nuclear Regulatory Commission, Washington, D.C., October 1987.

Hill, S.G., Iavecchia, H.P., Byers, J.C., Bittner, A.C., Zaklad, A.L., & Christ, R.E. *Comparison of Four Subjective Workload Rating Scales.* Human Factors, 34(4), pp. 429-439, 1992.

Hogg, D.N., Follesø, K., Torralba, B., & Volden, F.S. *Measurement of the Operator's Situation Awareness for Use within Process Control Research: Four Methodological Studies.* HWR-377, OECD Halden Reactor Project, Halden, Norway, 1994.

Hooper, K. N., Coury, B.G., & Terranova, M. Team Performance in Dynamic Systems. In *Proceedings of the Human Factors Society 35th Annual Meeting*, September 2-6, San Francisco, CA, 1991.

Huey, B.M., & Wickens, C.D. (Eds.). *Workload Transition: Implications for Individual and Team Performance.* National Academy Press, Washington, D.C., 1993.

Kantowitz, B.H., & Casper, P.A. *Human Workload in Aviation.* Chapter in *Human Factors in Aviation* (Ed. Weiner, E., & Nagel, D.), San Diego: Academic Press, pp. 157-187, 1988.

Meister, D. *Behavioral Analysis and Measurement Methods.* New York: John Wiley and Sons, Inc., 1985.

Montgomery, J.C., & Hauth, J.T. *Team Interaction Skills Evaluation Criteria for Nuclear Power Plant Control Room Operators.* NUREG/CP-0114, Vol. 1, 1991.

Montgomery, J., Gaddy, C., & Toquam, J. *Team Interaction Skills Evaluation Criteria for Nuclear Power Plant Control Room Operators.* In *Proceedings of the Human Factors Society 35th Annual Meeting*, pp. 918-922, 1991.

Montgomery, J.C., & Hauth, J.T. *Team Interaction Skills Evaluation Criteria for Nuclear Power Plant Control Room Operators.* In *Proceedings of the U.S. Nuclear Regulatory Commission Eighteenth Water Reactor Safety Information Meeting.* U.S. Nuclear Regulatory Commission, Office of Nuclear Regulatory Research, Washington, D.C., 1992.

Morgan, B.B., Jr., Glickman, A.S., Woodard, E.A., Salas, E., & Blaiwes, A. *Measurement of Team Behaviors in a Navy Training Environment.* Technical Report 86-014. Prepared for the Office of naval Research and Human Factors Division (Naval Training Systems Center), Orlando, FL, 1986.

Moroney, W.F., Biers, D.W., Eggemeier, F.Tl, & Mitchell, F.A. A *Comparison of Two Scoring Procedures with the NASA Task Load Index in a Simulated Flight Task.* IEEE Proceedings, pp. 734-740, 1992.

Nygren, T.E. *Psychometric Properties of Subjective Workload Measurement Techniques: Implications for Their Use in the Assessment of Perceived Mental Workload.* Human Factors, 33(1), pp. 17-31, 1991.

O'Hara, J.M. *Advanced Human-System Interface Design Review Guidelines.* In *Proceedings of the U.S. Nuclear Regulatory Commission Eighteenth Water Reactor Safety Information Meeting*, Rockville, MD, 1990.

Selcon, S.J., & Taylor, R.M. *Evaluation of the Situational Awareness Rating Technique (SART) as a Tool for Aircrew Systems Design.* NATO AGARD Aerospace Medical Panel Symposium, pp. 5-1 - 5-8, 1989.

Westinghouse Electric Corporation. *AP600 Standard Safety Analysis Report*, Rev. 0, Simplified Passive Advanced Light Water Reactor Plant Program Report DE-AC03-90SF18495, Prepared for U.S. Department of Energy, San Francisco Operations Office, June 16, 1992.

Wheatley, P.D., et al. *Evaluation of Operational Safety at Babcock and Wilcox Plants, Volume 2 - Thermal-Hydraulic Results.* NUREG/CR-4966, U.S. Nuclear Regulatory Commission, Washington, D.C., November 1987.

Wierwille, W.W., & Eggemeier, F.T. *Recommendations for Mental Workload Measurement in a Test and Evaluation Environment.* Human Factors, 35(2), pp. 263-281, 1993.

Winer, B.J. *Statistical Principles in Experimental Design (2nd Edition).* McGraw-Hill Book Company: New York, 1971.

"Policy Statement on Engineering Expertise on Shift," Federal Register (50 FR 53621), October 21, 1985.

Human-System Interface Design Review Guideline: The Development of Draft Revision 1 to NUREG-0700

John O'Hara, William Stubler, and William Brown
Brookhaven National Laboratory
Upton, NY 11973

Jerry Wachtel and J Persensky
U.S. Nuclear Regulatory Commission
Washington, D.C. 20555

ABSTRACT

Advanced human-system interface (HSI) technologies are being developed in the commercial nuclear power industry. These HSIs may have significant implications for plant safety in that they will affect the ways in which the operator interacts with and supervises an increasingly complex system. The U.S. Nuclear Regulatory Commission (NRC) reviews the HSI aspects of nuclear plants to ensure that operator performance and reliability are supported. The NRC is developing guidance to support its review of these advanced designs. The guidance consists of an evaluation methodology and an extensive set of human factors guidelines which are used in one aspect of the evaluation. The paper describes the guidance development of the evaluation methodology and the guidelines.

INTRODUCTION

One significant outgrowth of the Three Mile Island accident was that the U.S. Nuclear Regulatory Commission (NRC) required all licensees and applicants for commercial nuclear power plant operating licenses to conduct detailed control room design reviews to identify and correct human factors design problems. The NRC developed guidance (NRC, 1981) to support these reviews. Following this activity, the NRC has continued to focus on issues for which there were uncertainties in the scientific data needed to support the review of aspects of plant design and operation that affect human performance and plant safety. One such issue was the introduction into control rooms (CRs) of advanced, computer-based, human-system interface (HSI) technology; a technology which was not used in plants constructed in the 1980s and before. The term "advanced" refers to HSI technologies such as touch-screen controls and large-screen displays which are advanced relative to the HSIs implemented in most current nuclear power plants. Advanced HSIs are emerging in nuclear plants as a result of several factors including: (1) replacements and upgrades of existing CR HSIs with computer-based technologies, and (2) development of advanced CR concepts as part of new reactor designs. These developments could have significant implications for plant safety in that they will affect the role (function) of personnel in the system, the method of information presentation, the ways in which personnel interact with the system, and the requirements imposed upon personnel to understand and supervise an increasingly complex system (O'Hara and Brown, 1994).

The NRC has established programs to review the human factors engineering (HFE) aspects of design and implementation of significant changes to existing CRs and advanced CR designs in order to help assure that the incorporation of advanced technology enhances the potential safety benefits and minimizes the potentially negative effects on performance and plant safety. Because the available HFE review guidance was developed more than ten years ago, well before these technological advances, it did not adequately address these new HSI technologies. Accordingly, updated guidance was needed to serve as the basis for NRC HFE reviews. Thus, the *Human-System Interface Design Review Guideline,* Draft NUREG-0700, Revision 1 (O'Hara et al., 1995) was developed.

This paper addresses the development of updated guidance which consists of an evaluation methodology and HFE guidelines which are used as criteria for part of the evaluation.

HSI DESIGN REVIEW METHODOLOGY

The design review methods used in earlier reviews (NRC, 1981) were modified to address design trends and human performance issues associated with advanced HSIs (O'Hara and Brown, 1994; O'Hara, Higgins, et al. 1994). The resulting methodology was based in general systems theory and the premise that a top-down approach was necessary so that the significance of individual review topics could be seen in relationship to the high-level functions supporting plant safety. Top-down refers to a review approach that starts at the "top" with high-level plant goals that are broken down into the functions necessary to achieve the goals. Functions are broken down into tasks and allocated to human and system resources. Operator tasks are analyzed to identify the alarms, information, and controls that will be required to allow the operator to accomplish assigned functions. The detailed design implementation is the "bottom" of the top-down process. Thus, the evaluation of the detailed HSIs "at the bottom" emphasizes the tasks and plant functions they are designed to support.

Within this context, the overall purpose of the HSI design review is to ensure that the HSI supports safe, efficient, and reliable personnel task performance. This is accomplished by ensuring that design deficiencies, called human engineering discrepancies (HEDs), that could adversely affect plant safety are systematically identified and resolved. The scope of the HSIs included in the review is defined on the basis of their function and not their physical location, e.g., in the CR. Relevant HSIs include all alarms, displays, controls, job performance aids, workstation and workplace layouts. Also included are the environmental conditions in which the HSIs are operated, such as lighting, noise, temperature, and humidity. The staff's reviews address the following methodological aspects of HSI evaluation:

Planning Phase - An HSI design review plan should be developed to ensure that the evaluation is adequately defined in terms of review goals and scope, review team, management process, and technical approach.

Preparatory Analysis Phase - The analyses that make up the preparatory phase provide valuable information which supports the establishment of requirements for the HSI design process. These analyses also provide the technical basis and criteria for the conduct of HSI design verifications and validation; i.e., they identify human performance issues and task requirements with which the HSI should be evaluated. A systems approach should be used to identify HSI design requirements. Three main analyses include:

Operating Experience Review. A review of operating experience should be performed, including examination of plant performance reports and other documents, and a survey of personnel to identify HSI-related human performance issues.

Function and Task Analysis. A review of system functions and personnel functions and tasks should be performed to identify HSI requirements and performance criteria for personnel tasks.

HSI Inventory and Characterization. An inventory of the HSI should be developed, including a description of characteristics, functions, and performance features.

HSI Design Verifications and Validation Phase - HSI design verifications and validation should be performed to ensure that HEDs have been appropriately identified and documented. Because no one method is likely to be sufficiently comprehensive, it may be necessary to perform a series of analyses:

HSI Task Support Verification. This evaluation verifies that the HSI supports all identified personnel task requirements as defined by task analyses. HEDs are identified for: (1) personnel task requirements that are not fully supported by the HSI, and (2) the presence of HSI components which may not be needed to support personnel tasks.

HFE Design Verification. This evaluation verifies that the HSI is designed and implemented to

account for human capabilities and limitations. HEDs are identified if the design is inconsistent with HFE guidelines. The HFE guidelines for this evaluation are described in the next section.

Integrated System Validation. This evaluation validates that the integrated HSI design enables the accomplishment of task performance requirements for safe operation without imposing excessive workload. HEDs are identified if task performance criteria are not met or if the HSI imposes a high workload on plant personnel.

HED Resolution Phase - This phase should ensure that HEDs have been assessed and that important ones have been resolved. The assessment evaluates the safety significance of HEDs. HEDs that have no particular safety significance may be analyzed for improvement, but on a lower priority basis. Once corrective actions have been identified, a plan for their implementation should be developed, including: (1) evaluation of the installation and operation of all HSI modifications, and (2) correction of any implementation problems that are identified.

HSI DESIGN REVIEW GUIDELINES

The effort to develop HFE guidelines in support of HFE Design Verification began with the identification of a set of high-level design review principles based upon an evaluation of research and industry experience related to the integration of personnel into advanced systems (Flach, 1990; Shneiderman, 1987; Smith and Mosier, 1986; Vicente and Rasmussen, 1990). These principles address the generic HSI characteristics necessary to support operator performance, i.e., the operator's primary task of monitoring and controlling the process without imposing excessive demands associated with managing the interface itself such as window manipulation, display selection, and navigation. They also address whether the HSI supports recognition and tolerance of human error, and recovery from such errors when they do occur.

More detailed review guidelines were then developed for specific HSI topics (e.g., graphic displays, touch screens, and expert systems) through the application of a general guidance development process (see Figure 1). The process reflects an effort to develop valid guidance in the most cost effective manner possible. Validity is defined in term of two components: Internal and external validity. Internal validity referred to the degree to which the individual guidelines have a documented empirical or research basis. External validity referred to the extent to which the guidelines conformed to accepted human engineering practices which is established through independent peer review. When available source documents do not adequately meet these criteria, validity is addressed as part of our guidance development process.

Guidelines can be developed from a variety of sources, e.g., existing guideline documents or focused experiments conducted to provide information upon which guidelines can be developed (see Figure 1). These sources are listed in order from least effort (top box) to most effort required. The development of our guidelines began with the identification of primary sources, i.e., guidance documents that were judged of high validity. If the primary source documents were inadequate to serve as a basis for guidance development, appropriate guidance was sought in secondary sources (those having either internal or external validity) and tertiary sources (those without established validity). If these sources provided an inadequate basis, the results from basic technical literature were analyzed. Industry experience, such as published case studies and surveys/interviews with knowledgeable domain experts, was another potentially valuable source for identifying human performance issues and tested design solutions. Although such information might lack a rigorous experimental basis, it would have the benefit of direct relevance to nuclear plants.

Finally, if sufficient data could not be found in the sources described above, original research could be conducted. This approach has the advantages of being focused on specific issues of interest and providing a sound technical basis upon which to develop guidelines. However, this approach is least desirable because of the time and cost required.

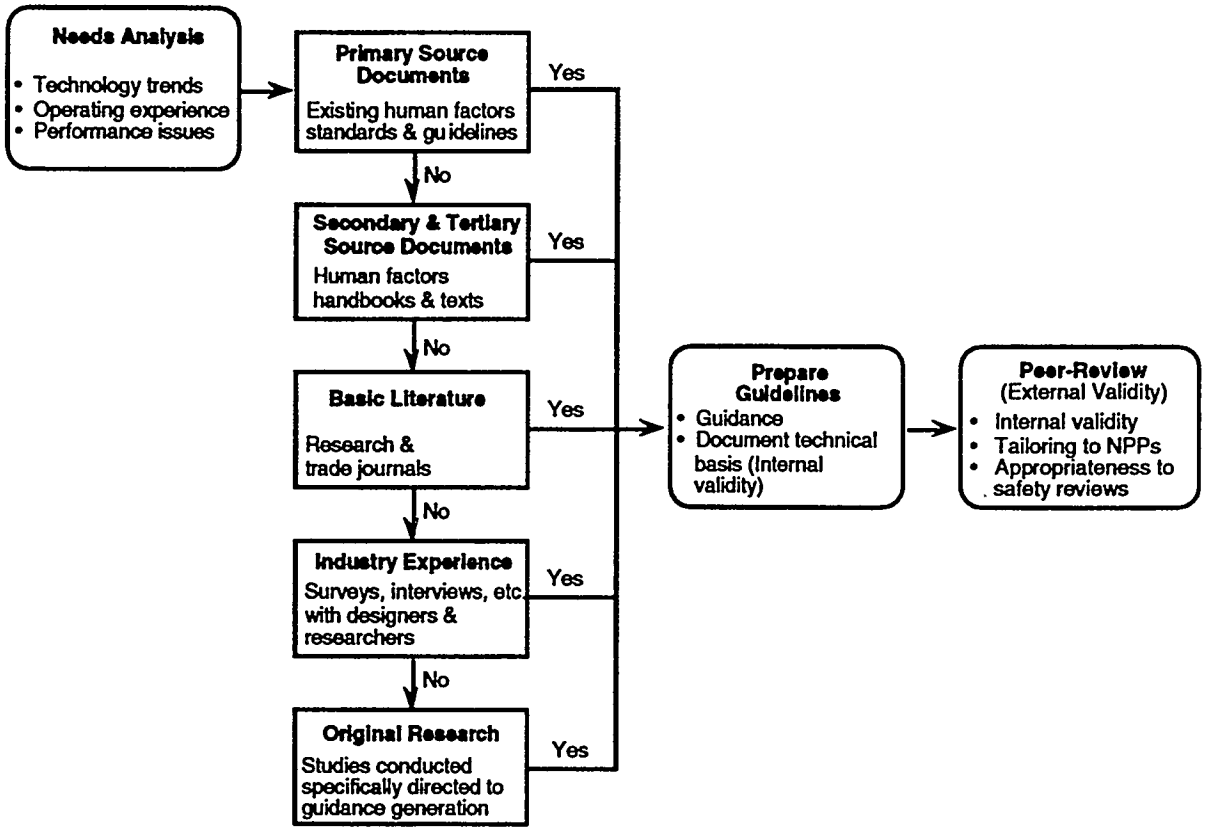

Figure 1. HFE guideline development process

The HFE guideline development process was applied to several areas and the results were documented: for information on general computer-based display and control systems, see O'Hara and Brown (1994); on advanced alarm systems, see O'Hara, Brown, Higgins, and Stubler (1994); and on local control stations, see Brown, Higgins, and O'Hara (1994). Portions of the guidance were evaluated with respect to its scope, technical content, and usability using two approaches (O'Hara and Brown, 1994). First, the guidance was used by experienced human factors reviewers in advanced control room environments. Second the guidance was evaluated in a peer-review workshop. In addition to the above, the workshop provided an evaluation of the validity and the technical basis of the guidance. The general results were very supportive and the guidance was modified based upon the feedback from these evaluations.

The specific HSI review methods and HFE guidelines from these individual efforts were then integrated with an update of the NRC's guidance for the review of conventional CR technology (NRC, 1981) to form a single design review guideline document, Draft NUREG-0700, Rev. 1. Draft NUREG-0700, Rev. 1 addresses both advanced and conventional HSIs and covers topics such as information display, user-system interaction (e.g., dialog formats and navigation), process control and input devices, alarms, analysis and decision aids, inter-personnel communication, workplace design, and local control stations.

In addition to a hard-copy document, the guidance has been developed as an interactive, computer-based review tool suitable for use on a portable computer (see O'Hara and Brown, 1994, for

a complete description of the computer-based review tool). It will facilitate on-site reviews by simplifying guideline access for a specific review, evaluating the interface, and preparing reports. The guidelines are stored in a database composed of several primary fields: guideline number, title, guideline statement, additional information, and source (link to primary source document). Other reviewer-support fields are also provided, e.g., a note pad for reviewers to append comments related to specific guidelines. The interactive review aid provides for many document functions such as immediate access to the table of contents, context index, glossary, and placemarkers. Reviewers can automatically go to desired sections by clicking on a table of contents or index entry. The interactive version will also make it easier to edit the guidelines and incorporate new guidelines as they become available.

PUBLIC COMMENT

Following the document preparation, NUREG-0700, Rev. 1 was made available for public comment. Comments were received from five sources. The majority of comments addressed specific aspects of the HFE guidelines. Many of these comments identified the need to clarify guideline criteria or to break-up compound guidelines into individual guidelines in order simplify their application. There were also requests for additional guidance in some of the areas that were not addressed in the current revision, such as updating of guidance on environmental factors. Such comments were noted and may be addressed in future revisions of the document. In the process of resolving these comments, a number of changes were made to improve the document.

SUMMARY

HSI design review guidance consisting of an evaluation methodology and HFE guidelines has been developed to support the NRC HSI reviews. The HFE guidance development process has been designed to support the updating of the HFE guidelines as technology changes, and to maintain the guidance as an up-to-date source of HSI review criteria. The effort to establish valid guidelines with a documented technical basis is a key aspect to the process. Thus, in addition to the main guidance document, detailed technical reports on the guidance development process and their technical basis were developed.

ACKNOWLEDGEMENTS

This research is being sponsored by the U.S. Nuclear Regulatory Commission. The views presented in this paper represent those of the authors alone and not, necessarily, those of the NRC.

REFERENCES

Brown, W., Higgins, J., & O'Hara, J. (1994). *Local control stations: Human engineering issues and insights* (NUREG/CR-6146). Washington, D.C.: U.S. Nuclear Regulatory Commission.

Flach, J. (1990). The Ecology of Human-Machine Systems I: Introduction. *Ecological Psychology*, 2, 191-205.

Moray, N., and Huey, B. (1988). *Human factors research and nuclear safety*. Washington, D.C.: National Research Council, National Academy of Sciences.

O'Hara, J., Brown, W., Stubler, W., Wachtel. J., & Persensky, J. (1995). *Human-system interface design review guideline* (Draft NUREG-0700, Rev. 1). Washington, D.C.: U.S. Nuclear Regulatory Commission.

O'Hara, J. and Brown, W. (1994). *Advanced human system interface design review guideline* (NUREG/CR-5908). Washington, D.C.: U.S. Nuclear Regulatory Commission.

O'Hara, J., Brown, W., Higgins, J., and Stubler, W. (1994). *Human factors engineering guidelines for the review of advanced alarm systems* (NUREG/CR-6105). Washington, D.C.: U.S. Nuclear Regulatory Commission.

O'Hara, J., Higgins, J., Stubler, W., Goodman, C., Eckenrode, R., Bongarra, J., & Galletti, G. (1994). *Human factors engineering program review model* (NUREG-0711). Washington, D.C.: U.S. Nuclear Regulatory Commission.

Shneiderman, B. (1987). *Designing the user interface: Strategies for effective human-computer interaction.* Reading, MA: Addison-Wesley.

Smith, S. and Mosier, J. (1986). *Guidelines for designing user interface software (Department of Defense ESD-TR-86-278).* Washington, D.C.: Office of Management and Budget.

U.S. Nuclear Regulatory Commission, (1981). *Guidelines for control room design reviews* (NUREG-0700). Washington, D.C.: U.S. Nuclear Regulatory Commission.

Vicente, K., and Rasmussen, J. (1990). The ecology of human-machine systems II: Mediating direct perception in complex work domains. *Ecological Psychology, 2,* 207-249.

LESSONS LEARNED FROM DEVELOPMENT AND QUALITY ASSURANCE OF SOFTWARE SYSTEMS AT THE HALDEN PROJECT

by

Thorbjørn J. Bjørlo, Øivind Berg, Morten Pehrsen, Gustav Dahll, Terje Sivertsen

OECD Halden Reactor Project
P.O. Box 173, Os Allé 4
N-1751 Halden, Norway
Phone: + 47 69 183100
Fax.: + 47 69 187109

ABSTRACT

The OECD Halden Reactor Project has developed a number of software systems within the research programmes. These programmes have comprised a wide range of topics, like studies of software for safety-critical applications, development of different operator support systems, and software systems for building and implementing graphical user interfaces. The systems have ranged from simple prototypes to installations in process plants. In the development of these software systems, Halden has gained much experience in quality assurance of different types of software. This paper summarises the accumulated experience at the Halden Project in quality assurance of software systems.

The different software systems being developed at the Halden Project may be grouped into three categories. These are plant-specific software systems (one-of-a-kind deliveries), generic software products, and safety-critical software systems. This classification has been found convenient as the categories have different requirements to the quality assurance process. In addition, the experience from use of software development tools and proprietary software systems at Halden, is addressed.

The paper also focuses on the experience gained from the complete software life cycle, starting with the software planning phase and ending with software operation and maintenance.

1. INTRODUCTION

The OECD Halden Reactor Project has developed a number of software systems within the research programmes in the man-machine systems area. These programmes have comprised a wide range of topics, like studies of software for safety-critical applications, development of different operator support systems, and software systems for building and implementing graphical user interfaces. The systems have ranged from simple prototypes to installations in process plants. In the development of these software systems, Halden has gained much experience in quality assurance of different types of software, and this paper summarises the lessons-learned from these activities.

The different software systems developed at the Halden Project may be grouped into three categories. These are plant specific software systems (one-of-a-kind deliveries), generic software products, and safety critical software systems. This classification has been found convenient as the categories have different requirements to the quality assurance process. In addition, this paper addresses the experience from use of software development tools and proprietary software systems at Halden. The paper will also focus on the experience gained from the complete software life cycle starting with the software planning phase and ending with software operation and maintenance.

2. SOFTWARE DEVELOPMENT AND TESTING PROCESS

2.1 Project Oriented SW Development (one-of-a-kind deliveries)

2.1.1 Software Quality Assurance Handbook

The use of formal software quality assurance activities at the Halden Project was introduced in bilateral software projects as the Gullfaks Training Simulator, developed for the Norwegian State Oil Company, see reference /HWR-225/, and the SCORPIO core surveillance system developed for the Ringhals NPP in Sweden. Since then, software quality assurance has been considered a natural part of most bilateral software projects. In 1990, a Project Handbook for Software Quality Assurance was developed at IFE /SQA90/. It was based on experience and established standards, such as IEEE-730, IEEE-828, IEEE-829, AQAP-13 and others. This handbook was updated during 1994/1995 to include the "Guidelines for the application of ISO 9001 to the development, supply and maintenance of software" - ISO 9000-3. The following sections highlight some of the main issues from the SQA Handbook.

2.1.2 Software Development Model

The primary activities that comprise the software design and development process include: establishing requirements, translating these into preliminary and complete designs, implementing the design in code, testing the code, and integrating the tested code with hardware and/or other software.

Classical project management is based on completing and reviewing each of the activities prior to proceeding to the next one. The strictly sequential phasing of development activities is referred to as the waterfall model and is the basis for most software development standards. The waterfall model is illustrated in Figure 1.

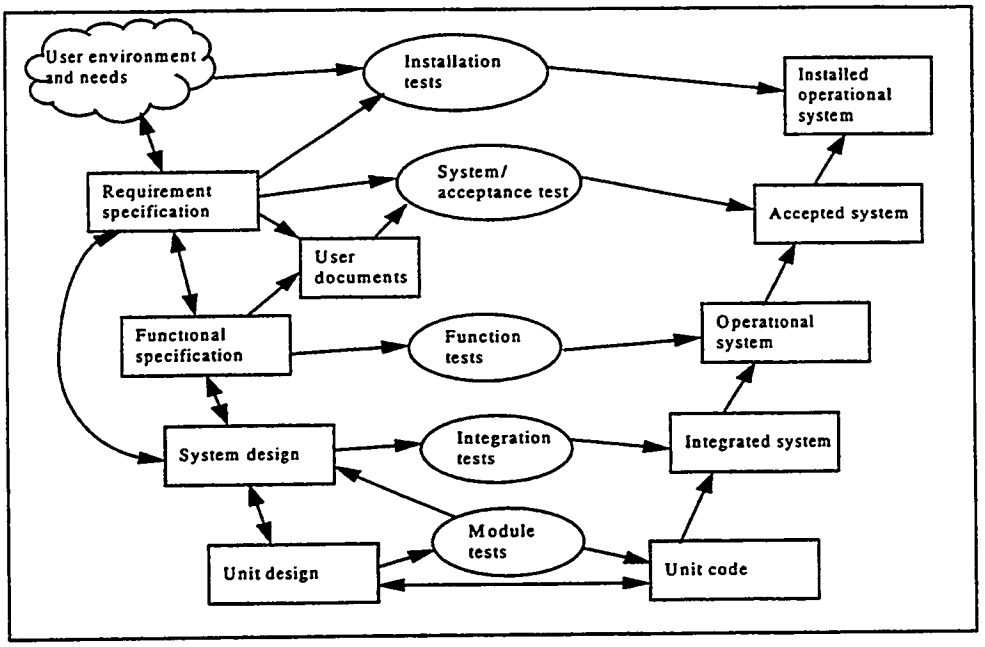

Figure 1. The waterfall system development model

Development Activities

A functional requirements specification of sufficient quality is critical to the overall success of the software development. The requirements should include all aspects necessary to satisfy the customer's need, and they should be stated precisely enough to be used in the validation and acceptance of the software product.

The requirements specification is either provided by the customer or by Halden Project personnel in co-operation with the customer. However, the requirements specification must be accepted by the customer before proceeding to the next project phase. The specification is reviewed by both parties, the customer and representatives from the Halden Project. It is important to ensure that all aspects regarding the customer requirements are considered and handled properly. The requirements specification may include functional requirements, software performance requirements, user interface requirements, and acceptance criteria.

The functional specification is a full narrative description of the functional system and describes what the system actually does, which functions can be performed, and how the functions are implemented.

The system design describes the system solution for hardware and software modules. The solutions shall fulfil the requirements in the specification, and the motivation for and nature of the chosen solutions shall be described. The software design activities specify the software architecture and continue the breakdown of functions identified in the requirements specification into necessary detail.

The detailed design will include definitions of the actual algorithms and equations as well as the detailed control logic and data operations that are to be performed. They provide the basis for the implementation activity, and each elemental unit is defined in sufficient depth to enable programmers not having a knowledge of the overall system to produce these programs.

During the unit coding and implementation phase, the detailed software design is translated into an appropriate level programming language which eventually will be translated into executable object code.

- *Testing activities*

Software verification is the process of determining whether or not the products of a given phase of the software development cycle fulfil the requirements established during the previous phase. Software validation is the process of evaluating software at the end of the software development process to ensure compliance with software requirements.

As the waterfall model indicates, software verification and validation tests are defined in parallel with the phases of the software development process. The code verification activities begin with unit testing and continues by a bottom-up strategy until the complete software system is tested. The SQA Handbook provides test guidelines for unit tests, integration tests, factory acceptance tests, and site acceptance test.

At the unit level, the software is not yet integrated into the system, therefore it can be extensively tested. The purpose of unit testing is to show that each module performs its intended function and does not perform unintended actions.

The purpose of integration testing is to show at the earliest stage of development that functionally related units correctly interact to perform the intended function. All units to be integrated must have passed the defined unit tests.

After integration testing, a functional test is performed on the operational system to verify all functions specified in the functional specification.

A Factory Acceptance Test, FAT, is an acceptance test performed at the Halden Project, i.e. the site where the software is developed. The purpose of the FAT is to test the complete software system against the acceptance criteria. The test specification is made on the basis of the requirements specification, and preferably before the design phase starts. Representatives from the customer and the Halden Project participate in the test activity.

A Site Acceptance Test, SAT, is in fact the same test as FAT. The only difference is that it is performed at the customer's site and within its intended operational environment. It is the customer's responsibility to perform the test, and report discrepancies.

2.1.3 Critical Steps and Considerations

In addition to the development activities described above, there are also "support" activities which are not in the main line of product development. These will mainly be parallel, independent activities. In this category of activities are: management, co-ordination and administration, planning and monitoring, technical development support, as the provision and support of tools for development, quality assurance and control, and customer training.

Project management and quality assurance are the key issues of a successful project, and the software development should be handled in a controlled manner with the ultimate goal to deliver the right product to the right time at the right cost.

2.1.4 Work Breakdown Structure

In order to make detailed plans, measure progress, include reviews, audits and tests, the development and support activities are broken down and grouped in Configuration Phases where each configuration phase is terminated in a Configuration Baseline, see Figure 2.

In each phase a number of items is produced, i.e. documents, pieces of hardware or software. Some of these will form part of the deliverable product. Others will merely form the basis for further development work. We define a baseline in terms of these baseline items which must be present in order for the phase activities to be complete.

However, the mere appearance of such items is not sufficient to ensure that the phase is complete. We review them for quality and completeness, and their suitability as the basis for the next phase and/or for inclusion in the product. Baselines are thus not only measurement points but also important aspects of the quality assurance.

- ***Unit Level Activities***

Each of the baselines B2 to B8 represent major project milestones but from B2 to B5 most of the work is in fact done in parallel. Following baseline B2, when the development task has been split into pieces, each unit of the design can be allocated to different people. These operations can proceed in parallel and need not be synchronised until the integration phase. For example, software units can be developed independently, and will have their own unit milestones (UMs).

- ***Integration Activities***

Integration begins before all units are completed. Integration of a project of large complexity is liable to be the area of highest risk within the development process so the earlier it begins the better. It is also planned and monitored carefully. The easiest way of achieving this is to make use of a build strategy. This implies a number of demonstrable subsets of the final system which can form integration milestones for progress checking purposes.

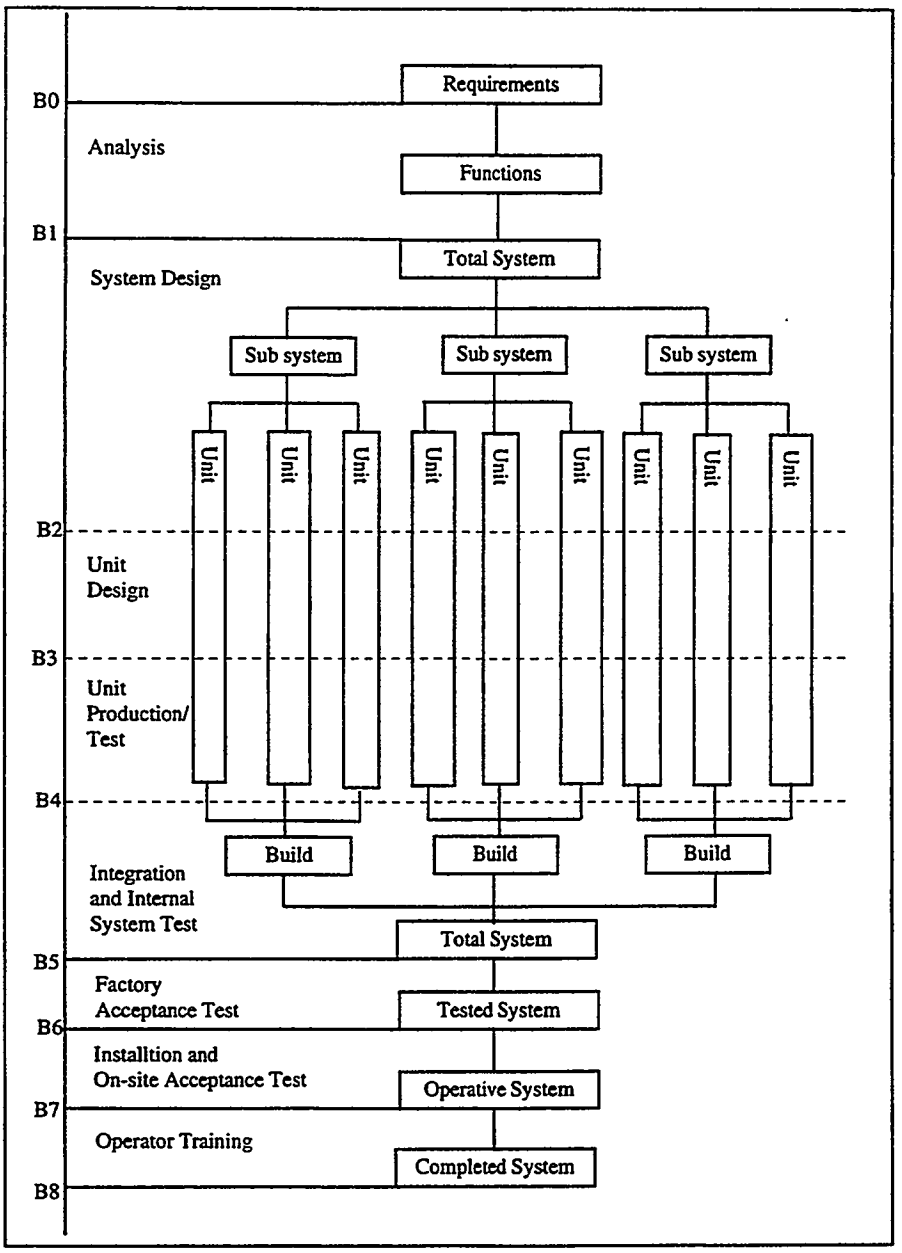

Figure 2. Configuration phases and baselines

Within this process the Unit Implementation Baseline, B4, represents the system level checkpoint at which the last unit is implemented and ready for integration. This is shown in Figure 3.

As each integration milestone (IM) is completed, tests are carried out on the subset of the final system that it represents, in parallel with its use as a basis for the next IM. This requires careful code change control procedures.

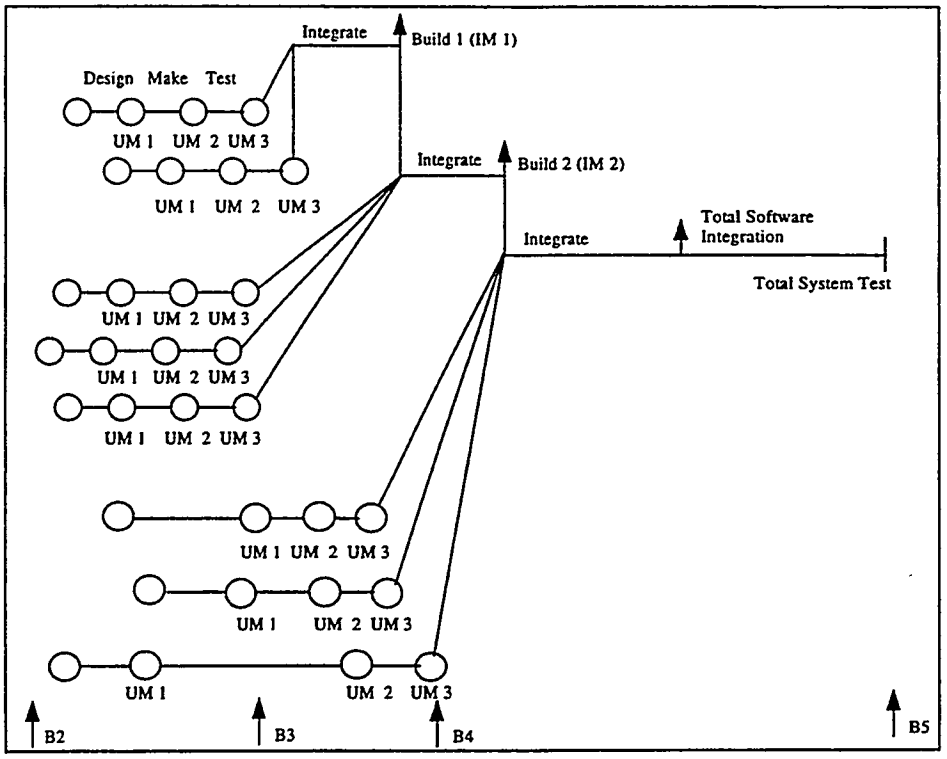

Figure 3. Integration Activities

2.1.5 Project Planning

Thorough planning of the project is one of the key factors in obtaining the outlined quality concept. The plans describe a disciplined environment in which a project can be run in a controlled manner and its evolution recorded and monitored easily and effectively. The plans incorporate organisational, technical, commercial and quality activities.

- ***Project Plan***

The Project Plan is the overall documentation of the total project and is worked out for all types of software projects. A Project Plan contains the following elements: project organisation, task identification and resource allocation, time schedules and work load estimates, quality assurance procedures, baselines and milestones for project monitoring, and project budget.

- ***Software Quality Assurance Plan***

The purpose of quality assurance during a software project is to control all activities affecting quality, and to ensure that the specified quality is achieved. Performance of quality assurance activities in accordance with the defined and documented procedures and work instructions for software is an important contribution towards the ultimate success of the project.

Analogous with the progress planning and reporting, reviews and audits shall be performed to ensure that the established procedures are followed.

A quality assurance plan for any part of the project should be issued prior to the commencement of any work on that part of the project and should be subject to review and approval before issuance.

The quality assurance plan should specify:

- quality objectives, what should be focused on during QA-audits (e.g. program-code, interfaces, functional requirements, compliance with specified standards and SQA Handbook, etc.)
- time schedule for QA-audits, a detailed plan should be provided specifying which items to be inspected and when specific responsibilities for quality activities are appointed such as:
  - reviews and tests
  - configuration management and change control
  - defect control and corrective action
  - detailed planning of test, verification and validation activities to be carried out, including schedules, resources and approval authorities

- ***Additional plans***

In larger software projects the following plans are also needed: purchase plan, document plan, training plan, installation plan and maintenance plan.

2.1.6 Project Tracking

Project tracking covers the verification, checking and action phases of the quality control. In general, the project tracking comprises: monitoring of the progress of the tasks, costs, results; identification of deviations from specifications and plans; and definition and initiation of corrective actions.

2.1.7 Configuration Management

When a software unit is placed under Configuration Management, this means that there exists a version of the software unit which is functioning according to specification after unit testing is completed. This means that the unit in principle is complete, and that any integration with other software, changes to the functionality and error detection must be handled on a formal level, identifying causes and consequences to any change to the software.

Configuration management is a mechanism for identifying, controlling and tracking the versions of each software item. In many cases, earlier versions still in use must be maintained and controlled.

The configuration management system should:

- Uniquely identify the version of each software item
- Identify the version of each software item which together constitute a specific version of a complete product
- Identify the build status of software products under development or delivered and installed
- Control simultaneous updating of a given software item
- Provide co-ordination for updating of multiple products in one or more locations
- Identify and track all actions and changes resulting from a change request, from initiation through to release.

The configuration management information is extremely valuable in order to be able to tailor new releases to fit each customer's configuration and operational environment. The procedures described in the SQA Handbook ensure that the items are submitted to configuration management at an appropriate point. It also defines procedures for modifying items already placed under configuration management.

The following items should be submitted to configuration management:

- Documents (specifications, designs, manuals, etc.)
- Software (source code, object code, executable files, specific test software, standard software as compiler, linker, operating system, libraries, system utilities and system parameters)
- Data (input data, databases, etc.)

2.1.8 Continuous Documentation

Documentation comprises all written information received and produced during the software project. The documents within a software project may be represented on paper and/or in electronic form. All documents are submitted to document control. The documents connected to a software development project may be:

- Contracts for development and maintenance
- Requirements specification
- Project plans (e.g. master plan, document plan, quality plan, review plan, configuration management plan, integration plan, test plan, and maintenance plan)
- Design, development and test documents (e.g. system design documents, detailed functional specification, unit development folders, test folders)
- Status and revision documents, progress reports
- Manuals (e.g. system documentation, user manuals)

The Unit Development Folders (UDF) and Test Folders (TF) are considered to be the most important procedures concerning documentation, progress, and quality assurance of software development projects at the Halden Project. These documents are mandatory in all projects and a description of these development documents is given below.

- ***Unit Development Folders***

At the start of the delivery project, a Unit Development Folder (UDF) is established for each of the units that have been defined during the system design phase. It consists essentially of a loose-leaf binder, and its electronic equivalent, with standard sections. These sections are completed as the project progresses. Besides forming the development documentation for the unit, the UDF is also the basis for quality control operations at this level and for planning and monitoring. The standard contents of the UDF are as follows: unit plan and estimates, unit requirements specification, unit design, unit code and implementation material, unit test definitions, unit test results, unit development notes, and revision log.

- ***Test Folders***

A test plan is worked out for all project level tests. The purpose of such a test plan is to prescribe the scope, approach, resources, and schedule of the testing activities, and to identify the items being tested, the features to be tested, the testing tasks to be performed, the personnel responsible for each task, and the risks associated with this plan.

The Test Folders document these test plans and project level tests and are similar in form to the UDF's. The contents are: test development plan and estimates, test specifications, requirements, environmental needs, design of test cases, implementation material (actual test programs etc.), test results, test reports, test notes, and revision log.

There is one Test Folder (TF) for each of the integration milestones, one for system/acceptance tests and one for site tests. If necessary, each may be split into more than one physical document.

2.2 Generic Software Products

The Halden Project develops a few generic software products, i.e. general software packages delivered to a number of customers. Such products are steadily improved and new releases of the product appear at regular intervals. The user interface management system Picasso /HWR-226, HWR-271, HWR-288/ and the computerised procedures system, COPMA /HWR-319/, are Halden software products belonging to this category. Quality assurance programmes for these products require some special considerations, in particular regarding configuration and version control, and error handling and correction routines. To illustrate this the quality assurance procedures of the Picasso development are described below.

2.2.1 Picasso QA Program

The development of Picasso-2 has been a continuous activity from the start-up in 1985 and its evolution has been influenced partly by the original design, partly by the use of Picasso-2 in different projects. Being used in delivery projects, new functionality has been demanded and optimisation has been requested, particularly to handle large amount of data. Several projects have been executed in parallel which imply parallel development of different software modules in Picasso-2. During the last 2-3 years Picasso-2 also has been ported to different hardware platforms and different versions of UNIX.

A problem occurred concerning keeping one updated version of the Picasso-2 source code modules. The main reason for this was that often more than one person was changing the same source code module in connection with different external projects where Picasso-2 was used. After some time, typically 2-6 months, the different new source codes had to be merged with the original source code, a time-consuming process and subject to introduction of errors. Experience showed that even if the new functions developed separately had been tested and functioned as expected, other functions were influenced by the changes. This often cause malfunctions when the new merged system was taken in use as a new version in the different projects.

To minimise the possibilities for introducing errors when adding new functions and to handle reported errors in the Picasso-2 system, a special QA-programme has been implemented, for maintenance of the existing Picasso-2 system and the follow up of registered external Picasso-2 customers. External Picasso-2 customers having signed a maintenance contract will be handled according to the specific terms in the agreement.

These quality assurance procedures cover what is defined as minor changes in the program code. Larger extensions where new modules have to be developed or system design modifications are required, follow the general QA-assurance procedures described in the SQA Handbook.

2.2.2 Quality Assurance Procedures

The Picasso-2 Development Group is responsible for handling the following tasks:

- Correcting errors reported by the users
- Customer support in general
- Implementing new functions
- Updating the documentation when new functionality is added
- Distributing new versions to users according to maintenance agreements
- Managing the document archive

- ***Error reports***

Error reports are accepted in written form only, using a standard error reporting form or by Electronic mail.

Reported errors are transferred to the Picasso-2 Error Report document for further handling. This document contains standard forms, one page pr. error.

When an error is corrected, a copy of the corresponding page in the Error Report document is sent to the source of the error report. A full document copy is supplied when updating customers with program releases.

The person responsible for handling the error assigned to him discusses the error and possible strategies for corrective actions. An analysis is done to check that other modules are not influenced. The error report contains information of which modules are influenced.

- ***Change proposals***

Change proposals can be requested by any user and shall only concern additional functionality which does not influence system compatibility. Change proposals are logged in the Change Proposal Log document using standard forms.

The extent of the change is evaluated, and for small changes the resulting design is documented in the Change Proposal Log document. For larger changes a separate design document has to be written and a project plan made according to the SQA Handbook.

When a larger change is completed, it is described in the Change Log Description document. The description will at least include a detailed description of the new functionality, and a list of all source files modified.

When a change has been completed, the Picasso-2 Users Manual is updated according to the detailed description of the new functionality.

The Change Log Description is included when a new Picasso-2 version is released.

- ***Version control***

The configuration co-ordinator is responsible for managing the different Picasso-2 versions. There are two different version categories: frozen versions and development system.

Frozen versions reside on directories locked for writing and are never changed. These directories contain complete source code, executable files and documentation.

The development system is used for correcting errors and implementing new functions.
When required a new version will be released, at this point the development system will be frozen, see Fig. 4.

Customers having reported errors which are fatal will receive an intermediate version using the current development version.

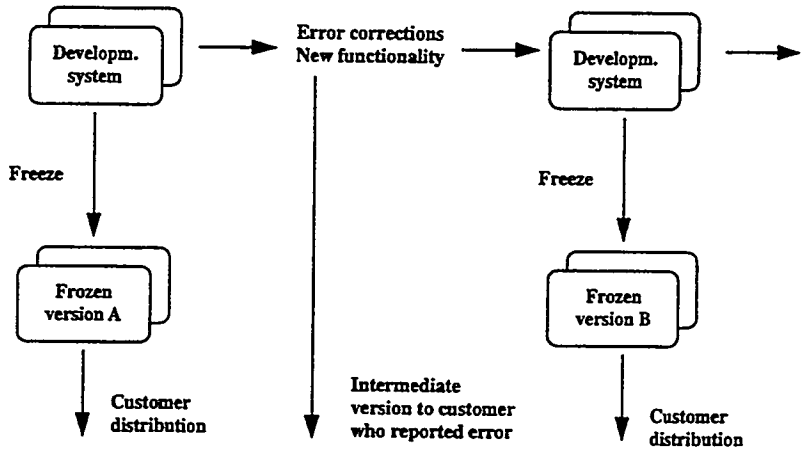

Figure 4. Version control

The different version releases are indicated by an identification letter, e.g. 2.4b, 2.4c.

New version releases that are downward compatible with the previous version are indicated by a new letter suffix. Incompatible versions are indicated by sequence numbering change, i.e. 2.4 to 2.5.

For each version and release there is platform dependent generated executable code.

- ***Porting***

The Picasso-2 system is prepared for compilation for all supported platforms. The scripts and makefiles for system generation will automatically detect on which platform the system generation is executed.

The source code contains platform dependency to cope with the platform specific code so that there is only one source code.

All problems detected when compiling/generating the system for a new platform type are described in the document Picasso-2 Porting.

- ***Testing***

The test procedures include:

- Testing of the specific function corrected
- Testing of the complete system on all platforms
- Testing of specific customer applications
- Checking with the software testing tool Purify

The function specific test verifies that a correction of a reported error has fixed that specific problem. Realistic test environments are used in the test. The test is carried out for all supported platforms.

A complete system test on all platforms is carried out using the Picasso-2 test system when a new version is to be frozen.

Testing of customer applications is connected to the maintenance contract. Whenever a new release or an intermediate version is delivered to a customer it will be tested on the test system.

All modified program modules are checked using Purify to minimise the probability for memory leaks and pointer errors before a new version is to be frozen.

- ***Source Code Changes***

When source code is changed because of error corrections or additional functionality, the following procedures are followed:

- The source file(s) changed shall be listed in the Change Description Log or the Error Log
- The source file header of the files(s) shall be updated to describe the change, the date of change and the person responsible (initials)
- Changed or added source code shall be indicated by comments

The comments shall at least contain the date and the initials of the person responsible.

2.2.3 Document Archive

The document archive contains the following documents:

Picasso-2 Users Guide,
Picasso-2 Tutorial,
Picasso-2 Course,
Picasso-2 Course Overheads,
Picasso-2 Quality Assurance Procedures,
Picasso-2 Error and Change Description Log,
Picasso-2 Porting,
Picasso-2 Distribution, and
Picasso-2 Procedures for making a delivery tape of the Picasso-2 software

All documents reside on the Picasso-2 document file directory.

The document co-ordinator is responsible for keeping the archive up to date.

In addition to these documents, a file containing all Picasso-2 maintenance contracts is kept and maintained in a central file.

2.2.4 Picasso-2 Distribution

When new versions are released all customers having signed a maintenance contract are supplied with a complete program system update and document update.

Customers not having a maintenance contract will be modified that a new version is released and have to order a new version covering the distribution costs.

A list of customers is maintained in the document Picasso-2 Distribution.

3. SAFETY CRITICAL SOFTWARE SYSTEMS

The Halden Project has carried out two projects in which a safety critical software system has been developed from initial specification to final testing.

3.1 The PODS Project

The PODS (Project On Diverse Software) /HPR-323/ project was a joint project between the Safety and Reliability Directorate (SRD), Central Electricity Research Laboratory (CERL), UK; VTT, Finland; and the HRP. The main objective of the project was to provide a measure of the relative merits of using diverse programs, as compared with any one of the programs replicated in all channels, in a 2-out-of-3 majority voting protection system. Three different programs based on the same specification and a test harness were developed (see fig. 5). The three programs were tested back-to-back with large numbers of data chosen from different test data selection profiles.

- ***Quality Assurance in the PODS Project***

At the inception of the PODS project it was decided that rigorous quality control would be applied to all phases of the project through to acceptance testing, as would be the case if the software was to be used in a high reliability application such as a nuclear reactor protection system.

As no universally accepted software quality standards existed at the outset of the project, it was agreed by all project members, that a set of quality assurance guidelines should be issued. This was an advisory document providing the ground rules on which each team was to base its own local quality assurance procedures. The guideline comprised a table of events which would normally be required to be executed during each of the specification, design, code, implementation, acceptance testing and back-to-back testing phases of the project. The activities of each QA representative were defined. The guideline was based upon the EEA QA guide /Eea81/.

The quality assurance activities were conceptually divided into two parts, viz. global and local quality assurance. Global quality assurance was the responsibility of SRD, who acted in a managerial role in relation to the local quality assurance representatives responsible to each team. The local quality assurance was performed by each team, who appointed a QA responsible, who was answerable to the SRD global quality assurance representative. The terms of reference of the local representative were as follows:

- To implement the quality assurance guidelines laid down by SRD.
- To provide written evidence to the global representative at regular intervals to demonstrate that quality assurance was being satisfactorily progressed.

Within these constraints, the local quality assurance representative was given freedom to choose and implement his own particular methods.

- ***Lessons Learned From The PODS Quality Assurance Programme***

The lessons learned from the quality assurance activities in the software development in the PODS project are as follows:

- The use of a well defined documentation process throughout the project enabled the global QA representative to review progress even though the companies were widely dispersed geographically.
- The implementation of error reporting and change control processes proved to be very effective as a way of controlling change.

- The local quality assurance plan produced by each team provided the details for implementation of the QA guide. These documents defined the responsibilities of each local team member, together with the development and programming techniques required.
- The formal quality assurance procedures were successful in that no implementation errors from the design and code phases were found in back-to-back testing, only specification-based errors.
- At all sites, inspection meetings, individual inspections and a formal design walk-through were held. The QA inspector checked that fault reports and change notices were being maintained correctly. These procedures were considered extremely useful.
- Reviews and walk-throughs were very efficient methods of revealing design and coding errors. Many of these errors, especially those found by walk-through, would have caused difficulties if they had slipped through to the coding phase. To increase software reliability, such methods should have been applied at earlier phases, i.e., the customers' specifications and the manufacturers' specification. This would probably have revealed many of the misinterpretations of the specifications, that later became apparent.

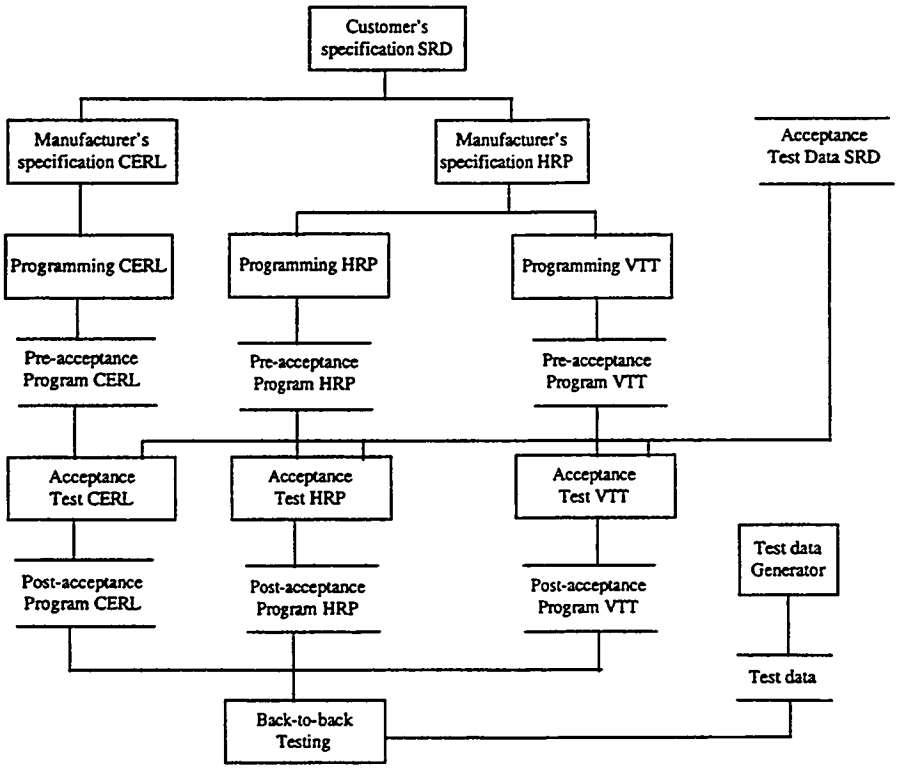

Figure 5. Experimental set-up for first back-to-back test

3.2 The EvalFM Case Example

The EvalFM project was established in order to investigate the applicability of formal methods in the development of safety-critical software based systems. The overall goal was to explore the strengths and limitations of formal specification- and development methods, through practical experience on a realistic example. To reach this goal, the project attempted to identify problems related to development of safety critical software-based systems, and to see how formal methods can be used to address these problems. In particular, the project evaluated the applicability of algebraic

specification and the theorem prover developed at the Halden Project (HRP Prover) as a basis for formal software development.

An example system was selected, based on the following criterion: it should be a realistic, preferably a real, safety-critical system related to nuclear power plant operation. Furthermore, the system should be of reasonable size to keep the effort needed reasonable. After consultation with Sydkraft (Barsebäck NPP) and ABB Atom in Sweden, it was decided to use the computer-based power range monitoring (PRM) system installed at Barsebäck NPP as an example system for the project. The project did not address ABB's implementation of the example system, but the development of a similar system using formal methods. The purpose of the PRM system which was of particular interest in the project is the monitoring of the average power emission of the core (the average PRM value). When high power emission is monitored, the system must trip the high level alarms.

- ***QA Plan for the EvalFM Case Example***

In the EvalFM project, the required abstract functionality of the example system was formulated within algebraic specification. An important aspect of this formulation was the derivation of the abstract functionality from the technical descriptions provided by the customer. Because the requirements specification described the desired functionality of an analogue system implementation, certain adaptations had to be made in order to use the specification as a basis for the development of a digital system. This corresponds to the common practice where the requirements specification is used as a basis for the derivation of other specifications for software, hardware, configuration, etc. In this process, experienced developers are usually well trained on treating the words and symbols in the requirements specification as specifying functions on a more abstract level.

In a formal development project, it is crucial that the developer's formal specification can be validated against the customer's requirement specification. The EvalFM project demonstrated how animation and theorem proving could be applied in this process. It was also demonstrated how the extensive use of a mathematical tool-kit made it possible to specify most of the system in a comprehensible and concise way. Furthermore, it was demonstrated how the system could be designed and implemented efficiently by utilising the design and implementation of the mathematical tool-kit. Through verified design steps, a concrete specification was developed which could be translated systematically into a program in a so-called "safe subset" of Pascal.

The use of the HRP Prover formed an important part of the development of the case example. This tool made it possible to detect syntactic errors in the specification, execute the specification as an early prototype of the system, prove properties of the specification, and prove correctness of the design steps. All these activities involve a large amount of symbolic manipulation, and the provision of a powerful theorem prover is therefore essential for the success of the method. Nevertheless, the use of a theorem prover, advanced as it may be, would not be sufficient in an industrial development project. The methodology would be easier to use if it was integrated in an application-oriented environment which included the theorem prover, relevant text editors, graphical user interfaces, transformation tools, etc. Furthermore, it would be essential to ensure that this environment were sufficiently reliable. For safety-critical applications, this would suggest that several of the tools included, the theorem prover in particular, should be formally developed.

- ***Lessons learned from the EvalFM project***

- The results from the EvalFM project strongly indicate that formal methods can be utilised to advantage in the development of a safety-critical system. However, to fully utilise the potentials of formal methods it is important that the customer's requirements document allows flexibility with respect to solutions for design and implementation.

- A large part of the effort involved in a formal development project is invested in the production and assessment of the specification. In most cases, only a minor part is invested in the actual implementation.
- Execution of the specification is an effective means for detecting specification errors and can be performed incrementally during the production of the specification. Further, execution of the specification increases its comprehensibility, and thereby facilitate communication between persons with varying technical background, e.g. person producing customer's requirements specification and system developer.
- Efficient use of theorem proving in specification and design requires that the specification language is supported by a powerful theorem prover. Use of a theorem prover alone is, however, not sufficient, for an industrial project a reliable, integrated development environment is needed.
- The development method based on algebraic specification can be used both for specification and design, and allows for implementation in a wide variety of programming languages. Further, it supports implementation of programs which avoid undesired features of the chosen implementation language. However, algebraic specification provides little support for important non-functional requirements, such as requirements to technical performance and accuracies.

4. PROPRIETARY SOFTWARE AND TOOLS

In recent years the trend has been to generate higher-level development tools to implement software systems. High-level tools close the gap between the design and the programming, and guide the developer in generating a software system based on the design. The major advantage of using high-level development tools is that the developer does not have to worry about technical programming solutions, thus the possibilities for introducing programming errors in the program code is limited. Another benefit of using such tools is that the implementation effort is reduced. However, this type of high-level programming requires a reliable development tool, tested and proven by experience.

At the Halden Project software development tools have been applied in a number of projects. Below some of these tools are listed together with experience at Halden from use of these tools.

4.1 Graphical User Interface Tools

TeleUSE is a tool for building graphical user interfaces based on the OSF/Motif style standard for look and feel. The system is delivered by Thomson Software Products (a company owned by Thomson-CSF). The Halden Project has used TeleUSE for building the user interface of the COPMA-II computerised procedure system.

UIM/X (earlier called Interface Architect) is a Graphic User Interface (GUI) builder. UIM/X enables the software developer to interactively create, modify, test, and generate code for the user interface portion of the applications. UIM/X is fully integrated with the OSF/Motif toolkit. Developers use a What You See Is What You Get (WYSIWYG) editor to graphically choose from any of the OSF/Motif widgets (such as push-buttons, scrollbars, popup menus, etc.) and draw their interfaces.

UIM/X also contains a built-in C interpreter. From within UIM/X, developers can create the C-code link between the user interface and their application. They have on-line access to their own compiled functions, and to an optional library of UIM/X convenience functions. UIM/X generates C or C++ code, as well as a customisable main program and makefile. It can also run the makefile.

- ***Halden Experience***

- Our main experience is that TeleUSE meets its specifications and has proven to be a flexible, reliable and usable tool for building graphical user interfaces. TeleUSE has contributed to savings

in implementation time and source code volume, and has facilitated the development of a well-structured and easily maintainable software structure. We have not experienced significant trouble caused by bugs or severe technical limitations in the product.

- When applying TeleUSE to develop graphical user interfaces based on OSF/Motif, one must be knowledgeable about the OSF/Motif widget set. Detailed knowledge about the OSF/Motif widgets, their attributes and behaviour, and how to combine widgets for building a user interface is still needed.
- OSF/Motif defines a limited set of user interface components that does not cover all possible needs. However, TeleUSE has proven to be open and flexible with respect to implementing lower-level programming using the Motif (Xm) library, the X Toolkit Intrinsics (Xt) library, and the X (Xlib) library functions.
- The only area where we have had significant problems with TeleUSE relates to installing TeleUSE run-time libraries on UNIX platforms other than the one used for system development
- The overall experience with UIM/X is that this is a very powerful tool enabling fast prototyping and testing of user interface applications. Application code may be developed within the UIM/X or developed in an external editor and linked to the system during compilation. Another important benefit is the generation of executable code making the final application independent of the UIM/X system. Thus, there is no need to install an expensive environment at the customers site.

4.2 Expert System Tools

G2 from Gensym Corporation is an expert system shell which is especially suited for the construction of real time expert systems. It is normally run on engineering workstations, and it uses the latest ideas in computer software technology. The structure of the knowledge base is for instance heavily object-oriented, and the interaction with the user rely on modern interface techniques. Thus the data objects in the knowledge base are shown as graphical symbols (e.g. a valve symbol), and they can be manipulated by means of mouse/menu techniques.

There are two important building blocks within G2, the rules and the general data objects. Starting to construct the general dataobjects in G2 is very much like using a graphical editor. The G2 programmer sets up an icon library, consisting of for instance valves, tanks and pumps. On the basis of this library, he can create instances of valves, tanks and pumps and put them on various windows (workspace) within G2. The programmer may connect objects on the same workspace by drawing lines between them.

The general data objects do not only consist of the graphical appearance. In addition, every data object has an associated set of attributes. In the case of a tank it could for instance be volume, inflow and outflow. Those attributes are given values later on when running the expert system.

Rules can also be used to give values to the attributes. The rules are special data objects which are used by the inference mechanism in G2. Generally, a rule consists of two parts, an antecedent(condition) and a consequent. Whenever the inference mechanism uses the rules and the antecedent is true then the inference mechanism implements the actions specified in the consequent part.

- ***Halden Experience***

- As a software development tool, the G2 system has satisfied most of the needs for building large, rather complex, quality assurance sensitive programs.
- G2 is a commercially available expert system shell, which is oriented towards real-time applications. This means that it can handle large input/output volumes automatically with

acceptable time response. However, G2 requires a lot of processing power. Even though the flexibility of the system is desirable it "costs" in terms of processing power.

- The G2 system also keeps a strict control of memory allocation. In this way, unpredictable time response due to garbage collection problems is avoided.
- G2 is a closed system in the sense that the developer only has access to the G2 data objects through the G2 interface. There are certainly cases where one would like the knowledge base to be in ASCII-readable format and where it should be editable from text editors such as EMACS.
- The real strength of the G2 system is not only flexibility as other systems are more flexible (e.g. KEE, Knowledge Engineering Environment, Intellicorp) in some respects. The real strength of G2 is the compromise between response time and flexibility.

4.3 Formal Development Tools

The formal specification language Larch together with a set of associated tools was used in the SAP (Safety Assessment of Programs) project. These tools are developed and available as free software from MIT. Several front end tools are available for making specifications towards a particular implementation language, e.g. C, C++, Ada or Modula 3. The Larch Prover (LP) can be used to prove theorems in the underlying logic. LP is an interactive theorem proving system for multisorted first-order logic. Unlike most theorem provers, which attempt to find proofs automatically for correctly stated conjectures, LP is intended to assist users in finding and correcting flaws in conjectures, an important activity in the early stages of the design process. LP is currently used elsewhere to reason about designs for circuits, concurrent algorithms, hardware, and software.

- ***Halden Experience***

- The formal specification language, Larch, works efficiently on large problems, has important user amenities and can be used by programmers with limited experience in formal methods.

4.4 Project Management Tools

The commercial Project Management and Planning Tool SuperProject Expert has been used a couple of times in larger bilateral projects at the Halden Project. This program offers project management techniques like PERT, Gantt Charts, Work Breakdown Structure (WBS), and Critical Path Method (CPM) to simplify the scheduling, costing, reporting, and updating of simple and complex projects. The program may also be used for several projects simultaneously, thus enabling levelling of resources between projects.

The program is inexpensive and runs on a PC.

- ***Halden Experience***

- SuperProject Expert requires substantial effort when entering the various project data such as tasks, task duration, sequence dependencies, start and finish dates, resources, etc. into the program. However, when this data is entered, the time "investment" pays back during the monitoring and controlling phases of the project.
- An inexperienced user requires a good deal of time to learn the system.
- Inexpensive tools like SuperProject Expert are not complete in e.g. graphics capability, thus additional tools are required.

4.5 Case Tools

Relational DataBase Management Systems (RDBMS) have been utilised in several projects at Halden. Further, the Case tool software Oracle Co-operative Development Environment (CDE) has been used.

The purpose with these tools is to create database applications more effectively and make the system documentation and maintenance work easier. Oracle CDE consists of several tools to support the entire development cycle. CDE consists of the Oracle CASE tools, and the Oracle 4GL tools. The Oracle CASE tools consist of CASE*Dictionary, CASE*Designer and CASE*Generator. The 4GL tools include PL/SQL, Oracle*Forms, Oracle*Graphics and Oracle*Reports.

- ***Halden Experience***

- Case tools like Oracle CDE offer a variety of facilities. Automatic generation of forms and reports, as well as other capabilities, enable prototyping and testing of functionality in co-operation with the customer at an early stage.
- However, one should remember that case tools are extensive systems requiring methodic coursing and expert consultancy in the initial stages.

4.6 Proprietary Software In Safety Related Applications

Proprietary software can be purchased "off the shelf" as a commercially available product. It consists mainly of re-useable modules (together with some customised modules) hence it is generally re-useable for other applications or by other people and/or organisations. Such software is often used in the control of Nuclear Power Plants, also in safety related applications. A typical example is the use of configurable systems, i.e. systems which are built up by standard software components in the same way as a hardware system is built up by standard hardware components.

A project (the SAMPS project) is performed at the Halden Project with the objective to investigate and develop techniques and methods which could be used to undertake a safety assessment of proprietary software in safety related application systems. In order to assess a system, it is necessary to obtain information on it. The amount of information that is available to an assessor varies between proprietary software manufacturers. This may lead to a number of different assessment approaches determined by the information obtainable from a manufacturer.

An important task within the SAMPS project was to undertake a market survey of proprietary software manufacturers to gain an understanding of the information which is available to enable an assessment of such systems to take place /HWR-372/.

- ***Lessons Learned From SAMPS Project***

- The general impression from information received from companies producing proprietary software for safety-related systems is that they follow high-quality standards in software development.
- An argument for the use of proprietary software in safety-related applications is that the wide user experience grants high reliability. To prove that this is the case requires data, both on failures and on applications. However, even if the companies are willing to reveal information and state that the documentation is available the needed information may be missing. This is particularly true for data needed when applying quantitative reliability models. Such models require quite detailed information on failure statistics and operation data, whereas the available data is often only correction reports and version documentation.

5. SUMMARY OF LESSONS LEARNED FROM HALDEN SOFTWARE DEVELOPMENT PROJECTS

The lessons learned from quality assurance of various software projects carried out at Halden are summarised in this section. It represents a synthesis of the accumulated experience from the different projects, and the lessons learned are grouped with respect to the different phases of the software life cycle.

5.1 Software Development Phases

5.1.1 Software Planning

- Good project planning is essential for the successful implementation of a software project. The waterfall model for system development with configuration phases, baselines, and unit milestones provides a solid foundation for the detailed development plans.
- In addition to the time schedules, the software quality assurance procedures to be implemented in the project must be chosen in advance. Also, a software quality assurance plan (with reviews and audits) must be included to ensure that the established procedures are followed. The procedures, methods, and guidelines given in the SQA Handbook have proven very useful when establishing such procedures.
- Detailed time schedules for all phases - design, implementation, testing, and integration - have proven to be a necessity. It is vitally important that the unit responsible does his own planning within the given timeframe.
- The activity plans made by the unit responsibles form the basis for progress reporting. The more detailed the unit plans are with respect to detailed sub-tasks and unit milestones, the easier and more accurate the progress reporting will be.
- The time schedule should be worked out in several levels, e.g. top level (contract schedule), sub-level, and unit level. A wise thing to do during the time scheduling is to introduce float or slack time (extra amount of time) in the critical path.
- Software estimation is a critical factor in the planning phase. Several estimation formulas and techniques have been developed throughout the years, but the best method seems to be an intuitive estimation based on knowledge and experience from similar projects. Thus, evaluating the project data when a project is finished gives information on how realistic the plans were made and might also identify where the plans went astray. Such an evaluation is beneficial for making better, more accurate budgets in later projects.

5.1.2 Software Requirements Analysis

- Spending much work on system specification is valuable for clarifying the functional requirements and focusing on the specific needs of the end-users by discussing and reviewing the specification.
- Information presentation must match the end-user requirements. For instance, the decision to make a system that could be used by reactor operators must have been made in the planning phase.
- Usually in contractual projects, the requirements specification, cost, and timeframe are fixed. However, open discussions with the customer at an early stage is important to get a common understanding of the product to be delivered.
- Testing the principles and methodology by means of a prototype on a simulator before plant installation was important for an advanced alarm system like the model-based early fault detection approach.

- Much of the effort involved in a formal software development project is in the production and assessment of the specification. In most cases, only a minor effort is invested in the actual implementation.
- The potentials of formal methods increase whenever the customer's requirements allow for a higher flexibility with respect to design and implementation.
- Execution of a formal specification is an effective means for detecting specification errors and can be performed incrementally during the production of the specification. Execution also increases the comprehensibility of the specification, and thereby facilitates the communication between persons with widely varying technical backgrounds.
- Formal specification can be facilitated by the use of some library of pre-defined data type specifications.

5.1.3 Software Design

- Designing the software units in detail with respect to functionality, data structures, interfaces, algorithms, and tests before actually writing the code, is extremely valuable.
- The unit design chapter in the Unit Development Folder (UDF) is such that another person/programmer may take over and continue the development of the unit. This is useful when re-planning and re-organisation is necessary during the project.
- Detailed design documents have proven very important when a system is extended and exported to other computer platforms several years after the original development team is finished and other personnel are involved.
- The detailed design documents may form part of a Detailed Functional Description, a document delivered to the customer for final discussion and acceptance. This is the last chance to reveal any misinterpretations made during the requirement specifications. A mandatory paragraph in this document should highlight any deviations, restrictions, and assumptions made with respect to the requirements.
- During the unit design, various checklists have proven valuable in the reviews and audits of each unit.
- A carefully designed database paves the way for easy future extensions.
- A lesson learned is to look carefully into how an expert system should be interfaced and integrated with an operator interface systems in a control room. Check if the display software contains the necessary functions required by the expert system or if new features have to be added.
- To reduce the software maintenance cost and probability of errors, the displays should be generated based on the content of the knowledge base and when the knowledge base is changed, the displays are changed accordingly.
- Expert systems also need access to a wide range of time-tagged process data on-line. The interface to the plant computer database should be examined carefully to secure that all the data needed is made available in an easy way software-wise. It should be easy to add new data tags when needed by the expert system, or all plant data could be made available to the expert system from the beginning. One should choose higher level programming tools suitable for expert system technology. The benefit of this is that the inference engine and more complicated reasoning logic can be validated and tested in many applications to remove errors.
- Efficient use of theorem proving in formal software development requires that the specification language is supported by a powerful theorem prover. For safety-critical applications, such a tool should be developed using formal methods to assure sufficient reliability of the tool.
- Several design steps in a formal development process follow specific transformation rules and can to some extent be automated.

5.1.4 Software Coding and Component Testing

- During the unit coding and testing phases various checklists have proven valuable in the reviews and audits of each unit. Walk-through of code, either by unit responsible or by another programmer, is extremely effective for revealing errors early in the project. This requires common standards concerning code comments, file headers, and identifier naming conventions implemented in the project.
- System configuration is simplified when plant-specific data are separated from the computer code. However, an object-oriented data structure will simplify the configuration task even more by avoiding double definitions in several data files. Also robustness in the software source code when reading data files must be emphasised to avoid using wrong data.
- Introduction of a user-interface management tool like Picasso-2 has reduced the need for low-level programming and testing in development of operator support systems.
- The development of an extended FORTRAN language, EFFORT, a precompiler and a data-base generator in the Early Fault Detection project has made it possible to avoid typical programming errors in FORTRAN, has improved readability of the code and has reduced maintenance requirements.
- Two test tools are heavily used at the Halden Project: Purify and Quantify (Pure Software Inc.). Purify is a program that detects programming errors concerning memory leaks and pointer errors. In some cases, such errors can be introduced at an early stage in the programming and may cause problems immediately. In other cases, such errors are potential "bombs" that can be released later when modifying the code. These errors can be very difficult to track and make debugging time-consuming. Using the Purify tool is now part of the procedures and the checking is performed immediately after a code segment is compiled and become executable.
- The Quantify tool gives valuable statistics about where a program consumes CPU-time and is used to pinpoint code which can possibly be optimised to improve system performance.

5.1.5 Software Integration Testing

- Integration testing should begin before all units are completed. Integration in a project of large complexity is liable to be the phase with highest risk in the development process, so the earlier it begins the better. The easiest way of achieving this is to make use of a build strategy. This implies a number of demonstrable subsets of the final system which can form integration milestones for progress checking purposes.
- Configuration Management is an important mechanism for identifying, controlling and tracking the versions of each software item. When a software unit is placed under Configuration Management, a version of the software unit exists and functions according to specification following testing. This means that the unit in principle is complete and that any integration with other software, changes to the functionality, and error detection must be handled on a formal level to identify causes and consequences of any change to the software.
- The integration request procedure and the error/change proposal procedure used during Configuration Management and Change Control are some of the most important procedures in the SQA Handbook. When a unit shall be integrated (transferred to the "freeze" user) or an already integrated unit has to be changed, special forms must be completed, reviewed, and signed. After approval, the work may begin and a copy of the form is filed in the UDF. All source codes have a mandatory file header where a history log is kept and updated. Traceability between source code, updates of the source code, and documentation is ensured by the forms identification number and the reference to this number in the history log.

5.1.6 Software System and Installation Testing

- The Test Folder document contributes significantly to the planning, specification, design, and documentation of the various system tests. The same template can be used for all tests from integration to final acceptance. Involving the customer in specification of the Factory Acceptance Test (FAT) and Site Acceptance Test (SAT) has proven very valuable.
- Verification of the total system with respect to time responses during high load conditions should be documented.
- Modifications to the system during the time between the validation and installation must be verified formally. A system for QA by means of change control requests should be followed. A system responsible and a QA responsible must be appointed.
- The testing procedures of the Picasso-3 system are currently based on manual execution and checking the results. Testing is performed on functional level of the changed or added code and on system level using applications. The experience with these procedures is that they need to be automated. The plan is to purchase a tool for this purpose. Much work must be done to define the tests for this tool, but once defined, the testing can be carried out frequently to see whether the changes done in the system have introduced unexpected errors or problems. The tests will also be continuously extended, e.g. when a bug is fixed a test is introduced for that particular function.

5.1.7 Software Operation and Maintenance Testing

- The main activity on the Picasso-2 system now concerns debugging and adding some new functions when required. After having introduced the QA-procedures, the traceability of reported errors and corrections have been improved. Use of a source code control system is not defined as part of the QA-procedures but there have been no practical problems doing this manually since the number of changes is quite low.
- The work on the Picasso-3 system is divided in two main categories: further development and debugging. A source control system has been developed based on SCCS. This control system requires developers to follow defined procedures. The experience using such a system is that there are some overhead compared to working directly with source files, but considerably more time is gained by having full control and documentation of all changes. The conclusion is that a source control system is a necessity in this type of software development and maintenance.
- Most of the errors and request for new functions are received by E-mail. Handling information this way is very convenient as the mail is distributed to all members of the development group and reach a person who can handle the mail within reasonable time. The mail is sorted by a person responsible for further handling which ensures that no information is lost. Overall E-mail has substituted the procedures of distributing papers and has decreased the time spent on handling.

5.2 Project Management and Quality Assurance

- Good project management is a key to success. Even though the rational, analytical aspects of project management are necessary to reach the overall goal of delivering the right product, at the right time and right cost, the "human" aspects are the most important factors. Thus, one should bear in mind that there is no analytical short-cut to good project management, and the ultimate goal of a successful project lies very much in the hands of the project manager.
- At the very beginning of the project a kick-off meeting or seminar is arranged. In this meeting the project specification, breakdown structure, organisation, plans, quality assurance, etc. are presented. A good idea is an open discussion and exchange of experience to get acceptance for the working procedures to be followed in the project.

- Regular meetings are necessary to highlight any problems and the project's progress to the project participants. One should not forget to allocate time to the meeting activities during the planning phase.
- The extent of a project's quality assurance system has to be adjusted to each specific application.
- The Unit Development Folders (UDF) and Test Folders (TF) are considered to be the most important procedures concerning documentation, progress, and quality assurance of software development projects at the Halden Project. These development documents are mandatory in all software projects at the Halden Project.

6. REFERENCES

/Eea 81/ *Guide to Quality Assurance of Software*, Electronic Engineering Association 1981

/HPR-323/ M. Barnes et al.,: *PODS (The Project on Diverse Software),* Halden Project Report, June 1985

/HWR-225/ T.J. Bjørlo and E. Stokke: *Quality Assurance and Control - A Practical Approach in Simulator Delivery Projects*, Halden Project Report, May 1988

/HWR-226/ A. Hornæs, T. Hveding, G. Pettersen, R. Storkås: *PICASSO-2. A Highly Automated Man-Machine Communication Design Tool for Real-Time Applications*, Halden Project Report, May 1988

/HWR-271/ F. Pettersen, A. Hornæs, R. Storkås: *PICASSO - An Advanced Graphic User Interface Management System*, Halden Project Report, January 1990

/HWR-288/ K.A. Barmsnes, A. Hornæs, R. Storkås: *PICASSO-3 System Design*, Halden Project Report, May 1991

/HWR-319/ F. Handelsby, E. Ness, J. Teigen: *COPMA-II On-line Functional Specification,* Halden Project Report, February 1992

/HWR-372/ Martin Brewer and Gustav Dahll: *A Survey on Proprietary Software Systems*, Halden Project Report, 1994

/SQA 90/ J. Kvalem and M. Pehrsen: *Project Handbook - Software Quality Assurance*, Institute for Energy Technology, March 1990

Assessment of Fiber Optic Sensors and Other Advanced Sensing Technologies for Nuclear Power Plants

H.M. Hashemian

Analysis and Measurement Services Corporation
AMS 9111 Cross Park Drive
Knoxville, Tennessee 37923 USA

Phone: (423) 691-1756
Fax: (423) 691-9344
E-mail: info@ams-corp.com

ABSTRACT

As a result of problems such as calibration drift in nuclear plant pressure sensors and the recent oil loss syndrome in some models of Rosemount pressure transmitters, the nuclear industry has become interested in fiber optic pressure sensors. Fiber optic sensing technologies have been considered for the development of advanced instrumentation and control (I&C) systems for the next generation of reactors and in older plants which are retrofitted with new I&C systems.

This paper presents the results of a six-month Phase I study to establish the state-of-the-art in fiber optic pressure sensing. This study involved a literature review, contact with experts in the field, an industrial survey, a site visit to a fiber optic sensor manufacturer, and laboratory testing of a fiber optic pressure sensor. The laboratory work involved both static and dynamic performance tests.

This initial Phase I study has recently been granted a two-year extension by the U.S. Nuclear Regulatory Commission (NRC). The next phase will evaluate fiber optic pressure sensors in specific nuclear plant applications in addition to other advanced methods for monitoring critical nuclear plant equipment.

1. INTRODUCTION

Measurement of pressure in industrial processes is performed by a variety of sensors, most of which operate by converting the applied pressure to a mechanical movement. The mechanical movement is then measured by a displacement sensor and converted to an electrical signal. In conventional pressure sensors, the displacement is typically measured by electromechanical devices such as strain gages, differential transformers, and capacitance sensors. In fiber optic pressure sensors, the displacement is measured by altering light delivered by a fiber optic transmission system to the sensing element. The intensity or another characteristic of the return light is used to measure the displacement of the sensing element, and correlate that to a pressure change.

Fiber optic pressure sensors have several advantages over conventional pressure sensors. This includes high sensitivity, resistance to electromagnetic and radio frequency interference (EMI/RFI), reduced calibration requirements, fast response time, and electrical isolation. However, fiber optic pressure sensors have different failure mechanisms and failure modes than conventional pressure sensors and adequate data and experience do not currently exist on long term performance of these sensors in industrial processes. Therefore, substantial research is needed to establish the technical basis for the use of these sensors in nuclear power plants.

A number of industrial and government organizations including the Electric Power Research Institute (EPRI), National Aeronautics and Space Administration (NASA), National Institute of Standards and Technology (NIST), National Science Foundation (NSF), and the U.S. Department of Defense have expressed interest in fiber optic sensing technologies. Research and development efforts are underway at these organizations as well as several universities to design and develop fiber optic temperature, pressure, vibration, and other sensors for industrial applications. Presently, fiber optic pressure sensors are used in limited applications in medical, aerospace, chemical, and automotive industries.

2.0 PRINCIPLE OF OPERATION OF FIBER OPTIC SENSORS

Figure 2.1 illustrates the basic components of a fiber optic sensing system. A transducer modulates a light signal according to the value of the process parameter being sensed. This modulated light signal travels through a fiber optic communication link to an interface unit. The communication link is typically in the form of a fiber optic cable or cables. Note that in some cases the transducer may be the cable itself. This intrinsic sensing is accomplished by allowing the process to alter the optical properties of the fiber core resulting in direct modulation of the light signal. The interface unit is used to either process the incoming light signal (i.e., convert it to an electrical signal) or condition and multiplex it with light signals from other fiber optic instrumentation.

The basic operation of a fiber optic sensor involves a light source which provides light to a transducer. The transducer modulates the light that is then sent to an optical detector and then to the signal processing equipment. The light source for a fiber optic sensor is typically a light emitting diode (LED) or a laser. Both of these sources convert electrical power into light with distinct spectral characteristics. For fiber optic systems involved in telecommunications, which involve long distance signal transmission, a laser is usually used as the light source because of its higher optical power output. However, fiber optic sensors typically utilize LEDs because of their availability, high reliability and low cost. In a distributed control system containing many fiber optic process sensors, one light source can be shared among several sensors. This is accomplished using optical couplers using a distributed system that uses time division multiplexing (TDM). The number of sensors which can be "daisy-chained" in this manner depends on the optical power requirements of the sensors and signal detection instrumentation and to the optical power output of the light source.

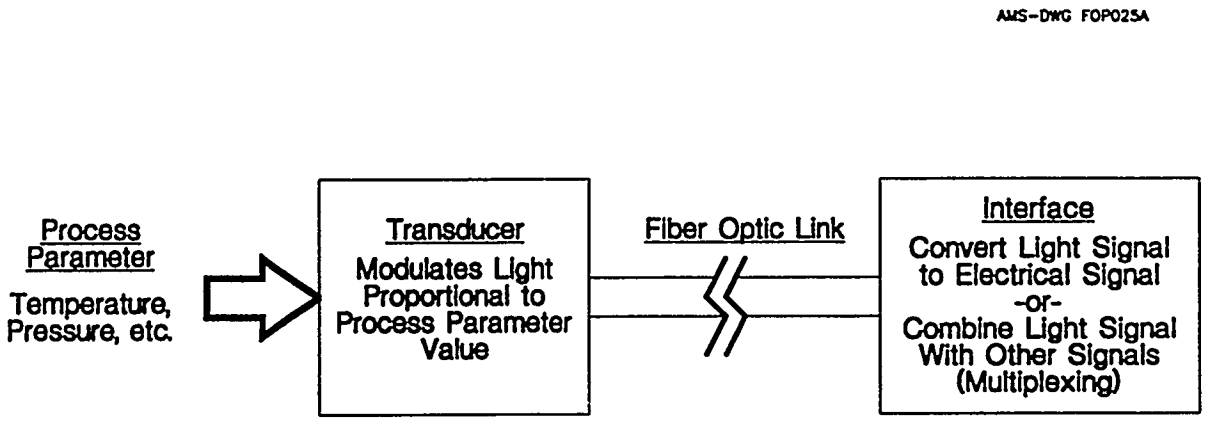

Figure 2.1 Illustration of the Basic Components of a Fiber Optic Sensing System

3.0 ADVANTAGES AND DISADVANTAGES OF FIBER OPTIC PRESSURE SENSORS

3.1 Advantages

Some of the relative advantages which fiber optic pressure sensors possess over conventional sensors are given in Table 3.1. Although not all fiber optic pressure sensors demonstrate every advantage listed in this table, many demonstrate most of these advantages.

Since fiber optic cables are dielectric and the sensing mechanisms used are usually optic and optomechanical, fiber optic pressure sensors are immune to radio frequency interference (RFI) and electromagnetic interference (EMI). This property allows high signal-to-noise ratios and transmission without shielding requirements in electrically noisy environments. As with EMI and RFI, noise emission and cross-talk among fiber optic cables is nonexistent. Optical fibers may be bundled together and several bundles may be run in close proximity.

The dielectric property of fiber optic cables eliminates shock hazards, as well as the need for surge protection and signal isolation. Fiber optic sensors are immune to ground faults and electrical hazards (e.g., ground loops, common mode voltages, and changes in ground potential). Typical materials used in fiber optic cables are chemically inert in most process environments. This property both protects the integrity of the cable and prevents undesirable chemical reaction with or contamination of the process environment.

Transmission loss, or attenuation, is generally much smaller in optical fibers than in the electrical leads of conventional process sensors. With the inherent multiplexability of many fiber optic sensors, several sensors can be used with a single transmission cable. Since some fiber optic sensing modulation techniques are digital in nature, fiber optic sensing is easily made compatible with digital control systems. Many fiber optic transducer designs are extremely small and lightweight. This allows sensor placement in locations previously inaccessible with conventional sensing technologies.

The small size and weight of fiber optic transducers renders them less vulnerable to vibration and shock. Fiber optic pressure sensors offer significantly greater sensitivity and dynamic range than conventional pressure transmitters, and can provide advantages in the following areas: linearity, stability, reliability, and response time.

High temperature environments can introduce diaphragm "creep" and unpredictable and non-repeatable measurements in conventional pressure transmitters. Many fiber optic pressure sensors have been designed so that they are unaffected by elevated temperatures. For this reason, as well as tolerance to vibration and shock, fiber optic pressure sensors can be used in adverse environments.

3.2 Disadvantages

Fiber optic sensors have some disadvantages when compared to conventional sensors. These may include fragility of the sensing element and fiber optic cable, poor compatibility with process environments, radiation-induced darkening of the fiber optic cables resulting in increased attenuation, complex and expensive signal processing equipment and, in certain cases, poor performance in static pressure measurements.

Many fiber optic sensors, especially of the intensity-modulated variety, are particularly vulnerable to fluctuations in the transmission characteristics of the fiber optic cables due to environmental and mechanical stressors, as well as variations in the sensitivity of detectors and the efficiency of light sources with temperature and aging. These specific problems are usually eliminated or reduced with the application of compensation techniques (e.g., use of a reference fiber or dual-wavelength measurement), and are not necessarily present with other modulation techniques.

TABLE 3.1

Advantages of Fiber Optic Pressure Sensors

Optical Isolation Advantages
EMI/RFI Immunity
Noise, Crosstalk, and Ground Loop Immunity
Elimination of Spark and Shock Hazards
Useful in Explosive Environments
Low Signal Attenuation for Remote Measurements
Physical Factors
Small in Size and Mass
Resistant to Harsh Environments
High Temperature Tolerance
Chemically Inert
High Tolerance to Vibration and Shock
Performance Characteristics
High Resolution
High Dynamic Range
Good Linearity
Temperature Compensation or Low Temperature Sensitivity
Multiplexing Capability

4. SURVEY OF THE FIBER OPTIC INDUSTRY

A critical aspect of the Phase I research project was the accumulation of knowledge from the individuals and organizations involved in fiber optic sensing technologies. This was accomplished by an informal survey of the fiber optic manufacturers and interviews with the experts in this field.

4.1 Description of Survey

Approximately one hundred individuals and organizations in the United States, Canada and European nations were contacted during the Phase I effort. These contacts represented a wide variety of expertise in fiber optic sensing technology. Figure 4.1 gives a breakdown of the contacts made during the project by identifying their involvement in fiber optic sensing. The majority of the organizations contacted were manufacturers of fiber optic sensors and related components.

Two questionnaires were used in performing the survey; one for the survey of manufacturers and another for interviews of industry experts, scientists, authors, etc. One of the most important questions asked during the survey involved the potential of fiber optic pressure sensors for safety-related measurements in nuclear power plants. Although a wide variety of responses were given to this question, the overall response was positive. Most manufacturers and industry experts felt that the necessary technology is currently available to design a fiber optic pressure sensor that can meet or exceed the nuclear industry design and qualification criteria. However, because of the current lack of research and testing into such items as long term radiation effects, this may not be possible in the near future.

4.2 Manufacturers Survey

As mentioned above, most of the organizations contacted were manufacturers of fiber optic sensors and fiber optic sensing system components. These manufacturers were identified through the literature review, searches of manufacturing indices, as well as through information obtained from various individuals contacted during the project. Over sixty companies were contacted in order to establish their involvement in fiber optic sensing, as well as to determine their interest in supplying products to the nuclear industry.

Figure 4.2 gives a breakdown of the involvement of the manufacturers surveyed in the development of fiber optic pressure sensors. As shown in this figure, only a small number (five) of manufacturers actually stock fiber optic pressure sensors. However, most of these sensors are intended for specific industrial uses such as in the chemical, medical, automotive and aerospace industries. Therefore, intercomparisons of the sensors manufactured by these companies was not possible.

Custom manufacturers were defined as those organizations that only design and fabricate fiber optic pressure sensors per customer requirements on an as-needed basis. These companies also typically manufacture fiber optic sensors for measuring other process variables. The manufacturers listed under the "R&D Phase" category in Figure 4.2 are companies that are currently developing a fiber optic pressure sensor for commercialization. However, as for the manufacturers that stock sensors, these companies are typically targeting a niche market.

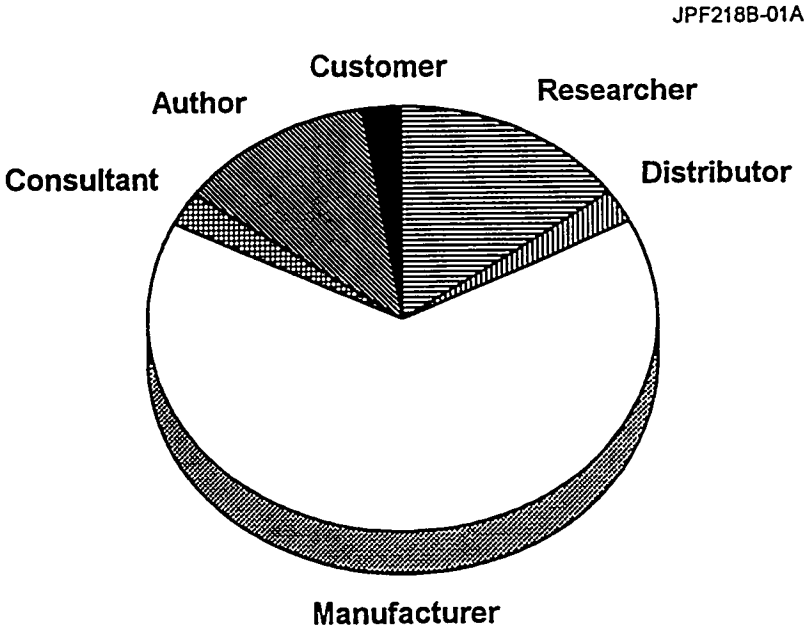

Figure 4.1 Contacts Made During the Fiber Optic Industry Survey

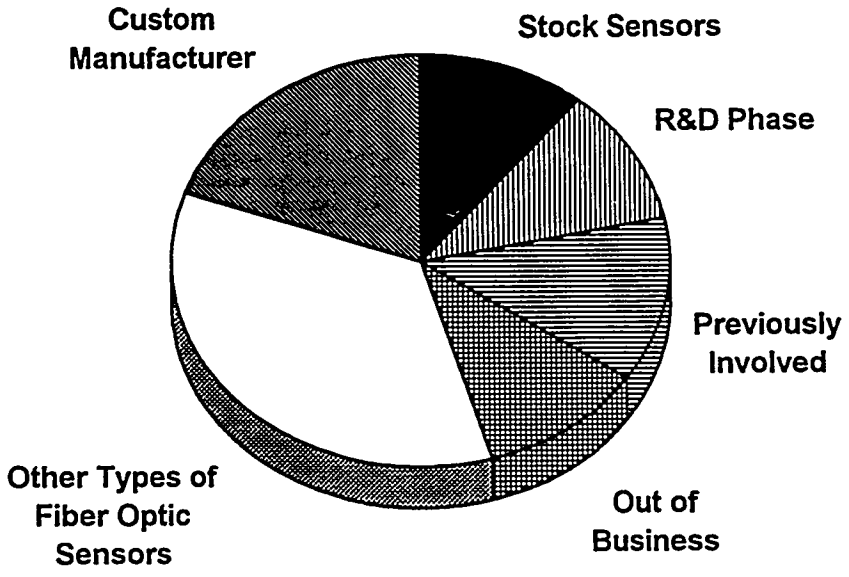

Figure 4.2 Involvement of the Manufacturers Surveyed in Fiber Optic Pressure Sensing

The three remaining categories shown in Figure 4.2 are companies that manufactured fiber optic pressure sensors at one time but are no longer involved in the technology, companies that went out of business, and companies that only manufacture fiber optic sensors that measure process variables other than pressure. Not shown in Figure 4.2 are companies that manufacture fiber optic system components only. These components include optical sources and detectors, as well as fiber optic cables. Information from these contacts was very helpful in establishing the characterizations and failure modes of the components that make up a fiber optic pressure sensing system.

The Phase I research showed that the four most popular fiber optic technologies were spectrum modulation, inferometry, frequency modulation and intensity modulation. Figure 4.3 shows the results of the manufacturers survey in terms of the popularity of these four sensing techniques. The main reasons given for the popularity of the intensity modulation technique over the other three was its simplicity, ruggedness and low cost.

An important part of the manufacturers survey was to establish the current interest of fiber optic pressure sensor manufacturers in entering the nuclear market. Although most were interested, all of these manufacturers had some reservations. Their reservations were mostly due to the design and qualification criteria, as well as skepticism concerning the interest of the nuclear industry in procuring such technologies. Most could not see an economic benefit for meeting the nuclear utility industry's requirements at this time. Also, note that most of the fiber optic pressure sensor manufacturers surveyed were companies with no previous involvement in the nuclear industry. The manufacturers that currently supply conventional pressure sensors to the nuclear industry are only moderately interested in developing fiber optic pressure sensors. A few have performed some limited investigations into this technology for nuclear power plants, but none are vigorously pursuing this issue.

5. LABORATORY TEST RESULTS

In an attempt to enhance the information compiled in the project, a fiber optic pressure sensor was obtained from Paroscientific, Incorporated of Redmond, Washington, for laboratory testing. This testing included measurements of the static and dynamic performance of the sensor.

5.1 Description of Sensor

The particular fiber optic pressure sensing system obtained from Paroscientific was a temperature-compensated demonstration unit which consists of a quartz crystal resonance pressure transducer, an electronic interface unit, and two fiber optic cables. The sensor is used for barometric pressure measurements between 11.5 and 16 PSIA (PSI absolute).

An interface unit supplies the optical power to the transducer through one of the fiber optic cables. The transducer then modulates the light according to the measured pressure and returns the modulated light to the interface unit through the second fiber optic cable. A drawing of the Paroscientific system showing the setup and the dimensions of the transducer and the interface unit is given in Figure 5.1.

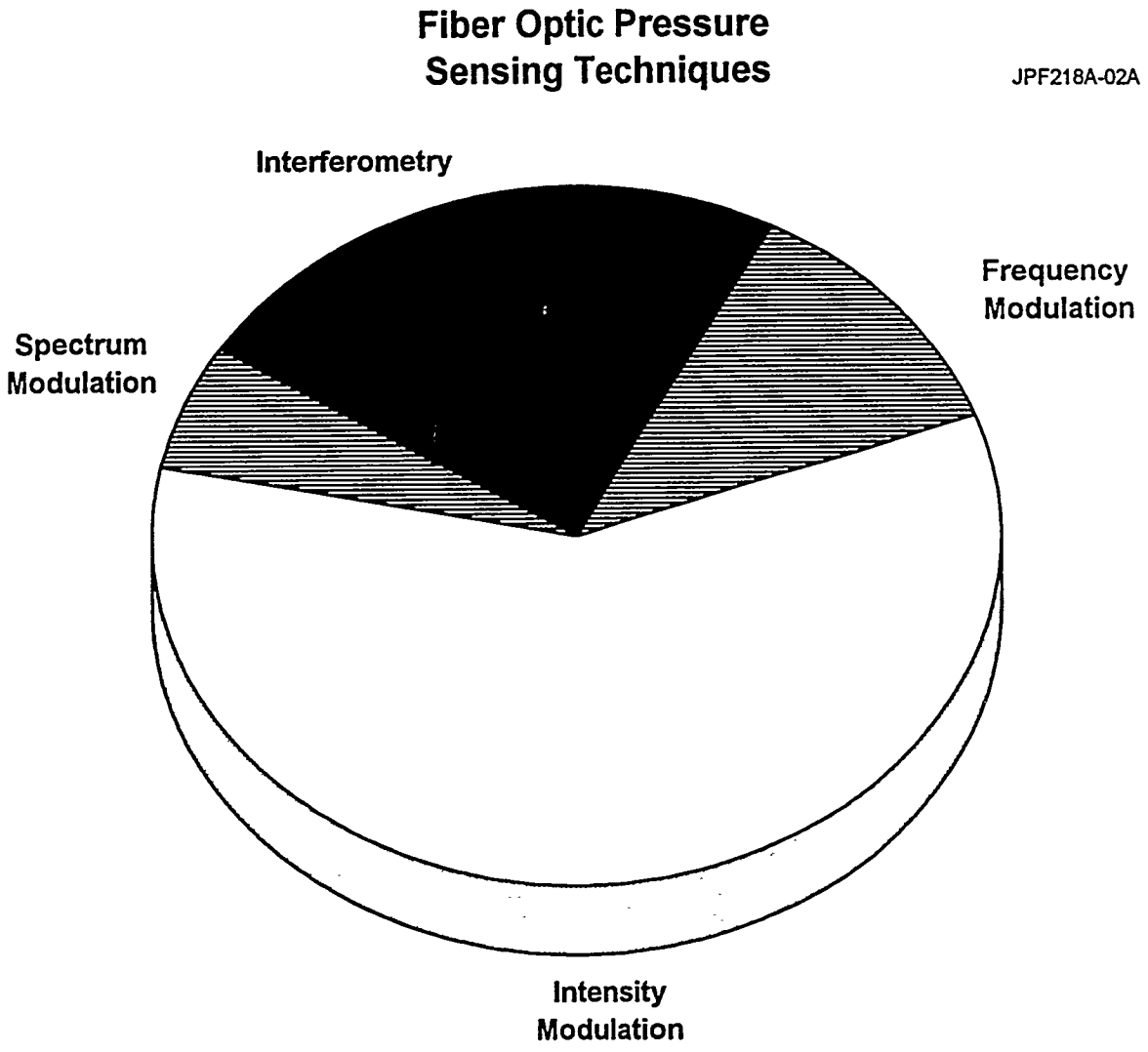

Figure 4.3 Popularity of the Four Main Fiber Optic Pressure Sensing Techniques

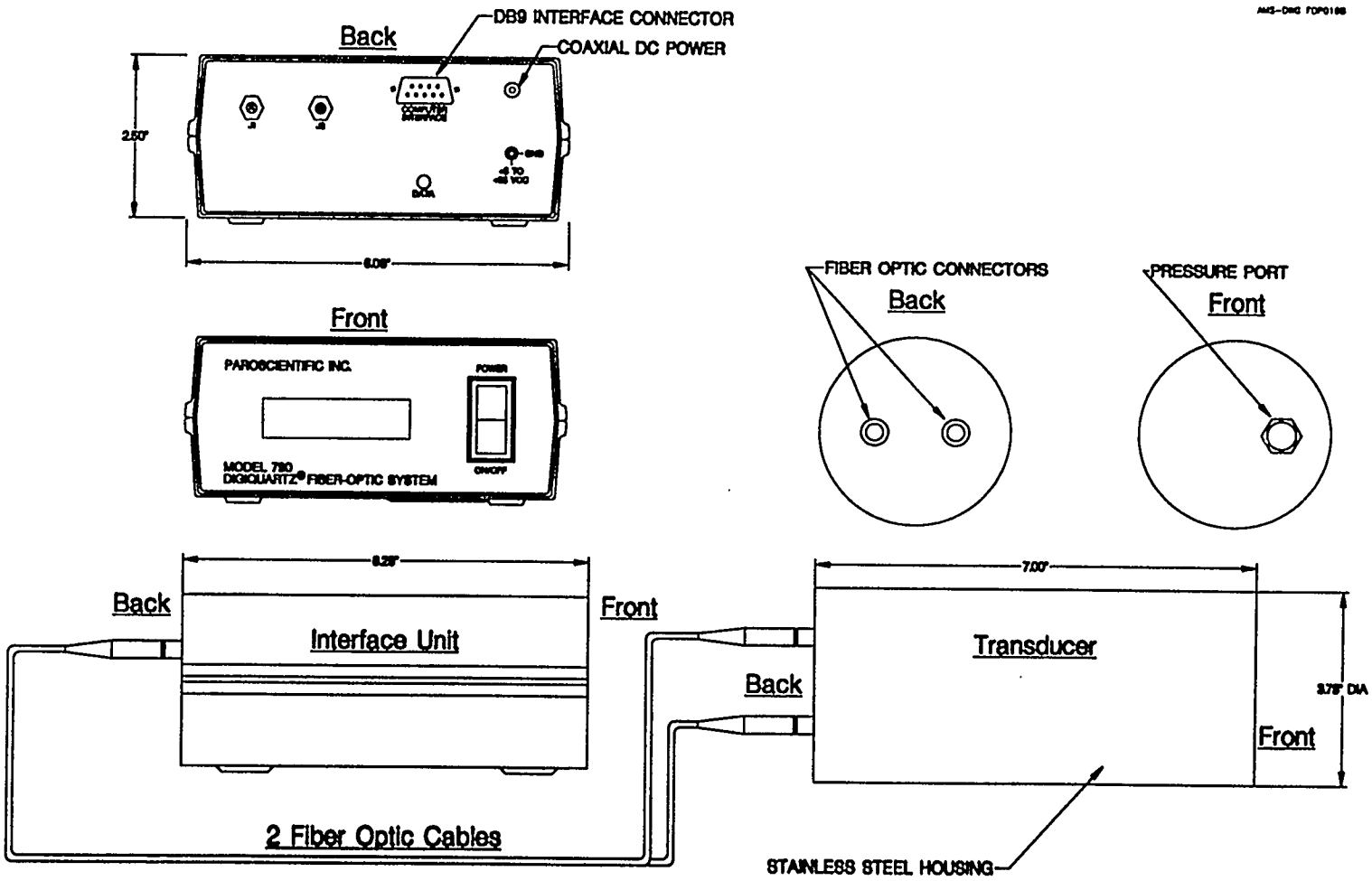

Figure 5.1 Drawing of the Paroscientific Fiber Optic Sensing System

5.1.1 Principle of Operation

The fiber optic pressure transducer tested in the laboratory uses quartz crystal resonance technologies to modulate the frequency of the light signal according to both the sensed pressure and the temperature inside the transducer. This is accomplished by using two quartz crystals, one for pressure and one for internal temperature, which resonate at different frequencies depending on the values of the measurands. The light beams that exit the transducer have frequencies which are dependent upon the resonating frequencies of the crystals. The resonant frequency of the pressure sensing crystal is primarily dependent on the sensed pressure but is somewhat affected by temperature. Therefore, the internal temperature sensing crystal, which has an optical frequency output dependent on temperature alone, is used to compensate for this small effect on the pressure crystal. The temperature range of this particular transducer is -65 to 225 degrees Fahrenheit although similar transducer designs can go up to approximately 250 degrees Fahrenheit.

The major advantages of the frequency modulation techniques for fiber optic pressure sensing are high accuracy, repeatability, low hysteresis and power consumption, along with long term stability. This particular sensor offers a 0.01% accuracy and its stability is comparable to timepieces which use crystal oscillators. However, the quartz crystals themselves are very sensitive to shock, vibration, and other stresses. The results of overstressing the crystals are typically catastrophic in terms of the performance of the sensor. In order to alleviate the potential for such problems, the crystals are mounted on mechanical isolation systems and mounting pads. Balance weights are also included to reduce the sensitivity of the sensor to acceleration, shock and vibration. The applied pressure is transferred to the quartz crystal through a bellows configuration in this particular sensor, although a Bourdon tube configuration is used in transducers which measure higher pressures.

5.1.2 Fiber Optic Cables

The light beams are sent to and from the pressure transducer through fiber optic cables which may be up to 500 meters long. The fiber optic cables for the sensor were supplied by the SpecTran Specialty Optics Company. They are multimode step index fibers with a high numerical aperture. Their high numerical aperture make them very tolerant to improper connections as well as macrobending. It also allows a greater amount of the light source to enter the cable thereby increasing optical power and allowing the use of less expensive light sources and optical detectors. Their ruggedness and low cost make them ideal for fiber optic instrumentation.

5.1.3 Interface Unit

The electronic interface unit, which can be located remotely from the pressure transducer, supplies light to the transducer and interprets the modulated light signals from it. A digital display is provided with the interface unit to provide local pressure readings. A computer can be linked to the interface unit through a standard RS-232 communications interface. This allows the user to control the interface unit display, receive pressure and temperature measurements with the desired format and resolution, and control other features of the sensing system. The communications protocol used with this system is such that up to 98 different transmitters can be attached to a single RS-232 port and controlled by a single computer.

Figure 5.2 is a block diagram of the entire sensing system that illustrates how the individual components of the interface unit function. The optical receiver/demodulator converts the incoming modulated light signals to electrical pulses. A digital counter, which is driven by a high frequency digital clock, is used to count the number of pulses that occur in a specific amount of time. The time between pulse counts is called the period and is inversely proportional to the frequency of the incoming light signal. A microprocessor is used to control the counter which is multiplexed to allow it to measure the period of both the temperature and pressure signals. The period measurements are then processed by the output circuitry according to the coefficients stored in the memory of the interface unit. This memory is in the form of an Erasable and Programmable Read-Only Memory (EPROM) that contains unalterable information as well as an Electrically Erasable and Programmable Read-Only Memory (EEPROM) that contains measurement conversion characteristics, display modes, and other parameters, which can be changed by the host computer.

5.2 Laboratory Test Results

The laboratory testing performed with the fiber optic sensor was aimed at providing a better understanding of the operation of fiber optic pressure sensors. The testing involved both static and dynamic characterizations of the fiber optic sensor and demonstrated its temperature compensating abilities.

5.2.1 Temperature Cycling

As mentioned earlier, the Paroscientific sensor uses a second crystal in the design that measures the internal temperature of the device. Because of the protective enclosures placed around the sensing elements, there is a significant lag between the external temperature and the temperature seen by the sensing elements. This temperature lag is shown in Figure 5.3. An environmental chamber that had been used in previous instrumentation aging research projects was utilized for the temperature cycling tests.

In order to demonstrate the temperature compensation capabilities of the Paroscientific sensor, a conventional pressure sensor was placed outside the environmental chamber as a reference while the fiber optic sensor remained inside. The temperature in the environmental chamber was cycled from room temperature, approximately 70 degrees F, to 150 degrees F. The temperature was then held constant for a period of approximately 13 hours before the heating was stopped and the environmental chamber was allowed to cool down to room temperature.

Figure 5.4(a) shows the temperature of the environmental chamber versus the internal temperature of the fiber optic sensor for one test run. Figure 5.4(b) shows the output of the conventional sensor versus both the uncompensated and temperature-compensated pressure signals coming from the fiber optic sensor. The uncompensated pressure signal, as shown in this figure, follows the outline of the reference sensor output but shows an increasing deviation as the internal temperature increases. The temperature-compensated pressure output, however, more closely follows the outline of the conventional sensor. Note that the intent of this test was to demonstrate the temperature compensation abilities of the fiber optic sensor and not to determine its accuracy. Figure 5.4(c) illustrates the temperature compensation more clearly by showing the deviation of the temperature-compensated measurement from the uncompensated output of the fiber optic sensor.

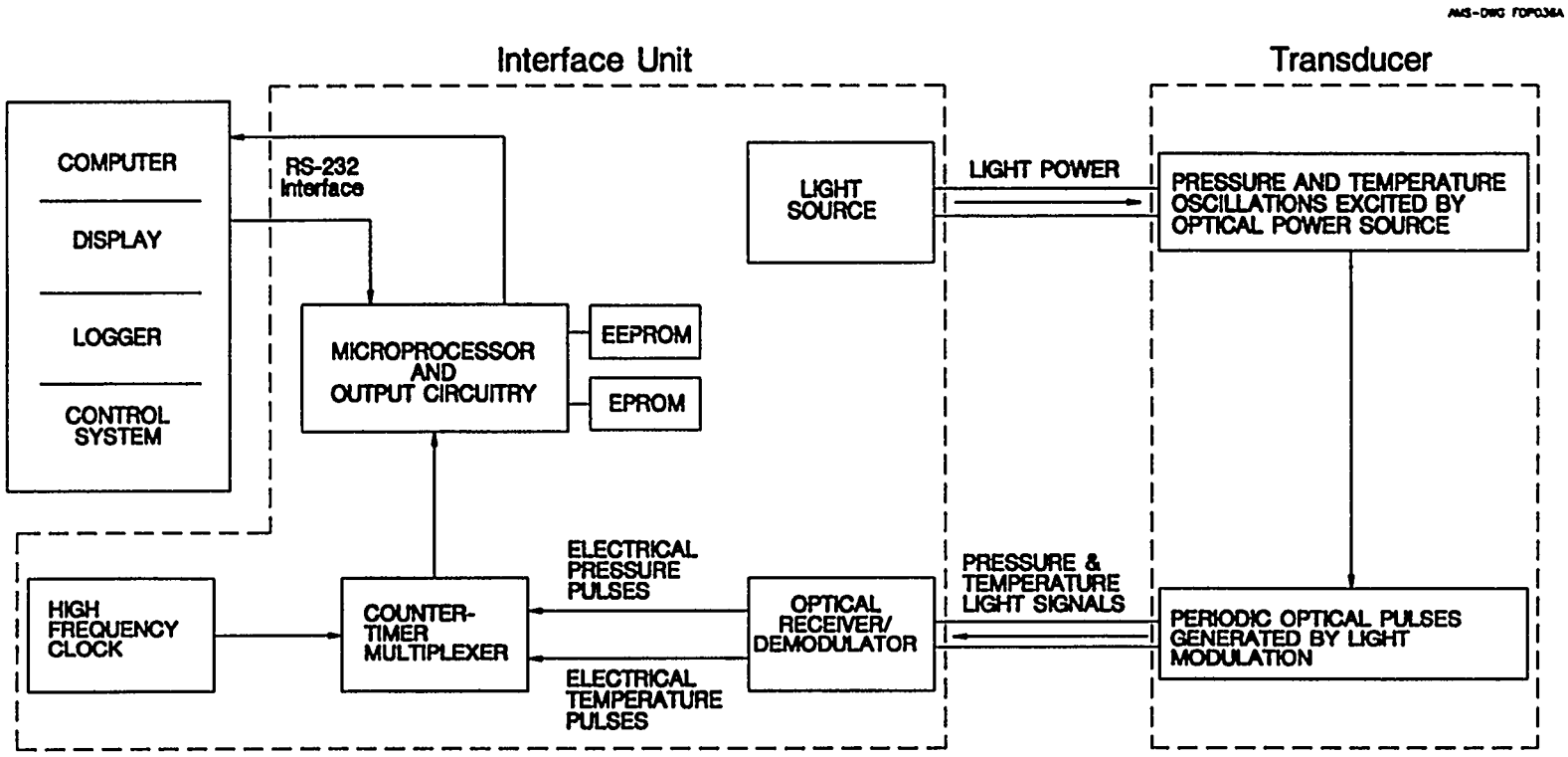

Figure 5.2 Block Diagram of the Paroscientific Pressure Sensor Showing the Components of the Transducer and the Interface Unit

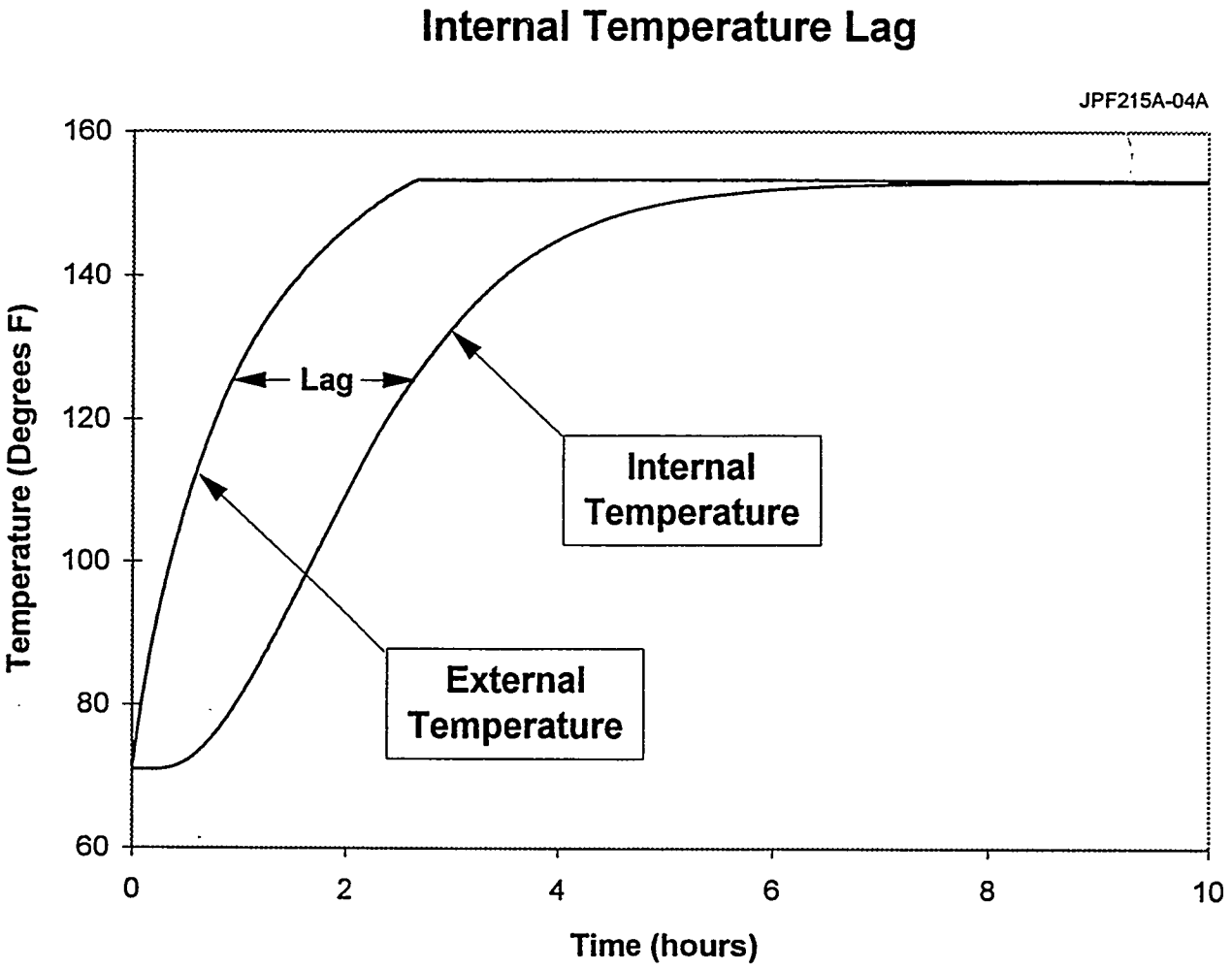

Figure 5.3 Temperature Lag Between the External and Internal Temperature Seen by the Fiber Optic Pressure Transducer

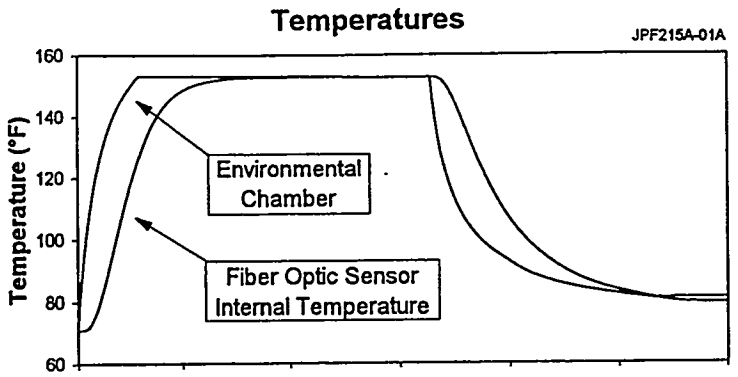

(a)

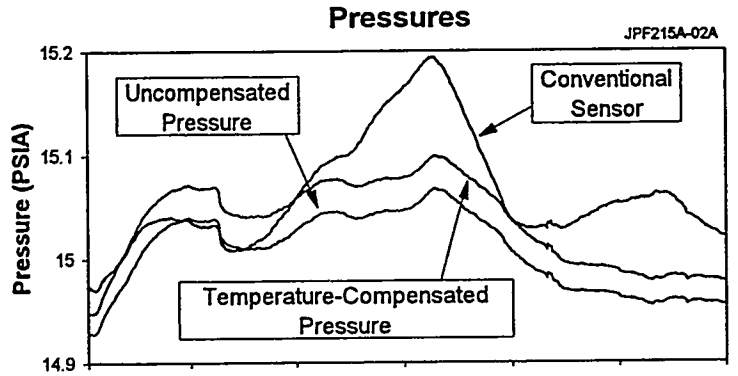

(b)

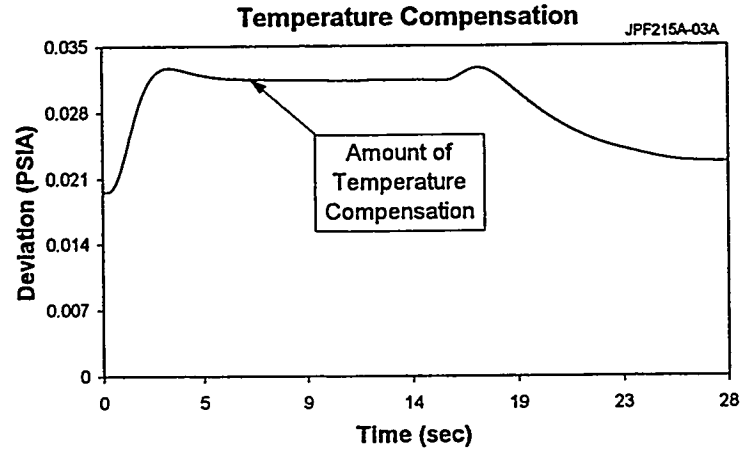

(c)

Figure 5.4 Results of One Series of Temperature Cycling Tests

5.2.2 Vibration Testing

One of the major concerns with fiber optic sensors is the potential damage to the sensing crystals due to vibration and other mechanical stressors. As mentioned above, a mechanical isolation system including mounting pads and balance weights is employed in this sensor to reduce the adverse effects of such stressors and protect the crystals. Because the Paroscientific sensor was a demonstration unit on loan for this research project, destructive vibration testing could not be performed. Therefore, the intent of the vibration testing was to demonstrate the ability of the fiber optic sensor to measure pressure accurately despite induced vibration.

The fiber optic sensor and a conventional sensor were fixed to a vibration beam and exposed to the same pressure source. The beam was pinned at one end to restrict movement to only one direction. A motor was fixed to the other end of the beam to induce vibration. Various size weights were attached to the shaft of the motor to produce an imbalance and thereby increase the vibration of the beam. Figure 5.5 shows the results for one set of vibration tests by comparing the output of the Paroscientific sensor to that of the conventional sensor. The motor was periodically turned on and off, as shown in this figure, to illustrate that the induced vibration had no effect on the output of the fiber optic pressure sensor.

5.2.3 Dynamic Testing

One of the potential advantages of fiber optic sensors over conventional pressure sensors is faster dynamic response. The transmission of the pressure signal to the remote electronics utilizes light beams which makes it almost instantaneous. Therefore, the limiting factors are the sensing elements that convert the process measurement to a mechanical displacement and the remote electronics that convert the incoming light signal to a measured pressure. The dynamic testing performed on the Paroscientific sensor attempted to establish its dynamic response characteristics.

Figure 5.6 illustrates the test setup for the ramp testing performed on the fiber optic pressure sensor. As seen in this figure, the pressure ramp was applied to both the fiber optic sensor and a pressure transmitter produced by the Validyne Engineering Corporation which was used as a reference sensor. The Validyne transmitter is a high-speed reference transmitter with a response time of less than 10 milliseconds. A computer initiated the ramp test by triggering a solenoid and then acquired data from both the reference sensor and the fiber optic sensor. A manually-controlled needle valve was used to control the rate of the pressure ramp.

Figure 5.7(a) shows the results from one ramp test while 5.7(b) shows the same results zoomed in on the first part of the transient. As seen in this figure, the dynamic response of the fiber optic pressure sensor is faster than that of the Validyne transmitter.

6. ADVANCED SENSING TECHNOLOGIES

As stated earlier, the Phase I project described in this paper has been granted a Phase II extension by the NRC to expand the study to include other advanced sensing technologies such as ultrasonic flow sensors and use of neural networks for nuclear plant applications. These are described below:

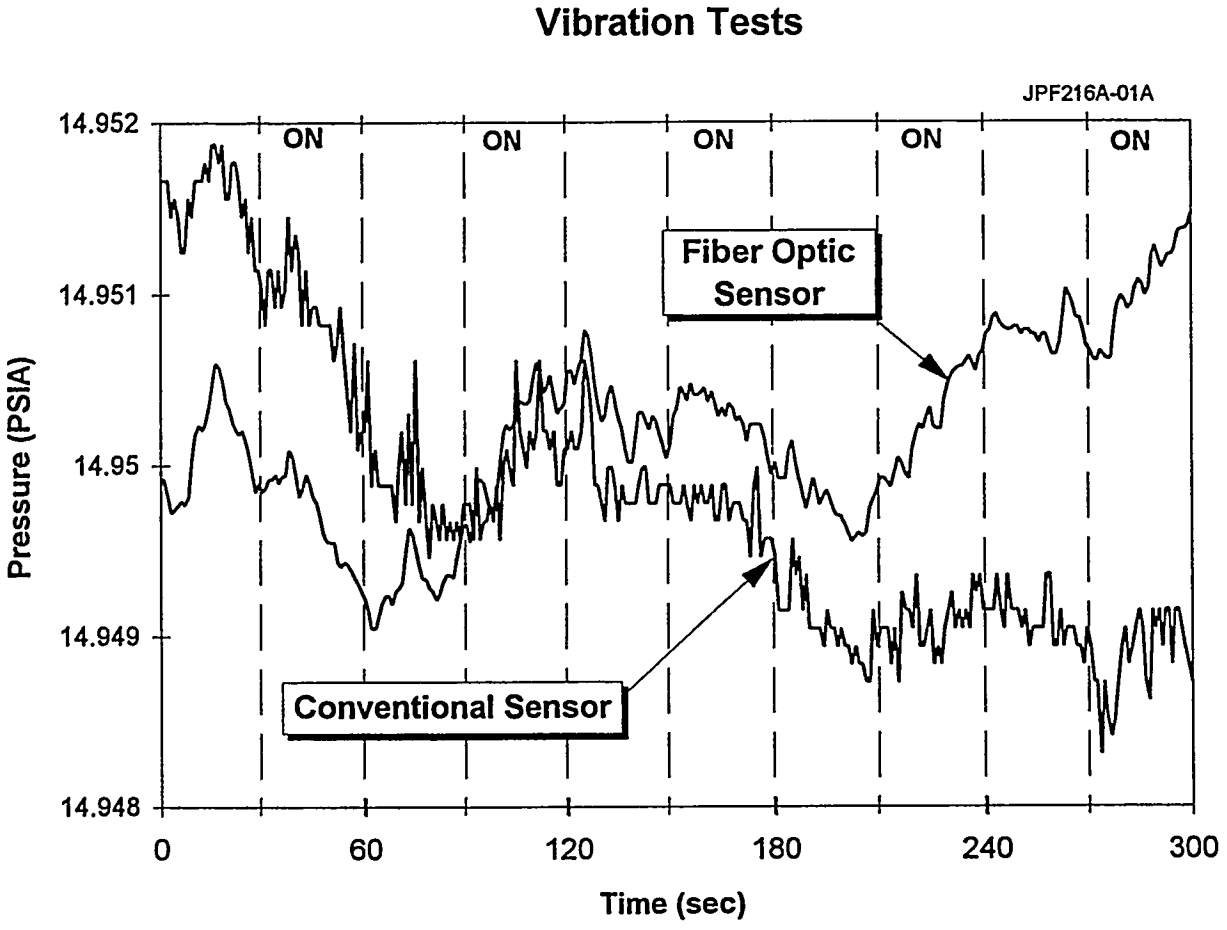

Figure 5.5 Results of One Series of Vibration Tests Showing no Visible Effect on the Fiber Optic Sensor Output as the Vibration Beam Motor was Cycled On and Off

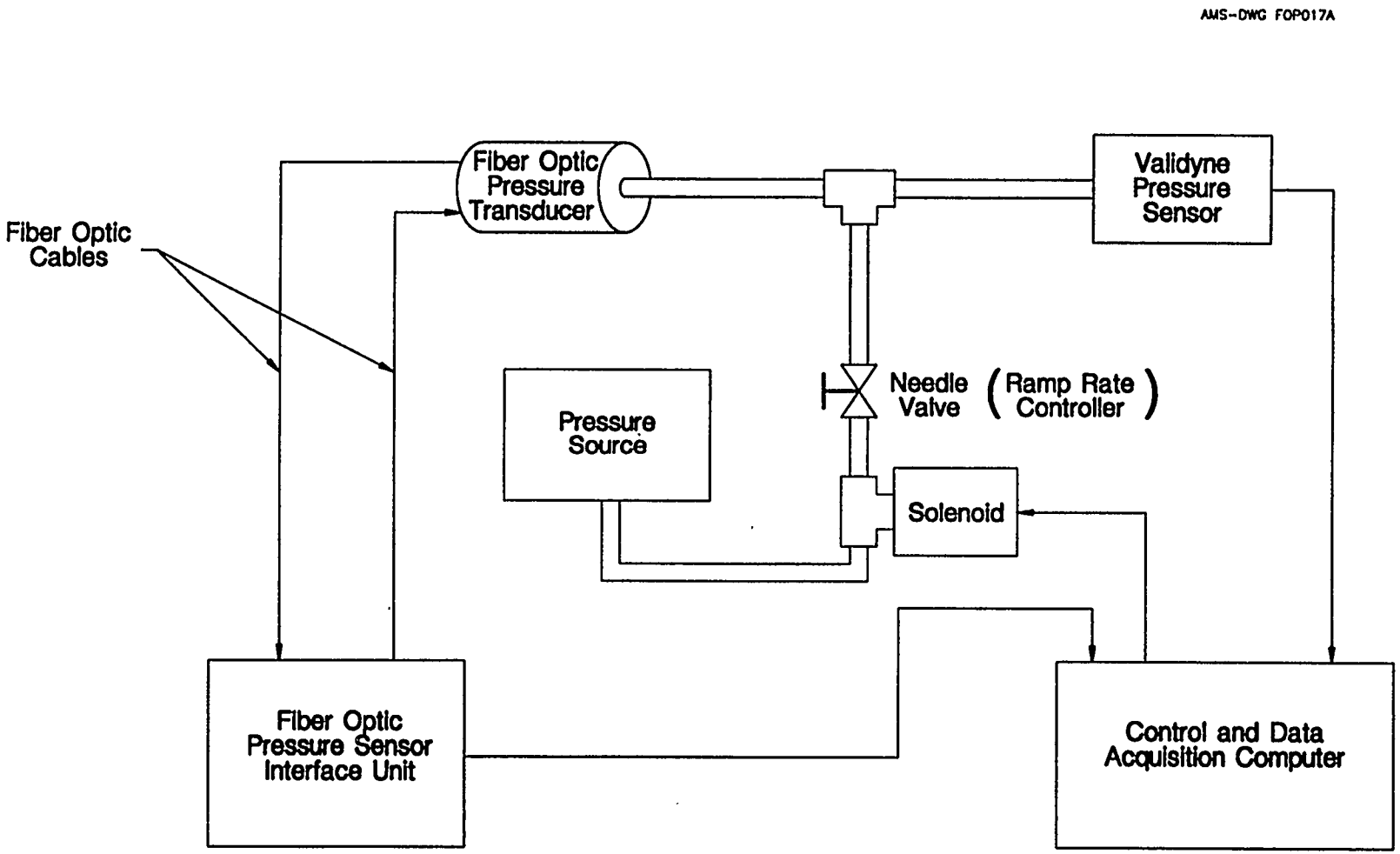

Figure 5.6 Illustration of the Test Setup for Dynamic Ramp Testing

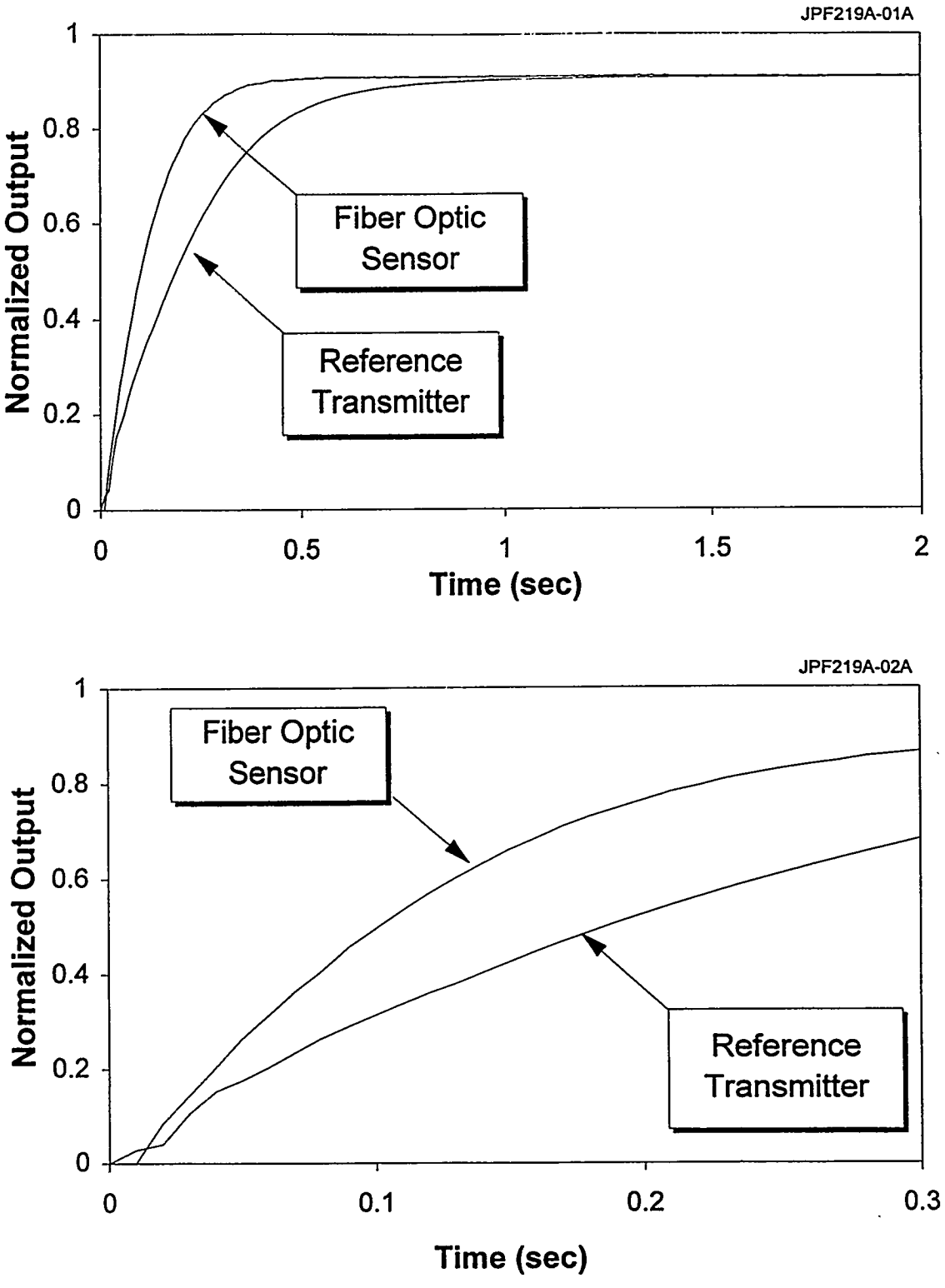

Figure 5.7 Results of an Increasing Pressure Ramp Showing the Faster Dynamic Response of the Fiber Optic Pressure Sensor versus the Reference Sensor

6.1 Ultrasonic Flow Sensors

In addition to fiber optic temperature and pressure sensors, the Phase II project will evaluate ultrasonic flow sensors. These sensors are currently used in a number of PWRs, primarily on a demonstration basis, for measurement of feedwater flow and primary coolant flow. They are also used, to a lesser extent, for measurement of primary coolant temperature. For measurement of temperature, two transducers are clamped to the pipe so that their signals are perpendicular to the flow. A signal is sent through the fluid from one side of the pipe and received on the other side. The time that it takes for the signal to travel through the fluid is measured by the ultrasonic transducers. This information and the pipe diameter are used to calculate the speed of sound through the fluid, which is a function of fluid temperature and density. Using existing correlations, the fluid temperature and density are identified.

For measurement of fluid flow rate, the transducers are installed on the pipe at an angle. The travel times of the two signals are identified and using this information and the angle between the two transducers on the pipe, the flow velocity can be identified. The velocity along with the fluid density (identified earlier) and the cross section of the pipe can be used to calculate the mass flow rate.

It has been suggested by several organizations, including EPRI and the Department of Energy, that ultrasonic flow sensors should be formally evaluated for nuclear safety-related applications. Ultrasonic flow sensors can measure fluid flow much more accurately than venturi-based flow meters that are currently used. Presently, large uncertainties are assigned to flow measurements from venturi flow sensors in nuclear power plants. Reducing these uncertainties could allow plants to operate more efficiently.

Ultrasonic sensors have not been qualified for nuclear safety-related applications and there is no independent assessment of their accuracy and reliability. These problems will be addressed in this Phase II project to determine the potential of these sensors for use as safety-related equipment in nuclear power plants.

6.2 Measurement of Flow Using Cross-Correlation of Signals

Fluid flow rate can also be measured by cross-correlation of signals from various pairs of sensors in a plant. Figure 6.1 illustrates a case where two thermocouples are used to measure fluid temperature at two different locations in a pipe. During plant operation, there are inherent temperature fluctuations in the process due to the flow of fluid and turbulence in the pipes. These fluctuations manifest themselves on the DC output of thermocouples and can be extracted from the output. To extract the temperature fluctuation, the DC component of the sensor outputs are nulled by adding a negative bias or using a high-pass electronic filter. The signal is then amplified and sent through a low-pass filter to remove the extraneous noise and provide for anti-aliasing before the signal is sampled by an analog-to-digital convertor for analysis by a computer. The analysis can be performed in the frequency domain and/or time domain to obtain the fluid transit time between the two thermocouples. This information along with the distance between the two thermocouples is used to calculate the fluid flow rate.

Although a pair of thermocouples was used here to describe the principle of flow measurements with the cross-correlation technique, almost any pair of existing signals in an operating plant that are sensitive to flow changes may be used for this application. For example,

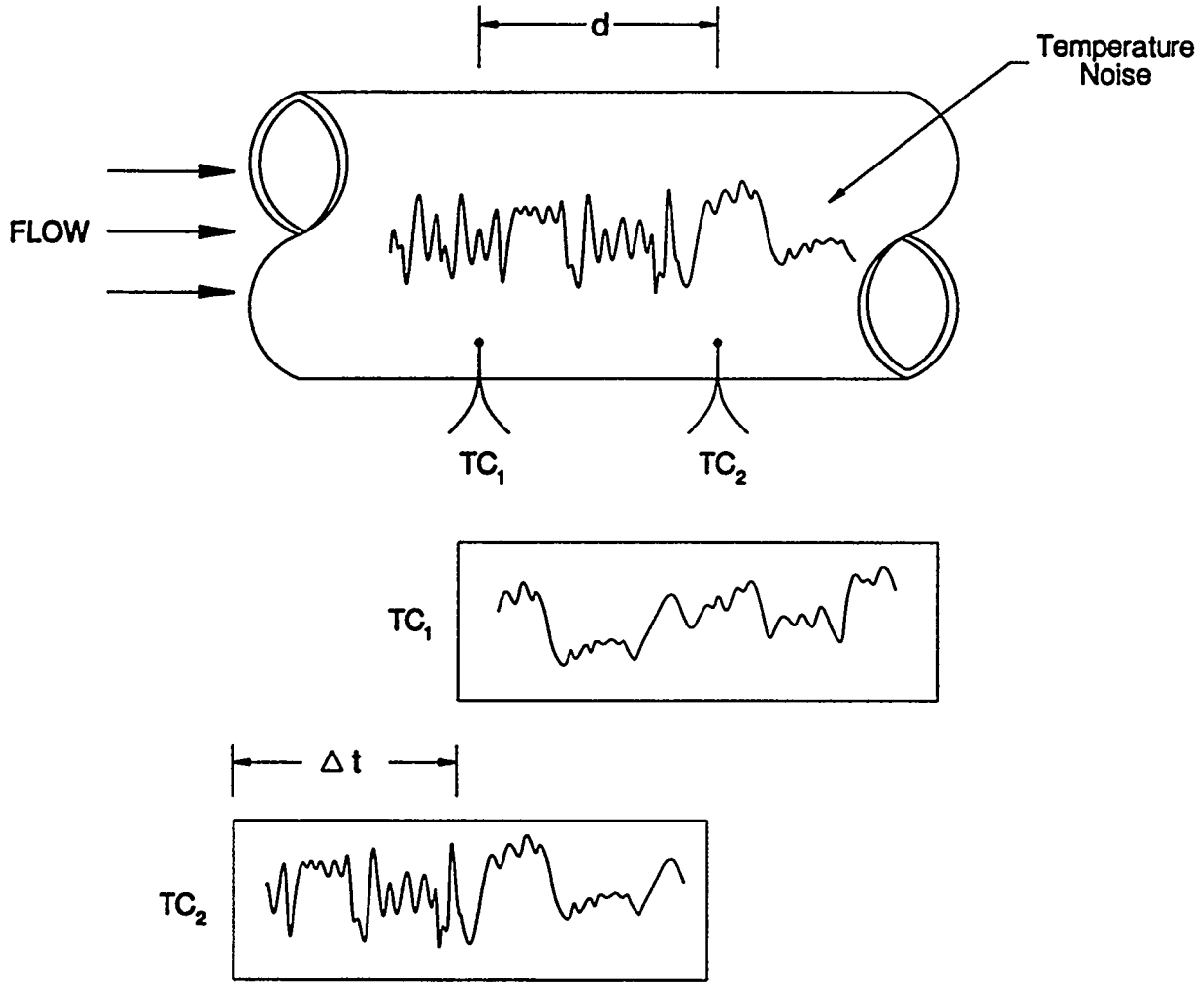

$$\text{Flow Velocity} \approx \frac{d}{\Delta t}$$

TC: Thermocouple

Figure 6.1 Illustration of Principle of Flow Measurement by Cross-correlation of Thermocouple Signals

neutron detectors and core exit thermocouples in a PWR can be used to measure the reactor coolant flow through the core.

The cross-correlation technique for measurement of primary coolant flow is not new. Analysis of N-16 gamma noise has been used in nuclear power plants to measure reactor coolant flow. What is new with the cross-correlation flow measurement method proposed here is that it does not require a particular noise source such as N-16 gamma and radiation detectors to measure the noise. Almost any appropriate pair of like or unlike signals can be cross-correlated to identify the transit time of the fluid. The validity of this method will be determined in Phase II by performing extensive laboratory tests.

6.3 Neural Networks

In the last five years, neural networks have been introduced in the nuclear power industry for a variety of applications, such as detection of venturi fouling in feedwater flow sensors, heat exchanger clogging, check-valve monitoring, vibration analysis, and other predictive maintenance applications. Neural networks are based on fitting the normal inputs and outputs when the system is operating normally. The fitting process is referred to as the "training" of neural networks. Once the neural network is trained, it can be used to detect off-normal conditions. If the neural network model for this system is trained during normal operation, it can be used to predict the flow rate at a later time. The results can be compared with the measured flow to determine drift or other anomalies in the flow sensor or to detect clogging in the heat exchanger.

Figure 6.2 illustrates the principle of neural networks. Basically, neural networks are a form of empirical modeling. In empirical models, a number of inputs are given to the model (an empirical equation developed by the user) and the output of the model is calculated. In neural networks, a similar procedure is followed, but the user does not have to develop the model. Generic neural network models are available for a variety of applications. The neural networks are trained using a set of real inputs and outputs. During training, the neural networks use the inputs and a generic model to reproduce the output. The output from the network is compared with the measured output and weighing factors in the neural network models are changed as necessary to match the neural network's output with the measured output. This process is repeated many times until the measured output and neural network's output converge within a prespecified criteria. The neural networks can then be used to determine if the input/output relationship that was established during training still exists. If not, the characteristics of the system have changed.

7. CONCLUSIONS

The results of a six-month Phase I research project funded by the Office of Nuclear Regulatory Research of the U.S. Nuclear Regulatory Commission are documented in this paper. The purpose of this effort was to establish the state-of-the-art in fiber optic sensing and determine if these sensors can be used for safety-related applications in nuclear power plants. The study included experimental work involving a fiber optic pressure sensor that was tested at the AMS laboratory. Furthermore, an informal survey of over one hundred fiber optic sensor manufacturers, researchers, authors, and others was performed using questionnaires that were

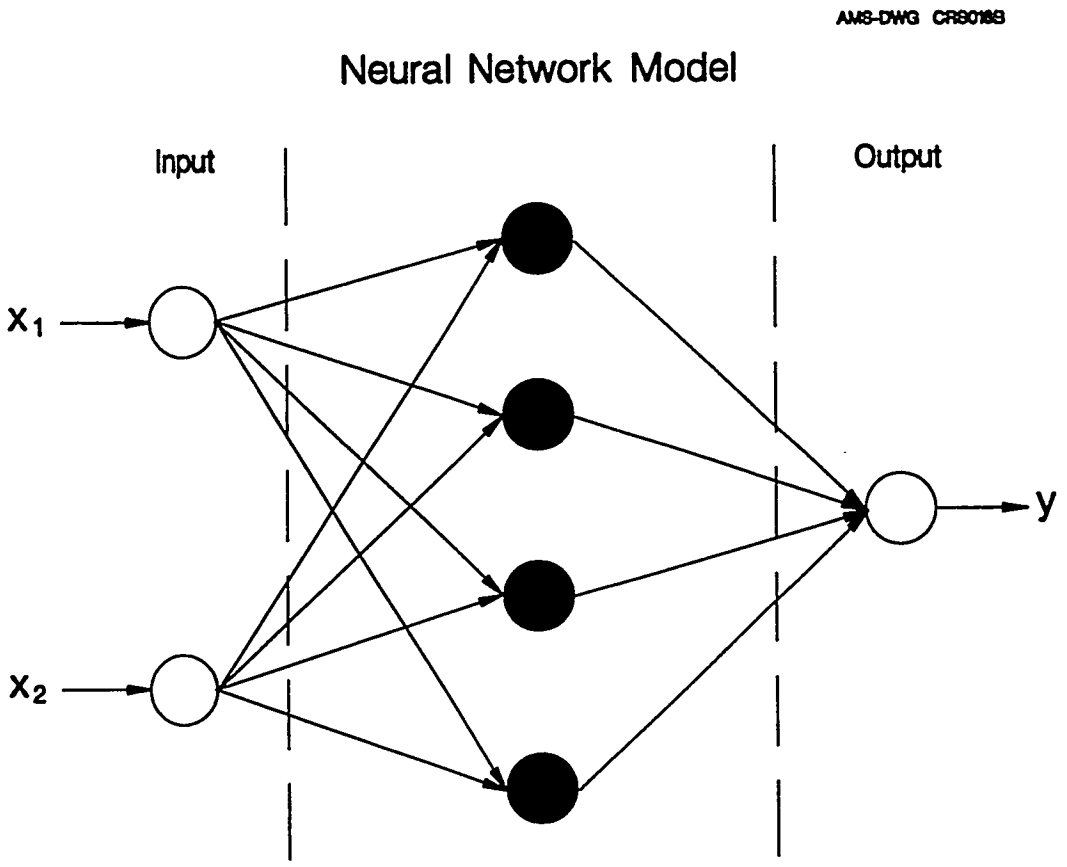

Figure 6.2 A Simplified Neural Network Model

sent out and followed by telephone contacts. These efforts, in addition to an extensive literature review, have led to the conclusion that although fiber optic pressure sensors have several advantages over the conventional pressure sensors, they are not presently ready for use in nuclear power plants because fiber optic sensing technologies are still evolving and their performance has not been extensively demonstrated for nuclear plant applications. In addition, fiber optic pressure sensors are currently much more expensive than conventional sensors.

The NRC has granted a Phase II extension of the project to address these shortcomings and evaluate the feasibility of using fiber optic sensors, including temperature sensors, in specific nuclear plant applications and determine the steps that must be taken to introduce fiber optic sensing technologies to the nuclear industry. In addition, other sensing technologies including neural networks and fluid flow measurement using ultrasonic flow sensors and cross-correlation of sensor outputs will be evaluated for use in nuclear power plants.

Preliminary Studies on the Impact of Smoke on Digital Equipment*

Tina J. Tanaka
Sandia National Laboratories
Albuquerque, NM 87185-0747

Kofi Korsah
Oak Ridge National Laboratory
Oak Ridge, TN 37831-6010

Christina Antonescu
United States Nuclear Regulatory Commission
Washington, DC 20555

Abstract

Last year the USNRC initiated a program at Sandia National Laboratories to determine the potential impact of smoke on advanced safety-related digitial instrumentation. In recognition of the fact that the reliability of safety-related equipment during or shortly after a fire in a nuclear power plant is more risk significant than long-term effects, we are concentrating on short-term failures. We exposed a multiplexer module board to three different types of smoke to determine whether the smoke would affect its operation. The operation of the multiplexer board was halted by one out of the three smoke exposures. In coordination with Oak Ridge National Laboratory, an experimental digital safety system was also smoke tested. The series of tests showed that smoke can cause potentially serious failures of a safety system. Most of these failures were intermittent and showed that smoke can temporarily interrupt communication between digital systems.

*This work was supported by the U.S. Nuclear Regulatory Commission and was jointly performed by Sandia National Laboratories and Oak Ridge National Laboratory. Sandia National Laboratories is operated by Lockheed Martin for the U.S. Department of Energy under contract DE-AC04-94AL85000. Oak Ridge National Laboratory is managed by Lockheed Martin Energy Systems, Inc., for the U.S. Department of Energy under contract DE-AC05-84OR21400.

Introduction

In recent years nuclear power plants have been experimenting with new digital equipment for use in safety systems.[1] Replacement of the older analog equipment with newer systems has raised questions because of the compact nature of the digital systems, the possibility that many functions will be multiplexed in the same equipment, and the potential that new common-mode failure mechanisms might be introduced. The Advisory Committee for Reactor Safeguards (ACRS) has been concerned about these changes and how the replacement of these safety systems will be regulated. In particular, the reaction of digital equipment to smoke has been questioned. These concerns about smoke are raised partly in reaction to the experience of the telecommunications industry which includes one case in which a fire in a central switching center caused extensive smoke damage to electronic equipment.[2] As a result of this fire, the industry has changed their requirements on cable insulation so that the insulation, which supplies a large fraction of the fuel in an accidental fire, is less corrosive if burnt.

While smoke is a known hazard for electronic equipment, very few tests have been performed to determine the reliability of electronic equipment in a smoke atmosphere. In 1994 the U. S. Nuclear Regulatory Commission (USNRC) began a program at Sandia National Laboratories (SNL) to assess the vulnerability of digital equipment to smoke and other synergistic fire conditions. As a preliminary test in this program, SNL exposed operating multiplexer modules to smoke in December 1994. Oak Ridge National Laboratory (ORNL) is investigating the effect of various environmental conditions on digital equipment, and hence, this first test was conducted on equipment suggested by ORNL and with software written by ORNL. One module failed intermittently during the tests, but could be restarted after the completion of the smoke exposure.

In May and June 1995, a series of smoke exposure tests were conducted on an experimental digital safety system designed and built by ORNL. This system was developed to identify short-term environmental stress-related vulnerabilities of technologies that are likely to be used in safety-critical applications in nuclear power plants. The stresses tested by ORNL were elevated temperature, humidity, electromagnetic and radio frequency interference (EMI/RFI), and smoke. The smoke exposures were modeled after likely fire scenarios in nuclear power plants based on past fire events and fire testing. These exposures also showed some failures, however, assuming good engineering design, no failures likely to prevent a safety system from performing its function were identified.

SNL is now performing a series of smoke exposure tests on digital components and printed circuit boards. One of the primary objectives is to measure the impact of smoke on the insulation resistance between contacts in typical components. The smoke environment will be varied to simulate different scenarios such as a high burning temperature versus a smoldering fire and high or low ambient humidity levels. This series of experiments will also compare different methods of component protection, such as conformal coatings and mounting the components in a box.

Studies on the reliability of digital equipment in a fire are rare, at least in part because smoke environments are not easy to quantify and reproduce. Standardized tests have been developed by professional groups such as the American Society for Testing and Materials (ASTM) and the National Institute of Standards and Technology.

At this time, the standardized tests of the behavior of smoke and electronics are limited to measuring the corrosive effects of smoke from various fuels on metals. These tests measure the relative amount of metal lost or the acidity of the smoke. Smoke-induced corrosion, however, typically damages electronic equipment over weeks, while our preliminary exposures show that smoke can damage components in other ways within minutes of a fire.

Recently, a group of researchers in the telecommunications field (in a collaboration among DuPont, Underwriters Laboratory, and AT&T)[3] have become concerned about another potential mode of failure for electronic systems: soot on electronics can bridge conductors. Instead of measuring metal loss or smoke acidity, these researchers are measuring the loss of insulation resistance. This loss and the resulting short circuit can cause immediate failure of a digital system.

This failure mechanism coincides with the concerns relevant to nuclear power plants. That is, for safety reasons, nuclear power plant operators are concerned about the failures that take place during or shortly after a fire—those that happen within minutes or hours rather than weeks.

Although the failure mechanism that DuPont/UL/AT&T are studying is more useful for nuclear power plants than corrosion studies, this group is not investigating the reactions of the digital equipment itself. Instead, it is investigating the surface insulation resistance of a printed circuit board exposed to smoke from a variety of materials. The USNRC is interested in the effect of smoke on the digital equipment itself and how any problems that may result may be mitigated. Because of the lack of a standard test method, SNL has adopted an approach to testing that includes features from standardized smoke corrosivity tests being developed by the ASTM. This report describes three test series on (1) multiplexer modules, (2) an experimental digital system, and, (3) circuit bridging of typical digital components.

Equipment Tested

Analog-to-Digital Modules and Multiplexer

The first smoke tests on components at SNL evaluated the effect of smoke deposited on the analog-to-digital (A-to-D) modules, multiplexer, and backplanes from Analog Devices®. These components were selected by ORNL for testing because they incorporate technologies that are likely to be used in safety systems of nuclear power plants.

Analog Devices sells a series of plastic-encased modules that can perform different functions: measure voltage, measure thermocouple or resistive temperature device (RTD) output, and then output current or voltage. All of these modules plug into a printed circuit-type board called a backplane that is powered with a 5-V dc power supply. The backplane has ports for both RS232 and RS485 connections that allow the backplane to send and receive information from a computer over a serial port.

The commercial computer program that is provided with the modules was used to configure an output module to produce a 0 to 20 mA current to serve as a reference source. The output current was passed through a precision resistor so that the voltage could be measured. An input module was configured to convert the analog voltage to a digital output for the computer. The input module, acting as the test specimen, resistor, and backplane were placed in the smoke exposure chamber while the output module remained outside, along with the interrogating computer (see Figure 1). During the smoke exposure, the input module measurements were compared with the output module readings. Ideally, the measurements should match exactly.

The software for assessing the performance of the test modules was developed ORNL as a "Turbo Basic" program. For the test, the computer directed the output module to feed a known current to the input module. The computer read the actual output module current and the input module voltage measurements. Each voltage measurement was repeated 6 times at 1-second intervals. The computer then changed the output current and repeated the readings. To scan the range of possible output currents, the current started at 0 and was incremented by +0.1 mA steps up to 20 mA. After the output current reached 20 mA, the data from the entire scan were recorded in a data file. The process was then repeated.

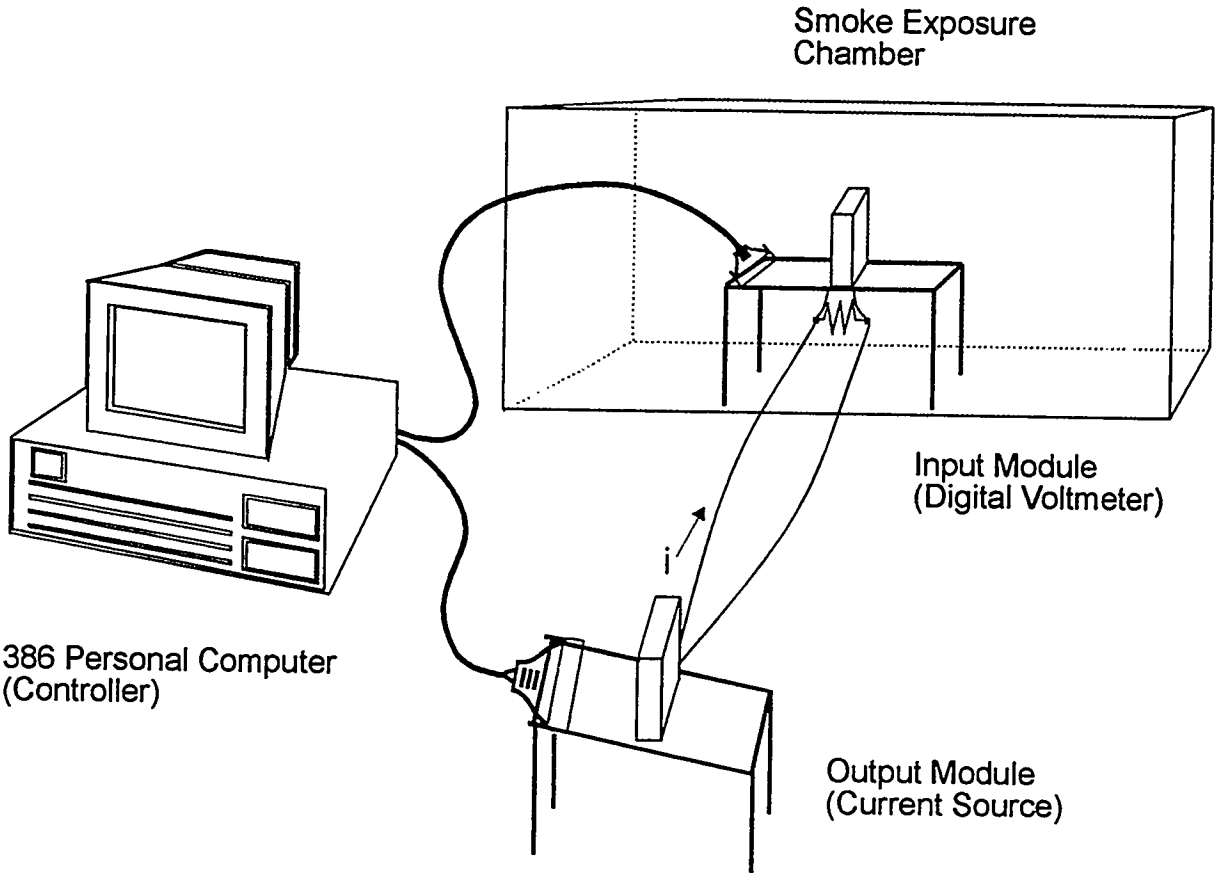

Figure 1. Multiplexer Test Setup.

Experimental Digital Safety System

A reactor trip system typically consists of four divisions of process channels that are eventually interconnected at some points, typically in 2 out of 4 voting logic configurations, for final safety system actuation. For the purposes of the tests described in this document, only one division of a typical system was fully implemented. The functions typically performed by the three other divisions were implemented by a single computer or host processor. This approach was necessary to meet budgetary constraints but did not compromise the objectives of the task since the safety channel implemented incorporated a full complement of the various technologies of interest, namely multiplexers, computers, fiber optic line drivers, a fiber distributed data interchange (FDDI) network, and optical/electrical interfaces.

In order to test these systems at SNL for different exposure conditions, the equipment was cleaned and reused in multiple tests. The process multiplexing unit (PRS/MUX) was exposed four times to smoke while the digital trip computer (DTC) was exposed three times to smoke and once to CO_2. The fiber optic modules (FOMs) were exposed to a smoke environment as well as high temperature tests since it was determined that they are very sensitive to heat.

A block diagram of the experimental digital safety channel (EDSC) is shown in Figure 2. A description of the various subsystems follows:

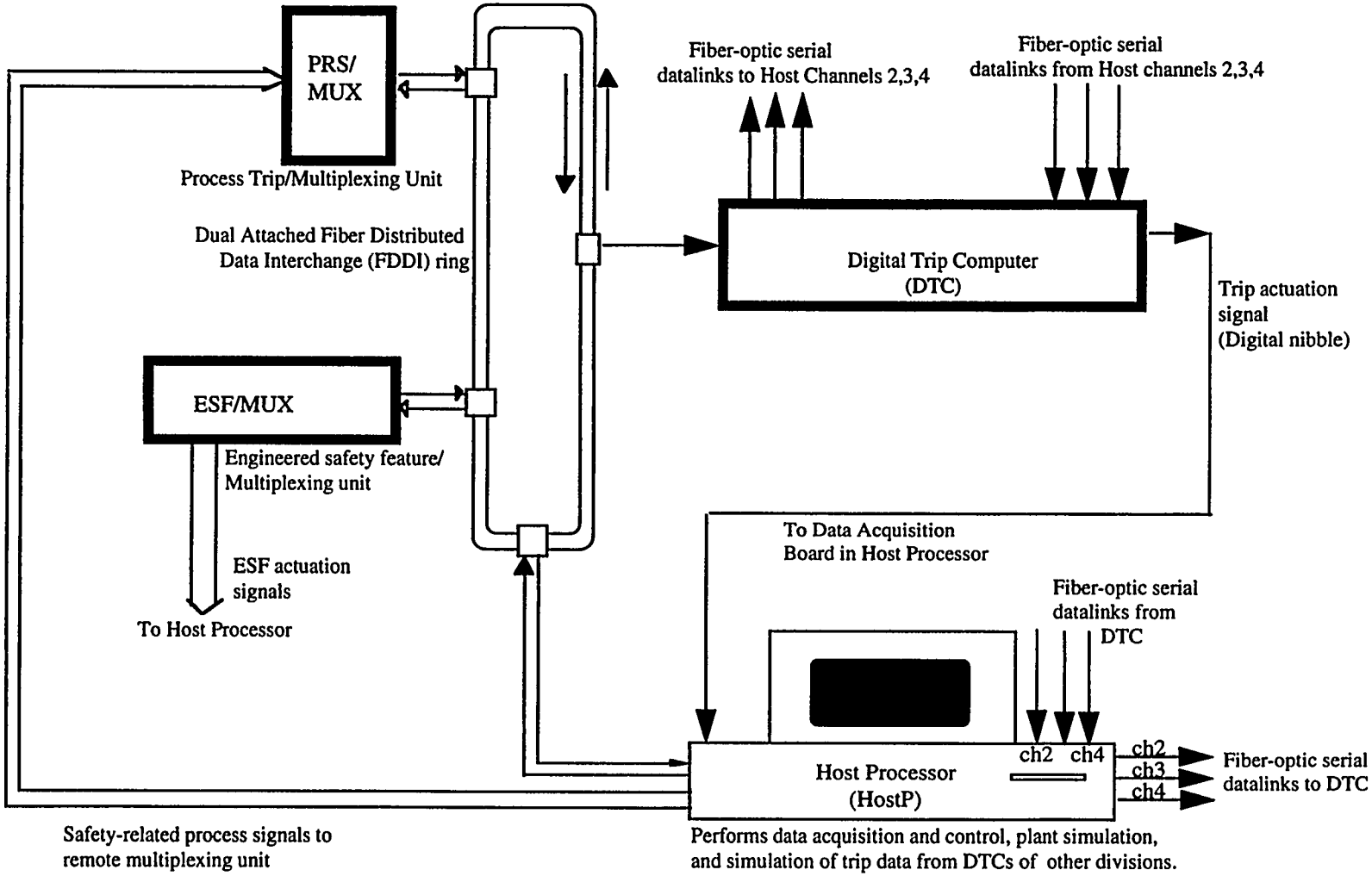

Figure 2. Block diagram of the experimental digital safety channel.

Process Multiplexing Unit (PRS/MUX)

The function of the PRS/MUX is to acquire analog data from the host processor (HOSTP), digitize these data, and format them into frames suitable for transmission over an FDDI network. In an actual plant, these process signals would come from field instrumentation such as transmitters. In this implementation, however, the signals are generated by a 16-channel digital-to-analog (D/A) plug-in card inside the HOSTP.

Digital Trip Computer (DTC)

The DTC polls the network to acquire the digital values of the process signals from the PRS/MUX. It then compares individual process values with trip setpoint values and sends a trip/no trip indication for each variable over three independent fiber optic serial datalinks to the host processor. (Note that in an actual protection system, these fiber optic datalinks would go to three other digital trip computers belonging to the three other divisions, the functions of which are being simulated by the host processor in the EDSC.) At the same time, the host processor sends trip/no trip information for each variable to the DTC via three independent serial datalinks. The DTC performs 2 out of 4 voting (local coincidence) on each set of process trip/no trip information received (note that for each process parameter, there are four trip/no trip data to vote on—one calculated from the process data received via the fiber distributed data interchange (FDDI) network, and three received from the host via the serial datalinks).

The Host Processor (HOSTP)

The host processor performs the following functions:

1. Simulates process signals typical of either normal or accident conditions. These signals are hardwired to the PRS/MUX.
2. Sends a command via the network to the PRS/MUX requesting it to begin acquiring process data.
3. Acquires the analog process data sent over the network by the PRS/MUX. (Note that the data from the PRS/MUX are also acquired by the DTC.) In this way the HOSTP verifies that the process voltage values it sent to the PRS/MUX have not been corrupted.
4. Simulates the trip functions of three other divisions by generating process trip/no trip data for each of ten process signals and sends them via fiber serial links to the DTC.
5. Performs 2 out of 4 voting based on the internally generated trip/no trip information and the trip/no trip information sent from the DTC via the serial datalinks.
6. Provides specified pump, valve, and other ESF actuation signals to the ESF/MUX via the FDDI network.
7. Monitors the ESF/MUX outputs via a plug-in analog-to-digital (A/D) card inside the host.
8. Performs error logging functions.

The Engineered Safety Feature Multiplexing Unit (ESF/MUX)

The ESF/MUX demultiplexes the digital information sent by the host via the FDDI network into the appropriate analog signals.

Circuit Bridging

There will be 28 circuit bridging tests to determine the amount of insulation resistance between contacts on different chip packages and on the surface of a printed circuit board when they are exposed to smoke and soot. As of the writing of this paper, three tests have been completed. The chip packages include both hermetically sealed ceramic packages and plastic packages and both

surface mount and through-hole mount styles. The printed circuit board tests consist of a set of four interdigitated comb patterns on one board with different dc voltages across each comb (see Figure 3). This printed circuit board pattern is similar to the standard pattern that the DuPont/UL/AT&T team will use for developing a new corrosivity standard.

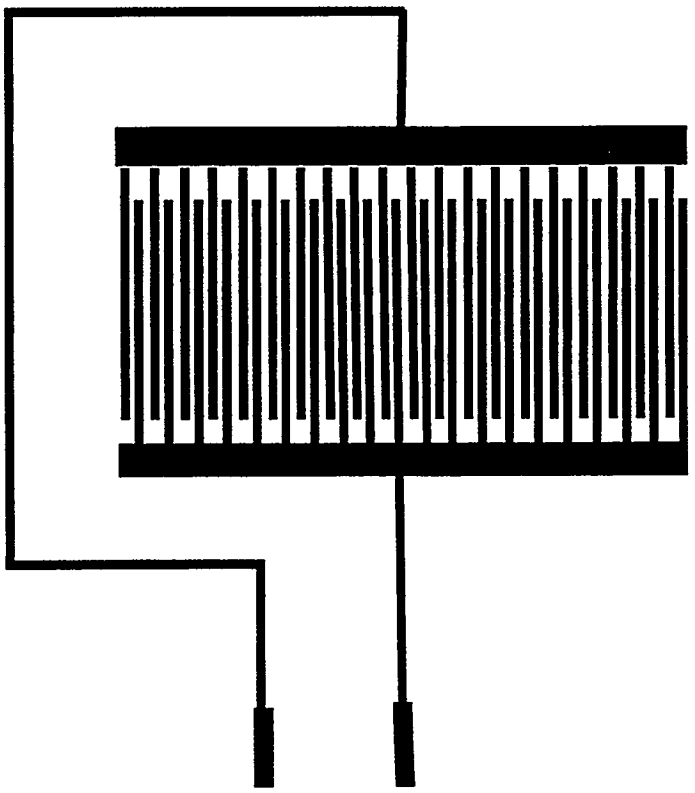

Figure 3. Comb Pattern for Measuring Insulation Resistance of Printed Circuit Boards

Other devices such as plastic-packaged optical isolators and memory chips are also being exposed to smoke and tested for functionality. The optical isolators are being tested during exposure to smoke while the memory chips are being tested before and after the exposure. The memory chips are powered up during the smoke exposure and are housed in one of two different packages, a plastic package and a hermetically sealed ceramic package.

Description of tests

The composition of smoke can vary, depending upon characteristics of a fire such as burn temperature, oxygen availability, material burned, and whether the fire is smoldering or openly flaming. In order to produce smoke in a standard and reproducible way for these preliminary tests, the ASTM draft corrosivity test standard produced by the Subtask E5.21.70 group was followed. This draft standard was based on a standard toxicity test that has been in use for many years. The primary measurement of this draft standard is the loss of metal from a corrosion probe as a function of the material burned. Although the objective of this ASTM test (relative corrosivity) is different from SNL's objective of testing the reliability of electronic equipment in a smoke environment, the methods of smoke production and the time of exposure to the smoke were adopted as the basis for producing a "standard" smoke environment and exposure scenario.

The procedure for exposing electronic equipment to smoke is as follows: The exposure chamber is a sealed Lexan box that contains the electronic equipment and into which all of the smoke is collected. The combustion cells, which are located underneath the exposure chamber, contain the fuel and are connected to the exposure chamber by a stainless steel chimney. Up to four such cells may be used depending on the total fuel load. Tungsten-quartz lamps located outside the combustion chamber provide radiant heat through the cell to the fuel inside. To aid in igniting the hot fuel, an electric sparker or a butane pilot flame is positioned above the fuel. The lamps are powered for 15 minutes each. For multiple cell burns, the lamps are powered sequentially. The equipment is exposed to the smoke for 1 hour after the smoke is first introduced. In the case of the multiplexer module, humidity was added to the exposure chamber after the 1-hour period from a portable steamer and in the case of the experimental digital system, by water heated with the radiant lamps. In the case of the circuit bridging components, humidity is added to the chamber by venting out the smoke and exposing the equipment to the environmentally controlled chamber that contains the testing equipment.

SNL has built two smoke exposure units, one following the dimensions of the ASTM draft standard (0.2 m^3 in volume), and a larger 1-m^3 unit required to test the experimental digital system built by ORNL. This is a static experiment in the sense that that all of the smoke produced is enclosed within the exposure chamber until the end of the exposure period. The 0.2-m^3 volume includes one combustion cell, while the 1-m^3 unit had four cells. The multiple combustion cells allow us to add smoke when desired and provided enough smoke to simulate a high fuel-load fire. The smoke production and exposure equipment is illustrated in Figure 4. The radiant heat lamps are adjusted so that a fixed heat flux level of either 50 kW/m^2 or 25 kW/m^2 is produced at the fuel surface to simulate full flaming and smoldering fires respectively. The heat flux is measured with a Schmidt-Boelter (thermopile) heat flux meter before each test to determine the amount of heat that would be incident on the fuel at the beginning of the test. Small variations in the positions of the lamps can affect the heat flux that is incident on the sample. As smoke is produced, the quartz chamber becomes coated with some soot and so the heat flux is reduced. No attempts were made to compensate for this effect..

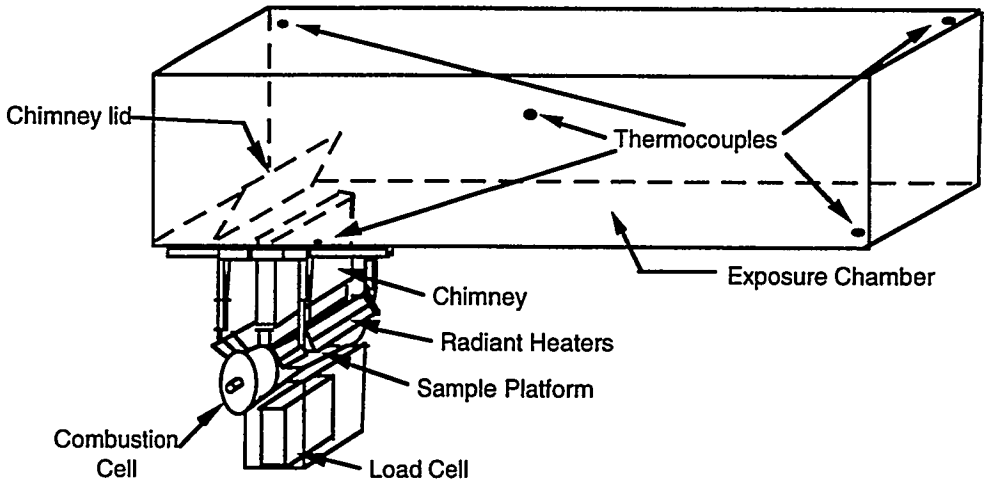

Figure 4. Small Smoke Exposure Chamber

Measurements of the condition of the smoke environment were also recorded. These included temperature, humidity before and after the exposure, smoke optical density, soot deposition on horizontal and vertical planes, chemical composition of gas, and soot. For the tests of the multiplexer modules, the copper lost from a standard corrosion probe was also measured. This measurement has been discontinued because of the cost and a lack of consistency.

Nowlen[4] reported on the types of fires that take place at nuclear power plants and their typical fuel load, where the fuel load is defined as the ratio of the weight of fuel consumed to volume of air. The highest fuel load occurs in small confined cabinet fires because of the limited volume of air in the cabinet. Of course, if the fire is very large, it will burn up all of the equipment in the cabinet, but for a small-to-moderate fire, the equipment may survive the heat and flames but not the smoke. For these preliminary smoke exposures, the fuel load was selected to simulate this high fuel load condition of 75 g/m^3. Fuel loads of 2.8 g/m^3, 20 g/m^3, and 160 g/m^3 were burned for the digital system tests. The lowest level of smoke represents the smoke density present in a location in the control room far away from a large cabinet fire located in the control room. The middle level represents the amount of smoke in the general areas around the plant (not the control room) given a fire in another cabinet nearby, and the highest level represents the amount of smoke present during a small fire if the equipment were located in the same cabinet as the fire. In the circuit bridging tests, some of the exposures correspond to low fuel loads, while others will correspond to high fuel loads.

Since the most abundant fuel in a nuclear power plant is cable insulation and jacketing material, cables were used to produce the smoke. The amount of cable material burned was determined by stripping the insulation material from a sample cable piece and weighing the fraction of the total cable weight that is made up of insulation. Typically, the insulation and jacketing materials comprised 50 to 75% of the total mass of the cable. Approximately 75 g/m^3 of fuel load was burned for each multiplexer test.

We expected that the type of fuel would determine how destructive the smoke would be. In a power plant there are several different types of cables used for instrumentation, power, and control. In addition, there are cables with insulation types that are no longer used, such as polyethylene and polyvinyl chloride (PVC), but which remain in place at the plants. For the multiplexer module tests, three types of cables were burned, one type in each test. Multiplexer test 1 used Brand Rex cable made with cross-linked polyethylene (XLPE) insulation with a chlorosulfonated polyethylene (CSPE) jacket. This cable is the third most frequently used cable in nuclear power containment.[5] Multiplexer test 2 used Anaconda Flameguard cable made with ethylene propylene rubber (EPR) insulation and a CSPE jacket. This is the most common combination of materials used for insulation in containments. Multiplexer test 3 used a Belden, non-nuclear qualified PVC jacketed and insulated cable. Although PVC cables are no longer widely used in nuclear power applications, they are still found in power plants and represent one of the most corrosive of cable insulation materials.

For the multiplexer tests, an electric sparker was run continuously to provide an ignition source for hot gases produced by the radiant heat lamps during the entire 15-minute period (consistent with the ASTM draft standard.) After 15 minutes the lamps were shut off, the chimney damper was closed, and a small fan mixed the smoke vapors. Since this was a static smoke exposure, the smoke was contained within the exposure chamber for the first hour of the test. The smoke chamber was sealed as well as possible to prevent smoke leaks. To allow for the expansion of air and smoke vapors caused by the initial heating and subsequent cooling of the contained air volume, an empty plastic bag was placed over one of the ports. One hour from the beginning of the test the smoke was vented.

In test 1, no humidity was added for the first 24 hours so that the equipment was exposed to a relative humidity (RH) below 20%. Since the draft standard recommends holding the RH at 75%, we attempted to do this after the preliminary 24 hours by setting a beaker of hot water in the exposure chamber. The test unit was left in the humid environment for 3 days. In test 2 we added humidity right after venting the smoke, using a portable hot steam humidifier. The humidity was adjusted by opening doors and running fans, but there was no control over the humidity overnight. In test 3 we added humidity right after venting the smoke. This humidity was added with a portable hot steam humidifier, but in a more controlled way than for tests 1 or 2.

For the experimental digital safety system, we burned a mixture of cables that would be found in power plants, as reported by Bustard and Holzman.[5] The amount of fuel was determined by the conditions we were trying to represent—control room for DTC and other more general areas for the PRS/MUX. Humidity was added by heating water with the radiant heat lamps. Carbon dioxide from

a fire extinguisher was added to the tests of the DTC to represent one of the fire suppressants available in the control room. Table 1 shows the smoke conditions in which the experimental digital safety system was exposed. There were 3 levels of smoke for these tests; 3 g/m^3, 20 g/m^3 and greater than 65 g/m^3. In smoke exposure 3 on the FOMs, each of the three levels of smoke were tested, but the equipment was not cleaned between tests. Instead, after a 1 hour test period for a particular smoke level, an additional amount of smoke was added to bring the smoke to the new level. Six FOMs were exposed at a time. For the first two smoke levels, three of the FOMs were exposed without their plastic casings. Since these failed after the 20 g/m^3 smoke level, three additional FOMs were placed outside of the smoke exposure chamber and added to the circuit so that the testing program could continue.

Table 1. Smoke Conditions for Experimental Digital Safety System

Test Name	Experiment Unit	Fuel burned (g/m^3)	Notes
1	PRS/MUX	3.3	No added humidity, electric sparkers
2	PRS/MUX	2.8	Added humidity, electric sparkers
3	DTC, no FOMs	2.63	No added humidity, electric sparkers
4a	DTC, no FOMs	None	2.64 lb. CO_2 added.
4b	DTC, no FOMs	2.8	With sparkers–channel trip errors, restarted without sparkers, added 2.48 lb. CO_2
5	DTC, no FOMs	20.39	No added humidity, butane lighter
6	PRS/MUX	19.97	Added humidity, butane lighter
7	PRS/MUX	160.13	No added humidity
8a	FOMs	None	Temperature scan only
8	FOMs, some of these without case	2.43	No added humidity for next three tests
8	FOMs	15.45	Smoke added to previous amount
8	FOMs, replaced open FOM's that failed.	46.42	Smoke added to previous amounts

The general procedure adopted for all the exposures was as follows:

1. The equipment under test (EUT) was placed in the exposure chamber and "baseline" data was obtained over a period of at least 3 h. This baseline test was performed on unexposed or cleaned equipment to assure the functionality of the equipment prior to the smoke exposure. (Note: The 1 m^3 exposure chamber is located inside of an environmental chamber). The environmental chamber was maintained at 75°F and 30% relative humidity (RH).
2. A predetermined mixture of different types of cables was burned to produce a desired smoke density in the exposure chamber. Most of these cables burned within 5 minutes.
3. In the case where the test called for smoke and humidity, a predetermined amount of water was heated inside the exposure chamber to provide the appropriate humidity.
4. The EUT was exposed to smoke for a total of 1 h. The smoke was then vented from the exposure chamber.
5. The EUT was left in the exposure chamber and monitoring continued for approximately 20 h. Chamber temperature was maintained at approximately 75°F and 30% RH.

6. The EUT was examined for damages/malfunctions and thoroughly cleaned. In general the cleanup involved removing the boards and blowing them with compressed air. The boards were then sprayed with Tech Spray no. 1677-125 Universal Cleaner Degreaser or Chemtronics Electronics Cleaner/Degreaser 2000.

The system tests were performed using spark ignition for the first three tests. During test 3, errors in the operation of the DTC started soon after the smoke was being produced. During the fourth exposure the same errors were found to be caused by the spark igniter. The DTC seemed to be more susceptible to errors caused by operating the sparker than the PRS/MUX. For tests on the DTC after test 4 a butane pilot lighter was used instead.

Results of tests

Preliminary Scoping Tests Using Multiplexer Board

Before each smoke exposure, the test units were assembled and tested to verify functionality. The test program was then run continuously throughout the smoke exposure and postexposure periods. The results of the multiplexer board exposures are listed in Table 2. The XLPE/CSPE cable (Brand Rex) and PVC cable (Belden) both ignited, while the EPR/CSPE cable (Anaconda Flameguard) only smoldered.

Table 2. General Results of Smoke Exposure

Test	Cable	Equipment performance
1	XLPE/CSPE	No change
2	EPR/CSPE	No change
3	PVC/PVC	Intermittent failures

The smoke affected the equipment by stopping the host computer program rather than changing the reading for the current values as we had expected. The program stopped twice during Test 3. The first stoppage occurred at 0:08 (8 minutes) after the start of the test, while the radiant heat lamps were still on. The computer showed a timeout error, indicating that it was not receiving data from the input-output module. The program was restarted and the data were normal. The next malfunction occurred at about 1:00 (1 hour) when the chamber was beginning to be vented. The program did not stop; however, the numbers in the data file were unusual and the printout on the screen was shifted. At 1:20, steam was added to the environment so that the relative humidity of the chamber was 75% RH. The program stopped again at 1:29 and showed the same timeout error as before.

The smoke-exposed equipment from tests 1 and 2 both operated normally throughout and after the smoke exposures. Although the equipment showed some visible soiling, this did not affect its performance. Steel parts that were exposed to test 3 were especially corroded after exposure.

To further explore failures that occurred during test 3, the equipment was periodically tested for 1 month after the exposure to smoke. The equipment continued to operate normally until humidity was added in the form of mist from a cool water mister. The mist condensed on the backplane and caused it to short. When the backplane began to short, the interrogation program stopped again and produced the same timeout error message as at 0:08 and 1:29 into the smoke exposure. This time, however, the equipment was permanently damaged and would not restart.

Preliminary Results From System Tests

The smoke exposures to the experimental digital safety system caused a variety of system errors. The explanation of the types of system errors that occurred for each test is shown in Table 3. It is important to note that after the various units were exposed to smoke, the baseline tests were no longer error free. Communication errors were observed at all levels of smoke, ranging from network retransmissions at low smoke densities to serial link timeout errors at higher smoke densities. Although errors were observed, no functional failures occurred during the tests related to general area fires. Therefore there is evidence that digital equipment exposed to a small control room fire is likely to perform properly during a reasonably short period of exposure provided that the equipment is not located in the same cabinet as the fire source.

Table 3. Failure Types from Smoke Exposures.

	B1	S1	B2	S2	B3	S3	B4	S4A	S4B	B5	S5	B6	S6	B7	S7	S8
Timeout from F.O. serial link to Host chn 2									☢							☢
Timeout from F.O. serial link to Host chn 3									☢							☢
Timeout from F.O. serial link to Host chn 4									☢							☢
DTC had to retransmit data to Host		☢	☢	☢			☢	☢			☢	☢	☢	☢	☢	
	(18h)	(1h) PRS/ MUX	(18h)	(1h) PRS/ MUX	(18h)	(1h) DTC w/o FOMs	(18h)	(2h) CO2 only	(1h) DTC w/o FOMs w/CO_2	(18h)	(1h) DTC w/o FOMs	(18h)	(1h) TRP/ MUX w/HI RH	(18h)	(1h) TRP/ MUX	(4h) FOMs only

B = Baseline test.
S = Actual smoke test (i.e., EUT was subjected to smoke during this time).
For the actual smoke tests (S1 through S8), the number in parentheses indicate the smoke exposure time, after which the test chamber was vented.
The failure modes indicated occurred within this window. For the baseline tests the numbers in parentheses indicate the test duration (the EUT was not subjected to smoke during this time).

It is important to note that an actual power plant safety system can, and typically is designed so that communication failures will not prevent the safety channel from performing its function. For example, the channel can easily be designed so that failure to receive data in a specified time will cause that channel to trip.

The computers under test exhibited no failures resulting from smoke particle deposition although soot was spread throughout each chassis by the computer's fan. It is believed that the conformal coating applied during fabrication of the main microprocessor boards served as an extra layer of protection against circuit bridging by conductive particles. This result suggests that packaging and integrated circuit fabrication techniques may provide some of the most important elements of a digital system's capability to withstand smoke exposure.

Preliminary Results of Circuit Bridging Tests

The circuit bridging tests have begun at Sandia National Laboratories to determine how the insulation resistance of chip packages and printed circuit boards is affected by smoke. The devices being tested include through-hole devices such as a DIPs (dual-in-line packages) and transistor outline cans. Surface-mounted chips such as SOICs (small-outline integrated circuits), flat packs, and leaded and leadless chip carriers are also included. Interdigitated combs to measure the surface insulation resistance are being tested at dc voltages ranging from 5 V to 160 V. Figure 5 shows an example of the results for a 160-V-biased comb from the very first test. The comb was exposed to 2.8 g/m^3 of

smoke from a mixture of cables burnt at a high radiant temperature in flaming mode. This fuel load corresponded to the exposure that a piece of equipment would be expected to experience if it were located across the room from a small fire. The combs were exposed to smoke for 1 hour and then to a 75 °F and 75% RH environment for 23 hours.

The relative resistance of four combs is plotted in Figure 5. These resistances are normalized to the value of resistance of each comb at the start of the smoke exposure. The uncoated comb was exposed directly to the smoke; the coated comb was sprayed with an acrylic conformal coating and then exposed to the smoke after drying overnight. The third uncoated comb was placed in a computer chassis whose fan was running, and the fourth uncoated comb was placed outside the smoke exposure chamber but inside an environment chamber which was controlled at 75 °F and 75% RH. The smoke exposure began after the first set of resistance values was measured. The insulation resistance of the uncoated board decreased a few minutes after the exposure began. Post-test examination of the uncoated board revealed a blackened spot on the comb, which is a likely area of low resistance. The conformal coating seems to be an effective way to prevent smoke from changing the insulation resistance of the printed circuit board. The comb in the chassis was affected by the smoke for a short time during the smoke production, but it seemed to recover later. This behavior may be related to the short-term failures observed in the tests of the multiplexer modules and experimental digital system.

Conclusions

Smoke can affect the operation of digital equipment. It particularly impedes communication transfer from one instrument to another, as shown in the experimental digital safety system. These problems in communication transfer, however, were mostly temporary and with adequate software could be compensated by repeated attempts in transferring the data. The temporary nature of these problems was similar to that encountered with the multiplexer tests. In both cases, this indicates that smoke may be causing intermittent shorts between circuits. These shorts may be temporary because the material that caused the short may be burnt away by the current that passes through it.

Humidity may also be an important factor in creating temporary shorts. Water is one of the combustion by-products of most fires. Water from sprinklers and misters is also used to combat fires. As shown in the PVC multiplexer module test, the addition of humidity was a factor contributing to communication errors.

Another fire suppressant, CO_2, was applied to the experimental digital safety system. This test was conducted while all digital parts were encased in a chassis, so the equipment was somewhat protected from the drastic change in temperature that discharging this gas causes. The addition of CO_2 had very little effect on the equipment.

Exposure of the experimental digital safety system to smoke was important to show that smoke can indeed affect the operation of a trip channel; however, because the equipment was repeatedly exposed to smoke after cleaning, it is not known how much smoke would cause faulty operation if the equipment had not been previously exposed. Other unknowns that could affect equipment may become apparent as the tests progress.

The results from the circuit bridging tests are promising. The insulation resistance seems to confirm the behavior of the full digital systems by decreasing when smoke is applied and in some cases returning to the starting value after the smoke deposition stops. The advantage to these tests is that the effects on the components are simple to diagnose, each part that is tested has not been previously exposed, and many factors, such as smoke conditions and protection of the boards, may be varied.

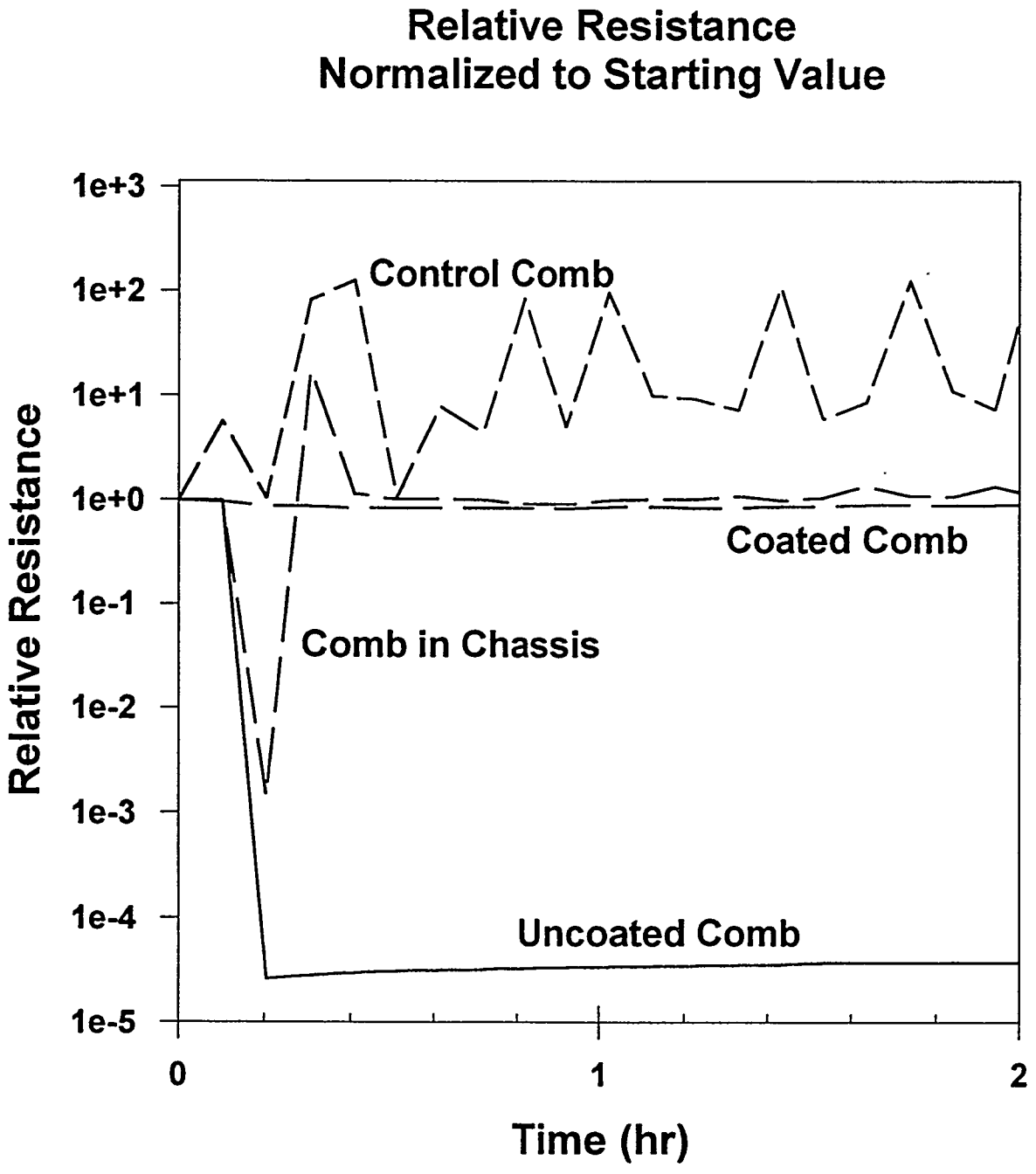

Figure 5. Circuit Bridging Test on 160 V Comb pattern.

Summary

The program to assess the impact of smoke on digital equipment has discovered that the important failure mechanisms are not only long-term effects such as corrosion, but also short-term and perhaps intermittent effects of circuit bridging. Work in this program is continuing in an effort to determine what methods of protecting equipment are effective and what smoke conditions are most damaging. These results may improve the safety of our nuclear plants as they modernize and replace their analog with digital equipment.

References

1 Miller, M. H., "Engineering Development of a Digital Replacement Reactor Protection System at an Operating US PWR Nuclear Power Plant," NUREG/CP-0140, Vol. 1, pp. 87-97.

2 Joint Report of Office of the State Fire Marshall and Illinois Commerce Commission Staff, "Hinsdale Central Office Fire," March 1989.

3 One of the authors attended meeting of Dupont/AT&T/UL at Bell Laboratories, Murray Hill on April 27, 1995.

4 Nowlen, S. P., Letter report on "Defining Credible Smoke Scenarios," dated September 30, 1994.

5 Bustard, L., and Holzman, P. "Low-Voltage Environmentally Qualified Cable License Renewal Industry Report; Revision 1," TR-103841, published by Electric Power Research Institute, July 1994.

DEVELOPMENT OF ELECTROMAGNETIC OPERATING ENVELOPES FOR NUCLEAR POWER PLANTS*

Paul D. Ewing and Stephen W. Kercel
Oak Ridge National Laboratory
P.O. Box 2008, Oak Ridge, Tennessee 37831-6006

ABSTRACT

This paper discusses the development of recommendations by Oak Ridge National Laboratory (ORNL) staff for electromagnetic operating envelopes to augment the electromagnetic interference/radio-frequency interference (EMI/RFI) and power surge test criteria and test methods recommended in NUREG/CR-5941, *Technical Basis for Evaluating Electromagnetic and Radio-Frequency Interference in Safety-Related I&C Systems*. Little is currently known about the prevailing ambient EMI/RFI and power surge environment in nuclear power plants. This lack of information makes it difficult to establish electromagnetic operating envelopes for safety-related instrumentation and control (I&C) systems with a high degree of confidence in their adequacy. Thus, ORNL staff are presently performing long-term EMI/RFI measurements at selected plant sites. Observations at the plant sites began in August 1994 and will conclude in November 1995. The EMI/RFI measurement data will be provided to NRC and should prove useful in developing electromagnetic operating envelopes suitable for the nuclear power plant environment. It is of interest to note that the data collected thus far is consistent with operating envelopes recommended by the Electric Power Research Institute for digital upgrades of I&C systems in nuclear power plants. In the meanwhile, interim electromagnetic operating envelopes are being recommended by ORNL staff to augment the recommended test criteria and test methods. The recommended interim operating envelopes are being based on operating envelopes for similar environments and are being documented in NUREG/CR-6304, *Recommended Interim Operating Envelopes for Safety-Related I&C Systems in Nuclear Power Plants* (draft).

1 INTRODUCTION

Instrumentation and control (I&C) systems in advanced nuclear power plants are expected to make use of both analog and digital equipment and will be significantly different from the totally analog-based I&C systems currently in use. Limited operational experience with digital technology and advanced analog electronics within the U.S. nuclear industry has caused concern about possible upsets and malfunctions in safety-related I&C systems due to electromagnetic interference/radio-frequency interference (EMI/RFI) and power surges. Hence, Oak Ridge National Laboratory (ORNL) staff have been tasked by the U.S. Nuclear Regulatory Commission (NRC) Office of Nuclear Regulatory Research to develop the technical basis for regulatory guidance on EMI/RFI and power surge withstand capability (SWC) issues.

*Research sponsored by the Office of Nuclear Regulatory Research, U.S. Nuclear Regulatory Commission, under Interagency Agreement 1886-8946-5A and performed at the Oak Ridge National Laboratory, managed by Lockheed Martin Energy Research Corp. for the U.S. Department of Energy under contract DE-AC05-96OR22464.

Recommendations on EMI/RFI and SWC test criteria, test methods, and installation practices have been reported in NUREG/CR-5941, *Technical Basis for Evaluating Electromagnetic and Radio-Frequency Interference in Safety-Related I&C.*[1] However, little is currently known about the prevailing ambient electromagnetic environment in nuclear power plants and this lack of information makes it difficult to develop recommendations for electromagnetic operating envelopes — that is, the level of interference that safety-related I&C systems should be able to withstand without upset or malfunction — with a high degree of confidence in their adequacy. ORNL staff are presently performing long-term EMI/RFI measurements at selected plant sites. The EMI/RFI measurement data will be provided to NRC and should prove useful in developing electromagnetic operating envelopes suitable for the nuclear power plant environment. In the meanwhile, interim electromagnetic operating envelopes are being developed by ORNL staff for recommendation to NRC to augment the test criteria and test methods proposed in NUREG/CR-5941. The recommended interim operating envelopes are being based on operating envelopes for similar environments and are being documented in detail in NUREG/CR-6304, *Recommended Interim Operating Envelopes for Safety-Related I&C Systems in Nuclear Power Plants* (draft).[2] The methodology for developing the recommended interim electromagnetic operating envelopes and a preliminary look at the EMI/RFI data collected at plant sites are discussed in this paper.

2 EMI/RFI AND SWC TEST CRITERIA

The EMI/RFI test criteria listed in Table 1 were extricated from Military Standard (MIL-STD)-461C, *Electromagnetic Emission and Susceptibility Requirements for the Control of Electromagnetic Interference,*[3] and recommended in NUREG/CR-5941 to evaluate the effects of EMI/RFI in safety-related I&C systems. Table 2 lists the corresponding counterparts to the recommended MIL-STD-461C test criteria found in the latest revision of the standard, MIL-STD-461D.[4] The test criteria are specified by alphanumeric codes: the first designation declares the criterion to be either radiated (R) or conducted (C), and the second designation specifies whether it covers emissions (E) or susceptibility (S). This alphabetic designation is followed by a numbering system that is specific to the particular test criterion. Note that the MIL-STD-461D test criteria are designated by the 100 series numerical nomenclature.

The rationale for the recommendation of these criteria is that NRC can take advantage of the military services' considerable experience in evaluating EMI/RFI effects. Also, close study of the test criteria indicates that the full range of electromagnetic compatibility issues is addressed in that the criteria cover the gamut of associated problems — conducted and radiated interference, transients, exposure to electric and magnetic fields, and noise coupling through equipment power and control leads. Corresponding test methods in MIL-STD-462, *Measurement of Electromagnetic Interference Characteristics,*[5] are used to demonstrate compliance with the MIL-STD-461C test criteria. The MIL-STD-462 test methods are well developed in that they have been reviewed and updated on a periodic basis since their inception in 1967.[6] The latest revision of the test methods can be found in MIL-STD-462D[7] and demonstrates compliance with the corresponding MIL-STD-461D test criteria. With the specification of the test criteria in Tables 1 and 2 (and their associated test methods), a definitive conclusion should be reached on whether equipment and subsystems can be expected to function properly in the presence of EMI/RFI.

Table 1 Recommended MIL-STD-461C test criteria

Criterion	Description
CE03	Conducted emissions, power leads, 15 kHz to 50 MHz
CS01	Conducted susceptibility, power leads, 30 Hz to 50 kHz
CS02	Conducted susceptibility, power and interconnecting control leads, 50 kHz to 400 MHz
CS06	Conducted susceptibility, spikes, power leads
RE02	Radiated emissions, electric field, 14 kHz to 10 GHz
RS01	Radiated susceptibility, magnetic field, 30 Hz to 50 kHz
RS02	Radiated susceptibility, magnetic and electric fields, spikes and power frequencies
RS03	Radiated susceptibility, electric field, 14 kHz to 10 GHz

C = conducted, E = emissions, R = radiated, and S = susceptibility.

Table 2 MIL-STD-461D counterparts to applicable MIL-STD-461C test criteria

Criterion	Description
CE102	Conducted emissions, power leads, 10 kHz to 10 MHz
CS101	Conducted susceptibility, power leads, 30 Hz to 50 kHz
CS114	Conducted susceptibility, bulk cable injection, 10 kHz to 400 MHz
CS115	Conducted susceptibility, bulk cable injection, impulse excitation
CS116	Conducted susceptibility, damped sinusoidal transients, cables and power leads, 10 kHz to 100 MHz
RE102	Radiated emissions, electric field, 10 kHz to 10 GHz
RS101	Radiated susceptibility, magnetic field, 30 Hz to 100 kHz
RS103	Radiated susceptibility, electric field, 10 kHz to 10 GHz

C = conducted, E = emissions, R = radiated, and S = susceptibility.

The SWC practices described in IEEE Std C62.41-1991, *Recommended Practice on Surge Voltages in Low-Voltage AC Power Circuits*,[8] are recommended in NUREG/CR-5941 to control upsets in safety-related I&C equipment caused by ac power surges. It is acknowledged that although the waveforms described in IEEE Std C62.41-1991 cannot possibly represent complex real-world surge environments, they

nonetheless define a manageable set of surge waveforms selected to simulate real world conditions. Tests employing these waveforms should provide meaningful and reproducible results that, in turn, should provide a reasonable degree of assurance that problems associated with power surges are averted.

Test procedures for the IEEE Std C62.41-1991 practices are described in IEEE Std C62.45-1987, *Guide on Surge Testing for Equipment Connected to Low-Voltage AC Power Circuits*.[9] Hence, IEEE Std C62.45-1987 should be used as a companion document to IEEE Std C62.41-1991. The test procedures are recognized throughout the power industry and have been endorsed by a number of equipment manufacturers and utilities.

3 APPROACH TO PERMANENT OPERATING ENVELOPES

The EMI/RFI operating envelopes in MIL-STD-461C and -461D are specified according to the particular application and the expected environment in which the equipment must operate. The military EMI/RFI operating environment may vary from low interference levels at ground-based locations to extremely high levels on the decks of aircraft carriers. In past surveys of nuclear power plant environments,[10] the radiated emissions from most equipment were found to be *moderate or less*. Nevertheless, equipment was identified that could not be expected to operate reliably in its intended environment. From the results of these surveys, it is reasonable to assume that a nuclear power plant could possibly be categorized as an industrial environment, with its electromagnetic ambient being less harsh than that of a typical military environment.

In nuclear power plant areas where safety-related I&C systems are to be installed, long-term radiated and conducted emission levels are being measured, and electromagnetic operating envelopes will be recommended accordingly. Stringent operating envelopes require specialized test equipment and thereby drive up testing costs. Hence, a choice of envelopes less stringent than those specified in MIL-STD-461C and -461D can aid in the avoidance of unnecessary testing. Recommendations for permanent EMI/RFI operating envelopes for the nuclear power plant environment will be based on I&C system emissions and susceptibility levels developed from the long-term radiated and conducted plant emission profiles for various sites. Such profiles should provide an assessment of the probable ambient electromagnetic environment; a safety margin can then be added to ensure the operability of the equipment under conditions more adverse than ambient. This type of approach should prove useful in establishing suitable EMI/RFI operating envelopes.

The establishment of SWC operating envelopes should take a different approach. Given the dynamic nature of power systems, power surge measurements are very much site dependent, and prediction of the future environment may require several years of monitoring.[11] Also, the surge environment is so complex that no set of test waveforms will completely represent the real world. Hence, it may be prudent to use the representative surge waveforms in IEEE Std C62.41-1991 as a baseline environment. As discussed in NUREG/CR-5941, the typical environmental conditions in a nuclear power plant could be represented by the two standard waveforms — that is, the ring wave and combination wave — and the electrically fast transients (EFT) waveform. Descriptions of the waveforms are given in Table 3. Location categories and exposure levels are outlined in IEEE Std C62.41-1991 and define applicable amplitudes for the surge waveforms that should provide an appropriate degree of SWC.

Table 3 Representative power surge waveforms

Parameter	Ring Wave	Combination Wave		EFT
Waveform	Open-circuit voltage	Open-circuit voltage	Short-circuit current	Pulses in 15-ms bursts
Rise time	0.5 μs	1.2 μs	8 μs	5 ns
Duration	500 kHz ringing	50 μs	20 μs	50 ns

4 RATIONALE FOR INTERIM OPERATING ENVELOPES

For the present, in lieu of developing EMI/RFI operating envelopes based on actual long-term emission profiles, interim envelopes are being recommended to correspond with those typically used to evaluate equipment in military environments thought to be similar to those of nuclear power plants. Of the environments described for the classes of military equipment and subsystems listed in MIL-STD-461C and -461D, the *military ground facilities* environment seems to most closely resemble the environment of a nuclear power plant. The military envelopes are being employed as the foundation for recommended interim electromagnetic operating envelopes and adjustments are being made to these envelopes based on the short-term EMI/RFI test data collected in nuclear power plants during a 1994 study conducted by the Electric Power Research Institute (EPRI). Results of the EPRI study are reported in TR-102323, *Guidelines for Electromagnetic Interference Testing in Power Plants*.[12]

In lieu of developing SWC operating envelopes based on knowledge of the surge environment, recommended interim envelopes are being developed based on assumptions made about the nuclear power plant environment. First, the location of safety-related I&C systems could likely be classified as *Category B* since this line impedance designation covers feeders and short branch circuits (<10 m) inside an industrial plant.[13] The increasing line impedance between the service entrance and equipment remotely located within a building will limit the rate of surge current change (di/dt) that can occur because rapid current changes require a large driving voltage that will in turn result in a disruptive discharge. Consequently, these discharges cut off high amplitude surges and prevent them from traveling to distant locations. Second, a *Low to Medium Exposure* level to induced surges could be assumed since it covers an industrial environment in geographical areas known for low to medium lightning activity, or with significant switching transients.

5 EMI/RFI MEASUREMENT DATA

ORNL staff are presently performing long-term EMI/RFI measurements at selected plant sites. Observations at the plant sites began in August 1994 and will conclude in November 1995. The measurements differ from previous EMI surveys in several ways.[14] First, the measurements are long term, featuring at least a week of continuous round-the-clock data collection at each observation point and at least a month of observations at each plant site. Second, the measurements are automated and unobtrusive and the actual ambient electromagnetic environment is observed during typical plant operations. Third, the measurements feature simultaneous time and frequency localization, allowing the capture of peak effects without sacrificing frequency information.

Figures 1 through 3 show some of the preliminary EMI/RFI measurement data for both radiated and conducted fields. In reviewing the data, some of the following conclusions can be drawn:

1) Although the ORNL survey is looking at the ambient electromagnetic environment from a different perspective than the EPRI survey of 1994, the ORNL observations thus far do not contradict the EPRI findings;

2) Routine operations at all of the survey sites resulted in significant EMI/RFI events, but these occurred with an extremely low rate of occurrence; and,

3) Although the EPRI study reports no radiated magnetic field data for the frequency range 50 to 100 kHz, the ORNL surveys observed significant radiated fields in this frequency range at all locations. Note that in this context significant is defined as falling within the dynamic range of the EMI/RFI monitoring equipment; it does not mean disruptive EMI/RFI levels.

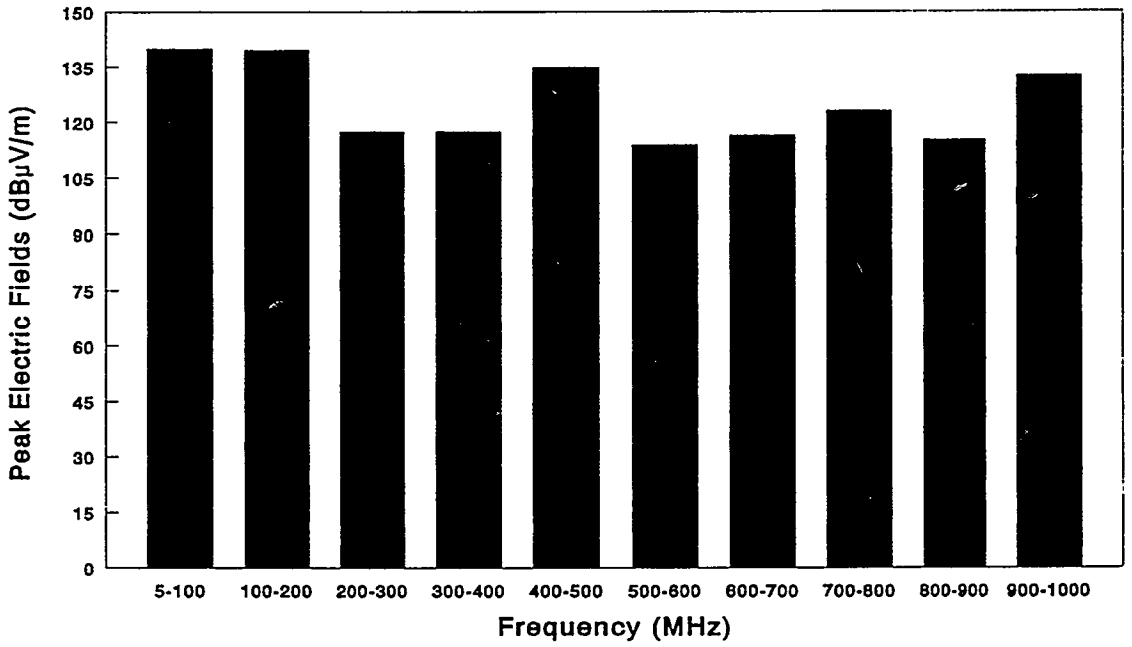

Fig. 1 Highest observed electric fields

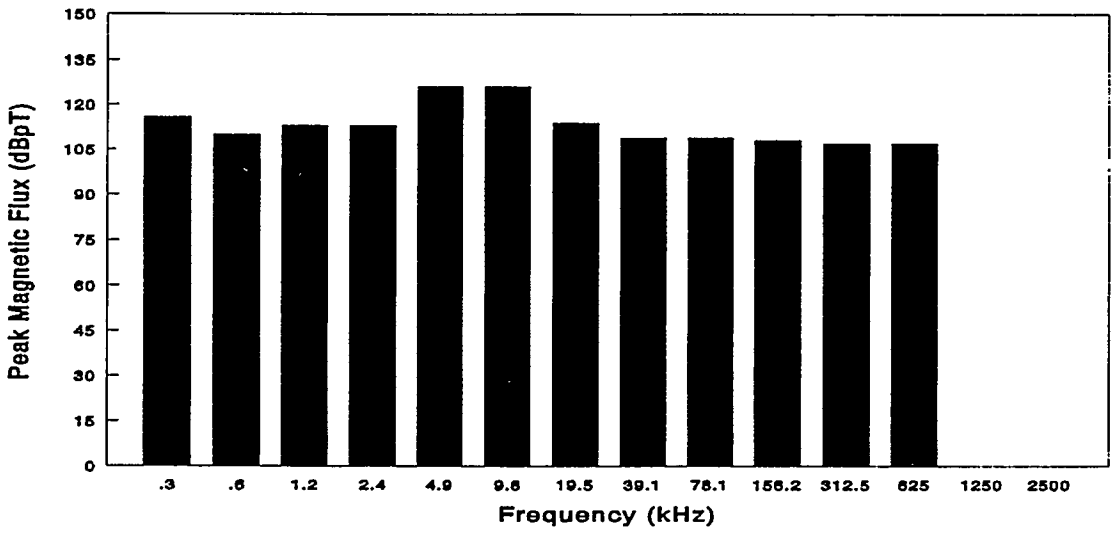

Fig. 2 Highest observed magnetic flux

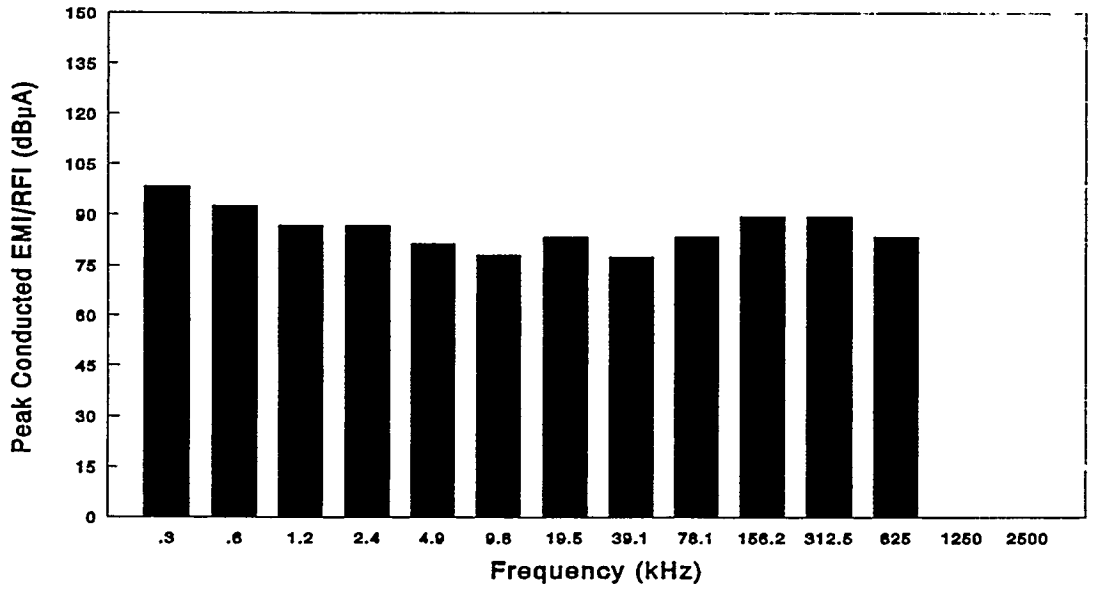

Fig. 3 Highest observed conducted EMI/RFI

6 SUMMARY

So far as the authors are aware, there is presently no NRC document that describes electromagnetic operating envelopes expected for the nuclear power plant environment. However, interim electromagnetic operating envelopes are being developed by ORNL at this time and recommended permanent operating envelopes based on plant measurements will follow. For the present, the recommended interim electromagnetic operating envelopes should ensure that EMI/RFI and power surge problems in nuclear power plants are averted with safety-related I&C system upgrades and the installation of new systems. Some conclusions have been drawn from the preliminary analysis of some EMI/RFI measurement data, but it is still too early to predict the results of the ORNL study. A detailed report will be issued after the completion of the EMI/RFI data collection at the survey sites.

7 REFERENCES

1. P. D. Ewing and K. Korsah, *Technical Basis for Evaluating Electromagnetic and Radio-Frequency Interference in Safety-Related I&C Systems*, NUREG/CR-5941, U.S. Nuclear Regulatory Commission, April 1994.

2. P. D. Ewing, *Recommended Interim Operating Envelopes for Safety-Related I&C Systems in Nuclear Power Plants*, NUREG/CR-6304, U.S. Nuclear Regulatory Commission, September 1995 (draft).

3. MIL-STD-461C, *Electromagnetic Emission and Susceptibility Requirements for the Control of Electromagnetic Interference*, U.S. Department of Defense, Aug. 4, 1986.

4. MIL-STD-461D, *Electromagnetic Emission and Susceptibility Requirements for the Control of Electromagnetic Interference*, U.S. Department of Defense, Jan. 11, 1993.

5. MIL-STD-462, *Measurement of Electromagnetic Interference Characteristics*, U.S. Department of Defense, July 31, 1967.

6. D. P. Rollinger, "The ABC's of MIL-STD-461: An Overview of Military EMC Standards and an Insight into Procurement Procedures," *EMC Test and Design*, pp. 19-25 (September/October 1991).

7. MIL-STD-462D, *Measurement of Electromagnetic Interference Characteristics*, U.S. Department of Defense, January 11, 1993.

8. IEEE Std C62.41-1991, *IEEE Recommended Practice on Surge Voltages in Low-Voltage AC Power Circuits*, Institute of Electrical and Electronics Engineers, approved Feb. 25, 1991.

9. IEEE Std C62.45-1987, *IEEE Guide on Surge Testing for Equipment Connected to Low-Voltage AC Power Circuits*, Institute of Electrical and Electronics Engineers, approved Sept. 25, 1991.

10. J. Cirillo and M. Prussel, "Electromagnetic Compatibility in Nuclear Power Plants," 1986 WATTEC Conference, Knoxville, Tennessee, Feb. 11–14, 1986.

11. F. D. Martzloff and T. S. Gruzs, "Power Quality Site Surveys: Facts, Fiction, and Fallacies," *IEEE Trans.*, IA-24 (6), pp. 100-118 (November/December 1988).

12. EPRI TR-102323, *Guidelines for Electromagnetic Interference Testing in Power Plants*, Electric Power Research Institute, September 1994.

13. IEEE Std C62.41-1991, *IEEE Recommended Practice on Surge Voltages in Low-Voltage AC Power Circuits*, p. 40.

14. S. W. Kercel, "A Confirmatory Research Approach to the Measurement of EMI/RFI in Commercial Nuclear Power Plants," *Proceedings of Twenty-Second Water Reactor Safety Information Meeting*, NUREG/CP-0140, U.S. Nuclear Regulatory Commission, pp. 31-51, April 1995.

Performance Evaluation of Fiber Optic Components in Nuclear Plant Environments

M.C. Hastings
D.W. Miller
The Ohio State University
206 West 18th Ave.
Columbus, OH 43210-1107

R.W. James
Electric Power Research Institute
3412 Hillview Ave.
Palo Alto, CA 94304

23rd Water Reactor Safety Information Meeting
October 23-25, 1995
Bethesda, MD

Abstract

Over the past several years, the Electric Power Research Institute (EPRI) has funded several projects to evaluate the performance of commercially available fiber optic cables, connective devices, light sources, and light detectors under environmental conditions representative of normal and abnormal nuclear power plant operating conditions. Future projects are planned to evaluate commercially available fiber optic sensors and to install and evaluate performance of instrument loops comprised of fiber optic components in operating nuclear power plant applications.

The objective of this research is to assess the viability of fiber optic components for replacement and upgrade of nuclear power plant instrument systems. Fiber optic instrument channels offer many potential advantages: commercial availability of parts and technical support, small physical size and weight, immunity to electromagnetic interference, relatively low power requirements, and high bandwidth capabilities. As existing nuclear power plants continue to replace and upgrade I&C systems, fiber optics will offer a low-cost alternative technology which also provides additional information processing capabilities. Results to date indicate that fiber optics are a viable technology for many nuclear applications, both inside and outside of containments. This work is funded and managed under the Operations & Maintenance Cost Control research target of EPRI's Nuclear Power Group. The work is being performed by faculty and students in the Mechanical and Nuclear Engineering Departments and the staff of the Nuclear Reactor Laboratory of the Ohio State University.

Introduction

Fiber optic technology presents opportunities to provide a cost-effective alternative for replacing/upgrading existing I&C systems in nuclear power plants while improving system reliability and introducing new functional capabilities. EPRI has therefore initiated a series of projects to evaluate the reliability and performance of commercially available fiber optic cables, connective devices, transmitter, receivers, and sensors in normal and post-accident environments typical of nuclear power plants. The overall objective of these research activities is to establish criteria under which commercially available fiber optic components can be used in nuclear plant instrument applications, especially those for which radiation or potentially severe post-accident conditions could exist.

As equipment testing and maintenance costs increase due to decreasing vendor support, equipment aging, and increasing performance demands, nuclear plants are replacing or upgrading selected I&C systems. Given that existing U.S. nuclear plants are licensed to operate for an average of 20 more years, and assuming that plant life extension and/or construction of new plants will occur domestically and/or internationally, these replacement and upgrade activities are expected to continue.

Fiber optic technology has the potential to meet existing functional requirements with lower installation and maintenance costs. First, it is a well-developed technology which continues to expand and is extensively supported in the vendor community due to its applications in many other fields, e.g.: communications, computers, medical equipment, and non-process signal processing and sensing. These facts not only help to assure the continued availability of a robust technology, but also benefit the power industry in terms of lower material costs. Fiber optics also offer many advantages. The physical size and weight of fiber to carry process data are much, much less than for conventional copper conductors. Consequently, fiber optic cable is much less likely to impact seismic loading calculations associated with cable trays. Physically smaller cables mean less potentially combustible material to address in fire loading analyses. Also, optical signals are insensitive to electromagnetic interference.

Development and application of fiber optics in nuclear plants will also position utilities to take advantage of several new capabilities. Sensors which produce an optical signal can be very sensitive and accurate. The bandwidth of optical fiber is large, and substantial signal multiplexing is possible. Coupled with more fault-tolerant data architectures (e.g. mesh rather than bus-loop), it is possible to develop systems using less cabling but with equal or improved reliability. Optical sensors combined with optical fiber and signal processing reduces the need for signal conversion, a source of instrument loop uncertainty.

The purpose of the EPRI program is to explore these issues and to assess the viability of fiber optics in nuclear plant applications. Currently, this research consists four projects, one of which is completed, one of which will be completed in 1995, and two of which are planned. The initial project, published as EPRI report TR-100367, "Optical Fibers in Radiation Environments", was initiated in 1989 and completed in 1992. This project examined performance of various commercially available communications grade optical fiber under exposure to mixed neutron/gamma and gamma radiation. The second project, underway since 1993, will be completed this year. This project is evaluating performance of both optical fibers as well as connective devices, transmitters, and receivers under mixed neutron/gamma and gamma radiation, and under a typical LOCA pressure/temperature steam environment. Two additional projects are planned. One will address environmental testing of commercially available fiber optic sensors, and the other will entail a demonstration of a fiber optic instrument loop in an operating nuclear power plant. Each of these projects will be described in this paper. An overview of results obtained to date will be presented.

Other Completed EPRI Fiber Optics Work

For several years, other EPRI technical groups have also performed fiber optics-related research. These activities are briefly summarized below:

- Demonstration of Fiber Optic Link Applications in Utility Plant Multiplexed Instrument and Control Systems (NP-1322, Oct. 1980)

  This project conducted a demonstration of early fiber optic technology in a fossil power plant. Results indicated that fiber optics were viable for power plant applications and identified several design, installation, and operational criteria to be considered for fiber optic systems. Many of these issues have been resolved through evolution of fiber optic technology since then.

- Development of a Fiber Optic Doppler Anemometer for Bubbly Two-Phase Flows (NP-2802, Jan. 1983)

  Development of fiber optic anemometers for measurement of vapor and liquid velocity as well as void fraction was investigated. Tests of prototype sensors were also presented.

- Optical Temperature Sensors for Transformers (EL-4376, Jan. 1986)

  This project developed an optical temperature sensor for measurement of hot spots in transformers over a temperature range of 0-200 °C. Test results indicated a sensor resolution of ± 1 °C and an accuracy of ± 2 °C.

- Ruggedized Optical Temperature Sensor for Transformers (EL-4377, Jan. 1986)

  This project developed a ruggedized version of an optical temperature sensor for measurement of hot spots in transformers over a temperature range of 0-200 °C. Calculated sensor life under typical operating conditions exceeds 700 years. (This project was completed in conjunction with EL-4376; see above.)

- Distributed Fiber-Optics Hot Spot Sensor (EL-5568, Dec. 1987)

  This project investigated the feasibility of a distributed fiber optic temperature sensor for electrical systems. Test results indicated the feasibility of such a sensor.

- Using Optical Pyrometry to Measure Gas Turbine Blade Metal Temperatures (AP-6020, Dec. 1988)

  This project evaluated the use of an optical pyrometer to measure gas turbine blade surface temperatures for evaluation of turbine component service life. Results indicated that the pyrometer could accurately measure blade surface temperatures in excess of 1000 °F.

- Improved Temperature Sensors for Large Generators (GS-6338, Apr. 1989)

  This project evaluated the feasibility of a fiber optic generator stator winding temperature sensor for large steam turbines and hydroelectric generators. The project concluded that such a sensor was feasible, based upon blackbody radiation measurement.

- Research Planning Study of Fiber Optic Sensors (ER-6428, Aug. 1989)

  This study evaluated potential utility applications for fiber optic sensors and limitations in their application. The study concluded that several viable applications for fiber optics sensors in power plants existed.

- High-Temperature Optical-Fiber pH Sensors (NP-6932, Aug. 1990)

  This project evaluated options for measuring pH using fiber optic sensors for temperatures up to 300 °C. Several variations of fluorescence techniques were identified as feasible.

- Phase-Modulated Fiber-Optic Current Transformer/Voltage Transformer (EL-7421, Jul. 1991)

  This project evaluated the feasibility of a fiber optic sensor for measurement of current and voltage in distribution systems. A prototype system suitable for laboratory testing using single-mode fiber was built and evaluated. The project concluded that such a sensor was feasible.

- Fiber-Optic Voltage and Current Sensors for Distribution Systems (TR-100291, Oct. 1992)

  This project was conducted in conjunction with EL-7421 (see above). A prototype system suitable for laboratory testing using multi-mode fiber was built and evaluated. The project concluded that such a sensor was feasible.

- Stability of a Fiber Optic pH Sensor at 100 Degrees °F (TR-101972, Feb. 1993)

  This project evaluated the life of an optical pH probe immersed in water at 100 °F. Changes in fluorescence and absorption properties of organic dyes were recorded. Results indicated that such a probe will yield stable measurements over periods of one year.

- Fiber Optic Distributed Temperature Sensor Demonstration (TR-101950, Mar. 1993)

  This project developed a distributed fiber optic sensing system to monitor peak winding temperature in stator and rotor windings. The system was tested both in the laboratory and on a fossil plant switchgear device. (See also ER-5568 above).

- Fiber Optic Electric Field Micro Sensor (TR-103395, Jan. 1994)

  This project developed and tested a prototype fiber optic sensor for detection of electric fields over a wide range (0-400 kV/m). Limitation and design improvements were identified.

- Optical Fiber pH Sensors for High Temperature Water (TR-104196, Nov. 1994)

  This project developed optical pH sensors capable of measurement in water up to temperatures of 50 °C with the capability to detect pH changes corresponding to morpholine concentration changes on the order of 1 ppm. Substantial drift was also observed.

Completed Fiber Optics Radiation Testing

The evaluation from the first project, published in EPRI TR-100367 in February 1992, focused exclusively on communications grade optical fiber and measurement of its performance characteristics under mixed neutron/gamma and under gamma irradiation.

A review of existing research was first performed to obtain results from related, prior research and to evaluate mechanism through which radiation causes degradation of fiber performance. Over eighty references were included in the scope of this review. This review yielded some general observations:

- Susceptibility to radiation is a strong function of type of dopants and the degree of doping in the fiber.

- Gamma radiation damages the lattice structure of the fiber, which in turn makes the strain on silica bonds in the fiber an important attribute. This attribute correlates to the method by which the fiber is drawn.
- High temperature and/or high light powers can cause some annealing of radiation-induced damage.

Six types of optical fiber typically used in communications applications were tested for combinations of different attributes: three different wavelengths, and single mode and step/graded index, doped and undoped cores. Table 1 below describes the different types of fiber tested; the particular fibers shown were evaluated because specimens were donated to the project by their manufacturers.

Table 1 - Description of Fibers Tested in EPRI TR-100367

Manufacturer	Abbreviation	Description	Core/Clad Diameter (μm)	Buffer/Jacket Diameter (μm)	N.A.
3M	1300 SM	Singlemode	/125±3	250±15	0.16
3M	1550 SM	Singlemode	/125±3	185±15	0.15
3M	3M Low OH	FT-200-LMT Pure Silica Core Proprietary 3M Hard Cladding Tefzel® 210 Buffer	200±5/ 230+0-10	500±30	0.37
3M	3M High OH	FT-200-UMT Pure Silica Core Proprietary 3M Hard Cladding Tefzel® 210 Buffer	200±5/ 230+0-10	500±30	0.37
Mitsubishi		ST-R100B-SY Step Index Pure Silica Core Doped Silica Cladding Silicone resin buffer Polyamide Jacket	100±3/140±3	400/900	0.20±0.02
AT&T		Graded Index Doped Silica Core (Germanium)	62.5/125	250	

Test conditions were varied over several factors:

- Type of radiation: gamma or mixed neutron/gamma
- Temperature: 25 °C or 100 °C
- Signal power level: 1 nW or 1 μW
- Wavelength: 850 nm, 1300 nm, or 1550 nm

Mixed gamma/neutron exposures were produced in the 10 kWt Ohio State University Research Reactor (OSURR). Specimens were irradiated at a neutron dose rate of 32 Gray/hr (SiO_2) and at a gamma dose rate of 1,870 Gray/hr (SiO_2) for 2 hours, equating to a total dose of approximately 3,800 Gy. Gamma-only exposures were produced in the University of Cincinnati ^{60}Co irradiation facility at an equivalent dose rate of 658 Gray/hr (SiO_2) for 2 hours, equating to a total dose of approximately 1,300 Gy. Table 2 identifies the combinations of the above factors for which test results were obtained.

Results were measured in terms of added signal attenuation as a function of dose and as a function of time after irradiation was completed. General conclusions from this work are that:

- Results are consistent with those documented in existing literature.
- Pure silica core fiber has a significantly lower radiation response than germanium doped silica fiber.
- Longer wavelength fiber exhibited lower additional signal attenuation due to irradiation than shorter wavelength fiber.
- The best-performing fiber exhibited additional attenuation < 5 dB/km.
- Fluorescence in fibers is a concern in the presence of radiation and with low signal power.

Table 2 - Description of Optical Fiber Tests in EPRI TR-100367

	Gamma exposure							Mixed neutron/gamma exposure					
T = 25 °C													
P = 1 nW													
λ	AT&T	Mitsu-bishi	3M 1300 ST	3M 1550 ST	3M High OH	3M Low OH		AT&T	Mitsu-bishi	3M 1300 ST	3M 1550 ST	3M High OH	3M Low OH
850 nm		✔			✔			✔	✔			✔	
1300 nm			✔		✔	✔		✔		✔		✔	✔
1550 nm				✔		✔		✔			✔	✔	✔
P = 1 μW													
λ	AT&T	Mitsu-bishi	3M 1300 ST	3M 1550 ST	3M High OH	3M Low OH		AT&T	Mitsu-bishi	3M 1300 ST	3M 1550 ST	3M High OH	3M Low OH
850 nm	✔				✔			✔	✔			✔	
1300 nm	✔							✔					✔
1550 nm	✔					✔		✔					✔
T = 100 °C													
P = 1 nW													
λ	AT&T	Mitsu-bishi	3M 1300 ST	3M 1550 ST	3M High OH	3M Low OH		AT&T	Mitsu-bishi	3M 1300 ST	3M 1550 ST	3M High OH	3M Low OH
850 nm		✔			✔			✔	✔			✔	
1300 nm			✔		✔	✔		✔		✔		✔	✔
1550 nm				✔		✔		✔			✔	✔	✔
P = 1 μW													
λ	AT&T	Mitsu-bishi	3M 1300 ST	3M 1550 ST	3M High OH	3M Low OH		AT&T	Mitsu-bishi	3M 1300 ST	3M 1550 ST	3M High OH	3M Low OH
850 nm	✔				✔			✔	✔			✔	
1300 nm	✔							✔					✔
1550 nm	✔					✔		✔					✔

Current Research

The second project (EPRI WO2409-25), currently underway, is a substantial expansion of the first project. It consists of two major tasks: performance evaluation of fiber optic components and benchtop performance evaluation of prototype sensor channels. The project was initiated in late 1993. To date, the majority of component testing has been completed. Testing of prototype instrument channels comprised of test components will be conducted in late 1995.

Environmental tests consist of mixed neutron/gamma irradiation, gamma-only irradiation, and exposure to high temperature and pressure steam in a pressure cell. Mixed gamma/neutron exposures were produced in the Ohio State University Research Reactor (OSURR) facility. Gamma exposures were produced in the Ohio State University Nuclear Reactor Laboratory Cobalt Irradiator Facility (OSUNRL-CIF). The steam environment testing was performed at Ohio State in a pressure cell. Test conditions replicated a main steam line break profile as defined in the EPRI Equipment Qualification Manual (TR-100516), which is consistent with the requirements of IEEE 323. The gamma-only exposure tests delivered a dose of approximately 1.4×10^4 Gray (SiO_2) over a period of about 3 hours. The mixed neutron/gamma exposure tests delivered a total neutron fluence of approximately 10^{17} n/cm^2.

Several different types of transmitters, receivers, couplers, splices, and connectors are being tested; the particular components shown in Table 3 were selected because specimens were donated to the project by their manufacturers. These components were operated at a wavelength of 1300 nm for the tests in this project. Other than the JDS coupler, two samples of each component were tested.

Table 3 - Description of Optical Fiber Components Tested in EPRI WOP2409-25

Transmitters	Receivers	Couplers	Connectors	Splices
AT&T ODL 125	AT&T ODL 125	FIS 2x2 F1-93205-M	FC Molex MM 86152-1000	AMP Finger Splice 608119-5/1x1
Hewlett-Packard HFBR-1312T	Hewlett-Packard HFBR-2316T	Gould 1x2 15312005022101	SC Molex MM 86161-1000	Fusion Splice (Fiberlign Micro Fusion Splicer)
Laser Diode TS-2143	Laser Diode RT-2714	JDS Fitel 1x2 AC1100-B2	ST OFTI 504021	GTE Fastomeric Splice WO4200/1x1
				Ultra Splice US-128

Different performance characteristics were evaluated to assess the effects of radiation and other environmental effects. Table 4 summarizes the performance characteristics evaluated for each component type:

Table 4 - Evaluated Fiber Optic Component Performance Characteristics

Component	Performance Characteristic Evaluated
Transmitters	• Risetime • Falltime • Average power output
Receivers	• Risetime • Falltime • Sensitivity
Couplers	• Coupling loss • Insertion loss
Splices and Connectors	• Insertion loss

At the time of preparing this paper, complete results from the mixed neutron/gamma exposures were not yet available due to the radioactivity of test samples, although tests were completed. Results from the gamma-only exposures yielded the following observations:

- Transmitters
  - increase in risetime of ~15%
  - increase in falltime of ~25%
  - decrease in output of ~10%
- Receivers
  - increase in risetime of ~10%
  - decrease in falltime of ~5%
  - decrease in sensitivity of ~5%

- Couplers
  - no change in coupling loss
  - increase in insertion loss of ~15%*
    (*Note: one of the couplers performed 20-30 times more poorly than the remainder of the group; the above value excludes this coupler)
- Splices
  - increase in insertion loss of ~10%
- Connectors
  - increase in insertion loss of ~10%

The above test samples were also baked in a laboratory oven to assess temperature effects on performance. This was done to facilitate separation of temperature and radiation effects in evaluating the mixed radiation exposure data. Samples were heated over a period of ~ 2 hours to a temperature of approximately 190 °F and held at that temperature for ~ 4 more hours. The results for all component types indicated a degradation in performance of only a few tenths of a dB for loss characteristics or approximately 10% for other performance characteristics.

A second phase of this project involves assembly and integral performance evaluation of prototype instrument channels under radiation and post-accident steam environments. Each channel consists of a receiver, transmitter, splices, a coupler, and a sensor. Two channels are being tested, one with an optical strain sensor and the other with a conventional differential pressure transmitter and electro-optical signal conversion. Figures 1 and 2 show a schematic view of each test channel.

Figure 1 - All-Optical Test Instrument Channel in EPRI WO2409-25

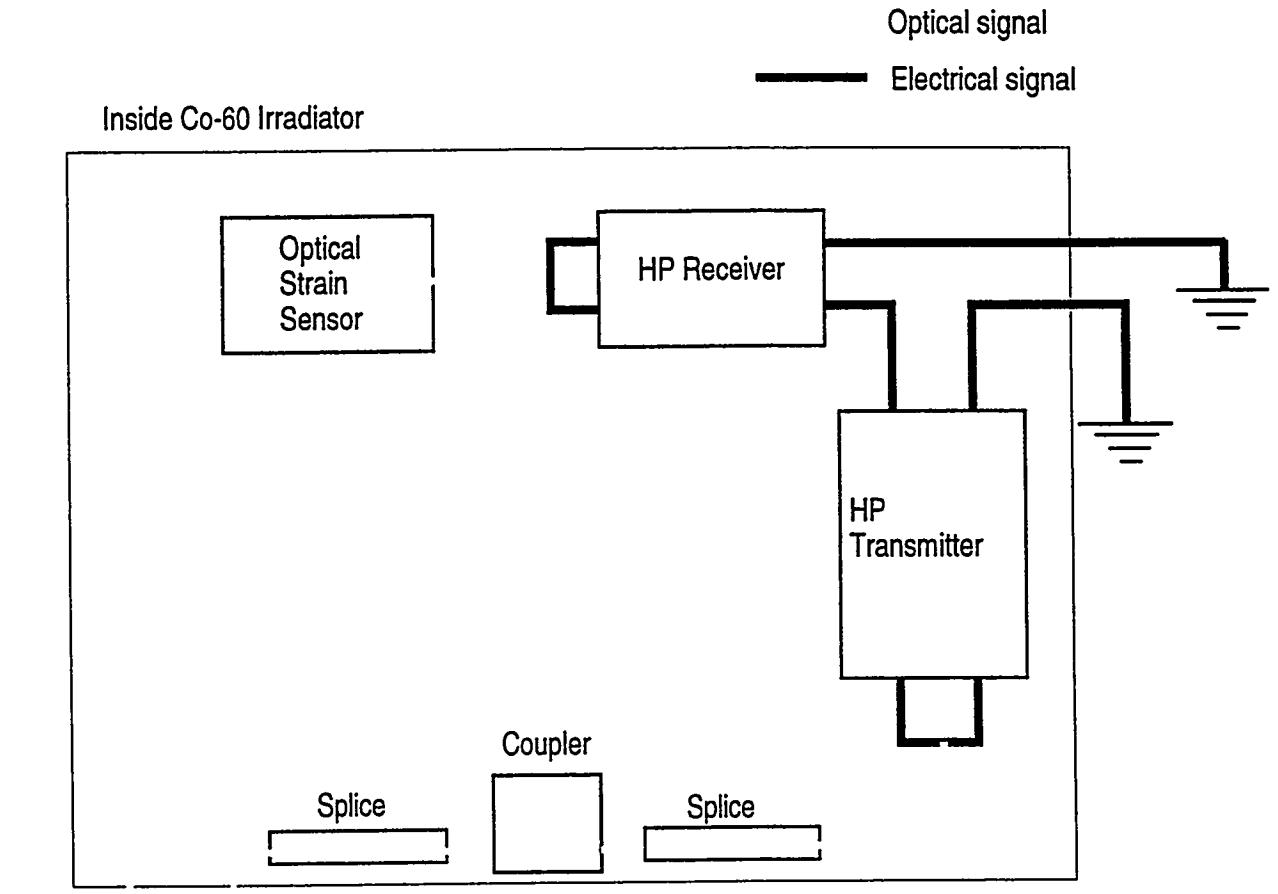

In the test channel shown in Figure 1, the strain sensor is equipped with its own light source. The sensing principle is the relation between the pressure induced on the strain sensor and the attenuation of the light signal. The receiver converts the light to an electrical signal, which drives the transmitter. This arrangement is being used to allow simultaneous testing of a receiver and a transmitter. The output light signal of the transmitter is routed through the components shown before detection.

Figure 2 - Electro-Optical Test Instrument Channel in EPRI WO2409-25

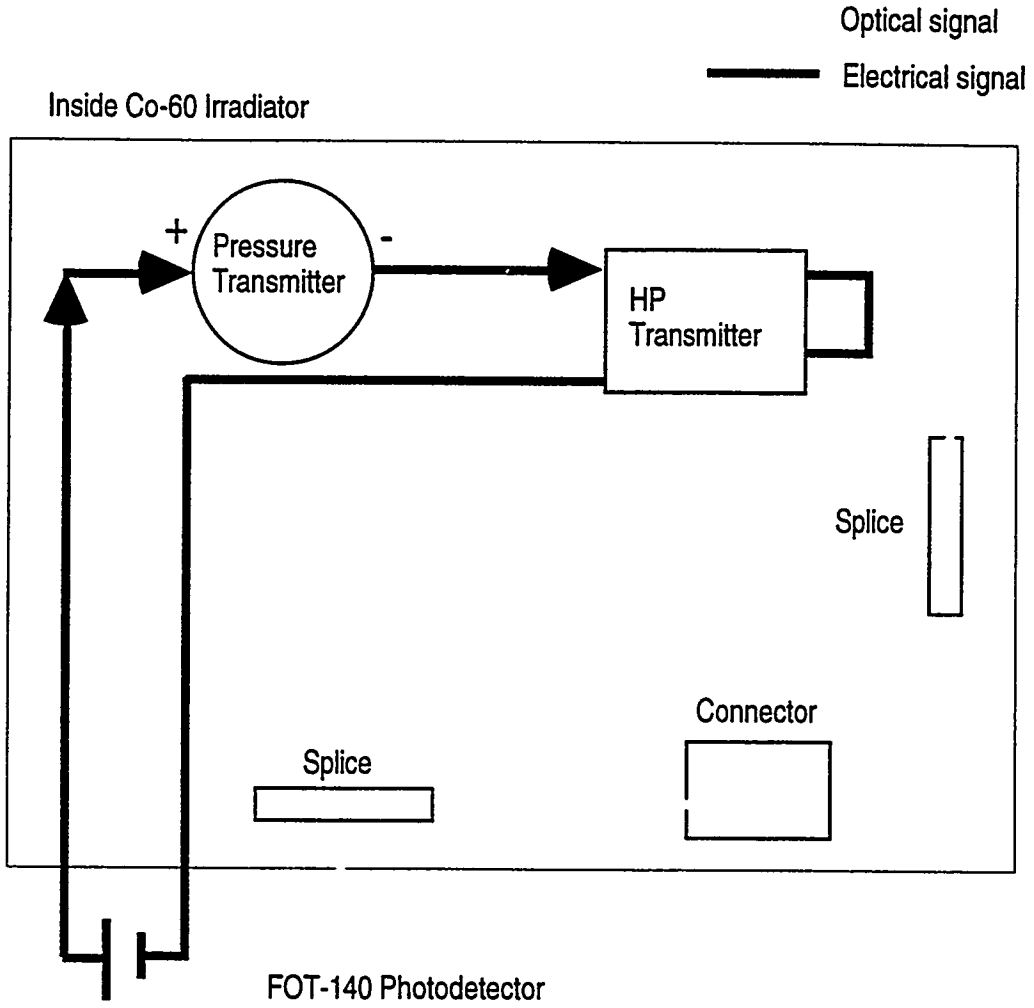

In the test channel shown in Figure 2, a conventional capacitive differential pressure sensor produces a current signal proportional to pressure. A constant amount of pressure is applied to the pressure sensor, which generates a constant current. This current drives the transmitter, which produces a light signal. The output light signal of the transmitter is routed through the components shown before detection.

Each of the above test channels will be exposed to a typical LOCA high temperature/pressure steam environment and left in the resulting high humidity environment for 30 days, during which performance measurements will be made.

Planned Research

Two additional projects are planned as part of this program. Initial funding and planning have been completed for a third project to perform evaluation of commercially available fiber optic sensors similar to that described above for components. The objective of this project would be to evaluate the viability of commercially available fiber optic sensors in operating nuclear plant applications and to conduct integrated tests of simulated channels using these sensors. This project will be completed in 1996. Planning for a fourth project to design and install a fiber optic instrument loop at a nuclear power plant as a demonstration of fiber optic technology has been initiated. A host plant has been identified, and the initial project scope and schedule are being discussed. The specific application under consideration is pressurizer relief tank pressure, which would be an in-containment installation. Funding is not yet approved for this project.

Summary

EPRI is completing a series of projects to evaluate the viability of fiber optic technology in process instrumentation applications at nuclear power plants. These projects are aimed at assessing the effect on performance of environmental factors typical of nuclear plants. EPRI has also completed several related projects evaluating prototype fiber optic sensors in other electric power applications.

To date, performance evaluation of optical fiber, transmitters, receivers, splices, connectors, and couplers has been completed under radiation, temperature, pressure, and humidity conditions representative of normal and post-accident nuclear plant conditions. Results thus far have been consistent with data previously available in the technical literature. Based on the results of this program, the following conclusions have been reached:

- Longer wavelength, pure silica core optical fiber is the most suitable for gamma radiation environments, and experience minimal signal attenuation due to radiation damage to the fiber.

- Transmitters, receivers, and connective devices experience performance degradation due to gamma radiation on the order of 10-25% (typical) at low power levels ($\leq 1\ \mu W$).

- Exposure to moderately high temperatures does not appear to significantly affect fiber optic component performance.

- Preliminary conclusions regarding fiber optic performance in mixed neutron/gamma radiation environments does degrade significantly.

- At this time, performance evaluation in high pressure/ temperature/humidity environments has not been completed.

- Commercial grade fiber optic technology is viable for many nuclear applications.

Successful application of fiber optic instrumentation loops will provide several advantages compared to conventional technology, and many new capabilities will also be accessible. Due to its active development and application in other industries, fiber optic components and optical fiber are relatively inexpensive. Fiber optics are insensitive to electromagnetic interference. The small size and low weight of optical fiber minimizes seismic loading issues and fire combustible loading issues. As fiber optics are introduced, new capabilities will also exist: multiplexing, different, more fault-tolerant process data acquisition architectures, and digital signal processing with less signal conversion.

An average of 20 years remains on most nuclear plant licenses, meaning that existing plant I&C systems must be maintained and operated cost-effectively for a substantial minimum period of time. Complete replacement of the 22% of U.S. electricity generating capacity represented by nuclear plants is also unlikely in this period of time, making nuclear plant life extension a strong possibility that must be considered in utility planning. Incremental replacement/upgrade of components and loops using fiber optic technology can provide a technically and economically viable approach to addressing these needs.

RESOLUTION OF THE DIRECT CONTAINMENT HEATING ISSUE FOR ALL WESTINGHOUSE PLANTS WITH LARGE DRY CONTAINMENTS OR SUBATMOSPHERIC CONTAINMENTS

Martin M. Pilch, Michael D. Allen, and Eric W. Klamerus
Sandia National Laboratories
Albuquerque, NM 87185

ABSTRACT

This report uses the methodology and scenarios described in NUREG/CR-6075 and NUREG/CR-6075, Supplement 1, to address the direct containment heating (DCH) issue for all Westinghouse plants with large dry or subatmospheric containments. DCH is considered resolved if the conditional containment failure probability (CCFP) is less than 0.1. The methodology calls for an initial screening phase in which the CCFP for each plant is calculated based on loads versus strength evaluations using plant-specific information. The DCH issue is considered resolved for a plant if the CCFP calculated in the screening phase is less than 0.01. This value is more stringent than the overall success criterion of 0.1. The CCFPs for all of the Westinghouse plants with dry containments were less than 0.01 in the screening phase calculations, and thus, the DCH issue is resolved for these plants based on containment loads alone. No additional analyses are required.

1.0 INTRODUCTION

In a light-water reactor core melt accident, if the reactor pressure vessel (RPV) fails while the reactor coolant system (RCS) is at high pressure, the expulsion of molten core debris may pressurize the reactor containment building (RCB) beyond its failure pressure. A failure in the bottom head of the RPV, followed by melt expulsion and blowdown of the RCS, will entrain molten core debris in the high-velocity steam blowdown gas. This chain of events is called a high-pressure melt ejection (HPME). Four mechanisms may cause a rapid increase in pressure and temperature in the reactor containment: (1) blowdown of the RCS, (2) efficient debris-to-gas heat transfer, (3) exothermic metal-steam and metal-oxygen reactions, and (4) hydrogen combustion. These processes, which lead to increased loads on the containment building, are collectively referred to as direct containment heating (DCH) when they have the potential to occur simultaneously. It is necessary to understand factors that enhance or mitigate DCH because the pressure load imposed on the RCB may lead to early failure of the containment.

DCH is a prominent severe accident issue because of its potential for early containment failure. The Nuclear Regulatory Commission (NRC) has identified DCH as a major issue for resolution in the Revised Severe

Accident Research Plan (NRC, 1992) and has sponsored programs at Sandia National Laboratories (SNL) to resolve the DCH issue.

NUREG-1150 was the first attempt to treat DCH from a probabilistic risk assessment (PRA) perspective that integrates sequence probabilities with uncertainties associated with initial/boundary conditions and phenomenological uncertainties associated with predicting containment loads. NUREG-1150 addressed only a small number of reference plants and the DCH database was largely nonexistent at the time, so there was no way to validate these early attempts to predict DCH loads. More recently, the Individual Plant Examinations (IPEs) have also addressed the DCH issue from a PRA perspective. Their strength is that plant-specific sequence information is fully integrated into the assessment for every plant. On the other hand, the approaches taken to assess containment loads are inconsistent and poorly tied to the existing database.

This paper, extracted from NUREG/CR-6338 (Pilch et al., 1995b) performs loads/strength evaluations in a consistent manner for all plants. The phenomenological modeling is closely tied to a now substantial database. Plant-specific analyses are performed, but sequence uncertainties are enveloped by a small number of splinter scenarios without assignment of probabilities.

The NRC-sponsored experimental program has played a major role in developing an understanding of the key physical processes in DCH. The technical basis for these scaled experiments was developed by the Severe Accident Scaling Methodology Technical Program Group (SASM-TPG) (Zuber et al., 1991) and by Pilch et al. (1992). The extensive database from counterpart experiments by Sandia National Laboratories and Argonne National Laboratory (ANL) has allowed the development and validation of simple analytical models for predicting the containment loads. In particular, the two-cell equilibrium (TCE) model is based on insights from the experimental program and is used in the analyses presented here. The TCE model takes into account the coherence between the entrained debris and the RCS blowdown steam. Any noncoherence in the entrainment process potentially limits the interactions that result in debris-to-gas heat transfer and in chemical reactions that produce hydrogen.

The first step in the DCH issue resolution process was writing NUREG/CR-6075 (Pilch et al., 1994a): "The Probability of Containment Failure by Direct Containment Heating in Zion." NUREG/CR-6075 assesses the probability of containment failure by DCH for the Zion nuclear power plant (NPP) and establishes the basic methodology that will be used to address DCH for all NPPs. The report was extensively reviewed by a panel of 13 experts representing national laboratories, universities, and industry (see Appendix A, Pilch et al., 1994b). The review process included written comments by the reviewers, responses by the authors, and rebuttals by the reviewers. Following this process, two working group meetings of selected members of the original peer review group were held to resolve two residual concerns: initial conditions and validity of the model.

Supplement 1 of NUREG/CR-6075 (Pilch et al., 1994b) was written in response to the peer review process to close the DCH issue for the Zion plant. It contains the additional analyses that the working groups indicated were necessary to strengthen the original conclusions. The working groups defined four new scenarios for analysis using the methodology in NUREG/CR-6075 and suggested using system-level codes to ensure consistency of the DCH initial conditions. They recommended using insights from core melt progression analyses performed by the Idaho National Engineering Laboratory (INEL) with SCDAP/RELAP5 in order to achieve consistency in quantifying initial conditions. These analyses indicated that failure of the hot leg or surge line resulting in depressurization of the primary system was observed well before core relocation and lower head failure. However, the calculations were continued until the lower head failed in order to gain insights about

conditions at lower head failure, such as the melt mass and composition, reactor coolant system pressure, melting of upper plenum steel, and relocation of metallic core blockages into the lower plenum. These insights were applied in developing the distributions for the new scenarios. The CONTAIN code, using sources from SCDAP/RELAP5, was used to ensure consistency in containment initial conditions prior to vessel failure. Load versus strength evaluations were performed using the TCE/LHS code, which uses the two-cell equilibrium model to calculate containment loads and Monte Carlo sampling to compute the load distribution (Pilch et al., 1994b). The containment strength was described in probabilistic terms using a fragility curve taken from the IPE. The conditional (on core damage) containment failure probabilities (CCFPs) for each of the new scenarios was determined. There were no intersections of the loads and strength distributions, and thus the probability of containment failure by DCH is low enough so that the issue is resolved for the Zion plant.

NUREG/CR-6109 (Pilch et al., 1995a) used the methodology and scenarios described in NUREG/CR-6075 and NUREG/CR-6075, Supplement 1, to address the DCH issue for the Surry plant. Consistency of the initial condition distributions was again ensured by using insights from systems-level codes, specifically SCDAP/RELAP5 and CONTAIN. The most useful insights are that the RCS pressure is low at vessel breach, metallic blockages in the core region do not melt and relocate into the lower plenum, and melting of upper plenum steel is correlated with hot leg failure. The SCDAP/RELAP5 output was used as input to CONTAIN to assess the containment conditions at vessel breach.

The loads evaluations for Surry in NUREG/CR-6109 (Pilch et al., 1995a) showed no intersections of the loads distributions with the containment strength distribution, and thus the DCH issue for Surry was resolved based on containment loads alone. However, the likelihood of high RCS pressures at vessel breach was evaluated for Surry. The probability of RCS pressures greater than 1.38 MPa for all station blackout scenarios without power recovery or operator intervention was found to be low ($\approx$0.077). This probability could have been factored into the containment failure probability for Surry if there had been significant intersections of the loads and strength distributions.

SCDAP/RELAP5 is the NRC's more mechanistic tool for performing integrated analyses of core melt progression. However, the peer review of SCDAP/RELAP5 noted that models and the existing database for late-phase core melt progression are often inadequate. Consequently, we anticipate that continued research will improve our understanding and capabilities in this area. Nonetheless, an integrated perspective of core melt progression was recommended by previous working groups to guide the selection of melt mass and composition distributions for DCH analyses.

Extrapolation of the DCH issue resolution beyond the Zion plant was first envisioned in NUREG/CR-6075 (Pilch et al., 1994a) where it was argued that most plants would have load distributions similar to Zion. Similarity of containment loads coupled with an anticipation that there would not be any significant deviations from the Zion fragility curve for containments of a similar class led to the tentative conclusion that DCH could be resolved for most pressurized water reactors (PWRs). Two concerns were expressed in the peer review (by a 13 member NRC appointed panel) of this work. First, peer reviewers recommended that consensus be achieved on the Zion resolution before proceeding with extrapolation to other plants. This recommendation has been satisfied by the establishment of two working groups to resolve residual concerns for Zion and the publication of NUREG/CR-6075, Supplement 1 (Pilch et al., 1994b), which documents modifications in the methodology arising from working group recommendations.

The peer reviewers of NUREG/CR-6075 also expressed concern that plant-specific differences in nuclear steam supply systems or plant geometry were not adequately addressed. In response to this concern, the NRC has instructed INEL to perform best estimate calculations of core melt progression using SCDAP/RELAP5. When complete, SCDAP/RELAP5 calculations will be available for representative plants from each supplier of nuclear steam supply systems. Insights from the calculations performed to date are factored into the current analyses. Concerns arising from differences in plant size, plant parameters, or plant geometry are addressed in this paper by performing analyses for each individual plant or site using plant-specific input.

This paper addresses the DCH issue for all Westinghouse plants with dry containments, which include 34 plants with large dry containments and 7 plants with subatmospheric containments. Westinghouse plants with ice condenser containments are excluded. The methodology developed in NUREG/CR-6075 and NUREG/CR-6075, Supplement 1, was used to perform a load versus strength evaluation for each of these plants using plant-specific data gathered from IPEs, Final Safety Analysis Reports (FSARs), and when necessary, direct contacts with plant personnel. The same enveloping accident scenarios (splinters) that were used in NUREG/CR-6075, Supplement 1, and NUREG/CR-6109 were used for these plant evaluations; these scenarios establish important input parameters for the loads calculations, e.g. the RCS pressure at vessel breach, the RPV breach size, the containment pressure and composition at vessel breach, etc. The melt mass and composition distributions developed for Zion (a four-loop plant) in NUREG/CR-6075, Supplement 1, were used for all of the four-loop plants. For all of the three-loop plants, the melt mass and composition developed for Surry (a three-loop plant) in NUREG/CR-6109 were used. For two-loop plants, the prescription given in NUREG/CR-6075, Supplement 1, was used to develop the melt mass and composition distributions. These assessments are more completely described for all PWRs (including Combustion Engineering and Babcock & Wilcox plants) in Appendix B of NUREG/CR-6338 (Pilch et al., 1995b).

Plant-specific data were gathered for each of the Westinghouse plants with dry containments for the loads versus strength evaluations. As much as possible, similar plants were grouped to facilitate the DCH assessments. For example, cavity drawings from all 41 Westinghouse plants were reviewed, along with the IDCOR (1985) categorization, and it was decided for coherence purposes that the cavities could be grouped into three types: Zion-like, Surry-like, and other. Only South Texas 1 and 2 fall into the "other" category. The cavity dispersal and coherence assessments are summarized in Section 4. A more detailed description is given in Appendix C of NUREG/CR-6338. The likelihood of water being present in the cavity at vessel breach is also assessed in Appendix C of NUREG/CR-6338. Cavities are grouped according to whether they are dry, wet, or deeply flooded.

Furthermore, review of the drawings of the lower compartment configurations of all 41 Westinghouse plants indicated that they could be grouped into four types (Zion-like, Surry-like, two-loop plants, and other). The only plants that fall into the "other" category are H.B. Robinson and South Texas 1 and 2. This grouping facilitated the assessment of the debris transport through the subcompartments to the containment dome. These assessments are also summarized in Section 4. A more complete description is given in Appendix C of NUREG/CR-6338 (Pilch et al., 1995b). Quantification of DCH phenomena is addressed in Section 5.

The containment fragility curve was extracted from the IPE for each plant. The fragility assessments are summarized in Section 6 and are compiled in Appendix D of NUREG/CR-6338. The TCE/LHS code was used to perform a load versus strength evaluation to determine the CCFP for each of the Westinghouse

plants with dry containments. The results of these calculations are presented in Section 7. The conclusions and recommendations are given in Section 8.

2.0 RESOLUTION METHODOLOGY

The methodology is aimed at grouping each PWR into one of two categories:

1. PWRs in which the threat of early containment failure is shown to be ≤ 0.1, and

2. PWRs in which the threat is > 0.1.

We consider DCH "resolved" for those plants that fall into the first category. The figure of merit by which resolution is judged is the mean conditional containment failure probability (CCFP). We emphasize that the containment failure probability is ultimately conditional on core damage. Based on NRC recommendations, the DCH issue for any PWR will be considered resolved if a CCFP ≤ 0.1 is reasonably demonstrated. We recognize that DCH must be considered in the plant-specific context of all early containment modes when this success criterion is applied; however, DCH is thought to dominate early containment failure for most plants. The DCH issue for plants falling into category 2 (CCFP > 0.1) may ultimately be considered resolved if the NRC chooses to view resolution from a broader perspective that convolutes the CCFP with the core damage frequency (CDF), or if the NRC chooses to perform a cost/benefit analysis.

Figure 1 provides an overview of the DCH resolution methodology. Consistent with peer review recommendations on NUREG/CR-6075, the first step in the methodology was to work through the key issues for Zion. When consensus was reasonably achieved through the peer review process and follow-on activities, the process was demonstrated a second time for Surry. In both cases, containment loads were calculated using simplified models and distributions on the dominant initial condition parameters. The Two-Cell Equilibrium (TCE) model was used for Zion and Surry, and the Convection Limited Containment Heating (CLCH) model was used for Zion. Three splinter scenarios were analyzed with the intent to envelop the expected range of initial conditions. The CCFP was calculated by convoluting the predicted loads distribution with a structural response distribution obtained from the IPEs. We note here that the CCFP was conditional on the splinter scenario since no attempt was made to assign probabilities to the various splinter scenarios. The analyses are documented in NUREG/CR-6075 and NUREG/CR-6075, Supplement 1, for Zion (Pilch et al., 1994a,b) and in NUREG/CR-6109 for Surry (Pilch et al., 1995a). For both Zion and Surry, there were no intersections (CCFP $\ll 0.1$) of the load distribution with the strength distribution.

The second step in the methodology is to repeat the process quantitatively used for Zion and Surry to all remaining PWRs using plant-specific input. This report executes this step for all Westinghouse (W) plants with large dry or subatmospheric containments. Two additional efforts are scheduled: the first will focus on all Westinghouse plants with ice condenser containments. We expect that CONTAIN will be used to calculate loads in this effort because it has models for the ice beds. The second will include all Combustion Engineering (CE) plants and all Babcock & Wilcox (B&W) plants.

Convolution of the containment load distribution with the containment fragility is performed for each plant using plant-specific information. The key plant-specific information used in these analyses are listed below with a brief description of how extrapolation is performed.

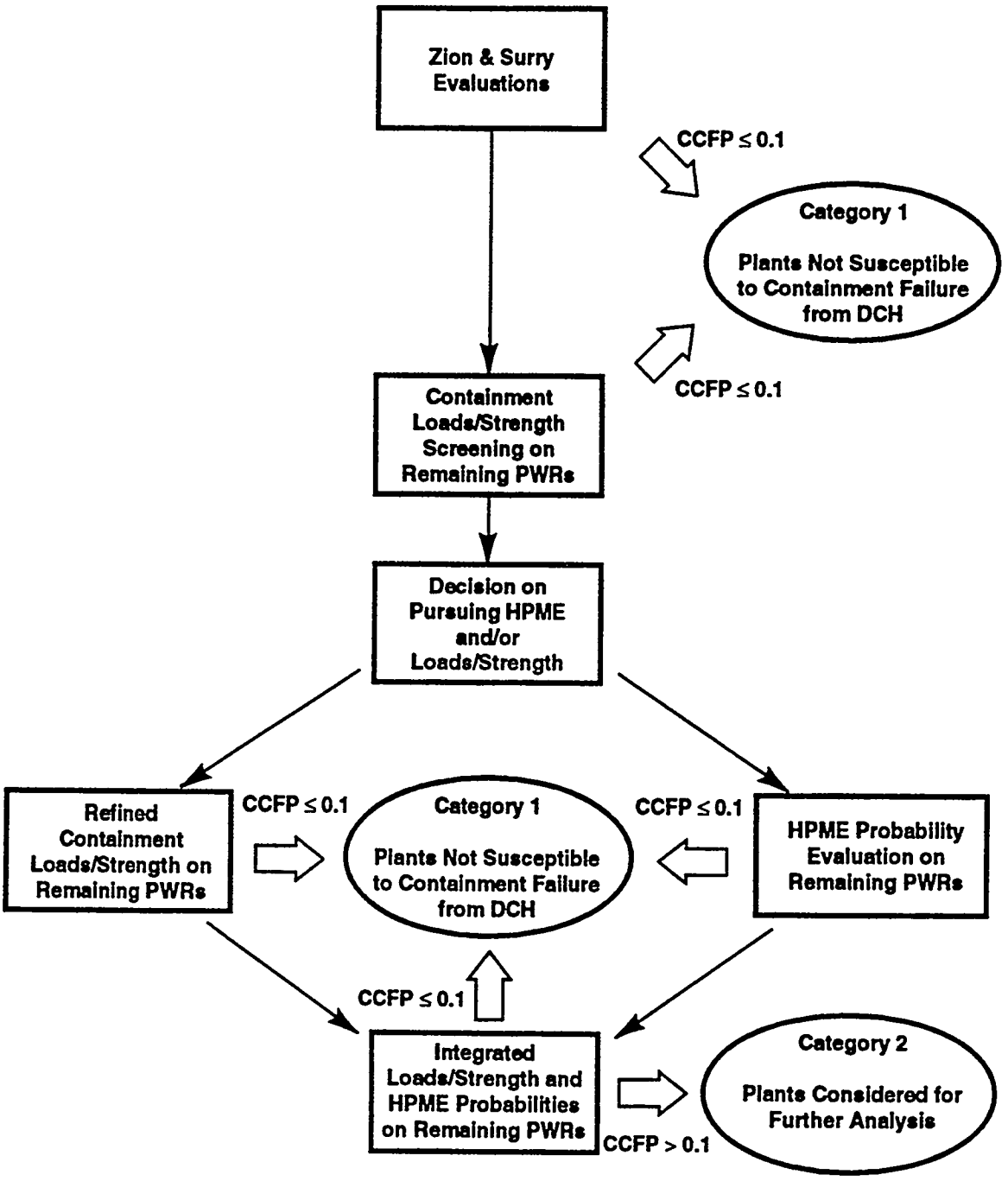

Figure 1. Methodology for resolution of the DCH issue for all PWRs.

1. RCS Initial Conditions: Two splinter scenarios are analyzed based on the Zion/Surry resolution efforts. RCS pressures and temperatures were specified for the splinter scenarios in the Zion/Surry resolution documents. Plant-specific RPV geometry and core compositions are employed and tabulated in Table 4.3 of NUREG/CR-6338 (Pilch et al., 1995b).

2. Melt Mass Distributions: A simple prescription for determining melt mass based on core size was developed as part of the Zion/Surry resolution effort. The bounding nature of this prescription was validated by SCDAP/RELAP5 for Zion, Surry, Calvert Cliffs, and ANO-2. The core size for Westinghouse plants can be grouped according to whether the plant has four, three, or two-loops. Existing melt mass distributions for Zion and Surry are applied to all four and three-loop plants, respectively. The same prescription used to develop melt mass distributions for Zion/Surry is used (Appendix B of NUREG/CR-6338) to develop a melt mass distribution for all two-loop plants.

3. Plant Geometry: Plant-specific geometry is used in these analyses and tabulated in Table 4.3 of NUREG/CR-6338. The coherence ratio and dome transport are two geometry specific phenomenological parameters that receive special attention in their assignments in Sections C.2.2 and C.3, respectively, of NUREG/CR-6338. Reactor cavities are grouped into three categories: Zion-like, Surry-like, and other. Existing coherence correlations for Zion and Surry are applied to all Zion-like and Surry-like cavities, respectively. A biased coherence correlation is applied to cavities that are neither Zion-like or Surry-like. Dome transport is calculated using plant-specific areas for flow around the RPV and for line-of-sight flow paths from the cavity exit.

4. Fragility: Plant-specific fragility curves are cataloged from the IPEs as part of Appendix D of NUREG/CR-6338.

We refer to the initial attempt at extrapolation as screening because the models are tied to the Zion and Surry database and other plants have different geometries and flow paths, which necessitate some judgment in application of the models. In addition, Zion and Surry were very well characterized. Complete plant drawings were available and SNL staff who were knowledgeable about DCH issues participated in tours of the plants. The primary sources for plant information are preliminary safety analysis reports (PSARs), FSARs, IPEs, and other plant safety analyses (PSAs). Of these, the IPEs proved most useful, but they do not carry the same level of detail that was available for Zion and Surry. In general, the plant data employed here has not been reviewed by the plant owners, except in a few cases where uncertainties were judged significant. To allow for any potential nonconservatisms or possible residual modeling concerns in the screening stage, we recommend a tighter resolution criterion, CCFP $\leq$ 0.01. Like the Zion and Surry efforts, the screening process will focus on a small number of splinter scenarios; consequently, the computed CCFPs will be conditional on the splinter scenario since no attempt will be made to assign probabilities to the splinters. Utilities may wish to employ some of the methods or results of this report when revising their PSAs to provide a more integrated perspective on this issue; however, this is beyond the scope or needs of the current effort.

Plants that do not pass the initial screening will then be examined more carefully to determine whether they can meet the CCFP $\leq$ 0.1 criterion with more detailed analyses, and therefore be considered resolved. This can be accomplished by one of three processes: refined load/strength analyses, consideration of HPME probabilities given core damage (i.e., assign probabilities to the splinters), or some integration of load/strength analyses and HPME probabilities. Additional analyses for plants that

do not meet the success criterion for the initial screening phase (i.e., CCFP ≤ 0.01) will be formally documented in a separate report to the NRC. This step will ensure that any plant that does not pass the initial screening test will receive close scrutiny that will be publicly documented. The best course of action must be judged for each individual plant. Some potentially fruitful options are discussed below.

Several options exist for refined load/strength analyses. They are listed here in order (roughly) of increasing effort.

1. The CCFP may not be very sensitive to potential uncertainties in the containment fragility. It is possible that the CCFP ≥ 0.01 in the screening study (using mean fragility curves) while the use of a high confidence fragility curve could still meet the resolution criterion, CCFP ≤ 0.1. This may occur if the plant has a long flat tail at the low end of the fragility curve.

2. Refine the accuracy of the TCE/LHS input. This can be accomplished by obtaining detailed plant drawings or by consulting with knowledgeable plant personnel.

3. Best estimate CONTAIN calculations could be performed that may result in lower predicted loads than those calculated using the TCE model. Lower loads were generally predicted in CONTAIN/TCE comparisons that were performed for NUREG/CR-6109 (Pilch et al. 1995a) for Surry.

4. Side failure of the RPV could retain ~25 - 50 percent of the melt in the RPV. Credit was taken for this in NUREG-1150 for Sequoyah. The likelihood of side failure, however, has yet to be resolved in a definitive way.

Demonstrating that the probability of HPME events is sufficiently low offers an independent path to resolving the DCH issue. Integration of sequence or HPME probabilities with conditional failure probabilities (for each splinter) was not performed or needed in this study. The plant's accident management procedures can be examined to determine if the operators will depressurize the RCS. We note that many plants can depressurize even in station blackout accidents because the PORVs have DC power. Recent SCDAP/RELAP5 calculations for Zion, Surry, ANO-2, and Calvert Cliffs support a body of evidence indicating that natural circulation processes will result in hot leg or surge line failure long before melt relocation to the lower plenum and bottom head failure. These natural circulation processes will lead to spontaneous and complete depressurization of the RCS for core melt accidents that involve no operator intervention. Thus, in station blackout accidents and in recovered accidents there is a high likelihood that the RCS will be depressurized at the time of vessel breach.

Recovery attempts without depressurization could have various consequences. Recovery at Three Mile Island-II (TMI-II) did not immediately arrest the core melt progression, but it was instrumental in preventing lower head failure. On the other hand, the margin to failure seems to have been small and recovery actions disrupted energy transport to the hot legs and surge line, thus preventing their failure. Consequently, attempts to demonstrate low HPME probabilities must address both spontaneous depressurization and the consequences of recovery. The necessary plant-specific information may be summarized from the IPEs, but the basis for the utilities quantifications should be reviewed. For perspective, the NUREG-1150 study for Sequoyah showed that ~40 percent of the core damage accidents involved accident recovery in sufficient time to preclude vessel failure. Resolution can be

achieved solely on HPME probabilities if their likelihood is shown to be ≤ 0.1. If independent resolution is not achieved, then HPME probabilities can be combined with the CCFPs to complete an integrated approach to resolution.

3.0 PROBABILISTIC FRAMEWORK

The probabilistic framework can be structured in the manner illustrated in Figure 2. As shown in this figure, the initial melt parameters are to be quantified as independent probability density functions, representing modeling uncertainty in the parameters. Variations from stochastic processes are assessed as insignificant relative to modeling uncertainty. These functions are formed into a joint probability density function and then combined with a causal relation (CR1) for the containment load, under the parameter distribution function that represents model uncertainty for the DCH processes, coherence ratio (R_t), to obtain a probability density function for the peak containment pressure. This distribution function for peak containment pressure is combined with the set of containment fragility curves (probabilistically distributed themselves) to obtain a probability distribution of containment failure frequency. In the current assessments, only a single fragility curve is available, but the discussion here has been generalized to accommodate desired improvements in information. Each fragility curve is expressed in terms of failure frequency, and this frequency expresses the statistically meaningful variations (based on actual experience) in containment strength. These containment strength variations are due to variations in material and workmanship and are characterized by the fraction that failed in a nominally similar population of structures subjected to the same load. On the other hand, the probability assigned to each fragility curve expresses a subjective degree of belief as to the appropriateness of it in meeting the intended task.

Sandia has developed software to perform either traditional Monte Carlo sampling or stratified Monte Carlo sampling. The software, called LHS, is user friendly and has an established quality assurance pedigree, including code assessment and verification. Sandia chose to use this numerical tool based on Latin hypercube sampling (LHS) to propagate distributions through the probabilistic framework. The resulting software was applied in NUREG/CR-6075, Supplement 1 (Pilch et al. 1994b), where it is described more fully in Appendix B. The same software was used in NUREG/CR-6109 (Pilch et al., 1995a), and it is used here without modification.

4.0 QUANTIFICATION OF INITIAL CONDITIONS

4.1 Introduction

DCH has traditionally been examined for a rather narrow range of hypothesized severe accident conditions: unmitigated station blackout at full system pressure; formation of a metallic blockage with an overlying ceramic crust in the core that contains a large fraction of core in a molten state; sudden failure of this blockage and crust, resulting in a massive relocation of the melt into the lower plenum; failure of a penetration passing through the lower head of the reactor pressure vessel; rapid ablation of the resulting hole in the RPV from 5 to about 40 cm (Pilch and Tarbell, 1985); and high-pressure melt ejection from the single hole followed by high-pressure steam blowdown. In attempts to address the DCH issue from either a systems point of view or an accident management point of view, intentional depressurization of the primary system has been examined (Hanson et al., 1990). Experiments have shown that the pressure must be very low (less than 1 MPa) to preclude the onset of dispersal from the

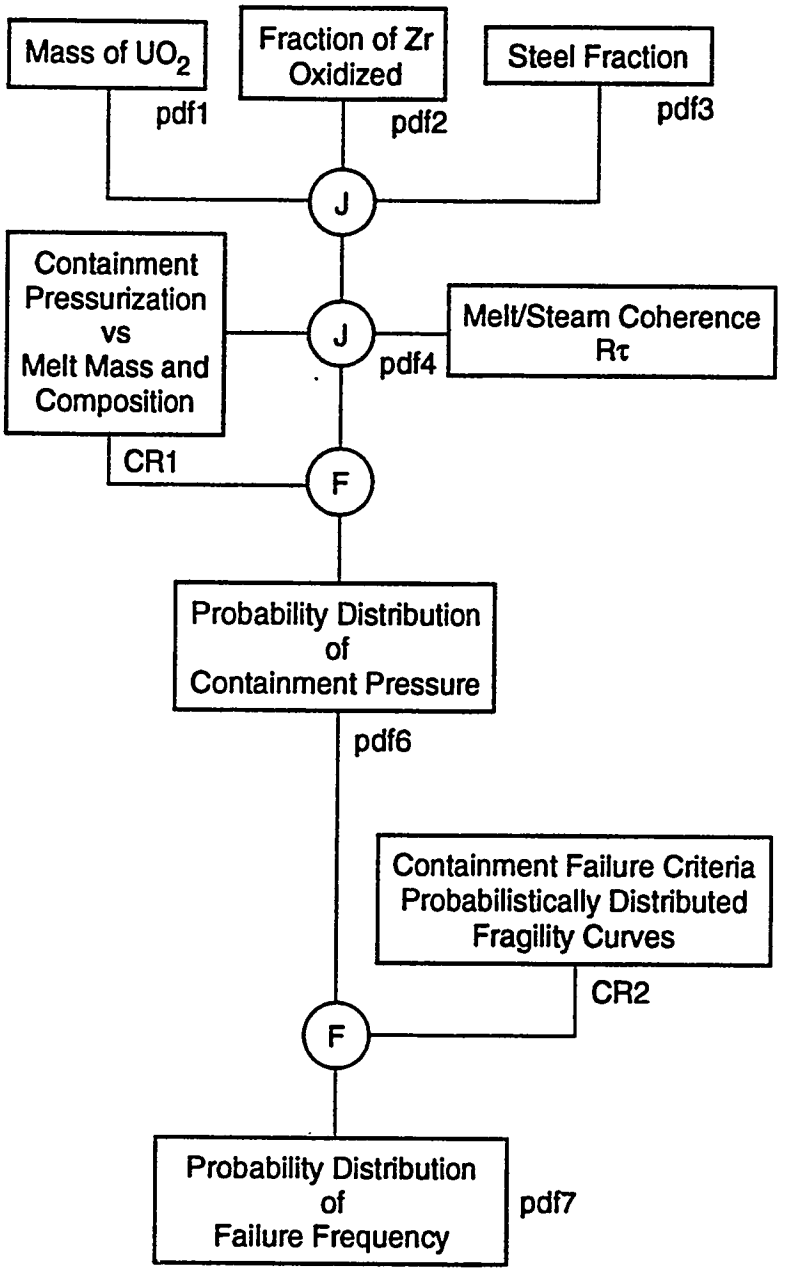

Figure 2. **The probabilistic framework for containment failure under direct containment heating scenarios. The (J) and (F) are the "joint" and "function" operations, respectively, as described in the text.**

cavity and to prevent the possibility of DCH (Tutu et al., 1988). Bounding calculations (Pilch and Tarbell, 1986) suggest that as little as 20 percent of the core (participating in DCH) could pose a threat for the containment. With this traditional understanding, containment-threatening loads from DCH can only be precluded if the RCS is almost fully depressurized. However, based on early CONTAIN calculations (Williams and Louie, 1988) the understanding developed in NUREG/CR-6075 (Pilch et al., 1994a, b), a substantial reduction of DCH loads is achieved without having to rely upon nearly complete depressurization of the RCS.

Quantification of melt release conditions was developed by attempting to envelop physically possible behavior in a comprehensive and systematic manner. This means that we needed to examine all reasonably conceivable severe accident scenarios, identify key aspects of their phenomena and respective ranges of behavior, and establish the few scenarios that envelop the DCH challenge to the containment.

Reviewers raised the following questions (Appendix A in Pilch et al., 1994b) regarding the completeness of the splinter scenarios considered in NUREG/CR-6075 (Pilch et al., 1994a) for the Zion application:

1. Can full-system pressure cases be ruled out?

2. Should operator intervention scenarios be analyzed?

3. Can dry core scenarios lead to melting and relocation of the metal (Zr) blockage from the core to the lower plenum?

Generally, the reviewers characterized initial condition quantifications in NUREG/CR-6075 (Pilch et al., 1994a) for Zion as "optimistic." Specifically, they expressed concern that ~8 MPa RCS pressure might not be adequately bounding, that the melt mass distributions were too narrow, and that the melt composition did not contain sufficient metallics (Zr and steel). The reviewers also stressed that SCDAP/RELAP5 analyses should be performed and used in a consistent manner in establishing initial conditions.

The NRC convened a working group to make recommendations on how to resolve these concerns for Zion. Their minutes are included in Appendix A of Pilch et al. (1994b). Residual concerns were fully resolved for Zion (Appendix A in Pilch et al., 1994b) and it is our intent to follow the prescription for quantifying initial conditions for all Westinghouse plants. The melt mass and composition distributions developed for Zion (a four-loop plant) in NUREG/CR-6075, Supplement 1, were used for all of the four-loop plants. For all of the three-loop plants, the melt mass and composition developed for Surry (a three-loop plant) in NUREG/CR-6109 were used. For two-loop plants, the prescription given in NUREG/CR-6075, Supplement 1, was used to develop the melt mass and composition distributions. These assessments are more completely described for all PWRs (including Combustion Engineering and Babcock & Wilcox plants) is given in Appendix B of NUREG/CR-6338 (Pilch et al., 1995b).

SCDAP/RELAP5 calculations were performed to provide confirmatory insight into the working group recommendations for Zion (Knudson, Appendix E in Pilch et al., 1994b) and for Surry (Knudson

and Dobbe, 1993; Quick and Knudson, Appendix E in Pilch et al., 1995a). The relevant insights are summarized as:

1. The amount of molten fuel at vessel breach never exceeded ~60% of the fuel inventory,

2. Insignificant quantities of zirconium relocate with the melt into the lower plenum,

3. Incore oxidation of zirconium ranged from 20-60%, and

4. Hot leg failure was induced long before lower head failure in station blackout accidents.

Quantification of our initial conditions envelop existing SCDAP/RELAP5 predictions. A complete tabulation of all initial conditions and their justification is given in NUREG/CR-6338 (Pilch et al., 1995b). The initial conditions can vary according to the splinter scenarios defined below.

4.2 Splinter Scenarios

Working group recommendations (Appendix A in Pilch et al., 1994b) focused on four splinter scenarios as shown in Figure 3. The intent was to place greater reliance on systems-level codes (SCDAP/RELAP5) in order to achieve better consistency between RCS pressure at vessel breach with melt mass and composition. Specifically, the working group emphasized that there were correlations between RCS pressure and melt composition; high RCS pressures and oxidic melts are correlated predominantly with operator intervention; metallic melts are correlated with reduced RCS pressures associated with pump seal leaks of sufficient magnitude that hot leg failure does not occur. The new scenarios either bound the scenarios in NUREG/CR-6075 or stress greater consistency in the conditions at vessel breach; thus, the new scenarios are intended to replace those in NUREG/CR-6075. The rationale leading to these splinter scenarios is discussed next.

The working group felt that there was no compelling need to analyze scenarios with penetration failures. The INEL lower head failure analysis (Rempe et al., 1993) and the OECD- NEA-TMI-2 vessel investigation project (Stickler et al., 1993) both concluded that rupture was much more likely than a penetration-type failure. Marshall (1988) performed some scoping experiments on tube ejection. Specifically, he confirmed that binding caused by differential thermal expansion could prevent ejection of a penetration from the lower head (for the conditions and materials tested); however, ballooning of the lower head, which could induce ejection of a penetration as a precursor to rupture, was not modeled in these experiments. Fauske and Associates, Inc. (FAI) (Hammersley et al., 1993), under the sponsorship of the Electric Power Research Institute (EPRI), has examined melt penetration into in-core instrument guide tubes. Pressure-driven melt was observed to travel approximately 2 m, which is far enough to carry it well beyond the lower head. However, the melt mass is too small to threaten the integrity of the guide tube. These limited experiments confirm INEL and OECD conclusions that penetration-type failures are unlikely. NUREG/CR-6075 (Pilch et al., 1994a) showed that a penetration failure followed by ablation of the lower head would produce a hole about the same size as would be expected for a local rupture of the lower head. Finally, work reported in NUREG/CR-6075 (Pilch et al., 1994a) showed that predicted loads for rupture scenarios bound predicted loads for penetration failure scenarios; consequently, penetration failures need not be considered further in the extrapolation activities.

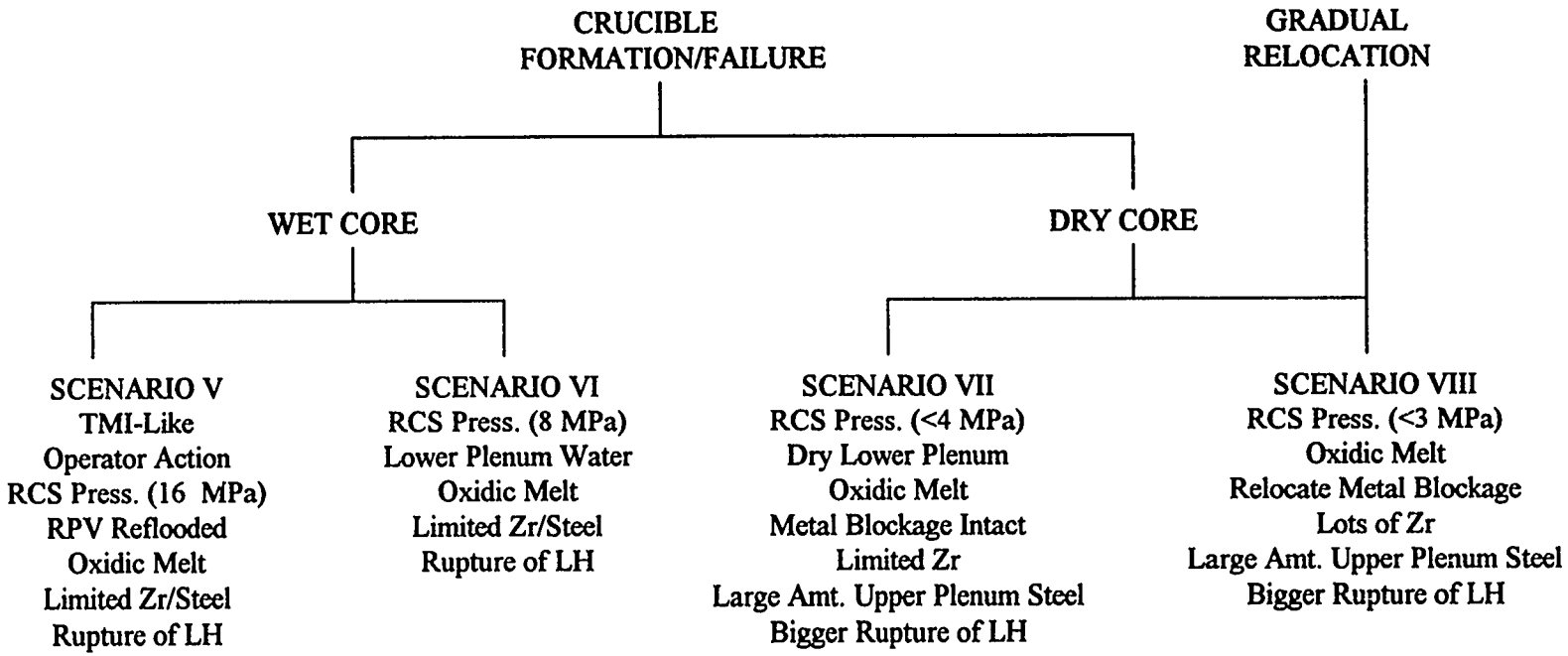

Figure 3. Splinter DCH scenarios reflecting working group recommendations.

Scenario VI is very similar to Scenario II in NUREG/CR-6075. Here, the working group wanted to emphasize the presence of water in the lower head. They recommended the addition of a new TMI-like scenario (Scenario V) characterized by reflooding and repressurization (~16 MPa) of the RCS as a result of operator actions. Scenarios V and VI were envisioned as having water in the core (at least covering the bottom) during much of the core melt progression; consequently, slumping core material would form a crucible which could fail only locally. The melt composition would be largely oxidic, with most unoxidized Zr permanently retained as a metal blockage in the core. Scenarios V and VI envelop those scenarios in which operators attempt to manage or recover an accident but fail to prevent severe core damage, which then leads to failure of the RPV lower head.

The working group then recommended consideration of scenarios (VII and VIII) in which core melting would proceed without water in the core region and largely without water in the lower plenum. It was their expectation that these scenarios would evolve to much lower RCS pressures (< 4 MPa) at vessel failure for typical small break loss-of-coolant accidents (SBLOCAs). Confirmatory calculations using SCDAP/RELAP5 indicate that complete depressurization of the RCS can be expected. At the lower pressures, the possibility of the upper plenum steel melting without also failing the hot leg becomes possible; thus, both scenarios VII and VIII augment the oxidic melt with large quantities of upper plenum steel. Scenario VIII is distinguished from Scenario VII in that the metal blockage is also assumed to remelt, allowing large quantities of unoxidized Zr to relocate to the lower plenum.

NUREG/CR-6075 considered a gradual relocation that progressed under high pressure (~8 MPa) with complete melting of upper plenum steel. Working group discussions pointed out that this scenario is overly conservative and that melting of upper plenum steel is strongly correlated with hot leg failure. In fact, gradual relocation has been predicted in only one MELPROG calculation for the Surry plant (Heames and Smith, 1987); and even here, hot leg failure was predicted to occur before core relocation into the lower plenum. Should a gradual relocation occur, working group members believed that it would look like Scenario VIII at the time of vessel failure.

SCDAP/RELAP5 calculations have been performed (based on working group recommendations) to confirm the basic features of Scenarios VII and VIII for Zion (Appendix C in Pilch et al., 1994b) and for Surry (Quick and Knudson, Appendix E in Pilch et al., 1995a). Three cases (representing short-term station blackout accidents) were run for Zion with SCDAP/RELAP5 representing the full spectrum of expected pump seal LOCAs: no leaks, 250 gpm/pump, and 480 gpm/pump. The key conclusion for Zion, however, is that hot leg failure will occur before core relocation for all pump seal LOCAs, leading to complete depressurization of the RCS before lower head failure. Earlier SCDAP/RELAP5 calculations for Surry (Knudson and Dobbe, 1993) also predicted that hot leg failure would occur before core relocation for these cases except for the 480-gpm/pump RCP leak. The earlier Surry calculations, however, were intentionally biased to accelerate core melt progression and lower head failure. Consequently, the NRC asked INEL to perform a best-estimate SCDAP/RELAP5 calculation for a 480-gpm/pump RCP leak at Surry. This best-estimate calculation also led to hot leg failure and complete depressurization of the RCS before lower head failure. Appendix E in Pilch et al. (1995a) presents these calculations in detail. Depressurized events such as this are of no interest to DCH. Consequently, Scenarios VII and VIII are not further analyzed in this report. Should the vessel fail, gravity drainage of melt into the cavity could pose risks that are beyond the scope of the current work.

In addition to RCS conditions, we must also envelop the range of containment conditions that can exist at vessel breach. Short-term station blackout accidents lead to the highest containment pressures (and steam concentrations) prior to vessel breach. These conditions are ascribed to Scenarios V and VI directly. Most DCH

relevant accidents involve operator intervention and the associated possibility that active containment cooling (i.e., fan coolers or sprays) could be operational. Such was the case at TMI-II. We analyze these splinters with no steam in the atmosphere (as an extreme), as Scenarios Va and VIa depending on whether the RCS pressure is high or at intermediate levels. Limited sensitivities were performed for containment pressures midway between the extremes noted above. The predicted loads were lower than the extremes, thus supporting the enveloping nature of the splinter scenarios.

In summary, DCH is only of concern if the reactor pressure fails while the RCS is still at elevated RCS pressure. Consequently, we exclude here from further analysis any scenarios with low RCS pressure at the onset of core damage, scenarios where the RCS is intentionally depressurized in compliance with accident management procedures or other forms of operator intervention, and sequences where the RCS unintentionally depressurizes as a natural consequence of core melt progression. SCDAP/RELAP5 calculations show that hot leg failure and RCS depressurization is likely unless the operators intervene in the accident. We envelop the RCS pressure with high pressure (16 MPa) and intermediate pressure (8 MPa) splinter scenarios, which are noted as Scenarios V and VI, respectively. We envelop containment conditions by considering splinters with and without active cooling in the containment; these are noted as Scenarios Va and VIa, respectively, depending on whether the RCS is at high or intermediate pressure. These four splinter scenarios adequately envelop the full range of RCS and containment conditions for the few DCH relevant scenarios.

5.0 QUANTIFICATION OF THE DCH PHENOMENA

The quantification of the DCH phenomenon is carried out by means of a causal relation (CR1) for the containment load. CR1 is fulfilled here by the two-cell equilibrium model, which is developed in Appendix E of NUREG/CR-6075 (Pilch et al., 1994a). Refinements to the hydrogen combustion models are documented in Appendix E of NUREG/CR-6075, Supplement 1 (Pilch et al., 1994b). In the TCE model, the containment pressurization can be written in terms of the various energy sources (blowdown, latent and sensible heat of debris, oxidation of metallic debris constituents, and hydrogen combustion) that can contribute to DCH,

$$\frac{\Delta P}{P_c^0} = \eta \frac{\Sigma \Delta E_i}{U^0(1 + \psi)}, \qquad (1)$$

where η is an efficiency of containment pressurization due to the combined processes of blowdown, heating of the atmosphere, and hydrogen combustion. The efficiency accounts for compartmentalized geometry of the containment and accounts for mitigation that is due to the noncoherence of debris dispersal and blowdown processes. The TCE model has been validated against the extensive database that is summarized in NUREG/CR-6075 (Appendix E). The TCE model attempts to represent the dominant processes contributing to DCH loads using a fast running code that meets the needs of the issue resolution effort; there is no claim that it captures every detail of DCH phenomenology.

Appendix C of NUREG/CR-6109 (Pilch et al., 1995a) gives an overview of other available models that have been used to predict DCH loads. In particular, the convection limited containment heating (CLCH) model (Yan and Theofanous, Appendix D in Pilch et al., 1994a) has been used (along with TCE) in resolution of the DCH issue for Zion, where TCE and CLCH gave similar results. The CONTAIN code has also been used extensively in DCH analysis of containment loads. Appendix G in NUREG/CR-6109 (Pilch et al., 1995a) compares CONTAIN and TCE predictions for conditions near the upper end of our distributions. CONTAIN

predicts loads comparable to or less than the TCE model. Consequently, we do not expect different modeling approaches to yield significantly different loads for comparable conditions.

NUREG/CR-6075 (Pilch et al., 1994a) identified the need to catalog the extent of cavity flooding prior to vessel breach. This is accomplished in Section C.2.3 of NUREG/CR-6338 (Pilch et al., 1995b), where assessments are taken from the IPEs under two limiting cases: with/without injection of the RWST into the containment. The assessments are quite plant-specific, but cavities are predominantly dry (26 dry, 11 wet, 4 unknown) if the refueling water storage tank (RWST) is not injected, and predominantly flooded (21 flooded, 11 wet, 7 dry, 2 unknown) if the RWST discharges fully. A deeply flooded cavity usually, but not always, means that the lower head of the RPV is at least partially submerged in water increasing the potential for in-vessel retention. Consistent with limited data, we ignore the potential impact of cavity water in our analyses.

We further categorize reactor cavities as *excavated* (29 plants) or *free standing* (12 plants). Free standing cavities are potentially vulnerable to damage in the event of high cavity pressures resulting from explosive or non-explosive fuel coolant interactions (FCIs) in the cavity. The failure pressure for each free standing cavity is not known; but should cavity failure occur, the debris will be dispersed onto the containment floor thus minimizing DCH interactions. Structural damage has the potential to enhance dome transport also in some unquantifiable manner; however, containment loads are insensitive to dome carryover in plants with high compartmentalized geometry. Excavated cavities are not vulnerable to damage from high cavity pressures. Detailed assessments of FCIs and their impact on cavity structures is outside the scope of this paper.

The working group discussions from NUREG/CR-6075, Supplement 1 (Appendix A in Pilch et al., 1994b) defined two new scenarios (V and VI) which involve significant quantities (~10-75 mt) of water that would be coejected with the melt into the reactor cavity. This is a situation that has not been addressed by the existing database; however, the working group (Appendix A in Pilch et al., 1994b) expressed an opinion that water in the primary system at vessel breach is expected to mitigate the impact of DCH. We note that a related experiment involving large quantities of cavity water (Allen et al., 1993; 1994) suggests that DCH energies went entirely into vaporizing water, pressurizing the containment to levels comparable to containment pressures observed in (essentially) dry DCH tests. RPV water (unlike cavity water) will partially flash to steam during isentropic blowdown. The contribution to containment pressure from this mechanism is less than ~0.075 MPa for ~75 mt of water in Zion. The calculations and results presented here are performed by ignoring any impact of coejected water. The margins to a significant DCH threat are high enough for Westinghouse plants so that the impact of coejected water can be ignored in these analyses. However, there are substantial uncertainties concerning the amounts and enthalpies of RPV water present at vessel breach, and additional study of the effects of coejected water would be warranted if future work indicates that large amounts of near-saturated water could be present. Towards this end, the NRC is sponsoring a 1:10th scale experiment in Calvert Cliffs geometry (CE) that will address the issue of coejected water. These experiments are scheduled for completion in the winter of 1995.

Most inputs to the TCE model are related to initial conditions and material properties. Four supplemental phenomenological models are required to complete evaluation of the TCE model:

1. a model for the coherence ratio as a function of hole size and cavity geometry,
2. a model for the hole size,
3. a model for the amount of preexisting hydrogen burned on DCH time scales, and
4. a model for the amount of dispersed melt that is transported to the dome.

Quantification of the second and third elements is consistent with prior efforts (Pilch et al., 1994a,b) and requires no additional explanation here. The first and fourth elements require special treatment when extrapolating beyond the Zion/Surry database.

Appendix E in NUREG/CR-6075 (Pilch et al., 1994a) develops a correlation for the coherence ratio based on experiment values obtained by a procedure best suited to the TCE model. The correlation can be expressed as

$$R_\tau = \frac{\tau_e}{\tau_b} = C_{R\tau}\, f_d \left(\frac{T^0_{RCS}}{T^0_d}\right)^{1/4} \left(C_d\, \frac{M^0_d}{M^0_g}\, \frac{A_h V^{1/3}_{cav}}{V_{RCS}}\right)^{1/2}, \qquad (2)$$

where $C_{R\tau}$ is a cavity-specific (weakly) multiplier that is determined from experiment data.

The database on which the coherence ratio correlation is based contains Zion-like geometries and Surry-like geometries, and the lead constant on the correlation is a weak function of the cavity type. For the purpose of quantifying the coherence constant and a relative standard deviation for each plant, we have categorized all Westinghouse cavities into one of three groups: Zion-like, Surry-like, and other. We have consulted the IDCOR descriptions of reactor cavities and applied our own subjective assessments based on IPE figures when making the assignments. Our basis is described more fully in Appendix C of NUREG/CR-6338 (Pilch et al., 1995b).

We define Zion-like cavities as having a U-tube layout with a slanted riser section, and we define Surry-like cavities as having a U-tube layout with a vertical riser section. Only two plants, South Texas 1 & 2, can not be characterized as Zion-like or Surry-like. Westinghouse cavities (41 total) are 27 percent Zion-like, 68 percent Surry-like, and 5 percent neither. There are variations within these groupings, so it is useful to explore how sensitive loads are to variations in the coherence ratio that could potentially arise due to variations in cavity geometry. Towards this end, sensitivities were run for Zion, Surry, and South Texas. A 30% increase in the recommended coherence produced only ~ 1% increase in containment loads.

Having further grouped the cavity designs, we assign the lead constant and relative standard deviation appropriate to Zion to all Zion-like cavities. A similar procedure is followed for Surry. Only two plants, South Texas 1 & 2, can not be characterized as Zion-like or Surry-like. In the case of South Texas 1 & 2, we biased (in the conservative direction) the lead constant for the combined Zion/Surry database by one standard deviation and then assigned the relative standard deviation appropriate to the combined database to the biased correlation. Uncertainties resulting from a geometry significantly outside the current database are bounded in this fashion while still maintaining a generous uncertainty distribution.

There are two primary debris transport pathways from the reactor to the containment dome in Westinghouse plants: (1) through the annular gap between the RPV and the biological shield wall, and (2) from the in-core instrument tunnel through the lower compartments. We express the dome transport fraction as

$$f_{dome} = f_{gap}(1 - f_{noz/shld}) + f_{sub}(1 - f_{gap}). \qquad (3)$$

Section C.3 of NUREG/CR-6338 (Pilch et al., 1995b) quantifies the various contributions to dome transport for each Westinghouse plant; however, we briefly summarize our approach. The gap contribution is determined

primarily by available flow areas, and the subcompartment contribution is determined by inertially dominated flow through the seal table room. Thus, to first order, we expect dome transport to be independent of RCS pressure. The gap contribution is determined primarily by available flow areas, and the subcompartment contribution is determined by inertially dominated flow through the seal table room. Thus, to first order, we expect dome transport to be independent of RCS pressure and constant for all scenarios. Although it is within the capabilities of the existing methodology and coding, uncertainty distributions on dome transport were not considered in the belief that the current quantifications are adequately bounding. We performed an arbitrary sensitivity study for the most sensitive plant (H.B. Robinson) and for the most sensitive scenario (VIa). The dome carryover fraction was increased by 30 percent from 0.621 to 0.807, and this resulted in only a 3 percent increase in the loads at the upper end of the loads distribution.

Transport of debris through the gap is calculated from a simple area ratio,

$$f_{gap} = \frac{A_{gap}}{A_{gap} + A_{cavity}}. \qquad (4)$$

This simple model was developed and validated against the DCH database in Appendix I of NUREG/CR-6075 (Pilch et al., 1994a). Based on experiments conducted by Bertodano (1993), we take nominal credit ($f_{noz/shld}$ ~0.10) for the missile shield and diversion of gap flow back into the subcompartments through the nozzle cutouts in the biological shield wall.

After reviewing the IPE drawings of all 41 Westinghouse (W) plants, we were able to categorize the lower compartment geometries into four distinct types (1) Zion-like (17 plants); (2) Surry-like (15 plants); (3) two-loop plants (6 plants); and (4) others (3 plants). For all of the plants that are Zion or Surry-like, a transport fraction (f_{sub}) from the cavity exit to the upper dome of 0.05 will be used in the extrapolation calculations, which is consistent with NUREG/CR-6075 and NUREG/CR-6109. In all of these plants, there are at least two floors between the cavity exit and the upper dome (usually the seal table room floor and ceiling, which is the operating deck level) and there are no significant line-of-sight debris transport pathways to the upper dome.

We note that the Zion and Surry experiments typically showed ~9 percent dome transport, which contains an unspecifiable amount of contaminants such as concrete. The quantification used here (0.05) is deemed conservative:

a) because the experiments did not model the vast array of in-core instrument guide tubes that may be dispersed from the cavity with the debris (Allen et al., 1990),

b) because the experiments did not model the steel hatches or "penthouses" (which restrict personnel access to the cavity) that will be blown upward into the seal table opening,

c) because most of the experiments did not model the seal table and because the seal table did not fail or fail completely in those experiments (Blanchat et al., 1994) that did model the seal table,

d) because the experiments did not model any of the equipment in the seal table room, and

e) because most of the experiments did not model the "plug" in the roof of the seal table room and because the plug was not always dislodged in the experiments (Allen et al., 1994) that did model the plug.

We note that more recent separate effects experiments for Zion (Wu, 1995) conducted at Purdue show dome carryover fractions of ~ 3 - 5% for the conditions of interest here. The enhanced carryover in the SNL/ANL IET tests could have resulted from the distorted cavity exit which was 2.7 times longer than prototypic. Wu's experiment show that dome carryover is comprised of a line-of-sight contribution that passes through the seal table room and very fine particles (~ 60 μm) that are carried by gas through the subcompartments and through vents into the dome. These very small particles are not fully effective when they reach the dome because oxidation is likely complete and some heat transfer has occurred prior to their arrival in the dome. We note that the TCE model is conservative in this regard because all debris transported to the dome is considered to be fresh, carrying its full undiluted energy content.

The two-loop plants have two floors between the cavity exit and the upper dome, i.e., the seal table room floor and the operating deck floor. However, there is a direct line-of-sight debris transport pathway that will allow some debris dispersal directly to the dome should the seal table fail. There are three plants (H.B. Robinson and South Texas 1 & 2) that are categorized as "other" in Table C.5 of NUREG/CR-6338. These plants do not look either like Zion or Surry and do not appear to meet the criteria for using the debris transport fractions used for Zion in NUREG/CR-6075 and for Surry in NUREG/CR-6109. The H.B. Robinson plant has two floors but appears to have significant direct line-of-sight debris transport pathways to the upper dome. In South Texas 1 & 2, the instrument guide tubes are sealed by 2 feet of concrete and the only debris transport pathway out of the cavity besides the RPV annular gap is through a manway that leads to a tortuous path to the upper compartments in the containment. There is no direct vertical debris transport pathway from the cavity except through the annular gap between the RPV and biological shield wall, so for South Texas 1 & 2 the fraction of debris that can be transported through the lower compartments is assumed to be zero.

Debris transport through line-of-sight flow paths to the dome is controlled by flow into and out of the seal table room,

$$f_{sub} = \min\left\{\frac{A_{str}}{\frac{1}{2}A_{cav\,exit}};1\right\}\min\left\{\frac{A_{op\,deck}}{A_{str}};1\right\} - 0.05, \qquad (5)$$

where nominal credit (0.05) is taken for the last array of equipment and structures that could impede flow into or out of the seal table room. These include: steel hatches or "penthouses" which restrict personnel access to the cavity, partial failure or nonfailure of the seal table, the array of in-core instrument guide tubes and their support structures that will be dispersed from the cavity with the debris, and equipment in the seal table room. A factor of ½ is multiplied by the area of the cavity exit ($A_{cav\,exit}$) because DCH experiments indicate that virtually all of the debris is ejected from the half of the opening furthest from the RPV.

6.0 QUANTIFICATION OF CONTAINMENT FRAGILITY

The Individual Plant Examinations (IPEs) for all operating Pressurized Water Reactors (PWRs) in the U.S. were assembled and containment fragility curves obtained. The containment capacity results from each of the IPEs were examined and briefly reviewed and the probability of containment failure was taken from them. In

many cases, this consisted of fragility curves showing pressure versus cumulative failure probability. In other cases, a mean or median failure pressure was specified along with uncertainty bounds. In some cases, only curves or points for various failure modes were given and a total probability of failure had to be constructed. In all these situations, a single fragility curve resulted that was intended to reflect both modeling uncertainty and stochastic uncertainties due to material property variations. In only two cases, confidence limits were derived and reported. Confidence limits are used to separate modeling uncertainties from stochastic uncertainties. A detailed assessment of the technical basis for the IPE fragility curves is beyond the scope of this paper.

For those IPEs presenting only a single curve, the curve was digitized, curve-fit with a spline program and failure probabilities determined at intervals of 1 psig. For IPEs which reported medians and uncertainties, a curve was developed and failure probabilities determined at intervals of 1 psig. The few which reported only median, 5 percent and 95 percent values, were fit to either a log-normal distribution, normal distribution or 3rd order spline function in order to get the best fit and failure probabilities determined at 1 psig intervals. In most situations where this occurred, only a third order spline provided an adequate fit to the three constraints.

Many of the IPE containment capacity analyses did not consider temperature or stated that increased temperatures would have little effect on the capacity. Other IPEs performed the analysis at either single or multiple accident temperatures. For those which determined the capacity at different temperatures, the analysis closest to 400 K (260°F) was selected as best representing the accident temperatures expected in the reactor containment building at the time of vessel breach.

We observed that the licensee's level of effort and our estimate of the reliability of these containment fragility curves varied significantly. In some cases, a detailed analysis was performed for every possible failure mode and an overall cumulative failure curve was determined by combining each mode of failure, while some IPEs simply used containment fragility curves derived from other containments or simply shifted other plant's fragility curves based on what they determined to be the difference in ultimate capacity.

Appendix D of NUREG/CR-6338 (Pilch et al., 1995b) briefly discusses how the fragility curves were determined from each IPE (when given enough information). In addition, the process of digitizing, fitting and tabulating the curves or data given in the IPEs is discussed for every plant, and the detailed results are also tabulated in Appendix D. We interpret our fragility curves as *mean* values, and our compilations, to the extent possible, strive for consistency in this regard.

Functional representations of fragility are subject to possible error when extrapolated to low failure frequencies because excessive extrapolation to low failure frequencies could lose or violate the physical basis on which most of the curve rests. In other cases, some IPEs conservatively tie the low end of the fragility curve to the design pressure. Consequently, the IPE fragility curves might be quite conservative in the tails.

On the other hand, the digitizing process is subject to human error and is dependent on the quality of the working curve. In a few cases, we supplied a curve fit to median, 5 percent, and 95 percent values, and extrapolation to lower failure frequencies may involve error. We will perform a sensitivity study by arbitrarily biasing the fragility curve 0.1 MPa to the left in order to assess the potential impact of these uncertainties.

Table 1 provides a concise summary of key plant-specific fragility data for each Westinghouse plant. The plants are grouped into one of four classes depending upon the type and construction of the containment. We see that large variations in containment strengths exist. H.B. Robinson has the least robust containment with a failure pressure of 88 psig at a failure frequency of 10 percent. Seabrook is the strongest containment with a failure pressure of 186 psig at the same failure probability. Thus, we conclude that a containment's fragility is plant-specific. It is to be anticipated that the fragility curves derived for a specific containment are sensitive to local design details, tolerances, and the design philosophy used for that particular containment. While it is likely that various submodels representing different local containment failure modes may be applicable to a variety of containments of a given type, it is also true that the combination of failure mechanisms existing in a given containment is unique. Thus, the reader is cautioned against reading any generic applicability into the fragility curves developed for any specific containment.

A common rule-of-thumb states that the ultimate capacity of a containment is ~ 2 - 3 times its design pressure. Table 1 confirms this rule-of-thumb, but the relative standard deviation is large, ~20 percent. Furthermore, the summary statistics for all entries indicates that you do better simply by citing a failure pressure (at a given frequency) based on the population mean. Consequently, the design pressure is a poor indicator of a containment's ultimate capacity.

We have provided summary statistics for each class of containment thinking that improvement could be realized by examining like kinds. Only Class 2 and Class 3 have sufficient entries for the statistics to be insightful. Unfortunately, no decisive improvement over population statistics is realized. Consequently, the DCH extrapolation study cannot benefit by grouping analyses based on the type of containment. We therefore use the plant-specific IPE fragility curve in our analyses.

Only two plants reported confidence limits (i.e., probability levels) on their fragility curve. Callaway (W) and Palisades (CE) are both large dry containments with a post-tensioned concrete cylinder with a steel liner. The high confidence fragility curve for these plants can be obtained (approximately) by shifting the mean curve to the left by ~0.1 MPa (15 psig) for Callaway and by ~0.07 MPa (10 psig) for Palisades. All other plants combine stochastic and modeling uncertainties into a single curve.

7.0 RESULTS AND SENSITIVITIES

Each scenario identified in Section 4, supplemented by the respective coherence ratio distribution and the plant-specific IPE fragility curve of Section 6, was run through the arithmetic defined by the probabilistic framework of Section 3 to produce a probability distribution for the containment pressure. Finally, the containment failure probability was computed. The process was repeated for all Westinghouse plants with large dry or subatmospheric containments using plant-specific input. The calculations were carried out using the computer code TCE/LHS as listed in Appendix B of NUREG/CR-6075, Supplement 1 (Pilch et al., 1994b) with 10,000 samples.

The figure of merit for DCH resolution is the mean (best estimate) conditional containment failure probability (CCFP), which is based on the mean containment fragility curve. Table 2 summarizes the results for each plant. The mean CCFP is ≤ 0.01 for each plant. Based on the merits of the screening study alone, DCH is considered resolved for all Westinghouse plants with large dry or subatmospheric containments, and no additional analyses are required.

Table 1 Similarity of containment fragility

PLANT	Design Press.	Cont. Press (psig) @			Cont. Press/Design Press @		
	psig	Prob.=0.01	Prob.=0.1	Prob.=0.5	Prob.=0.01	Prob.=0.1	Prob.=0.5
Class 1: Large Dry Containment; Steel Cylinder							
Kewaunee	46	113	130	150	2.46	2.83	3.26
Prairie Island 1,2	41	113	130	151	2.76	3.17	3.68
Class 2: Large Dry Containment; Reinforced Concrete Cylinder With Steel Liner							
Comanche Peak 1,2	50	95	104	114	1.90	2.08	2.28
Diablo Canyon 1,2	47	100	117	140	2.13	2.49	2.98
Indian Point 2	47	87	101	126	1.85	2.15	2.68
Indian Point 3	47	102	115	134	2.17	2.45	2.85
Salem 1,2	47	75	92	112	1.60	1.96	2.38
Seabrook	65	164	186	216	2.52	2.86	3.32
Shearon Harris	45	104	121	153	2.31	2.69	3.40
Class 3: Large Dry Containment; Post-Tensioned Concrete Cylinder With Steel Liner							
Braidwood 1	61	81	101	124	1.33	1.66	2.03
Braidwood 2	61	81	90	98	1.33	1.48	1.61
Byron 1	61	81	101	124	1.33	1.66	2.03
Byron 2	65	81	90	98	1.25	1.38	1.51
Callaway	60	104	123	134	1.73	2.05	2.23
Farley 1,2	54	98	105	114	1.81	1.94	2.11
Ginna	60	115	121	129	1.92	2.02	2.15
H.B. Robinson	42	70	88	130	1.67	2.10	3.10
Point Beach 1,2	60	127	146	161	2.12	2.43	2.68
South Texas 1,2	56	71	88	113	1.27	1.57	2.02
Summer	55	105	127	141	1.91	2.31	2.56
Turkey Point	59	118	131	150	2.00	2.22	2.54
Vogtle 1,2	52	100	119	139	1.92	2.29	2.67
Wolf Creek	60	88	108	128	1.47	1.80	2.13
Zion 1,2	47	97	118	133	2.06	2.51	2.83
Class 4: Subatmospheric Containment; Reinforced Concrete Cylinder With Steel Liner							
Beaver Valley 1&2	45	81	101	128	1.80	2.24	2.84
Millstone 3	45	88	103	118	1.96	2.29	2.62
North Anna 1,2	45	81	101	129	1.80	2.24	2.87
Surry 1,2	45	81	101	129	1.80	2.24	2.87
Summary Info							
Mean on Total	52.7	96.8	113.1	133.3	1.9	2.2	2.6
STD on Total	7.4	19.6	20.4	22.1	0.4	0.4	0.5
STD/Mean Total	0.14	0.20	0.18	0.17	0.20	0.19	0.20
Mean on Class 2	49.7	103.9	119.4	142.1	2.1	2.4	2.8
STD on Class 2	5.9	26.3	28.8	33.0	0.3	0.3	0.4
STD/Mean Class 2	0.13	0.25	0.24	0.23	0.14	0.13	0.14
Mean on Class 3	56.9	94.5	110.4	127.7	1.7	2.0	2.3
STD on Class 3	5.9	16.7	17.2	16.7	0.3	0.3	0.4
STD/Mean Class 3	0.10	0.18	0.16	0.13	0.18	0.18	0.19

Table 2 CCFP results

PLANT	Number of	Mean CCFPs				Est. CCFPs Using Biased Fragility			
	Loops	Scn V	Scn Va	Scn VI	Scn VIa	Scn V	Scn Va	Scn VI	Scn VIa
Class 1: Large Dry Containment; Steel Cylinder									
Kewaunee	2	0	0	0	0	0	0	0	0
Prairie Island 1,2	2	0	0	0	0	0	0	0	0
Class 2: Large Dry Containment; Reinforced Concrete Cylinder With Steel Liner									
Shearon Harris	3	0	0	0	0	0	0	0	0
Comanche Peak 1,2	4	0	0	0	0	0	0	0	0
Diablo Canyon 1,2	4	0	0	0	0	0	0	0	0
Indian Point 2	4	0	0	0	0	0	0	0	0
Indian Point 3	4	0	0	0	0	0	0	0	0
Salem 1,2	4	0	0	0	0	0	0.001	0	0.001
Seabrook	4	0	0	0	0	0	0	0	0
Class 3: Large Dry Containment; Post-Tensioned Concrete Cylinder With Steel Liner									
Ginna	2	0	0	0	0	0	0	0.001	0
Point Beach 1,2	2	0	0	0	0	0	0	0	0
Farley 1,2	3	0	0	0	0	0	0	0	0
H.B. Robinson	3	0	0.001	0.004	0.004	0.002	0.010	0.020	0.028
Summer	3	0	0	0	0	0	0	0	0
Turkey Point 3,4	3	0	0	0	0	0	0	0	0
Braidwood 1	4	0	0	0	0	0	0	0	0
Braidwood 2	4	0	0	0	0	0	0	0	0
Byron 1	4	0	0	0	0	0	0	0	0
Byron 2	4	0	0	0	0	0	0	0	0
Callaway	4	0	0	0	0	0	0	0	0
South Texas 1,2	4	0	0	0	0	0	0.001	0	0.003
Vogtle 1,2	4	0	0	0	0	0	0	0	0
Wolf Creek	4	0	0	0	0	0	0.001	0	0.001
Zion 1,2	4	0	0	0	0	0	0	0	0
Class 4: Subatmospheric Containment; Reinforced Concrete Cylinder With Steel Liner									
Beaver Valley 1&2	3	0	0	0	0	0	0.001	0.001	0.001
North Anna 1,2	3	0	0	0	0	0	0	0	0
Surry 1,2	3	0	0	0	0	0	0	0	0
Millstone 3	4	0	0	0	0	0	0.001	0	0

Most plants showed no intersections of the loads distributions with the fragility distributions. Only one plant, H.B. Robinson, showed a finite but negligible intersection of the load and fragility distribution for some of the scenarios. H.B. Robinson has containment loads that are about one standard deviation above the mean of all plants and has a significant line-of-sight flow path (i.e., a high dome transport fraction), which explains the higher loads. However, H.B. Robinson has the least robust containment of all the Westinghouse plants considered here. The higher loads for H.B. Robinson come about because of the higher dome transport fraction. The containment is actually somewhat larger than average compared to the fuel loading.

Severe accident issues, such as DCH, are judged based on their contribution to the mean containment failure probability, and this is the approach taken here. However, it is desirable and instructive to explore the margin in our analysis results. We address this need by recomputing the CCFPs for each plant using an estimate of the high confidence fragility curve or an arbitrarily biased fragility curve for each plant.

Only two plants reported confidence limits on their fragility curve, all other plants represent modeling and stochastic uncertainties in a single fragility curve. Callaway (W) and Palisades (CE) are both large dry containments having a post-tensioned concrete cylinder with a steel liner. The high confidence fragility curve for these plants can be obtained (approximately) by shifting the mean curve to the left by ~0.1 MPa (15 psig) for Callaway and by ~0.07 MPa (10 psig) for Palisades. For our study, we have also shifted the fragility curve of each plant 0.1 MPa to the left. This is equivalent to using high confidence fragility curves for Callaway and Palisades. This bias should be viewed as an arbitrary sensitivity study for all other plants.

All plants satisfy NRC's guidance that the CCFP ≤ 0.1 for DCH issue resolution using the biased fragility curves. Only H.B. Robinson shows CCFPs ≥ 0.01. Five additional sites show finite but negligible intersections with the fragility curves: Salem 1 & 2, Ginna, South Texas 1 & 2, Wolf Creek, and Beaver Valley 1 & 2. These are the more sensitive plants to DCH. NUREG/CR-6338 (Pilch et al., 1995b) provides a more complete ranking of plants based on sensitivity to DCH.

On average, intermediate RCS pressures (8 MPa) produced somewhat higher loads (0.530 MPa in Scenario VI and 0.574 MPa in Scenario VIa) than their higher RCS pressure (16 MPa) counterparts (0.454 MPa in Scenario V and 0.567 MPa in Scenario Va) at 99% probability level. This is attributed to the substantially larger melt masses (~20 mt more) ascribed to Scenarios VI and VIa compared to Scenario V and Va. We also note that scenarios with active containment cooling prior to vessel breach generally produced somewhat higher loads. Although failure of the RPV did not occur, the fan coolers were operational at TMI-II, which kept the steam concentration in the containment to negligible levels. Although the initial pressure in the containment is lower for those scenarios (Va, VIa) with active containment cooling, the final containment pressures following the DCH event are higher than similar scenarios (V and VI respectively) without active containment cooling. This is because a steam free atmosphere favors a more efficient contribution to DCH loads from combustion of preexisting hydrogen.

8.0 CONCLUSIONS AND RECOMMENDATIONS

This paper describes a process for extrapolating the methodology and scenarios developed in NUREG/CR-6075 and NUREG/CR-6075, Supplement 1 (Pilch et al., 1994a,b), to all other PWRs. The first step in the DCH issue resolution process is a screening phase in which loads versus strength comparisons are performed to evaluate the CCFP for each plant using plant-specific data. The results of the screening calculations show that

the CCFP based on the mean fragility curves is less than 0.01 for each Westinghouse plant with either a large dry or subatmospheric containment. In fact, only one plant showed a CCFP greater than 0.001. Thus, DCH is considered resolved for all Westinghouse plants, except those with ice condenser containments, and no additional analyses are required.

The CCFPs for each plant were recalculated using a biased fragility curve that is shifted to the left by 0.1 MPa. For Callaway and Palisades, the biased fragility curves are representative of high confidence fragility curves; and for all other plants, the biased fragility curves should be interpreted as arbitrary sensitivity studies. All plants have a CCFP less than the required success criterion of 0.1 even with biased fragility curves. Only H.B. Robinson has a CCFP greater than 0.01; for Scenario VIa, H.B. Robinson shows a CCFP of 0.028. H.B. Robinson appears to be the most sensitive of the plants analyzed because it has a large line-of-sight debris transport pathway to the containment dome and a containment fragility curve to the left of all other plants. Five other sites show finite but negligible intersections of the loads distributions with biased fragility curves: Ginna, Salem 1 & 2, South Texas 1 & 2, Wolf Creek, and Beaver Valley 1 & 2.

Three recommendations for confirmatory work were suggested in NUREG/CR-6075 and were addressed in this work. The recommendations from NUREG/CR-6075 are quoted below and are followed by a paragraph describing how the recommendation was addressed in NUREG/CR-6338 (Pilch et al., 1995b).

1. *Deeply Flooded Cavities*: "This plant-specific item is needed to identify any cases where geometry allows the build-up of water depths significantly higher than the condensate levels examined so far. Need for any additional evaluations will depend on the extent of such situations and on the particulars of each case."

   A plant-specific evaluation of the potential for having water in the cavity at vessel breach was performed and is provided in Table C.4 of NUREG/CR-6338. The plants are grouped as either dry (condensate water), wet, or flooded. If there is no RWST injection, then 26 plants will be dry, 11 plants will be wet, and 4 plants did not provide sufficient information. If the RWST tank empties, then 21 plants will be flooded, 11 plants will be wet, 7 plants will be dry, and 2 plants did not provide sufficient information. For cavities with significant amounts of water, existing analyses and experimental data indicate that HPME-induced containment loads are comparable to or less than the loads with dry cavities for oxidic melts. Table C.4 of NUREG/CR-6338 also classifies cavities as either excavated (29 plants) or free standing (12 plants). For cavities with significant amounts of water at vessel breach, the cavity loads due to fuel-coolant interactions could potentially damage or fail free standing cavities. Failure of a free standing cavity would not result in significantly higher DCH loads. In fact, if debris were dispersed directly into the containment basement, cavity failure might reduce the DCH load. Detailed assessments of potential FCIs and their impact on cavity structures was outside the scope of NUREG/CR-6338.

2. *System Pressure Level:* "Even though we show that melt expulsion with maximum primary system pressures do not lead to any significant concerns for Zion, we cannot categorically exclude system pressures above 8 MPa at this time for all plants. It may be worthwhile to determine if system pressures above 8 MPa can be excluded. This issue is explicitly addressed in integrated DCH issue resolution task."

   The initial conditions working group (NUREG/CR-6075, Supplement 1) recommended performing some DCH analyses at full system pressure to better envelop operator intervention accidents such as TMI-II. Scenarios V and Va were analyzed at 16 MPa and Scenarios VI and VIa were analyzed at 8 MPa. The splinter scenarios were analyzed at these high pressures even though SCDAP/RELAP5 analyses of Zion,

Surry, Calvert Cliffs, and Arkansas Nuclear One indicate that there is a high likelihood of system depressurization due to ex-vessel failures for station blackout scenarios without operator intervention.

3. *Containment Strength:* "It remains to be determined whether there are any significant deviations from the Zion fragility for containments of a similar class. Containment capability is affected by design details and must be examined on a plant-specific basis, possibly through the IPE or ongoing research sponsored by the NRC."

   Containment fragility has been compiled from the IPEs on a plant-specific basis and is summarized in Section 6 of this paper and compiled in Appendix D of NUREG/CR-6338. From these assessments, we made several important conclusions. The ultimate capacity of the containment does not correlate well with the design pressure. The average estimated failure pressure of all 41 plants at the 1 percent probability level is 97 psig with a standard deviation of ± 20 psig, i.e., the variation in plant fragilities is relatively large.

9.0 NOMENCLATURE

$A_{cav\ exit}$ = area of instrument tunnel exit
A_{cavity} = minimum flow area through the reactor cavity
A_{gap} = minimum flow area through the annular gap around the RPV
A_h = breach area in RPV
$A_{op\ deck}$ = area of the opening in the operating deck that is directly above the seal table
A_{str} = area of the seal table room opening
C_d = discharge coefficient (0.6)
$C_{p,w}$ = heat capacity of RPV steel
$C_{R\tau}$ = constant in coherence correlation
f_d = fraction dispersed
f_{dome} = fraction of dispersed debris that enters dome
f_{gap} = fraction of dispersed debris that enters the annular gap around the RPV
$f_{noz/shld}$ = fraction of dispersed debris that enters the RPV gap that flows back into the subcompartments through nozzle cutouts in the biological shield wall or that gets knocked down by the missile shield
f_{sub} = fraction of dispersed debris that enters the subcompartment and subsequently passes through to the dome
M^0_d = initial melt mass
M^0_g = initial RCS gas mass
P^0_c = initial containment pressure
R_τ = coherence ratio
T^0_d = debris temperature
T^0_{RCS} = RCS gas temperature
U^0 = total internal energy of containment atmosphere
V_{cav} = cavity volume
V_{RCS} = RCS volume

Greek

ΔE_i = energy contribution of DCH process
ΔP = pressure increase in containment due to DCH
σ = standard deviation
τ_b = characteristic blowdown time
τ_e = characteristic entrainment interval
η = pressurization efficiency
ψ = total heat capacity of dispersed debris divided by total heat capacity of the containment atmosphere

10.0 REFERENCES

Allen, M.D. et al. (1990). *A Demonstration Experiment of Steam-Driven, High-Pressure Melt Ejection: The HIPS-10S Test*, NUREG/CR-5373, SAND89-1135, Sandia National Laboratories, Albuquerque, NM.

Allen, M.D. et al. (1993). *Experiments to Investigate the Effects of Fuel/Coolant Interactions on Direct Containment Heating*, The IET-8A and IET-8B Experiments, SAND92-2849, Sandia National Laboratories, Albuquerque, NM.

Allen, M.D. et al. (1994). *Experiments to Investigate Direct Containment Heating Phenomena with Scaled Models of the Zion Nuclear Power Plant in the Surtsey Test Facility*, NUREG/CR-6044, SAND93-1049, Sandia National Laboratories, Albuquerque, NM.

Bertodano, M. Lopez de (1993). *Direct Containment Heating DCH Source Term Experiment for Annular Reactor Cavity Geometry*, Ninth Proceedings of Nuclear Thermal Hydraulics, 1993 ANS Winter Mtg., Nov. 14-18, 1993, San Francisco, CA, p. 111-120.

Blanchat, T.K. et al. (1994). *Experiments to Investigate Direct Containment Heating Phenomena With Scaled Models of the Surry Nuclear Power Plant*, NUREG/CR-6152, SAND93-2519, Sandia National Laboratories, Albuquerque, NM.

Hammersley, R.J. et al. (1993). "Experiments to Address Lower Plenum Response Under Severe Accident Conditions," *Proceedings of the International Topical Meeting on Probabilistic Safety Assessment* (PSA93), Clearwater Beach, FL.

Hanson, D.J. et al. (1990). *Depressurization as an Accident Management Strategy to Minimize the Consequence of DCH*, NUREG/CR-5447, U.S. Nuclear Regulatory Commission, Washington, DC.

Heames, T.J., and R.C. Smith (1987). "Integrated MELPROG/TRAC Analyses of a PWR Station Blackout," *Nuclear Engineering and Design*, Vol. 125, pp. 175-188.

IDCOR (1985). *Technical Support for Issue Resolution*, IDCOR, Technical Report 85.2, Fauske and Associates, Inc., Burr Ridge, IL.

Knudson, D.L., and C.A. Dobbe (1993). *Assessment of the Potential for High Pressure Melt Ejection Resulting from a Surry Station Blackout Transient*, NUREG/CR-5949, EGG-2689, EG&G Idaho, Inc., Idaho Falls, ID.

Marshall, B.W. (1988). *Reactor Safety Research Semi-annual Report July-December 1987*, NUREG/CR-5039, SAND87-2411, Vol. 2, p. 244, Sandia National Laboratories, Albuquerque, NM.

NRC (1992). *Severe Accident Research Program Plan Update*, NUREG-1365, Rev. 1, U.S. Nuclear Regulatory Commission, Washington, DC.

Pilch, M., and W.W. Tarbell (1985). *High Pressure Ejection of Melt from a Reactor Pressure Vessel: The Discharge Phase*, NUREG/CR-4383, SAND85-0012, Sandia National Laboratories, Albuquerque, NM.

Pilch, M., and W.W. Tarbell (1986). *Preliminary Calculations on Direct Heating of a Containment Atmosphere by Airborne Core Debris*, NUREG/CR-4455, SAND85-2439, Sandia National Laboratories, Albuquerque, NM.

Pilch, M.M. et al. (1992). "Counterpart and Replicate DCH Experiments Conducted at Two Different Physical Scales: The SNL/IET-1, 1R and the ANL/IET-1R, 1RR Experiments," Letter Report to the NRC, Sandia National Laboratories, Albuquerque, NM.

Pilch, M.M. et al. (1994a). *"The Probability of Containment Failure by Direct Containment Heating in Zion,"* NUREG/CR-6075, SAND93-1535, Sandia National Laboratories, Albuquerque, NM.

Pilch, M.M. et al., (1994b). *"The Probability of Containment Failure by Direct Containment Heating in Zion,"* NUREG/CR-6075, Supplement 1, Sandia National Laboratories, Albuquerque, NM.

Pilch, M.M. et al. (1995a). *"The Probability of Containment Failure by Direct Containment Heating in Surry,"* SAND93-2078, NUREG/CR-6109, Sandia National Laboratories, Albuquerque, NM.

Pilch, M.M. et al. (1995b). *"Resolution of the Direct Containment Heating Issue for All Westinghouse Plants with Large Dry Containments or Subatmospheric Containments,"* NUREG/CR-6338, SAND95-2381, Sandia National Laboratories, Albuquerque, NM.

Rempe, J.L. et al. (1993). *Light Water Reactor Lower Head Failure Analysis*, NUREG/CR-5642, EGG-2618, Idaho National Engineering Laboratory, Idaho Falls, ID.

Stickler, L.A. et al. (1993). *Calculations to Estimate the Margin to Failure in the TMI-2 Vessel*, TMI V(93)EG01, Idaho National Engineering Laboratory, EG&G Idaho, Inc., Idaho Falls, ID.

Tutu, N.K. et al. (1988). "Low Pressure Cutoff for Melt Dispersal from Reactor Cavities," in *Fourth Proceedings of Nuclear Thermal Hydraulics*, p. 29-37.

Williams, D.C. and D.L.Y. Louie (1988). "CONTAIN Analyses of Direct Containment Heating Events in the Surry Plant," ANS/ENS International Meeting, ANS Thermal Hydraulics Division, Washington, DC.

Wu, Q. (1995). "Transient Two Phase Flow and Application to Severe Nuclear Reactor Accidents," Ph.D. Thesis, Purdue University.

Zuber, N. et al. (1991). *An Integrated Structure and Scaling Methodology for Severe Accident Technical Issue Resolution*, Draft for Comment, NUREG/CR-5809, EGG-2659, EG&G Idaho, Inc., Idaho Falls, ID.

STATUS OF THE FARO/KROTOS MELT-COOLANT INTERACTIONS TESTS[a]

D. Magallon, I. Huhtiniemi, A. Annunziato, A. Yerkess, H. Hohmann
European Commission, Joint Research Centre
Safety Technology Institute, TP 421
I - 21020 Ispra (Va)

ABSTRACT

Results of FARO test L-19 are reported. It involved 155 kg of 80 w% UO_2+20 w% ZrO_2 at 3073 K quenched in 338-kg, 1-m-depth water at saturation at 5.0 MPa (i.e., 537 K). The test is compared with two former tests (L-06 and L-08) performed in similar conditions (1-m-depth water) but with reduced quantities of melt (18 and 44 kg, respectively). and with test L-14, performed with a similar quantity of melt (125 kg) but in 2-m-depth water. No fundamental differences with the former tests have been observed. Particularly, the quenching rate per unit melt mass was of the same order (0.5 MW). On the contrary, the portion of melt which remained as a cake on the bottom was larger (50% against a maximum of 30% in the previous tests. The possible reasons for these discrepancies are discussed. Recalculations of test L-19 by using COMETA and TEXAS are also reported and commented. Results from a new set of KROTOS tests conducted with Al_2O_3 to investigate further the differences already observed with corium melt are presented and discussed. In these tests the effect of melt superheat, water subcooling and ambient pressure on Al_2O_3/water system behaviour have been tested. In contrast with corium experiments, the results demonstrated that spontaneous explosions occur in the Al_2O_3/water system over all the range of parameters tested in highly subcooled conditions. Some TEXAS results for the latest KROTOS Al_2O_3 test, in which a violent steam explosion did occur, are presented and compared with experiment. During some KROTOS experiments there are large deformations of the bottom plate and hold-down bolts. Use is made of the 2-D axisymmetric code SEURBNUK-EURDYN to analyse these deformations of the test section and some results are presented.

1. FARO EXPERIMENTS

1.1 Background

The FARO tests have been designed to provide data on the integral corium melt jet/water mixing and quenching behaviour by using 150-kg-scale of UO_2-based melt in prototypical conditions. Basically, the penetration of the molten corium into the water of the lower plenum and its subsequent settling on the bottom head of the RPV are simulated.

Four tests performed in saturation conditions at 5.0 MPa with various quantities (18 to 151 kg) and compositions (UO_2-ZrO_2, UO_2-ZrO_2-Zr) of melt, and different depths of water (typically 1m and 2m) have been previously reported [1.1], [1.2]. In all the tests, significant breakup and quenching took place during the melt fall through the water. No steam explosion occurred. In the tests performed with a pure oxide UO_2-ZrO_2 melt, part of the corium (from 1/6 to 1/3) did not breakup and reached the bottom plate still molten whatever the water depth was. Data from test L-11, performed with 151 kg of UO_2-ZrO_2-Zr melt, suggest that full oxidation and complete breakup of the melt occurred during the melt fall through the

[a]The present FARO-LWR Test Programme is performed in collaboration with USNRC in the frame of Technical Exchange Agreement n° 4086-90-09 TG ISP USA.

water. A fraction of 64% of the total energy content of the melt was released to the water during this phase (~1.5 s), against 44% for a test performed in similar conditions but with a UO_2-ZrO_2 melt (L-14). The maximum temperature increase of the bottom plate was 330 K (L-14). The mean particle size of the debris ranged between 3.5 and 4.8 mm. These data have been extensively used for verification and validation of melt/water mixing codes such as CHYMES (AEA), COMETA (JRC), IFCI (SNL), IVA-KA (FZK), MC-3D (CEA) [1.3], and TEXAS (UW,JRC) [1.4].

Since October '94 experimental activities on FARO have included the execution of five tests (about one every 2.5 months), of which one only (L-19) was successful. It is worthwhile to mention briefly what induced the failure of four of the tests. In test L-15 the use of a new batch of ZrO_2 powder revealed to be inadequate and the melting of the corium could not be achieved. The former batch was used again for the next tests. In tests L-16 and L-17, amounts of melt around 150 kg were produced but remained trapped in the release vessel after delivery from the furnace, despite the release device functioned (see facility description in section 1.3). In fact, in L-17 about 8 kg of melt were delivered to the water through a hole of about 10 mm in diameter which formed in the centre of the corium front crust in the release vessel. The very reasons for failure of tests L-16 and L-17 are not fully understood. It is believed that, because of fatigue, the release vessel (which was the same used since test L-11) did not open properly. In L-18 the head of the furnace upper electrode was damaged before complete melting of the corium due to electrical power spikes. A spare electrode was available.

Thus, for performing FARO test L-19, the monitoring of the electrical power was modified for preventing spikes during the melting process, and a new release vessel was used. The results from this test are reported here. It involved 155 kg of w% 80 UO_2 + 20 ZrO_2 at 3073 K quenched in 330-kg, 1.1-m-depth water at saturation at 5.0 MPa (i.e., 537 K). The test concludes the series performed at 5.0 MPa system pressure. Comparisons with the former tests and progress in understanding the phenomena related to melt/water quenching are discussed. Test analyses by TEXAS [1.4] and COMETA [1.5] codes are presented.

1.2 FARO L-19 test objectives

The main objective for this test was to investigate the behaviour of a large mass (~150 kg) of dioxidic melt (80w%UO_2, 20w%ZrO_2) penetrating by gravity into a ~300-kg, 1-m-depth water pool at saturation temperature corresponding to 5.0 MPa, the cooling down of the melt debris and the early heating of the bottom plate. More specific objectives were the evaluation of the quenching rate of the melt during the penetration into water, the debris particle size distribution and the mass of fuel which has not experienced breakup.

Test L-19 was similar to tests L-06 and L-08 [1.1] for the water depth, having the same typical value of 1 m, but differed for the melt mass, with 155 kg of melt against 18 kg and 44 kg for L-06 and L-08, respectively. On the other hand, it was similar to test L-14 [1.2] for the melt mass (125 kg in L-14), but differed for the water depth (actually 1.1 m in L-19 against 2.05 m in L-14). Therefore, the most relevant issues to be investigated with L-19 was, on one hand, by comparison with L-06 and L-08, the effect of the quantity of melt, and on the other hand, by comparison with L-14, the effect of the water depth on melt fragmentation and quenching.

1.3 Test apparatus

A detailed description of the FARO facility and test procedure is provided in [1.2]. Only the features of special interest for test L-19 are mentioned here. The experimental arrangement is shown in Fig.1.1. The interaction vessel TERMOS is connected to the UO_2-ZrO_2 melting furnace via the release channel and isolated from it during interaction by the valve SO2. After melting in the FARO furnace, the melt is first delivered to the release vessel, and then released into the water. The test vessel TERMOS is connected

downstream to a condensing unit which operates only if the pressure in the interaction vessel reaches 9.3 MPa. The condensing unit is inerted with argon before the test.

Initially, the release vessel is at the same low pressure as the furnace (0.15 MPa). After transfer of the UO_2-ZrO_2 mixture to the release vessel, the intersection valve SO1 and the isolation valve SO2 are closed, and the release vessel is pressurised to the TERMOS pressure (i.e., 5.0 MPa) by using an argon supply. Upon pressure equalisation, the two melt catcher flaps automatically open. The lower flap allows the melt to be released to the water by gravity. The side flap, of the same diameter as the melt release flap, prevents against pressure differences between the release vessel and TERMOS during the melt release. After mixing with the water, the corium is collected in the debris catcher.

The principal quantities measured in the test vessel during the corium quenching are pressures and temperatures both in the freeboard volume and in the water, temperatures in the debris catcher bottom plate, water level swell. Tungsten ultrasonic temperature sensors are mounted in the release vessel for measuring the temperature of the melt. A total of about 250 signals are loaded to 6 different recorders of the data acquisition system. Pressure transducers and thermocouples are also installed in the various components of the condensing unit: piping, steam/water separator, condenser. A mass spectrometer is connected to the condenser for a qualitative indication of the gas composition. Water level measurements are made by differential pressure probes mounted both in the separator and in the condenser.

1.4 FARO L-19 test results

The experimental parameters and the main results from the test are summarised in Table 1.1. The melt temperature has been measured by a tungsten ultrasonic sensor installed in the outlet nozzle of the release vessel. A direct measurement of the duration of the release is not possible in the test conditions. The value indicated in the table has been calculated taking into account the actual geometry of the release vessel.

The pressure history in the TERMOS vessel, starting from the melt release time, is shown in Fig.1.2 for a time period of 100 seconds. In Fig. 1.3 the pressure during the first four seconds is presented together with its time derivative. According to thermocouples placed near the surface of the water, the melt leading front contacted the water at time 0.57 s, which is consistent with a pure gravity driven motion. At that time, the vessel pressure had increased by 0.38 MPa. The melt "leading edge" had a diameter around 300 mm at the time of contact with the water level. The melt velocity upon contact with the water was 6.9 m/s.

Starting from melt/water contact at time 0.57s two main phases are identified from Fig.1.2: from 0.57 s to 2 s (initial melt penetration in water, first pressure maximum at 8.2 MPa), beyond 2 s (medium term debris cooling phase).

In the first phase (0.57 s to 2 s) the pressure growth is essentially due to the steam generated by the heat exchange between the melt and the water. The mean rate of pressure increase during this phase was 2.0 MPa/s with a maximum of 4.0 MPa/s reached at time 0.95 s (see Fig.1.3). From centre-line thermocouples placed at different elevations in the water, melt down progression and velocity data could be established. The melt front progression in the water was rather uniform at a velocity of ~4 m/s. The contact of the melt front with the debris catcher occurred at time 0.83s. The level swell measurements indicated an increase of about 1.2 m in the time interval 0 - 1.9 s (Fig.1.4). Assuming that the melt trailing edge had the same velocity as the leading edge, one calculates that all the melt was below level 1100 at time 1.45 s. It must be noted however that, according to the level measurement, the water was at elevation 1900 at that time.

Table 1.1. FARO L-19 Experimental Conditions and Results

Melt	composition	w%	80 UO_2 + 20 ZrO_2
	temperature	K	3073
	discharged mass	kg	157
	hydrostatic head in release vessel	m	0.59
	Δp delivery		gravity
	initial jet diameter	m	0.10
	free fall in gas	m	1.99
	delivery time	s	0.88*
Gas Phase	initial composition	w%	96 steam + 4 argon
	volume	m^3	1.63
	initial temperature	K	537
Water	mass	kg	330
	initial height	m	1.10
	initial temperature	K	536
	fuel / coolant mass ratio		0.48
Test Vessel	diameter	m	0.71
	initial pressure	MPa	5.00
Results	maximum pressurisation during melt fall	MPa	3.2
	steam explosion		no
	energy released during melt fall: E_{fall}	MJ	82*
	ratio E_{fall} / E_{melt}		0.35
	maximum quenching rate	MW	88*
	maximum level swell	m	1.2
	broken up debris	kg	~80
	mean particle size of broken up debris	mm	3.7
	bottom plate temperature increase	K	252
	maximum heat flux	MW/m^2	0.5*

*calculated

The second phase starts after the first maximum at 2s. First, the pressure slightly decreased for ~200 ms from 8.2 to 8.16 MPa. Then, it increased again at a rate of about 0.03 MPa/s. The pressure increase noticed during this phase was due the debris cooling down. At time 35.7 s, when the pressure reached 9.2 MPa, the venting system operated for 3.7 s, transferring steam and inert gas to the condenser. The venting system valve (flow area 8.04×10^{-4} m^2) closed again at 39.5 s when the pressure reached 7.6 MPa. The amount of water in the condenser increased by 23 kg corresponding to the quantity of steam transferred. Fig. 1.5 shows the pressure increase in the condenser resulting from the transfer of inert gas. The pressure started to increase at time 10 s when the pressure in the test vessel reached 8.6 MPa, which is consistent with the vent valve characteristics. A mass spectrometer connected to the condenser indicated the presence of a noticeable amount of hydrogen after the venting valve operated. The quantity of hydrogen transferred could not be measured. However, the pressure increase in the condenser (0.07 MPa) was larger than what would have corresponded to the transfer of all the argon present in the test vessel. The initial amount of argon in TERMOS and the steam transferred to the condenser are known (1.45 and

23 kg, repectively). Thus, assuming that a uniform mixture steam-argon-hydrogen was vented to the condenser, one calculates that a total of about 0.4 kg of hydrogen was produced. This could correspond to the oxidation of 80 kg of UO_2 into U_3O_8, i.e., 100 kg of melt. Analyses of the debris are in progress to verify this hypothesis.

The L-19 debris consisted of a conglomerate ("cake") in contact with the bottom plate and overlaying fragments (loose debris). The fraction of melt which formed the cake was about 1/2 of the total. Particles which formed the loose debris were completely separated from each other in all the tests. The mean particle size of the loose debris is 3.7 mm. The maximum temperature increase of the bottom plate was 252 K measured in the centre of the contact face. The maximum heat flux to the bottom plate was calculated to be $5.x10^5$ W/m^2. The plate was not damaged, neither adherence to nor pitting was noticed.

1.5 Comparison with former FARO tests

Fig.1.6 and 1.7 show the energy released to the steam-water system and the corresponding quenching rate for tests L-11, L-14 and L-19, respectively. Table 1.2. summarises the main test conditions and data of use for the comparison. It is seen in Fig. 1.6 and 1.7 that the L-19 curves for energy and quenching rate are in between those of tests L-11 and L-14. Very early in the test, the quenching rates are more similar between L-19 and L-11 (melt with 4% of Zr metal) than between L-19 and L-14 (same melt composition as for L-19). This suggests that the higher free fall in L-19 with respect to L-11 and L-14, resulting in larger pre-fragmentation of the melt in the gas space and higher velocity upon contact with the water, induced at first an enhanced breakup and quenching of the melt. Later on, after ~1.2 s, when most of the melt is under water and the remaining melt contact the water at a higher elevation due to the level swell, the energy release and quenching rate are more in agreement with test L-14. On the contrary, for test L-11 the oxidation of the melt in water sustained a high level of breakup and quenching during all the time the melt progressed down into the water [1.2].

Table 1.2 indicates that two parameters are in good agreement between tests L-08, L-14 and L19, namely the released energy and quenching rate per kilogram of melt. The similarity is remarkable between tests L-08 and L-19 (also for the mean particle size), performed in similar conditions for the water depth, test section diameter and melt composition, but which differed by the melt quantity (157 kg for L-19 against 44 kg for L-08, respectively). It seems that, independently of the test conditions between L-08, L14 and L-19, the energy which can be received by the water is limited to a value around 0.5 MW/kg of melt. However, the results do not match when referred to the mass of broken up melt, because the fractions of particulate debris differed significantly between the test (see Table 1.2). These observations are apparently contradictory. One explanation may be found by analysing how the debris bed formed: does the cake come from part of the melt jet which did not breakup or partly from broken up particles which reaglomerated; alternatively, what fraction of the particulate debris comes from melt which fragmented during melt fall or form after the melt had settled. The tests do not allow to answer these questions. The codes are not in agreement on this point, essentially because they do not include debris bed formation and behaviour models. To draw more conclusions on this subject still requires further investigation.

The system behaviour during the debris cooling is not very different between L-19 and L-14 as well. Starting in L-19 from a higher pressure level in the vessel after the melt fall than in L-14 (8.2 MPa against 7.8 MPa, respectively), the pressure was near to reach its maximum value at 9.2 MPa (against a maximum at 8.4 MPa in L-14) when the venting system operated. The pressure rate was slightly higher in L-19. This may be due to the fact that less water than in L-14 was available, rather than to an increase of heat transfer due to the different characteristics of the debris.

Table 1.2. Summary of data of use for comparison between the FARO tests

Test n°		L-06	L-08	L-14	L-19	L-11
total melt mass	kg	18	44	125	157	151[a]
broken up debris	kg	12	30	105	80	151
melt free fall in cover gas	m	1.66	1.53	1.04	1.99	1.09
water depth	m	0.87	1.00	2.05	1.10	2.00
melt velocity at contact with water	m/s	6.0	10.0	5.6	6.9	5.7
mean melt velocity in water	m/s	2.3	3.7	4.8	4	2.5 /1.2[b]
mean particle size of debris	mm	4.5	3.8	4.8	3.7	3.5
energy of the melt: E_{melt}	MJ	27	66	188	236	225 (265[c])
energy released at first pressure maximum (~ melt fall): E_{fall}	MJ	6	24	83	82	170
ratio E_{fall} / E_{melt}		0.22	0.36	0.44	0.35	0.76 (0.64[c])
E_{fall} per kg of broken up melt	MJ/kg	0.50	0.80	0.79	1.03	1.13
E_{fall} per kg of melt	MJ/kg	0.33	0.55	0.66	0.52	1.13
maximum quenching rate: P_{max}	MW	7	22	57	88	157
P_{max} per kg of broken up melt	MW/kg	0.58	0.73	0.54	1.10	1.04
P_{max} per kg of melt	MW/kg	0.39	0.50	0.46	0.56	1.04

[a] UO_2 - ZrO_2 - Zr melt; [b] 2.5 m/s: mean value from level 2.00 m down to -0.6 m, 1.2 m/s=constant: from -0.6 m down to bottom plate; [c] Including the energy of the Zr/H_2O chemical reaction, i.e.-40 MJ.

1.6 Code application

1.6.1 FARO analysis with the code TEXAS-IV

The TEXAS-IV code [1.4] has now been modified to allow for more flexibility in specifying the fuel jet parameters (radii, velocity and temperature) during the outflow of the melt from the release vessel. In past calculations for FARO tests L-06, L-08, L-11 and L14 it was necessary to adjust one of these parameters, normally the initial diameter of the lagrangian particles describing the jet, to account for the pressure rise in the TERMOS pressure vessel. Now that the transient jet velocity can be accounted for during drainage, it is no longer necessary to modify the true jet diameter in order to have satisfactory agreement with the above mentioned FARO experiments. Furthermore, melt drainage times are now in better agreement with experiment.

This possibility to input a jet velocity profile to describe the flow of the fuel from the release vessel has also been exploited for FARO test L-19. The initial particle diameter chosen for the calculation was 0.092 m, the final discharge diameter measured in test L-14. This choice was made because the freezing code BUCOGEL [1.6] estimated a crust growth of only about 1 mm during melt drainage and so it was assumed that most of the crust was formed before drainage. Taking note of this tendency, one might also assume that the initial melt to drain from the release vessel could have a temperature much closer to the solidus than the rest of the bulk melt. Application of this latter assumption has lead to far better agreement in melt arrival times at the TERMOS debris catcher. The reason for this is that TEXAS assumes fragmentation will not occur when a particle becomes solid and since the first particles quickly solidify then they remain relatively large and thus arrive at the debris catcher earlier.

In Fig.1.8 the experimental and calculated pressures are compared. The initial pressure gradients, AB, and peak pressures at B are similar, however, the pressure rise (0.38 MPa) during the passage of the jet through the vapour phase is not reproduced. The slope of the pressure gradient after the formation of the debris bed, CD, was achieved by adjusting an input parameter that in principal determines the "effective" surface area of the agglomerated particles in the debris bed. Fig. 1.9 shows how the calculated total surface area of all melt particles varies with time, the maximum is 22.4 m^2 during the initial pressure rise and 1.3 m^2 after the formation of the debris bed. The maximum level swell was about 1.1 m and the net mass of water evaporated after 7 s was 11.7 kg. Fig. 1.10 shows how the melt particles start to break-up during their fall in the vapour medium at height 2 m and reach their minimum radius of 1.8-2.3 mm at about height 0.87 m, 0.23 m below the original water level (1.1 m). The first melt particles arrive at water surface and the debris bed at times 0.4 and 0.75 s, respectively. At height 0.67 m the melt particles commence to solidify (2873 K) and are still at this temperature on arrival at the debris bed.

1.6.2 FARO analysis with the code COMETA

The COMETA code [1.5] has been used to perform a pre-test prediction of the FARO test L-19. The calculation was performed with 125 kg and 3073 K, which were the expected best-estimate conditions for released mass and temperature of the corium. The overlay of predicted and measured pressure behavior is shown in Fig.1.11. The pressurisation rate was slightly underpredicted due to lower mass adopted, while the final pressure was overestimated. Valves opening was predicted at about 4 s while in the test they opened much later.

The reason for the pressure overestimation is the debris bed model actually present in the code. In COMETA three components are simulated: the jet, the fragmented drops and the fused debris or cake. The jet fragments into drops and the fraction of un-fragmented jet forms the cake; the drops, falling down, continue to fragment and upon reaching the bottom can enter the cake if their temperature is sufficiently high. The remaining drops on the bottom (Fig.1.12) continue to keep the same surface area, thus maintaining a great heat exchange with the surrounding coolant. In reality the "effective" surface area is smaller because embedded particles do not expose the whole surface to the coolant.

A post test analysis with the correct injected mass is shown in Fig.1.13. In this case the pressurisation rate is in better agreement with the experimental value. The problem of the over-pressurisation still remains for the reasons reported above. The total net energy and its derivative, that can be regarded as the quenching rate are very well predicted (Fig.1.14). The calculated average diameter is 2.8 mm where 3.7 mm were measured in the experiment. The mass of "cake" calculated by the code is 43 kg (27% of the injected mass), quite close to previous FARO tests with this water level, but in the experiment a mass of 77.5 kg (50%) was found as conglomerate. The correct prediction of the quenching rate and the almost correct evaluation of the average diameter could imply that in the experiment a larger fragmentation occurred and that part of the fragments re-entered the conglomerated cake after the fall. A more sophisticated and consistent debris model is necessary to account for this phenomenology.

1.7 Discussion and insights for further studies

The FARO tests performed so far at 5.0 MPa have significantly contributed to reduce the uncertainties associated to melt/water quenching predictions during the melt fall through the water. Results from COMETA and TEXAS codes presented as calculation examples in the paper show good agreement between the predictions for the melt fall phase. A broad agreement now also exist between all the codes presently used for analysing the FARO data [1.3].

The next step is to verify whether the mixing models calibrated on the FARO tests at 5.0 MPa are still valid in different conditions, e.g. at lower system pressure. For this purpose the next FARO test will be performed at 2.0 MPa. A blind prediction benchmark exercise has been set up for this purpose. AEA with CHYMES, CEA with MC-3D, FZK with IVA-KA, SIEMENS with IVA-4, University of Wisconsin with

TEXAS, ENEA and ENEL with IFCI, JRC with COMETA and TEXAS, have participated [1.7]. At the same time, performing a test at 2.0 MPa will make data available in conditions which are more in line with present accident management strategies in case of core melt down, namely to reduce the pressure in the RPV.

Concerning the debris bed formation (after melt fall) and cooling, the uncertainties are still large. The mixing codes do not presently includes detailed consistent models for describing the debris bed behaviour and downward heat transfer. On the other hand, it was not possible in FARO to determine the history of the formation of the debris (except for test L-11, where complete breakup of the oxidic/metallic melt occurred before the corium reached the bottom plate [1.2]). Only the final state of the debris and bottom structure heating data are available. Examining the long term pressure histories in the FARO tests may help to determine a typical surface exchange area for the debris (as proposed here with the TEXAS calculation), which in turn may give input for setting up debris bed models.

The similarity observed between test L-19 and former tests on the energy released per unit melt mass during the melt fall, apparently contrasts with the differences found on the fraction of melt which formed the cake. This suggest that there is not one single mechanism which governs the formation of the debris structure. Which part of the "cake" comes from not fragmented melt and which part comes from reagglomerated particles is not known. Test L-19 and former tests also suggest that, in the FARO conditions, increasing the melt mass (L-08, L-19) or decreasing the water depth (L-14, L-19), increases the amount of conglomerated debris (cake). This tendency is illustrated in Fig.1.15. Whether there is a limitation to this process is not clear from the test performed so far. Fig.1.15 indicates two possible evolutions (dotted lines) as a function of the melt mass. To answer these questions would require to use a larger melt mass, which is not possible in FARO. A compromise may consist to reduce the jet diameter in order to increase the melt delivery time, and to scale the conditions for the water (volume, height) according to the new melt delivery conditions. A jet of diameter down to 30 mm is possible, which would multiply by ten the delivery time (~10 s). By doing this, one has access to the debris configuration corresponding to a long (stationary) pour in conditions that are consistent with the present series, and more in agreement with melt delivery times expected in the reactor case. For the scaling, one may use dimensionless analysis based on the physical knowledge of the phenomena and on code predictions. Such an analysis is underway at JRC-Ispra with the use of COMETA.

The codes calibrated on the present series should be able to cope with the new conditions. In particular, they should be able to identify a possible water depletion effect in the mixing area during the melt fall, inducing a limitation of the breakup and an increase of the quantity of melt which arrives undisturbed on the bottom plate. Comparison with the test result should give indications on the scaling capabilities of the codes. However, consistent models for debris bed formation and behaviour are necessary in order to characterise the debris bed which forms in the test.

2. KROTOS EXPERIMENTS

2.1 Background

Active modelling work is currently underway in several research centres to investigate FCIs with particular emphasis on the different stages of pre-mixing, triggering, propagation and expansion (in the case of explosion), which determine the energetics and structural loading [2.1, 2.2]. In the light of these modelling efforts, fundamental experimental investigations are being performed in the KROTOS facility at JRC-Ispra. These experiments are aimed at providing benchmark data to examine the effect of fuel-coolant initial conditions and mixing on explosion energetics with both simulant materials such as alumina (Al_2O_3) and prototypical core material, corium (80 w% UO_2-20 w% ZrO_2).

Detailed data is needed where mixing and explosion processes occur under controlled conditions in a well-defined 1D geometry. With such data one can assess the mechanistic fuel coolant mixing models such as TEXAS, Univ. of Wisconsin [2.3], and explosion models such as IDEMO, IKE-Univ. Stuttgart [2.4], and TEXAS. These models are currently actively in use to analyse KROTOS test results with the aim to improve their predictive capabilities.

In the KROTOS test series with corium melt reported in [2.5], no energetic interactions occurred which is in sharp contrast with the supercritical explosions observed in preceding alumina test series in the narrow test section (of 95 mm inner diameter) [2.6]. However, the mixing of the corium melt with the coolant was limited by the rapid coolant vaporisation leading to a significant sweepout of the melt from the narrow test section used in these tests. Therefore, a decision was made to utilise a larger diameter test section (of 200 mm inner diameter). With this configuration the corium melt was successfully injected, but still no energetic interaction took place. This observation provided the motivation for the current test series in which tests with alumina were performed under similar condition as before (KROTOS 26-30) but with a larger diameter test vessel The importance of these data is twofold, first it facilitates the analysis of the observed differences in premixing behaviour between corium and alumina and, secondly it provides additional data on explosion propagation and energetics under various conditions (subcooling and ambient pressure).

2.2 KROTOS Facility

Fig. 2.1 illustrates the main components of the facility: the radiation furnace, pressure vessel and test section. In the following a brief description of the KROTOS facility is given, a more detailed description of the facility and test procedure is provided in [2.5].

The furnace consists of a cylindrical tungsten heater element which encloses the crucible containing the melt material. The furnace is operated with an electric power supply generating a maximum power of 130 kW. Depending on the crucible design and the desired melt composition, masses in the range of about 1 to 10 kg can be used. Maximum achievable temperatures in the furnace are of the order of 3300 K. The melt temperature is controlled by an optical pyrometer measuring the wall temperature of the crucible.

The crucible type depends on the desired melt temperature so that high temperature tests at 3073 K are performed with tungsten crucibles and lower temperature tests at 2400-2650 K with molybdenum ones. After having reached the desired melt temperature and when the crucible temperature has stabilised, it is released from the furnace and falls by gravity through a 4 m long release tube. Half-way down the tube, a rapid-acting slide valve separates the furnace from the test section below. This valve closes immediately after the crucible has passed. During its fall, the crucible cuts a copper wire generating the zero time signal for the data acquisition. Finally the crucible impacts onto a retainer ring at the end of the tube where a conical shaped metallic puncher breaks the bottom of the crucible, allowing the melt to pour into the test section. The melt jet diameter is defined by guiding the melt through a funnel of high temperature refractory material with an exit diameter of 30 mm.

The lower part of the KROTOS facility consists of a pressure vessel and test section, both made of stainless steel. The pressure vessel is designed for 2.5 MPa at 493 K. It is a cylindrical vessel of 0.4 m inner diameter and 2.21 m in height (volume: 0.290 m^3) with a flat bottom plate and flanged flat upper head plate. The test section consists of a strong stainless steel tube of inner diameter 200 mm and outer diameter 240 mm. The bottom of the test section can be closed by either a flat plate or with a gas trigger device (KROTOS 38).

In the gas trigger device, a gas chamber volume of 15 cm^3 can be charged to a pressure of up to 20 MPa (argon) and is closed by a 0.1-0.25 mm thick steel membrane. After melt penetration down into the

lower region of the test section, the mechanical destruction of the membrane delivers a pressure pulse propagating vertically upwards through the mixture of melt, water and steam. The gas trigger device is activated either by a thermocouple signal or by a backup time delay circuit.

Pressures both in the test section (K0-K5) and pressure vessel (C1-C3 and C11-C13), temperatures and water level swell histories are the main experimental parameters measured in every test. Temperature sensors (TC1-TC5) are located at the same elevations as pressure transducers (K1-K5), respectively (see Fig. 2.1). The location of K0 transducer is dependent on whether the gas trigger device is connected or not. In the case of a test without gas trigger (KROTOS 40-43) the K0 transducer is placed in the centre of the bottom plate.

2.3 Results

The experimental parameters and the main results from the current test series are summarised in Table 2.1. Table 2.2 summarises some more detailed results of the energetics of the tests with steam explosions. In this table the impulses, kinetic energy of the water slug and the energy conversion efficiency are given. The kinetic energy of the water slug is estimated from the impulse produced in the steam explosion assuming that this impulse causes no structural damage and it is solely absorbed in the water column thus accelerating it.

In the following the observations made in each test are briefly described and some comparisons are made with the data from previous test series. The timing in each test is referenced to a "trigger wire" which is cut by passing crucible in the release tube, see section KROTOS Facility.

KROTOS 38 test was essentially a repeat of the KROTOS 37 corium test [2.7] with alumina melt poured into subcooled water (T_{sub}=79 K). This test demonstrated significantly different premixing behaviour from the corium test as can be seen in Fig. 2.2 illustrating much lower steaming rates in the case of alumina during the mixing phase. A spontaneous explosion took place (at t=1.28 s) before the trigger device was operated. At this point the melt had penetrated down to TC3 level (550 mm from the bottom). The explosion dynamics is captured with the fast responding pressure transducers and is illustrated in Fig. 2.3. The explosion propagated up- and downwards from the K3 location. The observed peak pressure caused by the reflected shock wave exceeded 100 MPa at the bottom of the test section. The maximum explosion pressure of 69 MPa was recorded close to the surface at K5. The explosion efficiency was estimated to be about 1.5% (Table 2.2) which is comparable to the data from KROTOS 30.

The energetic interaction in the test section caused rapid compression of gas in the pressure vessel with the maximum pressurisation of 0.2 MPa. This is comparable to the pressurisation level of 0.18 MPa observed with the narrow test section (KROTOS 30). This fact together with the estimate of the explosion efficiency estimate would suggest that the energetics of the alumina interaction was not significantly altered by lessening the mechanical constraint of the narrow test section.

KROTOS 40 test was performed to address the significance of the radiative heat transfer from the melt jet as an explanation of the very strong initial steaming observed with corium melt which might have lead to a depletion of water in the mixing zone. The alumina melt was heated up to the same temperature as the corium melt in KROTOS 37 (3073 K). However, the incoming alumina melt produced an interaction at the melt/water contact which probably caused some pre-fragmentation of the melt jet above. Therefore, it is difficult to assess quantitatively how much of the enhanced steaming was due to the enhanced radiation heat transfer as opposed to having increased the surface area of the melt by pre-fragmenting it. Whatever the cause for higher steaming was, it was not sufficient to influence the mixing conditions in such a way that a spontaneous explosion could not happen. A spontaneous explosion took place at 3.1 s involving the melt mass not affected by the surface interaction. The longer mixing time (with respect to other tests with lower temperatures) implies that the overall melt temperature may have delayed the oc-

currence of the explosion. The dynamic pressures of this interaction are shown in Fig. 2.4. It can be seen that the explosion propagates from the bottom towards the surface with an average speed of 1000 m/s. The peak pressure is somewhat higher than in KROTOS 38 due to the higher thermal energy content of the melt and slightly higher inertial constraint (because the explosion was initiated close to the bottom of the test section). The pressurisation of the freeboard volume of 0.32 MPa was also somewhat higher than in the previous tests mainly because of the larger thermal energy content of the alumina melt

Table 2.1: KROTOS Experimental Conditions and Results in Alumina Tests

	KROTOS Test n°		38	40	41	42	43
Melt	discharged mass	g	1533	1470	1430	1539	1500
	temperature	K	2665	3073	3073	2465	2625
	initial jet diameter	mm	30	30	30	30	30
	free fall in gas	m	0.46	0.46	0.46	0.46	0.46
Water	mass	kg	34.5	34.5	34.5	34.5	34.5
	height	m	1.105	1.105	1.105	1.105	1.105
	initial temperature	K	294	290	368	293	295
	subcooling	K	79	83	5	80	89
Test	initial pressure (He)	MPa	0.1	0.1	0.1	0.1	0.2
Section	internal diameter	mm	200	200	200	200	200
	gas trigger		yes[a]	no	no	no	no
Results	confirmed penetration depth of the melt jet		TC3	TC1	TC1	TC2	TC1
	steam explosion		yes	yes	no	yes	yes
	time of explosion[b]	s	1.276	3.214	--	1.713	2.792
	max. dynamic pressure	MPa	69	86	--	57	117
	max. expansion vessel pressurisation	MPa	0.20	0.32	0.10	0.25	0.81
	total debris[c]	g	1523	1509	n.a.	1342	1687
	debris < 250µm	g	934	674	n.a.	781	721
	fuel volume fraction	%	1.6	n.a.	1.4	1.6	1.6
	coolant volume fraction	%	95.6	n.a.	83.0	97.6	95.6
	vapour volume fraction[d]	%	2.8	n.a.	15.6	0.8	2.8

[a]Spontaneous explosion took place before triggering. [b]Measured from the trigger wire. [c]Found in the test section and pressure vessel. [d]Integral data, calculated from the level swell measurements.

The following test, KROTOS 41, was performed to confirm the observation that spontaneous explosions with alumina are suppressed at low subcooling of the water (<10 K), see results from KROTOS 27. The water was heated to 95 °C and the alumina temperature was kept the same as in the KROTOS 37 test. A high level swell of 230 mm was measured corresponding to an integral void fraction of 16% which indicated significant steaming. No explosion occurred. The quenched alumina debris consisted of a small cake with some coarse debris which resembled the debris from the KROTOS 27 test. However, it is significantly different from the corium melt (in KROTOS 37), which fragmented to much finer debris, further demonstrating different fragmentation and mixing behaviour.

In the KROTOS 42 test, the melt superheat was lowered to 150 K in order to investigate if a superheat similar to that of corium melt would have been the cause for inhibiting an energetic interaction (in all the

previous tests with alumina the melt superheat has been higher than 250 K). The test was performed with subcooled water (T_{sub}=80 K). Again similar behaviour to that of KROTOS 38 was observed with very small steaming and level swell during the mixing phase prior to the explosion. The explosion did occur at 1.71 s and propagated in the test section as shown in Fig. 2.5.

Finally, in the KROTOS 43 test, the effect of the ambient pressure was investigated by performing the test at the elevated initial pressure of 0.2 MPa. It was interesting to investigate if the slight over-pressure, which is comparable to the initial rapid pressurisation level observed with corium (no steam explosions), would be enough to suppress an explosion. On the other hand, it can be noted that pressurising the system while keeping the water temperature at 295 K meant that the coolant was slightly more subcooled (T_{sub}=89 K). The melt temperature (2625 K) was again similar to that of the KROTOS 38 test and the former ones (KROTOS 26-30).

After melt injection, very little steaming was observed and the melt settled to the bottom of the vessel until an explosion emanated from the bottom at 2.79 s, see Fig. 2.6. Due to the inertial constraint of the water column along with the higher ambient pressure lead to high peak pressures of 117 MPa close to the bottom of the test section (at K1) which in turn resulted in deformation of both the bottom plate and the bolts holding the plate in place, see Figs. 2.7 and 2.8. Even though heavy structural damage was observed in this test, the observed peak pressures and the impulse generated were not significantly different from the KROTOS 38 test where less structural damage was observed.

Table 2.2: Explosion Efficiency in KROTOS Alumina Tests

	KROTOS Test n°		38	40	42	43
Melt	discharged mass	kg	1.533	1.470	1.539	1.500
Thermal	temperature	K	2665	3073	2465	2625
Energy	enthalpy	kJ/kg	4148	4727	3864	4091
	thermal energy, $E_{thermal}$	kJ	6359	6949	5946	6137
Kinetic	max. impulse location		K1	K1	K2	K1
Energy	max. impulse, I	kPa·s	76.2	60.5	72.5	68.4
Released	max. impulse at depth	mm	955	955	755	955
	water mass at depth, m_w	kg	29.9	29.9	23.6	29.6
	kinetic energy, $E_{kin}=(I \cdot A)^2/2m_w$	kJ	96.1	60.6	110.0	77.4
Efficiency	$E_{kin}/E_{thermal}$	%	1.5	0.9	1.9	1.3

2.4 Code application

2.4.1 KROTOS Analysis with the code TEXAS-IV

TEXAS-IV has been used for analysing the KROTOS experiments, tests 38 and 42. Since spontaneous explosions occurred in both experiments it was necessary to modify the code to take this into account. After saving the output data from a coarse mixing calculation the computations are continued using the fine fragmentation model found in TEXAS [2.3]. Spontaneous triggering is accomplished by simply introducing a small pressure into the Eulerian cell where the origin of the explosion, as deduced from the experimental pressure histories, takes place. The input data for the fragmentation model (proportional constant C=0.002, characteristic fragmentation time t = 0.001s) are similar to those used by Tang in reference [2.3] for alumina/water mixtures in the KROTOS tests 26 and 28 [2.6].

Fig. 2.9, centre, shows the TEXAS melt jet Lagrangian particle distributions for tests 38 and 42, at times 1.12 and 1.4 s, respectively. The void fraction is very small (<1%) throughout the water except in the vicinity of the melt, the maximum being about 6-7%. An instantaneous trigger pressure of 0.5 MPa was then applied in the Eulerian cells 11 and 9 for tests 38 and 42, respectively. Comparison of the computed and experimental pressures at gauges K1 to K5 reveal many quantitative and qualitative similarities, especially at gauge K3 and below, for tests 38 and 42, respectively. Following the initial upward moving shock, further important wave propagations are evidenced in the calculations at gauges K4 and K5. It should be noted that TEXAS does not take into account the physical presence of vapour bubbles, particularly those at the free surface, so that deviations from the true behaviour might be expected. The spontaneous trigger ruptured the membrane of the mechanical trigger in test 38. This was not taken into account in the calculation because its effect in producing fine fragmentation is expected to be relatively minor in comparison with that created by the spontaneous trigger.

Particle diameters after fragmentation were 0.57-0.73 mm for KROTOS 38 and 0.91-1.18 mm for KROTOS 42. It should be stressed that these diameters are not the diameters of the fine fragments but the diameters of the particles remaining after fine fragmentation. Fragmentation continues even after 3 ms but no more high pressures are produced, the region where the explosion occurred has a high void fraction and is continue to expand very rapidly.

2.4.2 KROTOS Analysis with the code SEURBNUK/EURDYN

The base-plate deformation observed in KROTOS 43 was calculated with the code SEURBNUK/ EURDYN [2.8]. A simplified finite element representation of the plate, using axisymmetric triangular elements, is shown in Fig.2.10. Since the code is two-dimensional it is not possible to model exactly the three-dimensional details in the region BC, see Fig.2.10. The six lugs through which pass the hold-down bolts that firmly hold the base-plate to the cylindrical test section are modelled as a complete annulus. The base-plate is assumed to be uniformly thick (40 mm), whereas in reality it is thinner (~ 36 mm) up to the radius of the flange (100 mm). The six hold-down bolts, diameter, 23 mm, are modelled using thin-shell elements as an equivalent annular ring, AB, height 50 mm, radius 130 mm and thickness 3.97 mm, where point A is considered fixed and point B is a node common to both the base plate and the annular ring.

In loading the base-plate the experimental pressure signal (thin line) at position K1 was approximated with the piecewise linear curve shown in Fig. 2.11. The computed maximum depression at the centre of the base plate with respect to the outer circumference was 9.5 mm and is in good agreement with the actual value (~11 mm). An independent computation for the modelling of the cylindrical test section, again using axisymmetric triangular finite elements, see Fig. 2.12, gave a similar value for the maximum hoop strain measured at position K1 (~0.6%). Similar calculations where only a fraction of the given load was applied to the structures demonstrated that for peak pressures above 50 MPa there will always be some permanent deformation

2.5 Discussion

The current test results clearly demonstrate the potential of alumina melt to produce a highly energetic spontaneous steam explosion when poured into subcooled water. As a consequence peak pressures exceeding 100 MPa are generated with large enough impulses to cause structural damage in the present test section geometry. The explosion propagation speeds are of the order of 1000 m/s. It is confirmed that a slight over pressure of 0.10 MPa is not sufficient to suppress the explosions. However, spontaneous explosions are suppressed when pouring the melt in the water with low subcooling, but if an external trigger is applied the system may still be triggered.

These observations are in sharp contrast with the previous corium tests where so far no steam explosion has been observed with or without an external trigger. The present data would suggest that the dif-

ferent premixing behaviour is the main factor reducing the potential for corium to produce an energetic interaction. Significant initial steaming in the case of corium implies high voiding and possibly water depletion in the mixing region. The alumina test with high melt temperature still produced an explosion albeit a delayed one. It is believed that increased radiation heat transfer combined with increased melt surface area due to pre-fragmentation (induced by the early surface interaction) was the reason for the longer mixing time. Therefore, the melt temperature had an effect on the timing of the explosion in this test. The alumina results with lower temperature demonstrated that explosions can also take place with a low melt superheat. Finally, the first test with an elevated initial pressure implied that the pressurisation taking place during the mixing phase is not sufficiently large to suppress explosions with alumina or that the higher subcooling level counterbalanced the stabilising effect of the elevated pressure.

The reported results would suggest that there is no particular single factor but rather a combination of the secondary effects due to the differences between material properties of the two different melts that causes alumina behave differently from corium under present conditions. Another factor that may suppress explosions in the tests with corium melt is the hydrogen produced during mixing. Even though corium used in KROTOS experiments is an oxide mixture, the results from the FARO tests have evidenced production of hydrogen with a mixture of similar composition. However, at present only qualitative data exists on hydrogen production and its effect on suppressing explosions is purely speculative.

An analysis of the KROTOS 38 and 42 tests with TEXAS model utilising simulated spontaneous triggering of explosions produced satisfactory results. Furthermore, the structural damage in the KROTOS 43 test was successfully simulated with SEURBNUK/EURDYN.

Another difference between the alumina and corium tests is the melt volume. The previous corium tests in the KROTOS facility have been performed with relatively small melt volumes (30% less volume than alumina). Therefore, more tests are planned in the KROTOS facility with larger corium melt masses. Tests will be also made with elevated trigger strengths and once the results from these tests are available, the current alumina data can be revisited to draw more conclusions which have significant importance regarding to alumina simulant tests performed currently in several research organisations.

ACKNOWLEDGEMENTS

The authors greatly acknowledge the work and efforts of the FARO and KROTOS teams.

REFERENCES

[1.1] D. MAGALLON and H. HOHMANN, High Pressure Corium Melt Quenching Tests in FARO, Nucl. Eng. Des. 155 (1995) 253-270.

[1.2] D. MAGALLON and H. HOHMANN, Experimental Investigation of 150-kg-Scale Corium Melt Jet Quenching in Water, NURETH-7, Saratoga Springs, NY, 10-15 September 1995.

[1.3] D. MAGALLON et al., High Temperature Melt/Water Mixing: Results and Calculations of FARO, PREMIX and MIXA Experiments, to be presented at FISA-95, Luxembourg, 20-22 November 1995.

[1.4] CHU C.C., CORRADINI M.L., HUHTINIEMI I., MURPHY J., TANG J., NILSUWANKOSIT S., "A Code Manual for TEXAS-IV: One Dimensional Transient Fluid Model for Fuel-Coolant Interaction Analysis", Nuclear Engineering and Engineering Physics Department, University of Wisconsin-Madison, WI 53706, October 1994.

[1.5] A. ANNUNZIATO, C. ADDABBO, "COMETA (Core Melt Thermal-hydraulic Analysis) a Computer Code for Melt Quenching Analysis", Proceedings of Int. Conf. "New Trends in Reactor Thermal Hydraulics", Pisa, June 1994.

[1.6] BERTHET B., GIBIAT D., LEMOINE F., SCHWARZ M., "Presentation of the Freezing Code BUCOGEL Version 2.1", CEA Cadarache, Note DRS/SEMAR 91/13 (English Version), November 1992.

[1.7] ANNUNZIATO A., C. ADDABBO and G. LEVA, FARO Test L-20 Benchmark Results, JRC Technical Note to be published.
[2.1] J. MURPHY and M. CORRADINI, An Assessment of Ex-Vessel FCI Energetics for ALWRs, Int. Conference on New Trends in Nuclear System Thermalhydraulics, Pisa 1994.
[2.2] T. THEOFANOUS and W. YUEN, The Prediction of Dynamic Loads from Ex-vessel Steam Explosions. Int. Conference on New Trends in Nuclear System Thermalhydraulics, Pisa 1994.
[2.3] J. TANG, Modeling of the Complete Process of One-dimensional Vapor Explosions, PhD thesis, Univ. of Wisconsin, 1993.
[2.4] M. BÜRGER, M. BUCK, K. MÜLLER and A. SCHATZ, Stepwise Verification of Thermal Detonation Models: Examination by Means of the KROTOS Experiments, CSNI Specialist Meeting on Fuel Coolant Interactions, NUREG/CP-0127, 1994.
[2.5] I. HUHTINIEMI, H. HOHMANN AND D. MAGALLON, FCI Experiments in Corium/Water System, NURETH-7, Saratoga Springs, 10-15 September 1995.
[2.6] H. HOHMANN, D. MAGALLON, H. SCHINS and A. YERKESS, FCI Tests in Aluminumoxide/Water System, Nucl. Eng. Des. 155 (1995) 391-403.
[2.7] H. HOHMANN, D. MAGALLON, I. HUHTINIEMI, A. ANNUNZIATO and A. YERKESS, Advance in FARO/KROTOS Melt Quenching Experiments, 22nd Water Reactor Safety Information Meeting, Bethesda, 1994.
[2.8] YERKESS A., BROADHOUSE B., SMITH B.L, "The Computer Code SEURBNUK/EURDYN, Part 2: Input and Output Specifications, EUR 10897 EN, 1987.

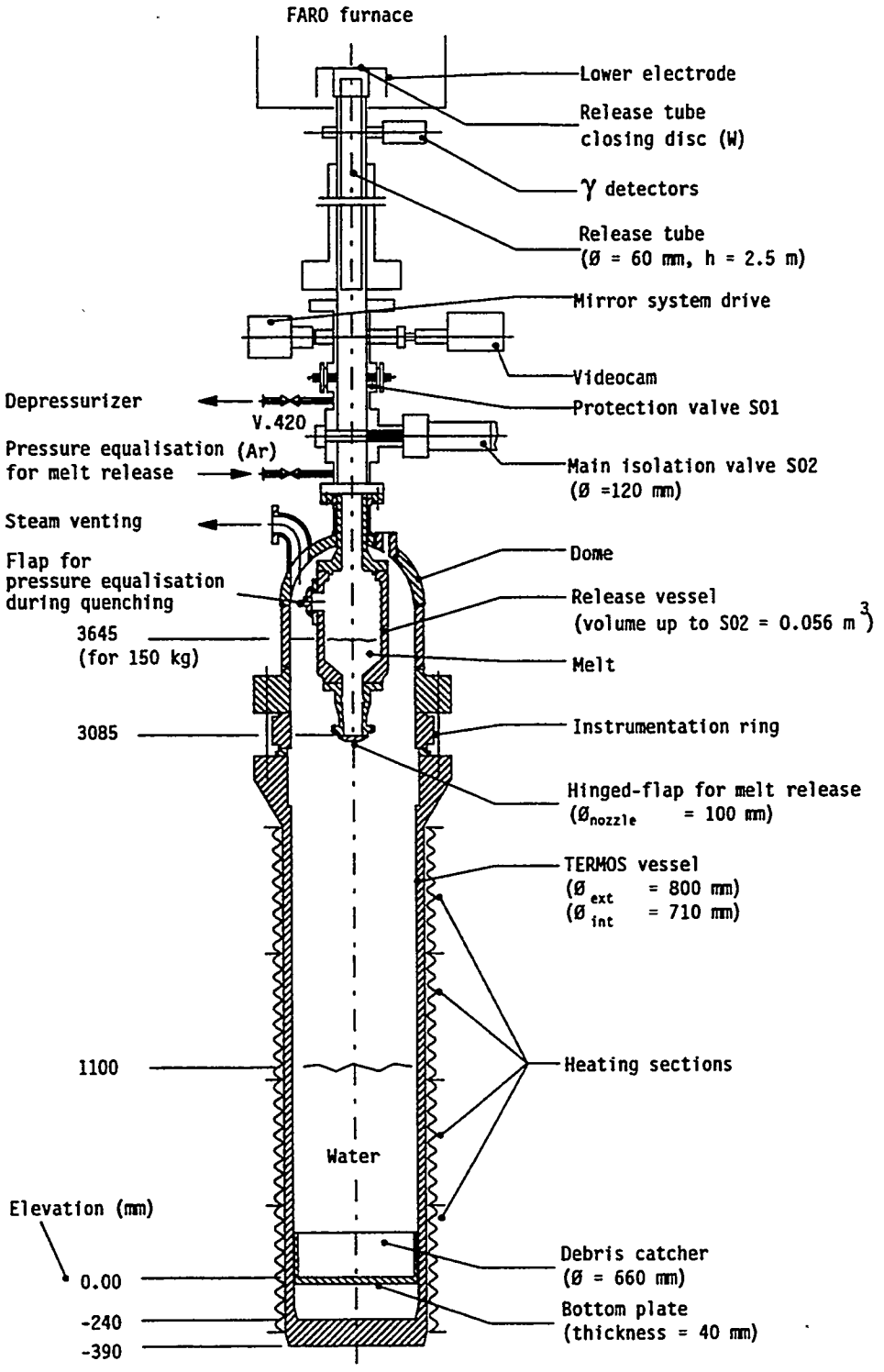

Fig. 1.1 - Experimental arrangement for FARO Test L-19

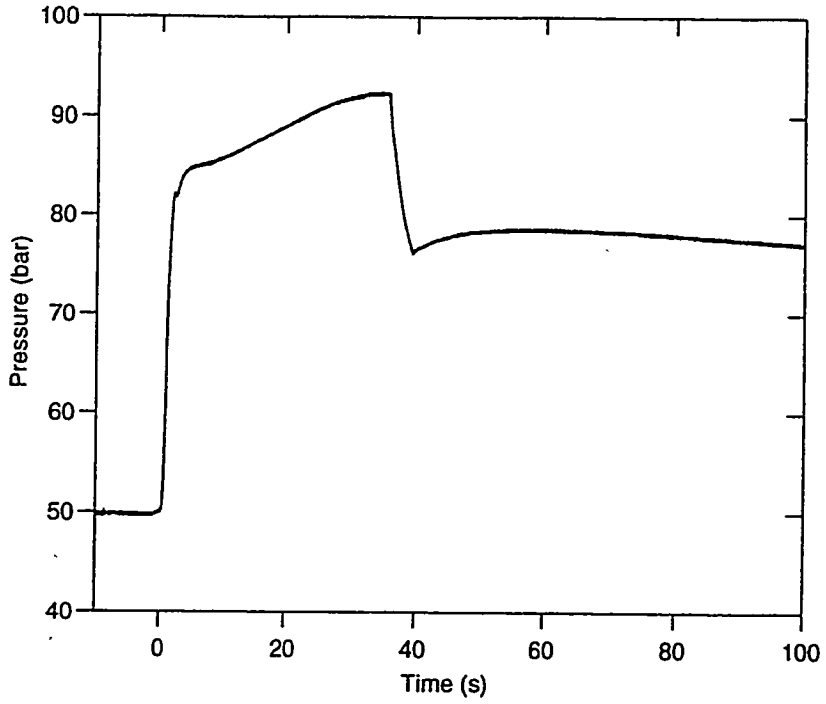

Fig 1.2 - FARO L-19 vessel pressure up to 100 s

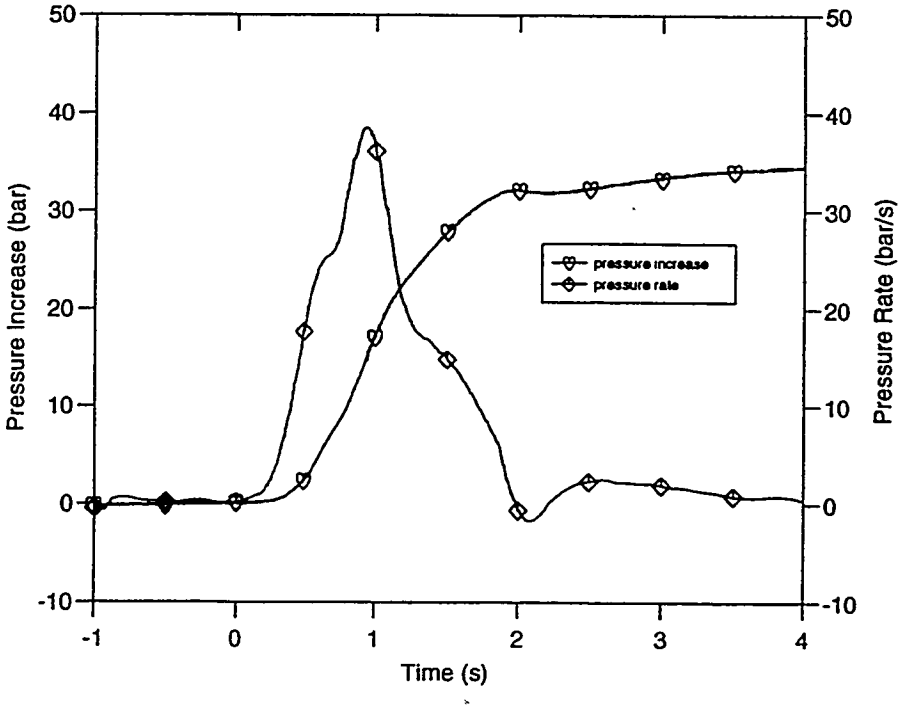

Fig. 1.3 - FARO L-19 pressure increase and rate during the first 4 s

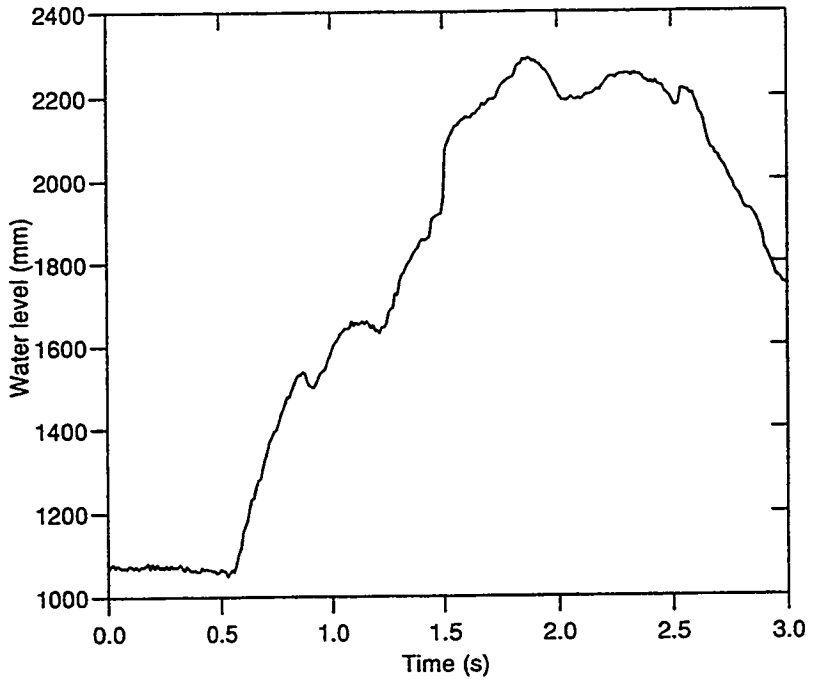

Fig. 1.4 - Water level in FARO Test L-19

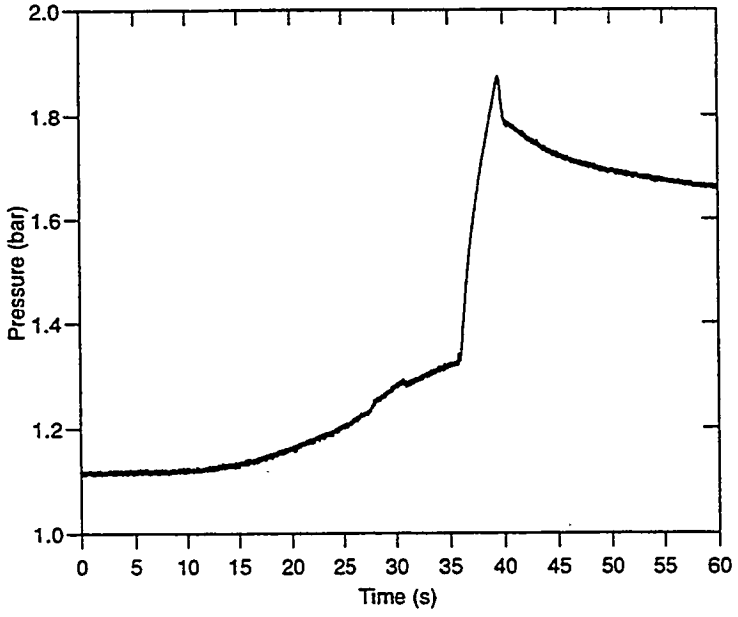

Fig. 1.5 - FARO L-19 Condenser pressure

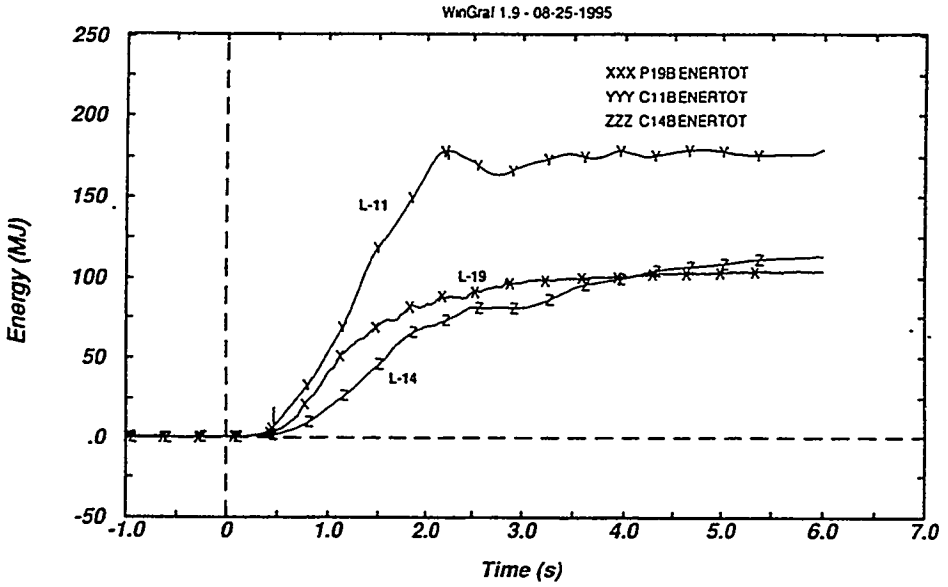

Fig. 1.6 - Comparison of energy released to the water in tests L-11, L-14 and L-19

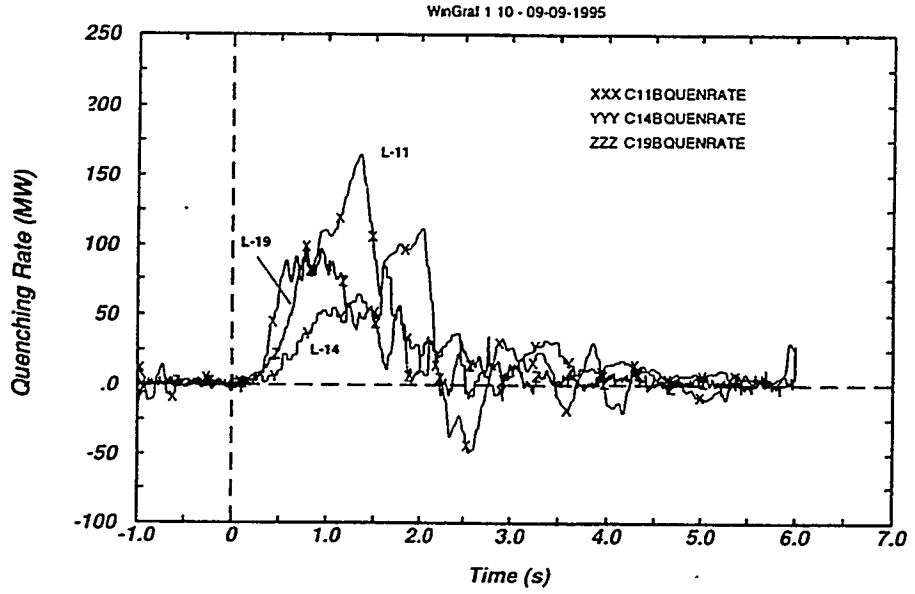

Fig. 1.7 - Comparison of quenching rates in tests L-11, L-14 and L-19

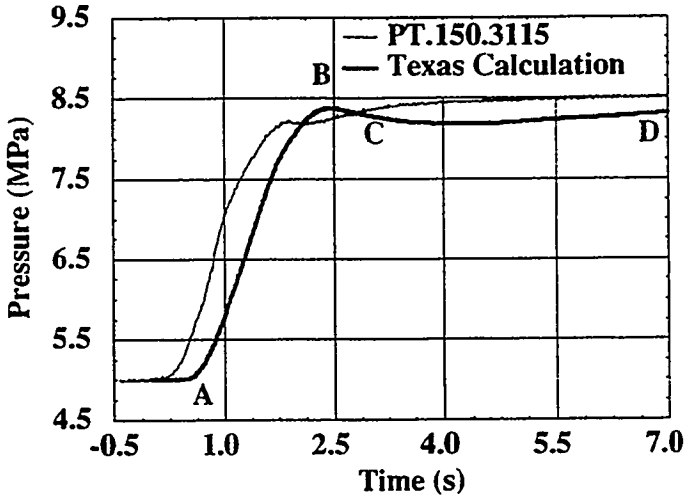

FIG. 1.8 -Comparison between TEXAS-IV and Experiment - FARO Test L-19

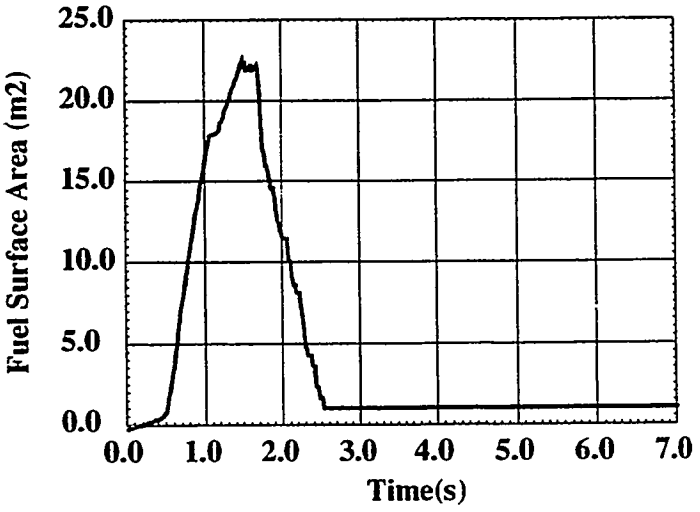

FIG. 1.9 - Variation of Fuel Surface Area for TEXAS-IV Calculation L-19

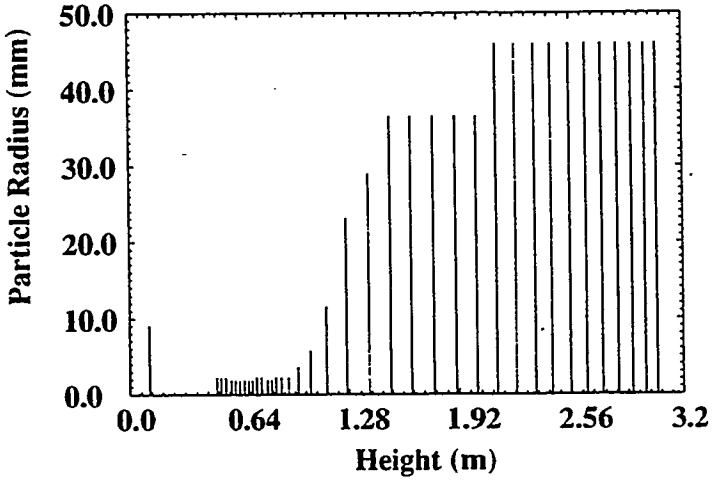

FIG. 1.10 -Variation of Particle Radius for TEXAS-IV Calculation L-19 at 0.8 s

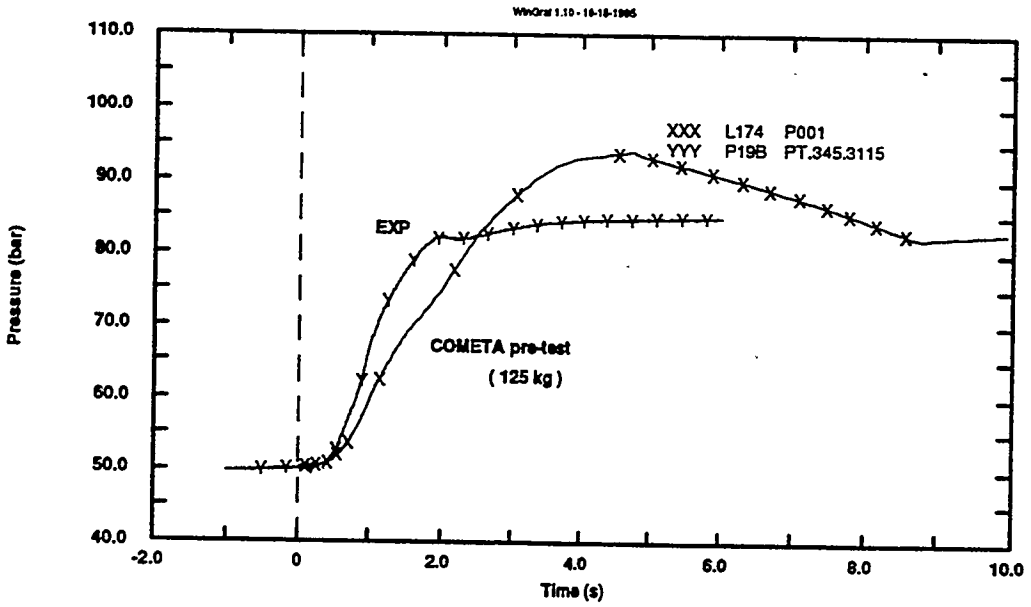

Fig. 1.11 - Pre Test prediction by COMETA code: Pressure

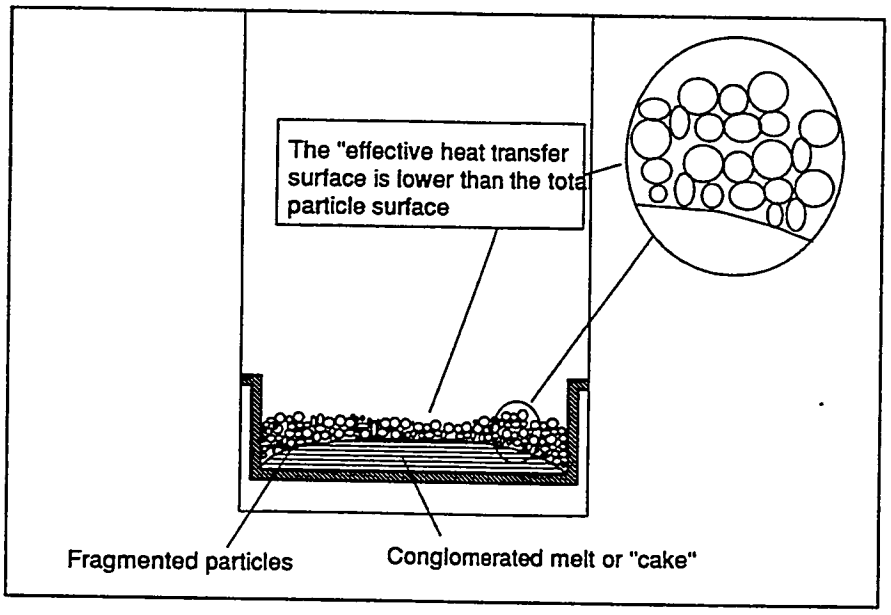

Fig. 1.12 - Representation of the debris bed configuration

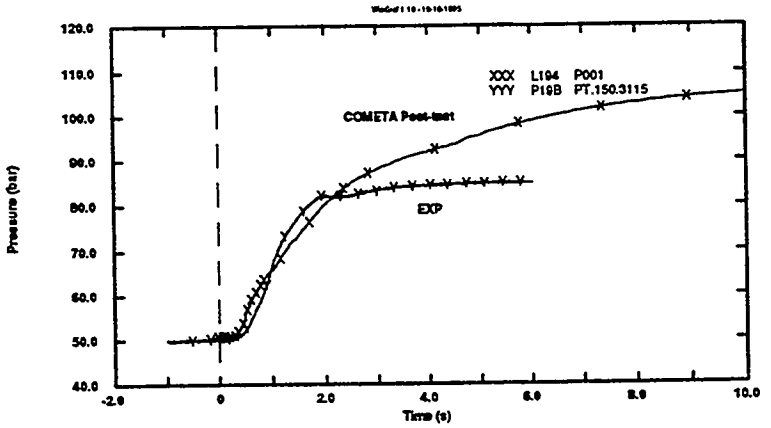

Fig. 1.13 - Post Test prediction by COMETA code: Pressure

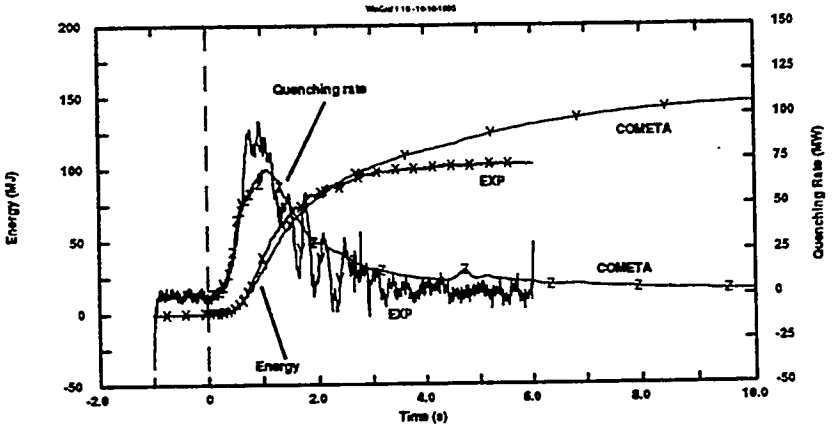

Fig. 1.14 - Post Test prediction by COMETA code: Total Energy

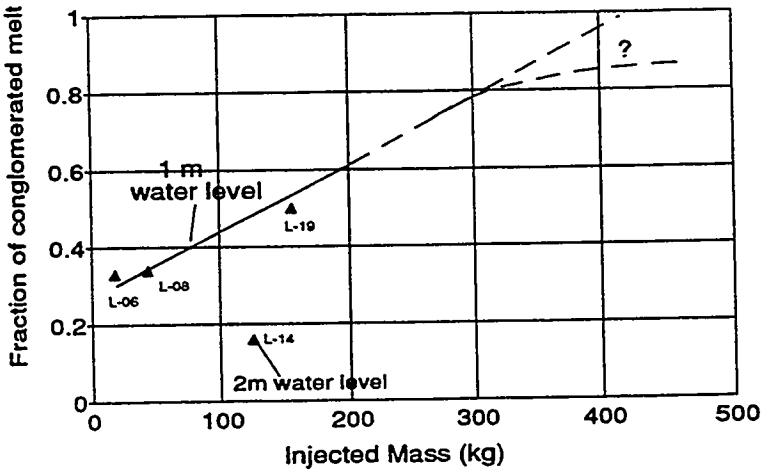

Fig. 1.15 - Fraction of conglomerate debris as a function of the melt quantities used in FARO and possible evolutions

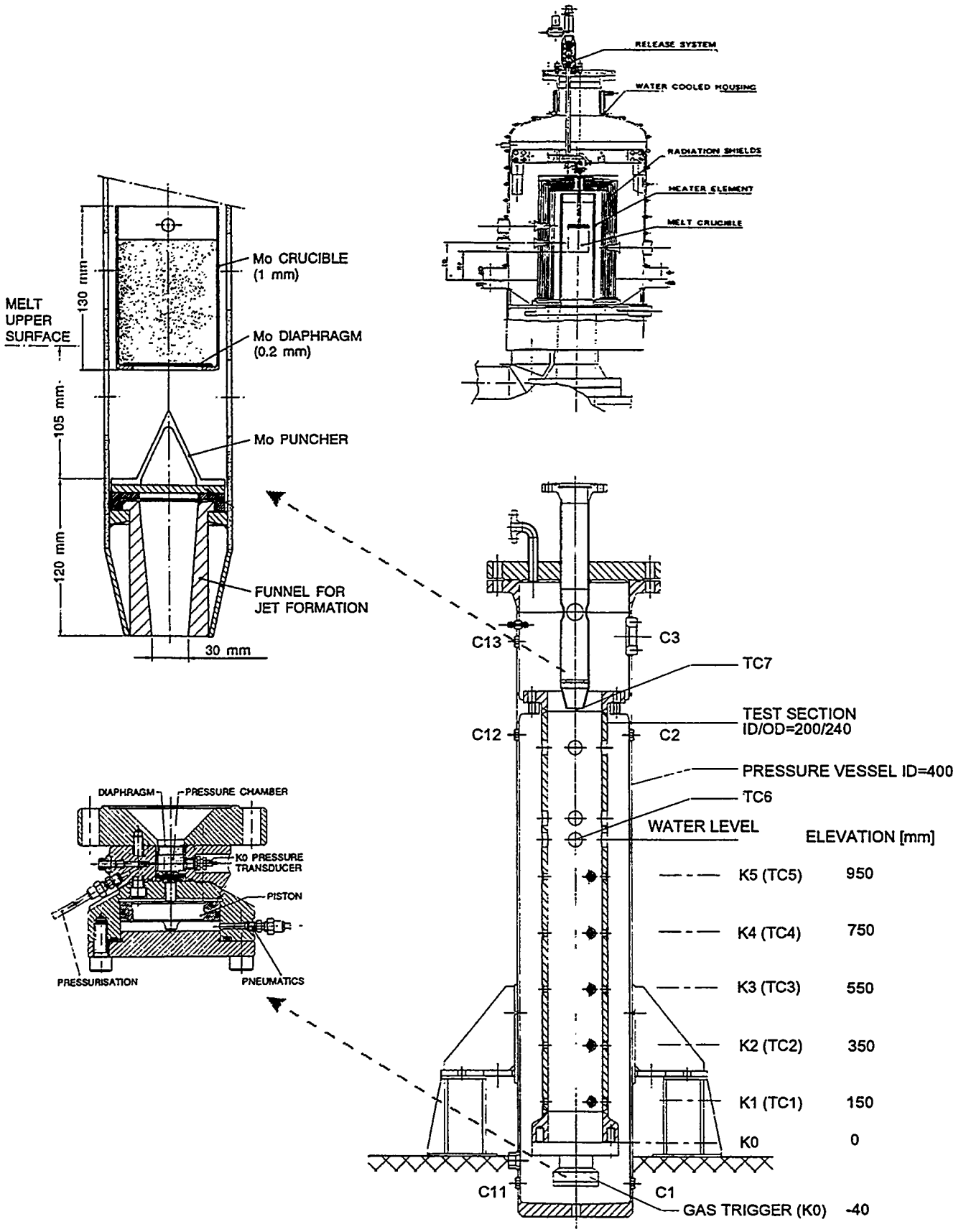

Fig. 2.1 KROTOS Test Facility

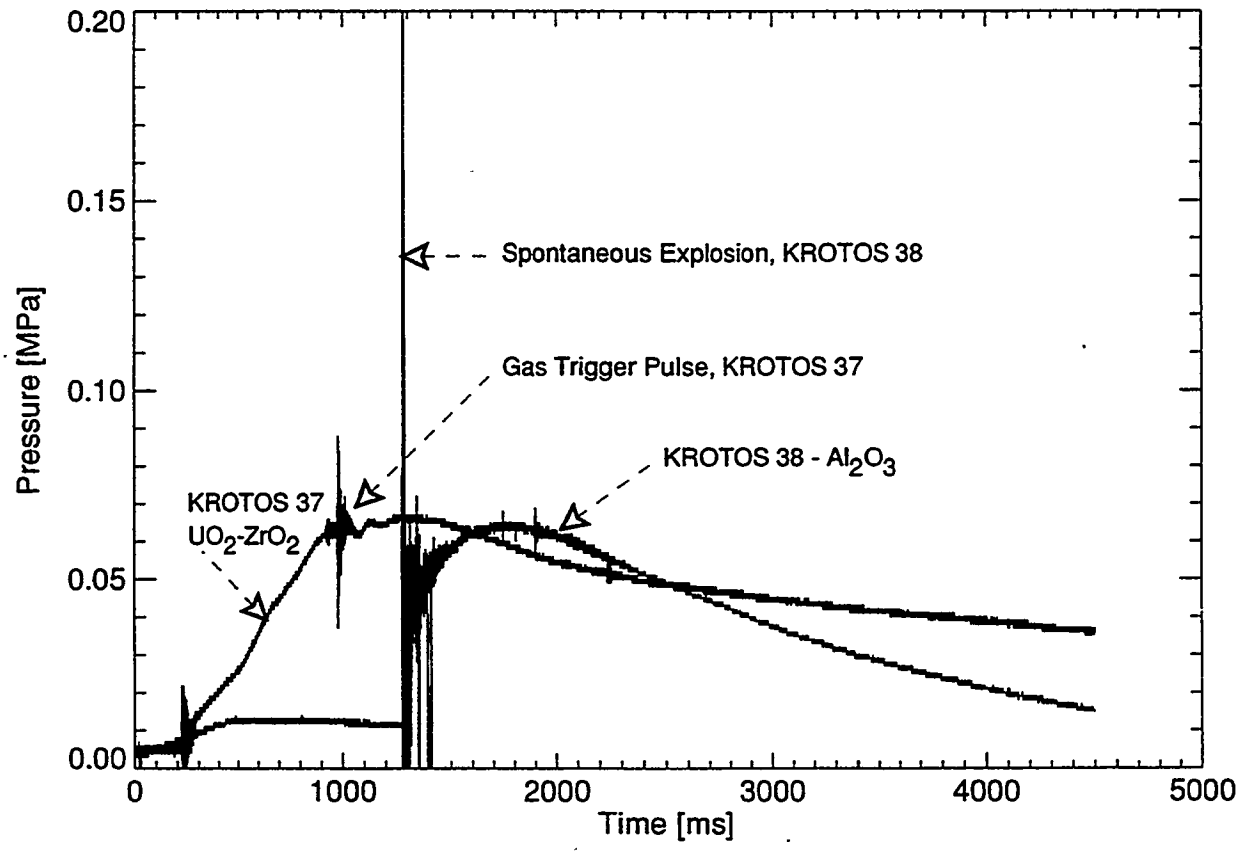

Fig. 2.2 Expansion Vessel Pressurisation, KROTOS 37 and 40

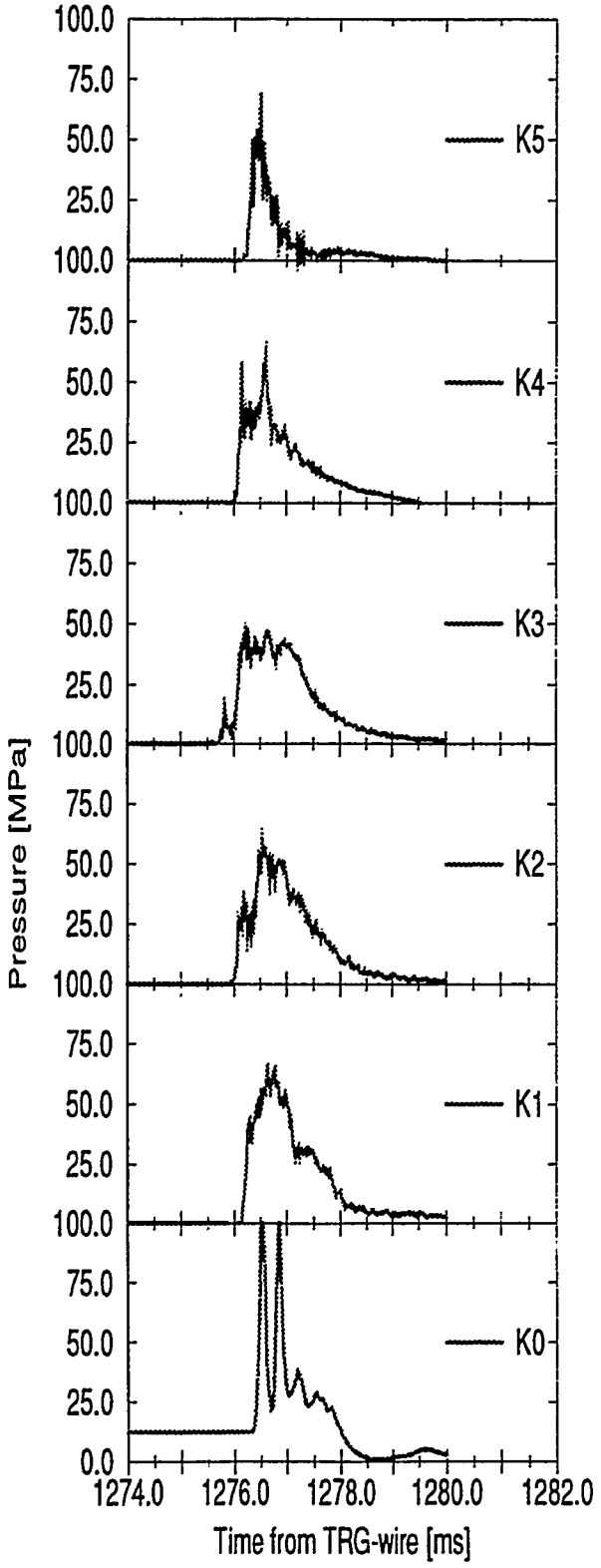

Fig. 2.3 Dynamic Pressures in the Test Section, KROTOS 38

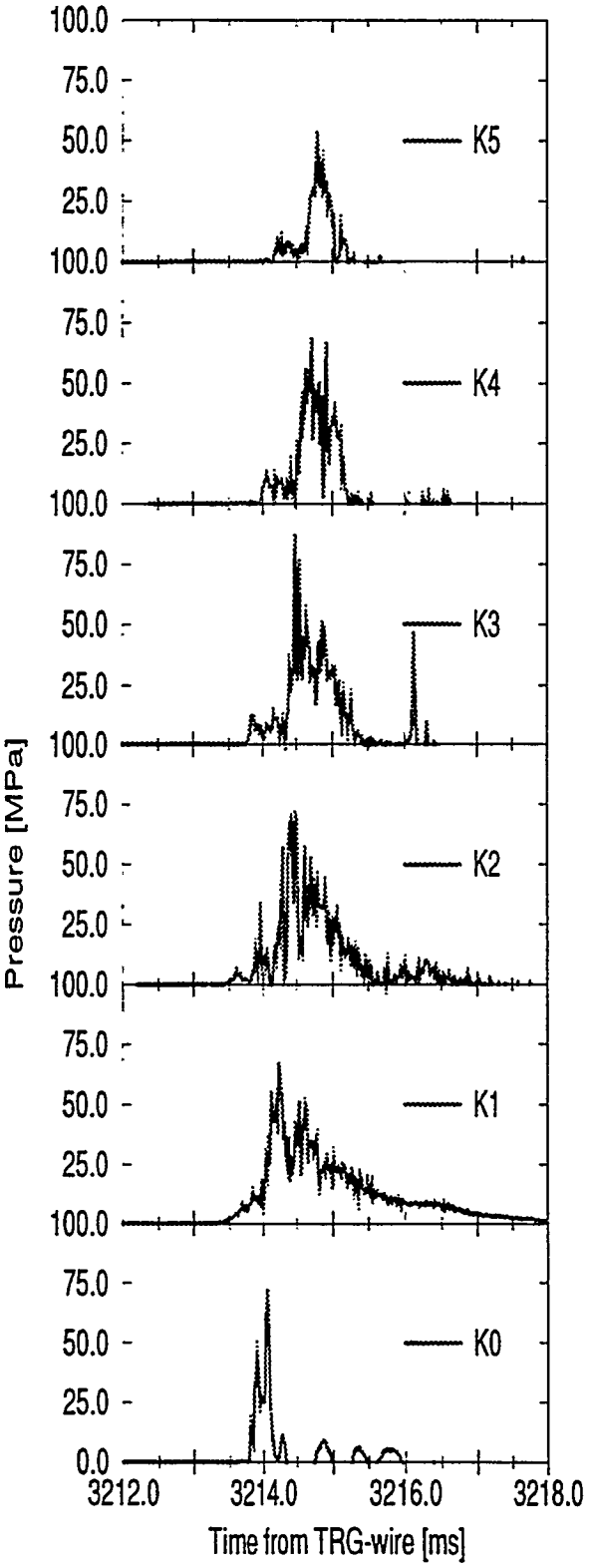

Fig. 2.4 Dynamic Pressures in the Test Section, KROTOS 40

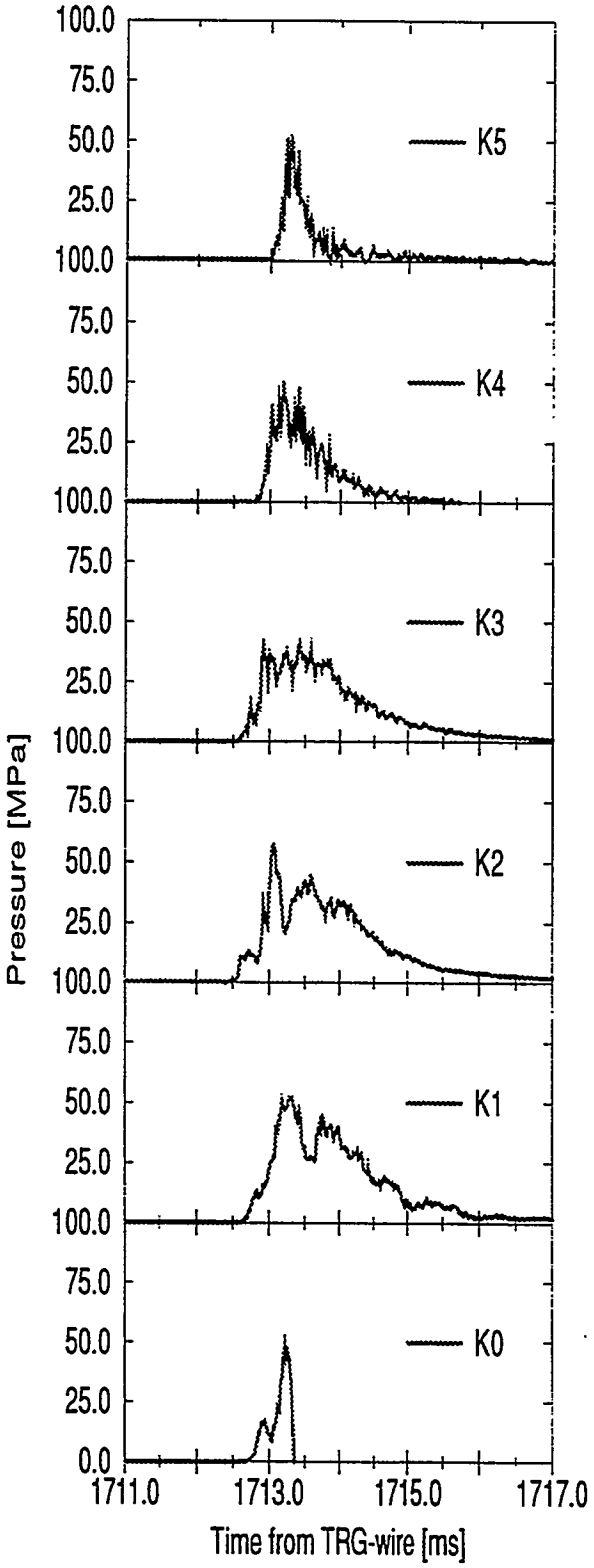

Fig. 2.5 Dynamic Pressures in the Test Section, KROTOS 42

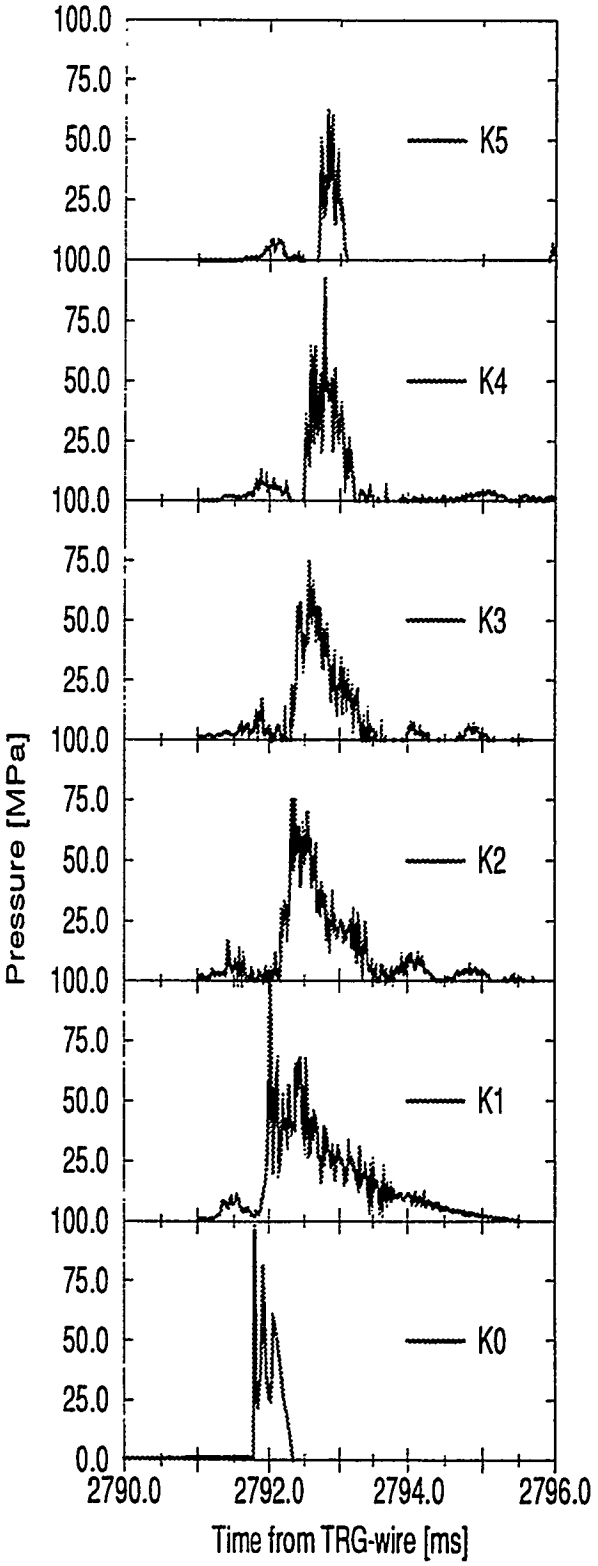

Fig. 2.6 Dynamic Pressures in the Test Section, KROTOS 43

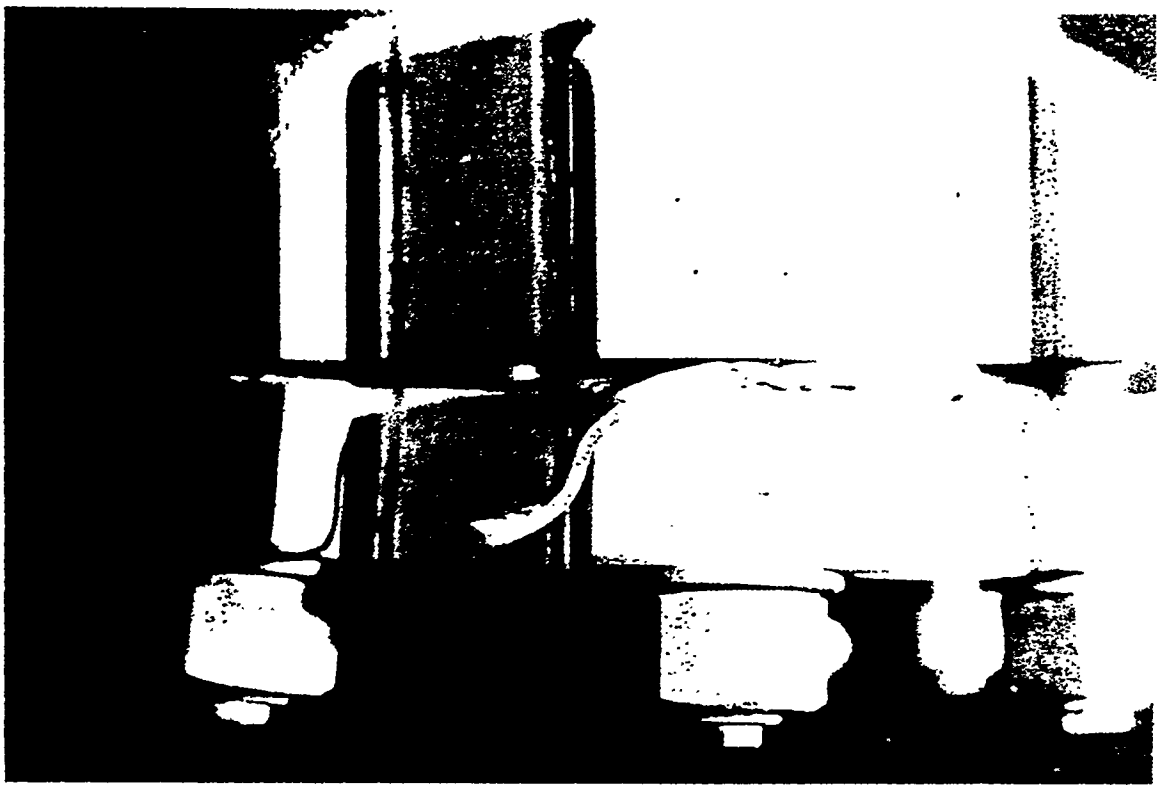

Fig. 2.7 Damage at the Bottom of the Test Section in KROTOS 43
(broken copper gasket ring visible)

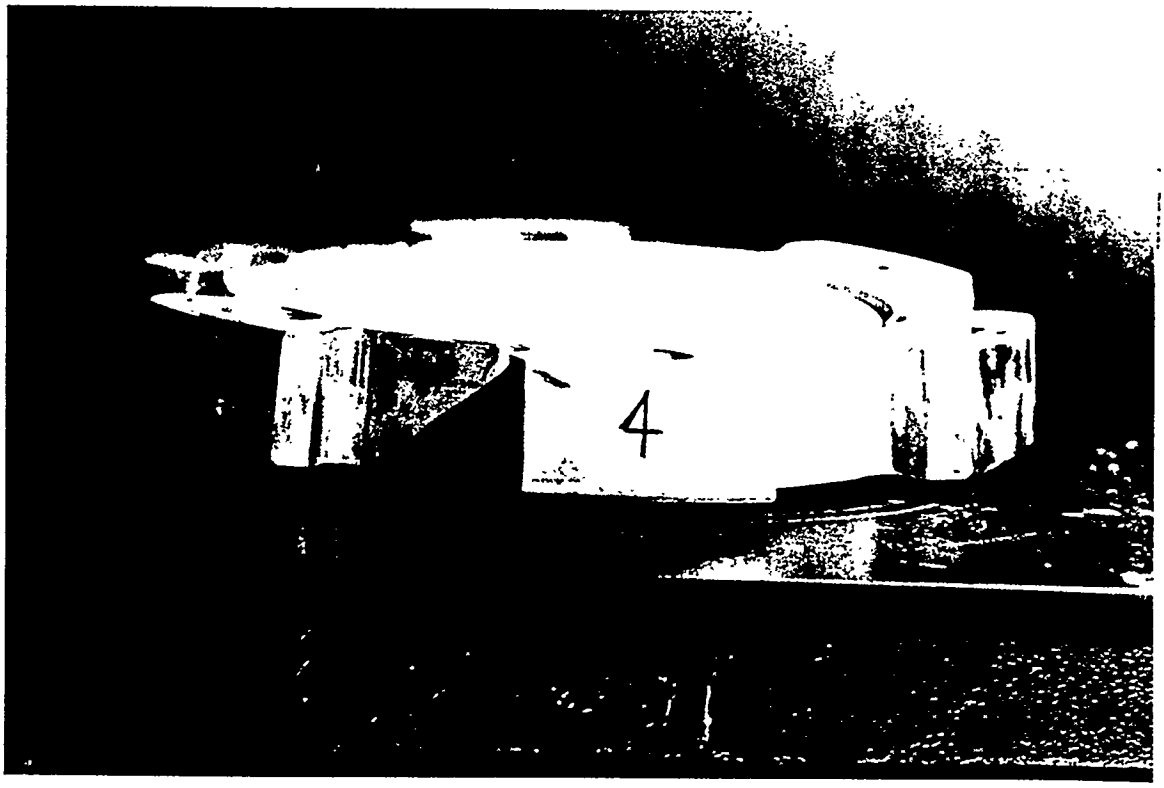

Fig. 2.8 Deformed Bottom Plate

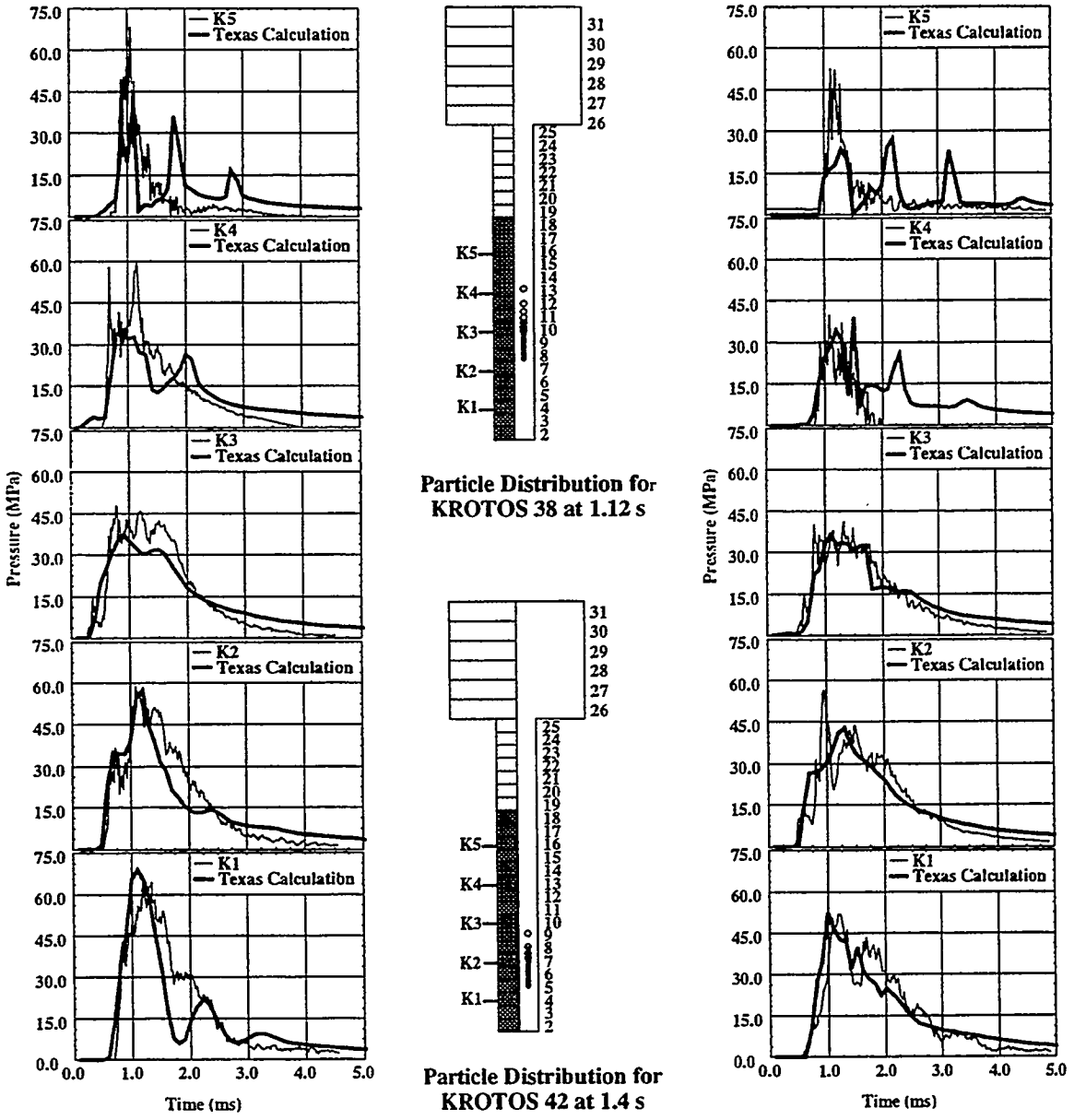

FIG. 2.9 - Comparison between TEXAS-IV and Experiment - KROTOS Tests 38 and42

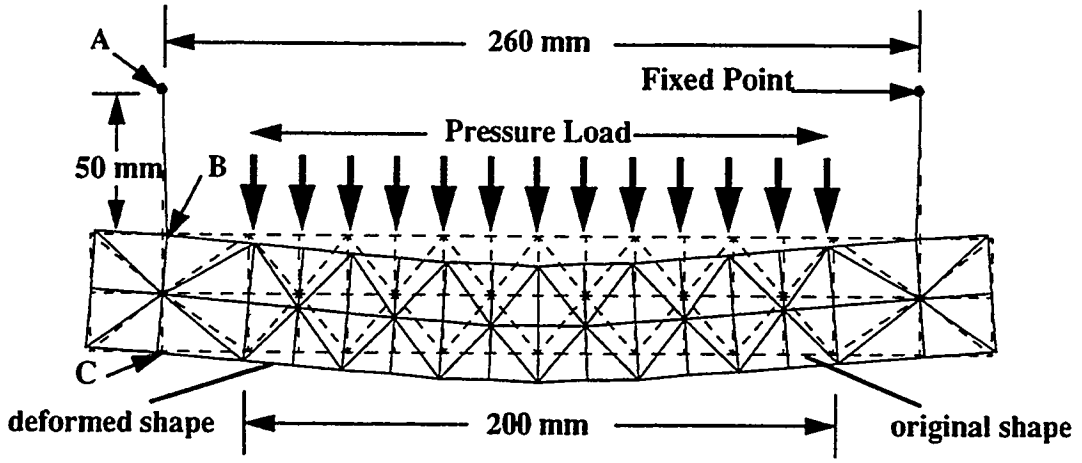

FIG. 2.10 - Pressure Loading of the KROTOS Test Section Base Plate - KROTOS 43

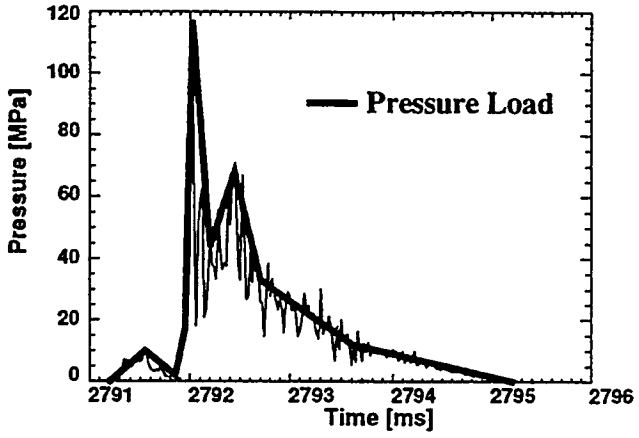

FIG. 2.11 - Gauge K1 Pressure Response

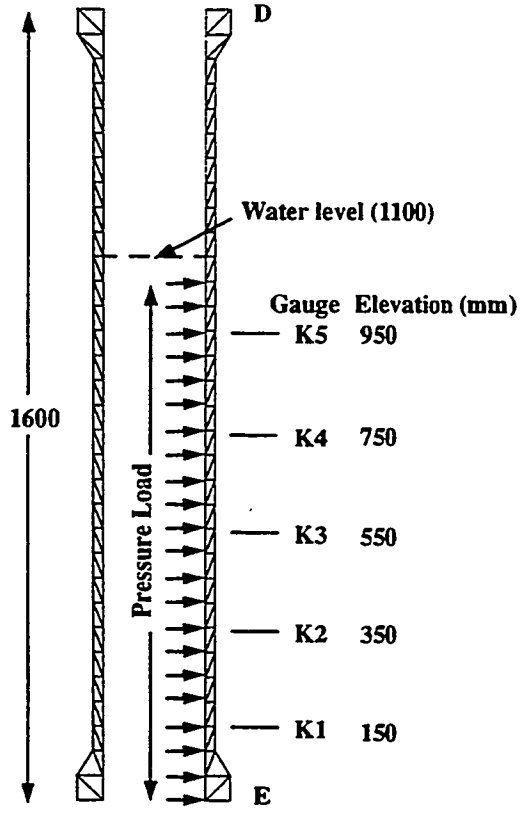

FIG. 2.12 - Pressure Loading of Cylindrical Test Section

AN OVERVIEW OF FUEL-COOLANT INTERACTIONS (FCI) RESEARCH AT NRC

S. Basu and T. P. Speis
Office of Nuclear Regulatory Research
U. S. Nuclear Regulatory Commission
North Bethesda, Maryland 20852

Abstract

An overview of the fuel-coolant interactions (FCI) research programs sponsored by the U.S. Nuclear Regulatory Commission (NRC) is presented in this paper. A historical perspective of the program is provided with particular reference to in-vessel steam explosion and its consequences on the reactor pressure vessel and the containment integrity. Emphasis is placed on research in the last decade involving fundamentals of FCI phenomenology, namely, premixing, triggering, propagation, and energetics. The status of the current understanding of in-vessel steam explosion-induced containment failure (alpha-mode) issue, and other FCI issues related to reactor vessel and containment integrity are reported, including the extensive review and discussion of these issues at the recently held second Steam Explosion Review Group Workshop (SERG-2). Ongoing NRC research programs are discussed in detail. Future research programs including those recommended at the SERG-2 workshop are outlined.

1. Introduction

The Fuel-Coolant Interactions (FCI) process involves transfer of energy from molten fuel to a surrounding coolant. During a postulated severe accident, the time scale for this mode of energy transfer may range from milliseconds to tens of seconds and even to hours. Interactions occurring in the milliseconds range could lead to energetic steam explosions which, if excessive, could challenge reactor vessel and containment integrity and, in turn, could lead to radiological releases to the environment. It is in this context that the FCI is considered a severe accident issue of potential risk significance and its resolution is sought in the framework of severe accident closure. Interactions occurring in the range of tens of seconds to hours are normally non-energetic and associated with quenching characterized by slow and partial fragmentation of melt and possible formation of a coolable debris bed. An understanding of the FCI issue associated with this form of interaction is important from the standpoint of debris coolability and subsequent arrest of accident progression. This paper gives an overview of the NRC-sponsored research on FCI in support of the above issues and the status of our understanding of these issues.

Energetic interactions could threaten reactor vessel or containment integrity either in the form of shock loading of structures over a very short time (typically less than ten milliseconds) or in the form of missile generation over longer times (typically up to few hundred milliseconds). The

failure mode induced by in-vessel steam explosion generated missiles was identified in the Reactor Safety Study, WASH-1400,[1] as the alpha-mode (or α-mode) containment failure, and was the primary focus in the early days of NRC-sponsored FCI research. In 1985, the first Steam Explosion Review Group (SERG-1) workshop was held to systematically evaluate the α-mode failure issue. The experts, who participated in that workshop, reviewed the then current understanding of the potential for containment failure from in-vessel steam explosions, and reached a consensus that the α-mode failure had a low probability. However, the experts recommended that more work would be necessary to develop a high confidence level in estimating the α-mode failure probability and in reducing the uncertainties in the estimates.

Much of the NRC-sponsored research since 1985 has been aimed at enhancing the technical basis for understanding this particular issue, estimating the bounds of potential energetics, determining conditions under which energetic interactions could occur, and resolving residual uncertainties in our understanding of fundamental processes involved in energetic FCI. Significant new research programs were also initiated during this period to investigate non-energetic FCI, i.e., melt quenching and coolability. Most recently, in June 1995, the second Steam Explosion Review Group (SERG-2) workshop was held to revisit the α-mode failure issue, and to evaluate our current understanding of other FCI issues of potential risk significance such as shock loading of lower head and ex-vessel support structures.

The overview in this paper covers the NRC-funded FCI research with particular emphasis on the progress made since the SERG-1 workshop, gives an account of the research on steam explosion fundamentals that has led to a better understanding of the α-mode issue and essential resolution of the issue from a risk perspective, and discusses NRC's ongoing programs on other FCI issues of importance, both energetic and non-energetic. The paper concludes with a brief discussion of future research direction based on recommendations from experts who participated at the SERG-2 workshop, and based on NRC's risk-oriented approach towards severe accident closure.

2. Past Research on Steam Explosion Fundamentals

The experts, who participated at the SERG-1 workshop in 1985, reached a consensus that the occurrence of an in-vessel steam explosion of sufficient energetics which could lead to α-mode containment failure had a low probability (median value $< 10^{-3}$ given a core melt accident, range of values between 10^{-1} and 10^{-5}). They acknowledged, however, that a degree of belief or subjectivity was associated with the individual failure probability estimates (see NUREG-1116[2]) for lack of a more complete "quantitative" understanding of the fundamental processes involved in FCI (e.g., premixing, triggering, and propagation). These estimates were based on a segmental approach to the overall sequence of events whereby the overall quantification is considered to be the product of probability measures for (1) melt initial conditions, (2) melt-water mixing and energy conversion, and (3) slug dynamics and missile loading. Most experts took a conservative approach in estimating the probability measure for melt initial conditions for lack of well validated data on core melt progression, melt relocation and transport to the lower plenum, and melt composition and properties. Many experts also took a similar conservative approach in estimating the probability measure for slug dynamics and missile loading. In

contrast, a wide range of probability measures from conservative to best estimate was provided by experts for melt-water mixing and energy conversion. The best estimate measures were based on the reasoning that only a limited melt mass would participate in an FCI, and also that the energy conversion in a large-scale system would be substantially lower than the theoretical thermodynamic limit. Consequently, further research on premixing to support the "limits-to-mixing" argument, became essential in developing a higher level of confidence to the α-mode failure quantification process.

In response to this need, the NRC funded a program at the University of California at Santa Barbara (UCSB) in 1989 to perform both theoretical and experimentally-oriented research on steam explosion fundamentals. In this program, Theofanous and his co-workers[3] investigated the water depletion phenomenon during premixing in support of the argument that only a limited melt mass is likely to participate in an FCI. The phenomenon refers to vaporization of substantial water mass from the mixing region due to rapid melt-to-coolant heat transfer, and displacement of remaining water mass away from the region caused by steam. As a result, the mixing region becomes largely void of water, and the steam produced from water vaporization acts as a barrier to further melt-coolant interactions. The concept of "microinteraction" for studying propagating steam explosions was also developed under this program. This concept provides a mechanism to study, in a systematic manner, various stages of escalation of an explosion from its initiation to sustenance of pressure waves in the melt-water-steam interaction zone to propagation of fully-developed shock waves.

Premixing Phenomena

The premixing phase of FCI is characterized by the breakup of one or more melt pour streams in contact with a coolant (water), melt droplet production and transport, vapor production, and water displacement from the melt-water interaction region. The objective of premixing research is to understand the underlying physics of the phenomena and to provide a basis for estimating the spatial distribution of melt, vapor (steam), and water at the instant a trigger is postulated to initiate a propagating interaction. This distribution is used in predicting the energy transfer from the fuel to the coolant.

Two contrasting concepts of premixing were developed in the early days, the first by Theofanous and Saito[4] and the second by Henry and Fauske[5], in the course of the Zion and the Indian Point PRA studies.[6] The Theofanous and Saito concept considered the premixing phenomena in terms of an interfacial stability in a two-phase medium, caused by hydrodynamic breakup of a gravity-driven coherent melt jet in contact with a surrounding coolant. The Henry and Fauske concept considered the phenomena also in terms of an interfacial instability, but caused by a thermally-driven jet fragmentation mechanism. Leaving aside the differences, both concepts led to a general observation that the mixing of melt and water was limited. In the case of hydrodynamic breakup, the limitation is imposed by a melt length scale, in particular, the ratio of melt flight path to melt jet diameter. In the case of thermal breakup, the limitation is imposed by the amount of coolant that can penetrate fragmented melt particles surrounded by a vapor blanket. In an earlier assessment of steam explosion-induced containment failure[7], Theofanous and his

co-workers recognized that both concepts required further investigation and some form of integration so that a stronger case could be made concerning their implications to the α-mode failure issue.

In subsequent work, Amarasooriya and Theofanous[8] extended the previous two-phase (melt and coolant) hydrodynamic treatment to three-phase (melt, coolant, and vapor) treatment in which both hydrodynamic and thermal aspects were considered. Under the NRC-funded research at the UCSB mentioned previously, Theofanous and co-workers performed the MAGICO series of experiments to characterize in detail the spatial-temporal evolution of the three-phase mixing zone. The experiments consisted of releasing kilograms of millimeter size hot steel spheres simulating a melt jet into a pool of saturated water in 1/8 and 1/4-scale lower plenum-like geometries, and studying the evolution of the three-phase interaction zone and the associated water depletion phenomenon. Control parameters varied in the experiments included pool depth (15, 25 and 50 cm), pour diameter (12 and 20 cm), freefall distance (5, 15 and 25 cm), particle size (1.5 mm and 2.4 mm), and particle temperature ranging from 823 to 1153 K. Key measurements in the experiments included local void fractions and global void fractions during a premixing transient. The local void fraction measurements capture the fluctuating characteristics of the voiding phenomenon at a local level (sample mixing volume several orders of magnitude smaller than the total mixing zone), whereas the global void fraction measurements are space averages of local fractions over a defined mixing domain (either the actual mixing volume or a cylindrical volume of height equal to the pool depth and radius equal to pour radius). The two measurements are complimentary to each other.

The results from MAGICO experiments demonstrated steam voiding around the hot spherical particles. The mixing region was found to be depleted of water, in part, as a result of its vaporization due to rapid melt-to-coolant heat transfer, and, in part, due to displacement of remaining water mass away from the interfacial region caused by steam. Substantial variations in the local void fraction measurements were observed, perhaps indicative of an interfacial instability during the transient. Generally, the global measurements showed certain trends when correlated with various experimental parameters. For example, the pool depth-averaged void fractions increased with decreasing pool depth. Overall, the MAGICO experiments provided a technique for quantifying the steam voiding phenomenon during premixing, and a data base for assessment of premixing codes.

The calculated global void fractions using, for example, PM-ALPHA were in reasonably good agreement with the MAGICO data, particularly, when the pool depth-averaged ones were compared. The code was also assessed against FARO quenching experiments L-6 (scoping test) and L-8 (quenching test QT2).[9] Comparison of predicted pressure history with the L-6 data was remarkably good, given that L-6 and all other FARO experiments use melt streams whereas the PM-ALPHA calculations are done with pre-fragmented melt particles.

The NRC-initiated FCI research program at UCSB continued in the recent years, however, under the auspices of the U.S. Department of Energy's Advanced Reactor Severe Accident Program (ARSAP). Additional MAGICO experiments were carried out under this program using cold (room temperature) and hot (up to 1800 K) particle clouds as well as single particles of oxidic (zirconium oxide and aluminum oxide), metallic (steel), and composite (silicon carbide)

materials. The cold experiments were conducted to study the space-time evolution of particle clouds under an isothermal condition. The hot experiments were extension of early MAGICO experiments to different melt simulants at higher temperatures. These experiments are described in detail in reference [10], and are mentioned here for the sake of completeness. In addition to providing a more expanded data base for the validation of premixing codes, these experiments are useful in studying a basic multiphase flow problem, i.e., that of film boiling from single spheres vs. spherical clouds. This distinction becomes important when particle-based codes are used for premixing calculations of continuous melt streams.

The premixing research, briefly discussed above, clearly indicates that the field is more mature now than in the past. There is general agreement among the majority of the experts who participated at the SERG-2 workshop, that substantial progress has been made in this area since the SERG-1 workshop. Most experts also agree that the existing analytical tools (premixing codes) may be adequate for performing premixing calculations in a multiphase system with a reasonable degree of accuracy. However, a more extensive assessment of these codes against melt jet experiments would be required to verify their robustness. More importantly, premixing research in the past few years demonstrated the water depletion phenomenon in support of the "limits-to-mixing" argument which is essential in resolving the α-mode failure issue.

Triggering Phenomena

Triggering is considered to be associated with the collapse of a vapor film locally around a melt droplet. The collapse is caused by an instability in the melt-coolant interaction zone resulting from a pressure perturbation or a flow perturbation. In reactor situations, numerous events may contribute to such perturbations, e.g., control rod dropping, sudden valve closure, pump cavitation, collapsing structures, and condensation, to name a few. The local vapor collapse produces fragmentation of the melt droplet, and an extremely rapid heat transfer to the surrounding coolant takes place resulting in a pressure spike and subsequently, a propagating wave. Clearly, triggering plays an important role in linking premixing and propagation, and in understanding these phenomena in an integral sense. By itself, however, triggering is a rather complex process that is difficult to model and to investigate experimentally. For this reason, most, if not all, experimental research on triggering is carried out in conjunction with integral FCI experiments.

Early NRC-funded research, which examined various aspects of triggering as part of the integral FCI or steam explosion experiments, includes steam explosion efficiency studies (open-geometry test series), the EXO-FITS series of tests, and the FITS series of tests, all performed at the Sandia National Laboratories (SNL). This extensive body of work is summarized in two review papers on steam explosion research by Corradini[11,12] and a third review paper, exclusively on triggering research, by Fletcher.[13] The last reference also cites another NRC-funded effort at the Argonne National Laboratory (ANL) dealing with fragmentation and quenching behavior of corium melt streams in water.[14] Additional triggering studies have been and continue to be performed by Corradini at the University of Wisconsin FCI facility, WFCI, and by researchers at the JRC/Ispra FARO/KROTOS facility. These studies will be elaborated further in this paper in relation to NRC's ongoing FCI research programs.

The SNL work led to a number of observations with potential implications to triggering of steam explosions in reactor prototypic situations. Of the experiments performed with prototypic reactor melts interacting with saturated to subcooled water at an ambient pressure of nominally 0.1 MPa, only one or two cases exhibited weak steam explosions either at high melt-to-coolant volume ratios or at high subcooling, and only when an external trigger was used. In contrast, many more cases using iron-alumina thermite and iron oxide as melt simulants produced strong steam explosions at a wide range of melt-to-coolant volume ratios, much lower subcooling to almost saturated conditions, same ambient pressure condition as that in the prototypic melt tests, and with or without the use of external trigger. Only at high ambient pressures and in the absence of an external trigger, steam explosion was suppressed in a few of these simulant experiments. The difficulty to trigger an explosion in a reactor prototypic melt-water system was also confirmed in the ANL experiments as well as in the FARO/KROTOS experiments.

Despite the above observations and similar findings from other non-NRC research programs, there is an overwhelming sense among the experts that the triggering process is poorly understood, due largely to its inherently random nature. The available data supports the assumption that a trigger would likely be available under accident conditions of interest in a reactor prototypic situation, but that the combination of material characteristics and the potential trigger strength would likely produce relatively weak steam explosions. Nevertheless, from the perspective of safety assessment and risk significance, most experts suggest a conservative approach to triggering, whereby it is assumed that an explosion would be triggered at the worst time during a premixing transient leading to trigger amplification or shock wave propagation.

Propagation Phenomena

The propagation phase of FCI is characterized by escalation of a trigger perturbation into a shock front that propagates through the multiphase interaction zone consisting of melt, steam, and water. The shock front is accompanied by an elevated pressure behind it, generated by the fuel-coolant energy transfer as a result of fine-scale fragmentation. The objective of propagation research is to investigate shock propagation in multiphase media, and to estimate the magnitude of fuel-coolant energy transfer and resulting pressurization, given a distribution (premixture) of fuel, steam, and coolant and their thermodynamic states.

As mentioned previously, the primary focus of NRC-funded FCI research in the early days was to understand and quantify the α-mode failure for which one needs only to calculate the thermal-to-mechanical energy conversion ratio, given a premixture (melt-steam-water distribution). Consequently, very little attention was paid in the early days to understand the underlying details of the propagation phenomena. This is because the experts generally share the view that the propagation phase can be treated conservatively from the standpoint of energetics using variants of the Hicks-Menzies or Board-Hall approach. At the conclusion of the SERG-1 workshop and based on the recommendations of experts who participated at that workshop, the NRC initiated a research program at the UCSB to study the fundamentals of propagation. The work, reported in reference [3], focussed on formulating the "microinteraction" concept, and performing hydrodynamic shock tube (SIGMA) experiments to verify the concept and to support its further development. This concept led to the development of the propagation code, ESPROSE.m.[15]

It is now a widely accepted view that the very early stages of an energetic FCI are dominated by thermally-induced fragmentation, whereas the very late stages (fully developed shock wave) are dominated by hydrodynamic fragmentation. It is the intermediate regime (escalation) where a strong coupling or feedback between the thermal and hydrodynamic fragmentation processes is believed to exist. The microinteraction concept provides a rational means to study this intermediate regime through the formulation of multidimensional pressure and velocity fields, taking into account the dynamic aspects of thermal-hydrodynamic interactions. The experiments, carried out at the SIGMA facility, consisted of releasing single drops of molten tin at different temperatures into the water-filled shock tube at two pressure levels, 6.6 MPa and 20 MPa, and measuring fragmentation using the X-ray imaging technique. Results from the SIGMA experiments show that at low to intermediate temperatures and low pressure, there is negligible fragmentation. However, at intermediate to high temperatures and high pressure, there is substantial fragmentation and it is thermally-driven.

The NRC-initiated propagation research at UCSB is continuing under the auspices of DOE. The work is described in reference [16], and is mentioned here for the sake of completeness.Besides the UCSB work, the NRC funded a research program in propagation and energetics at the University of Wisconsin. This program is continuing at present and will be discussed in detail later in the text.

While the current level of understanding of the propagation phase is adequate for estimating the net energy transfer to the coolant and hence, estimating the α-mode failure probability, it is recognized that understanding the consequences of localized FCI (shock loading of cavity structures, lower head loading, etc.) requires more rigorous treatment for which detailed propagation phase models are necessary. Nearly all experts agree that a two-dimensional propagation code is needed at a minimum. Some experts even recommend a three-dimensional code. It is also recognized that along with the development of multidimensional propagation codes, a more extensive experimental data base is necessary against which these codes can be assessed. Experimental work at UCSB, FARO/KROTOS, University of Wisconsin, and elsewhere are expected to provide the required experimental data.

3. Reassessment of the Alpha-Mode Failure Issue

As mentioned elsewhere in this paper, much of the NRC-funded FCI work since the SERG-1 workshop was aimed at enhancing the technical basis of the α-mode failure estimates given by the experts, and reducing uncertainties in the estimates in order to achieve an essential resolution of the issue from a risk perspective. Given the progress made in the last ten years in understanding the fundamentals of steam explosions, NRC convened the SERG-2 workshop in June 1995 to reassess the α-mode failure issue and to evaluate the current understanding of other FCI issues of potential risk significance. The reassessment and review were to be benefited from the significant progress in FCI research made in the U.S. and in other countries since the SERG-1 workshop.

To accomplish the objectives, a group of experts from academia, industry, and research community was invited to participate in the workshop. The experts were requested to provide

written responses, prior to the workshop, to a number of questions and issues focussing on major topical areas of FCI such as premixing, triggering, and propagation phenomena. FCI energetics, damage consequences, chemical augmentation, pressure suppression effect, and the role and importance of accident progression and melt relocation in providing initial conditions for FCI were also among the discussion topics. Furthermore, the questions focussed on residual uncertainties, if any, in resolving the alpha-mode failure issue, and on the status and capabilities of analytical tools.

Extensive discussions took place at the SERG-2 workshop among the experts, and consensus opinions on various topical areas emerged from such discussions. Of the eleven experts, all but two concluded that the α-mode failure issue was "essentially" resolved, meaning that this mode of failure is of very low probability, that it is of little or no significance to the overall risk from a nuclear power plant, and that any further improvement in our understanding of the various FCI phenomena and any further reduction in residual uncertainties are not likely to change the probability in an appreciable manner. For a more detailed discussion of the SERG-2 conclusions and recommendations, refer to the proceedings of the workshop (NUREG-1529).[17]

Table 1 summarizes the experts' estimates of the probability of α-mode failure given a core melt accident, compares the same with the estimates arrived at the SERG-1 workshop and with the WASH-1400 best estimate, and presents the status of resolution of the issue. Consideration of a number of factors was left to the judgement of the experts in arriving at their conclusions. These factors include: (1) potential differences between PWR and BWR geometries, (2) differences between low-pressure and high-pressure primary system initial conditions, and (3) the melt mass and other conditions in the reactor core prior to a postulated interaction of the melt with water in the lower plenum. The estimates of failure probability expressed by those SERG-2 experts, who also participated in the SERG-1 workshop, are generally an order of magnitude lower than the SERG-1 estimate. Note that the median value of the SERG-1 estimate is $<10^{-3}$, whereas the individual estimates range from 10^{-1} to 10^{-5}. Note also that the WASH-1400 best estimate failure probability is $<10^{-2}$. Some experts suggested the probability of the α-mode failure was vanishingly small so that there was no particular need to quantify the estimate. Some other experts noted that their estimates were still based, in part, on engineering judgement despite more quantitative information now available from FCI research. One expert was unable to provide a quantitative estimate suggesting that an adequate knowledge was still missing.

The dominant overall judgement of the experts is that the combination of events leading to α-mode containment failure is highly unlikely. The arguments related to fuel-coolant premixing, steam voiding and water depletion phenomena, discussed in the preceding section, played a key role in many experts' reasoning. These arguments pertain to the expected limited melt mass involved in a steam explosion, and the dynamics of the propagation phase which would be significantly mitigated by the presence of large void volume within the interaction zone. According to some experts, the limits-to-mixing argument alone may not be sufficient to preclude α-mode failure. Other mitigative factors, representative of real reactor situations, may contribute to low failure probability. These factors include expected limited thermal-to-mechanical energy conversion, and a range of dissipative phenomena involved in slug motion to the upper head.

Table 1. Alpha-Mode Failure Probability Estimates (Given a Core Melt Accident)

Participant	SERG-1 (1985)	SERG-2 (1995)	View on Status of Alpha-Mode Failure Issue
Bankoff	$< 10^{-4}$	$< 10^{-5}$	Resolved from risk perspective
Berthoud	--	$< 10^{-3}$	No statement on resolution
Cho	< WASH-1400*	$< 10^{-3}$	Resolved from risk perspective
Corradini	10^{-4} - 10^{-2}	$< 10^{-4}$	Resolved from risk perspective
Fauske	Vanishingly small	Vanishingly small	Resolved from risk perspective
Fletcher	--	$< 10^{-4}$	Resolved from risk perspective
Henry	--	Vanishingly small	Resolved from risk perspective
Jacobs	--	Probably low likelihood	Not resolved from risk perspective
Sehgal	--	$< 10^{-2}$	Resolved from risk perspective
Theofanous	$< 10^{-4}$	Physically unreasonable	Resolved from risk perspective
Turland	--	$< 10^{-3}$	Resolved from risk perspective

* WASH-1400 best estimate $< 10^{-2}$; SERG-1 consensus estimate $< 10^{-3}$

A proposed approach to an orderly closure of the α-mode failure issue, which would utilize and integrate the consensus opinions of experts on the subject, was briefly discussed. Most experts felt that the issue was essentially resolved from a risk perspective and, as such, a formal closure, though desirable, was not warranted at this point. Generally, however, the experts expressed a strong need for some additional research to further improve the understanding of physics underlying the steam explosion phenomena. This improvement of understanding, while not critical for further resolution of the α-mode failure issue from the risk perspective, is important for resolving other FCI issues such as lower vessel head integrity under a steam explosion load and shock loading of ex-vessel structures. As an added benefit, the improved understanding is expected to increase further the level of confidence associated with the α-mode failure probability estimate.

4. Current NRC Research Programs on FCI

The focus of current NRC research programs on FCI is on residual issues which are summarized in Table 2. Briefly, the issues addressed by the ongoing research programs are: large scale

Table 2. Fuel-Coolant Interactions: Residual Issues

Phenomena	Issue	Research Recommendations
Melt Relocation	• initial melt conditions	• improved late phase melt progression modeling
Premixing	• melt jet breakup • premixing of multiple jets • water depletion phenomena for melt jets • pressure effects on premixing	• assessment of premixing models and codes against melt jet experiments • improved melt fragmentation modeling • experiments to study pressure effects on premixing • plant safety assessment
Triggering	• pressure effect on triggerability • triggerability of prototypic melts • triggering of multiple explosions • trigger amplification vs. propagation	• experiments to study pressure effects on triggerability • experimental evaluation of triggerability of prototypic melts • scoping calculations for multiple explosions • minimum trigger requirements for propagation
Propagation	• melt fragmentation during propagation • multidimensional propagation modeling • fluid-structure interactions	• assessment of existing propagation models and codes against melt jet experiments • improved fragmentation modeling • modeling of fluid-structure interaction effects and experimental studies
FCI Energetics and Damage Consequences	• dissipative effects of internal structures • localized structural response	• experiments and modeling of dissipative effects • assessment of structural response models and codes
Other	• scaling issues: material and geometric • chemical augmentation	• development and validation of scaling principles • experiments with a range of simulant and prototypic materials • chemical augmentation experiments with metallic content in melts

integral experiments at FARO to investigate melt quenching and melt jet fragmentation, modeling of jet fragmentation, pressure effects on FCI phenomena (premixing, triggering, and propagation) and FCI energetics, propagation experiments (still predominantly in one dimension), chemical augmentation, and scale effects (both geometric and material). Other issues, listed in Table 2 but not addressed by NRC's ongoing FCI research programs, include improved late phase melt progression modeling, understanding of the basics of triggering phenomena, multidimensional propagation in multiphase media (both experiments and model development), dissipative effect of structures on FCI energetics, fluid-structure interaction modeling, assessment of structural response models and codes, and application of FCI analytical tools to plant safety assessment. Recommendations made by the SERG-2 experts to pursue further research on these issues are discussed in the next section in the context of future research plan.

FARO/KROTOS Program

The FARO/KROTOS program at the Joint Research Center (JRC), Ispra, is a long-range program that addresses premixing, quenching, propagation, and FCI energetics, in relation to melt jets. The NRC has been a participant in this program under a Technical Exchange Arrangement with the Safety Technology Institute of the Commission of the European Communities. The program originally started in 1990 as a four-year experimental effort to investigate interactions of prototypic (UO_2-ZrO_2) melt with water. The thrust of this program was in-vessel steam explosions and in-vessel debris coolability. A new four-year effort was initiated in 1995 with the emphasis on ex-vessel FCI and ex-vessel debris coolability. Further discussion here will focus on the ongoing effort, and on the recently completed previous effort, as appropriate.

Experiments in the FARO facility are designed to investigate the quenching and fragmentation of prototypic melt jets at a wide range of pressures (5 MPa to as low as 0.1 MPa). The high pressure experiments are prototypic of in-vessel scenario whereas, the low pressure experiments are prototypic of ex-vessel scenarios. Experiments in the KROTOS facility are designed to complement the FARO experiments in two ways. First, the basic FCI processes, particularly, the premixing and fragmentation phenomena are investigated in small-scale and well-instrumented KROTOS experiments. The results provide a basis for conducting FARO experiments at larger scales. Second, the KROTOS experiments utilize both simulant and prototypic melt materials so that the material effects in steam explosion can be investigated.

The progress of the FARO/KROTOS program was presented at various international meetings in the past,[18-20] and most recently, at the Twenty-Third Water Reactor Safety Meeting.[21] The FARO experimental setup is shown in Figure 1, and the KROTOS in Figure 2. The FARO setup consists of a melt furnace, a melt release vessel, and a water-filled interaction (test) vessel, TERMOS, equipped with a debris catcher and connected downstream to a condenser unit. Measurements in the FARO facility include pressure and temperature of the freeboard volume, water, and condensing system components; temperature of melt, debris catcher, bottom plate, and condensing system components; water level swell; and mass spectrometry for gas sampling. The components of the KROTOS facility are essentially similar, though at a smaller geometric scale, to those of the FARO facility. It has a melt generator (furnace and release vessel

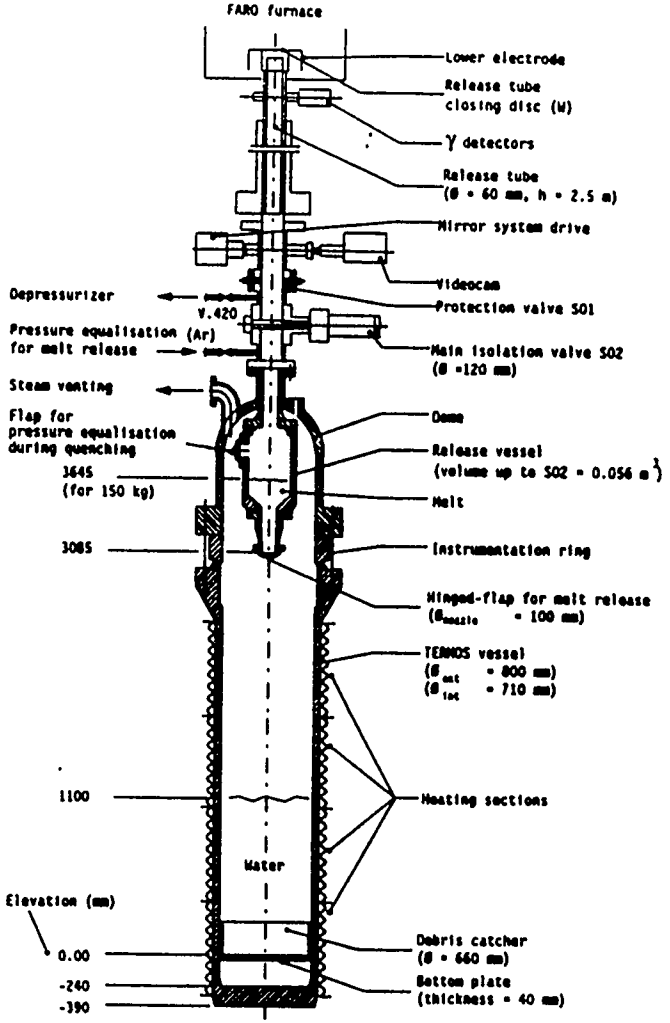

Figure 1. FARO Test Apparatus

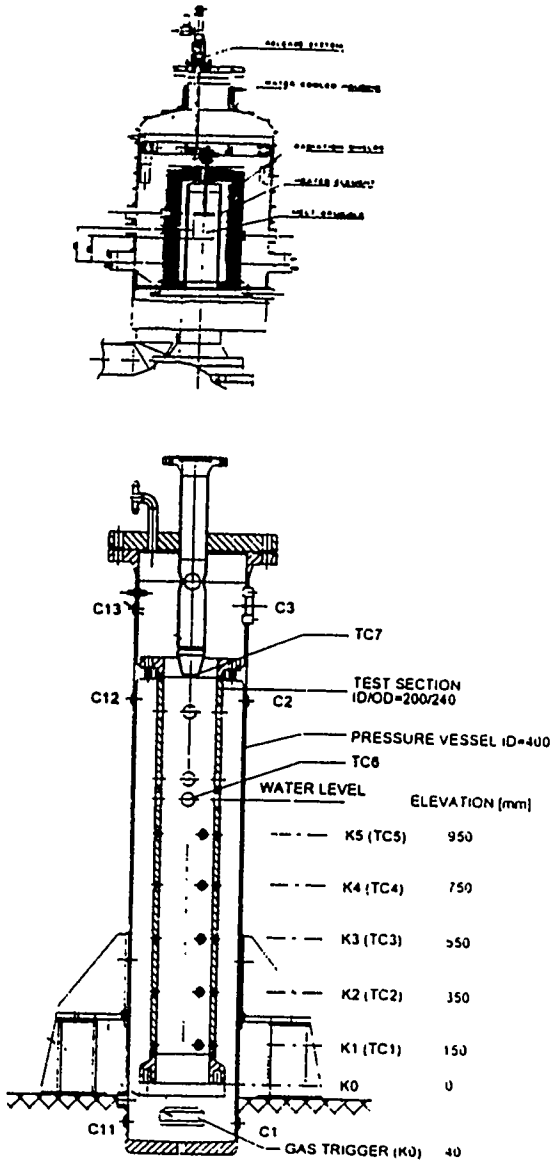

Figure 2. KROTOS Test Apparatus

combined) and a water-filled test section confined within a pressure boundary. A gas trigger is provided at the base of the test section, and there is no condenser unit in the KROTOS arrangement. Measurements in KROTOS are essentially similar to those in FARO. A comparison of some important features of the FARO and KROTOS facilities, as well as other FCI facilities used for the ongoing NRC-funded research is given in Table 3.

Table 3. FCI Experimental Facility Characteristics

Facility	Test Section Dia. (mm)	Melt Jet Dia. (mm)	Water Depth (m)	System Pres. (MPa)	Melt and Mass (kg)
FARO	470 - 1500	100	0.05 - 2.0	0.1 - 5.0	UO_2-ZrO_2 (w/ and w/o Zr and SS) 18 - 250
KROTOS	95 - 200	30 -50	1.0	0.1 - 1.0	UO_2-ZrO_2 Al_2O_3 1.4 - 6.0
WFCI	87 - 200	30	1.0	0.1	Sn 0.8 - 4.5 FeO, Fe_3O_4
ZREX	100	25 - 50	1.0	0.1	Zr (w/ and w/o ZrO_2) 0.2 - 1.0

To date, five successful FARO experiments (L-6, L-8, L-11, L-14, and L-19) have been performed, all at an ambient pressure of 5 MPa, using a UO_2-ZrO_2 melt composition (in L-11, a small amount of Zr was added). The initial and boundary conditions of the FARO experiments are summarized in Table 4, and the results are summarized in Table 5. Steam explosion was not observed in any of the five experiments. A relatively consistent quenching pattern was observed in all experiments with mean fragmentation sizes between 3 and 5 mm. Approximately 50 to 80 percent melt fragmented in these experiments with the exception of L-11 in which 100 percent melt fragmented. The temperature of the bottom plate, designed to simulate the lower head shell in these experiments, increased to a maximum of 330 K, and the plate was intact in all experiments. The oxidation of 4 w/o metallic zirconium in the initial melt composition is hypothesized to be responsible for complete fragmentation in the L-11 test, although there was no quantitative measurement of hydrogen generation (from zirconium oxidation by steam) to support this hypothesis.

A much larger number of KROTOS experiments have been performed during the same time period, due primarily to the relative ease of performing these small-scale experiments. The

Table 4. Initial and Boundary Conditions for FARO Experiments

Initial Conditions	L-6	L-8	L-11	L-14	L-19
Melt mass (kg)	18	44	125	151	155
Composition (w/o UO_2-ZrO_2-Zr)	80/20/0	80/20/0	77/19/4	80/20/0	80/20/0
Melt temp. (K)	2923	3023	2823	3073±50	3073
Water depth (m)	0.87	1.0	2.0	2.05	1.1
Water mass (kg)	120	255	608	623	334
Water temp. (K)	539	536	535	537	537
Vessel dia. (m)	0.470	0.710	0.710	0.710	0.710
Init. pres. (MPa)	5.0	5.8	4.9	5.0	5.0

Table 5. Summary of Results of FARO Experiments

Measured/observed Data	L-6	L-8	L-11	L-14	L-19
Steam explosion	no	no	no	no	no
Melt fragmented (kg)	12	30	151	105	77.5
Melt on bottom (kg)	6	14	0	20	77.5
Mean frag. size (mm)	4.5	3.8	3.5	4.8	3.7
Bottom plate state	intact	intact	intact	intact	intact
Bottom plate ΔT (K)	--	275	20	252	330
Maximum ΔP (MPa)	1.1	1.8	5.1	2.8	3.2
Water ΔT (K)	15	23	27	28	32
Max. level swell (mm)	130	410	1000	1100	1100

initial conditions of the most recent KROTOS experiments are summarized in Table 6, and the results are summarized in Table 7. Steam explosion was not observed in the experiments involving a prototypic melt composition at all water subcooling levels considered. However, in experiments involving simulant melt (Al_2O_3), steam explosions were observed with or without trigger, particularly at high water subcooling. One simulant experiment at saturated water condition showed a benign interaction. It is interesting to note that the melt superheat has virtually no effect on the occurrence of steam explosions. It also appears, based on a single data point at present, that a nominally higher ambient pressure (0.2 MPa as opposed to 0.1 MPa) may not suppress steam explosions. These experiments clearly indicate that the material behavior plays a critical role in the occurrence of steam explosions.

Table 6. Initial and Boundary Conditions for Recent KROTOS Experiments

Initial Conditions	37	38	40	41	42	43
Melt mass (kg)	3.22	1.53	1.47	1.43	1.54	1.50
Composition	UO_2-ZrO_2	Al_2O_3	Al_2O_3	Al_2O_3	Al_2O_3	Al_2O_3
Melt temp. (K)	3018	2665	3073	3073	2465	2625
Water depth (m)	1.1	1.1	1.1	1.1	1.1	1.1
Water mass (kg)	34.5	34.5	34.5	34.5	34.5	34.5
Water temp. (K)	294	294	290	368	293	295
Subcooling (K)	79	79	83	5	80	89
Init. pres. (MPa)	0.1	0.1	0.1	0.1	0.1	0.2
Gas trigger	yes	yes	no	no	no	no

In the past KROTOS experiments, there was no provision to measure directly the void fractions (vapor volume fractions). The global void fractions were calculated in these experiments based on the level swell measurements. Future KROTOS experiments are planned to be equipped with devices for measurements of local void fractions. Therefore, data from these experiments can be used more effectively to assess the premixing codes. Also, future FARO experiments may need to be equipped with a gas sampling device so that hydrogen generation, if any, can be quantified.

University of Wisconsin Program

The objective of the propagation experiments at the University of Wisconsin is to identify the combination(s) of fuel and coolant parameters that can lead to energetic FCI. The results can be used to define the conditions under which energetic FCI occurs and to provide quantification

Table 7. Summary of Results of Recent KROTOS Experiments

Measured/observed Data	37	38	40	41	42	43
Steam explosion	no	yes	yes	no	yes	yes
Max. ΔP (MPa)	0.07	69	86	0.1	57	117
Impulse (kPa-s)	--	76.2	60.5	--	72.5	68.4
Impulse depth (mm)	--	955	955	--	755	955
Kinetic energy (kJ)	--	96.1	60.6	--	110.0	77.4
Efficiency (%)	--	1.5	0.9	--	1.9	1.3
Debris< 250μm (g)	116	934	674	n/a	781	721

of such energetics. Moreover, the results may be extrapolated, with the help of a scaling methodology, to reactor prototypic situations.

The Wisconsin Fuel-Coolant Interactions (WFCI) is a one-dimensional test facility, an overall view of which is shown in Figure 3. The WFCI facility consists of a melt furnace, a remotely-operated melt delivery system, a one-dimensional test vessel fitted with a triggering device at the base, and an expansion tube connected at right angle to the test section at one end and to a quench tank at the other end. Measurements in the WFCI facility include temperature of melt and water, pressure at various locations (elevations) in the test section, water level swell, and slug displacement. The experiments to date, using a 87 mm diameter test section and tin simulant, were conducted in multiple series to investigate, in a controlled manner, the effect of fuel and/or coolant parameters on the steam explosion potential and on the conversion ratio. Description and objectives of these tests are summarized in Table 8. The initial and boundary conditions of the WFCI experiments (Series C through H) are summarized in Table 9, and the corresponding results are summarized in Table 10. All experiments were carried out at an ambient pressure of 0.1 MPa and using a constant water mass of 8.6 kg. Details of experiments and results can be found in references [22] and [23]. Note that Series A experiments were scoping tests, and Series B experiments were trigger tests with otherwise identical initial and boundary conditions as in Series A. these tests are not discussed further here.

The conversion efficiency was calculated from the experimental data as a ratio between work done to displace the slug mass and the steam explosion energy. The ratios calculated in this manner from different series of experiments are significantly lower (less than 1%) than the theoretical thermodynamic limits (Board-Hall, Hicks-Menzies, or some variants of these) suggesting that only a small melt mass is likely to participate in the FCI. Considering that a large fraction of the mechanical energy may be lost in the experimental circuit, the modified conversion efficiencies will still be significantly lower than the thermodynamic limit. it is

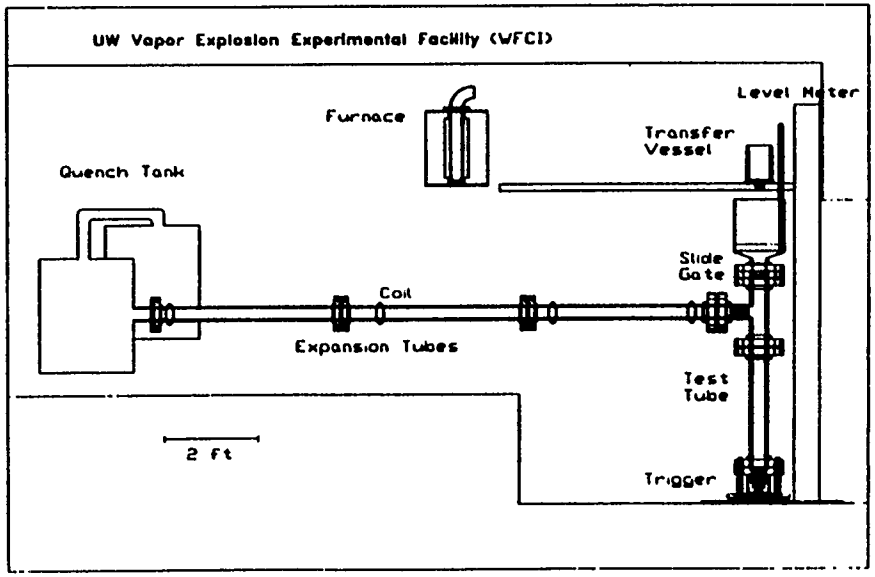

Figure 3. WFCI Experimental Setup

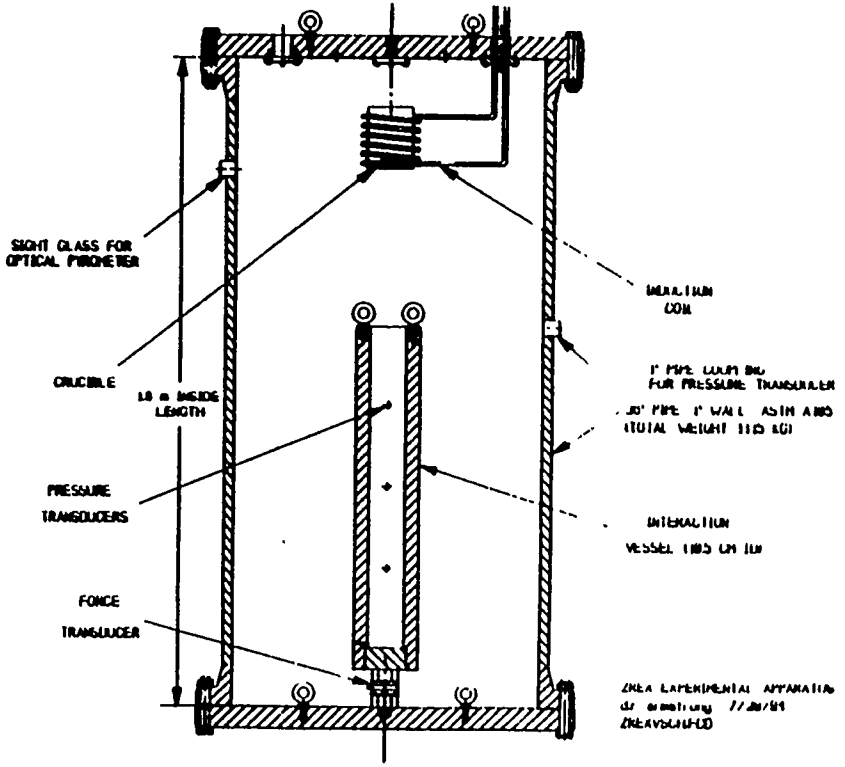

Figure 4. ZREX Test Apparatus

Table 8. Test Matrix for WFCI Experiments with Tin Simulant

Test Series	Test Objective and Description
A	Scoping tests to demonstrate reproducibility of data; six tests run, all triggered
B	Three tests run without external triggers, otherwise with identical initial conditions as in Series A to understand the effect of triggering
C	Six tests run with variable trigger strength to further understand the effect of triggering
D	Six tests run with variable slug mass to study the effect of system constraint on conversion ratio
E	Three tests run with variable melt temperatures to study the effect of melt superheat on conversion ratio
F	Three tests run with variable water temperatures to study the effect of subcooling on conversion ratio
G	Six tests run with variable coolant viscosities to study the effect of surfactant in suppressing steam explosion
H	Fifteen tests run with variable fuel/coolant mass ratios (alternatively, fuel/coolant volume ratios) to study the effect on conversion ratio

Table 9. Initial and Boundary Conditions for WFCI Experiments

Initial Conditions	C	D	E	F	G	H
Melt mass (kg)	3.1 - 3.3	2.9 - 3.5	0.7 - 3.9	1.0 - 1.5	0.8 - 3.7	3.5 -4.5
Melt temp. (K)	1154 - 1256	1092 - 1184	764 - 1063	1055 - 1144	1093 - 1157	1128 - 1173
Slug mass (kg)	23.4	0.5- 71.2	23.4	23.4	23.4	23.4
Water temp. (K)	356-360	356-360	359-366	300-345	298-306	355-361
Subcooling (K)	13 - 17	13 - 17	7 - 14	28 - 73	67 - 75	12 -18
Viscosity ratio	1.0	1.0	1.0	1.0	1.0 - 2.5	1.0
Init. pres. (MPa)	0.1	0.1	0.1	0.1	0.1	0.1
Trigger (MPa)	1.3 - 4.2	2.3 - 2.9	2.6 - 3.0	2.7	3.0	2.0- 3.4

Table 10. Summary of Results from WFCI Experiments

Measured/observed Data	C	D	E	F	G	H
Steam explosion	yes	yes	yes	yes	no*	yes
Max. ΔP (MPa)	3.8 - 17	8.8 -17	3 - 11	1.5 - 6.5	--	8 - 17
Impulse (kPa-s)	40 - 60	40 -75	2.5 - 8	2.5 - 8	--	40 -80
Kinetic energy (kJ)	2.4 - 3.7	2.4-4.9	2.7 - 3.4	n/a	--	2.7-4.8
Conv. ratio (%)	0.3-0.4	0.1-0.5	0.3-0.5	n/a	--	0.2-0.4

* steam explosion was observed in one case

interesting to note that there appears to be an optimal value of the conversion ratio with respect to fuel/coolant parameters. For tin simulant, the experiments show maximum value at a coolant-to-fuel volume ratio of about 12. It is hypothesized that other melt simulants, including prototypic melts, may exhibit similar qualitative trends. However, the tin simulant data has a relatively wide scatter. Moreover, this hypothesis has not been verified against the KROTOS or other data. Therefore, a definitive statement cannot be made at present as to how the tin simulant data can be scaled or extrapolated to reactor prototypic situations.

Concerning other parametric effects, the results of WFCI experiments indicate that coolant subcooling is more effective than melt superheat in destabilizing the premixture and initiating interactions. This is consistent with the results of KROTOS experiments. Also, limited data from experiments in which coolant viscosities were varied by adding surfactant, indicate that except in one case, the surfactant effectively suppressed steam explosions. Again, it is premature to generalize the results to reactor prototypic situations.

Chemical Augmentation Experiments

The chemical augmentation of FCI due to the presence of metal(s) in the melt is a distinct possibility. A varying degree of importance was assigned to this phenomenon by the SERG-2 experts. As one expert put it concisely, the relevant issues are: (1) the amount of zirconium (or, other metals) susceptible to oxidation at an explosion time scale, (2) consequences of chemical reaction on allowable void fraction for supercritical explosions, and (3) the extent of augmentation in terms of explosion energy, peak pressure, conversion ratio, etc. Note that the presence of zirconium in the melt is attributed as a factor for finer fragmentation of melt jet and correspondingly, a higher pressure peak, in the FARO L-11 quenching experiment. Generally, if the core melt contains significant quantities of metallic constituents which react chemically in the explosion time scale, all phases of FCI may be affected by such process. In a steam

explosion experiment, however, the presence of noncondensible gases (e.g., hydrogen) as a result of metal-water reaction is likely to increase the difficulty to trigger an explosion.

Noting the conflicting consequences of chemical augmentation and noting that there is hardly any data to render an informed judgement on this issue, the NRC has initiated an experimental program, ZREX, at ANL in the past year. The objective of the program is to investigate the possibility of chemical augmentation in a melt-water system containing metal. The ZREX experimental setup is shown in Figure 4. Like KROTOS and WFCI, the essential elements of the ZREX facility are: a melt generator and a delivery system, a one-dimensional test vessel fitted with a triggering device at the base, and a closed containment housing the test vessel. Measurements in the ZREX facility include temperature of melt, water, and freeboard volume, pressure at various locations in the test vessel, force at the base of the test vessel (measured by a force transducer on which the test section is mounted), containment pressure, and hydrogen generation. The experimental setup and plan are described in detail in an unpublished report by Cho and Armstrong.[24]

Only a limited number of scoping experiments have been performed to date at the ZREX facility. These tests examined the interactions of 200 g of Zr (Zircaloy) in a one meter water pool at 0.1 MPa ambient pressure. Both triggered and untriggered tests were conducted, but in the triggered tests, triggering was either delayed or did not function properly. Consequently, the results of the attempted triggered tests are essentially similar to those of the untriggered tests. Preliminary results from untriggered tests do not indicate any chemical augmentation, at least, none measurable. As an aside, two interesting observations are made from the scoping experiments. First, the results indicate that approximately 5 w/o Zr reacted with water during the FCI (based on gas sample analysis). Second, the entire melt fragmented to particles ranging from 5 to 20 mm in size, with a mass mean diameter of approximately 7 mm.

5. Future Research Needs

The future research needs, discussed in this section, are guided, in part, by the Commission Policy to maintain some expertise in the FCI area, and also, by the recommendations of the SERG-2 experts toward further understanding of broader FCI issues, i.e., FCI-related issues other than those associated with the α-mode of containment failure. It should be emphasized again that the α-mode failure issue is sufficiently understood from a risk perspective, and future research is not warranted solely on the basis of further improvement in understanding of this particular issue. However, an improved understanding of other FCI-related issues (e.g., shock loading of the lower head and the ex-vessel support structures) are relevant with regard to determining the efficacy of certain accident management strategies for operating reactors and the adequacy of certain passive system design features of advanced light water reactors. These other FCI issues are summarized in Table 2. Specific technical areas where research is needed to achieve further understanding of the issues include: (1) late phase melt progression modeling, (2) triggering fundamentals, (3) multidimensional propagation in multiphase media, (4) fluid-structure interactions and dissipative effects, (5) assessment of structural response codes, and extrapolation of small-scale FCI data to plant safety assessment. Additionally, further research is recommended in the areas of dynamics of melt jet fragmentation, chemical augmentation of

FCI energetics, pressure suppression effects on FCI, and possible scale effects (both geometric and material).

With regard to the late phase melt progression issue, the importance of accident progression and melt relocation in setting up initial conditions for FCI is clearly recognized. However, given the uncertainties underlying the late phase melt progression phenomena, a bounding approach is considered for FCI analysis. Likewise, it is recognized that the triggering process is poorly understood, due largely to its inherently random nature. Therefore, a conservative approach to triggering is recommended, whereby it is assumed that a trigger of sufficient strength would likely be available in a reactor prototypic situation. It is also determined that methods exist to calculate the FCI energetics and the damage consequences, perhaps without an undue conservatism, but these have not been assessed extensively for robustness or for their applicability to plant calculations. Finally, development of analytical tools in the past ten years focussed mostly on the premixing phase of FCI and, to a limited extent, on the propagation phase details. The assessment of these tools received even less attention than the development.

The future FARO program, in place through 1998 and with active participation by NRC, will examine quenching of a large mass (250 kg) of prototypic melt under different initial and boundary conditions such as shallow and deep water pools, intermediate (2 MPa) to low (0.5 MPa and perhaps, to 0.1 MPa) ambient pressures, and different w/o metal contents in the melt. Experiments are also planned to look into the ex-vessel melt spreading issue. The future KROTOS program (also, in place through 1998), will examine steam explosion behavior of prototypic and simulant melts under different initial and boundary conditions such as higher ambient pressures (to 1.0 MPa), presence of triggering, a range of water subcooling and melt superheats, and the possible effect of surfactant. These experiments will be instrumented to measure local void fractions so that the results can be used to assess the analytical codes.
The FARO experimental program described above will not address quenching of a large melt mass at low pressures in a water pool deeper than 2 m, which is relevant to ex-vessel FCI in a deep flooded cavity. Therefore, additional experiments at low pressures in a pool depth substantially greater than 2 m will be required to resolve this issue. Note that the planned KROTOS experiments, in particular, those at higher ambient pressures are expected to generate data on the pressure suppression effect.

Other experimental programs (non-NRC) investigating melt jet fragmentation include PREMIX experiments at Forschungzentrum Karlshrue (FZK) and ALPHA/STX experiments at Japan Atomic Energy Research Institute (JAERI), both using thermite melts. These programs, already in progress, complement the KROTOS program with regard to investigation of the premixing phenomena for melt jets. The planned JAVA program by the Institut de Protection et de Surete Nucleaire (IPSN) will also investigate the premixing phenomena involving prototypic melts.

At the conclusion of these experimental programs, it is expected that a more extensive experimental data base will be generated which will provide a better understanding of the jet fragmentation phenomena. The data base will be used to assess the analytical codes in order to verify and validate the water depletion phenomena and the limits-to-mixing argument for melt jets. The end product(s) will support the evaluation of such FCI issues as localized interactions,

and its effect on lower head integrity (for in-vessel explosions) as well as integrity of cavity structures including pedestals (for ex-vessel explosions).

The University of Wisconsin propagation experiments will be continued as part of the future research plan, however, with different simulants (oxidic and/or mixed) and using a larger diameter test vessel. The objective of the new series of experiments is to determine if the parametric effects on FCI energetics observed in the tin experiments can be reproduced in the oxidic or mixed simulant experiments, quantitatively or qualitatively. The objective is also to examine the effect of relaxing the radial constraint (through the use of larger diameter vessel) on FCI energetics. The results, along with those from future KROTOS and other experiments, will help develop and verify a scaling rationale for extrapolating the small-scale simulant data to reactor prototypic situations. Additionally, the results from these experiments can be used to assess the existing two-dimensional propagation models and codes.

Note that the SERG-2 experts strongly recommended continued development and assessment of multidimensional (two-dimensional at a minimum) analytical codes to provide a methodology for analyzing localized FCI and estimating the structural loading. These codes should have modeling features for shock-structure interactions, slug-structure interactions, and dissipative effects. The experts also recommended performing small-scale but well-instrumented propagation experiments with different melt simulants to understand the material scale effect, to determine the envelope of FCI energetics as a function of various fuel/coolant parameters, and to provide a data base for the assessment of analytical tools. Future FARO and KROTOS experiments in wider test sections are expected to provide some data on two-dimensional effects as are the University of Wisconsin experiments mentioned above. Also, ongoing BERDA experiments at FZK are expected to generate representative data on slug-structure interactions and dissipative effect of structures.

The NRC is continuing the chemical augmentation experiments at ANL using a metal-metal oxide-water system which is more prototypic of reactor situations. Due to facility constraints, these planned experiments will be performed using melt-water systems containing at most 20 w/o zirconium oxide (i.e., at least 80 w/o zirconium metal). The FARO program is expected to yield information on melt-water systems containing at most 5 w/o zirconium metal. Consequently, there will be a gap in the data for metal fractions in the range of 5 w/o to 80 w/o. In reactor prototypic situations, metal fractions above 5 w/o but substantially below 80 w/o may not be unlikely in some relocation scenarios (e.g., ex-vessel release of initially metallic melt mass followed by a gradually increasing oxidic melt mass). Therefore, there is a potential need, contingent upon the findings of the initial set of experiments, to perform additional experiments involving the above range of metal fractions.

Beyond the research programs mentioned above, the NRC plans to continue its active participation in the international cooperative programs in order to pursue jointly the experimental and analytical work on certain residual FCI issues, and intends to follow ongoing FCI research in other countries. It is recognized that FCI is fundamental to practically all severe accident issues. Therefore, in accordance with the Commission Policy, the NRC intends to maintain some expertise in the FCI area, and to assess the progress in FCI research at regular intervals to determine the regulatory implications of the results.

6. References

1. U. S. Nuclear Regulatory Commission, "Reactor Safety Study," WASH-1400, NUREG/75-0114, October 1975.

2. Steam Explosion Review Group, "A Review of the Current Understanding of the Potential for Containment Failure from In-Vessel Steam Explosions," NUREG-1116, U.S. Nuclear Regulatory Commission, June 1985.

3. T. G. Theofanous, et al., "Steam Explosions: Fundamentals and Energetic Behavior," NUREG/CR-5960, University of California at Santa Barbara, January 1994.

4. T. G. Theofanous and M. Saito, " An Assessment of Class-9 (Core-Melt) Accidents for PWR Dry-Containment Systems," Nuclear Engineering and Design, 66, 301 (1981).

5. R. E. Henry and H. K. Fauske, "Required Initial Conditions for Energetic Steam Explosions," Fuel-Coolant Interactions, HTD-V19, American Society of Mechanical Engineers, 1981.

6. U. S. Nuclear Regulatory Commission, "Preliminary Assessment of Core Melt Accidents at the Zion and Indian Point Nuclear Power Plants and Strategies for Mitigating Their Effects," NUREG-0850, November 1981.

7. T. G. Theofanous, et al., "An Assessment of Steam-Explosion-Induced Containment Failure," NUREG/CR-5030, University of California at Santa Barbara, February 1989.

8. W. H. Amarasooriya and T. G. Theofanous, "Premixing of Steam Explosions: A Three-Fluid Model," Nuclear Engineering and Design, 126, pp. 23-29 (1991).

9. S. Angelini, et al., "Premixing-Related Behavior of Steam Explosions," Proc. CSNI Specialists Meeting on Fuel-Coolant Interactions, NUREG/CP-0127, NEA/CSNI/R(93)8, pp. 99-133, March 1994.

10. S. Angelini, et al., "The Mixing of Particle Clouds Plunging into Water," Proc. 7th International Meeting on Nuclear Reactor Thermal-Hydraulics, NURETH-7, NUREG/CP-0142, Vol. 3, pp. 1754-1778, September 1995.

11. M. L. Corradini, et al., "Vapor Explosions in Light Water Reactors: A Review of Theory and Modeling," Progress in Nuclear Energy, 22(1), pp. 1-117, 1988.

12. M. L. Corradini, "Vapor Explosions: A Review of Experiments for Accident Analysis," Nuclear Safety, 32(3), pp. 337-362, 1991.

13. D. F. Fletcher, "A Review of the Available Information on the Triggering Stage of a Steam Explosion," Nuclear Safety, 35(1), pp. 36-57, 1994.

14. B. W. Spencer, et al., "Fragmentation and Quench Behavior of Corium Melt Streams in Water," NUREG/CR-6133, Argonne National Laboratory, February 1994.

15. W. W. Yuen, and T. G. Theofanous, "ESPROSE.m: A Computer Code for Addressing the Escalation/Propagation of Steam Explosions," DOE/ID-10501, University of California at Santa Barbara, April 1995.

16. X. Chen, et al., "On the Constitutive Description of the Microinteractions Concept in Steam Explosions," Proc. 7th International Meeting on Nuclear Reactor Thermal-Hydraulics, NURETH-7, NUREG/CP-0142, Vol. 3, pp. 1586-1606, September 1995.

17. S. Basu, and T. Ginsberg, "A Reassessment of the Potential for an Alpha-Mode Containment Failure and a Review of the Current Understanding of Broader Fuel-Coolant Interaction (FCI) Issues," Report of the Second Steam Explosion Review Group Workshop, NUREG-1529, 1996 (in preparation).

18. D. Magallon, and H. Hohmann, "High Pressure Melt Quenching Tests in FARO," Proc. CSNI Specialists Meeting on Fuel-Coolant Interactions, NUREG/CP-0127, NEA/CSNI/R(93)8, pp. 1-13, March 1994.

19. H. Hohmann, et al., "FCI Experiments in the AluminumOxide/Water System," Proc. CSNI Specialists Meeting on Fuel-Coolant Interactions, NUREG/CP-0127, NEA/CSNI/R(93)8, pp. 193-203, March 1994.

20. I. K. Huhtiniemi, et al., "FCI Experiments in the Corium/Water System," Proc. 7th International Meeting on Nuclear Reactor Thermal-Hydraulics, NURETH-7, NUREG/CP-0142, Vol. 3, pp. 1712-1727, September 1995.

21. D. Magallon, et al., "Status of the FARO/KROTOS Melt-Coolant Interactions Tests," Proc. Twenty-Third Water Reactor Safety Information Meetings, 1996 (in preparation).

22. H. S. Park, and M. L. Corradini, "The Effect of Constraint on Fuel-Coolant Interactions in a Confined Geometry," Proc. 7th International Meeting on Nuclear Reactor Thermal-Hydraulics, NURETH-7, NUREG/CP-0142, Vol. 3, pp. 1728-1742, September 1995.

23. H. S. Park, et al., "Experiments on the Trigger Effect for 1-D Large Scale Vapor Explosions," Proc. New Trends in Nuclear System Thermodynamics, pp. 271-289, June 1994.

24. D. H. Cho, and D. R. Armstrong, "Experiment Plan for Energetics of Molten Zircaloy-Water Steam Explosions," (unpublished ANL report), September 1994.

Progress on the MELCOR Code

Kenneth Bergeron, Randall Cole Jr., Arnold Elsbernd,
Salvador Rodriguez, Russell Smith, and Mark Leonard*
Modeling and Analysis Department
Sandia National Laboratories
Albuquerque, NM 87185-0739

Abstract

Sandia has made considerable progress in the past year on the MELCOR code for integrated severe nuclear reactor accident analysis:

Boron-Carbide Steam Reactions. We completed an upgrade of our treatment of chemical/physical interactions among water, B_4C, and stainless steel. These processes are important for tracking iodine inventories in BWRs.
Fission Product Vapor Scrubbing by Water Pools. We have upgraded the treatment of fission product scrubbing by replacing the earlier SPARC models with the more recent SPARC-90 models.
Core Flow Blockage and Generalized Axial Gradient Model. Perhaps the most fundamental improvement to MELCOR is our modified treatment of the effect on coolant flow of blockages due to core melt movement. A closely related model improvement was to extend MELCOR's sub-grid axial thermal gradient feature to conditions of arbitrary flow direction (e.g., reversed axial flow or radial flow).
VANAM (ISP-37). We have completed the calculations for the International Standard Problem, and have submitted them to the coordinator at Battelle Frankfurt.
Westinghouse Large-Scale Tests. We have assessed MELCOR's models for containment thermalhydraulics that are relevant for the passive containment cooling concept.
Accident Sequence Analyses. In view of the current interest in steam generator tube rupture (SGTR), we have conducted a series of studies of SGTR-induced accidents in the Surry plant. We have also completed an extensive series of accident sequence calculations for the Westinghouse AP600 reactor in support of the current ALWR certification process.
Current Work in Progress. We are currently in the process of implementing several new or improved models for MELCOR. These include models of fission product chemical reactions with surfaces, aqueous fission product chemistry, and an improved treatment of core structure support failure. We have two ongoing efforts to validate MELCOR against experimental data: an analysis of the Phebus FPT-0 experiment, and an evaluation of the new pool scrubbing model against EPRI experiments.

---

*Innovative Technology Solutions, Inc.

Introduction

The MELCOR code is a computational system for simulating the progression of events and phenomena in a nuclear power plant undergoing a hypothetical reactor accident. It was developed at Sandia National Laboratories (with important contributions from Oak Ridge National Laboratory and others) for the U.S. Nuclear Regulatory Commission. MELCOR is being developed with strict attention to configuration management, with numerous distinct versions released over the years. The most recent major release was version 1.8.3, which was released (with entirely new documentation) in September 1994.[1] To date, the code has been distributed to forty-eight organizations in twenty-two countries (see Table 1). Sandia personnel provide limited levels of assistance to these users. In addition, Los Alamos National Laboratory manages the MELCOR Code Assessment Program (MCAP) for the USNRC. Recent activities of MCAP are discussed in the paper by Boyack et al. in these proceedings.

Table 1. Countries (other than U.S.) to which MELCOR 1.8.3 has been distributed

Austria	Belgium	Croatia
Czech Republic	Finland	France
Germany	Hungary	Italy
Japan	Korea	The Netherlands
Republic of China	Russia	Slovak Republic
Slovenia	Spain	Sweden
Switzerland	Ukraine	United Kingdom

Considerable progress has been made at Sandia in the past year on MELCOR. In this paper, we will briefly describe the progress. The remainder of the paper is organized into five sections: ***Recent Improvements to MELCOR, Code Development in Progress, Validation of MELCOR, Validation Work in Progress, and Accident Analyses.***

Recent Improvements to MELCOR

The MELCOR project at Sandia (and corresponding work at Oak Ridge) follows a strictly controlled software development procedure, that incorporates a design phase, an external peer review phase, and an implementation phase that includes a limited degree of developmental testing. Releases of new versions of MELCOR also require, in addition, an extensive formal testing program. In this section, we will describe all the major code modifications that have been fully implemented since the release of MELCOR 1.8.3.

Boron Carbide Steam/Reactions. In MELCOR 1.8.3 there is a simple model for oxidation that has been found to be adequate for many situations, but which gives unsatisfactory results for reducing environments — it tends to seriously underpredict the methane generation rate, leading possibly to underestimation of the risk from the release of volatile methyl iodide. For this reason, we have developed an optional advanced boron

carbide reaction model, based on work done at Oak Ridge for the BWRSAR code and SCDAP/RELAP5.

This model uses a free energy minimization calculation that is constrained by limitations on the available masses of boron carbide and of steam. The boron carbide available is limited by a variety of processes, depending on the configuration of the core at the time of the calculation. For example, in the early stages of melt progression, no reactions will occur until a specified fraction of the stainless steel clad has been removed. Also, boron carbide that dissolves into the eutectic phase is not available for reaction. Steam available for reaction is limited by diffusion through oxidized layers for the geometry appropriate to the state of the core at the time of the calculation.

Fission Product Vapor Scrubbing by Water Pools. Numerous analyses and experiments involving the performance of pressure suppression pools have shown that removal of fission products from the primary system discharge is a very important mitigating process. An extensive experimental database exists upon which to base theoretical models. The modeling approach in MELCOR 1.8.3 is based on modifications of the SPARC code developed at Pacific Northwest Laboratories. Since their incorporation into MELCOR, improvements in the SPARC code have been made, culminating in the SPARC-90 code.[2] These improvements have now been incorporated, with as little modification as possible, into MELCOR.

Models for several aspects of fission product removal in SPARC-90 represent a significant upgrade to modeling capability and fidelity to measured data from that provided by the earlier release implemented in MELCOR. Among the more significant enhancements to modeling capability are the treatment of removal of iodine species that would be transported as vapors under typical reactor accident conditions (e.g., I_2 and organic iodides) and an explicit recognition of the dependence of bubble hydrodynamics and aerosol particle deposition efficiency on pool entrance geometry.

The capture of volatile iodine species in water pools is now represented in two regions of a water pool: local deposition upon entering the pool, resulting from thermodynamic equilibration with conditions in the neighborhood of the vent exit; and deposition at bubble/pool interfaces as the bubble swarm rises to the pool surface. Deposition in both regions of the pool is assumed to be limited by iodine species solubility at the interface. Changes in pool pH due to high radiation fields [which lowers the $H(I_2)$ partition coefficient] is not accounted for in the SPARC-90 models.

Numerous enhancements to the treatment of bubble hydrodynamics and aerosol particle deposition have been made in SPARC-90, most of which are based on observations and measurements from experiments performed by Battelle under the auspices of the Electric Power Research Institute (EPRI).[3,4] SPARC-90 (and MELCOR) currently offer the user a choice of three distinct pool entrance geometries, from which unique correlations for bubble breakup are applied, i.e., multi-hole vent such as the BWR T-quencher, horizontal vent, or vertical downcomer. Improved models are also implemented to describe the

hydrodynamics of, and particle deposition in, bubble swarms. Among the more important of these improvements is the recognition of the work of expansion generated by bubbles in the rising swarm. This term in the treatment of bubble thermodynamics produces conditions that favor enhanced particle condensation growth under certain thermodynamic conditions, thereby greatly increasing the potential for deposition.

Core Flow Blockage and Generalized dT/dz Model. MELCOR's strongly modular architecture treats core behavior and fluid flow separately, even allowing different nodalizations of the core region within the two modeling areas. This has several advantages for the code user, including modeling flexibility and the opportunity to trade off detail against calculational expense. It also simplifies maintenance for the code developer. There are some drawbacks: the flexibility of input imposes greater demands on the analyst, and separate modeling with the resulting numerically explicit interfaces imposes timestep limits for stability of the solution. Code improvements since release of MELCOR 1.8.3 have involved two areas affected by this structure: (1) the calculation of heat transfer between core structures and fluids and (2) representation of the effects of degraded core structures and/or relocated core materials on the resistance to fluid flow.

The first of these involves a model that has come to be called the "dT/dz" model. This model solves, within the core package, a numerically implicit representation of fluid flow and heat transfer using the core nodalization and boundary conditions from the hydrodynamics package. The resulting net heat transfer is passed as a numerically explicit source to the subsequent flow calculation. Although previous discussions of the model have tended to emphasize its function in allowing the core package to infer a more detailed temperature profile within a single hydrodynamic control volume, the implicit numerical method also stabilizes the calculation, permitting longer timesteps. The entire approach fails, however, if the flow patterns calculated by the hydrodynamic calculation are significantly inconsistent with those assumed by the heat transfer calculation.

In previous versions of MELCOR, the model was based on the assumption of upward axial flow. If the assumption was violated, calculated temperature profiles often appeared nonphysical and code performance suffered, sometimes to the point of a code abort. In addition, user input was required to define the source of upward flow, which proved a common source of errors. Improvements to the model have eliminated the need for user input and also removed the restriction on flow directions, allowing consistent treatment of flow patterns involving upward, downward, and radial flows. The improved model produces far more realistic results and, by reducing discrepancies between core and hydrodynamic temperatures, eliminates the cause of many previous numerical instabilities.

The second area of new modeling involves the hydrodynamic effects of relocation of materials in the core. This can substantially change flow geometry and alter the resistance to flow of coolant and/or coolant vapors through the core region, thus affecting the ability of the coolant to remove heat and also the ability of steam to reach and oxidize hot metal surfaces.

Previous versions of MELCOR have the capability to represent the increased flow resistance resulting from blockage of flow paths by core debris. However, this capability relies on a knowledgeable user defining effective valves based on appropriate control functions, and was rarely employed. For a flow path involving potential flow blockage by core materials, the new model calculates an additional friction term based on a correlation for flow in porous media in addition to adjusting the flow area; the only input required is a specification of which core cell or cells are associated with the flow path.

One anticipated effect of the new blockage model is that, by reducing the flow through highly blocked regions of the core that contain little fluid, it will relax the timestep limitation imposed by the material Courant condition in these regions. This may make it possible to run calculations with relatively detailed hydrodynamic nodalizations in the core region without the extreme performance penalties that have been observed with earlier versions of the code.

The new models allow greater fidelity in representing the behavior of a reactor system during a severe accident, while reducing the burden on the user to provide appropriate, often obscure, input. In addition, they have resulted in a much more robust code.

Code Development in Progress

Besides the completed code development work described above, we have a number of code improvements in progress.

Fission Product Reactions with Surfaces. Fission product releases from the primary system depend not only on generation and deposition mechanisms, but also on re-vaporization of volatile fission products from surfaces after deposition has occurred. Chemisorption at these surfaces can significantly inhibit re-vaporization. New models for chemisorption have been designed for MELCOR and, in addition, some improvements in the equations of state of fission products have been made to give more realistic re-vaporization behavior. The design report for this improvement has been externally reviewed and work on implementation has begun.

Fission Product Aqueous Chemistry. Accurate tracking of iodine inventories in the atmosphere and water pool requires improved modeling of aqueous chemical processes. Work has been initiated on a new model that treats diffusion through the pool surface boundary layer, radiolytic chemical reactions, and selected equilibrium chemistry. A key feature is tracking the pool pH, which is known to be a strong determinant of iodine chemistry equilibrium.

Core Support Structure Failure Model. MELCOR 1.8.3 has a model for failure of the core support plate that tends to affect accident progression results when the user changes timestep size, machine platform, or other variations to the code runs that should not impact the results. A thorough analysis of the reasons for these problems has been conducted, and a design for an improved model has been developed and documented. The improvements involve more careful treatments of axial and radial heat conduction, integral

incorporation of a creep-rupture failure model, and a user-controlled treatment of crust formation of the debris supported by the core support plate. Implementation of this model will take place following completion of the external peer review of the design document.

Validation of MELCOR

A major finding of the MELCOR Peer Review Committe[5] was that, given the importance of the code to safety and regulatory issues, there was inadequate documentation of systematic validation of the predictions of the code against experimental results (or against other codes that themselves were well-validated). In the past several years, Sandia and numerous other organizations have greatly expanded the base of validation results to address this deficiency. Below, we discuss two important new contributions.

International Standard Problem 37—the VANAM Experiments. VANAM M3 was a multi-compartment aerosol depletion test with hygroscopic aerosol material that was performed in the Battelle Model Containment (BMC) in Germany by Battelle Frankfurt in April 1992.[6] The experiment was intended to investigate thermal-hydraulic conditions and aerosol behavior in containment following a core meltdown accident with depressurization by pressurizer relief valve discharge (ND* scenario of German Risk Study B). The experiment was conducted in five phases that lasted a total of 29 hrs. Each phase was characterized by different combinations of air, saturated or superheated steam, insoluble aerosol, and soluble aerosol (NaOH). A key purpose of the experiments was to investigate the importance of hygroscopic aerosol behavior — i.e., the tendency of soluble aerosols to take up water even when the relative humidity is less than one.

MELCOR 1.8.3 does not have a model for hygroscopic water takeup by aerosols. For the purpose of this study, we developed a simple model and implemented it in a special version of the code. Our intention was not to establish a complete and robust implementation, but rather to create a minimal operational capability within the integrated MELCOR framework so that we could evaluate the importance of the effect and also the expected difficulty of a full implementation.

This interim model is based on the Mason equation, which gives the time rate of change of the particle radius as a function of aerosol composition and atmosphere conditions. The Kelvin effect, which modifies the equilibria to take account of the curvature of the particle surface, was also treated. The numerical implementation required coupling between the results of the water takeup process and the atmospheric conditions (which are calculated in a different module of MELCOR). Rather than attempting a careful implicit treatment, we used a "quasi-implicit" method, that during the aerosol calculation estimates thermal-hydraulic conditions at the end of the time step. This method was expected to generate some degree of numerical instability, and the results shown in Figure 1 are evidence of this. Fortunately, however, the oscillations in the results were bounded, and we successfully achieved numerical convergence throughout the calculation. Given the

oscillations, the accuracy of the solution is uncertain, but in general, this is an encouraging result with respect to the feasibility of implementing a model more rigorously.

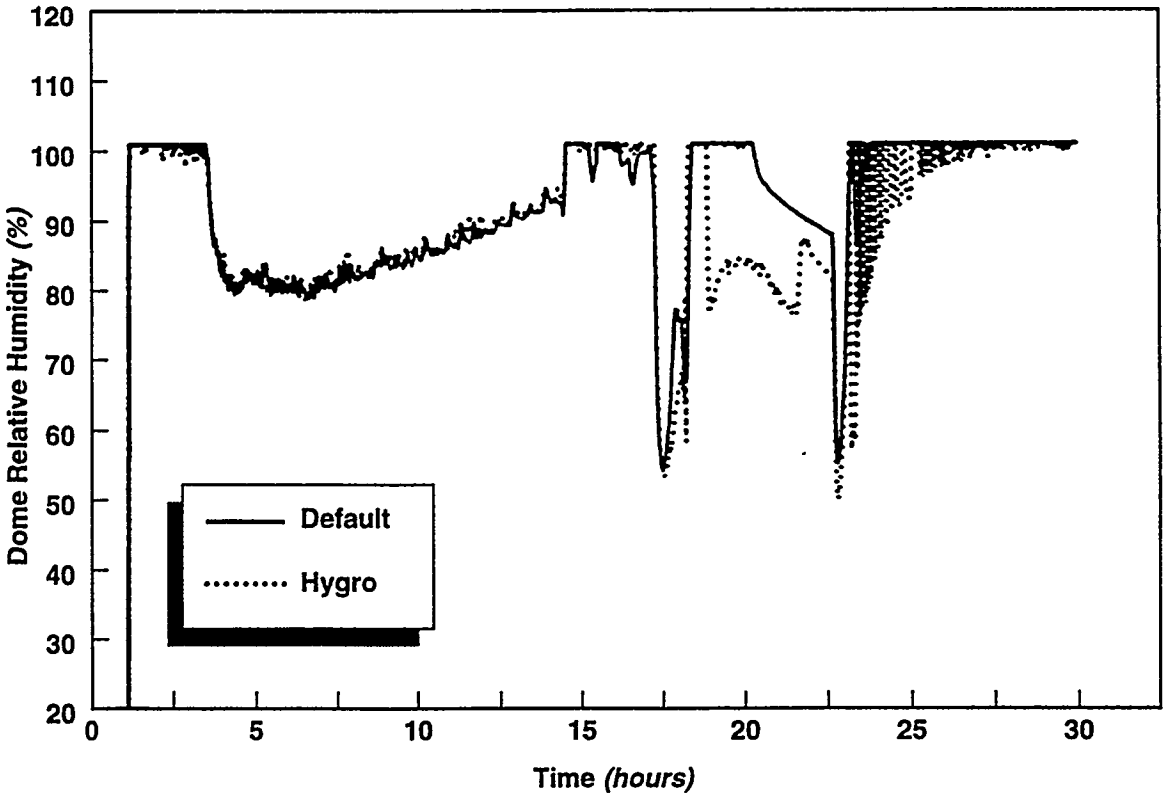

Figure 1. Relative humidity in the dome as predicted by MELCOR.

Figure 2 illustrates the calculated results of including the hygroscopic effect. As seen, the new (Hygro) model is closer to the experimental results for suspended soluble aerosol than is the default model. The new model successfully captures the trend seen in the experiments for accelerated water uptake to increase the rate of gravitational settling. No particular attempt was made to improve agreement for these calculations, because the severe numerical chatter seen in Figure 1 could be responsible for much of the deviation seen in Figure 2. Whether a proper numerical implementation of a hygroscopic model would give better agreement than shown here remains to be seen.

Westinghouse Large-Scale Tests. In order to provide confirmation of the Passive Containment Cooling System concept utilized in the AP600 advanced reactor design, Westinghouse has carried out a large number of tests at a scaled experimental facility. These experiments are known generically as Large-Scale Tests (LST), and provide an opportunity to validate a variety of MELCOR models, including recently developed capabilities for tracking water films on structure surfaces.

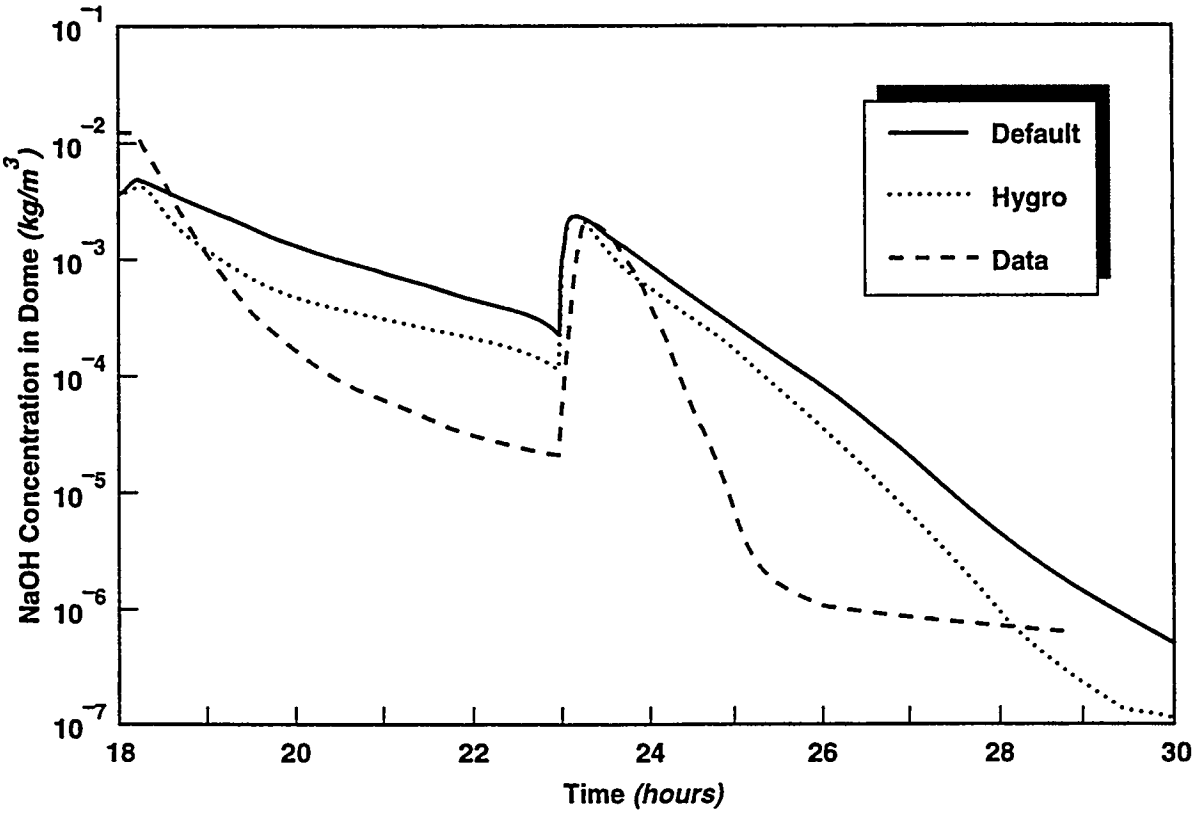

Figure 2. Soluble aerosol mass in atmosphere of the dome region of the VANAM experiment.

Post-test calculations were completed for Tests 202.3, 212.1, and 220.1 using MELCOR 1.8.3. The primary emphasis of the simulations is to demonstrate the adequacy of MELCOR to simulate containment phenomena and, secondly, to provide quantitative evaluation of the new film-tracking model in MELCOR. The film-tracking model is used to simulate the water flooding as it flows down from the top of the outer shell of the dome wall, carrying away sensible heat, and computes the amount of evaporation occurring in the liquid film. In addition, the model tracks the liquid film that develops as condensation occurs inside the dome wall.

During Test 212.1, steam was injected into the LST vessel until a quasi steady-state was reached. The process was repeated three times, with progressively higher steam-injection rates. Figure 3 shows the normalized measured and calculated pressure history (because of the proprietary nature of the data, pressures and time are shown only in arbitrary units). The figure shows that the calculated pressure remained mostly within 5% or less of the measured value. The dome vapor-temperature was typically calculated within 2 K or less of data. The measured temperature drops across the dome shell were calculated within 0.3 K of data and the calculated condensation rate was within 1.5% of data. The calculated inner- and outer-vessel heat transfer coefficients followed the data trend (i.e.

hand-calculated heat transfer coefficients based on measured data), were mostly inside the data band, and for the values outside the band, the coefficients were within the typical experimental error of +/- 25% found in the literature.

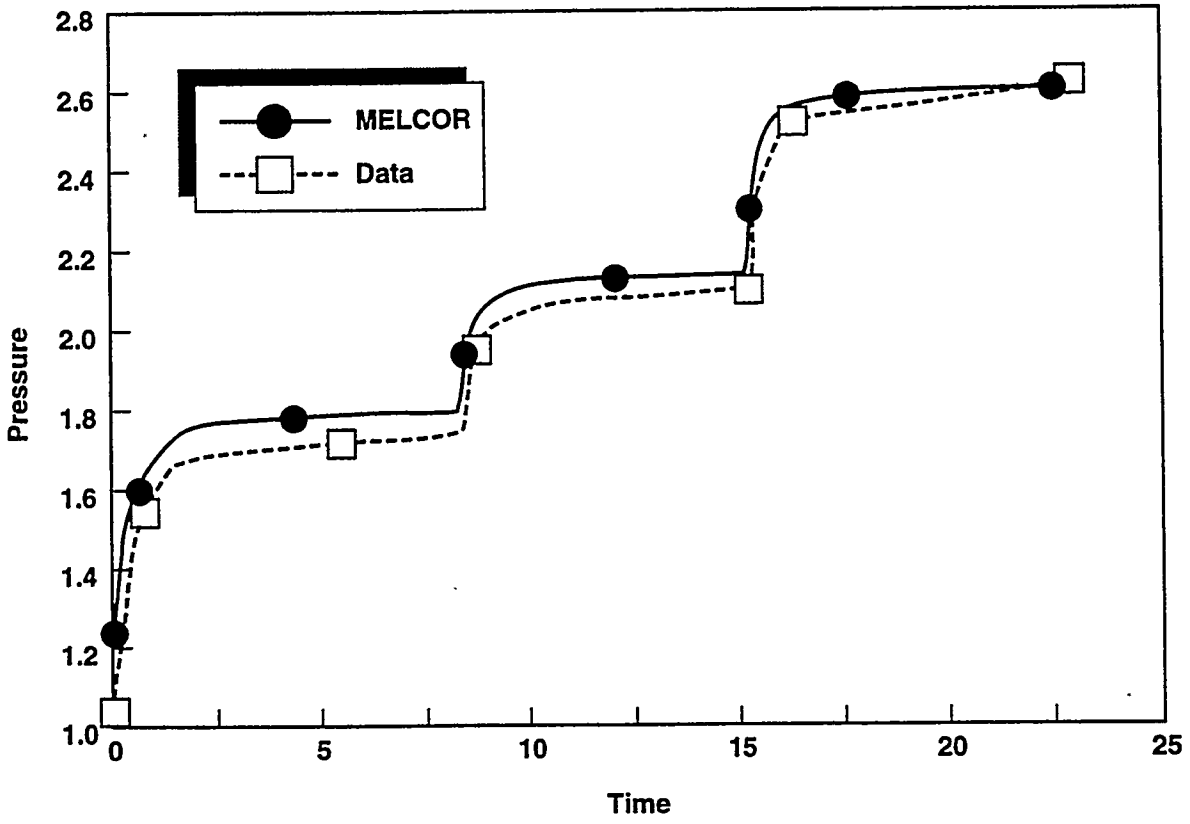

Figure 3. Normalized calculated and measured pressure for large-scale tests.

The adequacy of the film-tracking model was assessed by performing a code-to-code comparison (MELCOR-to-CONTAIN). The comparison was made because (1) no experimental data for the thickness was available and (2) the CONTAIN film models have been assessed previously and found to be in good agreement with data. The comparison showed that the MELCOR and CONTAIN film thickness were within 0.75 mm. Finally, as the MELCOR condensation film flowed downward, the film thickness increased at a consistent rate, as expected, and the evaporation film thickness decreased at a consistent rate as the film flowed downward, as expected.

Validation Work in Progress

Two MELCOR validation studies are currently underway at SNL. First, we are using EPRI data on fission product scrubbing in pools to assess the improved models (discussed above) from SPARC-90. Second, we are performing a series of calculations of the Phebus

FPT-0 integral severe accident experiment. For the latter, we have benefitted from the cooperation of several organizations that have previously performed MELCOR/Phebus studies. In particular, we have been provided with the MELCOR decks that were constructed by personnel at NUPEC in Japan; the Polytechnic University of Madrid, Spain; and KEMA in the Netherlands. We intend to pursue a series of calculations that will complement, rather than duplicate, the work already done by these institutions, and we are grateful for their cooperation.

Accident Analyses

Steam Generator Tube Rupture Sequence at the Surry Plant. Calculations have been performed with MELCOR to examine several aspects of severe accident progression during a postulated Steam Generator Tube Rupture (SGTR) accident sequence in a typical Westinghouse 3-loop PWR system. A key objective of these calculations was to provide thermal-hydraulic boundary conditions for a detailed assessment of fission product transport and deposition with the VICTORIA computer code[7] discussed in a paper by Bixler *et al.* in these proceedings. A second objective was to assess the potential for counter-current, vapor phase natural circulation flow patterns within hot leg piping during a single-tube SGTR. If natural circulation flow patterns could develop, the extent to which they influence fission product deposition was of interest. MELCOR calculations addressing natural circulation behavior are in progress, and are not discussed in the current paper. The discussion below is limited to results of preliminary (uni-directional flow) MELCOR calculations.

The calculations performed for the current study were restricted to an SGTR accident sequence in which only one tube is assumed to rupture as the accident initiating event. It is assumed that operator actions to depressurize the primary coolant system in response to detection of a ruptured U-tube (as directed by emergency operating procedures) are not successful. Under these conditions, the primary coolant system pressure remains elevated (~300 psia) during the period of core degradation and initial fission product release. A release path for fission products directly to the environment (i.e., bypassing the containment pressure boundary) occurs prior to the onset of core damage as a consequence of a presumed failure (in the open position) of a single relief valve on the faulted steam generator. Automatic actuation of the high-pressure emergency coolant injection system is assumed to occur when demanded to make up primary coolant mass lost through the ruptured tube, until the Refueling Water Storage Tank (RWST) inventory is depleted.

The preliminary MELCOR model used to simulate this accident sequence is based on the Surry plant configuration because a functioning MELCOR input deck was readily available from prior analyses performed by Sandia.[8] Modest modifications to this model were necessary to represent the SGTR accident sequence producing the hydrodynamic nodalization scheme shown in Figure 4. The faulted steam generator was arbitrarily selected to be "loop C" which contains the pressurizer. The combined volume and

behavior of the other two "intact" coolant loops are represented by a single, but separate, coolant flow circuit.

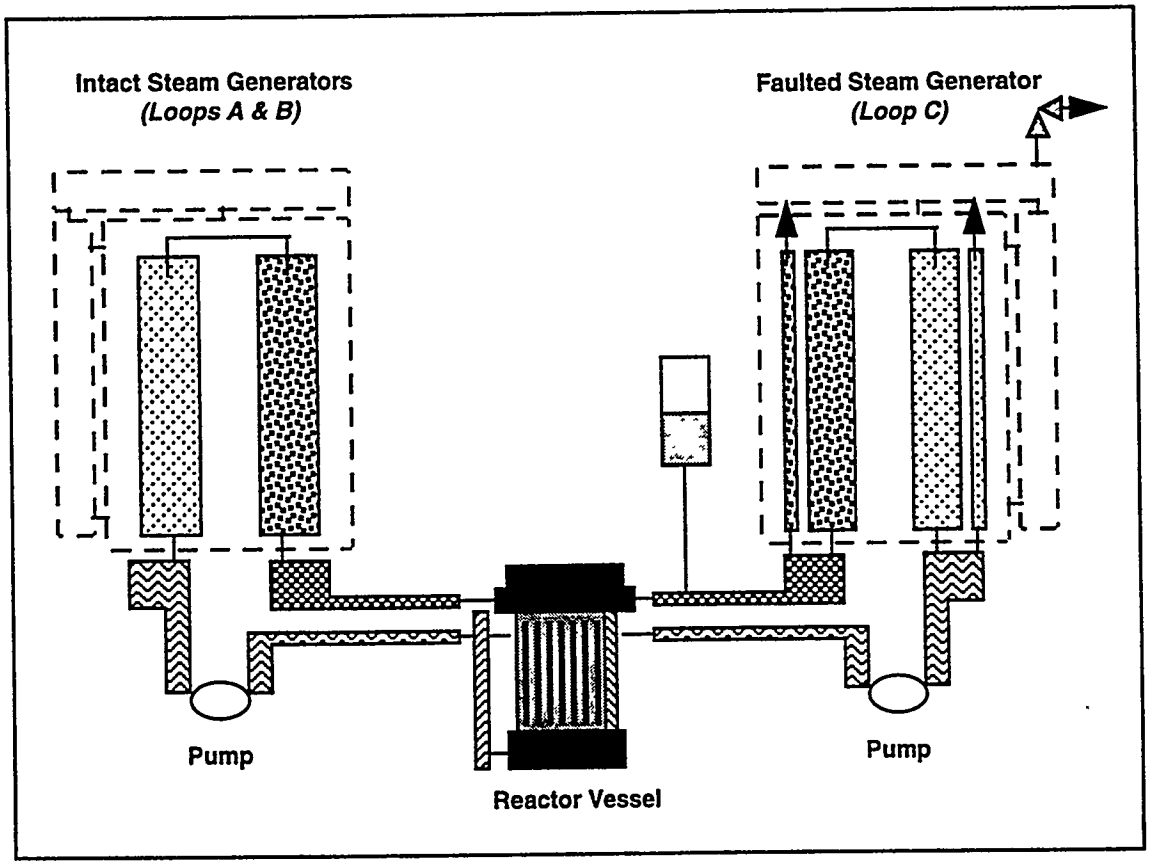

Figure 4. Nodalization for Surry SGTR sequence with "one way" hot leg.

The times at which key events in the SGTR accident sequence are calculated to occur are listed in Table 2. Due to the relatively small size of the break in the primary system, and the large volume of water in the RWST, the accident is very slow in evolving. For example, it takes approximately 16.2 hrs for the RWST inventory to be depleted, and the reactor vessel water level decreases below the top of active fuel at approximately 19 hrs after the initiating event.

Table 2. Timing of Key Events: MELCOR SGTR Simulation

Accident Event	Time After Initiating Event (s /hrs)
Guillotine rupture of one tube in the Loop C steam generator	0.0 / 0.0
Reactor scram on low pressurizer pressure	353.6 / 0.10
Main feedwater terminates/reactor coolant pumps trip and auxiliary feedwater initiates	358.7 / 0.10
High Pressure Injection (HPI) starts on low pressurizer pressure	376.0 / 0.10
Auxiliary feedwater terminates in Loop C due to high water level	1919.6 / 0.53
First cycle of the Loop C steam generator secondary coolant relief valve (RV)	3770.0 / 1.0
Secondary RV sticks open in the Loop C steam generator on the 55th cycle	7619.0 / 2.1
RWST depleted—HPI flow terminates	58,408.1 / 6.2
Reactor water level below top of active fuel	~68,000 / ~18.9
Gap release in Rings 1 & 2	105,671 / 29.4
Core Support Plate Failed	113,755 / 31.6
Lower head penetration failed -- debris ejected to cavity	113,804 / 31.6

The calculated pressure response of the primary coolant system, as well as the intact and faulted steam generator secondary coolant systems, are shown in Figure 5. Following an initial depresurization in response to the break, the primary coolant system stabilizes at a pressure of approximately 95 bar (1375 psia). When the RWST is depleted at approximately 58,000 s, the pressurizer water level drops below that allowed for pressurizer heater operation and primary coolant system pressure decreases sharply. The subsequent thermodynamic state of the primary coolant system becomes closely coupled to the response of the steam generator secondary systems after this point in time.

Accident Analyses for the Westinghouse AP600

In support of NRC's effort to review the AP600 design certification analysis, Sandia performed independent MELCOR analyses of accident progression and associated containment performance for a wide range of postulated severe accidents. Where meaningful, comparisons were made between results of the MELCOR calculations and corresponding MAAP4 calculations performed by Westinghouse in support of the AP600 Standard Safety Analysis Report (SSAR). Although the objective of the MELCOR calculations was to provide a general technical basis for NRC to evaluate the analyses presented in the SSAR, specific MELCOR calculations were also performed to examine

unique aspects of the AP600 design that are designed to mitigate severe accidents. For example, calculations were performed:

- To characterize the importance of hydrogen igniter system, Passive Residual Heat Removal (PRHR) system and Passive Containment Cooling System (PCS) operation to severe accident progression and containment loads;

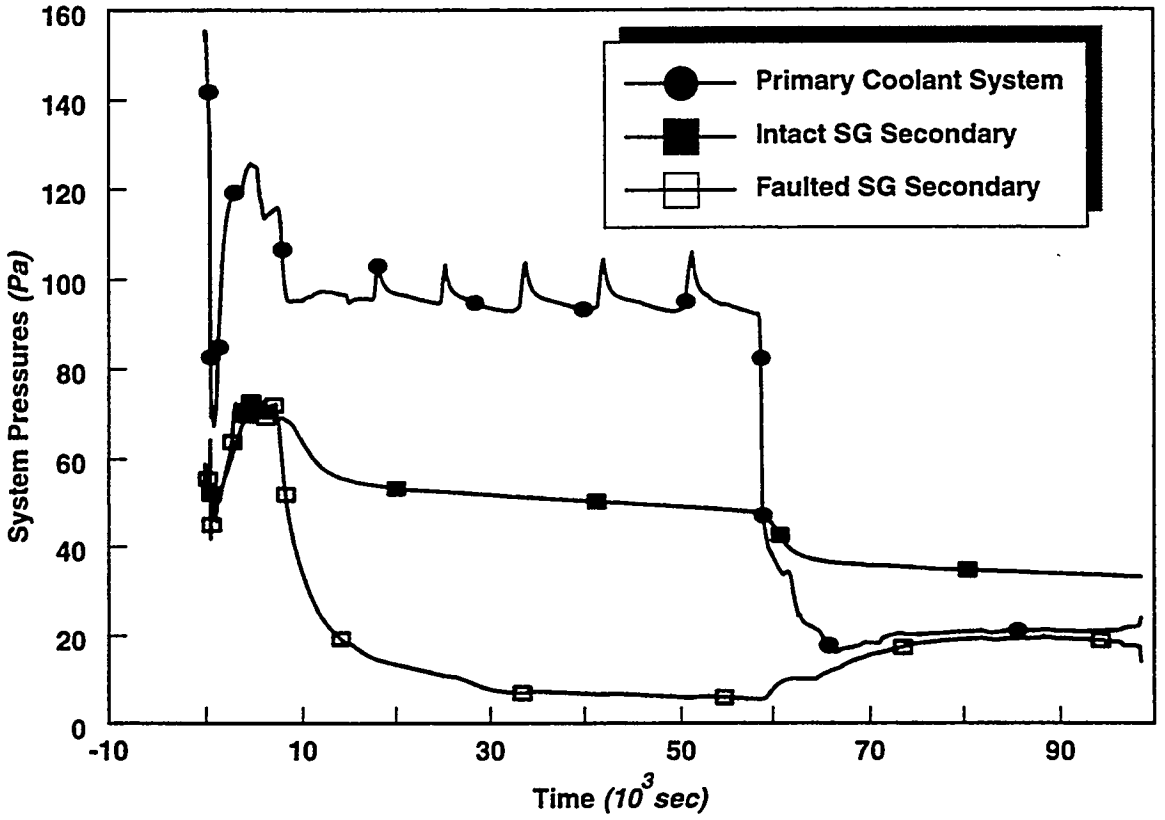

Figure 5. MELCOR calculations for Surry SGTR sequence with "one way" hot leg.

- To examine the conditions under which sufficient water would be available for maintaining external cooling of core debris via heat transfer to a flooded cavity (thereby preventing vessel breach); and

- To examine the impact of alternative modeling assumptions regarding corium-concrete interactions on long-term containment loads under conditions in which vessel breach would occur.

Results of these calculations are documented in a proprietary report.

REFERENCES

1. R. M. Summers, et al., MELCOR Computer Code Manuals, NUREG/CR-6119, SAND93-2185, Sandia National Laboratories, Albuquerque, NM (September, 1994).

2. P. C. Owczarski and K.W. Burk, "SPARC-90: A Code for Calculating Fission Product Capture in Suppression Pools," NUREG/CR-5766, PNL-7223 (1991).

3. D. D. Paul, et al., "Radionuclide Scrubbing in Water Pools - Gas-Liquid Hydrodynamics," NP-4113-SR, (ANS Topical Meeting, Snowbird, Utah), Electric Power Research Institute (1984).

4. J. C. Cunnane, et. al., "The Scrubbing of Fission Product Aerosols in LWR Water Pools under Severe Accident Conditions - Experimental," ibid.

5. B. E. Boyack, et al., MELCOR Peer Review, LA-12240, Los Alamos National Laboratory, Los Alamos, NM (March, 1992).

6. T. Kanzleiter, VANAM Multi-Compartment Aerosol Deposition Test M3 with Soluble Aerosol Material, Technical Report BIeV-R67.098-304, Battelle Institut e. V., Frankfurt am Main, Germany (July, 1993).

7. T. J. Heames, et al., VICTORIA: A Mechanistic Model of Radionuclide Behavior in the Reactor Coolant System Under Severe Accident Conditions, NUREG/CR-5545, SAND90-0756 (Rev. 1), Sandia National Laboratories, Albuquerque, NM (December, 1992).

8. L. N. Kmetyk, et al., Summary of MELCOR 1.8.2 Calculations for Three LOCA Sequences (AG, S2D S3D) at the Surry Plant, NUREG/CR-6107, SAND93-2042, Sandia National Laboratories, Albuquerque, NM, (March 1994).

INVESTIGATION OF A STEAM GENERATOR TUBE RUPTURE SEQUENCE USING VICTORIA

N. E. Bixler, C. M. Erickson,
Sandia National Laboratories
Albuquerque, New Mexico 87185-0739

and J. H. Schaperow
Nuclear Regulatory Commission
Washington, DC 20555

ABSTRACT

VICTORIA-92 is a mechanistic computer code for analyzing fission product behavior within the reactor coolant system (RCS) during a severe reactor accident. It provides detailed predictions of the release of radionuclides and non-radioactive materials from the core and transport of these materials within the RCS. The modeling accounts for the chemical and aerosol processes that affect radionuclide behavior. Coupling of detailed chemistry and aerosol packages is a unique feature of VICTORIA; it allows exploration of phenomena involving deposition, revaporization, and re-entrainment that cannot be resolved with other codes.

The purpose of this work is to determine the attenuation of fission products in the RCS and on the secondary side of the steam generator in an accident initiated by a steam generator tube rupture (SGTR). As a class, bypass sequences have been identified in NUREG-1150 as being risk dominant for the Surry and Sequoyah pressurized water reactor (PWR) plants. SGTR sequences are the most probable of the bypass sequences studied in NUREG-1150. However, at the time that the work supporting NUREG-1150 was performed, the capability did not exist to adequately account for attenuation of fission products in the primary and secondary sides of the steam generator and in the pipework leading from the steam generator and venting into the atmosphere. Assumptions that were made on attenuation of fission products in the steam generator and exiting pipework resulted in relatively small retentions. Following the publication of NUREG-1150, the possibility was brought out that, if fission product attenuation in the steam generator were significant, this class of accident sequences might be shown not to be risk dominant after all. The work presented here addresses this outstanding issue. More recent information from the Surry IPE also identifies SGTR sequences as significant contributors to core damage frequency and indicates that they would result in relatively large fission product releases to the environment.

The Surry plants, which are 3-loop PWRs of Westinghouse design, were chosen as the basis for this investigation. Thermal-hydraulic data were calculated using MELCOR. VICTORIA was used to analyze fission product release from the fuel and transport through the RCS leading to the broken steam generator tube, through the secondary side of the steam generator, out through the pipework leading from the steam generator to an atmospheric dump valve--which is assumed to stick open during the early portion of the accident--and into the atmosphere.

1. Introduction and Overview of VICTORIA

Release of radionuclides into the atmosphere is the main concern in the event of a nuclear reactor accident. The consequences of a severe reactor accident depend on the quantity, characteristics, and timing of the release of radionuclides from the reactor coolant system (RCS) into the containment, and finally into the atmosphere. In a by-pass accident, releases by-pass containment and pass directly into an auxiliary building or directly into the atmosphere. As a result, accurate determination of fission product attenuation in the primary and secondary circuits is paramount to the assessment of risk for the by-pass sequences.

The physical processes that influence the quantity and timing of a release are complex. In order to be able to predict the outcome of a nuclear accident, it is necessary to accurately model as many of the relevant physical processes as possible. VICTORIA [1] is a mechanistic computer code designed to model such releases from the RCS during a severe reactor accident.

The purpose of VICTORIA is to enable the prediction of the magnitude, speciation, physical properties, and timing of fission product release from the RCS of a nuclear reactor undergoing a severe accident. VICTORIA does not predict thermal-hydraulics, but requires such information as input. The heart of the code is in its mechanistic treatment of fission product release from fuel, chemistry, aerosol physics, transport, and decay heating. The coupled treatment of these phenomena make VICTORIA unique in its predictive capabilities. The following paragraphs describe briefly the current capabilities of VICTORIA.

VICTORIA contains models for release of fission products from both intact and degraded fuel geometries, including rubble beds and molten pools. For intact fuel, release mechanisms within fuel grains are either by advection and diffusion [2,3] or, alternatively, may include models for the effects of bubble formation, coalescence, and migration and the effect of grain boundary sweeping [4,5]. Transport through fuel pores is by surface and gaseous diffusion and by a model for advection due to calculated pressure gradients [1]. Chemical speciation and interaction with surfaces are also essential parts of this calculation because chemical reactions and phase changes drive the concentration and pressure gradients that produce diffusion and advection. Only gaseous transport is considered in the gap between clad and fuel, but both diffusion and advection are treated. Chemical speciation and interaction with the inner cladding surface are also modeled. Transport through a breached cladding is treated similarly to that in fuel pores. From the cladding, fission products diffuse through a boundary layer and into the bulk gas.

A model for pressurized rupture and release from silver-indium-cadmium control rods is available in VICTORIA. This model is based on the work of Powers [6], which defines the partial pressure of the vapor species above a molten alloy as a function of temperature and composition. This model also uses the experimental data of Bowsher et al. [7] to estimate the properties of the aerosol created during the burst. The models used to describe release from control rods are detailed further in Section 3 of Reference 1.

The chemistry models used in VICTORIA are largely based on thermodynamic equilibria; however, models also account for kinetically limited rates for several processes. These include oxidative volatilization of UO_2, tellurium-zircaloy interactions, and chemisorption of several cesium and iodine species onto structures. VICTORIA treats 288 chemical species composed of 26

elements. All of the chemistry models are described further in Section 4 of Reference 1. An optional nonequilibrium model treats the effects of chemical kinetics below a specified threshold temperature in a simple way. Below the threshold, kinetic effects are taken to be infinitely slow. This option has been dubbed the "frozen chemistry" model [8]. If this option is chosen, change of phase is modeled but chemical reactions are not allowed below the specified temperature threshold.

Bulk-gas processes include heterogeneous chemical speciation (the condensed phase forms aerosol particles), advection, diffusion, and aerosol phenomena, including formation, growth, agglomeration, and deposition. Agglomeration and deposition mechanisms include Brownian motion or diffusion, gravitational settling, turbulent shear, and turbulent inertia. Additional deposition mechanisms include thermophoresis and inertial deposition in pipe bends, sudden contractions, steam separators, and steam dryers [9]. A model for re-entrainment of deposited aerosols, based on the data of Wright et al. [10], has also been incorporated. These models are described further in Section 5 of Reference 1.

A model for radioactive decay heating is also available in the code [11]. This model simulates the heat-up of films and structures by decay heating from deposited radionuclides. It can be used to investigate the effect of decay heating on revaporization of the deposited material. This model is described in more detail in Section 6 of Reference 1.

2. Analysis of SGTR Sequence

Analysis of a steam generator tube rupture accident (SGTR) was performed for a sequence similar to the HINY-NXY sequence that was considered in NUREG-1150 [12]. This sequence is believed to be similar to the one investigated in the Surry individual plant examination (IPE) [13] as well, except that two tubes were assumed to rupture in that investigation, whereas only one was assumed to rupture in the HINY-NXY sequence and in this analysis.

As part of this effort, the predicted source term was compared with two earlier works, NUREG-1150 and the Surry IPE. In addition, predicted results were compared with the MELCOR calculation that was used to determine the thermal-hydraulic data needed as input to VICTORIA.

An objective of this analysis was to demonstrate that MELCOR thermal-hydraulic data could be used to drive VICTORIA. A previous calculation for a station blackout (TMLB') [14] had been performed using SCDAP/RELAP5 [15] thermal-hydraulic data to drive VICTORIA. The SGTR analysis presented here was the first attempt to perform a VICTORIA analysis using data from MELCOR [16,17].

3. Brief Description of the SGTR Sequence

The thermal hydraulics and fuel degradation analysis for the SGTR sequence was performed by MELCOR and is reported elsewhere [16,17]. Table 1 summarizes the timing of the major events, using the initiating event, a guillotine rupture of a single steam generator tube, as the reference time.

Table 1. Timing of Major Events in SGTR Sequence as Predicted by MELCOR

Event in Accident Sequence	Time (s)
Guillotine Rupture of Steam Generator Tube in Loop C	0
Reactor Scram	360
High-Pressure Injection (HPI) Starts	380
Secondary RV Sticks Open in Loop C	7620
RWST Depleted, HPI Terminates	58,400
Beginning of Core Uncovery	68,000
Beginning of Fuel Rod Failure	105,700
Rupture of Lower Head	113,800

Reactor scram occurs at 6 minutes following the initiating event. Shortly after that, high-pressure injection begins. All high-pressure injection systems are assumed to function. A secondary relief valve is assumed to stick open as soon as a significant amount of water is forced through it, which occurs at just over 2 hours. High-pressure injection terminates after 16 hours, when the water supply is depleted. Core uncovery begins about 2.5 hours following termination of high-pressure injection; however, the water level stays near the top of core for a considerable time and, as a result, fuel rods do not begin failing until after 29 hours. Rupture of the lower head occurs at about 31.6 hours, at which point the MELCOR calculation was terminated. Thus, the period for which fission product release and transport was calculated was only about 2.25 hours.

MELCOR predicts that, following the sticking open of the secondary relief valve, the system quickly depressurizes to between 10 and 15 bars. The maximum core temperatures do not exceed much over 2500 K and large portions of the core remain well below 2000 K for most of the transient. These are relatively low temperatures and do not permit large releases, especially for the less-volatile elements.

4. VICTORIA Representation of the Surry Plant

The VICTORIA analysis of the SGTR sequence was performed as five separate calculations. These were for the core region, the primary circuit excluding the two ends of the broken steam generator tube, each end of the broken tube, and the secondary circuit. The nodalizations for each domain and further details are given below.

The VICTORIA nodalization of the core region contained 15 cells and is shown schematically in Figure 1. Neither the lower plenum nor the core bypass were included in the nodalization since these did not participate in the release or transport of fission products. Instead, the steam that vaporized in the lower plenum was inserted as a source into the bottom cells of the core and the steam that flowed through the bypass was included as a source into the upper plenum. At the

earlier times when the water level was somewhere between the top and bottom of the core, the steam source was inserted just above the water level. The quantities of steam, hydrogen, fission product species, and structural materials that transported through the upper boundary of the core were saved and used later as sources of mass into the upper plenum. In addition, the aerosol size distributions were saved and used to determine aerosol sources into the upper plenum.

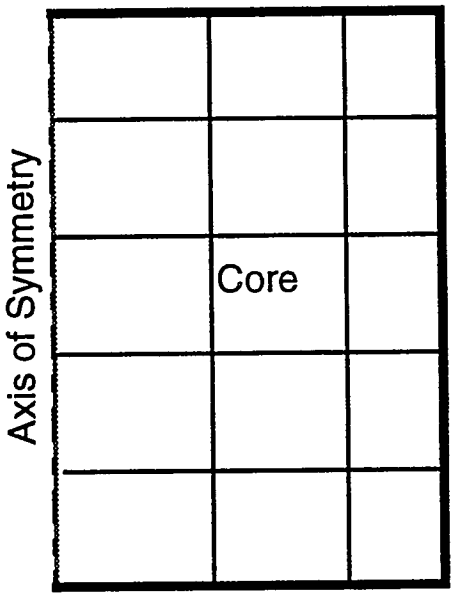

Figure 1. Schematic of the VICTORIA nodalization of the core region.

Figure 2 contains a schematic of the VICTORIA nodalization of the upper plenum, hot leg, and steam generator, including the broken tube. Since the ruptured tube is assumed to be completely severed, flows through both sides of the break can occur. The flow through the side connected to the steam generator outlet plenum, cell 7, is fed by steam flowing through the intact tubes, denoted in the schematic by cells 3 and 4. Flow through the other side of the broken tube, cell 6, is fed directly by steam from the steam generator inlet plenum, which is part of cell 2.

Separate VICTORIA calculations were performed for each end of the broken tube, cells 6 and 7 in Figure 2. This was advantageous because the velocities were much higher in the broken tubes than elsewhere in the primary circuit and, as a result, the time-step size had to be much smaller. Data flow between domains was handled in the same way as described above for species leaving the fuel region. In addition, data for each species leaving cells 6 and 7 was retained to be used as input sources in the analysis of the secondary circuit.

Figure 3 shows a schematic of the VICTORIA nodalization of the secondary circuit. Cells 1 and 2 represent the upper portion of the steam generator and cells 3 and 4 represent the steam line. Cell 1 contains the steam separators that are used to remove entrained water from the steam. Cell 2 contains the steam dryers. The VICTORIA models for aerosol deposition in steam separators and dryers were employed, respectively, in cells 1 and 2.

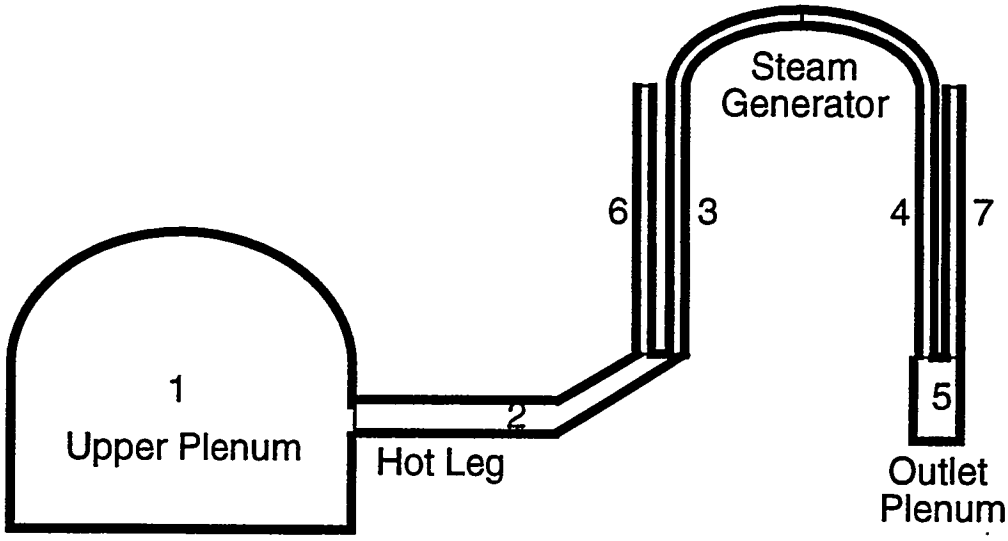

Figure 2. Schematic of the VICTORIA nodalization of the upper plenum and primary circuit.

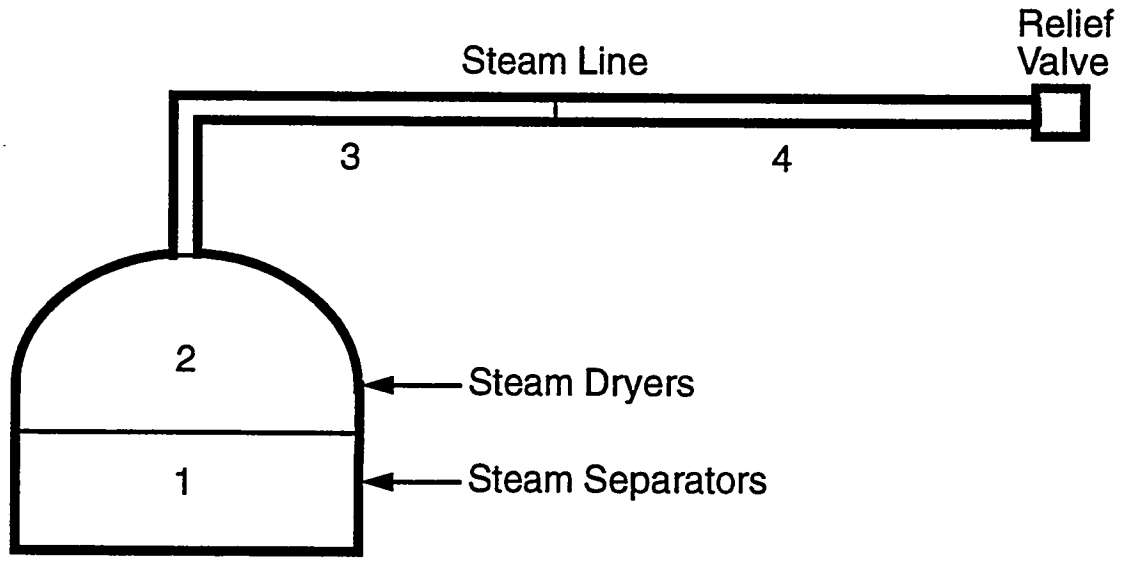

Figure 3. Schematic of the VICTORIA nodalization of the steam generator secondary and steam line.

Thermal-hydraulic properties, such as flow areas, hydraulic diameters, and surface areas, were taken to be consistent with the MELCOR input [16] used to generate the thermal-hydraulic data for this analysis. Twelve aerosol mass bins were used to represent the aerosol size distribution, which ranged from 10^{-21} to 10^{-10} kg by decade. The cladding failure temperature was chosen to be 1250 K to match the MELCOR predictions. The melting point for the cladding was chosen to be 2140 K. Matzke's recommendation for intragranular diffusion coefficient [18] was

used for all of the fission products. Other values were chosen to be the standard ones recommended for most VICTORIA calculations [1].

5. Analysis of the Core Region

Figure 4 shows the timing and magnitude, in terms of percent of fuel inventory, of the releases from the core region, i.e., the percent that reaches the upper plenum. Releases from the fuel rods are slightly higher than shown in this figure because some of the material released from the fuel is retained within the core region and so never reaches the upper plenum. Significant releases begin at about 110,000 s after the initiating event. Only iodine, cesium, and tellurium are seen to be released at a significant percent of fuel inventory.

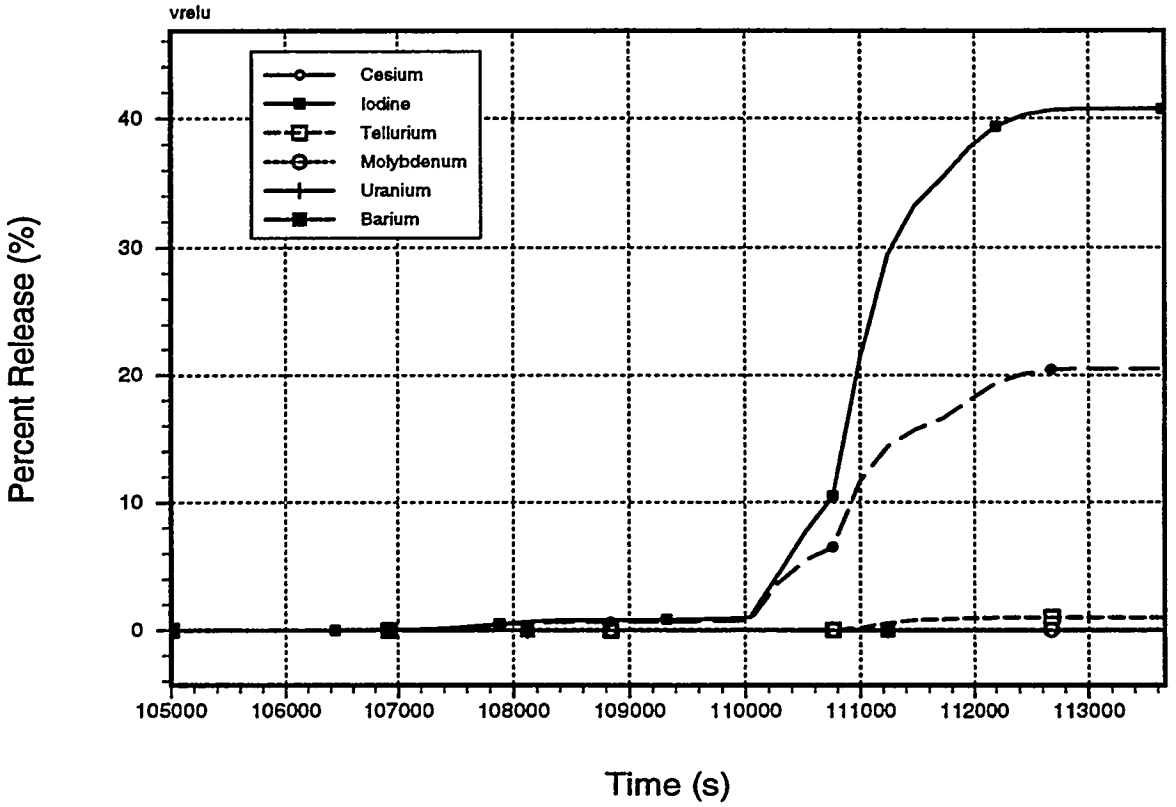

Figure 4. Release histories, as a percent of fuel inventory, for cesium, iodine, tellurium, molybdenum, uranium, and barium.

Table 2 displays information about the integral masses and percents released from the fuel rods over the transient. The values given in this table are somewhat greater than the final values displayed in Figure 4, as explained above. Table 2 also compares the results of this work with results from NUREG-1150 for the HINY-NXY sequence, the Surry IPE, and with the MELCOR predictions that were used to construct the thermal hydraulics for this same sequence. Table 2 shows that MELCOR predicts somewhat lower releases than the Source Term Code Package (STCP) or the industry code, MAAP. VICTORIA predicts even lower releases than MELCOR, es-

pecially for the low-volatility elements, such as barium, molybdenum, and ruthenium. It should be noted that MELCOR does not predict the release of antimony directly. Instead, it includes this element in a group for which the primary element is cadmium, which explains why the predicted value is so high.

Table 2. Elemental Releases from the Fuel Rods

Reference	This work			NUREG-1150 [11]	Surry IPE [12]	SGTR T-H [16,17]
Element	Inventory (kg)	Mass Rel. (kg)	% Rel.	% Rel. (STCP)	% Rel. (MAAP)	% Rel. (MELCOR)
Kr	16	11.7	73.16			69.3
Xe	225	164.5	73.11			69.3
I	9	4.1	45.48	92.5	99.0	69.3
Cs	118	30.1	25.48	92.8	99.0	69.3
Te	18	0.2	1.19	61.0	88.0	10.4
Ba	65	0.5	0.70			7.3
Sb	1	0.0	0.23			21.8
Mo	135	0.1	0.05			5.4
U	67530	0.1	$2x10^{-4}$			$1x10^{-4}$
Ru	100	0.0	$1x10^{-5}$			$2x10^{-3}$

The trend shown in Table 2 is that the more refined tools, which should give more realistic and less conservative predictions, give lower estimates of release. Differences between the MELCOR and VICTORIA predictions are probably due to differences in chemical properties, pressure effects, and differences in the treatment of temperatures of relocated fuel. (VICTORIA releases have been shown to depend on pressure [19]; MELCOR releases do not account for the influence of pressure.)

6. Analysis of the Primary Circuit

Figure 5 shows the VICTORIA predictions for the accumulation of masses in the upper plenum and primary circuit, i.e., the reactor coolant system. The largest deposited masses are for cesium, followed by iodine. Early in the transient, molybdenum is the third most abundant fission product element in the upper plenum and primary circuit; later in the transient, uranium followed by tellurium replaces molybdenum for dominance. The final deposited mass of fission products in

the RCS is about 20 kg. In addition, about 45 kg of tin, 50 kg of silver, 7 kg of indium, and 7 kg of cadmium are predicted to deposit in the RCS.

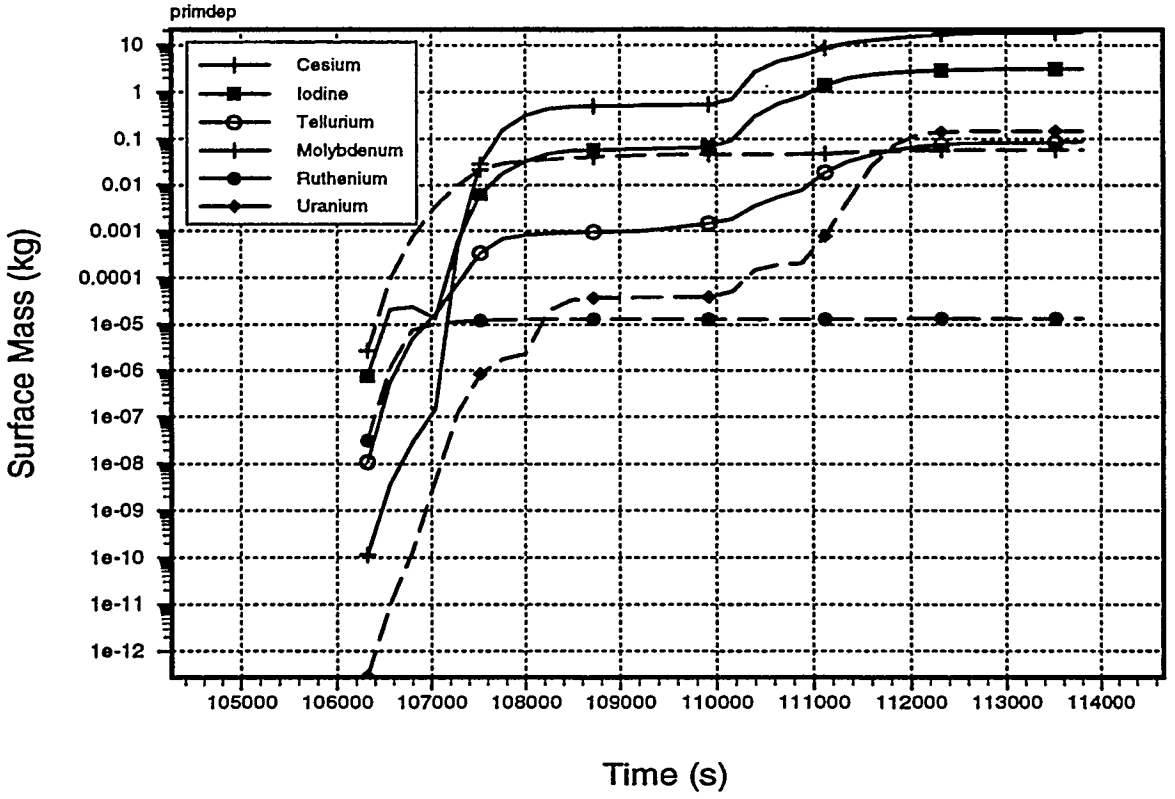

Figure 5. VICTORIA-predicted retention histories in the reactor coolant system.

Table 3 contains a comparison of predicted retentions in the RCS as percents of the mass released from the fuel. The intention in presenting this comparison was to normalize out any differences in release models by using the mass released from the fuel as a basis for comparisons further downstream.

Table 3. Percent of Material Released from Fuel Retained in RCS

Element	STCP [11]	MAAP [12]	MELCOR [16,17]	VICTORIA
Kr			3.7	3.2
Xe			3.7	3.2
I	40	32	*	99.2
Cs	41	32	80.1	93.6
Te	67	19	78.8	99.7
Ba			87.2	99.8

Table 3. Percent of Material Released from Fuel Retained in RCS

Element	STCP [11]	MAAP [12]	MELCOR [16,17]	VICTORIA
Sb			87.2	99.7
Mo			87.2	99.4
U			87.6	99.7
Ru			87.3	99.4

* Not available.

The MAAP results from the Surry IPE predict the lowest retentions; the STCP, used in NUREG-1150, predicts somewhat higher retentions in the RCS; MELCOR predicts retentions in the range of 80 to 90%; VICTORIA predicts, with the exception of cesium and the noble gases, retentions to be nearly 100%.

VICTORIA predicts that most of the deposited iodine is in the form of CsI; most of the deposited cesium is in the form of CsOH. Because CsOH is more volatile than CsI, less cesium than iodine is retained in the RCS. Species that are mostly in the condensed phase (as an aerosol) are retained at a very high fraction in the RCS. The primary retention mechanisms are gravitational settling in the upper plenum, deposition at the bends in the steam generator inlet plenum, and turbulent deposition in the broken steam generator tube where flow velocities are sonic for most of the transient.

7. Analysis of the Secondary Circuit

Figure 6 shows the retention of fission products and uranium in the steam generator secondary and in the steam line. The mass deposition on the secondary side is much smaller than on the primary side because a very small fraction of the mass is predicted to escape from the primary. In terms of mass, the dominant elements are cesium, iodine, uranium, and tellurium, in that order.

Table 4 gives comparisons for retention in the secondary circuit, i.e., in the steam generator secondary and in the steam line. MAAP predicts the highest retentions; the STCP and MELCOR predict retentions of about 5 to 10% of the mass released from the fuel; VICTORIA predicts retentions that are less than 1%, which is a result of the fact that most of the fission products are predicted to be retained in the primary circuit. Furthermore, VICTORIA predicts that much of the mass entering the secondary circuit is in the form of vapor, especially for cesium and iodine. In addition, sufficient thermal-hydraulic data were not available to treat thermophoretic deposition in the steam line. As a result, VICTORIA predicts fairly low retentions on the secondary side.

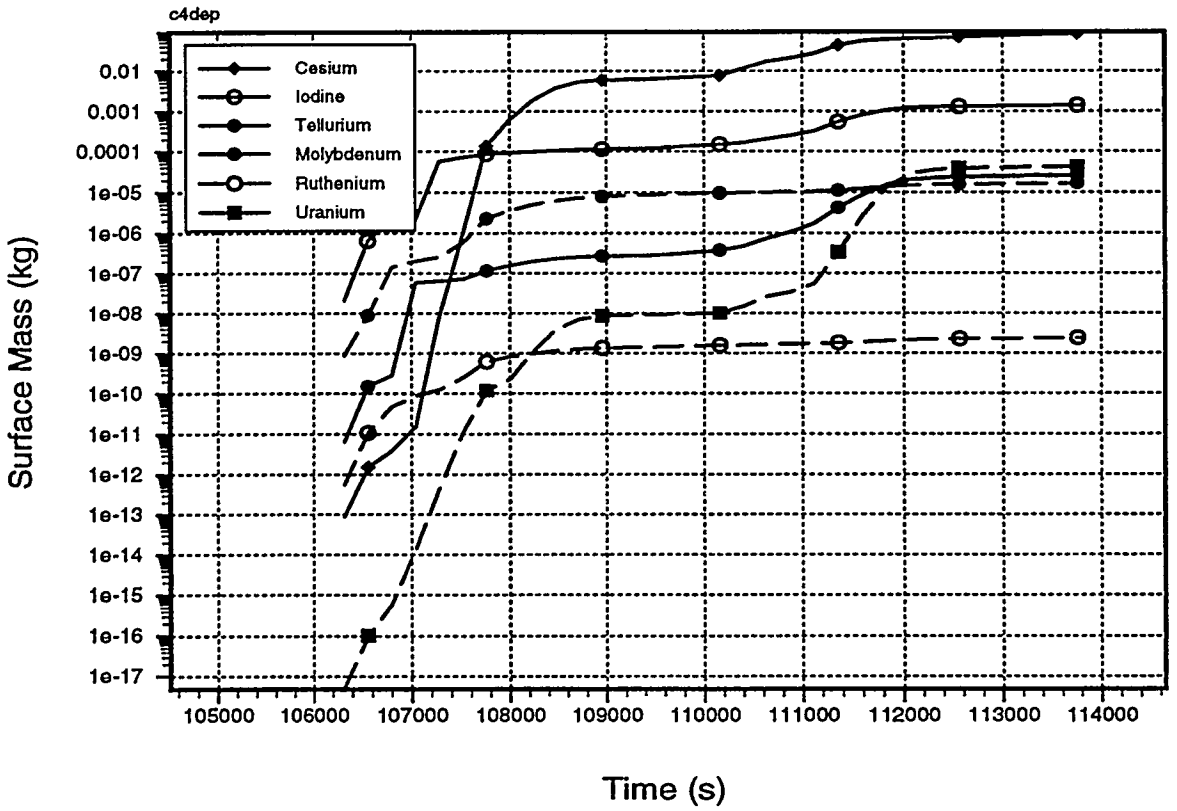

Figure 6. VICTORIA-predicted retention histories in the secondary circuit.

Table 4. Percent of Material Released from Fuel Retained in Secondary Circuit

Element	STCP [11]	MAAP [12]	MELCOR [16,17]	VICTORIA
Kr			0.5	0.2
Xe			0.5	0.2
I	6	22	*	0.1
Cs	6	24	9.3	0.4
Te	6	18	9.8	0.0
Ba			6.0	0.0
Sb			6.0	0.0
Mo			6.0	0.0
U			5.8	0.0
Ru			6.0	0.0

* Not available.

Table 5 shows comparisons of the most important result, the percent of the inventory initially contained in the fuel that is released from the secondary into the auxiliary building. The STCP and MAAP predict overall releases of the volatile fission products, iodine, cesium, and tellurium, to be roughly 50% of the initial fission product inventories. MELCOR predicts these releases to be 1 to 10%. VICTORIA, which is the most sophisticated in terms of fission product modeling, predicts these elements to be released at a level of about 1% or less. The VICTORIA predictions indicate a significantly lower risk to the public for SGTR sequences than those predictions given in NUREG-1150 and in the Surry IPE.

Table 5. Percent of Fuel Inventory Released from the Secondary Circuit into the Auxiliary Building

Element	STCP [11]	MAAP [12]	MELCOR [16,17]	VICTORIA
Kr			66.4	70.6
Xe			66.4	70.6
I	50.2	44.9	*	0.3
Cs	49.0	43.2	7.3	1.4
Te	15.9	55.0	1.2	$3x10^{-3}$
Ba			0.5	$1x10^{-3}$
Sb			1.5	$6x10^{-4}$
Mo			0.3	$3x10^{-4}$
U			$7x10^{-5}$	$6x10^{-7}$
Ru			$1x10^{-2}$	$6x10^{-8}$

* Not available.

8. Summary

Generally, VICTORIA predicts lower releases of fission products from the fuel and much greater retention of the released fission products in the upper plenum and primary circuit than had been predicted in earlier works, e.g., NUREG-1150 [11] and the Surry IPE [12].

Acknowledgments

This work was supported by the US Nuclear Regulatory Commission and performed at Sandia National Laboratories, which is operated for the US Department of Energy under Contract Number DE-AC04-94AL85000. Help and advice from Mark Leonard and Terry Heames of the ITS Corporation are also gratefully acknowledged.

References

1. T. J. Heames, D. A. Williams, N. E. Bixler, A. J. Grimley, C. J. Wheatley, N. A. Johns, and M. D. Vine, P. Domagala, L. W. Dickson, C. A. Alexander, I. Osborn-Lee, S. Zawadzki, J. Rest, and H. S. Bond, "VICTORIA: A Mechanistic Model of Radionuclide Behavior in the Reactor Coolant System Under Severe Accident Conditions, Revision 1" SAND90-0756, NUREG/CR-5545, Sandia National Laboratories, Albuquerque, New Mexico (1992).
2. A. H. Booth, "A Method of Calculating Fission Gas Diffusion from UO_2 Fuel and Its Application to the X-2-f Loop Test," CRDC-721, AECL Chalk River, Canada (1957).
3. N. E. Bixler and T. J. Heames, "Status of VICTORIA Development and Assessment," NUREG/CP-0114, *Proceedings of the Eighteenth Water Reactor Safety Information Meeting, Vol. 2*, U.S. Nuclear Regulatory Commission, Washington, DC, pp. 271-282 (1990).
4. J. R. Matthews and M. H. Woods, "Modelling the Transient Behaviour of Fission Gas," *Journal of Nuclear Materials, 84*, pp. 125-136 (1980).
5. J. Rest and A. W. Cronenberg, "Modeling the Behavior of Xe, I, Cs, Te, Ba, and Sr in Solid and Liquefied Fuel During Severe Accidents," *Journal of Nuclear Materials, 150*, pp. 203-225 (1987).
6. D. A. Powers, "Behavior of Control Rods During Core Degradation: Pressurization of Silver-Indium-Cadmium Control Rods," NUREG/CR-4401, U.S. Nuclear Regulatory Commission, Washington, DC (1985).
7. B. R. Bowsher, R. A. Jenkins, A. L. Nichols, N. A. Rowe, and J. A. Simpson, "Silver-Indium-Cadmium Control Rod Behaviour During a Severe Accident," AEEW-R1991, UKAEA, Winfrith, UK (1986).
8. N. E. Bixler and K. W. Boyack, "Frozen Chemistry Model for VICTORIA-92 and its Assessment Against Data from Falcon-ISP," Letter Report to the USNRC, Sandia National Laboratories, Albuquerque, New Mexico (1994).
9. K. H. Im, R. K. Ahluwalia, and H. C. Lin, "The RAFT Computer Code for Calculating Aerosol Formation and Transport in Severe LWR Accidents," NP-5287-CCM, Argonne National Laboratory, Argonne, Illinois (1987).
10. A. L. Wright, W. L. Pattison, and J. Y. King, "'SERIES -2' Aerosol Resuspension Test Data Summary Report," Oak Ridge National Laboratory, Oak Ridge, Tennessee, unpublished.
11. N. E. Bixler, "Model for Heat-Up of Structures in VICTORIA," SAND92-1506, Sandia National Laboratories, Albuquerque, New Mexico (1992).
12. NUREG-1150, Vol. 1, "Severe Accident Risks: An Assessment for Five U.S. Nuclear Power Plants," U.S. Nuclear Regulatory Commission, Washington, DC (1990).
13. Virginia Electric Power Company, "Individual Plant Examination Submittal for Surry," Sections 4.3 and 4.7.
14. N. E. Bixler and C. M. Erickson, "VICTORIA-92-01 TMLB' Calculation Using SCDAP/RELAP5 Thermal-Hydraulic Data," Letter Report to the USNRC, Sandia National Laboratories, Albuquerque, New Mexico (1994).
15. C. M. Allison, G. A. Berna, E. W. Coryell, K. L. Davis, D. T. Hagrman, J. K. Hohorst, R. R. Schultz, and L. J. Siefken, "SCDAP/RELAP5/MOD3.1 Code Manual Volume III: SCDAP/RELAP5 Users Guide and Input Manual," NUREG/CR-6150, EGG-2720, Idaho National Engineering Laboratory, Idaho Falls, Idaho (1993).
16. K. Bergeron, R. Cole Jr., A. Elsbernd, S. Rodriguez, R. Smith, and M. Leonard, "Progress on the MELCOR Code," NUREG/CP-0149, *Proceedings of the USNRC Twenty-Third Wa-*

ter Reactor Safety Information Meeting, U.S. Nuclear Regulatory Commission, Washington, DC, (1996).
17. M. T. Leonard and S. G. Ashbaugh, "MELCOR 1.8pz Calculations of a Steam Generator Tube Rupture Severe Accident Sequence in a 3-Loop Westinghouse PWR," ITS/SNL-95-07, Sandia National Laboratories, Albuquerque, New Mexico (1995).
18. Hj. Matzke, "Diffusion in Ceramic Oxide Systems," *Advances in Ceramics, 17*, pp. 1-54 (1986).
19. N. E. Bixler, "VICTORIA-92 Analyses of Phebus FPT-3: The Proposed High-Pressure Test," Letter Report to the USNRC, Sandia National Laboratories, Albuquerque, New Mexico (1994).

THE SEVERE ACCIDENT RESEARCH PROGRAMME PHEBUS F.P.: FIRST RESULTS AND FUTURE TESTS.

M. SCHWARZ (1) - P. von der HARDT (2)

(1) Institut de Protection et de Sûreté Nucléaire - IPSN
CEA CADARACHE - F 13108 SAINT PAUL LEZ DURANCE - FRANCE

(2) European Commission
Joint Research Centre - Safety Technology Institute
CEA CADARACHE - F 13108 SAINT PAUL LEZ DURANCE - FRANCE

ABSTRACT

PHEBUS FP is an international programme, managed by the French Institut de Protection et de Sûreté Nucléaire, Electricité de France and the European Commission in close collaboration with the USNRC (US), COG (Canada), NUPEC and JAERI (Japan) and KAERI (South Korea). Its objective is to investigate through a series of in-pile integral experiments, key phenomena involved in LWR severe accident such as the degradation of core materials up to molten pool, the subsequent release of fission products and of structural materials, their transport in the cooling system and their deposition in the containment with a special emphasis on the volatility of iodine.

After a general programme description, the paper focuses on the status of analysis of the first test FPT-0, which involved trace irradiated fuel and which has shown some quite unexpected results regarding fuel degradation and iodine behaviour, and on the upcoming test FPT-1 which will use irradiated fuel. The status of the preparation of the remaining tests of the programme is also presented.

1. INTRODUCTION

The PHEBUS FP programme [1] is the centrepiece of a world-wide co-operation on the investigation of severe accidents in Light Water Reactors, from the point of view of consequence assessment and the evaluation of possible accident mitigation measures. It provides a rather unique opportunity to check on a series of integral in-pile experiments that all the important phenomena controlling core degradation, from the early phase of cladding oxidation up to the late phase of pool formation, fission product release, their transport in the circuit and their subsequent behaviour in the containment, are correctly understood and properly modelled in the analytical tools used to assess the safety of Nuclear Power Plants.

The first experiment of the programme, FPT-0, was successfully performed in December 1993. As the first results were coming out, in particular the radio-tomograms, it became clear that FPT-0 has reached a more advanced state of bundle degradation than any previous in-pile experiment. Subsequently, a rather large amount of fission product was released from the trace irradiated fuel and made it possible to demonstrate the capability of the facility to reach the assigned objectives regarding fission product study.

The evaluation of the on-line experimental data as well as of the numerous post-test analyses is now almost complete with the exception of the bundle post irradiation examination which is still in progress. Extremely valuable information has already been obtained, which is now in the hands of analysts who are facing the challenging task of trying to explain the unexpected phenomena observed in the test, such as the early fuel degradation and the higher than expected concentration of iodine in the containment atmosphere.

Most of the analysis performed to date has concentrated on checking thermal-hydraulic and bundle degradation aspects. Consistency in fission product and structural aerosol measurements was also systematically checked. The results of this work was important to correct and improve the instrumentation and the test procedures in time for FPT-1, the next experiment of the programme. The test conditions are close to the FPT-0 ones, except for the use of fuel irradiated to a mean burn-up of 23 GWd/tU.

In parallel, review of the needs and priorities of safety analysis has led to revise the test matrix, giving more weight to the FPT-4 and FPT-5 experiments which will mostly address safety issues of the so-called late phase, in particular the release and transport of low-volatility fission products and transuranium elements under respectively very high temperature and high oxygen (air ingress) conditions.

After a brief review of the PHEBUS programme and facility, the status of the FPT-0 analysis will be presented. A description of the upcoming test FPT-1, as well as the status of preparation of the remaining tests of the programme will also be given.

2. PROGRAMME DESCRIPTION

2.1. Objectives

PHEBUS FP supplies data on core degradation and FP release under water reactor severe accident conditions.

The residual risk to the environment during and after a severe nuclear power plant accident with core damage resides mainly in the fission products (FP) emanating from the overheated core.

It is therefore necessary to evaluate FP quantity and nature (the reference source term) and to assess the efficiency of preventive and mitigative measures that can be implemented on a plant: operating and emergency procedures and specific hardware (engineered safety features and ultimate devices).

In this analysis, the chemistry aspect is essential to determine FP behaviour at various points in the plant and to evaluate the radiological impact of potentially large property variations between different species of the same FP. For these studies and from the point of view of code validation, the PHEBUS FP experiments offer a number of novel aspects :

1. A source representative as to composition and concentration of FPs, control materials, and structural materials. Hence one can expect representative chemistry - aerosol size distribution and composition, interaction between vapours and aerosols and between vapours and structures - that is difficult if not impossible to obtain with artificial sources or in small-scale experiments.

2. Circuit temperatures high enough to be representative of reactor primary system components. The circuit materials are Inconel and austenitic steel. It is presently thought that there is little difference in the degree of reactivity with regard to FP retention between both materials. The issue, however, is further examined by separate effects tests. Components at lower temperatures can be included (e.g. a steam generator tube), which can even be cold enough to induce steam condensation on the walls and onto aerosols.

3. A containment vessel with several systems for producing representative thermal-hydraulic conditions, including the sump and wall temperatures and the temperature of surfaces upon which condensation is to take place.

4. Design features of the containment that allow containment chemistry to be reproduced, including a realistic source, painted surfaces, free or controlled sump pH, and a high radiation level.

Code and model validation requirements that will be met by PHEBUS FP correspond in the main to these special advantages:

5. Data on the release of FPs and other core materials under conditions of advanced degradation (oxidising or reducing conditions, significant melting of fuel, and oxidised cladding). Data on the release of less-volatile FPs (Ba, Sr, and Ru) are of particular interest both for model validation-improvement and from the point of view of safety analysis.

6. With the realistic source and circuit temperatures, data on transport and deposition in circuit components. Items of particular interest are the role of multicomponent aerosols; vapour-aerosol interaction and revaporization as well as (with realistic source and thermal-hydraulic conditions) the
differential depletion of hygroscopic and nonhygroscopic aerosols; and the role of steam condensation on structures in aerosol removal.

7. New data on fission-product chemistry and iodine behaviour with a range of chemical conditions and in the presence of radiolysis.

2.2. Organisation

The program is managed by a Steering Committee (SC) that meets twice a year. The SC receives advice from three working groups (Fig. 1) :

- An analytical group (Scientific Analysis Working Group, SAWG), assisting in the test matrix definition, preparing the experiments by pre-calculations, and finally analysing the results obtained.

- A technical Group (TG) that assesses experimental equipment, instrumentation, and operating procedures proposed and analyses the in-pile performance of equipment, instrumentation, and procedures.

- A restricted financial group controlling the expenditures of the two major program partners according to the contractual definitions.

Between two SC meetings, PHEBUS FP is managed by a program group that has these mandates:

- Define and schedule the work of the different teams working for the program.

- Prepare and distribute the required information.

- Request SC decision for matters beyond day-to-day management.

- Prepare the SC meetings, together with the working group chairmen.

The Institut de Protection et de Sûreté Nucléaire (IPSN) and the European Commission (EC) have been major program partners since the signing of the basic contract in July 1988. Organisations from European Member States are represented in the SC by EC but participate directly in the work of the analytical and the technical groups. Electricité de France is also represented in the SC and the working groups.

Since 1988 several overseas partners joined the program: the US Nuclear Regulatory Commission, the Nuclear Power Engineering Test Centre (Japan) and Japan Atomic Energy Research Institute, COG Canada, and the Korean Atomic Energy Research Institute. The entry of new partners is under negotiation.

The collaboration of all participating organisations, particularly in the analytical and technical groups, is encouraged. Assistance in solving numerous technical problems and participation in precalculations and analysis of the experiments, on the other hand, safeguard the best possible expertise transfer to and from the PHEBUS FP Program.

2.3. PHEBUS facility [1] [2] [3]

The PHEBUS FP program required 5 years (1989-1993) and $80 million (US) for design and construction of buildings, reactor components, experimental equipment, and instrumentation & controls.

Experimental Equipment

In-Pile Section (Test Train). A horizontal section on driver core midplane (Fig. 2) shows the 20-rod test fuel bundle surrounded by a ceramic shroud fitted inside the pressure tube. The central position is occupied by a silver-indium-cadmium stainless steel clad control rod. Two Zircaloy grids with Inconel spacers are located at respectively 220 and 740 mm from the bottom of the fuel column. The thermal shroud consisted of two concentric, high-density, zirconia tubes in the FPT-0 test train. FPT-1 will be fitted with a new zirconia shroud and an inner thoria liner.

A remotely operated foot valve below the fuel bundle connects the inner test train volume to the surrounding high-pressure water loop during the fuel reirradiation phase. The valve is closed for the high-temperature transient phase. The upper plenum tube above the fuel bundle acts as a cooling water return pipe during reirradiation. It conducts the hot-steam-hydrogen-FP mixture towards the experimental building during the transient phase. The test fuel is 4.5% enriched UO_2 for the first test and preirradiated fuel for the remaining tests of the program. The irradiated fuel originates from the BR3 plant in Mol, Belgium. Before being shipped to Cadarache, the BR3 fuel pins underwent a lengthy characterisation program at JRC, Karlsruhe. The main objectives of these tests were checks on possible deformation and incipient cladding cracks. FP and heavy nuclei distribution, grain size, fuel stoichiometry, and burnup were measured. All pins for PHEBUS FP were « healthy ». In contrast to earlier test fuel from BR3, grain size and oxygen/metal (O/M) ratio correspond to commercial fuel data.

The test train is instrumented with about 70 thermocouples, two ultrasonic thermometers, miniature fission chambers, and a differential pressure transducer. Small bore tubes are provided for the injection of steam and noncondensable gases underneath the test fuel bundle. The test train sits in a double-walled in-pile cell, a fixed structure in the centre of the PHEBUS reactor core. Together with the double-contained components of the high-pressure water loop, the in-pile cell completes the three-barrier safety design principle as a protection against accidental radioactivity release from the experiment.

Primary Circuit (Simulated RCS). The test train upper plenum and the horizontal line (Fig. 3) are the first components of the primary circuit. Both fulfil the same function during the high-temperature transient: that is they convey the hot-steam-hydrogen effluents sweeping FPs and other aerosols out of the fuel bundle toward the experimental building. The upper plenum and horizontal line are Inconel-lined, trace heated to 970 K, and instrumented with thermocouples. As mentioned before, both components are part of the high-pressure cooling water circuit during the reirradiation phase.

For safety reasons, all experimental components are housed in a steel caisson, which continues the triple barrier principle mentioned previously. Major components of the primary circuit are two instrumentation groups at points « C » and « G », and a simulated steam generator. This latter device is operated in a noncondensing mode during the first two tests. For experiments in the later part of the test matrix, the steam generator could be condensing or replaced by a different primary circuit configuration.

Containment Vessel (Fig. 4). This 10-m^3 cylinder simulates the reactor containment building. Similar to the other experimental components, it is installed inside the safety caisson. Particular design features of the containment vessel are a sump and a group of three condensers in the upper part. They are designed to control steam condensation and to recuperate condensates with entrained FPs for analysis.

Painted surfaces on the condensers and in the sump support experiments about organic iodine formation during the containment « chemistry » phase. The condensers simulate the cold structures of a reactor building; they limit condensation onto the vessel wall, which could not be quantified accurately.

Note that the overall scaling factor for the main components (fuel, steam generator, containment volume and cooled structure area) is of the order of 1/5000 as compared to a 900 MWe Nuclear Plant.

Experimental instrumentation

The test results are elaborated through different devices and methods:

1. Thermal-hydraulic on-line instrumentation, like thermocouples, pressure transducers, and flowmeters

2. FP on-line instrumentation, like gamma spectrometers.

3. Sampling instruments, requiring post-test analyses (PTA) of their gaseous, liquid, and/or solid FP contents.

4. Post-irradiation examination (PIE) of the damaged fuel bundle.

Typical sampling instruments adapted to, or developed for, PHEBUS FP are inertial impactors, filters and coupons for aerosols, capsules for gas or liquid sampling, and selective iodine speciation samplers. Various primary circuit components, moreover, can be recovered after each test for analysis of FP deposits.

All sampling instruments are recovered by remote handling as soon as the experimental installation is back to atmospheric pressure and room temperature. They are transferred to a hot cell under the FP caisson where first inspections and gamma scans are carried out, beginning with those samplers which have to be scanned for iodine.

After a first selection, specimens are shipped to a number of laboratories for PTA with these objectives :

- An overall FP and other aerosol mass balance.

- Determination of elemental and isotopic composition and of the chemical speciation of the samples.

• Determination of aerosol granulometry and morphology in solid deposits.

The PTA plan has been elaborated together with the participating laboratories, who will use scanning electron microscopy, X-ray diffraction and fluorescence, energy-dispersive X-ray spectroscopy, inductively coupled plasma optical emission spectroscopy, electron microprobe analysis, and wet radiochemistry for the analytical work.

The PTA plan includes the horizontal line and the test train upper plenum. The lower part of the test train with the damaged fuel bundle is examined according to another program, largely based on more traditional destructive fuel PIE techniques. The objectives of PIE are the mapping of fuel debris and corium compounds and the quantification of remaining FPs.

2.4. Support projects

As a support to PHEBUS FP, out-of-pile (separate effects) experiments are required [1]:

• For phenomenological studies and code validation in areas not adequately covered by PHEBUS FP.

• As direct assistance to preparation, operation, and interpretation of the PHEBUS FP tests.

These experiments, partially performed by overseas programme partners, are not described in the scope of this paper.

3. THE FIRST TEST, FPT-0

The first test of the programme, FPT-0, using trace irradiated fuel, was performed from December 2 to 6, 1993.

3.1. Test conditions

The FPT-0 test section has already been described in 2.3. The main component of the circuit was a steam generator regulated at 420K to avoid any steam condensation under the pressure conditions (0.2 MPa) of the test.

The bundle was irradiated in the PHEBUS core during 9 days at nominal power, cooled by a forced flow of pressurised water. The objective of this pre-test phase was to build up a fission product inventory large enough for on-line and post-test gamma spectrometry and to induce radiolysis in the sump, providing iodine re-volatilisation inside the containment.

The bundle boundary conditions were set up in order to investigate fuel degradation, fission product release and transport under low pressure and oxidising (steam-rich) conditions. The objective was to reach and exceed the melting point of fuel.

The vessel boundary conditions were adjusted in order to limit the relative humidity ratio below about 70%, avoiding uncontrolled steam condensation on the walls which could force fission product deposition on undesirable non instrumented spots. The sump temperature was 90°C and a buffered acidic pH condition was achieved in order to maximise iodine re-volatilisation.

This test protocol was decided after years of pre-calculations by the various partners using different sets of codes all around the world [4].

3.2. Test scenario

The FPT-0 test scenario and the sequence of events observed during the test have been already reported in detail in [5] and [6] and will only be briefly summarised.

After the irradiation phase, the reactor was shut down for a period of 36 hours, in order to prepare all the circuits for the transient test and let the ^{135}Xe accumulated in the driver core decrease to a sufficient level to restart the reactor.

The bundle transient consisted in 4 main phases(see Fig. 5):

- a thermal calibration phase of 10000s with three different steady state bundle temperature levels (730K, 870K and 1200K) ;

- a cladding oxidation phase (10000 to 13000s) obtained by increasing stepwise the power level whereas a quite large steam flow rate was maintained in the bundle to avoid steam starvation ;

- a heat-up phase (13000 to 18138s) during which, after a power plateau for instrumentation check-out, steam flow rate was progressively reduced while the power level was increased stepwise. Melting of about 10 to 20% of fuel was aimed at during this phase of the test. Several events activated pre-defined criteria which terminated the bundle part of the test by reactor shutdown ; it is worth noting that the power level reached at that time was only about 60% of the maximum power foreseen according to the final test protocol.

- a bundle cooling-down phase which followed the reactor shutdown during which the steam flow rate was maintained to ensure the transportation of fission products and aerosol through the circuit to the containment.

The total duration of the degradation and the fission product release phases of the test was about 2.5 hours. After closure of the circuit, the experiment continued during 4 days during which long term chemistry effects were investigated in the vessel simulating the containment.

3.3. Main observations

A. Bundle behaviour

From the readings of the bundle thermocouples, which performed remarkably well up to the beginning of the heat-up phase, and from the qualitative information given by the On-Line Aerosol Monitor, it is possible to infer the global behaviour of the bundle (see Fig 5).

Prior to the last thermal calibration plateau, the fuel rod claddings failed, as expected, at a temperature of 1070K, because of their internal pressure. The control rod then failed at the beginning of the cladding oxidation period, at a temperature of 1540K, lower than the melting point of its stainless steel cladding, most probably due to the rather high level of the vapour pressure developed by Cadmium. It gave rise to a strong aerosol signal as seen on figure 5.

The steam-Zircaloy reaction took place in the upper part of the bundle and propagated downwards as the temperatures increased. Temperatures as high as 2750K were measured at 700 mm elevation, preceded by a fast temperature increase at a rate of 10K/s. As expected, a large hydrogen flow was produced, as deduced from measurements in the containment but, as planned, steam starvation was not (at least globally) reached at the outlet of the bundle. It is estimated that about 70% of the Zircaloy available in the bundle have oxidised during this phase.

Shortly after the heat-up phase was resumed (~ 13800s), there were evidences of several material relocation events inside the bundle which were followed by a rather strong event detected by the OLAM at 15180 seconds. In fact, all the thermocouples of the test section responded also to this event, showing a temperature spike. It was attributed to an accumulation of liquid materials on the lower grid, as inferred from a large increase in the shroud temperature at this level which resulted in a temporary flow blockage. The sudden sharp signal monitored by the OLAM was probably caused by a large transportation of aerosol when flow was restored.

At the end of the test, an increase of aerosol release was again observed simultaneously with an unexpected small increase of the driver core reactivity. This event is attributed to a coherent motion of the pool of fuel material accumulated on the lower grid.

The post-test non destructive examinations, in particular the numerous extremely valuable radio-tomograms taken along the fissile length, show clearly a very advanced stage of degradation (see Fig 6). About 50% of the fuel relocated, creating a large cavity and under it an accumulation of material on and below the lower grid. Intact rods can only be recognised in the first 100 mm at the bottom of the bundle where silver-rich probably mostly metallic materials have accumulated. Main fuel accumulation seems to consist in a central porous structure surrounded by a rather dense crust of materials. This crust is also seen above the refrozen pool on the partly eroded shroud wall, suggesting that the pool has moved downwards during the degradation process.

Peripheral rods, more intact in the upper part of the bundle, delimit the cavity left by the relocated inner ring of rods. Evidence of large fuel degradation (dissolution) is also seen above the upper grid.

Destructive examinations are in progress to determine the composition of the melt and try to infer the maximum temperature experienced by the bundle.

B. Aerosol and FP release

During the test, all the sampling devices and the gamma spectrometers operated well, except at the end of the radiation phase during which too high count rates were reached in the spectrometers located in the circuit. In addition, plugging due to high aerosol concentrations and too long sampling times was observed on several samplers.

From the gamma counting of the different samples after the test, it is seen that the fission product and aerosol release rates is not only correlated with the temperature level in the bundle but also with the bundle degradation process (see Fig. 7); it indeed appears that the formation of the liquid pool resulted in a large decrease of the release rates of volatile as well as less volatile fission products and structural aerosol. The final pool movement gave also rise to a large release rate of these elements, probably as a result of structural materials being incorporated in the moving pool.

The amount of fission products and control rod material released can be grouped in 3 categories :

1. large release (>50%) of the volatiles as I, Te, Cs
2. significant release (<50%) of structural element of Ag and In
3. low release (few %) of low-volatiles (Ba/La, Ru).

The Ba element was mainly released during the cladding oxidation phase (H2-rich flow) compared to Ru, mainly releases during the heat up phase under oxidising environment.

The post-test analyses are almost complete and have enabled fission product and aerosol concentrations to be determined at different time in the circuit and the containment. Aerosol composition appears quite homogeneous for any particle diameter. Estimations of depositions on the walls of the circuit and of the containment were also obtained from post-test gamma scanning measurements. They will be analysed in the next section.

3.4. Status of the analysis and interpretation

Some of the previous results were not expected, as in particular the fairly large state of bundle degradation, reached apparently quite early in the test, at a power level much lower than the calculated level to melt fuel. The analytical challenge to explain why and how these phenomena occurred was particularly important in view of the preparation of the following test FPT-1.

A. Bundle aspect

Most of the analyses [7] [8] [9] were performed using as analytical tool ICARE2 V2 Mod1, a bundle degradation computer code developed by IPSN.

The temperature transient measured during the cladding oxidation period (12000-12500s) as well as the hydrogen production are fairly well reproduced by ICARE2 (see Figures 8 and 9). This result was achieved taking into account the as measured shroud thermal conductivity, which turned out to be lower than the estimations made in the pre-test analyses, and with the aid of a modified clad failure criterion. The criterion previously used was mostly deduced from the analysis of the PHEBUS SFD series of tests and is quite empirical. In fact, these tests were largely conducted in two phases : a low temperature pre-oxidation phase followed by a steam-poor phase. These conditions are quite different from the steam-rich conditions achieved in FPT-0. To reproduce FPT-0, it was necessary to keep the cladding integrity for a longer time.

Due to the rather high temperature achieved on a short time scale in the upper half of the bundle, clad melting and some fuel dissolution are calculated by the code. Good agreement between calculations and measurements are obtained if relocating this mixture on the upper grid.

From about 14000 seconds onwards, the results of the ICARE2 calculations diverge progressively from the temperature measured in the shroud (see Fig 10). ICARE2 is systematically overestimating the temperatures measured between levels 400 and 700 mm. At about 15200 seconds, the temperature at levels 200 and 300 mm rises rapidly in the shroud and stabilises at a much higher level than calculated by the code (see Fig. 10).

A much better agreement can be obtained with calculations, assuming a gradual relocation of the equivalent of the 8 inner rods in between both spacer grids onto the lower grid. The inferred temperature level at which relocation took place is of the order of 2400-2500K.

To explain such a rather low fuel relocation temperature in a steam-rich environment, three main assumptions are being investigated :

- loss of geometry of the bundle as a result of the rather strong cladding oxidation and subsequent degradation of the radiative heat transfer, resulting in central temperatures being hotter than calculated ; fuel melting upon reaching UO_2-ZrO_2 liquidus ;

- relocation of some Zircaloy-rich mixtures during the oxidation period below the upper grid ; it then froze and melted again as the power rose again ;

- the failure of the control rod may have resulted in Zr/Ag/Fe drops being projected against the inner rods. Such mixtures are known to interact with Zirconia and Urania and to lower their dissolution temperature as observed in some CORA experiments [10].

It is difficult to determine from the measurements which is the actual process. Post-irradiation examination of the melt may help to resolve this issue. From the first results, it seems that iron and other metal oxides may have played an important role in the precocity of the FPT-0 bundle degradation.

The mass of liquid fuel in the resulting pool of liquefied material is estimated to be around 2 to 3 kg, according to last ICARE2 calculations, in good agreement with the results of the radio-tomogram analysis. The final movement of the pool at the end of the test has not yet been analysed.

B. Fission product behaviour in circuit

The release of the fission products and of the structural materials has not yet been compared to code calculations. It is however already clear that these codes will have to take into account the evolution of the material surface to volume ratio during the degradation of the bundle.

From the analysis of the samplings taken along the circuit and, in particular, from the gamma scan of the thermal gradient tube, it appears that all fission products but iodine were in a condensed form at 970K. This means that cesium was not transported as CsOH, contrary to what was expected. Iodine may have been transported as CsI, RbI or AgI, since these species have about the same vapour pressure. However, AgI is not predicted by thermochemistry codes under the conditions prevailing in the circuit.

In addition, it is uncertain whether all the iodine was condensed at the outlet of the steam generator (420K). Indeed, the analysis of one gas capsule mounted after an impactor tends to indicate the presence of 2% of volatile iodine. But mainly because of uncertainty in filter efficiency, this information has to be taken with care (i.e. iodine could also have been transported as a sub-micron aerosol). Gas sampling techniques was subsequently corrected in FPT-1 using high efficiency filters and capsules filled with zeolite.

In view of the rapid decay of the iodine present in FPT-0 and more generally due to the rather low fission product to structural aerosol mass ratio, very little information was obtained from the post test analysis on the chemical forms of the fission products transported in the circuit. The situation should be considerably improved in FPT-1 due to the use of pre-irradiated fuel.

In the steam generator tube, the flow is accelerated at the same time as it is rapidly cooled to the pipe wall temperature of 420K. Thermophoretic and turbulent deposition of fission product was expected to be high but the measured values were about 2 to 3 times lower. Studies with transport codes such as VICTORIA and SOPHAEROS are in progress to find an explanation for this behaviour. One possibility being explored is the validity of the thermophoretic formulations for metallic particles, since the aerosols observed in FPT-0 are mostly composed of silver and rhenium.

C. Fission product behaviour in containment

As explained before, a low humidity ratio was achieved in the vessel during the aerosol injection phase. Aerosol deposition as measured by gamma signals and samples can be rather well reproduced with reasonable assumptions on the particle size, although the partial retention (5 to 10%) on the outer containment surface is difficult to explain.

These aerosols were essentially composed of a mixture of structural materials transporting a quite homogeneous mixture of fission products. Most of iodine thus settled to the bottom of the vessel during this phase of the test.

However, a significant fraction of iodine (significant as compared to calculations, see Figure 11, but no more than a few percent) behaved as volatile species during this phase.

The sump chemistry was affected by the partial dissolution of the aerosols (mainly Re and Ag) settled at the bottom of the vessel and entrained during the washing phase at the end of the aerosol injection phase. This phase resulted in a strong decrease of the sump pH.

According to the gamma measurements, the entrained iodine after washing rapidly settled and/or deposited on the walls of the sump and of the recirculating loops. An explanation for this phenomena could be the rapid reaction of iodine in the aqueous phase with silver deposited on walls.

As a result of this reaction, the I2 production rate by radiolysis as calculated by the IODE code is quite low and cannot account for the iodine concentration observed in the vessel atmosphere (see Fig. 11). It can only be explained by the presence of very fine iodine-rich aerosol or gaseous iodine probably formed in the containment during the aerosol injection phase. The phenomena controlling the subsequent evolution of the airborne concentration are then dominantly surface depositions and desorptions.

As a lesson learnt from FPT-0, the iodine instrumentation was considerably reinforced in the FPT-1 vessel : gas capsules filled with zeolite after high efficiency filters, on-line gas analyser, more Maypacks ... Simultaneously, a review of the models used in the iodine codes has been initiated and analytical tests, investigating in particular the kinetics of reaction between silver and iodine, have been specified.

4. FUTURE TESTS

4.1. Overall test programme

The test matrix (table 1) is reviewed in regular intervals, as results from previous experiments and new requirements become available. In its present form it implies the sequence

FPT-0 -1 -4 -2 -5 -3

4.2. The second test, FPT-1

From the beginning of the Program, FPT-1 had been conceived as a repetition of FPT-0, but using high burn-up fuel. Several other parameters were also to be changed in circuit and containment. Considering the unexpected results of the first experiment (see paragraph 3 above) it was decided to limit the parameter variations between the two experiments.

At the time of the 23rd Water Reactor Safety Information Meeting (WRSM) the FPT-1 facility was ready and undergoing final testing & commissioning. Test termination criteria are being developed on the basis of the analysis of FPT-0 in order to limit the amount of liquefied fuel to about 2 kg. New phenomena linked to fuel burn-up, such as fuel foaming, are also being investigated.

4.3. Experiments nr. 3 and 4

At the time of the 23rd WRSM the option FPT-4 before FPT-2 was under discussion.

FPT-2, on the other hand, could be operated in two different modes without significant changes to the facility hardware, viz.

a. reproducing FPT-1, but under reducing conditions obtained with much lower steam flow rate, as to achieve steam starvation during the Zircaloy-water reaction phase in the upper test fuel bundle section, or with hydrogen injection at the inlet of the bundle;

b. reproducing FPT-1, still under oxidising conditions but with a lower steam flow rate plus a possible injection of boric acid.

FPT-4 has been conceived as an entirely different experiment investigating the release, transport, and settling of low-volatility fission products, uranium and transuranium elements. Referring to a late phase severe accident situation the test, scheduled for the fall of 1997, features a debris bed of high burn-up fuel inside a thoria crucible. The fuel is fission-heated up to partial melting through a series of steady states. Fission products and other elements are swept out by hot steam under different H_2/H_20 ratios and measured in the circuit and in the containment vessel.

Detailed objectives of the test, such as the need to avoid crust formation above the pool, are being discussed. In parallel, R&D work is underway to cope with rubbelized fuel handling, fabricate high temperature instrumentation to be installed in hot cell conditions and to develop sequential coupons operating at high temperatures. Circuit instrumentation and sampling as well as post-test operations are similar to those used for the earlier tests (see paragraph 2.3.), with special emphasis on elements like Ba, Eu, La, Ru, Sr, U, Np, Pu, Am.

4.4. The last two tests

FPT-5 uses a « normal » test fuel bundle, without the central control rod, with a 9 days' in-situ re-irradiation. During the high temperature transient air is injected rather than steam, in reference to air ingress reactor accidents (e.g. after lower bulkhead failure). Release, transport and deposition of fission and activation products are expected to differ from the FPT-0/FPT-1 scenarios, and are measured with the standard set of instruments and samplers.

The last experiment of the present test matrix is likely to be carried out in the years 2001/2002. FPT-3 has been maintained as a « spare » test with the idea of either repeating one of the earlier experiments(as a consequence of facility failure or poorly understood phenomena), or introducing new parameters like boiling water reactor conditions, higher circuit pressure, advanced fuel.

Secondary experiments could be carried out in the containment vessel during any of the tests mentioned above. They could involve spray systems, hydrogen recombiners, specific sump pH management etc. The impact on the main experimental program of the test concerned needs to be analysed in each case.

5. CONCLUSIONS

Carried out two years ago the first PHEBUS FP experiment has proven the feasibility of the envisaged test programme in the new installation, together with the right choice of post-test operations. The results, on the other hand, point to a number of unexpected phenomena, as much earlier and stronger fuel degradation than expected or the presence in the containment of larger volatile iodine concentration than predicted. However, prior to drawing any firm conclusion, in particular regarding iodine behaviour, it is necessary to wait for the results of the second experiment, FPT-1, which will involve more typical (higher) fission product concentrations thanks to the use of pre-irradiated fuel.

A large number of technical improvements and model / code adaptations could be accommodated between the tests. The major challenge presently consists in reducing the intervals between tests to about 18 months.

Future tests are expected to be yet more interesting and challenging from both technological and analytical points of view. Investigating the behaviour of non-volatile fission products as well as the transuranium elements in core meltdown situations will produce a quite unique experimental database.

A complete understanding of the PHEBUS experiments and the transposition of this understanding to the reactor case will require quite intensive efforts in the international community for the years to come.

6. REFERENCES

[1] P. von der HARDT, A.V. JONES; C. LECOMTE, A. TATTEGRAIN - Nuclear Safety Research. The Phebus FP Severe Accident Experimental Programme, *Nuclear Safety* 35(2), July-December; 1994, invited.

[2] P. von der HARDT and A. TATTEGRAIN - Phebus probes core melt-down behaviour : first results, NUCLEAR EUROPE WORLDSCAN (ENS) 9-10/95 (Sept.-Oct. 1995), invited.

[3] J.Y. BLANC, B. CLEMENT, and P. von der HARDT - Fuel bundle examination techniques for the Phebus Fission Product test, IAEA Techn. Committee Meeting on Behaviour of LWR Core Materials under Accident Conditions, Dimitrovgrad, Russia, October 9-13, 1995.

[4] A. MAILLIAT, F. SERRE, A.V. JONES, I. SHEPHERD - The calculational Programme to Prepare the First PHEBUS - FP Tests - USNRC 20th Water Reactor Safety Meeting, 21-23rd October, 1992

[5] G. REPETTO, P. von der HARDT, Ch. GONNIER, B. BERTHET; and B. CORNU - Experimental results of the PHEBUS FPT-0 test, ibid.

[6] G. REPETTO, P. von der HARDT, Ch. Gonnier, M. HAESSLER - The First PHEBUS Fission Product experiment FPT-0. General aspects of the experimental sequence concerning the fuel bundle degradation and FP release, ANS International Topical Meeting "Safety of Operating Reactors", Seattle (USA), September 17-20, 1995

[7] B. ADROGUER, I. SHEPHERD; C. JAMOND, S. BOURDON, and S. EDERLI - Analysis of the PHEBUS FPT-0 bundle behaviour with ICARE 2, CSARP Meeting, Bethesda, MD, 1-5 May 1995.

[8] C. JAMOND et al. - Status of the interpretation of the PHEBUS FPT-0 test with the ICARE 2 V2 mod 1 code, International Seminar on Heat and Mass Transfer in Severe Reactor Accidents, Cesme, Turkey, 21-26 May 1995.

[9] M. LIVOLANT et al., First results from the PHEBUS FP severe fuel damage test FPT 0 : Bundle aspect. 13th Int. Conf. on Structural Mechanics in Reactor Technology (SMIRT), Porto Allegre, Brazil, 13-18 August, 1995.

[10] P. HOFMANN, S. HAGEN, G. SCHANZ, and A. SKOKAN - Chemical interactions of reactor core materials up to very high temperatures, KfK 4485, January 1989.

PHEBUS FP TEST MATRIX
OBJECTIVES AND OVERALL PROGRAMME PLANNING

Table 1

N°	Main objective	Fuel bundle	Primary circuit	Containm. Vessel	Projected Test Date	Status, remarks
FPT 0	Core degradation and FP release from fresh fuel Oxidizing environment	Maximum volatile FP/aerosol release 20 % fuel melting	FP retention in the primary circuit of steam generator secondary side hot. Analysis of deposits for granulometry, composition and chemical species	Aerosol behaviour Iodine chemistry Sump pH = 5, buffered.	Dec. 1993	Post-test analyses and interpretation ongoing interpretation started. Final report : middle of 1996
FPT 1	As FPT-0, but with preirradiated fuel	As FPT-0	As FPT-0	As FPT-0, but with higher humidity	Early 1996	Under testing and commissioning
FPT 2	As FPT-1 but with boric acid injection in oxidizing environment. Alternative steam-poor conditions	Maximum volatile FP/aerosol release, in presence of boric acid aerosols	As FPT-0, with boric acid aerosols	As FPT-1 Recirculation spray with sump water	1997 or 1999	Basic parameters have been defined. Precalculations are ongoing
FPT 4	Debris bed to molten pool test. Low volatility FP release	Fuel degradation from debris bed to molten pool Release and speciation of low volatility FPs and transuranian elements	Deposition and retention of less volatile FPs and of transuranics	Deposition and retention of less volatile FPs and of other aerosols	1997 or 1999	Calculations and techn. preparations ongoing. Design study report : November 1994
FPT 3	Open test with options like : - repetition of an earlier test, - BWR conditions, - high pressure				2002	
FPT 5	Air ingress test	Fuel degradation under highly oxidizing conditions FP release and speciation No control rod	As FPT 0	As FPT 2	2000	Basic options defined

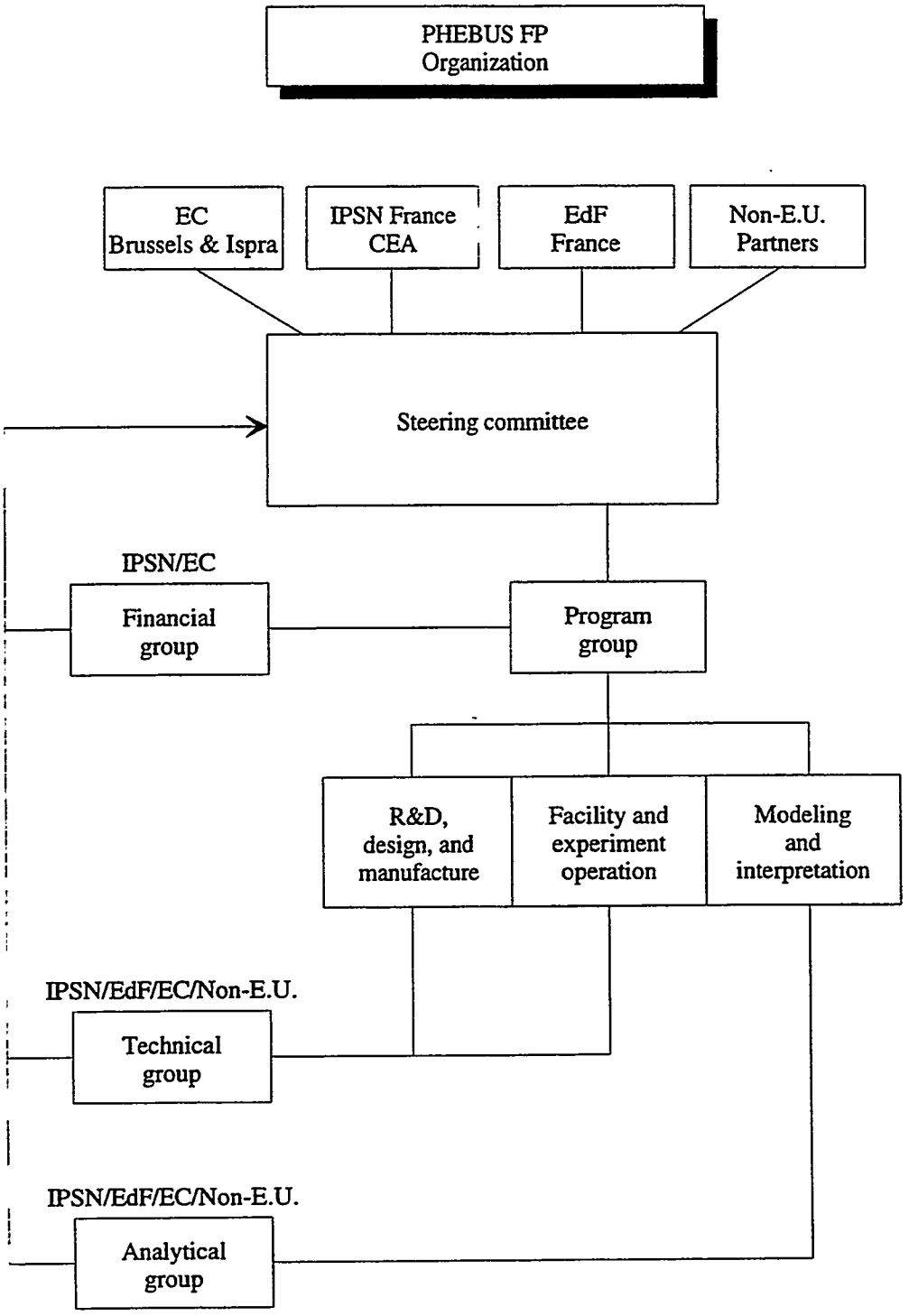

Figure 1 - Phebus FP organization chart.

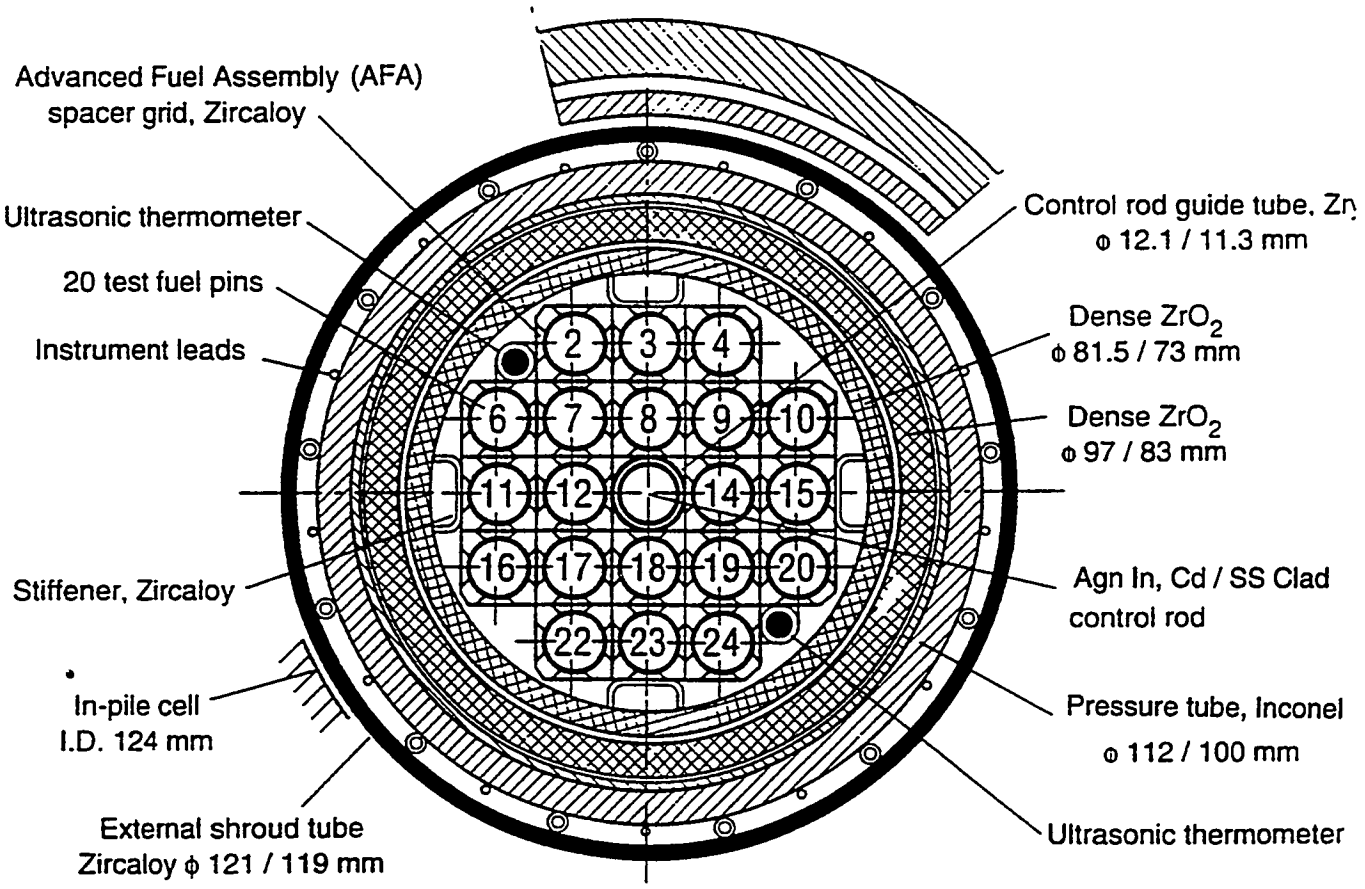

Figure 2 - FPT0 in-pile test section, horizontal section

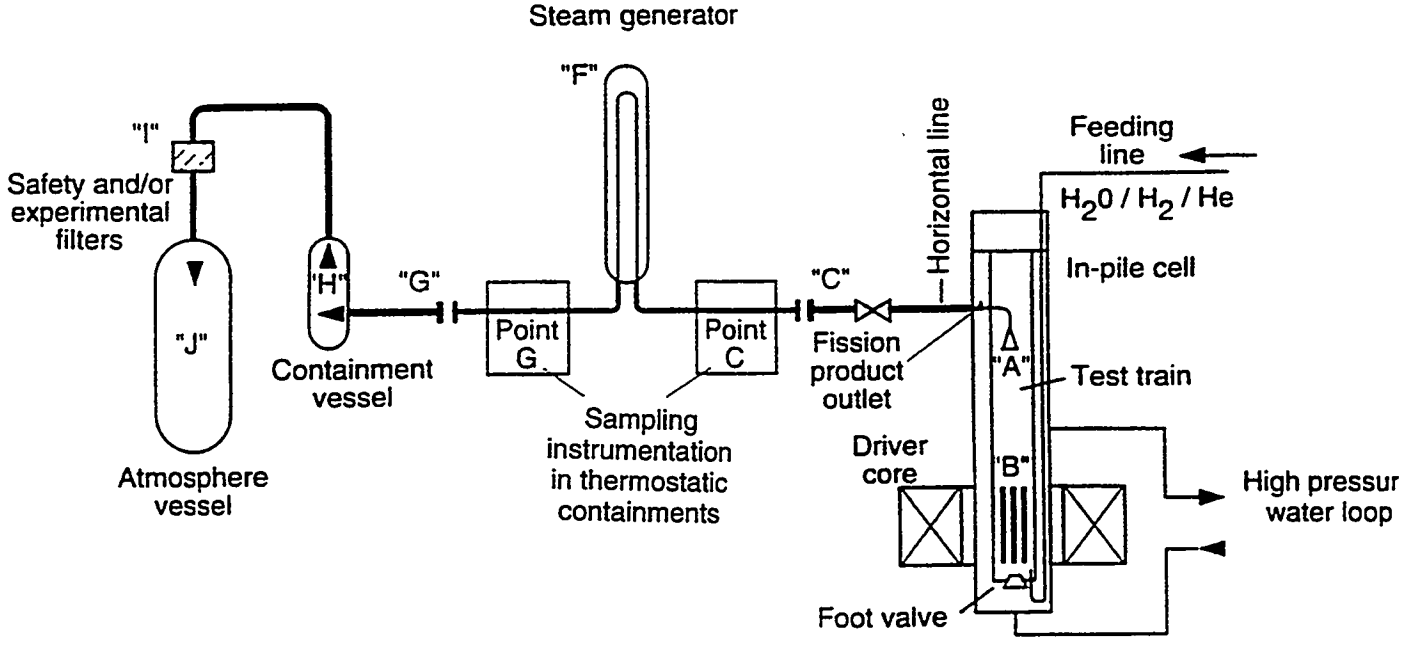

Figure 3 - FPT0 experimental circuit

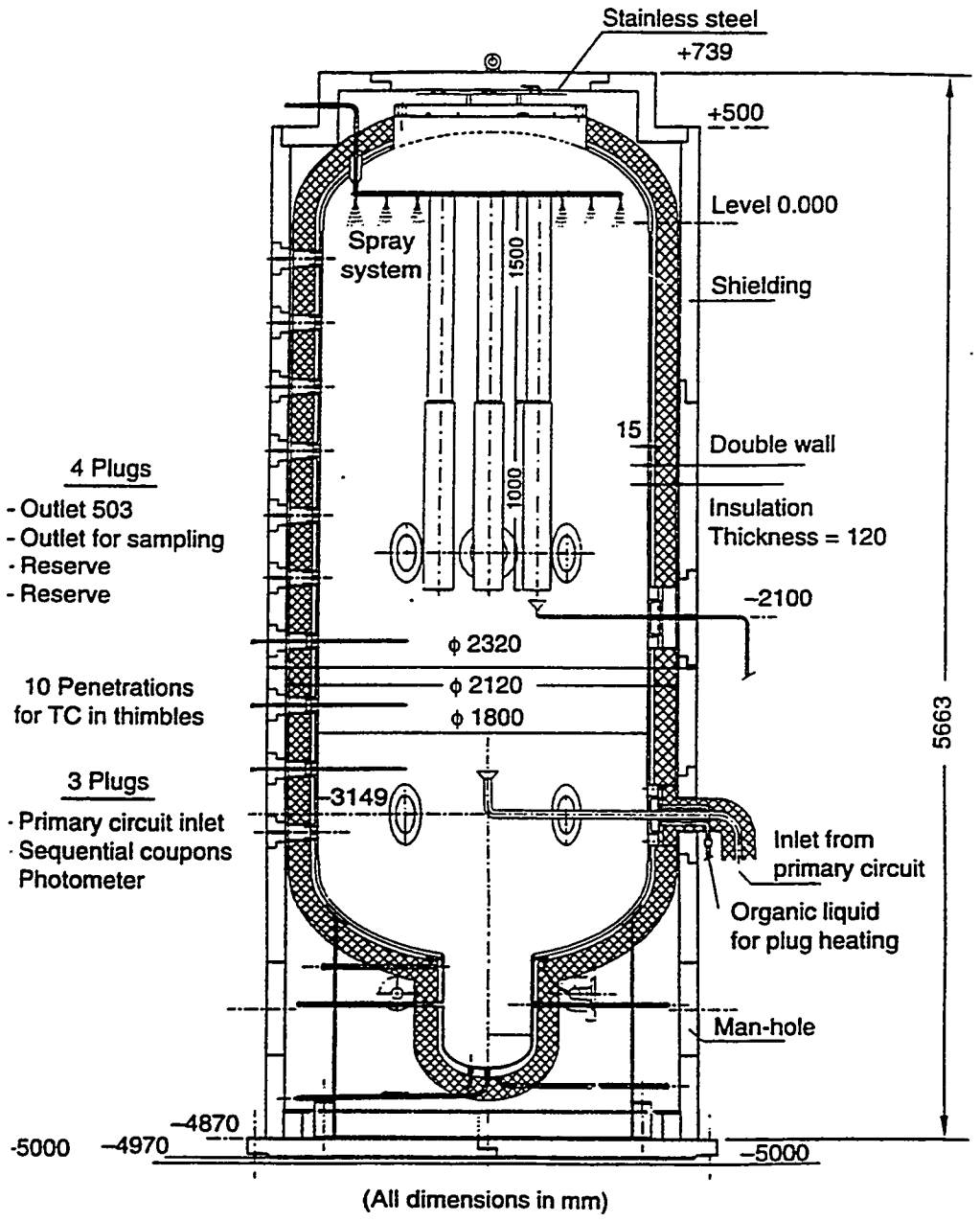

Figure 4 - Phebus FP REPF 502 containment vessel

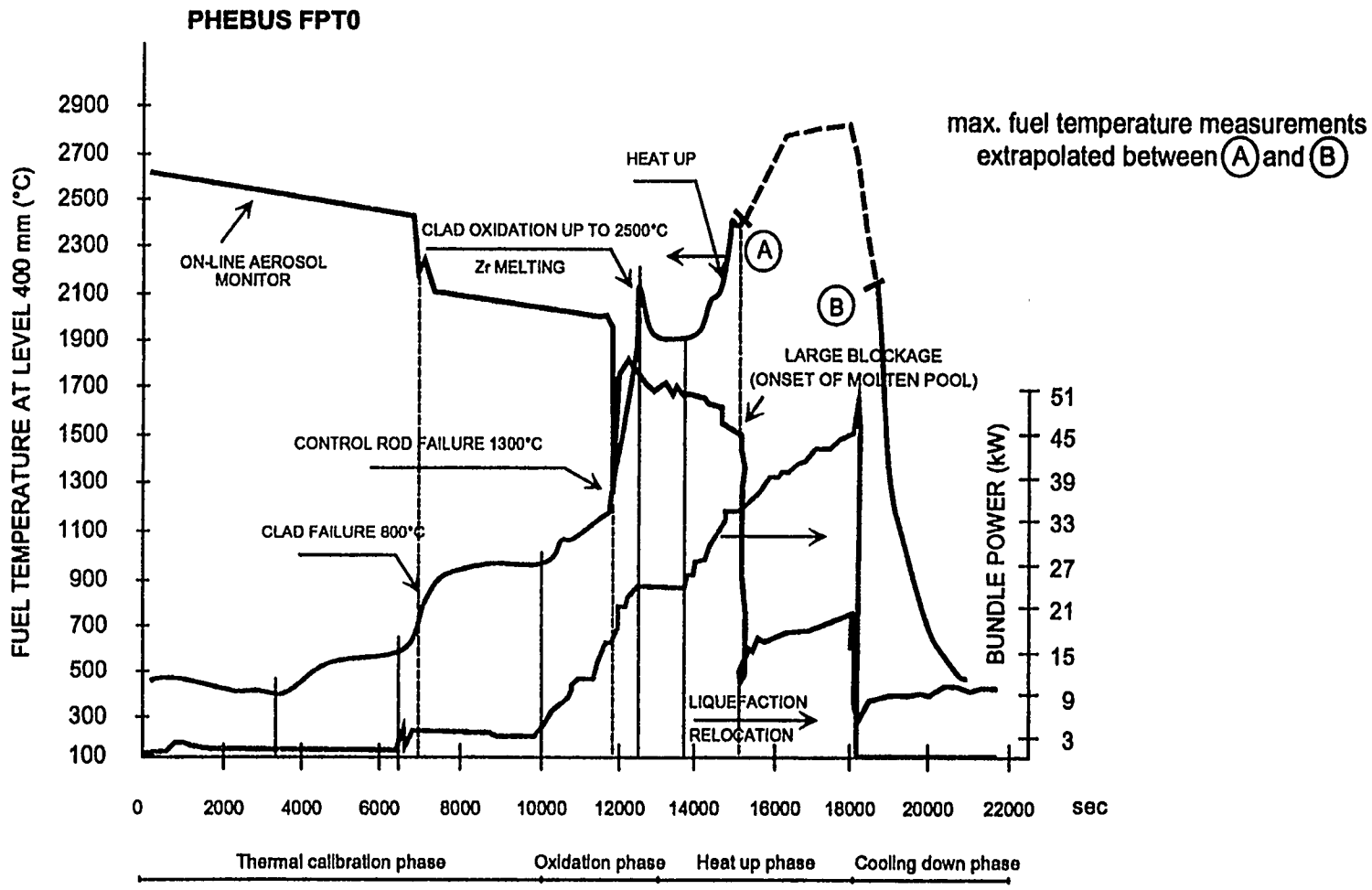

Figure 5 - FPTO Bundle Behaviour Main Results

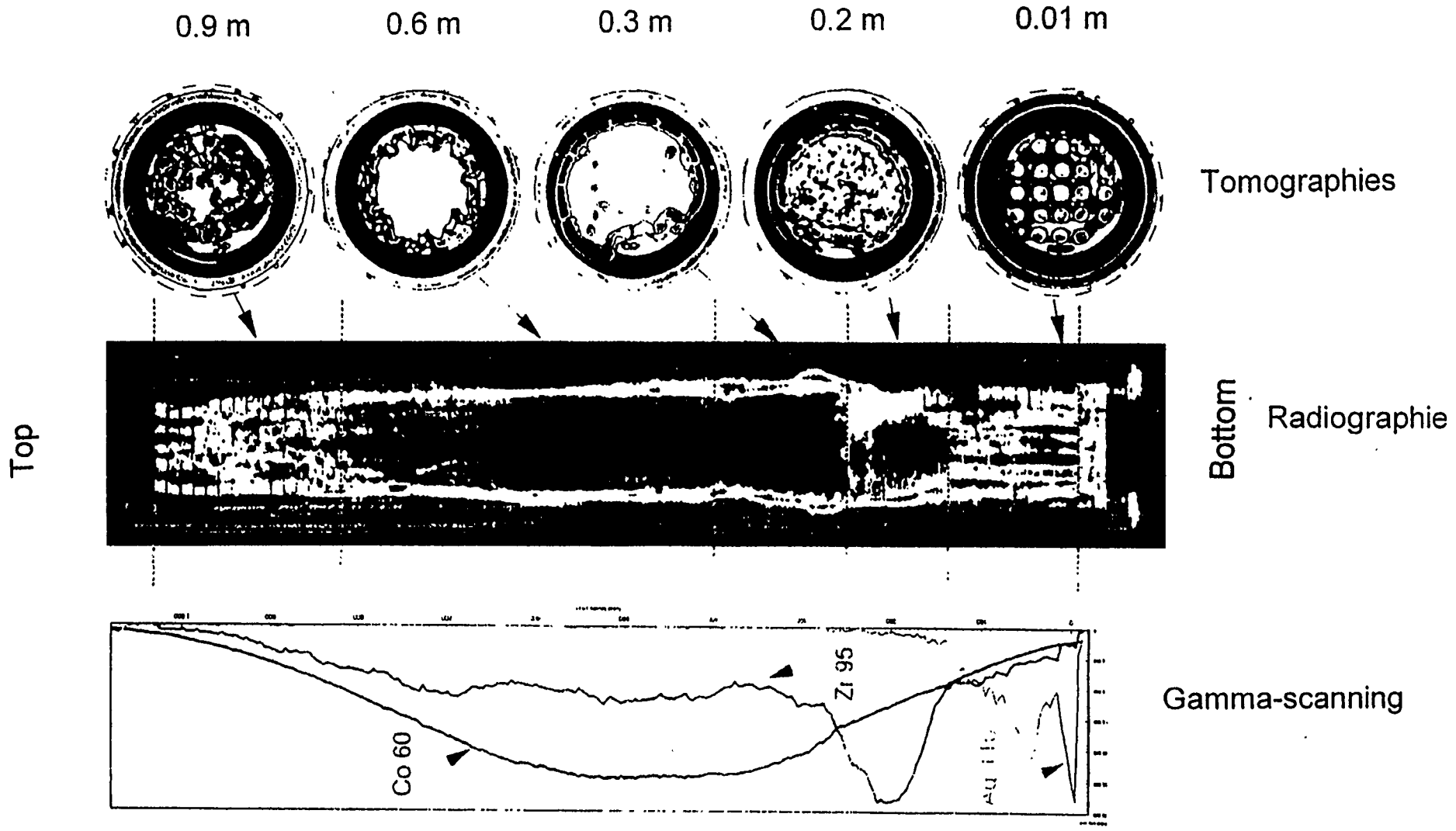

Figure 6 - FPTO Non-destructive Post-test examinations

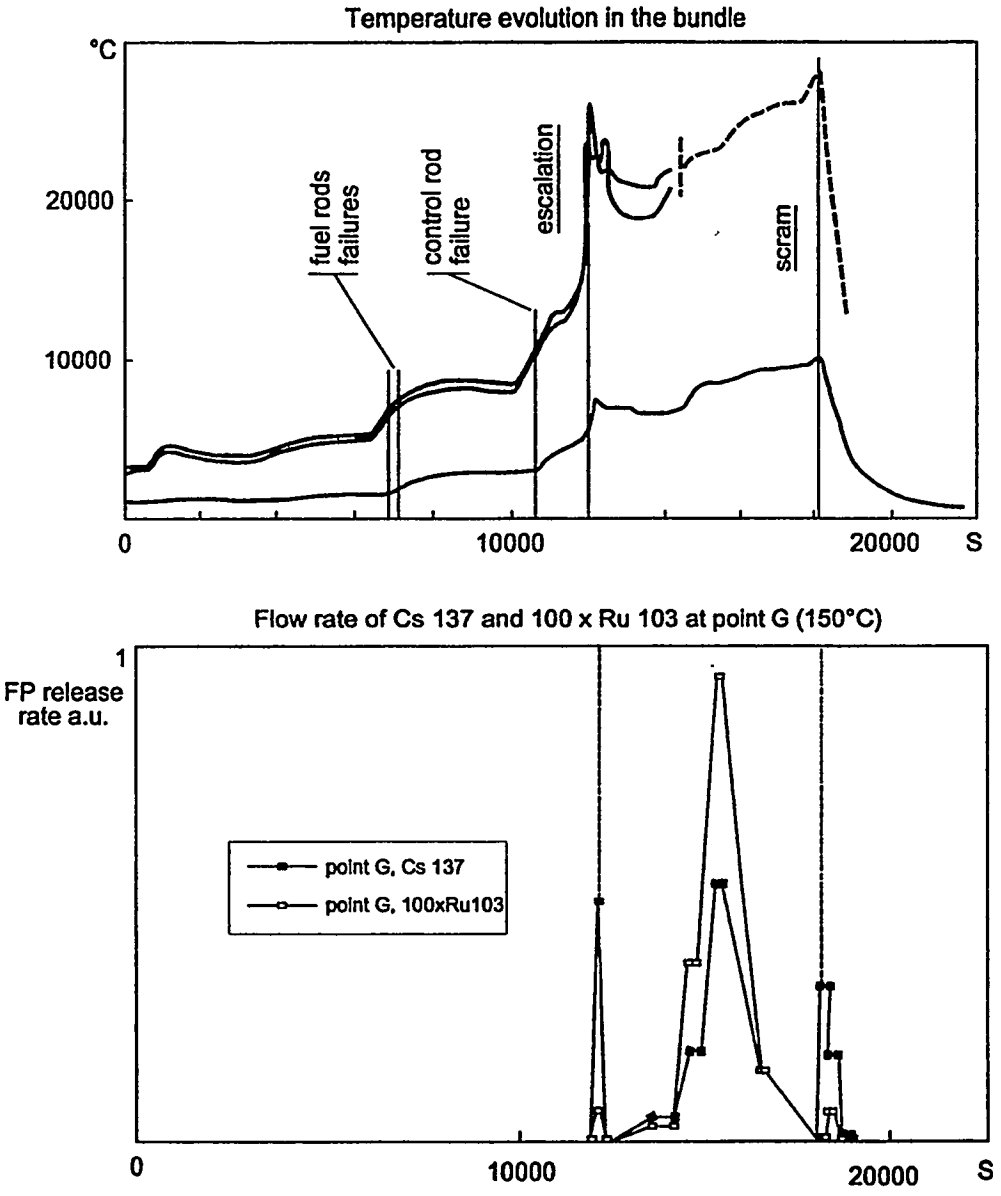

Figure 7 - FPTO FP release correlated to bundle degradation events.

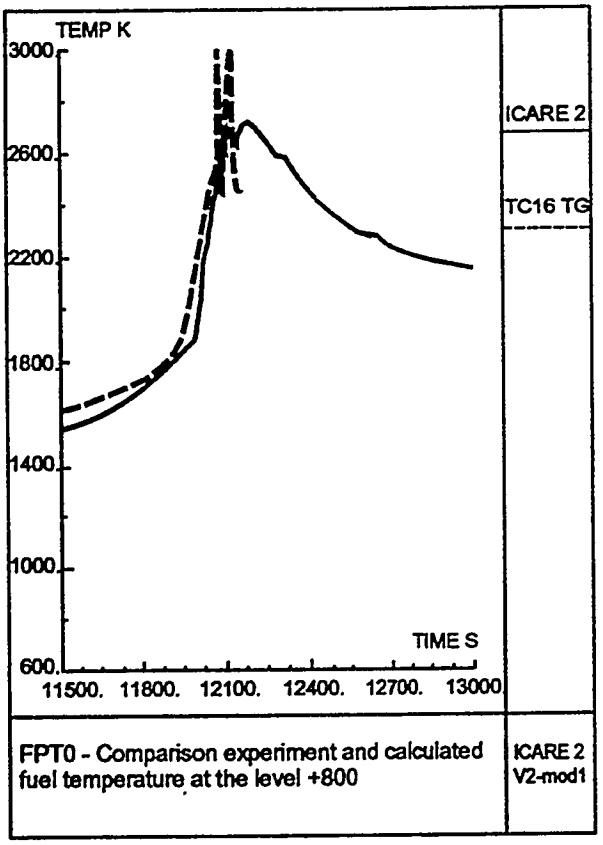

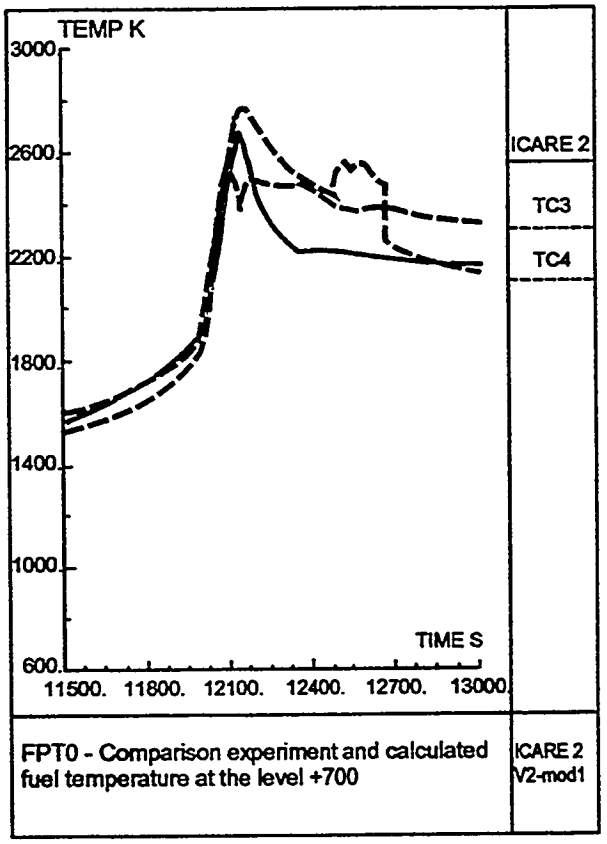

Figure 8

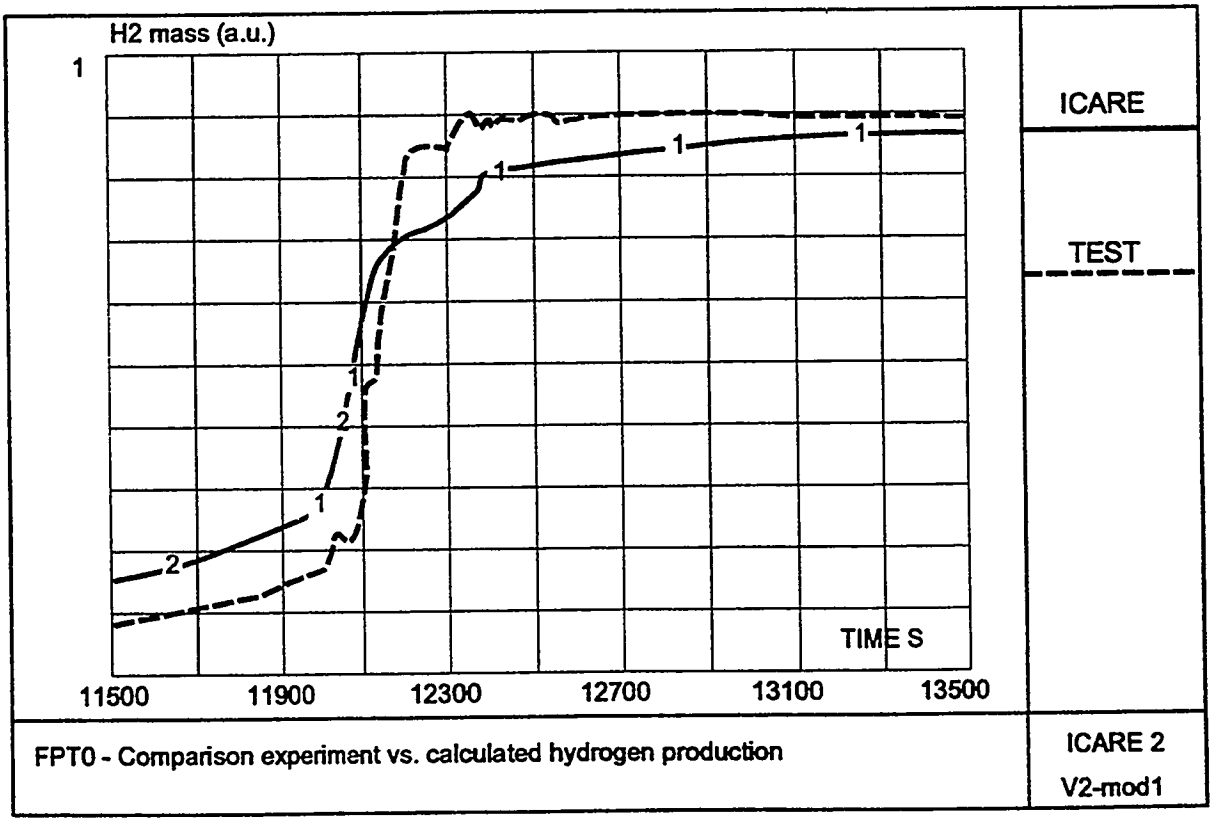

Figure 9

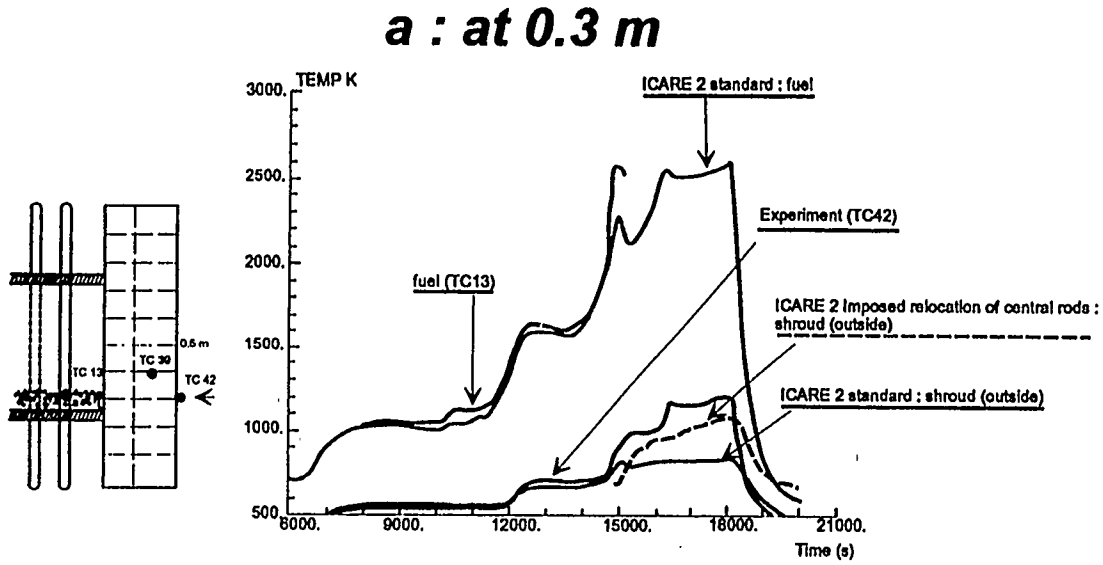

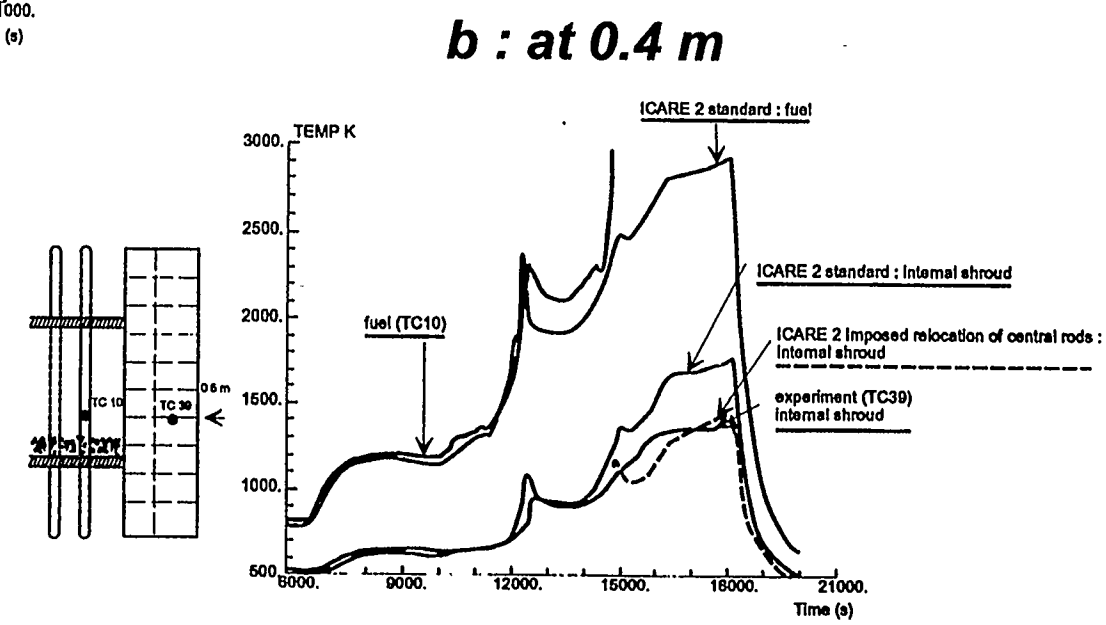

Figure 10 - Fuel and Shroud Temperatures
Experiment - Calculation Comparisons

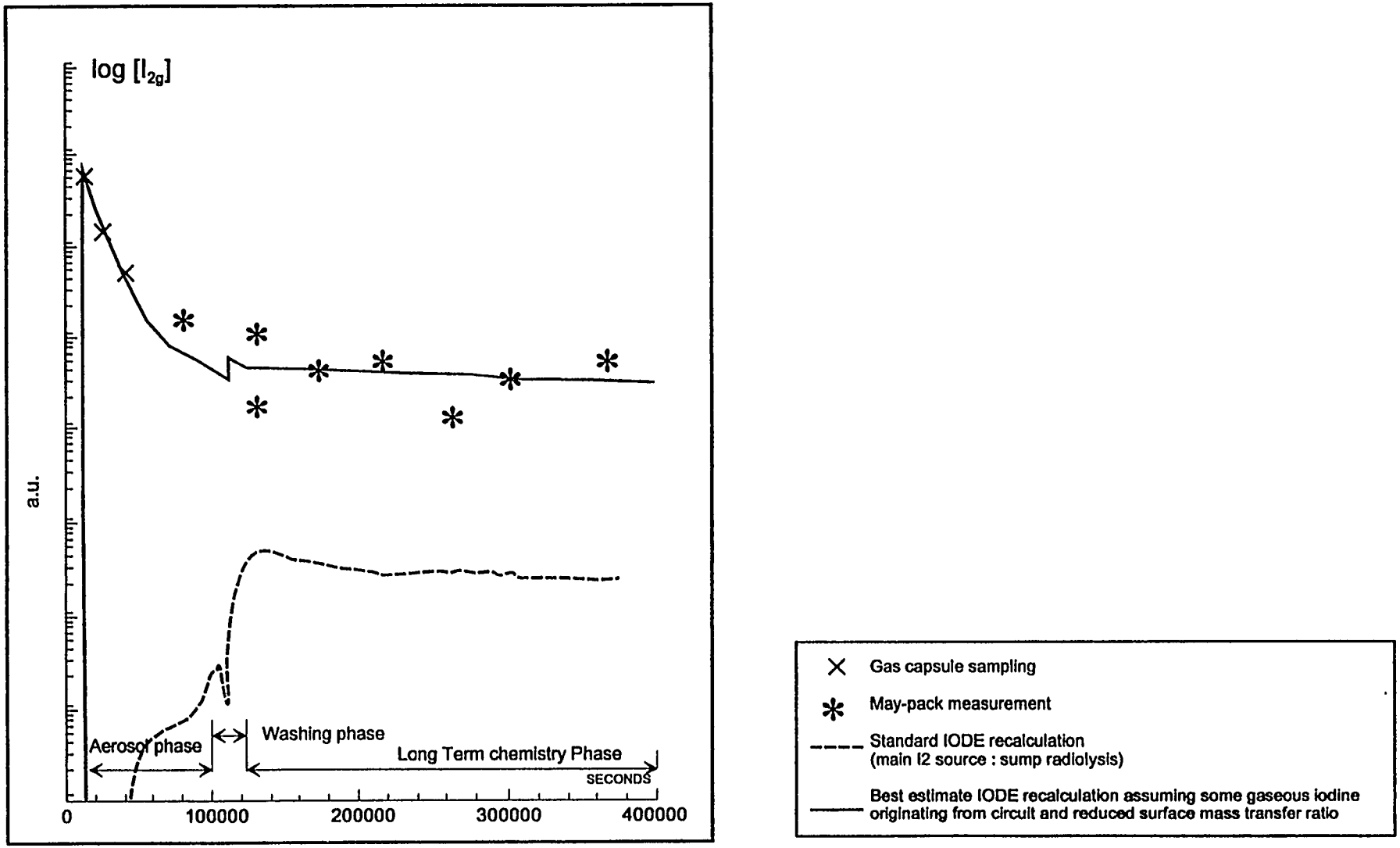

Figure 11 - Iodine Volatility in FPTO Containment

PRELIMINARY RESULTS OF THE XR2-1 EXPERIMENT

Randall 0. Gauntt and Paul H. Helmick,
Sandia National Laboratories, Albuquerque, NM
Larry Humphries
SAIC, Albuquerque, NM

ABSTRACT

The XR2-1 (Ex-Reactor) experiment, investigating metallic core-melt relocation in boiling water reactor (BWR) geometry, was performed on October 12, 1995, following two previous simpler XR1-series tests in August and November of 1993. The XR2-1 test made use of a highly detailed replication of the lower region of the BWR core, including the control blade and channel box structures, fuel rods, fuel canister nosepieces, control blade velocity limiter, and fuel support pieces, in order to investigate a key core melt progression uncertainty for BWR Station Blackout type accidents. The purpose of this experiment program is to examine the behavior of downward-draining molten metallic core materials in a severe reactor accident in a dry BWR core, and to determine conditions under which the molten materials drain out of the core region, or freeze to form blockages in the lower portion of the core. In the event that the draining metallic materials do not form stable blockages in the lower core region, and instead erode the lower core structures such as the lower core plate, then the subsequent core melt progression processes may proceed quite differently than was observed in the TMI-2 accident, with correspondingly different impact on vessel loading and vessel release behavior.

The results of the Ex-Reactor tests are preliminary. All of the tests conducted have shown a significant degree of channel box destruction induced by the draining control blade materials. The XR2-1 test further showed that the draining zircaloy melt causes significant disruption of the fuel rod geometry. All of the tests have shown tendencies to form interim blockages as the melts temporarily freeze, but that these blockages re-melt, assisted by eutectic interactions, resulting in the sudden draining of accumulated metallic melt pools. The sudden drainage of such pools can result in fast draining from the core region of a fraction of the metallic materials through flow pathways to the lower plenum that bypass the core plate.

1. Introduction and Background

The Ex-Reactor (XR) experiments are being conducted at Sandia National Laboratories to aid in the resolution of a major uncertainty in the core melt progression process associated with a severe accident in a boiling water reactor (BWR) where loss of reactor core coolant inventory has occurred. Specifically, the class of accidents of concern are those that involve core melting under dry core conditions, such as an unrecovered Station Blackout accident with manual vessel depressurization.[1] In these accidents, a manual vessel depressurization is expected to be carried out by the plant operators when the core water level drops to ~35% below the top of the core. This procedure is intended to cool down the reactor core before the onset of severe fuel damage from oxidation and over-temperature conditions by making use of the steam blowdown and cooling effect, and to permit the activation of any potentially available low pressure coolant injection systems. After vessel depressurization, the water level in the vessel is expected to be below the lower core plate, but above the jet pump intake nozzles. The procedure also delays severe

damage to the core by about a half an hour, assuming that reintroduction of water into the core does not subsequently occur. (Note, many variations to this accident can be imagined with varying degrees of operability of the control rod drive hydraulic system.) In the event that core cooling is not regained, the severe core damage processes resulting from the continued core heatup takes place under comparatively "dry core" conditions because of the low water level in the reactor vessel, with very low steam flow through the core.

Without vessel depressurization, "wet core" conditions would exist, with the lower core generating comparatively large amounts of steam from the boiling coolant present there. Wet core conditions were present in the TMI-2 accident, which, as a result of subsequent core melt progression processes, are believed, in general, to lead to a blocked core configuration with the formation of a growing molten ceramic fuel pool. The water in the lower core causes relocating molten core materials to freeze, forming a dense crust. Subsequent melt collects upon the crust blockage until a molten pool forms. Later, as the pool growth reaches a boundary of the core, the contents of the molten pool (principally molten ceramic fuel) will be released and relocation to the lower vessel head follows, as occurred in the TMI-2 accident. The blocked core "TMI-like" melt progression scenario is illustrated in Figure 1.

In the case of the BWR "dry core" melt progression scenario, it is not clear that the blocked core, molten pool configuration, discussed in the previous paragraph will result since the heat sink associated with water in the lower core is not present. An alternative "continuous drainage" melt progression pathway has been proposed for these dry-core conditions, which does not lead to the formation of a large in-core molten ceramic pool, but instead, follows a continuous drainage behavior, where molten material drains from the core region without the formation of any stable crusts or blockages. This alternative melt progression pathway is also illustrated in Figure 1, and can be seen to lead to very different melt relocation behavior and different vessel head loading conditions. The TMI-like blocked core pathway results in a sudden relocation of ~3000K molten ceramic fuel material, which subsequently comes into contact with the lower vessel head. The alternative continuous drainage pathway results in the gradual and continuous drainage of materials from the core region, first the lower melting point metallic core materials (control blades and zircaloy materials), and later solid or molten ceramic fuel materials. In this case, the metallic materials will collect on the lower head, followed later by overlying ceramic fuel materials. Because these two melt progression pathways lead to important differences in the timing and mode of vessel failure, in addition to differences in the rate, temperature and composition of those materials that are ultimately released into the containment environment, it is important to understand under what conditions which melt progression scenario will result, so that the consequences of these two different pathways can be assessed. Complicating the analytical assessment of these pathways is the complexity of the BWR lower core geometry, which is comprised of fuel canisters with rods, control blades, and inter-canister gaps, as well as lower canister nosepieces, control rod drive tubes, the lower core plate structure, and numerous flow pathways. These geometrical complexities are illustrated in Figure 2. These complexities, together with uncertainties concerning material eutectic interactions (Zr-Fe for example), stability of core structures during melt relocation,

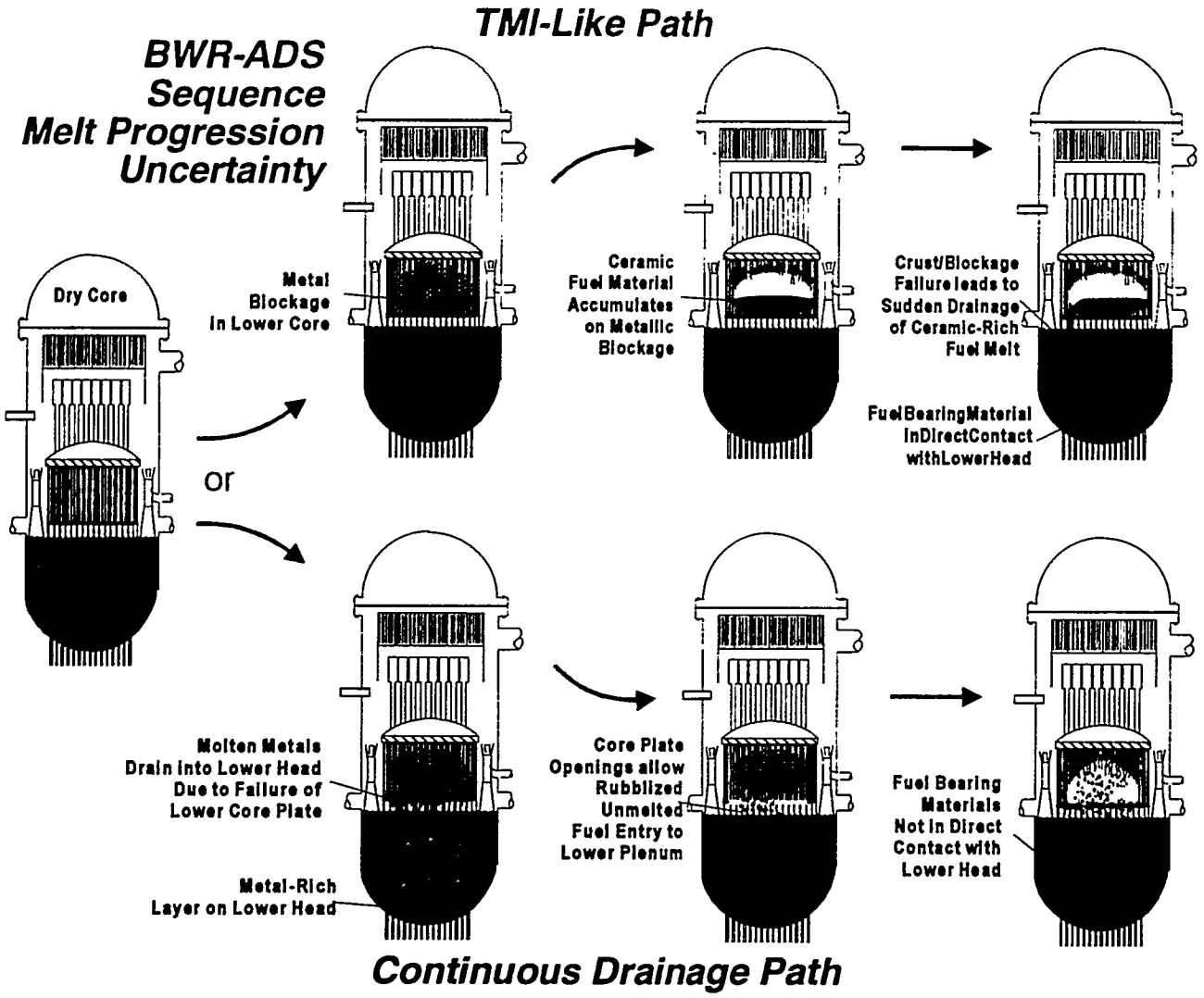

Figure 1. Illustration of the melt progression branchpoint uncertainty for "dry core" and "wet core" scenarios.

and the freezing and blockage behavior of relocating metallic melts has prompted an experimental, and companion analytical, program to address this melt progression issue. The Ex-reactor experiments are intended to provide the experimental evidence necessary to develop and assess predictive models of this phase of the melt progression process, which are required to resolve the uncertainty in this crucial melt progression pathway branchpoint.

2. Experimental Program

In order to determine the conditions under which BWR dry core melt progression will follow either the "blocked core, TMI-like" path, or alternatively, the continuous drainage pathway, a series of experiments is currently underway to characterize the behavior of the draining metallic core materials in the geometry of the BWR lower core region. If the molten metallic core materials form stable blockage configurations in the lower BWR core region under dry core conditions, then it is considered likely that the TMI-like melt progression pathway, involving the formation

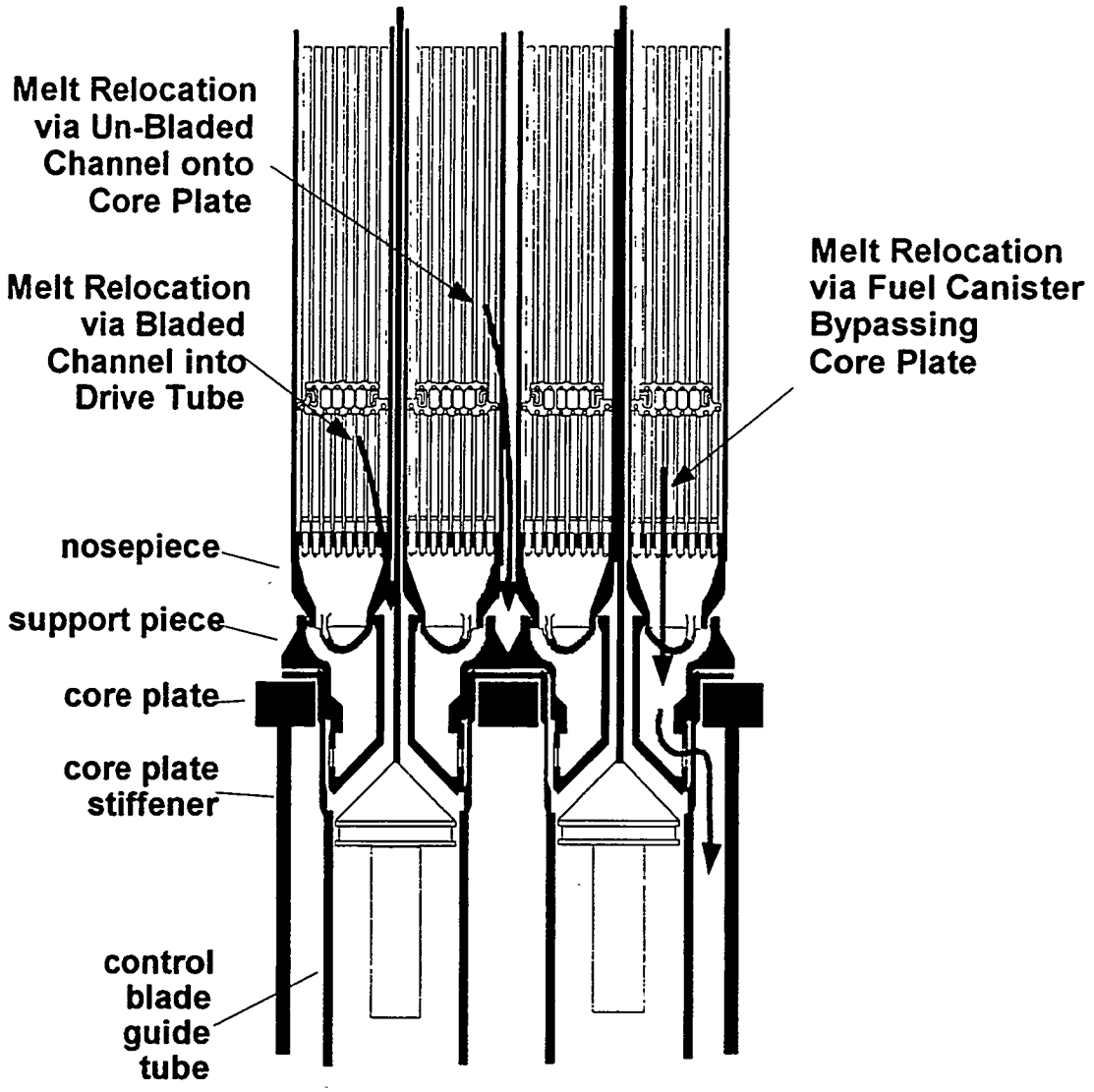

Figure 2: Diagram of the complex lower core structure in the BWR.

of a ceramic fuel melt pool, will also apply to BWRs. It should be realized, however, that under typical dry-core conditions, there is only marginally sufficient thermal heat sink available to freeze the relocating stainless steel control blade melt and the subsequently relocating zircaloy channel box and cladding materials. This together with the complex BWR lower core geometry, with many possible melt drainage pathways (Figure 2) and many potential material interaction effects, would suggest that stable blockages might not form, and that the continuous drainage melt progression pathway might be favored.

The general approach taken in the Ex-Reactor experiments is to simulate the lower 1/2 to 1 meter of the BWR core geometry in full scale at the time that the molten metallic core materials are beginning to drain from the upper regions of the core into the lowermost regions. A test section is constructed, including important geometrical features such as zircaloy fuel canister walls, B_4C-filled stainless steel

Lateral Geometry Considered in XR Series 1 and Series 2 Tests

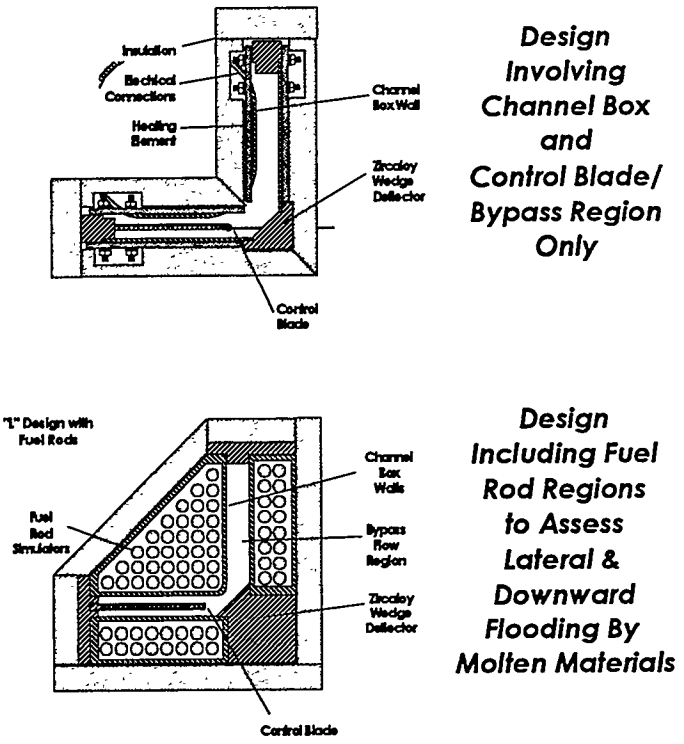

Design Involving Channel Box and Control Blade/ Bypass Region Only

Design Including Fuel Rod Regions to Assess Lateral & Downward Flooding By Molten Materials

Figure 3: Cross sectional views of test bundles for the XR1 (top view) and XR2 (bottom view) tests.

control blade structure, fuel canister nosepieces, lower core plate, bladed and unbladed inter-canister gaps, and so on. Prototypic materials are used in the conduct of these experiments. Figure 3 shows a cross sectional view of two test section designs used in these experiments. In the upper view, a simple channel design used in the XR1 tests is shown where only the fuel canister walls (channel box) and the control blade features are included. The lower view shows the cross section for the more prototypic geometry XR2 tests which include arrays of zircaloy-clad fuel rods in addition to the channel box and control blade structures. The lateral scale of the XR2 test section is designed to represent all of the lateral degrees of freedom with respect to the draining of molten materials, and was selected based on symmetry principles (the XR2 test section is approximately a 1/8 symmetric section extracted from the 4-canister repeating array of the BWR core).

The tests are conducted by pouring molten metallic materials (molten control blade steel and molten zircaloy components - fuel rod cladding and channel boxes) into the upper, open end of the heated test section, thereby simulating the melting and draining of the upper core metallic materials in the overheating reactor. The test sections are heated using electrical heating on the periphery so that a prototypic axial thermal gradient is imposed over the length of the test section. The object is to characterize the nature of any blockages that are formed as the melt enters the test geometry, and to provide information on melt drainage pathways through the lower core region.

Figure 4 shows the test facility used to conduct the XR experiments. The test section is placed within the argon-inerted test chamber to prevent air oxidation of the test section components and the draining metallic melts (control blade and zircaloy). The test section is instrumented with thermocouples to measure the thermal gradient prior to introducing the molten metals, and to characterize the melt flow and blockage behavior of the melt flowing into the test section. In addition to thermocouples, a real-time x-ray imaging system provides a video image of the melt flow as it enters the test section, showing flow behavior and blockage formation.

The melt flow in the package is provided by an inductively powered melter system, situated above the test section (Figure 4). The total amount of metallic melt delivered to the test section is representative of that available from the entire axial extent of the core above the lower 1/2 to 1 meter region, and so, the tests include the full amount of incoming melt mass and enthalpy that would be typical of actual accident conditions. The melt delivery system provides for molten control blade material to be delivered to the bladed section of the test bundle, and for molten zircaloy to be directed over both the fuel rods and the channel box walls. The timing and rate of melt flow into the test section is also controlled to correctly represent the accident conditions. The melt is prepared continuously by feeding wires of either control blade composition or zircaloy into the radiant cavity melter illustrated in Figure 4. The radiant cavity is held at ~2700K by inductive coupling with a 225 kW high frequency power supply. The melter system also provides a downward radiant heat flow of ~20 kW to the top of the test section which is situated below the melter, as shown in Figure 4. This downward-directed heat source is used to establish the desired axial thermal gradient in the test section prior to introducing the molten materials.

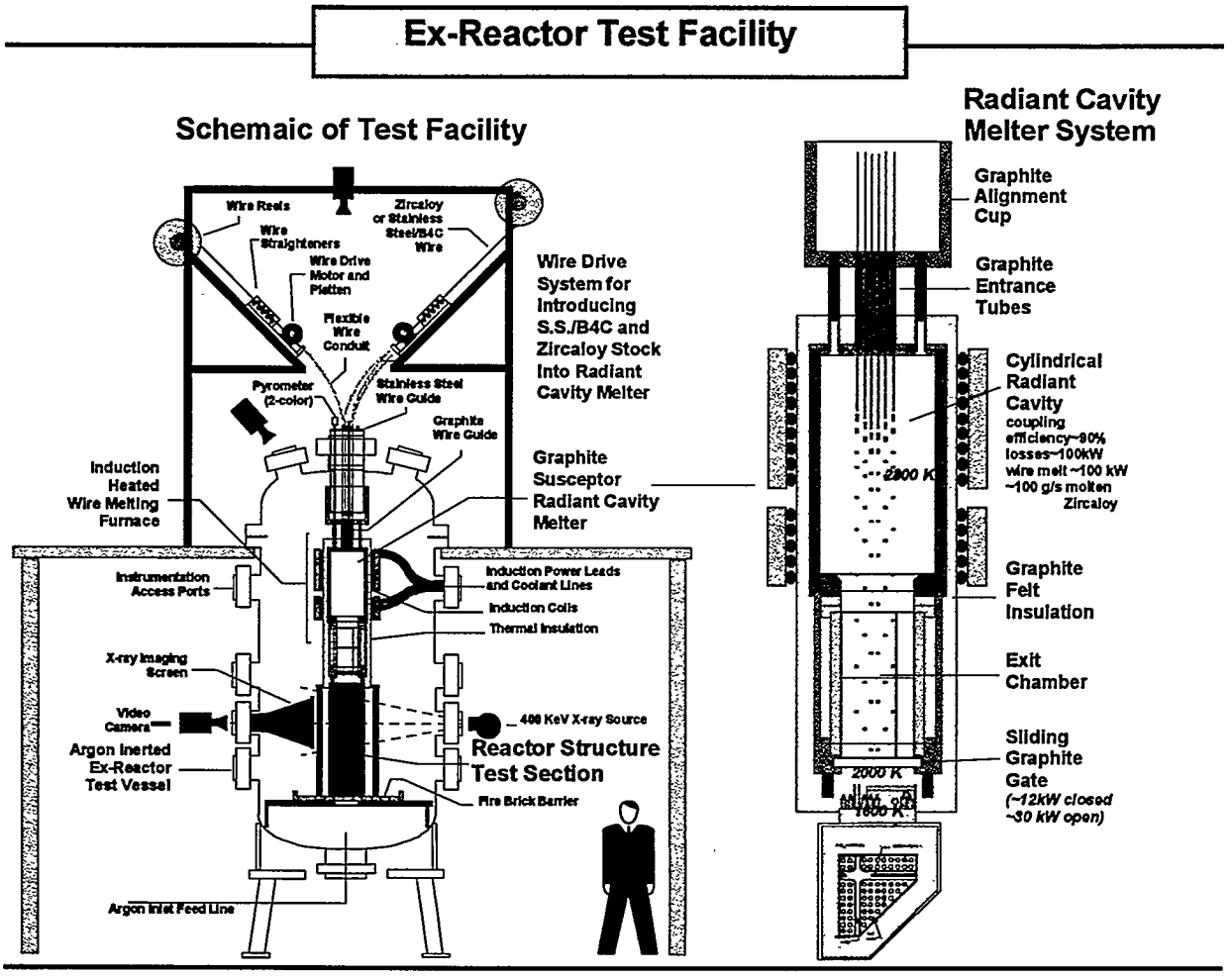

Figure 4: Facility for conducting the Ex-Reactor experiments.

3. Description of the XR2-1 Experiment

Two "Simple Channel" tests (XR1-1 and XR1-2) and one highly detailed test, XR2-1, have been performed in this program. A description of the more detailed XR2-1 test follows. The results of the XR1-series tests are described elsewhere.[2]

3.1 XR2-1 Test Section Geometry

The XR2-1 test section included a high degree of geometric realism and detail in its design. In addition to including the B_4C-filled stainless steel control blade structure that was investigated in the simple channel XR1 tests, the XR2-1 test section also included 62 UO_2-filled fuel rods with one simulated water rod. The rods were arranged into fuel canister structures as shown in the cross section view in Figure 3. Actual BWR zircaloy grid spacers were included in the rod bundles. The lower test section included highly detailed replication of the lower BWR core region, including the control blade velocity limiter, control blade guide tubes, core plate, fuel support pieces, and fuel canister nosepieces. Actual BWR structures were used in the fabrication of these test section components also. Finally, the zircaloy fuel rod cladding and fuel canister walls were oxidized in steam prior to assembly to form a ~40μm oxide layer in order to simulate the oxide layers normally present on components that have been in an operating reactor environment. Shown in Figure 5 are the BWR core components that were used in the fabrication of the XR2-1 test section, and Figure 6 shows the XR2-1 test section partially assembled.

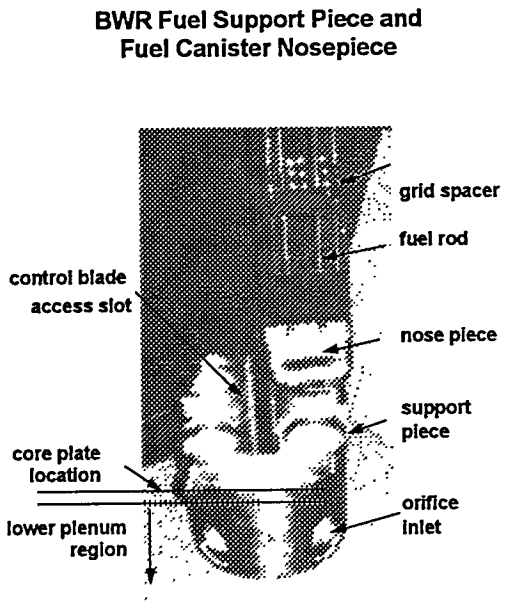

Figure 5: Photograph of BWR structural components that were used in the fabrication of the XR2-1 test section.

Figure 6. Photograph of the partially assembled XR2-1 test section showing fuel rods, nosepiece, and control blade structures.

3.2 Test Conditions

The test conditions used in the XR1 series and the XR2-1 test are summarized in **Table 1.** Note that the XR1 simple channel tests involved only a single pour of molten control blade alloy, whereas the XR2-1 test included a pour of molten zircaloy in addition to the initial pour of control blade melt. Note also that the melt masses correspond to the entire height of the reactor core above the lower .5m test section, resulting in full scaling with respect to lateral dimension (within the unit cell) and total melt mass.

Table 1 Nominal Target Conditions Used in the XR1-1, XR1-2, and XR2-1 Experiments

Test Condition	XR1-1	XR1-2	XR2-1
Fuel/Channel Length	1 m	.5 m	.5m
Axial Thermal Gradient	1000 K/m	2000 K/m	2000 K/m
Fuel Channel Surface Oxide Layer	2 μm	2 μm	40 μm
Melt Pour Duration	10 min	15 min	30 min
Control Blade Melt	12 kg	12 kg	12 kg
Zircaloy Melt	—	—	60 kg
Melt % B_4C	4.4w%	4.4w%	4.4w%

The thermal conditions applied to the XR2-1 test section and the melting/draining rate of control blade alloy and zircaloy materials for the test was determined by best estimate calculations performed using the SCDAP/RELAP5 code with enhanced BWR structure models, as described in reference 1. The results of those calculations are shown below in Figure 7 and Figure 8.

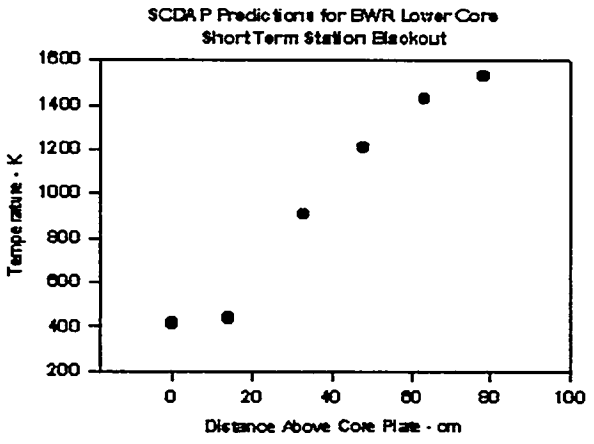

Figure 7: Target conditions for axial thermal gradient in the lower BWR core for Dry-Core (Station Blackout with depressurization).

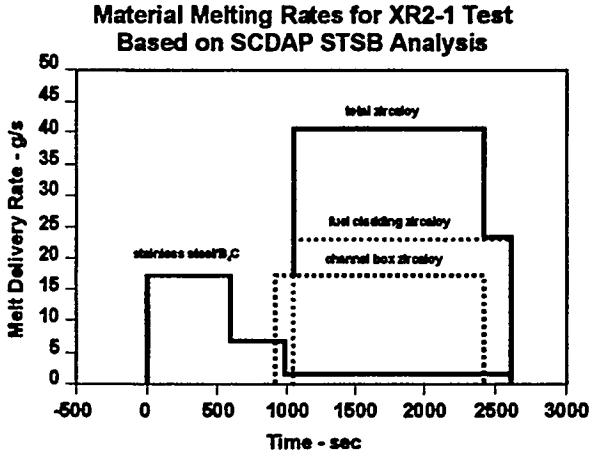

Figure 8: Target conditions for flow rate of molten metallic materials from upper core into lower core.

3.3 Preliminary Results of the XR2-1 Test

Following the preheating of the XR2-1 test section to obtain the desired initial thermal conditions, melt flow into the test section was initiated by feeding the bank of 10 stainless steel/B_4C alloy wires into the radiant cavity melt delivery system. The steel alloy wires were fed into the test section over a period of about 1000 seconds as shown in Figure 9. At the end of the steel melting period, 30 zircaloy wires were fed simultaneously into the radiant cavity melt delivery system, providing zircaloy melt delivery to the XR2-1 test section over the subsequent ~1000 seconds. Altogether, more than 3500 meters, or ~72 kg of steel alloy and zircaloy wire were fed into the radiant cavity melter and provided as melt to the test section, simulating the draining of molten core materials into the lower BWR core region.

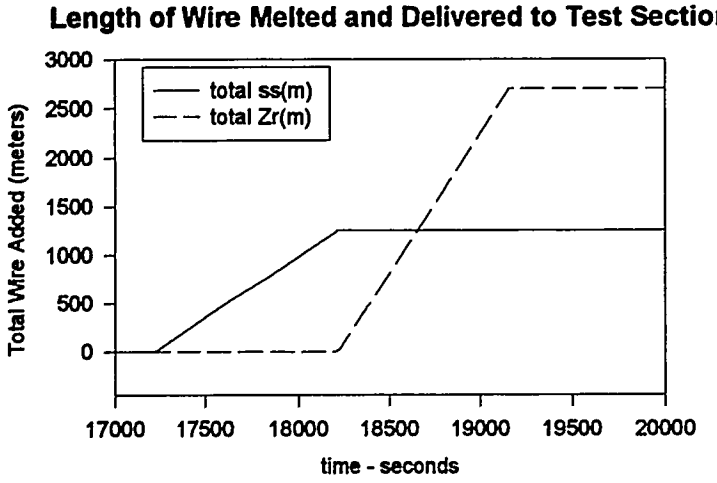

Figure 9. Wire feed history for the XR2-1 test.

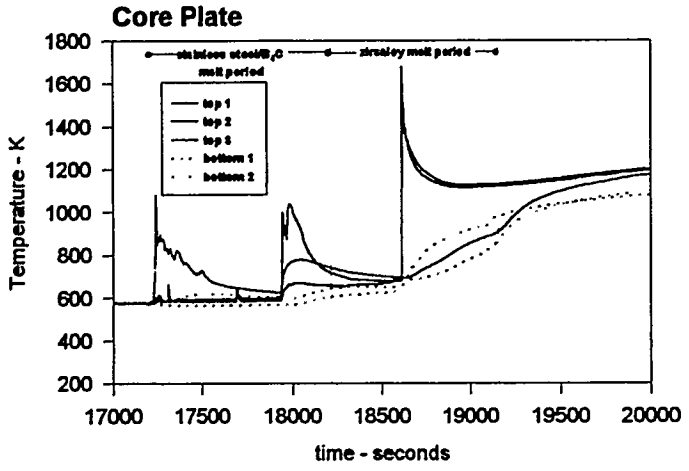

Figure 10. Thermal response of the XR2-1 core plate structure.

As the control blade melt was initiated into the XR2-1 test section, melt was initially observed to arrive at the lower core plate region, as indicated by the thermal response measured there (Figure 10). Note that although the control blade melt is delivered only over the control blade region, the draining materials quickly diverted laterally into the open channel region (unbladed bypass region) due to freezing and blocking of the bladed region, and drained to the core plate, which lies at the bottom of the unbladed intercanister gap. As can be seen from Figure 10, the initial thermal response observed at the core plate region subsides, indicating that no additional material reached the core plate after the initial arrival of melt there. This is believed due to the formation of blockages within both the bladed and unbladed channel gaps which retained the draining melt within the test section.

In time however, the blockage remelted, probably assisted by eutectic interactions between the molten steel and the zircaloy channel walls, allowing the retained accumulating melt to suddenly release, as evidenced by

the second transient response on the lower core plate toward the end of the steel melt pouring period at ~18,000 seconds. Similar behavior was observed for the draining control blade melts in the XR1-1 and XR1-2 simple channel tests. The formation of the blockage, the accumulation of melt over the blockage, and the draining of the accumulated melt following failure of the blockages were observed through the real-time X-ray imaging system developed for these experiments.

When the zircaloy melt pour phase was initiated, it is apparent that this melt initially did not drain to the bottom of the test section, and instead formed a blockage region higher in the test bundle. The blockage formation and melt accumulation were observed using the real-time x-ray imaging system. The zircaloy melt continued to accumulate until shortly after 18,500 seconds, when a large and sudden melt release event was observed at many locations in the lower test bundle, including the lower core plate and regions below the core plate. This relocation event resulted in significant heating of the core plate and lower test section, as seen from the thermal response in Figure 10. Some of the zircaloy melt released in this event drained to the bottom of the test section below the core plate, finding pathways through the fuel nosepiece and the lower support piece. A pool of molten zircaloy also appears to have formed on the core plate. The real-time x-ray images indicate that the upper pool level may have extended above the tops of the lower nosepieces. This would mean that the pool level was above the top of the support piece making it possible for melt to drain through the control blade access slots. In fact, there are some indications early on of molten material draining through the short control blade slot, but there are no immediate temperature signatures at locations on the long control blade slot or the velocity limiter indicating that this channel was probably blocked by control blade material.

The pool above the core plate continued to grow, and lower structures, including the lower control blade and guide slots, showed a gradual yet very significant increase in temperature. The molten zircaloy pool gradually reheated and remelted the control blade material that was blocking the core plate penetration until at 19,100 seconds when there was a rapid drainage of material through this channel onto the velocity limiter and into the lower catch basin. Real-time x-ray images showed material draining from both the control blade channel and the molten zircaloy pool in the unbladed bypass channel above the core plate.

The post-test condition of the XR2-1 test section reveals a large degree of disruption of the upper bundle features, as seen from Figures 11 and 12. The orderly rod array channel walls and control blade have been significantly disturbed with virtually no recognizable features remaining. In addition, some vertical compaction of the bundle occurred. The fuel rods in the top of the test section were denuded of cladding by the draining molten zircaloy and the radiant heat load to the top of the bundle, allowing the eroded UO_2 pellets to collapse to a rubble geometry.

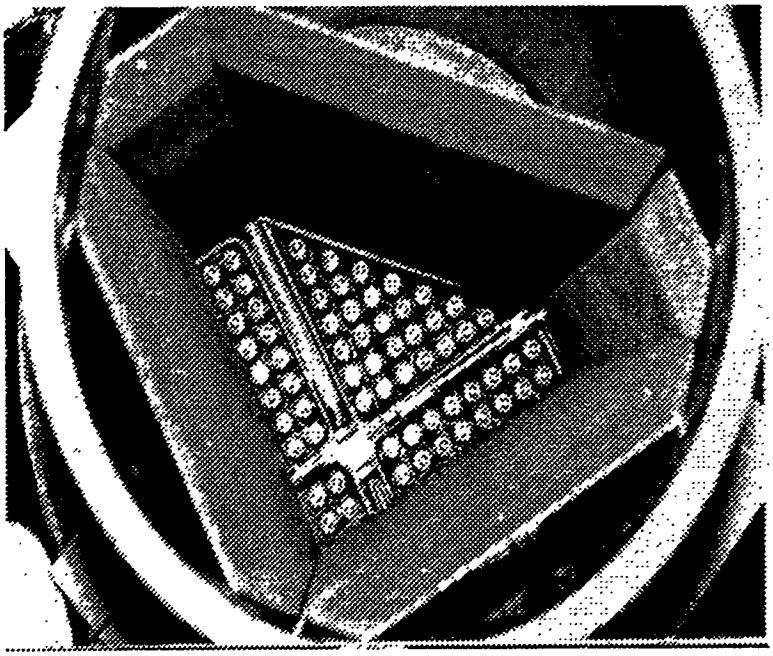

Figure 11. Pre-test top view of the XR2-1 test section showing fuel rods, channel walls and control blade.

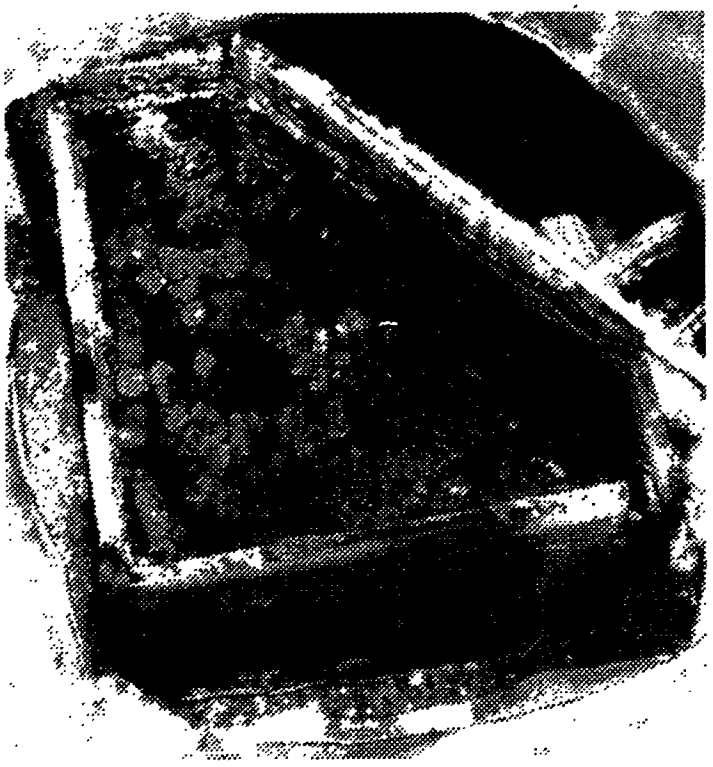

Figure 12. Post-test top view of the XR2-1 test section showing substantial disruption of ordered geometry.

Figure 13, showing two x-ray projection views of the XR2-1 post-test condition, reveals that some fuel rod features remain in the lower regions of the test section, although the rods are highly distorted. Blockages of refrozen melt are seen across the test bundle above the core plate, as well as on and below the core plate. Refrozen melt is visible within the fuel canister nosepieces and in the nozzle inlet region below the core plate. (The nozzle inlet region is the main coolant flow path by which water flows from the lower plenum below the core plate, up through the fuel support pieces, into the fuel canister nosepieces and up through the fuel channels in the normally operating BWR - see Figure 2 for clarification.) The nozzle inlet region is largely filled with refrozen melt, as is the control blade access slot in the drive tube region. Finally, a large accumulation of melt is seen to have solidified at the lower-most catch basin of the test section, apparently arriving there by way of the control blade access slot and the fuel canister nozzle inlet pathways. The top surface of the refrozen material in the lower catch basin is flat, indicating that this material arrived at a high enough transfer rate and with sufficient superheat to attain a flat upper surface, as

opposed to a "stalagmite" geometry typical of dribbling melts with little superheat. Eutectic behavior may play a role in the effective amount of superheat contained within the draining melts.

4. Conclusions

In the Ex-Reactor testing program, three melt progression tests have been performed, two simple channel tests (XR1-1 and XR1-2), and one full geometry test (XR2-1) which included highly realistic and full scale representation of the lower BWR reactor core region. The Ex-Reactor tests are nearly full-scale, both with respect to the geometry and the melt mass involved, and make use of prototypic materials to simulate as faithfully as possible the accident conditions expected for a Short Term Station Blackout accident in a US BWR. Evaluation of the most recent XR2-1 test results is preliminary. Similar general behavior was observed in all of the tests, the most significant being the initial formation of blockages by the draining metallic melts, and the subsequent catastrophic failure of those blockages, resulting in the sudden drainage of melt to lower regions. The drainage can result in metallic materials bypassing the core plate region by several different natural flow paths in the BWR lower core region (see Figure 2).

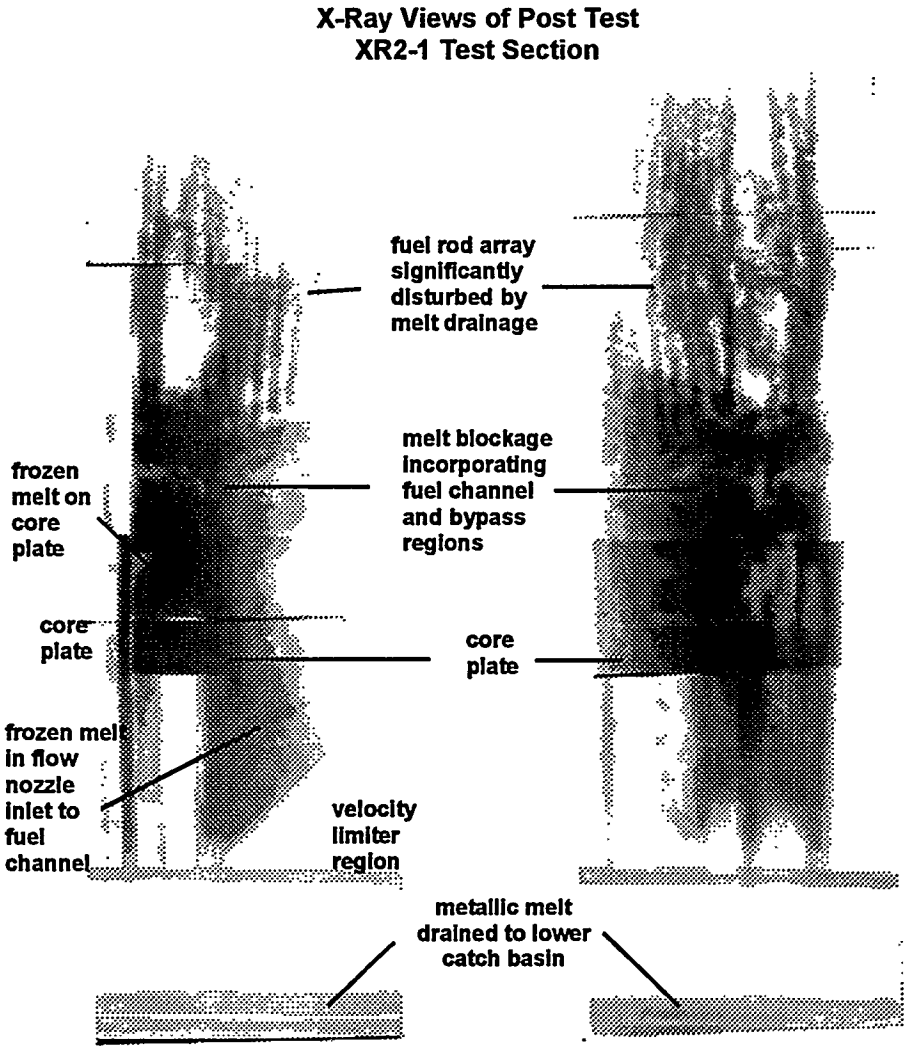

Figure 13. X-ray projection views of the XR2-1 test section.

It is also apparent from these tests that the BWR fuel canister/bypass geometry is degraded early in the core melt progression when the channel walls are destroyed by the highly aggressive eutectic action of the molten

control blade alloy. The subsequently draining zircaloy melt was observed in the XR2-1 test to cause significant disruption of the fuel rod configuration, and may be an early initiator for the transition from a rodded to a rubblized core geometry. Transfer of molten metallic materials to the lower plenum region under reactor accident conditions may be significantly enhanced by the aggressive material interactions, especially the Fe-Zr eutectic behavior observed in the Ex-Reactor experiments. Characterization of these tests is ongoing. Additional physical analyses will be performed to determine more precisely the end-state of the XR2-1 test section and the nature of key structural degradation mechanisms, and numerical analyses will be performed to infer the full impact of the phenomena observed in the Ex-Reactor tests on full BWR system behavior. While further analyses are required to resolve completely the "drainage versus blockage" issues at the focus of these experiments, it is apparent from direct observation that the failure of the BWR core plate is not a prerequisite for the transfer of important quantities of molten metallic materials into the lower water-filled plenum region.

REFERENCES

1 F.P. Griffin and L.J. Ott, "Development of the BWR Dry Core Initial and Boundary Conditions for the SNL XR2 Experiments," ORNL/NRC/LTR-94/38, 1994.

2 R.O. Gauntt, et al, Metallic Core-Melt Behavior in Dry-Core BWR Accidents: The Ex-Reactor Experiments, 1994 USNRC Water Reactor Safety Information Meeting, Bethesda, MD, October 1994.

STEADY-STATE OBSERVATIONS AND THEORETICAL MODELING OF CRITICAL HEAT FLUX PHENOMENA ON A DOWNWARD FACING HEMISPHERICAL SURFACE

F. B. Cheung and K.H. Haddad
Department of Mechanical Engineering
Pennsylvania State University
University Park, PA

ABSTRACT

Steady-state boiling experiments were performed in the SBLB test facility to observe the two-phase boundary layer flow behavior on the outer surface of a heated hemispherical vessel near the critical heat flux (CHF) limit and to measure the spatial variation of the local CHF along the vessel outer surface. Based upon the flow observations, an advanced hydrodynamic CHF model was developed. The model considers the existence of a micro-layer underneath an elongated vapor slug on the downward facing curved heating surface. The micro-layer is treated as a thin liquid film with numerous micro-vapor jets penetrating through it. The micro-jets have the characteristic size dictated by Helmholtz instability. Local dryout is considered to occur when the supply of fresh liquid from the two phase boundary layer to the micro-layer is not sufficient to prevent depletion of the liquid film by boiling. A boundary layer analysis, treating the two-phase motion as a separated flow, is performed to determine the liquid supply rate and thus the local critical heat flux. The model provides a clear physical explanation for the spatial variation of the CHF observed in the SBLB experiments and for the weak dependence of the CHF data on the physical size of the vessel.

INTRODUCTION

One essential element needed to assess the feasibility of external cooling of core melt in the lower head of a reactor vessel by cavity flooding as a severe accident management strategy, is the critical heat flux for boundary layer boiling on the vessel outer surface. To gather this important piece of information, the subscale boundary layer boiling (SBLB) test facility was developed to simulate the boiling phenomena on the external bottom surface of a reactor vessel. A large number of transient quenching experiments were conducted in the facility under both saturated and subcooled boiling conditions to determine the local boiling curves and the local critical heat flux on the vessel outer surface. It was found that the local CHF value increased by more than 100% from the bottom center to the upper edge of the heated vessel. The quenching data were presented in the 22nd Water Reactor Safety Meeting (Cheung and Haddad 1994).

In this study, steady-state observations of the boundary layer boiling phenomena on the outer surface of a heated hemispherical vessel were performed at high heat flux levels. The objectives were to seek a fundamental understanding of the two-phase boundary layer flow

behavior near the CHF limit and to confirm the spatial variation of the critical heat flux along the curved heating surface. Based upon the steady-state observations, theoretical modeling of the boundary layer boiling and CHF phenomena was made. The objectives of the modeling effort were: (i) to develop an advanced hydrodynamic CHF model specifically for pool boiling on a downward facing curved surface, (ii) to provide a physical explanation for the large spatial variation of the critical heat flux observed in the SBLB experiments, and (iii) to determine (if any) the dependence of the critical heat flux on the physical size of the heated vessel. The last item is needed for extrapolation of the subscale boiling data to full-scale reactor applications.

It should be noted that the mechanism responsible for the occurrence of CHF in pool boiling has been the subject of extensive investigation and debate in the past several decades. Kutateladze (1950) was the first to propose the analogy between the flooding phenomenon and the CHF condition. This analogy was first mentioned by Bonilla and Perry in 1941 as reported by Zuber (1959), but it appears that Kutateladze was the first to pursue the idea. He used dimensional analysis to derive the following expression for the critical heat flux:

$$q''_{CHF} = C_k \rho_g^{1/2} h_{fg} \left[\sigma g(\rho_\ell - \rho_g)\right]^{1/4} \tag{1}$$

where the constant C_k was assigned the value of 0.131 based on maximum heat flux data.

Chang (1957) proposed a similarity between the Taylor wave motion and the boiling crisis. This postulation, coupled with arguments that were published in the Soviet literature, influenced Zuber (1959) to develop a hydrodynamic CHF model based on Taylor wave motion and Helmholtz instability. In Zuber's model, burnout was assumed to attain when the interface of the large vapor columns leaving the surface became Helmholtz unstable. The vapor columns were separated from each other by a distance equal to the most dangerous Taylor wavelength. The critical heat flux was predicted by the following expression:

$$q''_{CHF} = 0.131 \rho_g \, h_{fg} \left[\frac{\sigma(\rho_\ell - \rho_g)g}{\rho_g^{\,2}}\right]^{1/4} \tag{2}$$

which is essentially the same as equation (1). Some refinements of Zuber's model was made by Lienhard and Dhir (1973), which resulted in a value of 0.149 for the constant coefficient rather than 0.131.

Lienhard and Hasan (1979) used the mechanical energy stability criterion to predict the CHF in pool boiling. They considered the boiling system to be in stable equilibrium when the change in the system energy was equal to or less than zero. For nucleate boiling, this implies that the mechanism of vapor removal remains stable as long as the net mechanical energy transfer to the system is negative. Violation of this condition marks the occurrence of CHF.

Using this principle, Lienhard and Hasan were able to show that the results of their analysis were consistent with Zuber's model. They also showed that their model eliminated the need for information on the Helmholtz unstable wavelength. However, this was replaced by the need for information on the bubble departure diameter corresponding to the breakup of the vapor column.

Haramura and Katto (1983) postulated that a liquid film existed underneath each vapor bubble growing on the heating surface. The vapor bubble hovered over a number of small jets that supplied the bubble with vapor mass, leading to a timely growth of the bubble until it was pulled upward away from the surface by buoyancy. The bubbles were arranged in a rectangular array with a spacing equal to the most dangerous Taylog wavelength whereas the liquid film thickness was one-fourth of the Helmholtz wavelength. Burnout was assumed to take place when the liquid film underneath the vapro bubble evaporated completely before the departure of the bubble. Accordingly, the following expression was derived for the critical heat flux:

$$\frac{q''_{CHF}}{\rho_g^{1/2} h_{fg}\left[\sigma(\rho_\ell - \rho_g)g\right]^{1/4}} = \left(\frac{\pi^4}{2^{11}3^2}\right)^{1/16}\left(\frac{A_v}{A_w}\right)\left(1-\frac{A_v}{A_w}\right)^{5/16}\left[\frac{1+\rho_\ell/\rho_g}{\left(1+11\rho_\ell/16\rho_g\right)^{3/5}}\right]^{5/16} \tag{3}$$

where A_v/A_w is the ratio of the cross-sectional area of the vapor jets to the heating surface area. This ratio was found to be a function of the density ratio, ρ_g/ρ_ℓ, of the fluid only.

From the above literature survey, it is evident that in all the existing CHF models developed by previous investigators, the critical heat flux was treated constant and uniform over the entire heating surface. Thus far, no attempt has ever been made to predict the spatial variation of the critical heat flux along the heating surface. While the assumption of a uniform critical heat flux is a good approximation for upward facing surfaces, it is not a valid assumption for downward facing surfaces. In the latter case, a two-phase boundary layer flow is likely to be induced by the boiling process owing to the downward facing orientation of the heating surface. With the development of a boundary layer flow, the local critical heat flux could be substantially modified by the flow, thus leading to a significant spatial variation of the CHF values along the heating surface in the flow direction. Conceivably, none of the existing CHF models is applicable to pool boiling on a downward facing heating surface. It should also be noted that correlations for the maximum pool boiling heat flux have been restricted to the geometrically averaged CHF value for the heating objects, as summarized by Carey (1992). The reported data on the spatial variation of CHF are limited to those by Cheung and Haddad (1994) and Theofanous et al. (1994).

EXPERIMENTAL METHOD

Flow observations and heat transfer measurements were made in the SBLB test facility under steady-state conditions, covering the entire range of heat fluxes in the nucleate boiling

regime. The SBLB facility, consisting of a pressurized water tank with a condenser unit, an interchangeable test vessel, a data acquisition system, and a high-speed photographic system, was developed specifically to simulate the phenomena of critical heat flux for downward facing boiling on the external bottom surface of a reactor vessel. A detailed description of the facility and its operating procedure is given by Cheung and Haddad (1994) and will not be repeated here. In this section, only the portion relevant to high-heat-flux nucleate boiling under steady-state conditions is discussed.

To facilitate steady-state observations and local heat transfer measurements at high heat flux levels, a new test vessel with segmented heating elements was fabricated. The vessel was made of aluminum and had two separate parts, i.e., a heated lower hemispherical part and an unheated upper cylindrical part. The upper part was 12" (0.305 m) in diameter and 24" (0.61 m) in height, whereas the lower part was 12" (0.305 m) in diameter and 6" (0.152 m) in height. These two parts were used to simulate the lower head and the cylindrical wall section of a reactor vessel. The lower hemispherical part was further divided into five segments, each having the same surface area. Uniformly spaced independent heating elements were installed on the interior side of each segment to simulate decay heating of the vessel wall by a corium pool. The power supply to the heating elements in each segment was controlled separately, with the resulting local heat flux covering the anticipated range up to 1.0 MW/m^2. This design allowed for the attainment of the critical heat flux condition in a local portion of the vessel outer surface with the neighboring portions still in the nucleate boiling regime.

Special precautions were taken in conducting the experiments as the heat flux level approached the CHF point. Local meltdown of the test vessel would occur if the power to the heating elements were not discontinued before local dryout took place on the vessel outer surface. To prevent this from happening, a temperature control system was employed. Thermocouples were embedded at various locations within the wall on the interior side of the lower segments. The temperature responses of these thermocouples were fed into a computer and then checked against a set point value. If any of the temperatures inside the test vessel wall exceeded the set point, the power to all the heating elements would be discontinued by triggering the solid state relays that were part of the heater circuits. To approach the CHF limit, the local heat flux level was raised by a small step each time. At a level below the critical heat flux, the local wall temperature would rise rather moderately toward a new steady-state value. Once the critical heat flux limit was exceeded, an abrupt increase in the local wall temperature beyond the set point value took place. The occurrence of the local CHF state was detected and monitored by observing the time response of the local wall temperature.

The local boiling events at high heat flux levels were recorded under steady-state conditions by a Kodak Ektapro high-speed photographic system consisting of a motion analyzer, an imager, a cassett conditioner and a TV set. The recorded vapor dynamics were analyzed in slow motion to determine the cyclic ejection frequencies, the characteristic times for the vapor-cover period and the waiting period, and the aspect ratio of the elongated vapor masses. In the meantime, the local heat fluxes were determined from the wall temperatures recorded by the

embedded thermocouples using an inverse heat conduction code. The local heat fluxes so determined were further confirmed by the power imput to each of the local segments.

The qualitative two-phase boundary layer flow behavior and vapor dynamics observed at high heat flux levels were employed in the development of an advanced hydrodynamic CHF model. On the other hand, the quantitative heat transfer data were used for model validation. Comparison of the steady-state results were also made with the nucleate-boiling protion of the local boiling curves obtained in the transient quenching experiments reported by Cheung and Haddad (1994).

THEORETICAL MODELING

Critical heat flux is a limiting mechanism in nucleate boiling involving the dryout of liquid on a heating surface. It represents the upper bound of the excellent state of nucleate boiling where the heating surface is wetted with liquid and the heat transferred to the liquid is absorbed by the latent heat of vaporization in the immediate vicinity of the heating surface. The occurrence of the CHF state may be a result of (i) deficiency in vapor removal from the heating surface, (ii) inadequate supply of fresh liquid to the heating surface, (iii) premature liquid depletion on the heating surface, or (iv) the combination of all three factors.

Most existing hydrodynamic CHF models were developed primarily for upward facing surfaces. The critical heat flux was treated as a peculiar point that was different radically from the nucleate boiling regime. Helmholtz instability was assumed to act on the CHF point only, causing a sudden collapse of the vapor removal path. The validity of these conventional models for downward facing surfaces is highly skeptical. The nucleate boiling phenomenon on the outer surface of a heated hemispherical vessel observed in the SBLB experiments clearly indicated that throughout the entire high heat flux regime, nucleate boiling was subject to Helmholtz instability with cyclic ejection of large elongated vapor masses or slugs from the downward facing curved heating surface. Underneath each vapor slug was a micro-layer consisting of a continuous liquid film with numerous micro-vapor jets penetrating through it. The size of the micro-jets was dictated by Helmholtz instability. The CHF limit was reached as a result of insufficient supply of liquid from the two-phase boundary layer to the micro-layer, leading to depletion of the liquid film, i.e., local dryout of the heating surface. In view of this, the CHF point is a continuation of the nucleate boiling region in the high-heat-flux regime. It simply represents the upper limit of nucleate boiling. Throughout the entire high-heat-flux regime including the CHF point, nucleate boiling is subject to Helmholtz instability. This important new feature is employed in this study to develop an advanced hydrodynamic CHF model for pool boiling on a downward facing hemispherical heating surface.

Behavior of the Micro-Layer

Figure 1 shows schematically the configuration of a micro-layer underneath an elongated vapor slug growing on a downward facing curved heating surface. The micro-layer consists of a

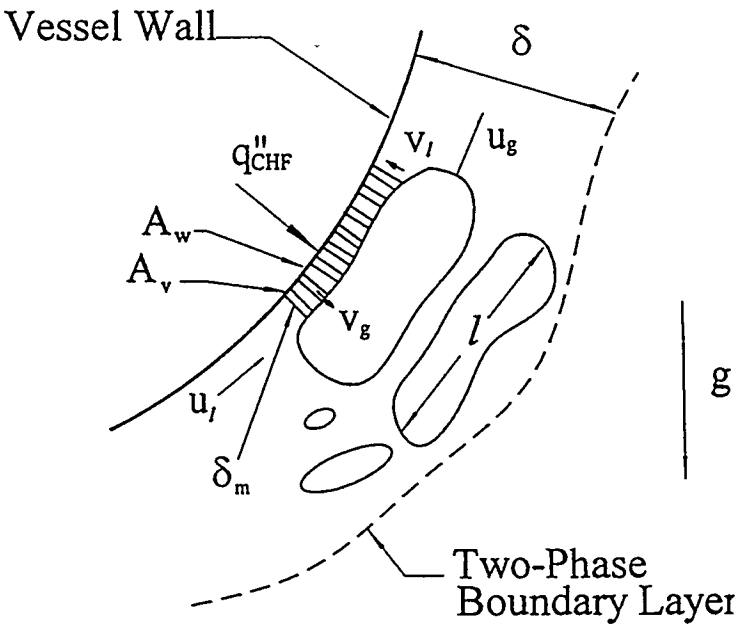

Figure 1. Schematic of the Micro-Layer Underneath an Elongated Vapor Slug.

continuous liquid film with numerous micro-vapor jets or stems penetrating through it. The thickness of the liquid film, δ_m, is the same as the length of the vapor stems. Under steady-state conditions, the mass flow rate of the vapor jets must be equal to the local rate of nucleate boiling, i.e.,

$$\rho_g v_g A_v = q''_{NB} A_w / h_{fg} \quad \text{or} \quad v_g = \frac{q''_{NB}}{\rho_g h_{fg}} \frac{A_w}{A_v} \tag{4}$$

where ρ_g is the vapor density, v_g the vapor jet velocity, A_v the surface area occupied by all the vapor jets, A_w the total heating area underneath the elongated vapor slug, q''_{NB} the local nucleate boiling heat flux, and h_{fg} the latent heat of vaporization. To satisfy continuity, the rate of liquid depletion of the micro-layer must be given by

$$\rho_\ell v_\ell (A_w - A_v) = q''_{NB} A_w / h_{fg} \quad \text{or} \quad v_\ell = \frac{q''_{NB}}{\rho_\ell h_{fg}} \frac{A_w}{A_w - A_v} \tag{5}$$

where ρ_ℓ is the liquid density and v_ℓ the velocity of the liquid in the micro-layer flowing vertically toward the heating surface.

According to the Helmholtz instability (Carey 1992), the relative velocity between the vapor jets and the liquid film in the micro-layer is given by

$$\left|v_g - v_\ell\right| = \left[\frac{2\pi\sigma\left(\rho_\ell + \rho_g\right)}{\lambda_H \rho_\ell \rho_g}\right]^{1/2} \tag{6}$$

where σ is the surface tension and λ_H the Helmholtz wavelength. The latter can be expressed in terms of the relative velocity by

$$\lambda_H = \frac{2\pi\sigma}{\rho_g}\left(1+\frac{\rho_g}{\rho_\ell}\right)\left|v_g - v_\ell\right|^{-2} \tag{7}$$

For the vapor jets to be hydrodynamically stable within the liquid film, the length of the jets should remain smaller than the Helmholtz wavelength. This implies that

$$\delta_m < \lambda_H \quad \text{or} \quad \delta_m = C_1 \lambda_H \tag{8}$$

where C_1 is a proportionality constant having a value less than unity.

Assuming a value of 0.25 for C_1, Haramura and Katto (1983) has shown that the micro-layer area ratio is a function of the density ratio of the fluid satisfying the following form:

$$\frac{A_v}{A_w} = 0.0584\left(\frac{\rho_g}{\rho_\ell}\right)^{0.2} \tag{9}$$

The above expression was found to match the conventional pool boiling data for water and R-113 very nicely. However, the liquid film thickness so predicted ($\delta_m \sim 0.056$ mm) was almost a factor of two smaller than the measured value ($\delta_m \sim 0.12$ mm). This discrepancy was evidently due to the assumption of $C_1 = 0.25$ which was somewhat arbitrary. To be general enough, the exact value of C_1 will not be assumed in this study and the following expression will be employed in place of equation (9)

$$\frac{A_v}{A_w} = C_2\left(\frac{\rho_g}{\rho_\ell}\right)^{0.2} \tag{10}$$

where C_2 is treated as an unknown constant having a value much less than unity. The use of these proportionality constants C_1 and C_2 will be discussed later.

For most fluids at moderate pressures, the density ratio is usually much less than unity, i.e., $(\rho_g / \rho_\ell) << 1$. It follows from equations (4), (5), and (10) that

$$\frac{\nu_\ell}{\nu_g} = \frac{C_2(\rho_g / \rho_\ell)^{1.2}}{1 - C_2(\rho_g / \rho_\ell)^{0.2}} << 1 \tag{11}$$

Hence the relative velocity between the vapor jets and the liquid film is essentially the same as the vapor jet velocity itself. Combination of equations (4), (7), (8) and (10) gives

$$\delta_m = C_3 \sigma \rho_g \left(1 + \frac{\rho_g}{\rho_\ell}\right)\left(\frac{\rho_g}{\rho_\ell}\right)^{0.4}\left(\frac{h_{fg}}{q''_{\mathrm{NB}}}\right)^2 \tag{12}$$

where C_3 is a new constant equal to $2\pi C_1 C_2{}^2$.

Occurrence of the Local CHF

Referring to Figure 1, the local rate of liquid supply, $\dot{m}_s$, from the two-phase boundary layer to the micro-layer is given by

$$\dot{m}_s = \rho_\ell u_\ell A_m \tag{13}$$

where u_ℓ is the local liquid velocity in the two phase boundary layer and A_{m} the flow area across the micro-layer. On the other hand, the local rate of depletion, $\dot{m}_d$, of the liquid film is given by

$$\dot{m}_d = q''_{\mathrm{NB}} A_w / h_{fg} \tag{14}$$

where A_{w} is the heating surface area underneath the elongated vapor slug. Local dryout of the liquid film is considered to occur when the local rate of liquid supply becomes smaller than the local rate of liquid depletion. In other words, the local critical heat flux limit is reached when the liquid supply from the two-phase boundary layer to the micro-layer is not sufficient to prevent local boil-dry of the liquid film. From equations (13) and (14), an expression for the local critical heat flux, q''_{CHF}, can be obtained by setting $\dot{m}_s$ equal to $\dot{m}_d$ and q''_{NB} equal to q''_{CHF}. The result is

$$q''_{\mathrm{CHF}} = \rho_\ell h_{fg} u_\ell \left(\frac{A_m}{A_w}\right) \tag{15}$$

where A_{m} is now the flow area across the micro-layer at the local CHF point.

Assuming the characteristic length of the vapor slug to be ℓ, the flow area A_m and the heating surface area A_w can be expressed by

$$A_m \sim (\delta_m)_{CHF}\ell \quad \text{and} \quad A_w \sim \ell^2 \tag{16}$$

where $(\delta_m)_{CHF}$ is the thickness of the micro-layer at the local CHF point, i.e., at q''_{CHF}. From the steady-state flow observations in the SBLB experiments, the characteristic length ℓ, is found to be proportional to the local two-phase boundary layer thickness, δ_0, in the bottom center region, i.e.,

$$\ell = C_4\delta_0 \tag{17}$$

where C_4 is a constant having a value very close to four. Substituting equations (16) and (17) into (15), the following expression is obtained for the local critical heat flux:

$$q''_{CHF} = \rho_\ell h_{fg} u_\ell (\delta_m)_{CHF} / C_4\delta_0 \tag{18}$$

where additional proportionality constants from equation (16) have been absorbed in C_4.

As discussed early, the CHF point is a continuation of the nucleate boiling region in the high-heat-flux regime. It simply represents the upper limit of the nucleate boiling heat flux. Helmholtz instability is acting upon the micro-layer throughout the entire high-heat-flux nucleate boiling regime including the CHF point. Hence, equation (12) should be applicable to the CHF limit. By setting q''_{NB} equal to q''_{CHF}, equation (12) becomes

$$(\delta_m)_{CHF} = C_3\sigma\rho_g\left(1+\frac{\rho_g}{\rho_\ell}\right)\left(\frac{\rho_g}{\rho_\ell}\right)^{0.4}\left(\frac{h_{fg}}{q''_{CHF}}\right)^2 \tag{19}$$

Substitution of Equation (19) into (18) gives

$$q''_{CHF} = B\rho_g h_{fg}\left[\frac{\sigma u_\ell}{\rho_\ell\delta_0}\left(1+\frac{\rho_g}{\rho_\ell}\right)\left(\frac{\rho_g}{\rho_\ell}\right)^{-1.6}\right]^{1/3} \tag{20}$$

where $B = (C_3 / C_4)^{1/3}$ is a new constant. Evidently, the local critical heat flux varies according to the 1/3 power of the local liquid velocity. This local flow quantity, which is expected to increase significantly along the heating surface in the flow direction, will be determined by treating the two-phase boundary layer motion as a separated flow.

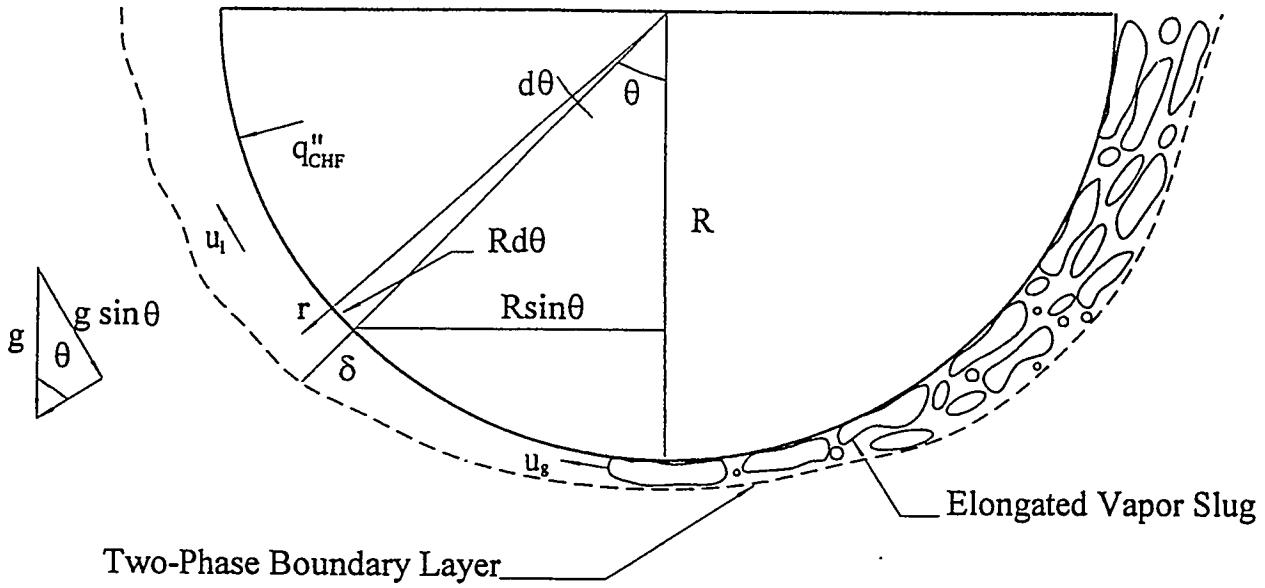

Figure 2. Configuration of the Two-Phase Boundary Layer on the Outer Surface of a Heated Hemispherical Vessel.

Two-Phase Boundary Layer Analysis

Figure 2 depicts the buoyancy-driven two-phase boundary layer flow on the outer surface of a hemispherical vessel. The vessel has a radius R and is heated from inside. The ambient liquid is quiescent and the boundary layer motion is induced entirely by pool boiling of the liquid on the vessel outer surface. To describe the boundary layer variables, an axisymmetric spherical coordinate system is employed. The radial and angular positions in the boundary layer is given by r and θ, respectively. The important length scales are the local heating length $R\theta$ and the local boundary layer thickness δ, whereas the important velocity scales are the local liquid and vapor velocities, u_ℓ and u_g, respectively. The latter two quantities are defined for the local velocities in the direction parallel to the heating surface. Under the influence of gravity, the buoyancy force driving the two-phase motion is proportional to $\alpha(\rho_\ell - \rho_g)g\sin\theta$, where α is the local void fraction of the two-phase mixture and $g \sin \theta$ is the local acceleration of gravity in the direction parallel to the heating surface.

According to Cheung and Epstein (1987), the momentum relation for the vapor-liquid mixture in the two-phase boundary layer is governed by the following differential equation applicable to any location θ along the hemispherical heating surface:

$$\frac{d}{d\theta}\left\{\left[\rho_g \alpha u_g^{\,2} + \rho_\ell (1-\alpha) u_\ell^{\,2}\right]\delta \sin\theta\right\} = \alpha\delta R g(\rho_\ell - \rho_g)\sin^2\theta - (\tau_w + \tau_i) R \sin\theta \tag{21}$$

where τ_w is the wall friction and τ_I the interfacial friction. These quantities are given by (Cheung and Epstein 1987):

$$\tau_w + \tau_i = 0.5 C_f \left[\alpha u_g + (1-\alpha) u_\ell\right]\left[\rho\alpha u_g + \rho_\ell (1-\alpha) u_\ell\right] \tag{22}$$

where C_f is a friction coefficient having the value of 0.005.

The local boundary layer thickness can be determined from the conservation of vapor mass. A mass balance on the two-phase boundary layer at any location θ gives

$$\frac{d}{d\theta}\left[\alpha u_g \delta \sin\theta\right] = \frac{q''_{CHF} R \sin\theta}{\rho_g h_{fg}} \tag{23}$$

where in deriving the above expression, the local wall heat flux on the heating surface has been assumed equal to the local critical heat flux. This corresponds to the critical heating condition for which the local CHF limit is reached in all upstream locations on the outer surface of the hemispherical vessel. This situation gives rise to the maximum local vapor velocity and boundary layer thickness that can possibly be attained at a given downstream location θ. Physically, the use of q''_{CHF} in equation (23) is consistent with the notion that CHF represents the upper bound of the excellent state of nucleate boiling. Beyond this upper limit, dryout will occur on the heating surface.

To close the governing system, an independent expression is needed for the relative velocity between the liquid and vapor phases. This is obtained by assuming that once the vapor mass departs from the heating surface, it would attain its terminal rise velocity relative to the liquid phase in the two-phase boundary layer. It follows that (Wallis 1969)

$$u_g = u_\ell + 1.53\left[\frac{\sigma g \sin\theta(\rho_\ell - \rho_g)}{\rho_\ell^{\,2}}\right]^{1/4} \tag{24}$$

where $g \sin\theta$ represents the local gravitational force tangential to the heating surface. As will be seen in the numerical solution, the relative velocity is important only in the upstream locations near the bottom center. In most downstream locations, the relative velocity is considerably smaller than the vapor and liquid velocities themselves. This is owing to the fact that the vapor

generation rate is extremely high at the CHF limit, resulting in very large vapor and liquid velocities in the two phase boundary layer. Thus any errors associated with the relative velocity used in equation (24) will not materially affect the predicted two-phase boundary layer flow behavior.

Inspection of equations (20) to (24) indicates that the following local boundary layer variables, namely, the dimensionless critical heat flux, Q_{CHF}, dimensionless boundary layer thickness, Δ, dimensionless vapor velocity, U_g, and dimensionless liquid velocity, U_ℓ, can be introduced to simplify the governing system:

$$q''_{CHF} = \rho_g h_{fg}\left[\frac{\sigma g(\rho_\ell - \rho_g)}{\rho_g^{\,2}}\right]^{1/4}\left(1+\frac{\rho_g}{\rho_\ell}\right)^{1/3} Q_{CHF} \tag{25a}$$

$$\delta = \left[\frac{\sigma R^2}{g(\rho_\ell - \rho_g)}\right]^{1/4}\left(\frac{\rho_g}{\rho_\ell}\right)^{-0.1}\Delta \tag{25b}$$

$$u_g = \left[\frac{Rg(\rho_\ell - \rho_g)}{\rho_g}\right]^{1/2}\left(\frac{\rho_g}{\rho_\ell}\right)^{0.1} U_g \tag{25c}$$

$$u_\ell = \left[\frac{Rg(\rho_\ell - \rho_g)}{\rho_\ell}\right]^{1/2} U_\ell \tag{25d}$$

In terms of the dimensionless local variables, equations (20) to (24) can be written as

$$Q_{CHF} = B(U_\ell / \Delta_0)^{1/3} \tag{26}$$

$$\frac{d}{d\theta}\left\{\left[\alpha U_g^{\,2} + \left(\frac{\rho_g}{\rho_\ell}\right)^{-0.2}(1-\alpha)U_\ell^{\,2}\right]\Delta\sin\theta\right\}$$

$$= \alpha\Delta\sin^2\theta\left(\frac{\rho_g}{\rho_\ell}\right)^{-0.2} - 0.5C_f L_b^{-1/2}\left(\frac{\rho_g}{\rho_\ell}\right)^{0.1}\sin\theta\left[\alpha U_g + \left(\frac{\rho_g}{\rho_\ell}\right)^{-0.6}(1-\alpha)U_\ell\right] \tag{27}$$

$$\left[\alpha U_g + \left(\frac{\rho_g}{\rho_\ell}\right)^{0.4}(1-\alpha)U_\ell\right]$$

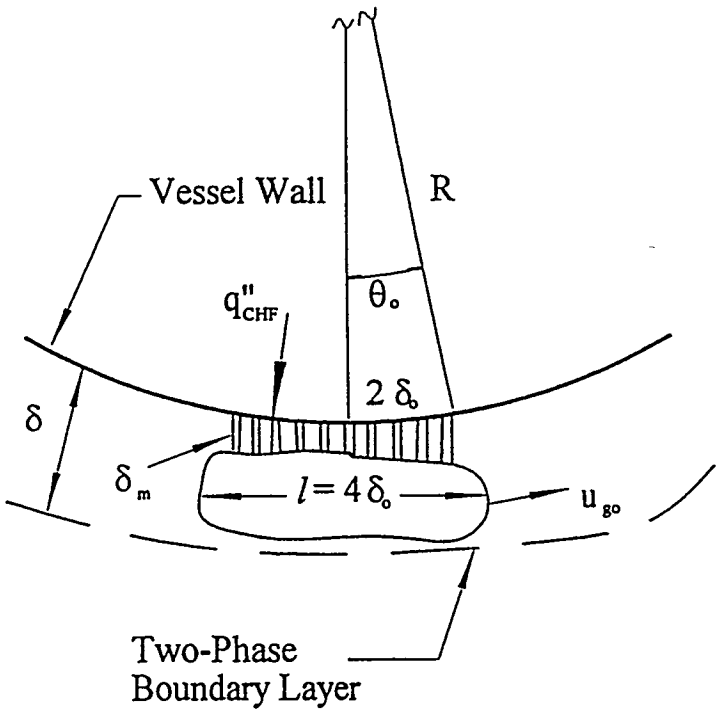

Figure 3. The Micro-Layer and the Vapor Slug at the Bottom Center of the Vessel.

$$\frac{d}{d\theta}\left[\alpha U_g \Delta \sin\theta\right] = Q_{CHF}\sin\theta \tag{28}$$

$$U_\ell = \left(\frac{\rho_g}{\rho_\ell}\right)^{-0.4} U_g - 1.53(L_b{}^2 \sin\theta)^{1/4} \tag{29}$$

where

$$\Delta_0 = \left[\frac{\sigma R^2}{g(\rho_\ell - \rho_g)}\right]^{-1/4}\left(\frac{\rho_g}{\rho_\ell}\right)^{0.1}\delta_0 \tag{30}$$

$$L_b = \frac{1}{R}\left[\frac{\sigma}{g(\rho_\ell - \rho_g)}\right]^{1/2} \tag{31}$$

Physically, the dimensionless parameter L_b represents the length ratio between the intrinsic bubble size and the vessel radius.

Initial Conditions and the Universal Constant

It remains necessary to determine the initial value, Δ_0, for the dimensionless boundary layer thickness. This requires considerations of the vapor mass that forms in the bottom center region of the heated vessel, as shown schematically in Figure 3. Based upon the vapor dynamics observed in the SBLB experiments, the aspect ratio of the vapor mass is very close to four, i.e., $C_4 = 4$ in equation (17).

The vapor velocity, u_{g_0}, at an initial location θ_0 near the bottom center can be determined by performing a mass balance, i.e.,

$$\rho_g u_{g_0} \alpha (2\pi R \delta_0 \sin\theta_0) = \frac{1}{h_{fg}} \int_0^{\theta_0} q''_{CHF} 2\pi R^2 \sin\theta d\theta \tag{32}$$

Since $\theta_0 << 1$, the local critical heat flux can be treated as a constant equal to $(q''_{CHF})_0$. An expression for u_{g_0}, may thus be obtained by carring out the integration in equation (32). The result is

$$u_{g_0} = \frac{(q''_{CHF})_0}{\alpha \rho_g h_{fg}} \left[\frac{1-\cos\theta_0}{\sin\theta_0}\right]\left(\frac{R}{\delta_0}\right) \tag{33}$$

For $\theta_0 << 1$, it can be shown that

$$\sin\theta_0 = \theta_0 \quad \text{and} \quad \cos\theta_0 = 1 - \frac{1}{2}\theta_0^2 \tag{34}$$

Substituting equations (34) into (35), the following expression is obtained for u_{g_0},

$$u_{g_0} = \frac{(q''_{CHF})_0}{\alpha \rho_g h_{fg}} \left(\frac{R}{\delta_0}\right)\frac{\theta_0}{2} \tag{35}$$

In terms of the dimensionless quantities, equation (35) can be written as

$$U_{g_0} = \frac{(Q_{CHF})_0}{\alpha \Delta_0}\frac{\theta_0}{2} \tag{36}$$

where U_{g_0} and $(Q_{CHF})_0$ are the initial values of U_g and Q_{CHF} at $\theta = \theta_0$. From equation (29), the dimensionless liquid velocity at θ_0 is given by

$$U_{\ell_0} = \left(\frac{\rho_g}{\rho_\ell}\right)^{-0.4} \frac{(Q_{CHF})_0}{\alpha \Delta_0} \frac{\theta_0}{2} - 1.53(L_b^2 \sin\theta_0)^{1/4} \tag{37}$$

For $\theta_0 << 1$, equation (37) can be written as

$$U_{\ell_0} = \left(\frac{\rho_g}{\rho_\ell}\right)^{-0.4} \frac{(Q_{CHF})_0}{\alpha \Delta_0} \frac{\theta_0}{2} - 1.53 L_b^{1/2} \theta_0^{1/4} \tag{38}$$

Applying equation (26) at $\theta = \theta_0$ and using equation (38), an implicit relationship can be derived for Δ_0. This is

$$\left(\frac{\rho_g}{\rho_\ell}\right)^{-0.4} \frac{(Q_{CHF})_0}{\alpha \Delta_0} \frac{\theta_0}{2} - 1.53 L_b^{1/2} \theta_0^{1/4} = \left[\frac{(Q_{CHF})_0}{B}\right]^3 \Delta_0 \tag{39}$$

Once Δ_0 is known, equations (26) to (29) can be solved simultaneously to determine the spatial variation of Q_{CHF}.

The above formulation results in one universal contant that needs to be determined from experimental data. To do this, the vapor dynamic and the local CHF limit at $\theta = \theta_0$ observed in the SBLB experiments are employed. Referring to Figure 3, the criterion for the occurrence of the local CHF limit in the bottom center region is based on the depletion of the liquid film in the micro-layer before the departure of the vapor mass from the heating surface. The mass of the liquid film is $\rho_\ell \delta_m (A_w - A_v)$ whereas the total rate of nucleate boiling heat transfer is $q''_{NB} A_w$. If the duration of the vapor ejection cycle is Δt_v, then local dryout would occur if $q''_{NB} A_w \Delta t_v / h_{fg}$ becomes equal to or larger than the mass of the liquid film. Thus the local CHF limit is given by

$$(q''_{CHF})_0 = \frac{1}{A_w \Delta t_v}\left[\rho_\ell (\delta_m)_{CHF} (A_w - A_v) h_{fg}\right] = \frac{\rho_\ell h_{fg} (\delta_m)_{CHF}}{\Delta t_v} \tag{40}$$

where the term involving the area ratio has been ignored as $A_v / A_w << 1$. Substituting equation (19) into (40) and rearranging, an expression for the universal constant can be derived. This is

$$C_3 = \frac{\Delta t_v}{\sigma \rho_\ell \rho_g}\left(1 + \frac{\rho_g}{\rho_\ell}\right)^{-1}\left(\frac{\rho_g}{\rho_\ell}\right)^{-0.4}\left[\frac{(q''_{CHF})_0}{h_{fg}}\right]^3 \tag{41}$$

In the SBLB experiments, the duration Δt_v, was found to be 0.25 s whereas the local CHF limit was 0.4 MW/m^2. Using the properties for water, i.e., σ = 0.0588 N/m, ρ_ℓ = 958 kg/m^3, $\rho_g = 0.598 \text{kg/m}^3$, and $h_{fg} = 2.257$ MJ/kg, the value of C_3 is calculated to be 0.00079. It follows that the universal constant in equations (26) and (39) is given by

$$B = (C_3 / C_4)^{1/3} = 0.0582 \tag{42}$$

where the value of $C_4 = 4$ has been used.

RESULTS AND DISCUSSION

Steady-State Flow Observations

Steady-state boiling experiments were conducted specifically for observing the local vapor dynamics and the two-phase boundary layer flow on the curved heating surface. The water was maintained at nearly 100°C in these experiments whereas the local wall heat flux was varied from 0.1 MW/m^2 to the vicinity of the local CHF limit. At these high-heat-flux levels, a cyclic vapor ejection process was clearly observed. Large and elongated vapor masses or slugs, being squeezed up against the wall by the local buoyancy force, were found to grow periodically on the heating surface. They were then ejected violently upward in all directions. The ejected vapor masses carried away the local vapor bubbles but tended to by-pass those large vapor slugs growing on the heating surface in the downstream locations.

As the heat flux level was increased toward the local CHF limit, the cyclic ejection of the vapor masses appeared to be explosive and highly chaotic, especially in the bottom center region. The characteristic frequency of the vapor ejection cycle tended to increase with the heat flux level. However, the frequency increased very slowly as the CHF limit was approached. A close-up view of the vapor slugs revealed the existence of a thin liquid film, i.e., a micro-layer, underneath each elongated vapor slug. The small vapor masses that were generated at numerous discrete locations on the heating surface were fed in a continuous manner to the large vapor slug through the liquid film in the micro-layer. These small vapor masses had the shape of micro-vapor jets similar to those depicted in Figure 1. Apparently, it was the thin liquid film underneath the large vapor slug that prevented local dryout of the heating surface from occurring.

Near the local CHF limit, the characteristic frequency of the vapor ejection cycle was found to be approximately 4 Hz. Thus the cycle duration was about 0.25 s. Over 90% of this duration, the heating surface was covered by the vapor slugs. The waiting period was less than 10% of the cycle duration. The overall two-phase boundary layer flow configuration was similar to the one depicted in Figure 2. At the bottom center of the vessel, only a single large vapor mass was present in the local boundary layer region. However, in the downstream locations, two or three large vapor slugs could be present in the local boundary layer region at the same time.

Upon departure, a vapor slug tended to flow around those that were growing on the heating surface in the downstream locations. The local boundary layer thickness increased considerably from the bottom center to the upper edge of the heated vessel.

The vapor dynamics and cyclic ejection frequencies recorded at various heat flux levels were analyzed in slow motions and compared. No apparent changes in the vapor dynamics and cyclic ejection process were observed as the CHF point was attained. The vapor/liquid morphology and the local flow behavior were essentially the same throughout the high-heat-flux regime up to the CHF point, although the characteristic frequency of the vapor ejection cycle tended to increase with the heat flux level. Clearly, the CHF point is a continuation of the nucleate boiling region and simply represents the upper limit of the high-heat-flux regime. Throughout the entire high-heat-flux region including the CHF point, nucleate boiling is subject to Helmholtz instability. The conventional assumptions that the critical heat flux is a peculiar point different radically from the nucleate boiling regime and that Helmholtz instability acts only on the CHF point causing a sudden collapse of the vapor removal path are not valid for downward facing surfaces.

Steady-State Heat Transfer Measurements

Steady-state boiling experiments were performed in the SBLB test facility under both saturated and subcooled conditions, with the water temperature varying from 90°C to 100°C. Measurements of the local boiling heat flux and the local wall superheat were made with the local input power to the heating elements in each segment of the test vessel as the key parameter. Input powers covering the entire range of nucleate boiling including the low-, intermediate-, and high-heat-flux regimes, were used in the experiments. The local wall superheat corresponding to a given power input was measured by thermocouples on the outer surface of the vessel. The local boiling heat flux, on the other hand, was determined by performing an inverse heat conduction analysis of the temperatures recorded by thermocouples embedded inside the wall. The boiling heat flux was found to agree satisfactorily with the local power input. The uncertainty in the embedded thermocouple locations was about ± 0.001 m, the maximum error in the temperature reading was ± 0.1°C, and the uncertainty in the calculated heat flux was ±7%.

Typical time responses of the local wall temperature following a step increase in the local wall heat flux observed in the SBLB experiments are shown in Figure 4. Curve (a) corresponds to the case for which the final steady-state wall heat flux was below the local CHF limit, whereas curve (b) corresponds to the case for which the final wall heat flux was at the local CHF limit. Initially, the wall temperature was at a steady state. Following a step increase in the wall heat flux, the local wall temperature rose rather moderately toward a new steady-state value in case (a). On the other hand, an abrupt increase in the local wall temperature beyond the set point was detected by the temperature control system in case (b) which triggered the solid state relay to cut off the power to all the heating elements. It should be noted that in the actual experiments, a

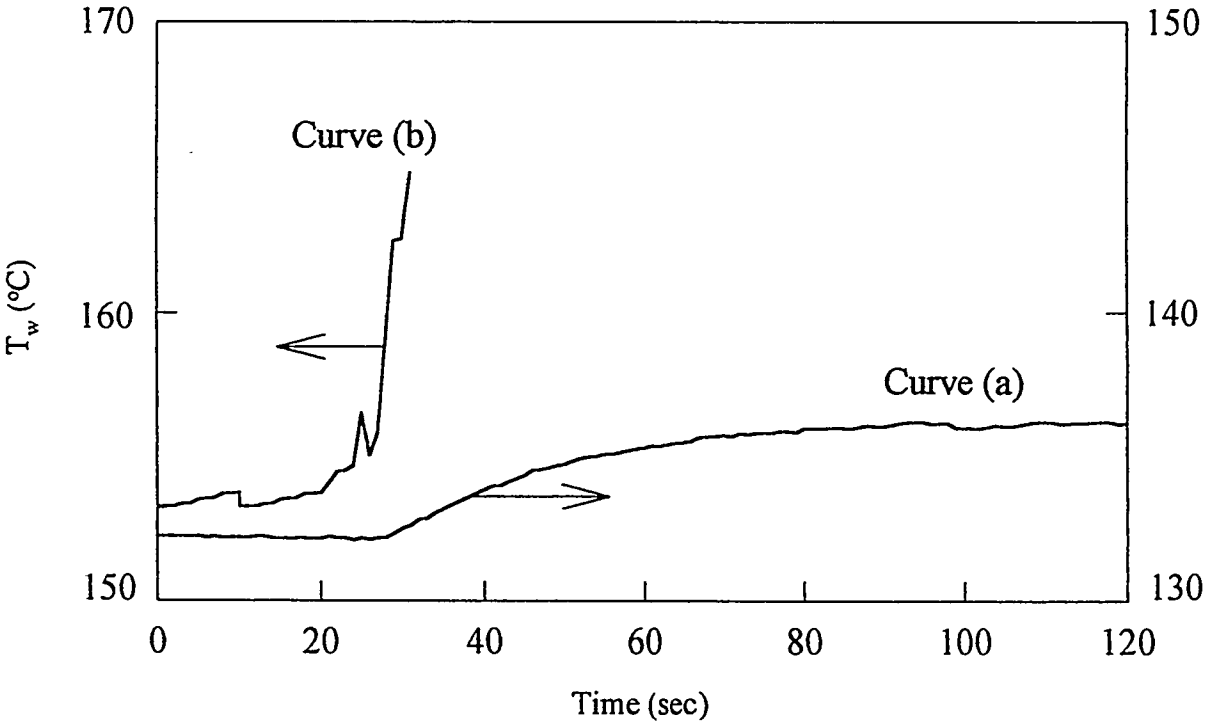

Figure 4. Typical Time Responses of the Local Wall Temperature Following a Step Increase in the Wall Heat Flux.

very small step increase (0.005 MW/m^2) was employed as the local CHF limit was approached. The relatively large step increase (0.1 MW/m^2) in curve (a) was used for illustration purposes.

The steady-state nucleate boiling data at the bottom center ($\theta = 0°$) and off-center ($\theta = 15°$) locations of the test vessel are shown in Figures 5 and 6. Four sets of data including both the cases of saturated and subcooled boiling are presented. In contrast to the conventional case of pool boiling for which subcooling has very little effect on nucleate boiling heat transfer, in the present case, a strong subcooling effect was observed at low-to-moderate heat flux levels. This is evidently due to the influence of the two-phase boundary layer flow. As observed in the SBLB experiments, the size of the vapor mass decreased drastically with an increase in the degree of subcooling. The decrease in the vapor size not only reduces the local bubble agitation but also decreases the two-phase boundary layer flow. As a result, the convective heat transfer associated with the the local bubble agitation and the two-phase boundary layer motion is considerably reduced. This reduction in the convective heat transfer cannot be compensated by the increase in the wall-to-liquid temperature difference. The net result is that the local boiling heat flux actually decreases as the degree of subcooling is increased. At high-heat-flux levels, however, latent heat transport dominates the convective heat transfer. Thus the subcooling effect becomes less important in the high-heat-flux regime.

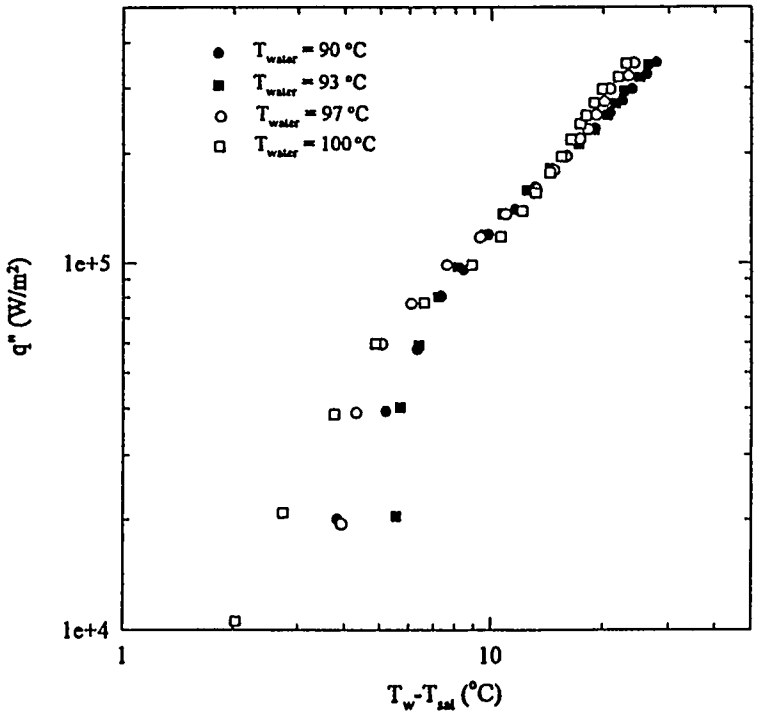

Figure 5. Steady-State Nucleate Boiling Data Measured at the Bottom Center of the Vessel (θ = 0°).

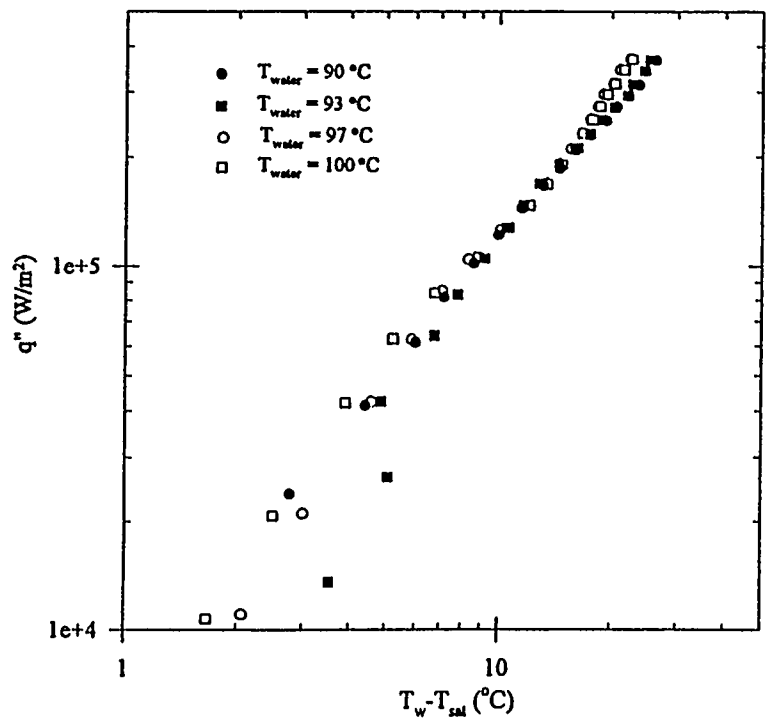

Figure 6. Steady-State Nucleate Boiling Data Measured at an Off-Center Location (θ = 15°).

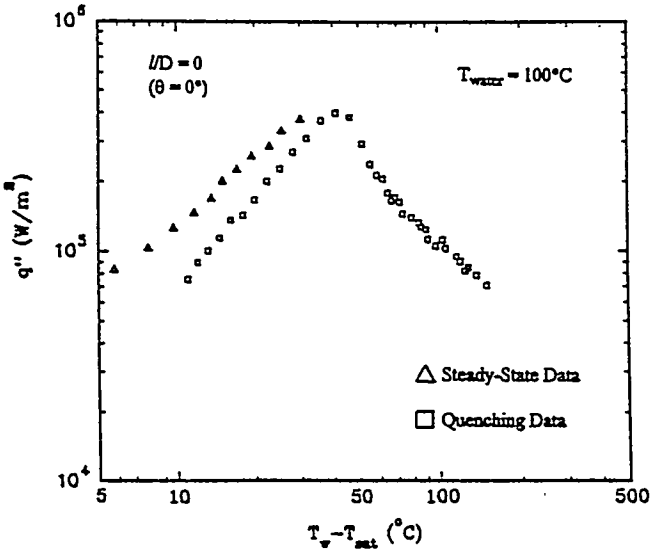

Figure 7. Comparison of the Steady-State and Transient Quenching Data for Water at 100°C.

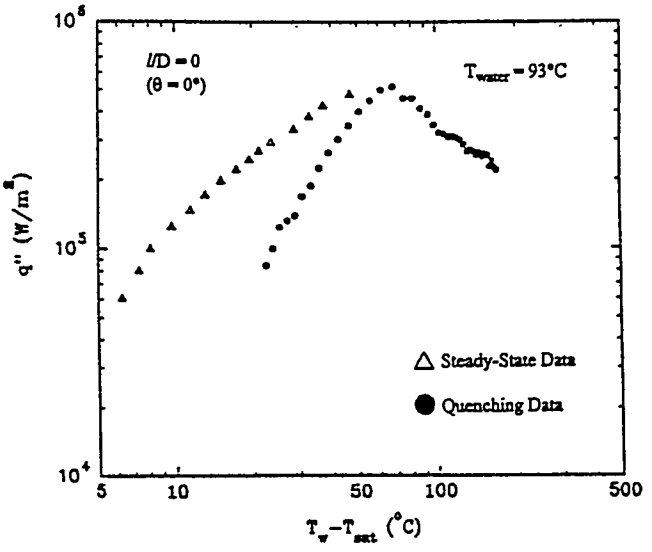

Figure 9. Comparison of the Steady-State and Transient Quenching Data for Water at 93°C.

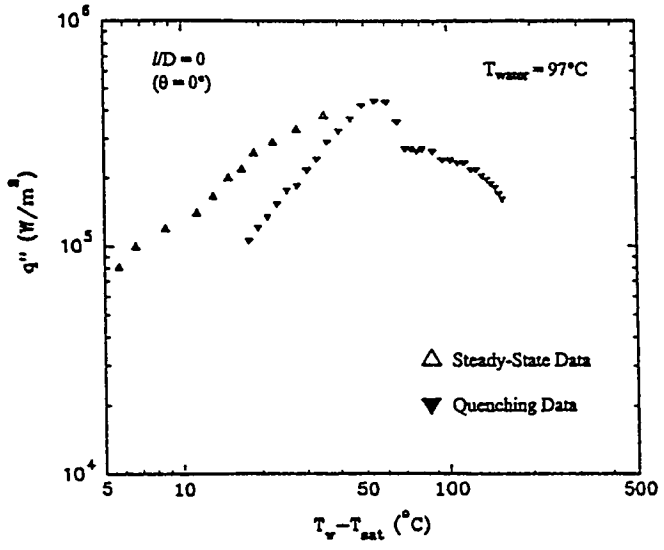

Figure 8. Comparison of the Steady-State and Transient Quenching Data for Water at 97°C.

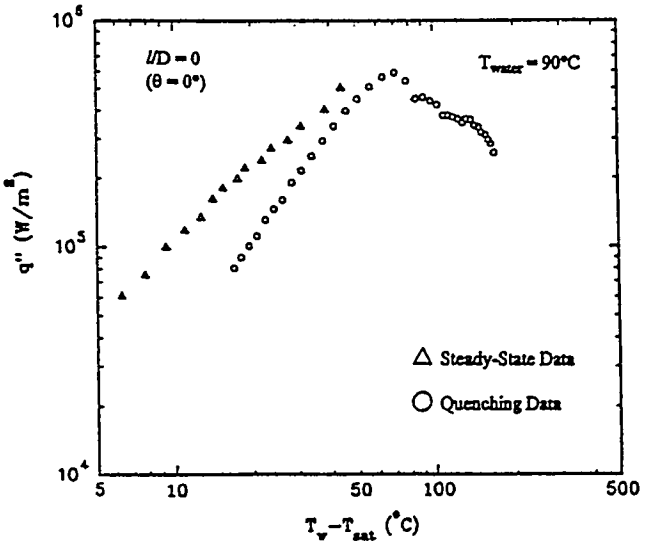

Figure 10. Comparison of the Steady-State and Transient Quenching Data for Water at 90°C.

A comparison of the steady-state results with the quencing data is shown in Figures 7 to 10 for four different water temperatures. It can be seen that for both saturated and subcooled boiling, the steady-state boiling data are consistently higher than those determined from transient quenching experiments, particularly at low heat flux levels. This is probably due to the fact that there were some errors associated with the data deduced from the transient experiments in the final stage of quenching. An order-of-magnitude analysis of the qunching process indicates that the time scales for the initial and intermediate stages of quenching were sufficiently large for the flow to establish a quasi-steady behavior. However, the time scale for the final stage of quenching was much too small for adequate flow development. As a result, the quenching data under-estimated the nucleate boiling rate. However, the difference between the steady-state and transient data becomes smaller as the heat flux level is increased. The local CHF limit obtained in the steady state experiments appears to be very close to those deduced from the quenching data.

Predictions of the Advanced Hydrodynamic CHF Model

Calculations of the local boundary layer flow quantities and the local CHF limits have been made over the range of $0 \leq \theta \leq \pi/2$ for water. In these calculations, the value of L_b has been set equal to 0.164, 0.0164, and 0.00164, corresponding respectively to a radius of 1.2" (0.0305 m), 12" (0.305 m), and 120" (3.05 m) for the heated hemispherical vessel under consideration. Results are shown in Figures 11 to 18.

The spatial variations of the boundary layer thickness predicted by the present model are presented in Figure 11 for the dimensionless quantity and Figure 12 for the physical quantity. For all values of L_b, the boundary layer thickness increases considerably from the bottom center to the upper edge of the vessel. The effect of L_b on Δ is important only for small values of θ and large values of L_b. This implies that the dimensionless boundary layer thickness is a weak function of the physical size of the vessel. The size effect is important only when the vessel diameter is very small. The actual boundary layer thickness, on the other hand, is a strong function of L_b. For $L_b < 0.05$, however, δ is almost inversely proportional to the square root of L_b. Thus for vessels larger than 0.1 m in diameter, δ would vary according to the square root of the vessel diameter whereas Δ is essentially independent of the vessel size.

The spatial variations of the vapor and liquid velocities are presented in Figures 13 and 15 for the dimensionless quantitites and Figures 14 and 16 for the physical quantities. For all values of L_b, the vapor and liquid velocities increase by more than an order of magnitude from the bottom center to the upper edge of the vessel. The relative velocity between the liquid and vapor phases is on the same order of the vapor and liquid velocities when θ is small. For large values of θ, the relative velocity is an order of magnitude smaller than the liquid and vapor velocities. The effect of L_b is quite strong on u_ℓ and u_g but very weak on the dimensionless quantities U_ℓ and U_g. For $L_b < 0.05$, both u_ℓ and u_g are almost inversely proportional to the

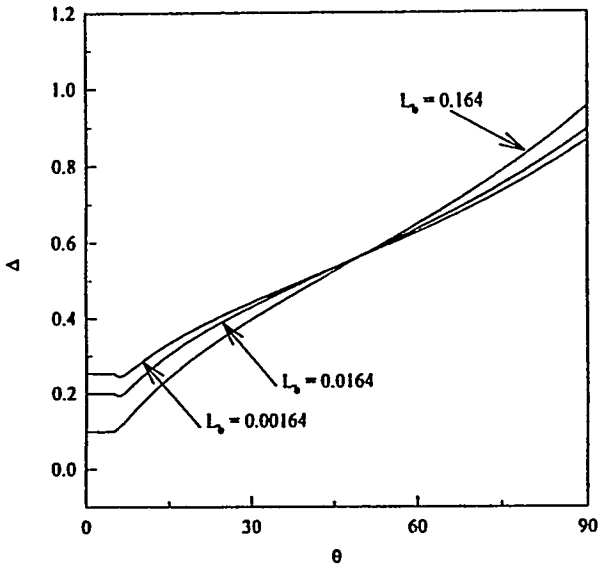

Figure 11. Predicted Variation of the Dimensionless Local Boundary Layer Thickness.

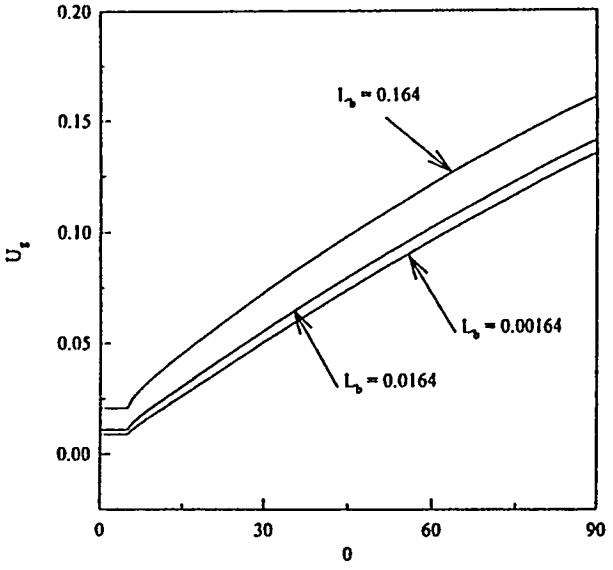

Figure 13. Predicted Variation of the Dimensionless Local Vapor Velocity.

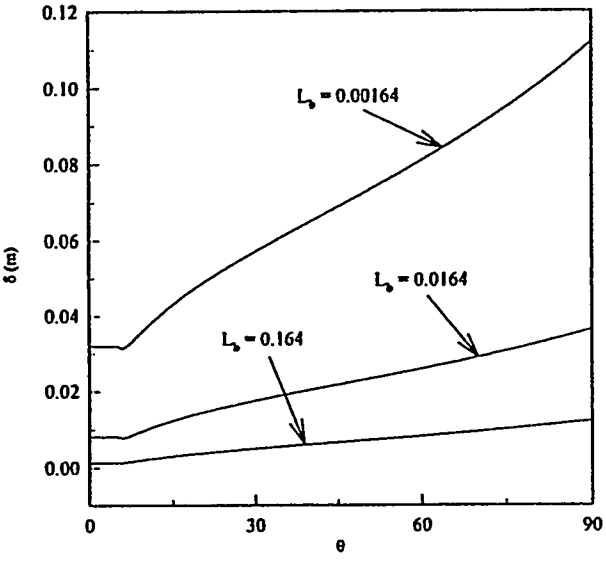

Figure 12. Predicted Variation of the Actual Local Boundary Layer Thickness.

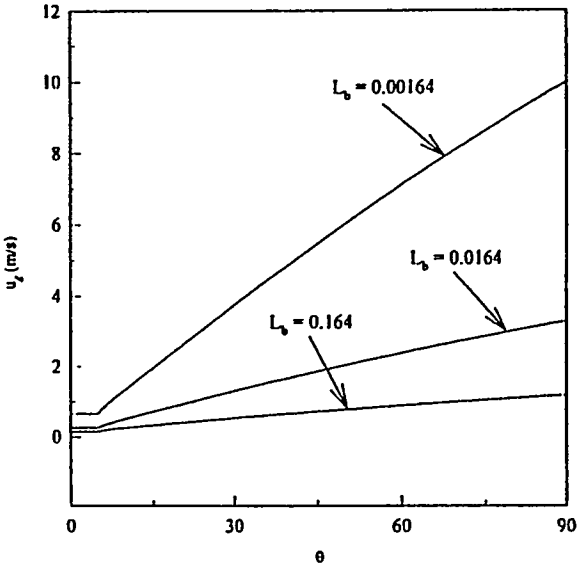

Figure 14. Predicted Variation of the Actual Local Vapor Velocity.

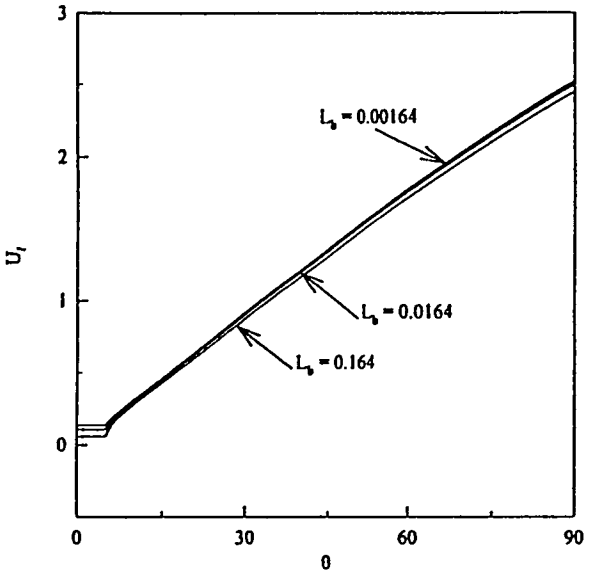

Figure 15. Predicted Variation of the Dimensionless Local Liquid Velocity.

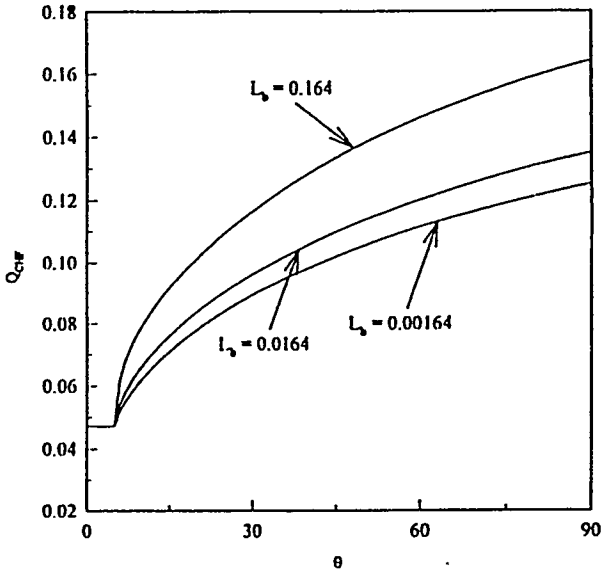

Figure 17. Predicted Variation of the Dimensionless Local Critical Heat Flux.

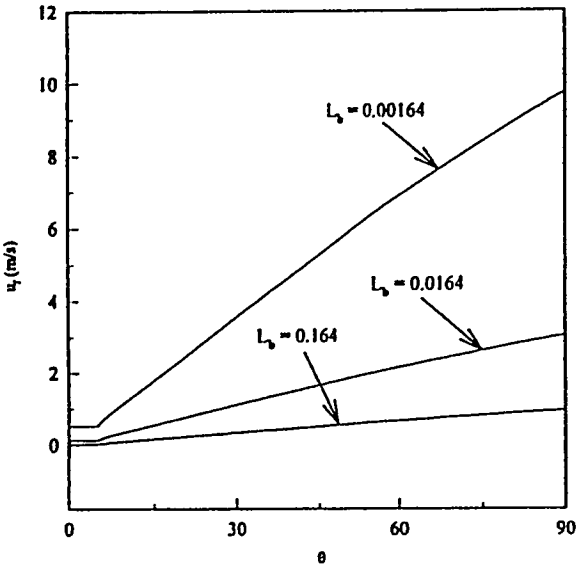

Figure 16. Predicted Variation of the Actual Local Liquid Velocity.

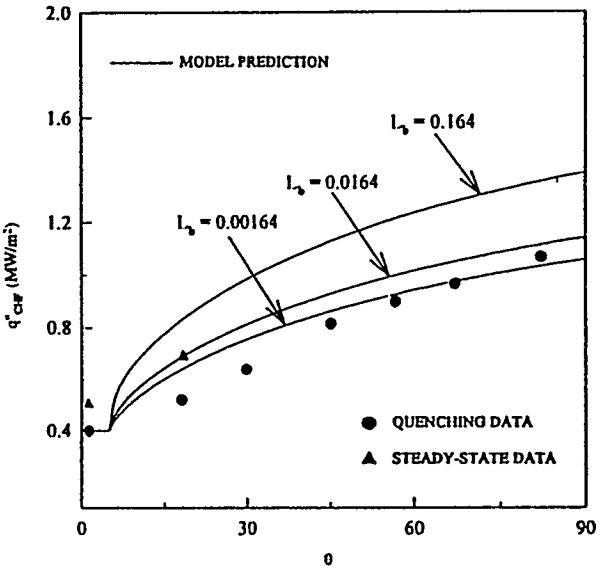

Figure 18. Predicted Variation of the Local Critical Heat Flux: Comparison with Experiments

square root of L_b. Thus for vessels larger than 0.1 m in diameter, u_ℓ and u_g would vary according to the square root of the vessel diameter whereas U_ℓ and U_g are essentially independent of the vessel size.

Figures 17 and 18 show the spatial variations of the dimensionless critical heat flux and the actual critical heat flux. Both Q_{CHF} and q''_{CHF} are weak functions of the size parameter L_b for the cases of L_b equal to 0.0164 and 0.00164. This clearly demonstrates the fact that for heated vessels with diameters considerably larger than the characteristic bubble size, the critical heat flux is weakly dependent of the vessel size. As given by equation (20), the local critical heat flux is given by the 1/3 power of the ratio between the local liquid velocity and the local boundary layer thickness. For $L_b < 0.05$, both u_ℓ and δ vary according to the square root of the vessel diameter. Thus the size effect on u_ℓ and δ_0 cancels out and q''_{CHF} becomes almost independent of L_b. Note that the local critical heat flux increases by more than 100% from the bottom center to the upper edge of the vessel. Physically this is because of the boundary layer flow effect. With the local liquid velocity increasing by more than an order of magnitude over the range of $0 \le \theta \le \pi/2$, there is a large increase in the local liquid supply rate, resulting in a significant spatial variation of the critical heat flux.

CONCLUSIONS

Based upon the experimental and theoretical results of this study, the following conclusions can be made:

1. For nucleate boiling on a downward facing surface, there is a micro-layer underneath each vapor slug growing on the surface. The micro-layer consists of a thin liquid film with numerous micro-vapor jets penetrating through it. In the entire high-heat-flux region including the CHF point, the micro-jets are subject to Helmholtz instability.

2. Local dryout of the surface occurs when the local rate of liquid supply to the micro-layer becomes smaller than the rate of depletion of the liquid film by boiling. This critical condition determines the maximum wall heat flux corresponding to the local CHF limit.

3. Owing to the effect of the two-phase boundary layer induced by boiling, the local rate of liquid supply increases significantly from the bottom center to the upper edge of the vessel, thus greatly enhancing the local CHF limit. This provides a physical explanation for the large spatial variation of the critical heat flux observed in the SBLB experiments.

4. For hemispherical vessels with diameters considerably larger than the characteristic bubble size, both the local liquid supply rate and the local boundary layer thickness are proportional to the square root of the vessel diameter. Since the critical heat flux depends only on the ratio of the liquid supply rate and the boundary layer thickness, the size effect tends to cancel

out altogether. As a result, the critical heat flux is independent of the physical size of the vessel.

5. The steady-state boiling data are consistently higher than the quenching data, particularly at low heat fluxes. However, the difference between the steady-state and quenching data becomes smaller as the heat flux level is increased. The local CHF limit obtained in the steady state experiments appears to be very close to those deduced from the quenching data.

ACKNOWLEDGMENT

This work was sponsored by the U.S. Nuclear Regulatory Commission under Contract No. NRC-04-93-061.

REFERENCES

Carey, V.P., 1992, "Liquid-Vapor Phase Change Phenomenon," Hemisphere Publishing Corporation.

Chang, Y.P., 1957, "A Theoretical Analysis of Heat Transfer in Natural Convection and in Boiling," *Trans. ASME,* Vol. 79, pp. 1501.

Cheung, F.B. and Epstein, M., 1987, "Two-phase Gas Bubble-Liquid Boundary Layer Flow Along Vertical and Inclined Surfaces," *Nuclear Engineering and Design,* Vol. 99, pp. 93-100.

Cheung, F.B. and Haddad, K.H., 1994, "Observation of the Dynamic Behavior of the Two-Phase Boundary Layers in the SBLB Experiments," *Proceedings of the 22nd Water Reactor Safety Meeting,* Washington, D.C.

Haramura, Y. and Katto, Y., 1983, "A New Hydrodynamic Model of Critical Heat Flux, Applicable Widely to Both Pool and Forced Convection Boiling on Submerged Bodies in Saturated Liquids," *Int. J. Heat Mass Transfer,* Vol. 26, No. 3, pp. 389-399.

Kutateladze, S.S., 1948, "On the Transistion to Film Boiling under Natural Convection," *Kotloturbostroenie,* No. 3, pp. 10.

Lienhard, J.H. And Dhir, V.K., 1973, "Hydrodynamic Predictions of Peak Pool-Boiling Heat Fluxes from Finite Bodies," *Trans. Am. Soc. Mech. Engrs.,* Series C, *J. Heat Transfer,* Vol. 95, pp. 152-158.

Lienhard, J.H. and Hasan, M., 1979, "On Predicting Boiling Burnout with the Mechanical Energy Stability Criterion," *Trans. Am. Soc. Mech. Engrs.,* Series C., *J. Heat Transer,* Vol. 101, pp. 276-279.

Theofaneous, T.G., et al., 1994, "Critical Heat Flux through Curved, Downward Facing, Thick Walls," *Nuclear Engineering and Design,* Vol. 151, pp. 247-258.

Zuber, N., 1959, "Hydrodynamics Aspects of Boiling Heat Transfer," AEC Rep., AECU-4439, June.

HYDROGEN DETONATION AND DETONATION TRANSITION DATA FROM THE HIGH-TEMPERATURE COMBUSTION FACILITY[1]

G. Ciccarelli, J. L. Boccio, T. Ginsberg, C. Finfrock, L. Gerlach,
H. Tagawa[2], and A. Malliakos[3]

Brookhaven National Laboratory
Department of Advanced Technology
Upton, N.Y. 11973

ABSTRACT

The BNL High-Temperature Combustion Facility (HTCF) is an experimental research tool capable of investigating the effects of initial thermodynamic state on the high-speed combustion characteristic of reactive gas mixtures. The overall experimental program has been designed to provide data to help characterize the influence of elevated gas-mixture temperature (and pressure) on the inherent sensitivity of hydrogen-air-steam mixtures to undergo detonation, on the potential for flames accelerating in these mixtures to transition into detonations, on the effects of gas venting on the flame-accelerating process, on the phenomena of initiation of detonations in these mixtures by jets of hot reactant products, and on the capability of detonations within a confined space to transmit into another, larger confined space. This paper presents results obtained from the completion of two of the overall test series that was designed to characterize high-speed combustion phenomena in initially high-temperature gas mixtures. These two test series are the intrinsic detonability test series and the deflagration-to-detonation (DDT) test series. A brief description of the facility is provided below.

1 INTRODUCTION

The concern over the possibility of a combustion event occurring in a water-cooled nuclear reactor during a severe accident was heightened following the Three-Mile Island Unit 2 (TMI-2) accident. After consideration of the pressure pulse induced during the TMI-2 accident, combustion research focusing on hydrogen-air mixtures was intensified. Due to

---

[1]This work was performed under the auspices of the U. S. Nuclear Regulatory Commission and the Japanese Nuclear Power Engineering Corporation.

[2]Visiting Research Engineer, Nuclear Power Engineering Corporation, Tokyo, Japan.

[3]Program Manager, U. S. Nuclear Regulatory Commission, Washington, DC.

the high dynamic pressures associated with the detonation mode of combustion, one of the main goals of the research was to determine the necessary geometric and thermodynamic conditions required for detonation initiation. This knowledge is essential in order to help predict the possibility of such an event during a postulated severe accident and to estimate the associated loading on containment.

Under most severe accident scenarios, a containment atmosphere consisting of hydrogen, air, and steam at initial temperatures up to 373K and pressures up to roughly three atmospheres can prevail. For this reason, most of the detonation research recently conducted were at these conditions (Tieszen et al., 1987). Calculations by Yang (1992) have shown that under certain accident scenarios, local compartment temperatures in excess of 373K can occur. Since relevant data at such temperatures is limited and confidence in the modeling of detonations is not high, the need arose to perform further investigations into high-temperature, high-speed combustion phenomena.

The High-Temperature Hydrogen Combustion Research Program at Brookhaven National Laboratory is jointly funded by the U.S. Nuclear Regulatory Commission and the Japanese Nuclear Power Engineering Corporation, sponsored by the Ministry of International Trade and Industry (MITI). The overall goal is to extend the capability to assess potential detonation-type loads in containment during severe accidents, characterized by initial high-temperature and large steam fraction hydrogen-air-steam mixtures. This paper presents the results from two elements of the High-Temperature Combustion Program, dealing with inherent detonability and fast-flame transition.

1.1 Objectives

The BNL High-Temperature Combustion Facility (HTCF) was constructed to investigate hydrogen combustion phenomena in gaseous mixtures of hydrogen-air and steam at temperatures up to 700K. The major component of the facility is a 27.3-cm inner-diameter, 21.3-m long heated detonation tube. The Small-Scale Development Apparatus (SSDA) was constructed to support the design of the HTCF and to augment the experimental data base. A detailed description of the SSDA can be found in NUREG/CR-6213.

The objectives of this phase of the overall experimental program are:

(1) Provide experimental data on the detonation cell size of hydrogen-air and steam mixtures as a function of initial mixture temperature, in order to determine the effect of temperature in the range of 300K to 650K on the sensitivity of the mixtures to undergo a detonation.

(2) Evaluate the ability of the ZND physical model to predict the effect of temperature on the detonation cell size of mixtures of hydrogen-air and steam and to compare the measured detonation velocity with the predictions from the classical theory.

(3) Determine the effect of initial temperature and steam dilution on flame acceleration and deflagration-to-detonation transition phenomena and evaluate the effects of temperature on flame-acceleration limits.

The purpose for acquiring these data and for performing these evaluations has been to enhance our knowledge base in estimating the likelihood of mixtures, prototypical to nuclear power plant severe accident conditions, to undergo a detonation or a high-speed combustion event.

2 EXPERIMENTAL DETAILS

2.1 Experimental Apparatus

The central feature of this facility is the large detonation vessel (LDV), which is a 27-cm diameter, 21.3-m long cylindrically cast, stainless-steel detonation tube, constructed in seven modular, ASME-certified, flanged, 3.05-m long sections. A photograph of the assembled vessels, which were fabricated by Fluitron, Inc., is shown in Figure 1. Four other test sections have been constructed, which can be individually attached to sections of the LDV, to investigate the effects of gas venting on flame acceleration and DDT phenomenon. The Maximum Allowable Working Pressure of the LDV is 10 MPa (100 atm). Each section of the vessel can be independently heated up to 700K, using ceramic heating blankets that surround each modular section of the LDV. Various combinations of hydrogen-air-steam test mixtures, with initial temperatures and pressures respectively ranging between 300K to 700K and 100 KPa to 300 KPa, can be quickly injected into the heated detonation tube. Additional gases, such as nitrogen, carbon dioxide and monoxide, and oxygen, can also be introduced as components of the test mixture. Ignition of the test mixture can be generated in one of several ways: directly by a high-energy spark discharge, by glow-plug igniters, and indirectly by the transmission of blast waves, from an oxy-acetylene gas driver, into the test gas mixture. Accommodations for using high-explosive (HE) discharges for detonation initiation were factored into the design of the LDV, but the use of blast waves, generated by the rapid combustion of a highly sensitive oxy-acetylene mixture (in lieu of a HE discharge), proved successful. Instrumentation and a data acquisition system permit the measurements of initial/final gas composition, dynamic pressure and temperature, flame velocity, detonation wave speed, and detonation cell width.

Some of the systems unique to this facility are described in the appendix. Further details can be found in Ciccarelli (1996).

2.2 Experimental Procedures

The following is a brief description of the steps taken to execute a detonation experiment at elevated initial temperature. Before the vessel heating system is started, a smoked foil is prepared and inserted into the back end of the vessel, after which the heating system is turned on at the remote control unit. The temperature set points for the vessel and other trace heaters are then entered into the computers in the control room. Since the driver is

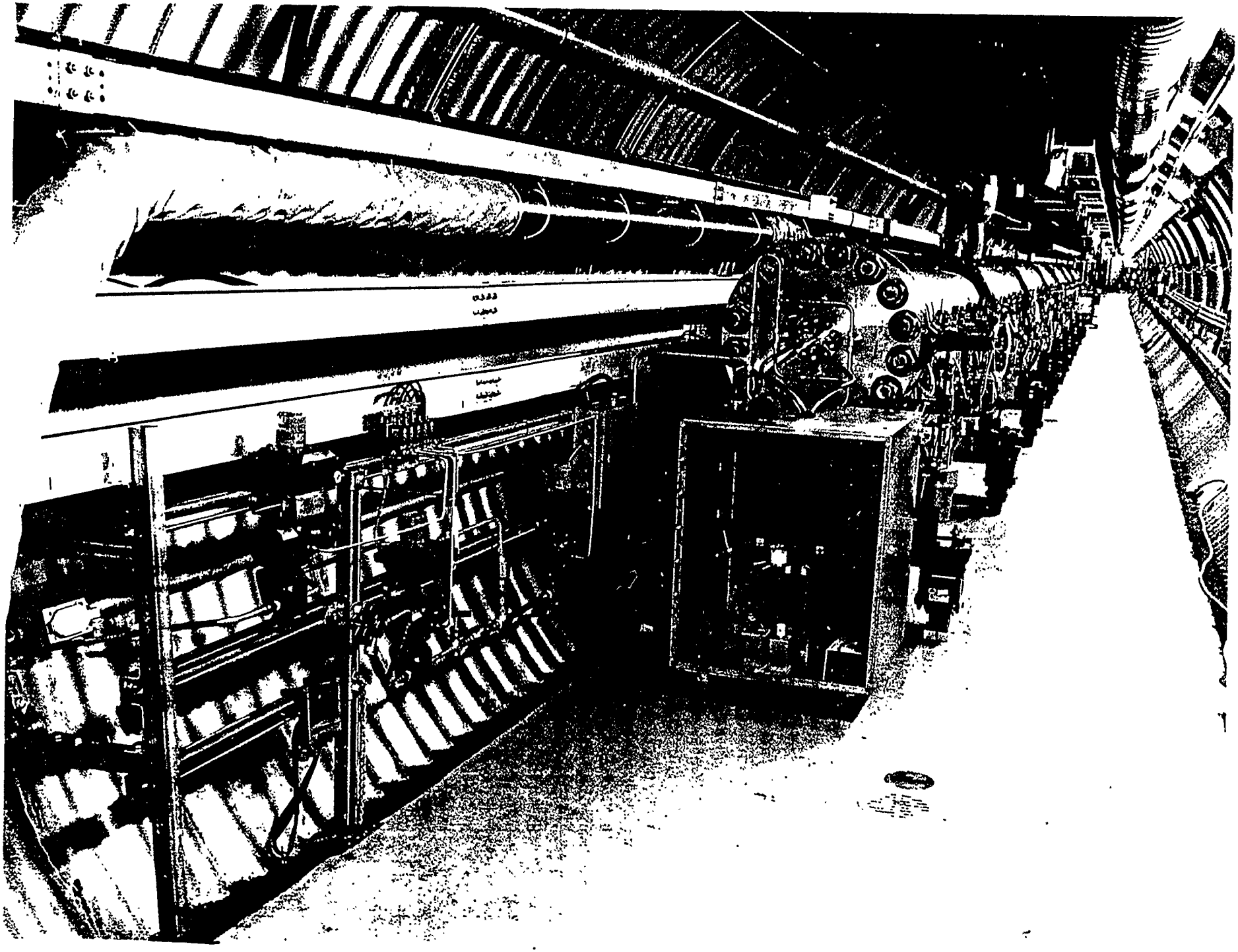

Figure 1: Photograph showing the driver-end of the test vessel inside the tunnel

not heated, the exploding wire used to initiated the detonation in the driver gas can be put into place at any time during the vessel heatup. After the wire is in place, the vessel vacuum can be started. When all the temperature set points have been achieved, all personnel are cleared from the area. The final step is the closure of a large plug door, which satisfies the facility's interlock system that permits the flow of combustible gases (i.e., releases instrument air to the valves) and the charging of the trigger system high-voltage capacitor.

With combustible gas flow enabled, the respective gas constituent flow settings and the various chart and log parameters are input at the computer terminal in the control room. The high-voltage capacitor for the triggering device is charged and the scopes are armed. The operator then starts a program which takes control of the gas filling and firing sequence. The first operation performed by the program is to start the flow of the constituent gases. Before injection into the vessel is initiated, the mixture flow bypasses the test vessel out the exhaust stack, until steady-state flow conditions are achieved. This bypass phase takes 20 seconds, after which the gas is directed into the vessel. The vessel is filled to a pressure just below the prescribed test pressure. After the test gas has been loaded: three test gas samples are taken, the sample bottles valved out, and the driver gas is injected raising the vessel pressure to the test pressure (e.g., one atmosphere). Note, the larger the driver partial pressure, the longer the driver slug is. Once the driver gas is injected, there is a 2-second delay, allowing the valves to close, and the exploding wire is triggered and the detonation is initiated. The combustion products in the vessel are then flushed out through a 7-m high exhaust stack using two 100-HP blowers located at each end of the test vessel. Only after purging has been completed are personnel allowed by the interlock system to enter the tunnel to remove the smoked foil and perform other duties in preparation for the next test.

Tests on flame acceleration and DDT are conducted in a similar fashion, except for this test series, a glow plug is used for ignition in lieu of the gaseous driver. Also to induce turbulence in the flow, equally spaced orifice plates having an inner diameter of 21 cm are installed in the vessel every 27 cm.

3 EXPERIMENTAL RESULTS

3.1 Gas Driver Characterization

One of the unique features of the HTCF is the use of a "diaphragmless" gas driver (i.e., no physical boundary between driver and test gas) to initiate detonations in the test gas. However, the driver gas slug is not as well defined as could be by a diaphragm separating the test gas from the driver gas. As the driver gas is injected into the test vessel, it mixes with preloaded test gas. The degree of mixing and the extent of driver gas convection down the vessel has to be determined in order to be able to calibrate driver conditions and assess driver performance.

3.1.1 Gas Driver Composition

A series of calibration tests were performed to determine the driver gas composition before injection into the vessel and the driver gas distribution inside the test vessel just after injection.

In the first set of tests, the vessel was evacuated, filled with a 20 percent (based on oxygen/acetylene delivery pressures) driver gas mixture to a vessel pressure of 0.05 MPa absolute, and then detonated. The measured detonation velocity down the length of the vessel was 2100 ± 9 m/s. Using the chemical equilibrium code STANJAN (Reynolds, 1986), the CJ (Chapman-Jouguet) detonation velocity for a 20 percent acetylene mixture was calculated to be 2160 m/s, which is only 3 percent higher than the measured velocity. This provided assurances on the calibration of the driver gas composition settings.

The driver gas distribution was measured in the next series by taking gas samples at various axial locations one second after driver gas was injected into an equimolar test gas mixture. Based on the amount of hydrogen detected in a sample, the fraction of the sample consisting of driver gas can be inferred.

The measured axial distribution of the driver gas is given in Figure 2, where the ratio of the driver gas volume to the total gas volume (i.e., driver plus test gas) is plotted versus axial distance from the driver section endplate. Note that the driver gas constitutes between 30 and 40 percent of the gas at the exploding wire location, i.e., the endplate. The driver fraction then drops off asymptotically with distance. From these tests, it appears that the effective driver length scales with the driver volume, or partial pressure.

To some extent, dilution of the acetylene-oxygen driver gas with test gas is advantageous since the detonation pressure in the driver gas will match more closely the detonation pressure in the test gas.

3.1.2 Effect of Driver Length on Detonation Transmission

Another series of experiments was performed in which the driver gas partial pressure, and thus the effective driver length, was varied, and the detonation velocity measured down the length of vessel to ascertain under what driver conditions are stable detonations achieved. The results from these experiments are illustrated in Figure 3. The theoretical CJ detonation velocity and pressure for this rather insensitive test gas is 1233 m/s and 0.377 MPa, respectively. As depicted in this figure, the detonation is initiated immediately in the driver (25 percent oxyacetylene mixture) where the propagation velocity is of the order of 2200 m/s. The detonation velocity quickly decays to a velocity just under the test gas CJ velocity. This figure shows that there is a clear correlation between the distance where the detonation falls off and the effective length of the driver gas depicted in Figure 2. The average terminal velocity for the different driver pressures is similar except for the largest driver (e.g., 1.0 psi), where the average velocity is somewhat higher. For a driver partial pressure of less than 0.2 psi, a detonation was not initiated in the test gas.

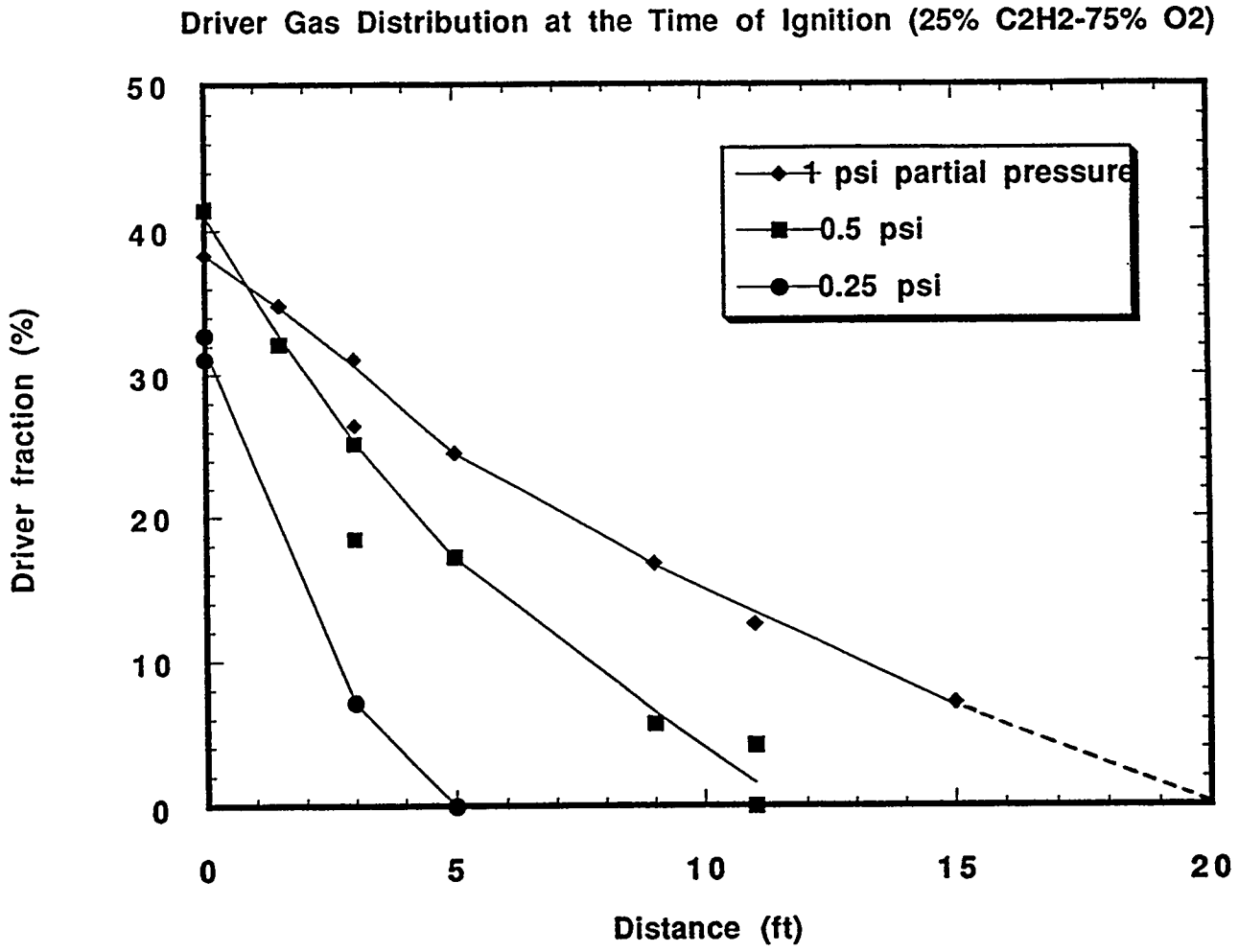

Figure 2: Experimentally measured driver-gas (C2H2 + O2) axial distribution in the test vessel at 1 second after driver-gas injection

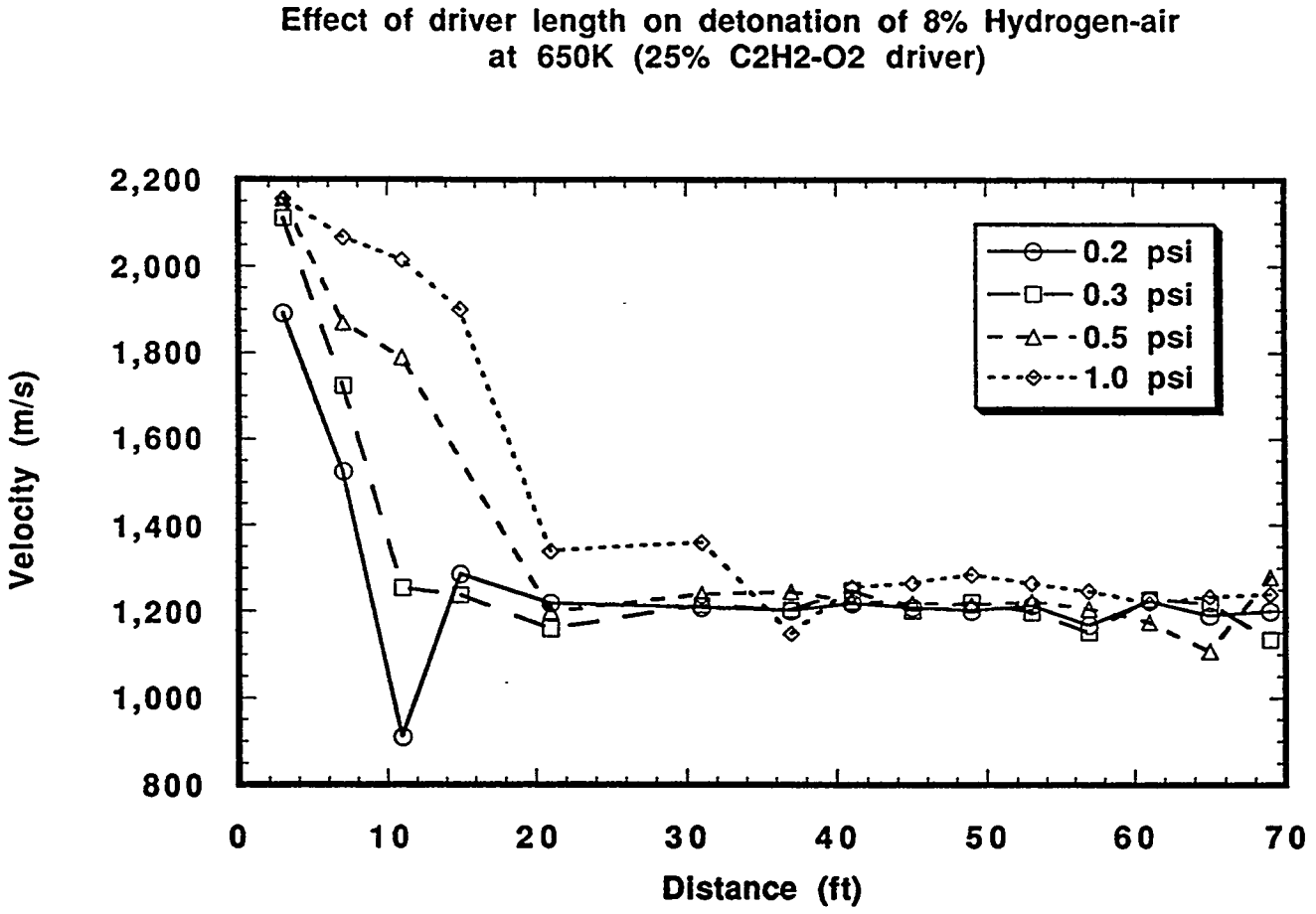

Figure 3: Effect of driver partial pressure (or length) on detonation transmission in an 8 percent hydrogen and 92 percent air mixture at 650K and 0.1 MPa

These experimental findings indicated that the optimum driver conditions for subsequently generating self-sustained detonations in the test gas and for obtaining reliable cell size data are a 0.25-psi driver with a composition of 25 percent acetylene and 75 percent oxygen.

3.2 Detonation Cell Size Measurements

Detonation cell size measurements from smoked foils are presented for hydrogen-air-steam mixtures over a range of initial temperatures and pressures. The cell size data reported are only for detonations that have generated more than three cells across the foil. For detonations generating less than three cells, it is possible that the detonation cellular structure is being influenced by the vessel confinement.

A code, developed by Shepherd (1986), based on the 1-dimensional ZND model of detonation, was used to calculate the thermodynamic structure of the reaction zone and the extent of the fast reactions in these mixtures. The input required by the ZND code is the initial mixture composition and thermodynamic conditions along with the mixture CJ detonation velocity, which is obtained from the equilibrium code STANJAN (Reynolds, 1986). For these tests, the reaction zone length is defined as the distance between the shock wave and the calculated point downstream where the temperature gradient is maximum (i.e., location of maximum energy release rate). The experimentally measured cell size is compared to the predicted cell size derived from the calculated ZND detonation reaction zone length, Δ. The predicted cell size is taken to be proportional to the reaction zone length (i.e., $\lambda = A\Delta$). Other studies have used different definitions for the parameter Δ.

3.2.1 Baseline Experiment at 300K and 0.1 MPa

Figure 4 presents the experimental cell size data from the HTCF as a function of the hydrogen mole fraction, between 15 and 55 percent. Also included in the figure are experimental data from the SSDA (Ciccarelli et al., 1994) and from Sandia's HDT (Tieszen et al., 1987). The plot of cell size versus hydrogen mole fraction results in the classical "U"-shaped curve where the minimum corresponds to the stoichiometric composition. The error bars on some of the SSDA results indicate the standard deviation in the cell size measurements from the smoked foil. The ZND model prediction of cell size, using a proportionality constant of 51 for all the mixtures, is shown as a solid line. The scaling factor was chosen by anchoring the SSDA experimental cell size data to the ZND model prediction at the stoichiometric composition (i.e., 30 percent hydrogen). The apparent agreement between the experimental and the model predictions is deceiving because of the logarithmic scale. Measurements show that the scaling factor is strongly dependent on mixture composition, especially for weaker (below 20 percent hydrogen) mixtures. Further details on the lack of a universal proportionality "constant," A, are given in Ciccarelli et. al. (1996).

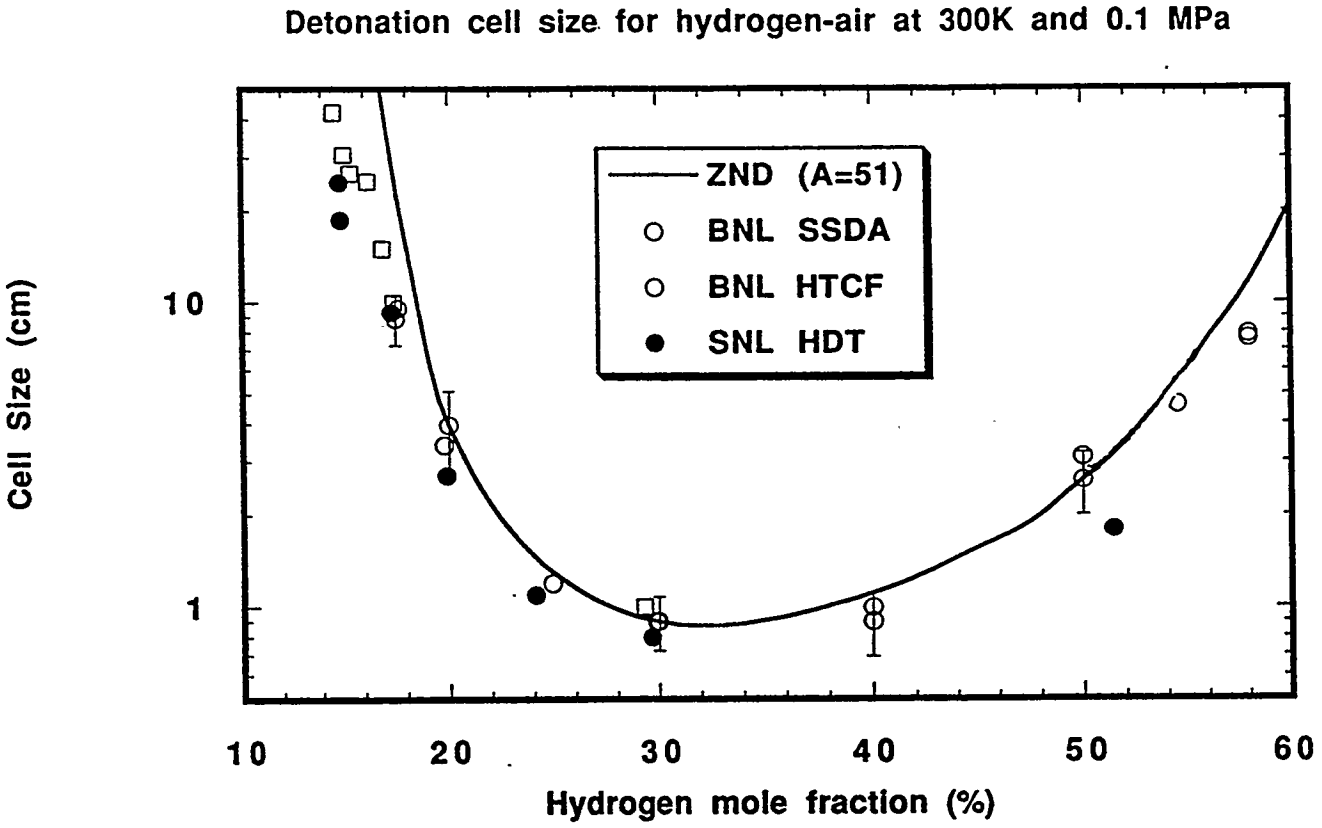

Figure 4: Detonation cell size for hydrogen-air mixtures at 300K and 0.1 MPa

3.2.2 Effect of Initial Mixture Temperature on Cell Size

The effect of temperature on cell size is illustrated in Figure 5, where the 300K data and the 650K data are superimposed. The general trend in the data (i.e., U-shaped curve) at both temperatures is about the same; the only difference is that the 650K curve is much broader than the 300K curve. This plot clearly shows that for a given hydrogen-air mixture, increasing the initial mixture temperature decreases the detonation cell size, especially for lean mixtures. For example, for a 15 percent hydrogen-air mixture, the cell size at 300K is 18.7 cm; and at 650K, the cell size is roughly an order of magnitude smaller (e.g., 1.6 cm). For a 30 percent hydrogen mixture, the effect of raising the temperature from 300K to 650K is to halve the cell size. The other important observation is that increasing the temperature has the effect of widening the detonability limit, i.e., lowering the lean detonability limit.

3.2.3 Effect of Steam Dilution on Cell Size

SSDA data on the effects of steam dilution were extended in the HTCF where sensitive hydrogen-air mixtures could be tested with higher steam dilutions. The HTCF data in conjunction with the SSDA data are shown in Figure 6. The data indicates that for a given mixture temperature, increasing the steam dilution increases the cell size and thus decreases the mixture sensitivity. However, as the mixture temperature is increased, the mitigating effect of steam addition is diminished. At 400K, for example, the maximum mixture steam content that could be tested is 20 percent; and at 650K, mixtures containing up to 40 percent steam resulted in detonations. The experimental data show reasonably good agreement with ZND model predictions with A = 51.

3.3 Deflagration-to-Detonation Transition

Extensive investigations in tubes have shown that the transition from a fast flame to a detonation can occur when the flame accelerates to a velocity equal to the sound speed in the combustion products. If DDT does not occur and the flame propagates at the speed of sound of the products (i.e., product flow is choked relative to flame), the propagation mode is referred to as the "choking" regime. To generate fast flames in a finite length tube, arrays of orifice plates are placed down the length of the tube to promote turbulence in the reactants and thereby enhance the burning process. For the stable propagation of a detonation wave down an obstacle-laden tube, Peraldi et. al. (1986) showed that the free flow diameter must at least accommodate one cell width ($d/\lambda \leq 1$). One of the objectives of this phase of the overall test program was to investigate the effects of initial temperature on the flame acceleration process within the detonation tube.

Flame acceleration and detonation transition tests were conducted in the HTCF at temperatures of: 300K, 400K, 500K, and 650K for lean to stoichiometric hydrogen/air mixtures. Selected tests were also performed with mixtures containing 10 percent and 25 percent steam. Parameters measured allowed for the choking and quasi-detonation limits to be determined as a function of mixture composition and initial temperature. Flame velocities, peak overpressures, and DDT run-up distances were also measured.

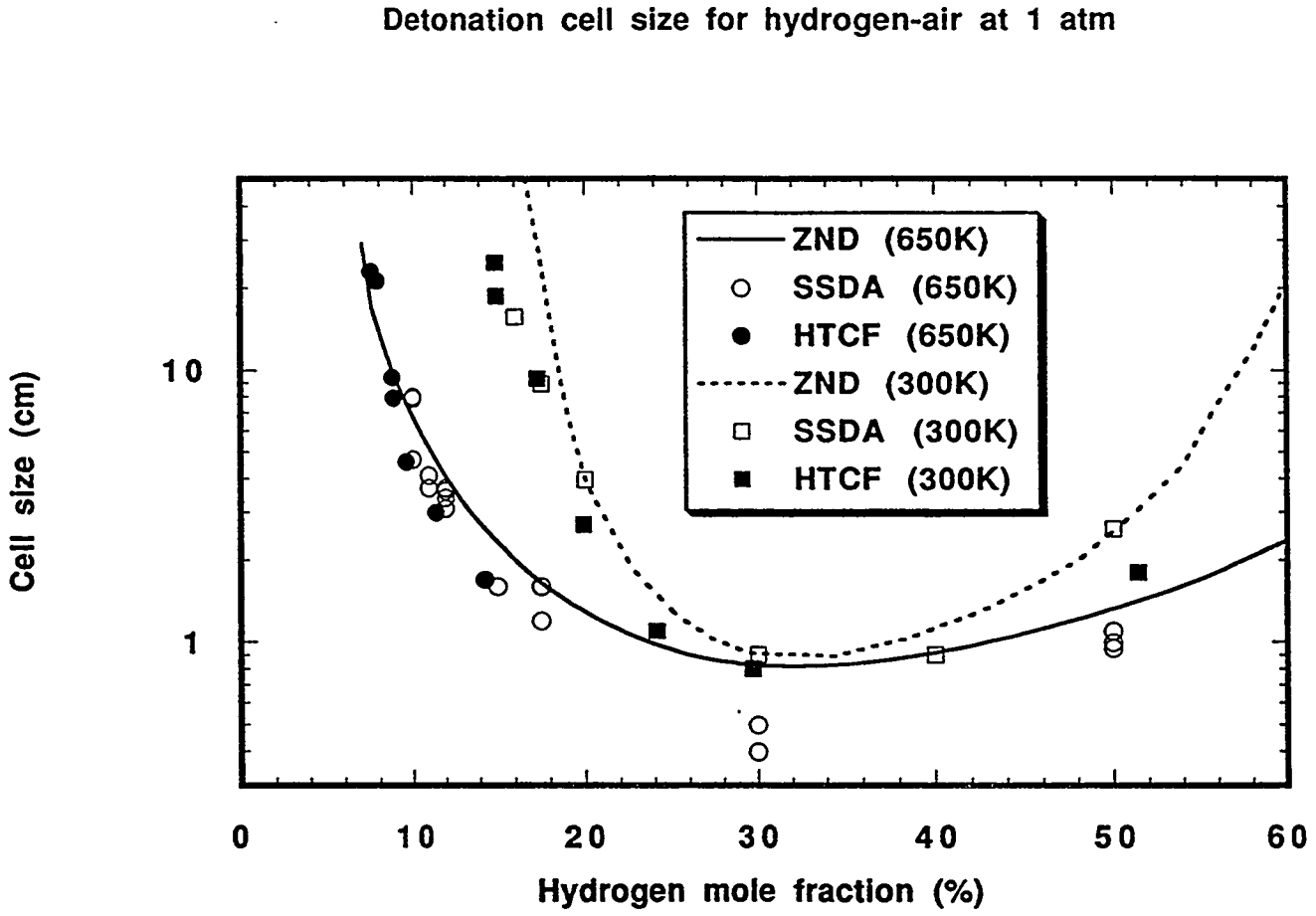

Figure 5: Comparison of detonation cell size for hydrogen-air mixtures at 300K and 650K at 0.1 MPa

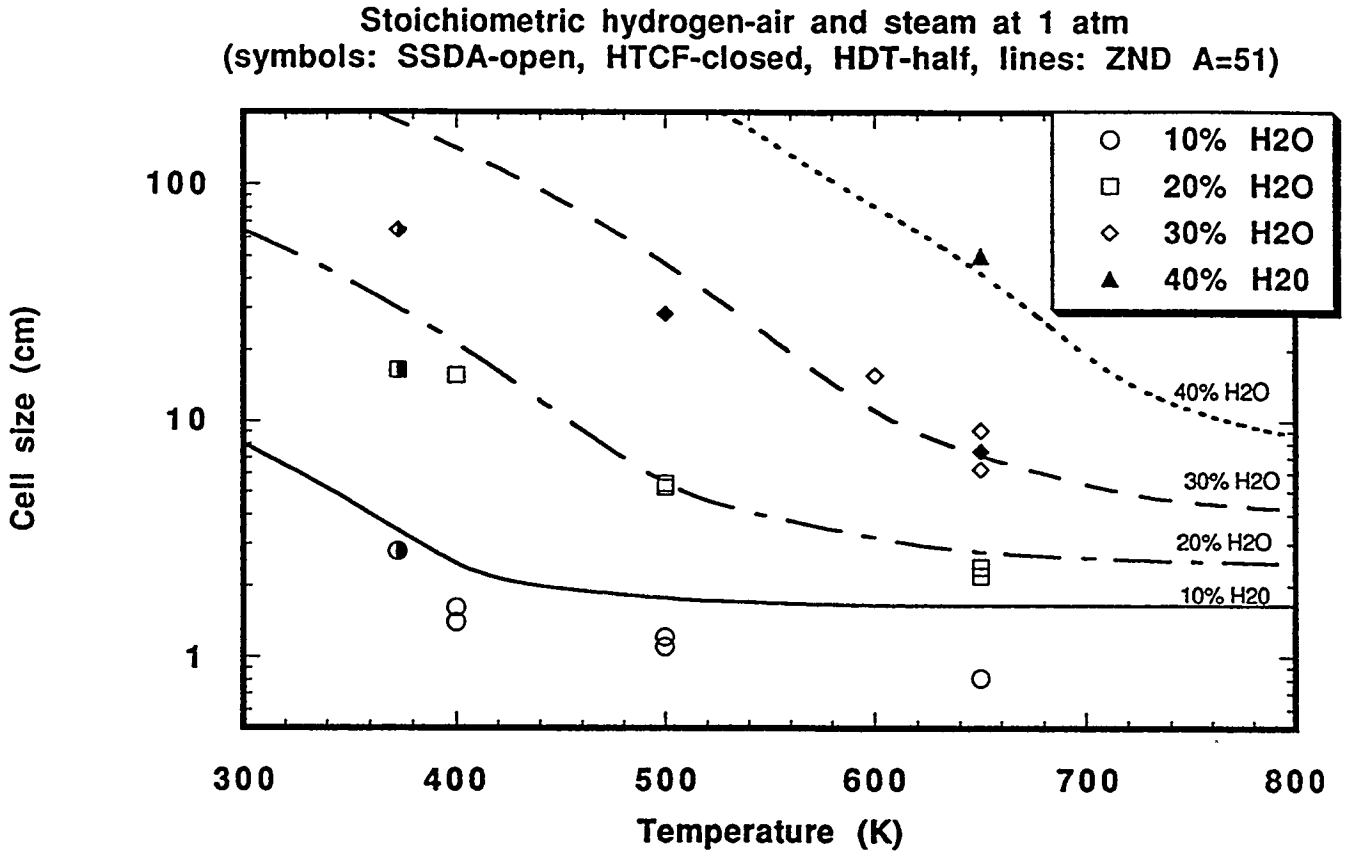

Figure 6: Detonation cell size as a function of temperature for stoichiometric hydrogen-air and steam mixtures at 0.1 MPa

Table 1 summarizes the results of temperature and steam fraction on the two flame acceleration limits. These data were obtained by conducting a series of tests where flame velocities were measured for a prescribed initial temperature and composition. Figures 7 and 8 typify the trends in measured flame velocity versus gas composition for tests conducted at 300K and 650K, respectively. Also indicated are the gas compositions where the flame speed is just above the isobaric sound speed of the combustion products and the calculated CJ detonation velocities. Figure 9 presents similiar data for tests conducted at 400K and 10 percent steam.

Further details on this phase of the High-Temperature, High-Speed Combustion Program can be found in Ciccarelli et. al. (1996).

4 SUMMARY AND CONCLUSIONS

For any hydrogen-air-steam mixture, cell size measurements have shown that increasing the initial mixture temperature in the range of 300K to 650K while maintaining the initial pressure of 0.1 MPa decreases the cell size and thus makes the mixture more sensitive. In the HTCF, the effect of steam dilution on cell size was tested in stoichiometric and off-stoichiometric (e.g., 18 percent hydrogen) hydrogen-air mixtures. Increasing the steam dilution (or partial pressure) in hydrogen-air mixtures at 0.1 MPa initial pressure increases the cell size and thus decreases the mixture sensitivity, irrespective of initial temperature. It was also observed that the desensitizing effect of steam on hydrogen-air detonability diminished with increased initial temperature. The maximum steam dilution resulting in a detonation was 50 percent steam in a stoichiometric hydrogen-air mixture at 650K and 0.1 MPa. Although not shown in this paper, a limited number of experiments were carried out to investigate the influence of initial mixture pressure on detonation cell size. There was very little effect observed in the pressure range tested, 0.1 MPa to 0.24 MPa, for relatively weak hydrogen-air-steam mixtures. It can be shown that the minimal sensitivity to pressure is also predicted by the ZND model.

A 1-dimensional, steady-state ZND model, with full chemical kinetics, has been used to predict cell size for hydrogen-air-steam mixtures at different initial conditions. The cell size is taken to be proportional to the calculated ZND reaction zone length ($\lambda = A\,\Delta$). Taking A to be a constant, the ZND model did a relatively good job at predicting the overall trends in the cell size data as a function of mixture composition and initial conditions. However, a comprehensive comparison of the theoretical predictions with the experimentally measured cell size has demonstrated that the two are not linked by a simple constant of proportionality, A. In this investigation, it has been shown that A is also a function of the initial mixture temperature, such that $\lambda = A(\phi, T_o)\Delta$.

Evaluations of the flame propagation regimes for these conditions and for the HTCF also indicate that cell size alone does not dictate the DDT limit.

TABLE 1

Flame Acceleration Limits for Hydrogen-Air Mixtures Without Venting

Temp (K)	Choking Limit	DDT Limits	
	% H2	% H2	d/λ
300	11	15	1.0
500	8	12	1.5
650	11	11	5.5

Flame Acceleration Limits for Hydrogen-Air-Steam Mixtures Without Venting

Temp (K)	% Steam	Choking Limit	DDT Limits	
		% H2	% H2	d/λ
400	10	12	18	0.7
500	25	14	24	1.5
650	25	16	19	0.8

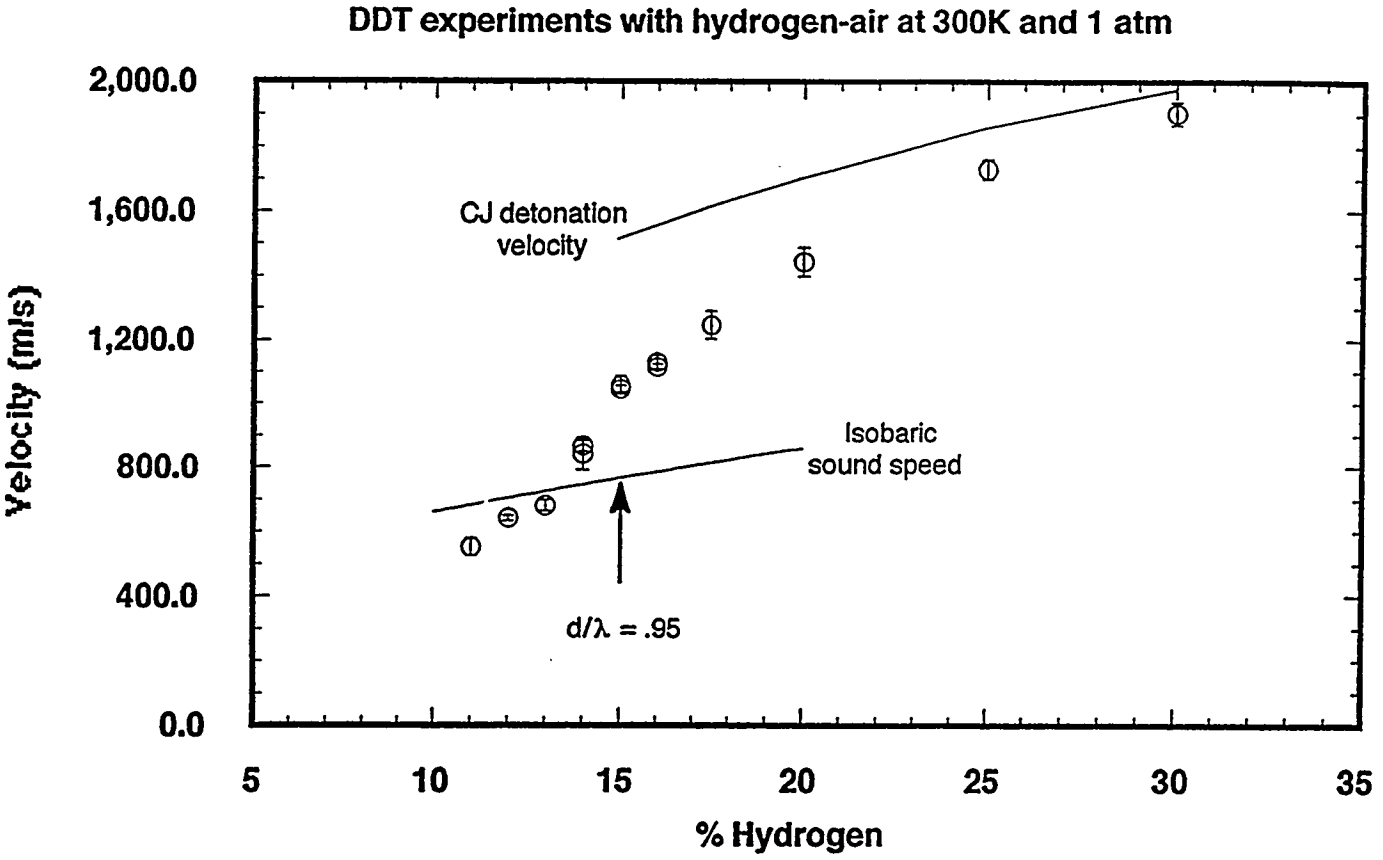

Figure 7: Measured flame velocity vs. gas composition for tests conducted at 300K

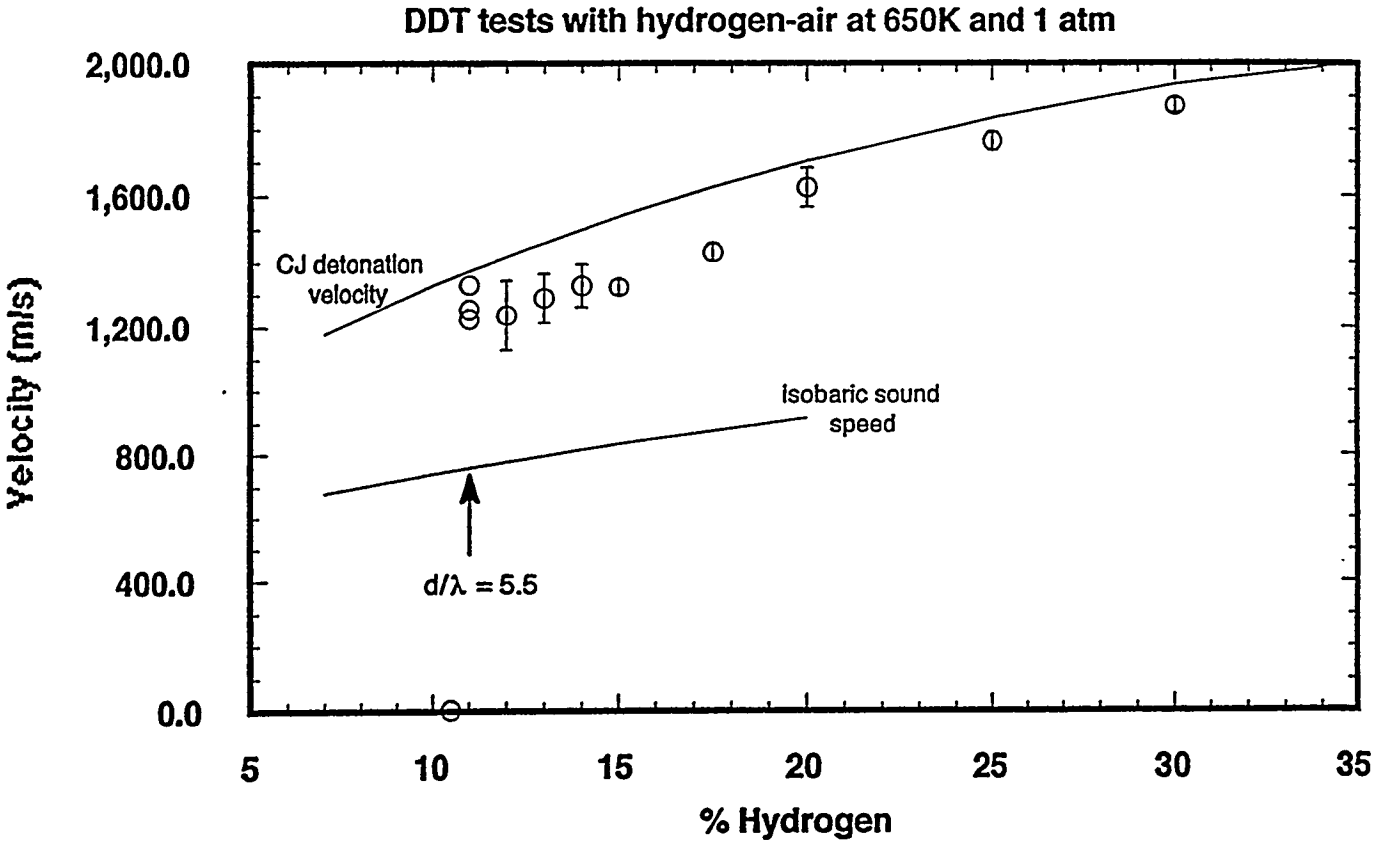

Figure 8: Measured flame velocity vs. gas composition for tests conducted at 650K

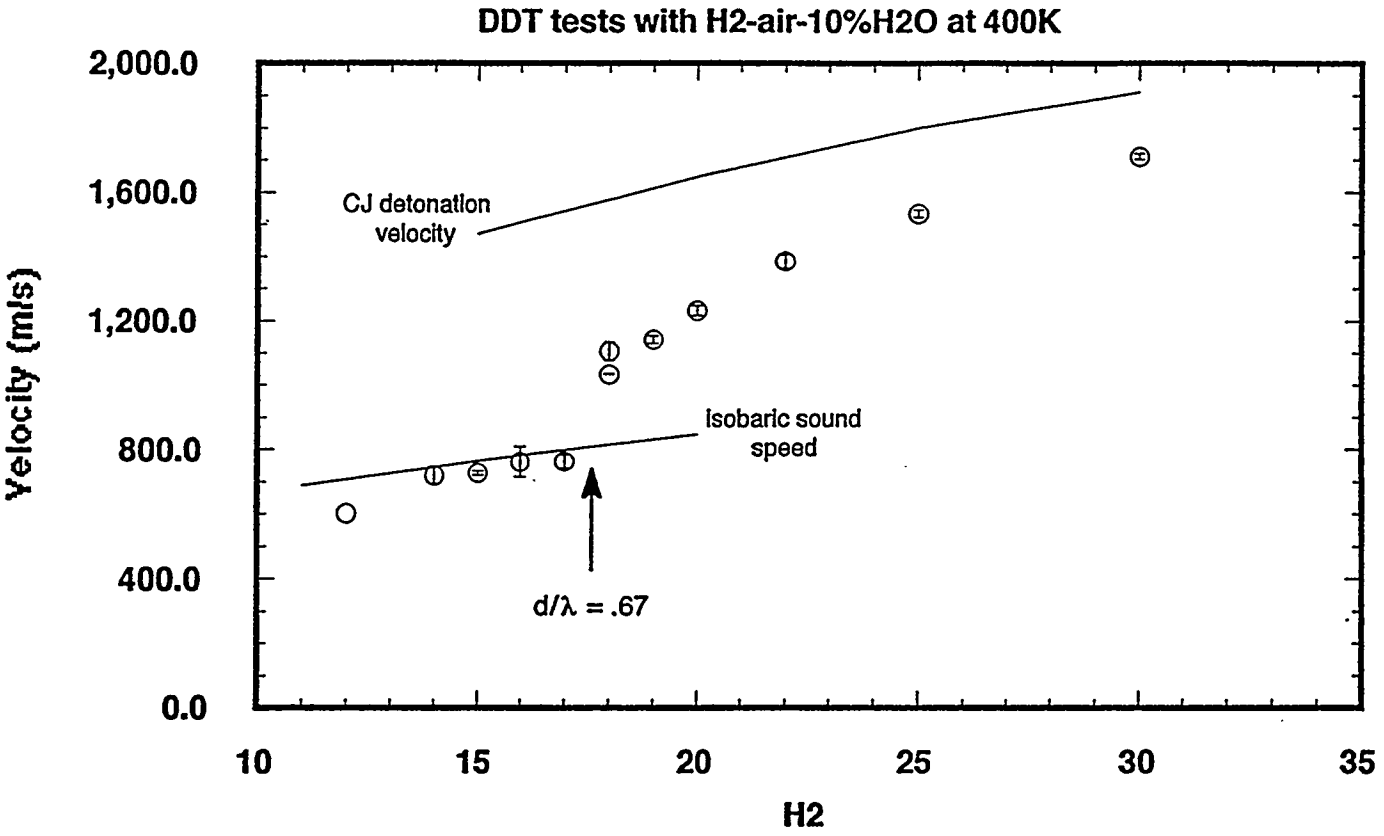

Figure 9: Measured flame velocity vs. gas composition for tests conducted at 400K and 10 percent steam

5 REFERENCES

Ciccarelli, G., et al., "High-Temperature Hydrogen-Air-Steam Detonation Experiments in the BNL SSDA," NUREG/CR-6213, BNL-NUREG-52414, 1994.

Ciccarelli, G., et al., "Detonation Cell Size Measurements and Predictions in Hydrogen-Air-Steam Mixtures at Elevated Temperatures," Combustion and Flame, 99, pp. 212-220, 1994b.

Ciccarelli, G., et al., "Detonation Cell Size Measurements in High-Temperature Hydrogen-Air-Steam Mixtures at the BNL High-Temperature Combustion Facility," NUREG/CR-6391, BNL-NUREG-52482, to be published, 1996.

Ciccarelli, G., et al., "Effect of Temperature on DDT Phenomena: Part 1- No Venting," to be published as NUREG/CR, 1996.

Peraldi, O., et al., "Criteria for Transition to Detonation in Tubes," 21st Symposium (International) on Combustion, The Combustion Institute, Pittsburgh, PA, 1986.

Shepherd, J. E., "Chemical Kinetics of Hydrogen-Air-Diluent Detonations," Progress in Astronautics and Aeronautics, 106, Dynamics of Explosions, J. R. Bowen, et al., eds., 1986.

Stamps, D. W., and S. R. Tieszen, "The Influence of Initial Pressure and Temperature on Hydrogen-Air-Diluent Detonations," Combustion and Flame, Vol. 83, pp. 353-364, 1991.

Reynolds, W. C., "The Element Potential Method for Chemical Equilibrium Analysis: Implementation in the Interactive Program STANJAN Version 3," Dept. Of Mechanical Engineering, Stanford University, Palo Alto, California, January 1986.

Tieszen, S. R., P. S. Martin, W. B. Bennedick, M. Berman, "Detonability in Hydrogen-Air-Diluent Mixtures," NUREG/CR-4905, SAND85-1263, 1987.

Yang, J. W., "High-Temperature Combustion in LWR Containments Under Severe Accident Conditions," Brookhaven National Laboratory, Technical Report L-1924 1/17/92, January 1992.

APPENDIX

SALIENT FEATURES OF THE HTCF

The High-Temperature Combustion Facility (HTCF) was designed and constructed with the objective of studying detonation phenomena in mixtures of hydrogen-air-steam at initially high temperatures. The central element of the HTCF is a 27-cm inner-diameter, 21.3-m long cylindrical test vessel capable of being heating to 700K ± 14K. A unique feature of the HTCF is the "diaphragmless" acetylene-oxygen gas driver which is used to initiate the detonation in the test gas.

Gas Driver Detonation System

A gas driver system is used to initiate the detonation in the HTCF test vessel. The concept, similar to that used in the SSDA, is to produce a short slug of acetylene-oxygen mixture at one end of the vessel and initiate a detonation in this mixture using an "exploding wire." The detonation from the driver gas slug is then transmitted into the test gas. For tests at elevated temperature, the driver section (i.e., the first 3.05-m long test vessel section) is unheated so that the acetylene-oxygen mixture does not burn upon injection.

The driver gas plumbing and the high-voltage trigger circuit used for the exploding wire can be seen in the foreground in the photograph in Figure 1. The acetylene-oxygen mixture is injected into the vessel via a sparger system consisting of four equally spaced perforated tubes. The driver gas composition can be varied either by the needle valves or by the bottle regulator delivery pressure. The acetylene and oxygen are mixed by flowing the two gases co-axially into a manifold chamber and then into the four sparger tubes, which penetrate 10 cm into the vessel through the endplate. The four tubes enter the vessel at equally spaced radial positions just inside the vessel inner-wall. Each tube is oriented to direct the oxyacetylene gas inwards toward the vessel centerline.

The detonation in the acetylene-oxygen driver is initiated by the shock wave produced by an exploding wire. The exploding wire is a fine copper wire fastened between two electrodes, mounted onto an instrumentation plug that protrudes into the center of test vessel through the driver endplate. The wire is made to explode by passing a large current through it, derived by shorting a 20-microfarad, 7.5-KV capacitor.

Heating System

The heating system was designed, manufactured, and installed by Cooperheat Inc. of Piscataway, New Jersey. The assembled, insulated test vessels are each capable of being heated to the maximum operating temperature of 700K in four hours.

The heating system is segmented into three major components, consisting of the heating elements, the power control unit, and a remote control unit. The remote control unit

houses two multi-zone PID temperature controllers which are adjusted through a computer located in the control room. This control unit is also the terminal for all the control zone thermocouples on the test vessel. The power control unit distributes the power to the various heating zones on the vessel. Each test vessel has a mounted junction box where the power cables enter and are terminated at a power distribution block. The heater element leads hang below the vessel and are connected to the appropriate power distribution block.

The heating elements, which are mounted directly on the vessel, are resistance wires woven into a ceramic pad that are fastened to the vessel using stainless-steel pipe clamps. The heater pads were custom designed to give maximum heater coverage on each test vessel section. The entire vessel is covered with two layers of 2.54-cm thick Kaowool insulation blankets. A typical 3.05-m long vessel pipe section has three heating zones which can be controlled independently, and each flange pair also has its own heating zone yielding a total of 29 heating zones for the entire vessel.

Instrumentation

The instrumentation used in the present experiments are identical to those used in the SSDA (Ciccarelli, 1994). Test gas thermodynamic conditions, such as temperature, pressure, and mixture composition, are all monitored and logged before a detonation is initiated. Standard K-type, exposed junction probe thermocouples with an accuracy of 1.2K are used to monitor the gas temperature. The vessel pressure is monitored using a strain gage Wika pressure transducers having an operating range of 0 to 0.34 MPa absolute with an accuracy of 0.1 percent of full scale. The flow rates in the test gas constituents are determined by fixing the upstream pressure in each of the choked Fox venturis. The Fox venturis have a manufacturer's quoted accuracy of 2 percent. Three gas samples are taken from the vessel, using pre-evacuated 150-ml gas cylinders, before each test. After the test, the samples are then analyzed as a further check on hydrogen content using a gas chromatograph (Carle Model 311H). The gas chromatograph is periodically calibrated using hydrogen gas standards with an accuracy of 2 percent. For tests with steam, the venturi mass flow rate is used to back out the steam content. Steam is provided through a 24kW Reimers boiler that can deliver 100 psig, saturated steam at 81 lbm/hr.

Detonation pressure is measured using fast-response PCB 113A24 quartz piezoelectric pressure transducers. Due to the high-temperature environment, the transducers are housed in special water-cooled adaptors. These transducers have a maximum pressure range of 6.8 MPa with a rise time of 1 μs. The accuracy of the transducer is less than 1 percent of full scale. Time-of-arrival of the flame or detonation front is measured using ionization probes. These probes consist of two electrodes which penetrate about 1.27 cm into the vessel. The electrodes are connected to a simple circuit which outputs a voltage signal when the electrodes are shorted by the passage of the reaction zone. The time-of-arrival is used in conjunction with probe spacing to determine the average detonation or flame velocity. For relatively low-speed flames, the output of thermocouples is also used to estimate the flame velocity.

Detonation cell size is measured using the "smoked-foil" technique. Aluminum foils are used, typically 2-m long, 0.5-mm thick, which when shaped into a cylinder can cover almost the entire vessel inner-wall. The foil ends were riveted to 3-mm thick, 5-cm wide steel rings placed on the inside of the foil for added strength. The inside of the foil is smoked after the rings are mounted. The cylindrically shaped foil is placed upright on one end, and a kerosene lamp is burned inside. The foil is sooted incrementally from the bottom to the top in sections roughly 30-cm high. As discovered from the SSDA tests, for experiments at elevated temperature, the best results were obtained when the foil was first coated with a very thin layer of silicone fluid before smoking.

Data Acquisition and Control

All data acquisition and control equipment is located in the control room. A 486 Gateway PC equipped with several commercially available Strawberry Tree data acquisition and control cards and software are used to run the experiments from the control room. Three ACPC 12-bit analog input cards (16 channels each) are used for monitoring pressure transducer and thermocouple signals. One ACPC digital input/output card (40 channels) is used for actuating valves and monitoring limit switches. One ACAO 12-bit analog output card (6 channels) is used to feed the set points to the three PID pressure regulators. A Personal 488 card is also installed to provide GPIB capabilities to the system. The cards are driven by an icon-based Strawberry Tree program called Workbench.

Two 100-MHZ, 4-channel LeCroy 314L digital oscilloscopes are used to capture the high-speed output signals from the piezoelectric pressure transducers and the ionization probes. Hard copies of the oscilloscope signals were made after each experiment.

RECENT EXPERIMENTAL AND ANALYTICAL RESULTS ON HYDROGEN COMBUSTION AT RRC "KURCHATOV INSTITUTE"*

S. B. Dorofeev, A. A. Efimenko, A. S. Kochurko, V. P. Sidorov

Russian Research Centre "Kurchatov Institute", Moscow, 123182, Russia

ABSTRACT

A review of hydrogen combustion research at Kurchatov Institute is presented. Criterion for spontaneous detonation onset possibility and its application to severe accidents in a nuclear power plant is discussed. Theoretical and experimental results on spontaneous detonation onset conditions are summarized. Three series of large scale turbulent jet initiation experiments have been carried out in KOPER facility (50 m3 and 150 m3). Series of jet initiation experiments in initially confined H2 - air mixtures have been carried out in KOPER facility (20 - 46 m3). Turbulent deflagration/DDT experiments were carried out in large scale confined volume of 480 m3 in RUT facility. Results showed, that the characteristic volume size should be used for conservative estimates in accident analysis. Series of experiments on detonation transition from one mixture to another of lower sensitivity has been carried in DRIVER facility. The experiments were aimed on the estimation of the minimum size of a detonation kernel. The received results are in a good agreement with the 7 cell width criterion. Results of combined hydrogen injection/ignition experiments are presented. The experiments are aimed on the investigation of possible consequences of deliberate ignition at dynamic conditions. Analysis of the experimental data showed applicability of 7 cell width criterion to dynamic conditions. .The sum of the results on the scaling of spontaneous detonations is discussed in connection with the strategy of hydrogen mitigation at severe accidents.

INTRODUCTION

Hydrogen release to the containment of nuclear power plant can be expected during severe accidents. Containment compartments contain air, which can be mixed with hydrogen forming a combustible mixture. Many potential ignition sources can be found in a containment in the course of severe accidents. That is why hydrogen combustion or explosion events are likely and can result in loading of the containment and its internal structures.

Different measures to mitigate hydrogen explosion hazard are discussed with the following main approaches. The first is an appropriate design of a containment which should be strong enough against loads from hydrogen combustion. This way cannot be thoroughly applied for existing plants. The second is inertization of containment atmosphere, which means, that oxygen should be removed from containment, and no combustion would be possible. Compete inertization resolves the hydrogen problem, but only partial inertization can really be discussed. The third way is a deliberate ignition of hydrogen-air-steam mixtures in order to avoid accumulation of dangerous hydrogen concentrations. Deliberate ignition, however, does not exclude a combustion event and corresponding loading to a

* Research sponsored by US NRC and Forschungszentrum Karlsruhe, Germany.

containment. The forth option is catalytic hydrogen recombination. Hydrogen source and consumption are distant in this case, and hydrogen combustion cannot be excluded.

The above examples show that there is no simple and universal engineering decision of the hydrogen problem. All possible scenarios of severe accidents cannot be studied experimentally. It is impossible, also, to run full scale experiments. At the same time corresponding mitigation measures have to be qualified. These are the reasons for continuing studies of hydrogen combustion phenomena relevant to severe accident conditions.

Hydrogen combustion research program at RRC "Kurchatov Institute" includes description of different combustion regimes, their threshold conditions, and loads. Slow deflagrations, accelerated flames and fast turbulent deflagrations, deflagration to detonation transition (DDT), local and global detonations are analyzed. Loads from these combustion modes are studied. Threshold conditions between slow combustion and explosion regimes (local and global detonations) and their scaling are analyzed. The objective of the research program is to elaborate corresponding numerical and analytical tools appropriately validated against experimental data.

Considerable progress has been made earlier in the description of the loads from different combustion and explosion modes[1-4]. The results have shown that local and global detonations and DDT events are capable to produce the most severe loads to the containment and its internal structures. Although the description of loads from fast turbulent deflagrations and transient explosion processes needs to be improved, the most important issue for safety analysis is the description of conditions for spontaneous detonations and scaling of these conditions. The purpose of the present paper is to describe the results obtained on the scaling of spontaneous detonations and to discuss their application for safety analysis.

SCALING OF SPONTANEOUS DETONATIONS

No satisfactory model is presently available that is capable of accurately predicting a complete flame acceleration and transition to detonation event. Numerical studies are difficult because they should include the computation of unsteady, turbulent, multidimensional, compressible reacting flows. A wide range of spatial and temporal scales exists in both the chemistry and fluid dynamics of these flows. Obviously, numerical simulation of the complete DDT process requires excessive computing resources and is not really practical at present.

Different modes of the onset of spontaneous detonation can be expected in severe accident conditions. In addition to DDT, these are turbulent jet initiation, and reflection of pressure waves. If scale limitations for the onset of a detonation can be found, they should control all these modes of initiation. The analysis of the effect of scale is important as a first step in this complicated problem. Numerous experimental data on detonation properties[6-8], and experimental results on detonation onset conditions[9-18] have been accumulated. These data can be useful for the analysis of the effect of scale.

Effect of scale on the onset of detonation

The processes of spontaneous initiation of a detonation can be divided into two separate phases: (1) the creation of conditions for the onset of detonation by processes of flame acceleration, vorticity production, and formation of jets; (2) the actual formation of the detonation wave itself. Processes in the first phase are scale dependent. They are particular to the specific initial and boundary conditions of the problem. However, the actual formation of the detonation appears to be the more universal problem. It is this phase, which can impose final scale limitations, that is addressed in the following discussion.

The second phase begins with the general situation of a sensitized volume of partially reacted and/or compressed gas surrounding autoignition centers. Different experimental observations indicate that

detonation is achieved through the formation of localized explosions, amplification of the pressure wave from these explosions, and finally through the transmission of the detonation complex from the sensitized to the unperturbed part of the mixture. This process is very complicated and numerous details can effect the chance of a detonation occurring. Different physical mechanisms are involved in the above sequence of events. Triggering of the localized explosions are discussed thoroughly by Urtiew and Oppenheim[19]. Lee's SWACER - mechanism (Shock Wave Amplification by Coherent Energy Release)[20] and the associated concept of Zel'dovich et al.[21] can describe amplification of the pressure wave. Triggering of the transverse wave structure is also of great importance.

At the same time, some global view of the problem seems possible. If all necessary conditions are fulfilled and a complex of a strong shock and reaction front is formed, the resultant wave has to pass from a preconditioned, sensitive mixture to the unperturbed mixture. During this process, the characteristic width of the reaction zone should grow continuously with decrease in the reaction rate. Increasing portions of reactants should be heated by the leading shock. Associated energy losses can be responsible for the failure of the wave. An additional interfering factor is the losses caused by continuous diffraction of the wave in the case of expanding waves. Both factors require a sufficiently large size of the preconditioned mixture for the transmission of a detonation. This minimum size can be defined for the one-dimensional problem, without expansion.

Following the above considerations it is possible to find a link between mixture composition and the minimum size of the preconditioned mixture that would allow creation of a detonation. This minimum size, L_m, would depend on the mixture properties. The question is what minimum volume of the preconditioned mixture should be created in order that a local explosion can result in a detonation? This scale limitation, representing the necessary condition, should be considered along with other necessary requirements.

Numerical Modeling of Detonation Self-Initiation

With the aim of evaluating detonation onset conditions, numerical modeling of the self-initiation phase has been undertaken[22, 23]. Two different problems have been considered. The first was detonation initiation via autoignition of locally nonuniform mixtures and pressure wave amplification (SWACER or "gradient" initiation mechanism). Initial nonuniformities were formed by spatial temperature distributions and distributions of an additional active chemical component. The second was the problem of detonation transmission through a mixture with decreasing reaction rate.

Finite-difference models for unsteady, multidimensional, inviscid, compressible reacting flow based on the conservation equations of mass, momentum, and energy in lagrangean and eulerian representations were used[1]. Calculations were for ideal gas equations of state (individually for products and reactants) and a one-step Arrhenius chemical kinetic model. Two-dimensional and three-dimensional versions of the codes were used first to determine the mixture properties (detonation cell width, blast initiation energy). Parameters were chosen to simulate two mixtures of different kinetics, with regular and irregular cellular structures. Corresponding dimensionless effective activation energies E_a/RT_{vn} used were 5.7 and 10.5 (T_{vn} - von-Neumann temperature, R - gas constant). The same numerical models were applied to study mixtures with one-dimensional (planar and spherical) nonuniformities.

In the SWACER problem, the minimum nonuniformity length allowing detonation formation beyond a sensitized region has been studied[22, 23]. Shapes of the nonuniformities have been varied. The results have shown that detonation initiation is much more difficult in the cases of divergent waves (spherical symmetry) and temperature distributions. The minimum characteristic nonuniformity size has been found to be at least 7 cell width of the unperturbed mixture. The results have shown also that the possibility of detonation initiation is strongly affected by the phase of wave transition to the unperturbed mixture.

The problem of detonation transition has been considered individually in an one-dimensional planar case[23]. A small high-pressure region was used to initiate the detonation wave. This passed through the region of decreasing reaction rate, which was varied by changing the dependence of the cell length versus distance. The possibility of detonation propagation and transmission to the ambient mixture was studied in a number of calculations. It has been found that both the results of SWACER modeling and transition study give similar values for the minimum nonuniformity size required for the onset of spontaneous detonation.

Analytical 1D consideration of the critical conditions for detonation propagation through sensitivity gradient[24] have shown that the critical gradient expressed in terms of characteristic reaction zone width l_r is given by $dR/dl_r \approx \alpha\cdot(E_a/RT_{vn} - 1/2)$, where α is a constant depending on specific heat ratios of products and reactants. For the mixture model used in numerical simulation of the transmission problem $\alpha \approx 30$, $l_r \approx \lambda/20$, $E_a/RT_{vn} \approx 5.7$, and critical gradient appeared to be $R/\lambda \approx 7$. This is in accord with the results obtained numerically. In addition, the difference in critical conditions found for $E_a/RT_{vn} \approx 5.7$ and $E_a/RT_{vn} \approx 10.5$ corresponds to the function of critical gradient on E_a/RT_{vn}.

The minimum scale requirements for detonation formation found out in the calculations can be estimated as 7λ in terms of the cell width beyond the sensitized region[23, 25]. This estimation corresponds to the planar case, optimum shape and nature of the nonuniformity. In the case of expanding waves (spherical symmetry), the minimum scale of nonuniformity should be increased due to additional requirements for the minimum curvature of the wave. The results also indicate that the minimum scale requirement is a function of the effective activation energy of the chemical reaction rate, but this function seems to be not strong enough to change the order of magnitude. Although 1D modeling cannot take into account some essential features of detonations, and the cell size is not enough to characterize the mixture sensitivity, the estimate obtained indicates an importance of scale for spontaneous detonation possibility.

APPLICATIONS TO SEVERE ACCIDENTS

Hydrogen Accumulation and Combustion

Table 1 illustrates qualitatively main possible ways of hydrogen accumulation and combustion during severe accidents.

Table 1
Local and Global Combustion Events

Steam condensation in H_2/air/steam atmosphere	H_2/steam (H_2) injection into air/steam atmosphere	
Slow increase of H_2 concentration in compartments and containment dome	Slow H_2 accumulation in compartments far away from the release point	Relatively fast H_2 accumulation near the break
Premixed initial conditions. Combustible mixture occupies several compartments		Dynamic initial conditions
Global combustion events		Transient or local combustion
FLAME, Battelle, HDR, BNL, Surtsey, KOPER, RUT(premixed) experiments and analysis		RUT dynamic injection experiments

Formation of a combustible mixture in compartments of a containment can result from steam condensation in hydrogen-air-steam mixture, or from injection of hydrogen (H_2-steam) mixture into air-steam atmosphere. In the first case, slow increase of H_2 concentration is expected in compartments and containment dome. In the second case, analogous slow accumulation of H_2 is expected in compartments far away from the release point. Relatively fast accumulation of hydrogen takes place near the break. If the increase of hydrogen concentration is slow, several compartments are occupied by premixed combustible mixture. A combustion of such a mixture can take place as a "global combustion event". If the increase of hydrogen concentration is fast (near the break), dynamic, non-premixed initial conditions are formed. Transient or "local combustion events" can be expected in this case. Most of the studies on hydrogen combustion behavior have been carried out for premixed initial conditions, which are typical for global combustion events. Dynamic conditions were studied in the RUT hydrogen injection/ignition experiments.

Global Combustion Events

The minimum scale requirement for the onset of a detonation gives a basis for the comparison of different experimental results in the case of premixed initial conditions. Such a comparison is presented in Fig. 1, in the form of a correlation of nonuniformity size, L, and the detonation cell width, λ. Experimental results on both detonation initiation by a turbulent jet of hot combustion products and the results on deflagration to detonation transition in large volumes have been collected. Experimental data on cell width[6, 7] were used. For the turbulent jet initiation experiments, the jet orifice diameter was used as a characteristic size, L. For DDT experiments, this becomes the size of the volume, which controls the possible macroscopic nonuniformity size. The results of the RUT premixed DDT experiments represent the largest scale and the least sensitive mixtures. The line represents the scale limitation, $L_m \approx 7\lambda$, described in the previous section.

Because the scale limitation represents the necessary (not sufficient) condition, no sharp demarcation is to be expected between "go" and "no-go" experiments shown in Fig. 1. For initial conditions corresponding to the lower part of Fig. 1 (below the line), the minimum scale requirement is satisfied, but this does not mean that detonations must be initiated. Other conditions concerning the early stages of the DDT must also be met. A more important point is that a detonation would not be expected in the upper part of Fig. 1, due to the scale limitation.

The accuracy of the cell width data is within a factor of 2 or so. The possible characteristic sizes, L, of a sensitized mixture have been approximately estimated from the experimental conditions. The minimum scale requirement $L_m \approx 7\lambda$ itself gives the order of magnitude. Nevertheless, the data of Fig. 1 with the variables ranging from millimeters to meters show clearly the effect of scale within these limits of accuracy. The proposed scale limitation $L_m \approx 7\lambda$ is in a good agreement with the experimental results, over a wide range of volumes and mixture compositions.

Another point concerns the use of the cell width to characterize a mixture sensitivity. Clearly, the cell width cannot be considered as a fundamental or reliable scaling parameter. Unfortunately, other parameters, such as the critical exit diameter or experimental ignition delays behind a shock wave, are not presently available for many mixtures and compositions. Possibly, computed reaction zone widths could principally be used for such a correlation. It may be that a single parameter is insufficient to characterize the sensitivity of a mixture to detonation. An example is that many relationships based on cell widths fail with changes in cellular structure regularity. The more surprising is the good agreement observed in Fig. 1. One reason may be that all the data shown are for the mixtures which have, more or less, the same type of irregular cellular structure. Small changes of effective activation energy do not significantly alter the minimum scale requirement[24]. The same correlation, however, does not seem to be

applicable for highly argon diluted mixtures. In spite of the obvious limitations of the cell width scaling, it is this condition $L_m \approx 7\lambda$ that has been used to define the mixture compositions for the given geometry of the RUT facility in the premixed DDT tests. It has been estimated that 12.5% H_2 should be the critical composition for the RUT scale. The tests started with this composition and the results have confirmed this expectation.

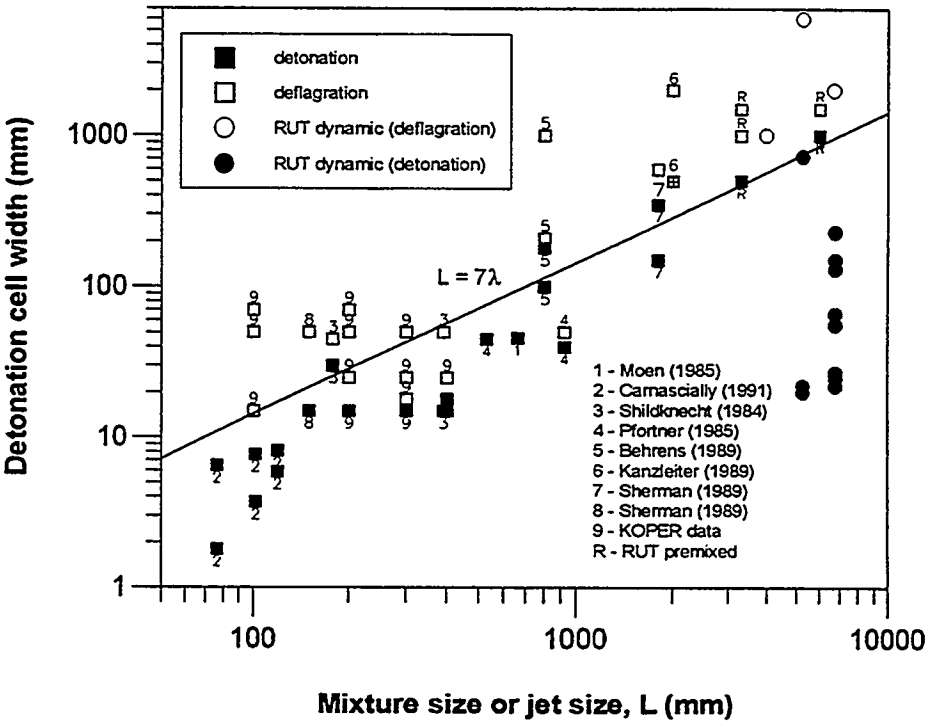

Figure 1. Experimental data on turbulent jet initiation and DDT in large confined volumes

Dynamic H_2 Injection/Ignition Experiments

Series of experiments with dynamic hydrogen injection and spark ignition have been carried out in the RUT facility. The objective of the tests was to study possible consequences of deliberate ignition in dynamic conditions. The scheme of the facility is presented in Fig. 2. Experimental variables were igniter location, ignition, time injection rate and location.

Experimental conditions. Initial volume of the enclosure was 310 m^3. Hydrogen injection rates were 0.6 - 1 kg/s, and 0.1 - 0.18 kg/s. Two different injection locations were used. The direction of hydrogen injection is shown in Fig. 2. Ignition was made by one electric spark operating at 0.1 Hz, and 1 Hz. The location of the igniter was varied. Distances from the injection point and igniter were approximately 5, 10, 15, and 20 m. The corresponding locations are shown in Fig. 2.

Experimental results. In the dynamic tests, hydrogen cloud was formed moving to the igniter position. Ignition occurred when the cloud boundary reached the igniter. For upper injection location much more hydrogen was accumulated in the cloud, than that for upward directed lower injection. Mean hydrogen concentration in the cloud was high enough to result in DDT for the upper location of H_2 injection. Fig. 3 shows flame propagation and transition to detonation for tests with upper location of hydrogen injection. Transition to detonation resulted in a high level of overpressures recorded inside enclosure. An example is shown in Fig. 4.

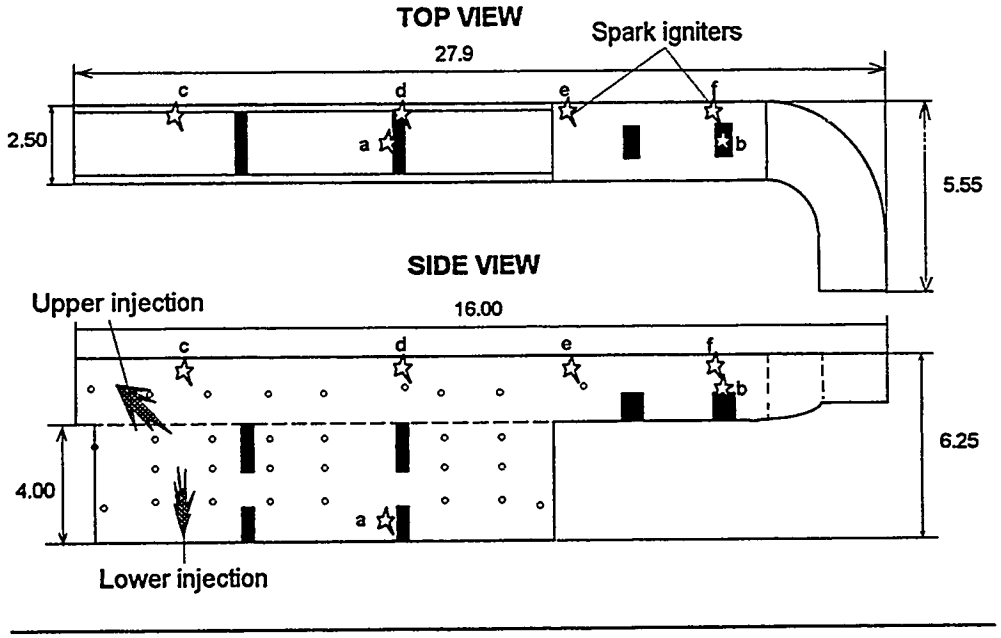

Figure 2. Scheme of RUT facility

Upward directed lower hydrogen injection resulted in early ignition of the hydrogen-air cloud. Hydrogen was distributed mostly near the ceiling of the enclosure. Hydrogen concentrations in the cloud were about 10% vol. or less. Ignition resulted in slow deflagrations (Fig. 5) generating low level overpressures (Fig. 6). The greater was the distance between injection and ignition points, the higher was the overpressure recorded.

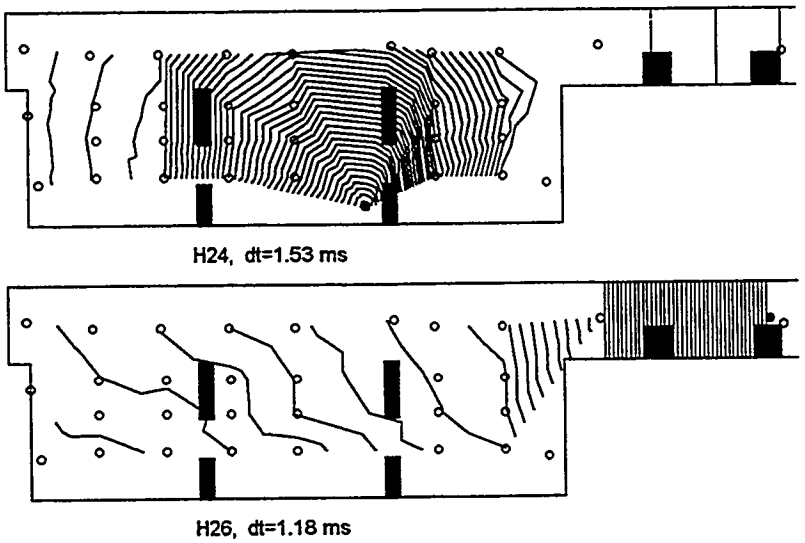

Figure 3. Flame positions as a function of time for tests 24 (upper) and 26 (lower). dt is time step.

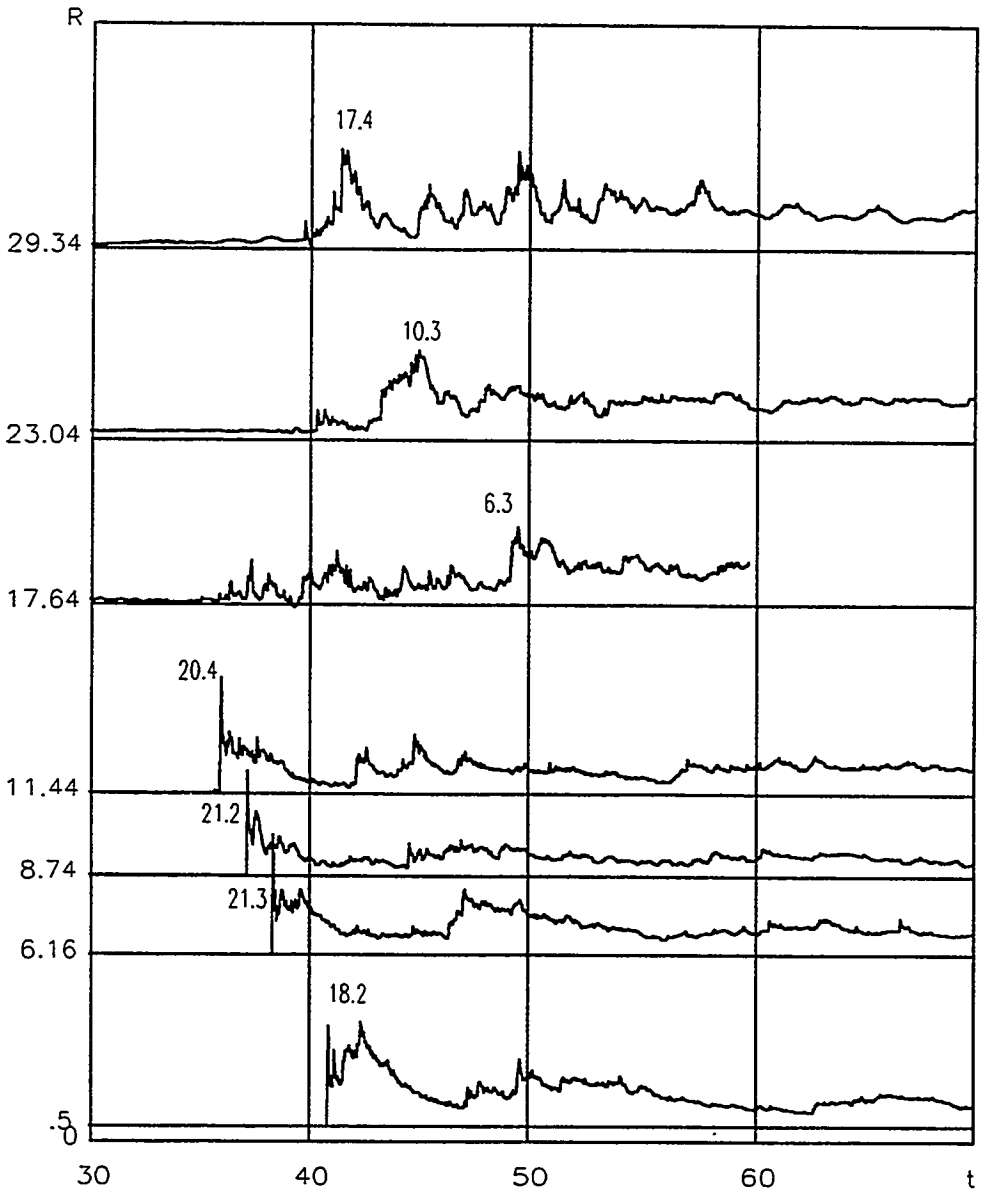

Figure 4. (R -- t) - diagram of pressure waves in test 28. R in meters, t in ms. Maximum overpressures (bar) are shown in the plot.

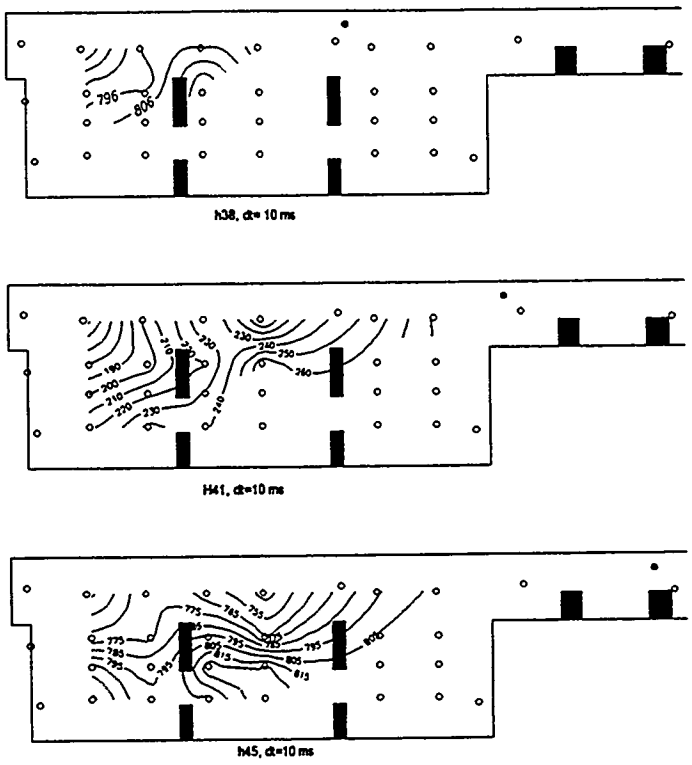

Figure 5. Flame shape as a function of time for tests 38, 41, and 45. dt is time step.

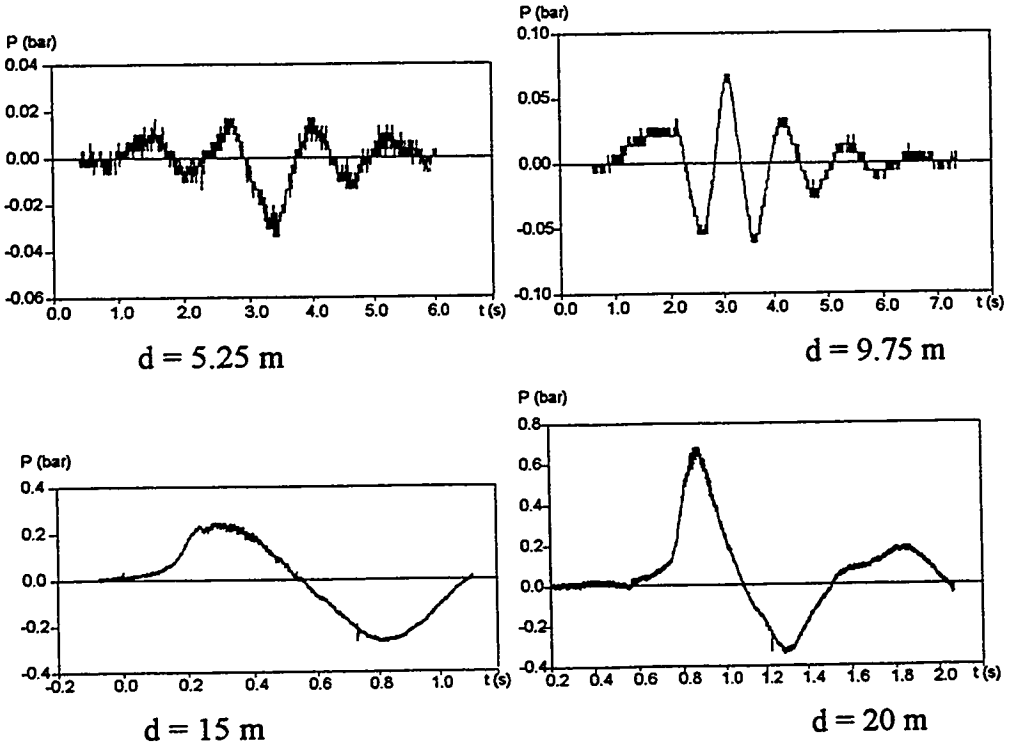

Figure 6. Pressure records for lower injection location (d - distance from igniter to injection point).

Summary of observations. The processes observed in the dynamic injection/ignition experiments included the cases of

(1) no ignition (H_2 is low at ignition time and igniter location);
(2) ignition, flame acceleration, DDT, and local detonation (upper injection location);
(3) ignition and deflagration (lower injection location).

Good local mixing and large-scale concentration nonuniformities were observed during hydrogen injection. Explosions observed under dynamic conditions are essentially local phenomena. The amount of hydrogen, which can be involved in local detonation, is limited by igniter location. The local explosions observed are not connected with global combustion events described earlier in this paper. Multiple explosions were also observed in the case of continuous injection. Explosions resulted in venting, re-addition of air, mixing, secondary explosion, venting, etc. Each of these explosions was of local character with limited amount of hydrogen involved.

DDT Conditions and Hydrogen Igniters

Main parameters that may effect the possibility of DDT in the presented tests are the distance between injection and ignition points and mean hydrogen concentration in the cloud at the time of ignition. The results of the tests are presented in these variables in Fig. 7. The mean hydrogen concentrations in the cloud were determined as the ratio of hydrogen volume to cloud volume at the instant of ignition. The latter is defined by cross-section of the enclosure and distance to igniter. It is clear that the possibility of DDT depends only on the mean hydrogen concentration in the cloud for the given size of the enclosure. The limit (12.5% vol. H_2) is exactly the same as for premixed DDT experiments in the same facility. Distance to igniter has an indirect effect on the possibility of DDT. For small distances, dangerous concentration of hydrogen cannot be accumulated before ignition.

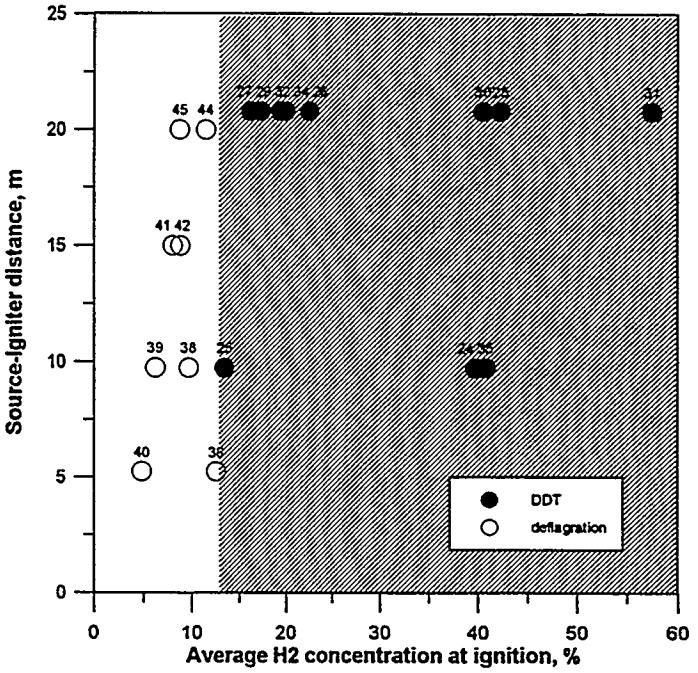

Figure 7. Range of parameters for DDT in dynamic injection/ignition experiments. Test numbers are shown in the plot.

The composition limit obtained is valid only for the particular size of the enclosure. The 7λ criterion can be used to scale these results for different sizes of compartments. If the detonation cell width is defined by the mean hydrogen concentration in the cloud, and the cloud size itself gives the characteristic

nonuniformity size, we can analyze data of dynamic tests in the same way as that of premixed experiments. Figure 1 shows that 7λ criterion can be applied for dynamic conditions also.

If the distribution of hydrogen concentration in some enclosure is known as a function of time, ignition time can be determined for a given ignition location. The possibility of DDT can be estimated on the basis of mean hydrogen concentration in the cloud and its characteristic size. If the mixture occupies all volume of the enclosure, its characteristic size should be used. Such a consideration gives a basis for estimation of a number and locations of igniters for deliberate ignition of hydrogen in the containment. First, detailed hydrogen distribution calculations are necessary. The calculations should provide data on the locations where the earliest ignition is possible. Usually such a location corresponds to high elevations and flow paths. For global combustion events, the maximum allowable distance between igniters can be estimated as 7 cell widths of the most sensitive part of the mixture at the time of ignition. For dynamic conditions (near the break) characteristic size of H2 cloud (compartment) at a time of ignition should be less than 7 cell width of average mixture composition in the cloud to avoid DDT.

CONCLUSIONS

Important problems of hydrogen combustion behavior during severe accidents in a nuclear power plant are determination of conditions for spontaneous detonations and scaling of these conditions. In the present paper, scaling of spontaneous detonations and its application for safety analysis are discussed. Results of theoretical analysis show that the formation of the detonation wave itself imposes the scale limitation for the transition to a detonation. The characteristic geometrical size of the mixture allowing a transition to detonation is shown to be strongly related to the mixture sensitivity. In terms of detonation cell width λ the minimum size can be estimated as 7λ. This criterion is confirmed by numerical and analytical studies, and by experimental data over a wide range of volumes and compositions.

Experiments with dynamic H_2 injection have been performed to study the consequences of deliberate ignition near hydrogen release location. The possibility of DDT is shown to depend on mean hydrogen concentration in the cloud at the time of ignition. This limit is in accord with earlier premixed DDT experiments and with cell size scaling of DDT conditions. The H_2 concentration at ignition time depends, in its turn, on the mutual position of hydrogen jet and igniter. Upward directed H_2 injection is shown to be least dangerous; igniter placing at highest elevations is preferable to others. Criteria for placing hydrogen igniters can be based on detailed distribution calculations and on the proposed cell size scaling of DDT conditions.

REFERENCES

1. Dorofeev, S. B., Efimenko A. A., Kochurko, A. S. and Chugunov, A. E., Numerical simulation of multidimensional structure of detonations. SR&DO Industrial Risk, Preprint IRIS-91/2, 1991 (in Russian).

2. Dorofeev, S. B., Sidorov, V. P., Kochurko, A. S., Bezmelnitsin, A. V., Breitung, W. *14th International Colloquium on Dynamics of Explosions and Reactive Systems*, University of Coimbra, Coimbra, 1993, Vol. 2, pp. D2.17.1-D2.17.10.

3. Efimenko A. A., Kochurko A. S., Dorofeev, S. B., Breitung, W. *14th International Colloquium on Dynamics of Explosions and Reactive Systems*, University of Coimbra, Coimbra, 1993, Vol. 2, pp. D1.17.1-D1.17.10.

4. Breitung W., Dorofeev S. B., Efimenko A. A., Kochurko, A. S., Redlinger R., Sidorov, V. P., *Proceedings of ARS'94 Int. Topical Meeting on Advanced Reactor Safety*. Pittsburg, PA, Vol. 2, pp. 733-745.

5. Dorofeev, S. B., Sidorov, V. P., Dvoinishnikov A. E., Breitung, W. *Combust. Flame* (to appear).
6. Guirao C. M., Knystautas R., Lee J. H., A Summary of Hydrogen-Air Detonations for Reactor Safety, Sandia National Laboratories / McGill University, NUREG/CR-4961, 1989.
7. Stamps, D. W., Benedick, W. B., Tieszen, S. R. Sandia National Laboratories, SAND89-2398, NUREG/CR-5525, 1991.
8. Ciccarelli, G., Ginsberg, T., Finfrock, C., Boccio, J., Economos, C., Kinoshita, M., Presented at CSARP Meeting Bethesda, MD May 2-6, 1994.
9. Moen, I. O., Bjerketvedt, D., Jenssen, A., and Thibault, P. A., *Combust. Flame* 61:285-291, (1985).
10. Schildknecht, M., Geiger, W., and Stock, M., in *Progress in Astronautics and Aeronautics* (A.L. Kuhl, Ed.), The American Institute of Aeronautics and Astronautics, Inc., Washington, 1985, Vol. 94, pp. 474-490.
11. Kanzleiter, T. F., presented at the 17th Water Reactor Safety Information Meeting -89, Rockvill MD, USA, 1989.
12. Dorofeev, S. B., Bezmelnitsin, A. V., Sidorov, V. P., Yankin, J. G., and Matsukov, I. D., *Fourteenth International Colloquium on Dynamics of Explosions and Reactive Systems*, University of Coimbra, Coimbra, 1993, Vol. 2, pp. D2.4.1-D2.4.10.
13. Sherman, M. P., Tieszen, S. R., Benedick, W. B., Fisk, J. W., and Carcassi, M., in *Progress in Astronautics and Aeronautics* (A.L. Kuhl, Ed.), The American Institute of Aeronautics and Astronautics, Inc., Washington, 1986, Vol. 106, p. 66.
14. Sherman, M. P., Tieszen, S. R., and Benedick, W. B., Sandia National Laboratories Report No. SAND85-12611, NUREG/CR-5275, 1989.
15. Sherman, M. P., Tieszen, S. R., and Benedick, W. B., Sandia National Laboratories Report No. SAND89-0859, 1989.
16. Carnasciali, F., Lee, J. H. S., Knystautas, R., and Fineschi, F., *Combust. Flame* 84:170-180 (1991).
17. Berman, M., *Nuclear Science and Engineering*, 93:321-347 (1986).
18. Behrens, U., Langer, G., Stock, M., and Winkler-Bott, *Nuclear Engineering and Design*, 130:43-50(1991).
19. Urtiev, P., and Oppenheim, A. K., *Proc. Roy. Soc. London*, A 295:13-28 (1966).
20. Lee, J. H. S., Knystautas, R. and Yoshikawa, N. *Acta Astronautica* 5, 971-982, (1978).
21. Zel'dovich, Ya. B., Gelfand, B. E., Tsyganov, S. A., Frolov, S. M. and Polenov, A. N., in *Progress in Astronautics and Aeronautics* (A.L. Kuhl, Ed.), The American Institute of Aeronautics and Astronautics, Inc., Washington, 1988, Vol. 114, pp. 99-123.
22. Dorofeev, S. B., Kochurko, A. S., and Chaivanov, B. B., *Sixteenth Symposium (International) on Loss Prevention and Safety Promotion in the Processes Industries,* Oslo, 1989, Vol. 4, pp. 22-1 - 22-19.
23. Dorofeev, S. B., Bezmelnitsin, A. V., Efimenko, A. A., Kochurko, A. S., Sidorov, V. P., Yankin, J. G., and Matsukov, I. D., RRC "Kurchatov Institute" Report, RRCKI-80-05/3, NUREG/CR-6072, 1993.
24. Kryuchkov S. I., Dorofeev, S. B. Submitted to *Combust. Flame*, 1995.
25. Dorofeev, S. B., Efimenko A. A., Kochurko, A. S. and Chaivanov B. B. *Nuclear Engineering and Design,* 148: 305-316 (1992).

SCDAP/RELAP5 CODE DEVELOPMENT AND ASSESSMENT*

C. M. Allison
J. K. Hohorst

Idaho National Engineering Laboratory
Applied Engineering Development Laboratory
Lockheed Idaho Technologies Company
Idaho Falls, Idaho 83415

ABSTRACT

The SCDAP/RELAP5 computer code is designed to describe the overall reactor coolant system thermal-hydraulic response, core damage progression, and fission product release during severe accidents. The code is being developed at the Idaho National Engineering Laboratory under the primary sponsorship of the Office of Nuclear Regulatory Research of the U.S. Nuclear Regulatory Commission. The current version of the code is SCDAP/RELAP5/MOD3.1e. Although MOD3.1e contains a number of significant improvements since the initial version of MOD3.1 was released, new models to treat the behavior of the fuel and cladding during reflood have had the most dramatic impact on the code's calculations. This paper provides a brief description of the new reflood models, presents highlights of the assessment of the current version of MOD3.1, and discusses future SCDAP/RELAP5/MOD3.2 model development activities.

INTRODUCTION

The SCDAP/RELAP5 computer code is designed to describe the overall reactor coolant system (RCS) thermal-hydraulic response, core damage progression, and fission product release during severe accidents[1,2]. The code is being developed at the Idaho National Engineering Laboratory (INEL) under the primary sponsorship of the Office of Nuclear Regulatory Research of the U.S. Nuclear Regulatory Commission (NRC). The current version of the code is SCDAP/RELAP5/MOD3.1e[2]. Although MOD3.1e contains a number of significant improvements since the initial version of MOD3.1 was released, a set of new models to treat the behavior of the fuel and cladding during reflood has had the most dramatic impact on the code's calculations. In particular, the ability to predict the accelerated heating and melting of hot, damaged fuel assemblies during water injection has been significantly improved. A brief description of the new MOD3.1 reflood models and the highlights of the assessment of the current version of the code are presented in the next section. The next

* Work supported by the U.S. Nuclear regulatory Commission, Office of Research, under DOE Contract No. DE-AC07-76IDO1570.

section discusses the ongoing model development and assessment activities for SCDAP/RELAP5/MOD3.2. A brief summary and conclusions are provided in the final section.

HIGHLIGHTS OF THE MOD3.1e ASSESSMENT RESULTS

As described in a previous Water Reactor Safety meeting paper[3], SCDAP/RELAP/MOD3 and previous versions of the code were unable to predict the experimentally observed behavior for experiments where hot, damaged bundles were reflooded. Although those versions of the code were able to predict the fragmention of the bundles, the accelerated or renewed bundle heating and melting and sharp increases in hydrogen production during bundle reflood were not predicted. In fact, it was noted the total hydrogen production in bundle reflood experiments could be underpredicted by as much as a factor of five. As a result, the influence of bundle reflood was a major focus of model development activities for MOD3.1 and subsequent versions of the code. These new models have been introduced in two steps as described in a recent paper presented at the NURETH-7 meeting[4] and MOD3.1e code manuals[2]. The initial version of SCDAP/RELAP5/MOD3.1, which was released in 1994, contained two bounding correlational-based models to treat the cracking of the oxidized fuel rod cladding. One model, a local model, assumed the protective oxide layer would crack at a given elevation when oxidation-embrittled Zircaloy cladding cooled rapidly to a temperature between 1150 to 1560 K. The other model, a global model, assumed the protective oxide layer would crack over the full height of the fuel rod cladding as soon as water was added. In both cases, enhanced oxidation and heating then occurred due to the oxidation of the hot Zircaloy layer exposed by the cracking of the protective oxide. Mass diffusion of steam to the surface of the cladding was the oxidation-rate limiting process once the oxide was cracked. The flooding rates and heat transfer during the reflood process were described using standard RELAP5 thermal-hydraulic constitutive models.

After a systematic assessment of these models, an additional model was then added to MOD3.1 to treat the oxidation of the liquefied U-Zr-O moving down the outer surface of the fuel rod cladding. During reflood, molten U-Zr-O is formed during the initial increase in temperature resulting from the oxidation of the hot Zircaloy layer exposed by oxide cracking. This model, based upon the observation of U-Zr-O rivulet and droplet flows in the German CORA experiments, describes the motion of droplets of liquefied U-Zr-O and the resulting oxidation of those drops as shown in Figure 1. As indicated in this figure, the droplets and rivulets of liquefied U-Zr-O are represented as a series of hemispherical droplets relocating down the outer surface of the cladding. The heat transfer between the droplet, coolant, and underlying cladding and fuel and the oxidation of the droplet are considered by the new model.

The assessment of MOD3.1e used code-to-data comparisons to evaluate the impact of the new models and other minor code modifications. The code-to-data comparisons included nine experiments from tests performed in the CORA facility (CORA experiments) in Germany[5,6,7], the NRU facility (Full Length High Temperature, FLHT, experiments) in Canada[8,9], and the Power Burst Facility (Severe Fuel Damage, SFD, experiments) in the United States[5,10]. The comparisons included (a) both electrically heated and nuclear heated experiments; (b) bundles with fuel rods only, fuel rod bundles with Ag-In-Cd control rod structures, and fuel bundles with BWR control blade/channel box structures; (c) initial heating rates varying from 0.5 to 1.0 K/s; (d) peak bundle temperatures between 2100 to 2900 K; and (e) both slow and

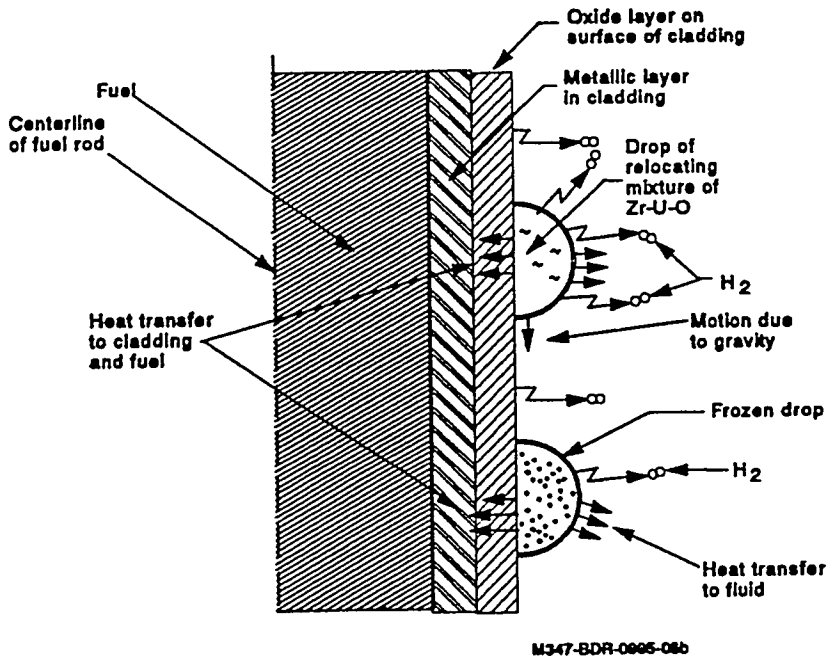

Figure 1 - MOD3.1e U-Zr-O droplet oxidation model.

rapid (bundle reflood and quenching) cool down.

Although thermocouple failure prevents a quantitative assessment of the bundle peak temperature history in these experiments, the overall calculated temperature response and heating rates during the initial heating phase of the experiments were in good agreement with that observed as shown in a sample taken from the CORA-17 comparisons, Figure 2. This experiment used a combination of electrically heated fuel rod simulators, fuel rods, and BWR control blade/channel box structures[5]. As indicated in the figure, this experiment is terminated by the reflooding of the bundle. The figure shows the calculated and measured temperatures at three elevations. The total heated length of this bundle is 1 meter. It can be seen that all of the thermocouples fail during the initial heating and melting phase of the experiment since many of the structures where the thermocouples are mounted melt as higher temperatures are reached. However, as shown in the figure, thermocouples in cooler regions of the bundle did survive, indicating that the calculated trends are consistent with the overall temperature response of the bundle. In addition, this figure also shows the sharp increase in the bundle temperature resulting from the start of bundle reflood even though the bundle had started to cool previously due to the termination of electrically heating. The calculated temperature spikes show the same trend. These spikes were not predicted with previous versions of the code.

A similar trend was observed for the CORA-13 experiment[7]. This experiment also used electrically heated fuel rod simulators but had a PWR Ag-In-Cd control rod and Zircaloy guide tube rather than the BWR structures used in CORA-17. Figure 3 shows the calculated and measured temperatures in the bundle immediately before and during reflood. The thermo-

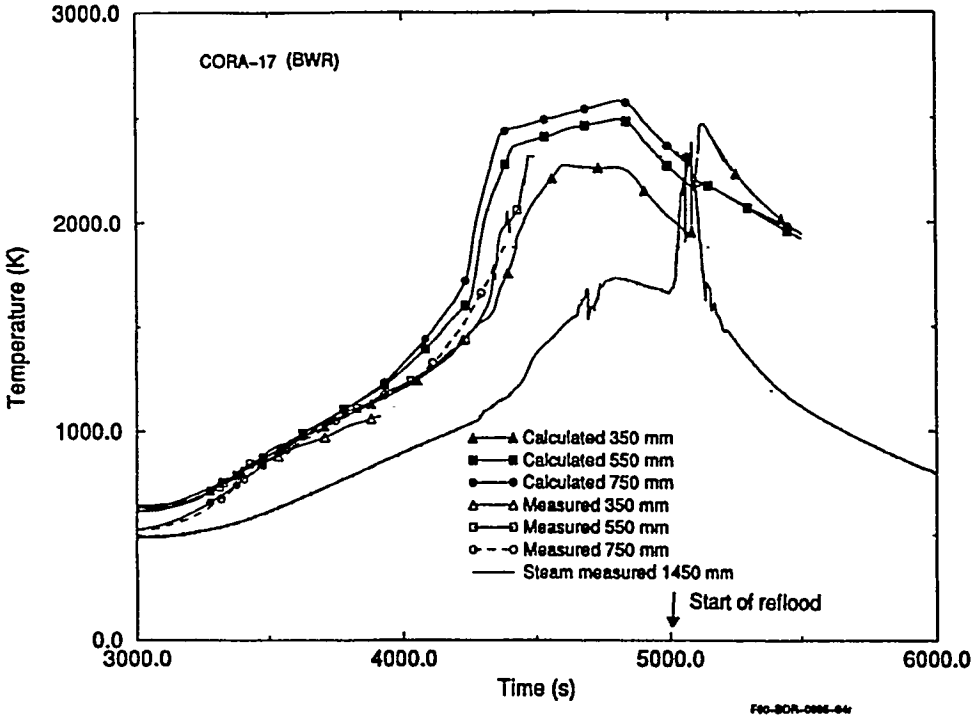

Figure 2 - Calculated and measured bundle temperatures for the CORA-17 BWR experiment.

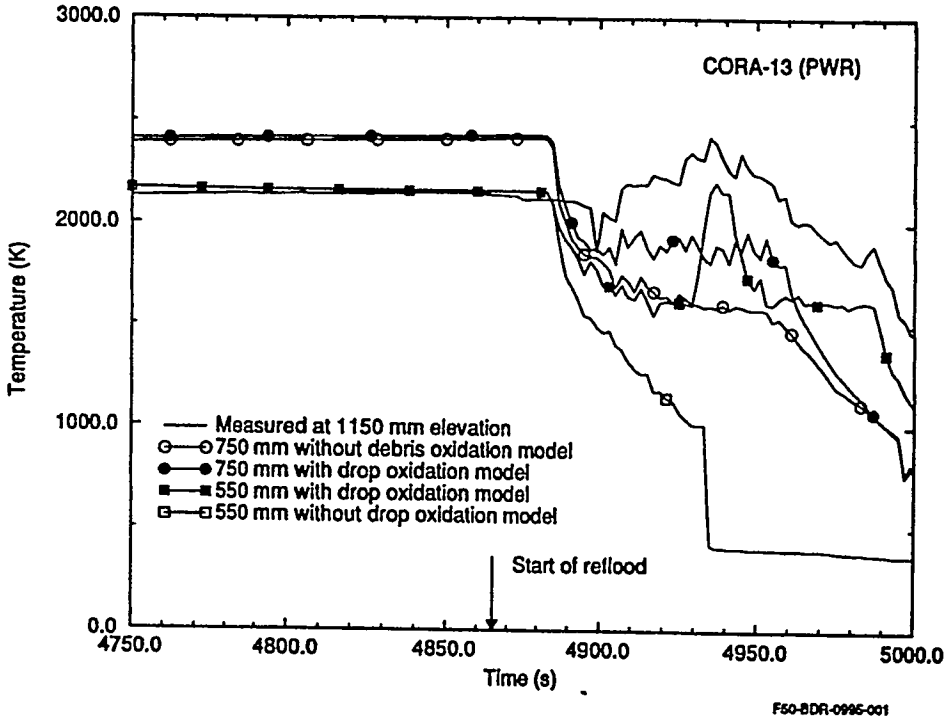

Figure 3 - Calculated and measured bundle temperatures during the reflood phase of the CORA-13 PWR experiment.

couples at the 550 and 750 mm elevations had failed previously so a thermocouple in a cooler region above the bundle is shown for comparison to the calculated temperatures in the hot region of the bundle. This figure shows a comparison where the MOD3.1e U-Zr-O droplet oxidation model is either included or not included, indicating that the new model plays an important role in the ability to predict the continued heating of the bundle even though the electrical heating of the bundle was terminated prior to reflood.

However, as shown in Figure 4, it was observed for the CORA PWR experiments, CORA-2 is shown, that the heating rates at temperatures above 1500 K were underpredicted. This trend was not observed in either the CORA BWR experiments or the experiments in the other facilities. This trend is also inconsistent with previous MOD3.1 calculations. The cause for this discrepancy is still under investigation, but has been attributed to the high concentration of Argon used in the experiments to help cool the experimental facility and changes in the MOD3.1e mass diffusion model.

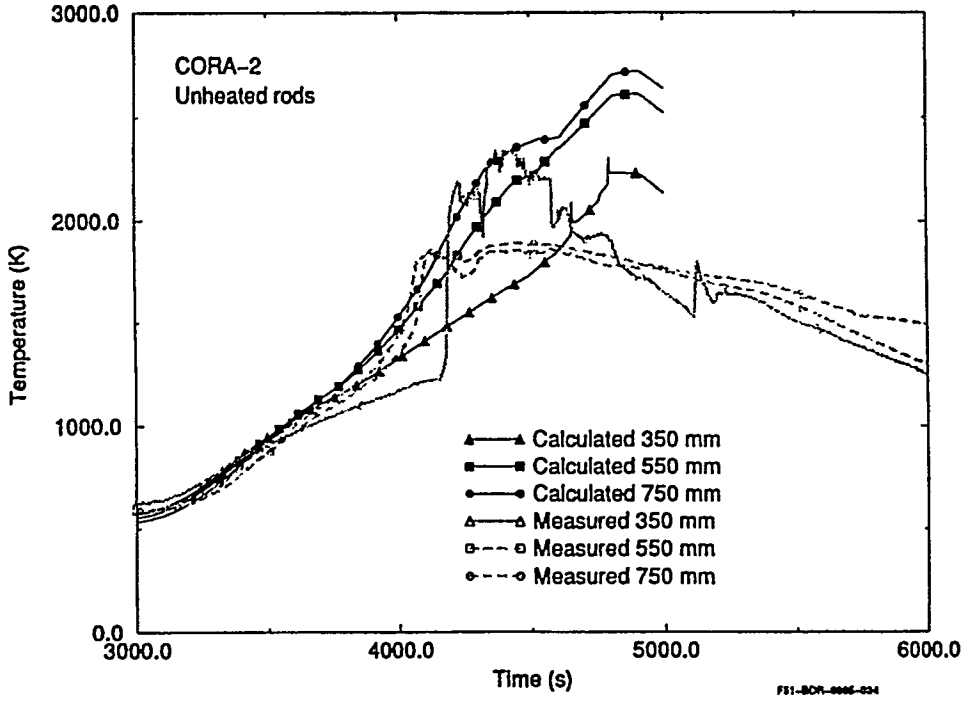

Figure 4 - Calculated and measured bundle temperatures for the CORA-2 experiment.

Two experiments, SFD-ST[10] and FLHT-5[9], were also used to assess the accuracy of the predicted water levels and dryout times. These were the only experiments used in the assessment that subjected the experimental bundle to a bundle boildown transient. All of the other experiments used superheated steam and argon mixtures. As shown in Figure 5, the predicted collapsed water levels and dryout times are consistent with those observed in the SFD-ST experiment. As indicated by the calculated and measured temperatures at the 0.5 m elevation, the intermittent dryout at the beginning of the transient is not predicted exactly but the temperature response once the bundle is starting to heat up is in good agreement. The sawtooth pattern on the predicted collapsed water level is an artifact of the nodalization

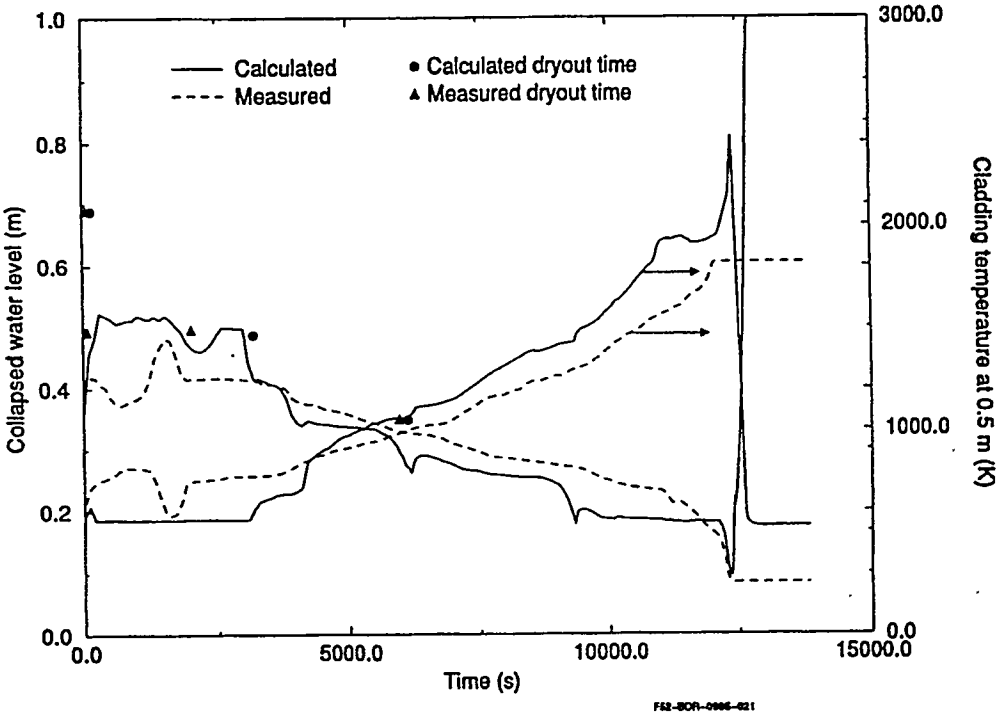

Figure 5 - Calculated and measured water levels and dryout times for the SFD-ST experiment.

and results as the water levels moves from one axial node to another. The calculated and measured heating rates for FLHT-5 once dryout had occurred were also in good agreement, but it was observed that there was a wide variation in the measured dryout times between the heated fuel rods and colder shroud around the bundle[2]. This radial variation was not predicted by the code since a single flow channel was used to represent the bundle.

The most dramatic improvement observed in the code-to-data comparisons was the predicted total hydrogen production for bundle experiments terminated by reflood and quenching. Even though the introduction of the ZrO_2 oxide cracking models into MOD3.1 eliminated much of the variation between calculated and measured hydrogen production for several reflood experiments, the calculated total hydrogen production rates were still consistently below that measured in the experiments[2]. In some cases the discrepancy was as much as a factor of two. However, with the addition of the MOD3.1e U-Zr-O droplet oxidation model, that systematic bias appears to be eliminated. For example, in the CORA-13 experiment, the total hydrogen calculated for MOD3.1 was 77 g while MOD3.1e calculated 222 g. The measured value was 210 g. For SFD-ST, the measured value was 172 ± 40 g; MOD3.1e calculated 146 g. The MOD3.1 predicted value was 81 g. For these two experiments the discrepancy between calculated and measured total hydrogen for MOD3.1e is now well within the estimated experimental uncertainty in the measurement. The calculated values are between +6% to -15% of the measured values. For comparison, for SFD-ST where an error estimate is provided, the experimental uncertainty is $\pm 23\%$.

The one notable outlier in the code-to-data comparison was the CORA-17 experiment, the only BWR bundle experiment that included reflood. In this case, the predicted total

hydrogen production was still below that measured. The measured value was 150 g, while the predicted value was only 63 g. Although the exact cause for this discrepancy has not yet been established, the experimentalists[11] attribute much of the total hydrogen production to the oxidation of the B_4C. Although the MOD3.1e BWR control blade/channel box model considers the oxidation of the B_4C, stainless steel, and Zircaloy, there are no specific models which address the possible cracking of the protective oxides or the fragmentation of these structures during reflood.

The possible variation in hydrogen production rates during different phases of the experiments was also assessed. However, this assessment is complicated by the large experimental uncertainties in these measurements. In the CORA experiments used in the assessment, where the hydrogen is measured downstream of the experimental bundle, large time delays have been observed between the actual hydrogen production in the bundle and the hydrogen sampled in the monitor. Although corrections have been developed for more recent CORA experiments, it was not possible to correct the data used in this assessment for those delays[11]. In addition, it has been observed that the measured hydrogen production rate is very sensitive to the type of hydrogen measurement used. Although the uncertainties in total hydrogen can be determined by a mass balance on oxidized material during post-test metallurgical examinations, the determination of experimental uncertainties in the hydrogen production rate is much more difficult. For example in the FLHT-5 experiment, three independent measures of the hydrogen production rate were obtained from a noncondensible flow meter, a Palladium-based meter, and a thermal-conductivity-based meter[9]. As shown in the integrated hydrogen production curves in Figure 6, the measured initial production rates are comparable, although significant time delays are apparent. In this case, it was determined

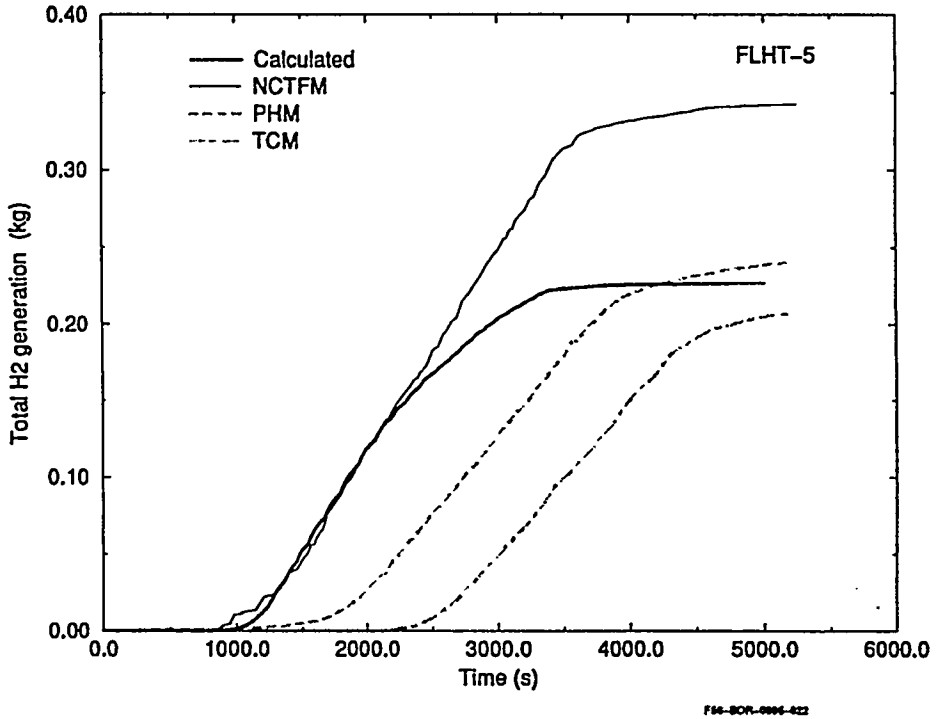

Figure 6 - Comparison of calculated and measured integrated hydrogen production for the FLHT-5 experiment.

by the experimentalists that the noncondensible flow meter was the most accurate measurement. Since this experiment was designed to establish the longer term hydrogen production rate for a bundle held at temperatures near the melting point of Zircaloy for an extended period of time, it was concluded that the oxidation of the bundle during the melting phase, following the initial heating and melting of the bundle, may be under predicted by the code. The total hydrogen production predicted for this experiment was 227 g as compared to an measured value of 300$\pm$30 g, a variation of -24%.

The calculated damage progression for MOD3.1e was also consistent with that observed in the experiments. Both the new PWR Ag-In-Cd control rod and BWR B_4C control blade/channel box models were more consistent with separate effects experiments where material interaction reaction rates have been measured, and integral bundle heating and melting experiments. In addition, as shown in Figure 7, the default ZrO_2 shattering model, the local model, provides the best overall agreement with the observed bundle end states

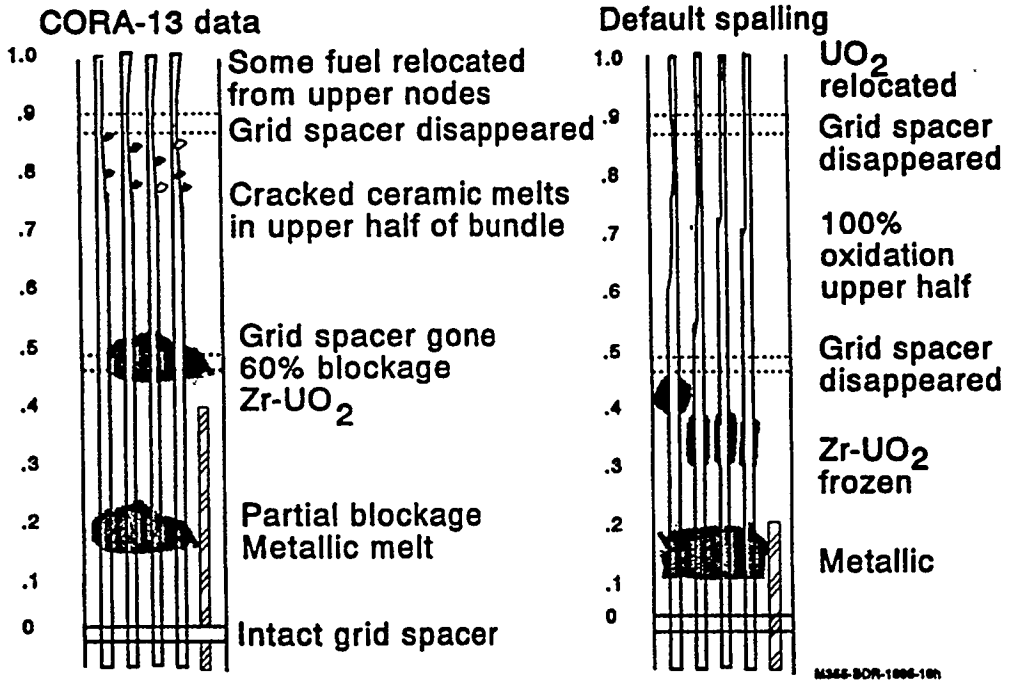

Figure 7 - Comparison of calculated and observed bundle end states for the CORA-13 PWR experiment with reflood.

following bundle reflood. The optional bounding reflood model, the global shattering model, consistently overpredicts the damage in the bundle.

SCDAP/RELAP5/MOD3.2 MODEL IMPROVEMENTS

The final set of peer-review-recommended[12] late phase model improvements is currently being implemented into SCDAP/RELAP/MOD3.2. This version of the code will be released in 1997 after the completion of a formal peer review of the improved models, model

implementation and testing, and developmental assessment. The MOD3.2 late phase model improvements include - (a) debris bed thermal-hydraulics, formation, heating, melting, and fission product release; (b) molten pool formation, growth, and crust failure; (c) the melting and failure of upper plenum and core plate structures; and (d) the interactions between the melt, structures, and water during the slumping of molten material from the core. In addition, the MATPRO material properties library[13] and associated physical models will be updated to include the effects of material interactions not currently considered, plant aging, and extended burnup of the fuel. In a number of cases, as described in more detail in the following discussion, the theoretical approach for the individual models has been defined and peer-reviewed. Model implementation and testing is currently underway for the models discussed.

The implementation of the improved models for debris bed thermal-hydraulics is the most advanced. The new models have been implemented and development assessment is currently underway. These new models replace the existing RELAP5/MOD3.1-based constitutive models with models developed specifically for porous materials. In thermal-hydraulic volumes described by either the in-core or lower plenum debris models, the flow area and volume terms in the conservation equations have been modified to account for the porosity and effective particle size distributions in those debris beds. The flow regime maps, flow resistance, and heat transfer correlations have also been modified in those regions. RELAP5/MOD3.1-based thermal-hydraulic conservation and constitutive models are used in the remainder of the thermal-hydraulic volumes throughout the system. The volume and junction flow regime maps for debris beds have been modified based upon a series of debris bed thermal-hydraulic experiments performed at UCLA (University of California, Los Angeles)[14,15,16]. As shown in the example given in Figure 8, the new models will follow the

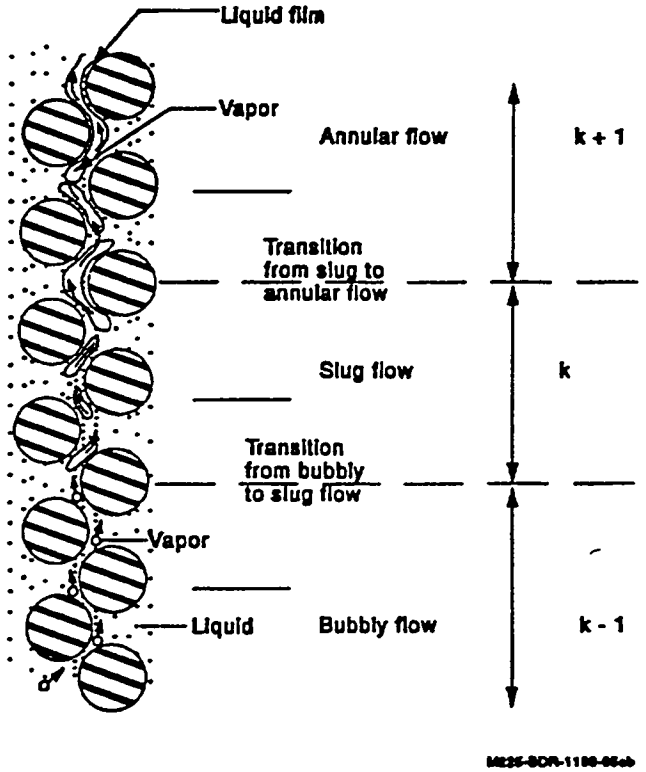

Figure 8. Schematic of pre-surface dryout flow regimes.

dryout of the debris particles through several regimes including bubbly, slug, and annular flow with reflood being treated in a similar manner. These new models are currently being assessed using the CORA and SFD-ST damaged bundle experiments noted in the previous section and debris quenching experiments performed at Brookhaven National Laboratory[17] and UCLA[18].

The new models for debris formation, heating, and melting have also been partially implemented. The primary change in these models is to allow for much more diverse, hetergenous debris beds. As shown in Figures 9-11, the type of debris beds that can be formed either through the liquefaction and refreezing of assembly materials or the fragmentation of the fuel rods can be very diverse. Although most of the experiments have shown that debris formed as a consequence of the freezing of liqefied material has limited open porosity available for internal cooling, the variation in closed porosity and the effective density and thermal conductivity of the material can vary subsubstantially depending upon the experimental conditions. For example, as shown on the right hand side of Figure 9, a cross-section through the ceramic blockage region for the OECD LOFT LP-FP-2 central fuel assembly[19], the internal porosity is limited even though an extensive network of cracks was formed during cooldown. On the other extreme, as shown on the left hand side of the figure, a cross-section from the DF-4 experiment which included a BWR control blade/channel box structure[20], the frozen material has extensive closed porosity with a foam-like appearance. The majority of the experiments also have shown that the fuel rods, and associated fuel pellets, remain relatively intact even during a rapid quench. However, the size of the resulting fuel debris and remaining fuel columns can vary over a wide range, depending upon the initial state of the fuel and conditions leading up to the formation of the debris. For example, Figure

Figure 9. Cross-sections from the DF-4 and OECD LOFT LF-FP-2 cohesive debris regions.

10 shows typical cross-sections taken from the SFD 1-1 and SFD 1-4 experiments[21,22] where relatively large fuel fragments are apparent even for fuel which has been irradiated. These experiments were slowly cooled. However, some experiments exhibited a complete desintering of the fuel, resulting in a very fine fuel power as shown in Figure 11, taken from the ESBU-2A experiment conducted in Germany[23]. As a result, the debris behavior models are being modified to allow for spatial varying debris bed porosities and particle size distributions. In addition, preliminary correlations for the characteristics of the debris beds have been developed based upon a preliminary review of the data from many of the bundle heating and melting experiments. However, the final correlations will be developed through the post-test examinations of the bundles from on-going experimental programs.

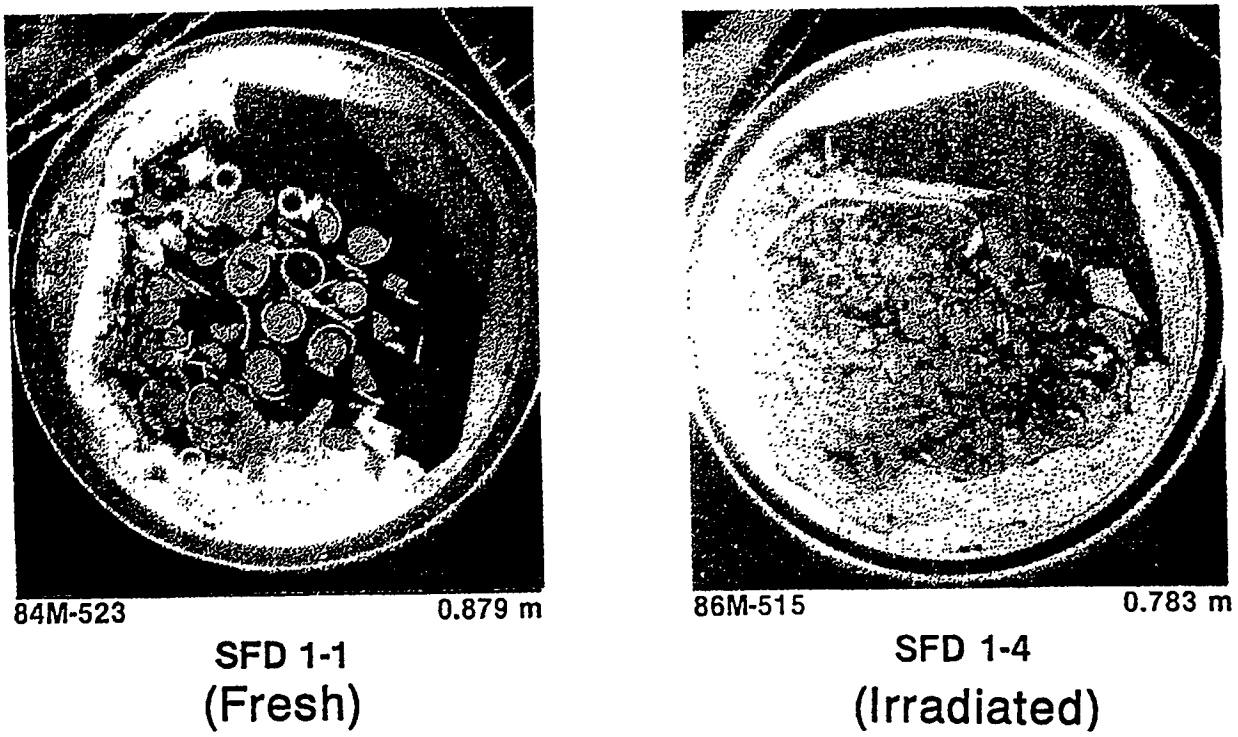

Figure 10. Cross-sections from the SFD 1-1 and SFD 1-4 upper debris regions with fresh and irradiated fuel.

Improved models for molten pool formation, growth, and crust failure have also been partially implemented into MOD3.2. Although the basic correlations for molten pool steady state natural circulation have been updated through the incorporation of additional experimental results, the dominant changes in the molten pool formation and growth models are related to (a) the development of a transient form of the correlations to account for the heat transfer from the molten pool prior to reaching steady state conditions and (b) incorporation of the effects of void formation in the natural circulation heat transfer associated with retained fission products or the vaporization of structural materials with relatively low melting temperatures[24]. As shown in Figure 12, the transient heat transfer from the molten pool, as indicated by the average Nusselt number for a representative size pool, can be substantially less than that occurring once steady-state conditions are reached. In addition, as shown in Figure 13, the incorporation of void formation effects on the molten pool natural

Figure 11. Desintered fuel region in the ESBU-2A experiment.

circulation heat transfer can have a significant impact as well. For Rayleigh numbers in excess of 10^{14}, typical of the molten pools in the reactor scale, an increase in the void fraction of the melt consistent with the end-state porosity observed in refrozen melts, can increase the heat transfer from the molten pool by 1 to 2 orders of magnitude. The changes in the crust failure models are also significant in that the new models account for the thermal and structural behavior of the crusts surrounding the molten pool. This will be particularly important for transients where the molten pool and crust is surrounded by water. For example, as may have occurred in the TMI-2 accident, even though the molten pool crust may reach thermal equilibrium and a stable thickness, variations in system pressure and other external conditions can lead to a structural failure of the crust. For example, as shown in Figure 14, a calculated failure map for the failure of a crust on the side of either a cylindrical or hemispherical molten pool, the mechanical failure of a thermally stable crust depends upon the pressure across the crust, due either to variations in the system pressure outside the molten pool or height of the pool, the thickness of the crust, and the temperature of the crust. The note on the figure shows the estimated crust thickness and pressure difference between the molten pool and the

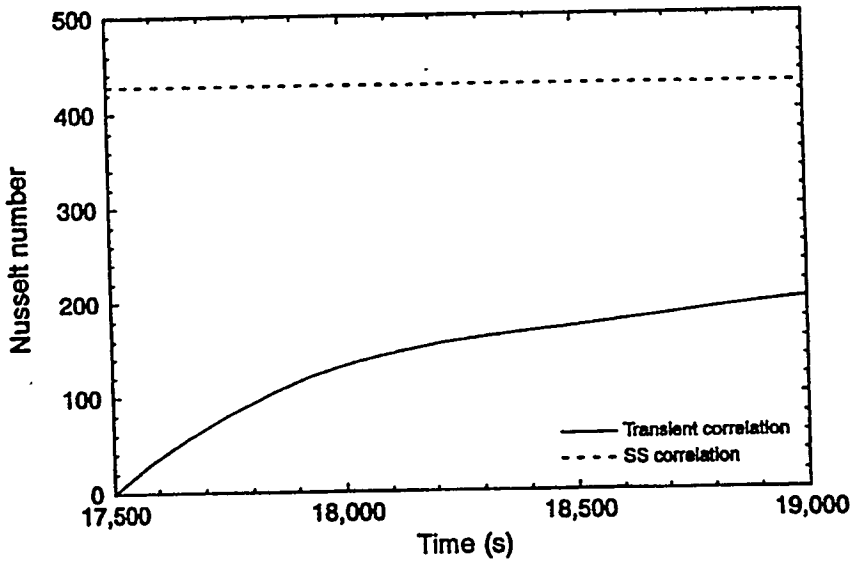

Figure 12. Comparison of steady-state and transient molten pool natural circulation heat transfer for a reactor scale pool.

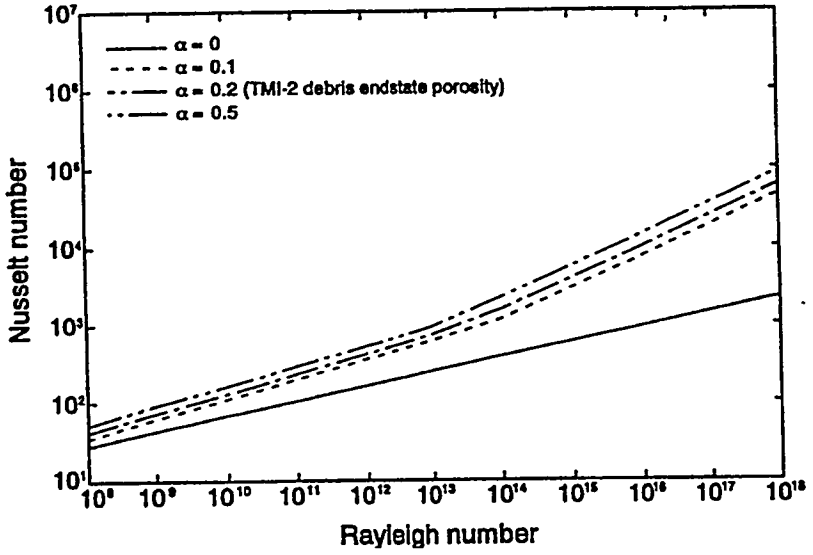

Figure 13. Comparison of the molten pool natural circulation heat transfer for different vapor void fractions in the melt.

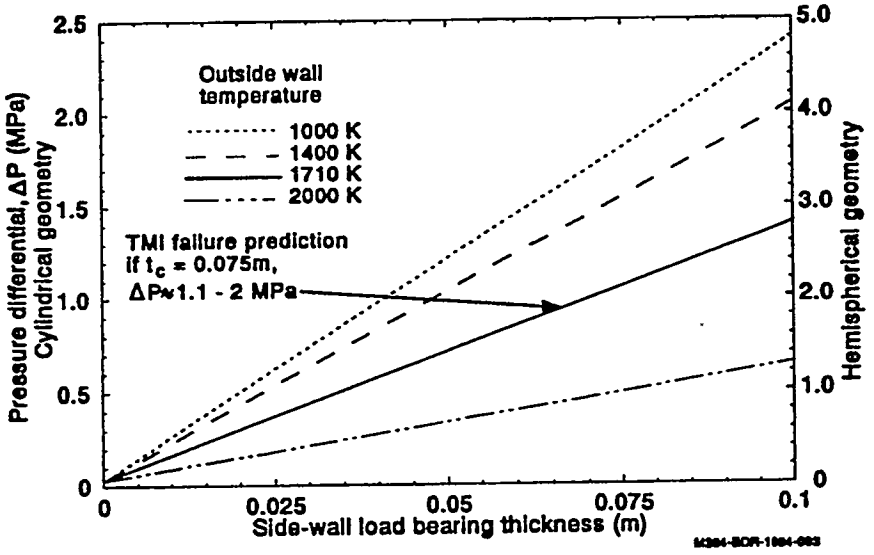

Figure 14. Side-wall failure map for a closed crucible with molten interior and linear through-wall temperature distribution.

coolant for TMI-2. The pressure difference was computed assuming that the crust had relatively limited permeability so the molten pool pressure could not follow the rapid system pressure fluctuations occurring near the time of molten pool slumping.

The remainder of the MOD3.2 models are still either in the preliminary design stages or in the early stages of implementation and will not be discussed in this paper. However, it should be noted that the overall MOD3.2 model improvement and assessment activities will also be an international activity over the next two years. New models for fuel rod and Ag-In-Cd control rod oxidation, melting, and fragmentation will be developed and assessed by the United Kingdom, Germany, and Russia. Over the longer term, Russia will be developing and assessing improved molten pool models, based upon experimental programs being performed in that country.

SUMMARY AND CONCLUSIONS

As discussed in the MOD3.1 assessment highlights section, the addition of new models to treat the cracking of the protective oxide film on the Zircaloy cladding and the oxidation of liquefied U-Zr-O had the most dramatic impact on the MOD3.1 calculations relative to previous versions of SCDAP/RELAP5. The current version of MOD3.1 now more accurately predicts the renewed heating and melting and dramatic increases in hydrogen production during the reflooding of hot damaged bundles. In addition, the incorporation of improved models for Ag-In-Cd control rods and B_4C control blade/Zircaloy channel boxes now better reflect the observations from separate effects material interactions experiments and integral bundle heating and melting experiments. It was noted that the heating rates above 1500 K were underpredicted for the CORA PWR experiments but not for the CORA BWR

experiments and experiments in other facilities. This discrepancy has been attributed to the presence of high concentrations of Argon used in the CORA experiments. It was also noted that the total hydrogen production was underpredicted for the CORA-17 BWR experiment with reflood. This has been attributed to oxidation of the B_4C. These descrepancies, and others identified through continued assessment of MOD3.1 for the early phases of a severe accident, will be the focus of modeling development activities in the United States and abroad.

Work is also well underway to incorporate the late phase modeling improvements recommended during the formal peer review of SCDAP/RELAP5/MOD3. These modeling improvements will be incorporated into SCDAP/RELAP5/MOD3.2 for release in 1997 once the developmental assessment of these new models is completed.

REFERENCES

1. SCDAP/RELAP5/MOD3.1 Code Manual, Volumes 1-5, NUREG/CR-6150, EGG-2720, Idaho National Engineering Laboratory, June 1995.

2. SCDAP/RELAP5/MOD3.1 Code Manual, Volumes 1-5, Revision 1, NUREG/CR-6150, INEL-95/0609 (Formerly EGG-2720), Idaho National Engineering Laboratory, To be Published.

3. C. Allison, et al., "SCDAP/RELAP5 Code Development and Assessment", Proceedings of the U.S. Nuclear Regulatory Commission Twenty-First Water Reactor Safety Information Meeting, NUREG/CP/0133, Vol. 2, April 1994.

4. L. J. Siefken, et al., "Oxidation During Reflood of a Reactor Core with Melting Cladding", Proceedings of the Seventh International Meeting on Nuclear Reactor Thermal-Hydraulics, NURETH-7, NUREG/CP-0142, Vol 3, pp 1851-1862.

5. S. Hagen, P. Hofmann, C. Allison,"Lessons on In-Vessel Severe Accidents from Experiments at KfK and the INEL", American Nuclear Society Transactions, 1993 Winter Meeting, San Francisco, November 14-18, 1993.

6. S. Hagen et al., "CORA Experiments on the Materials Behavior of LWR Fuel Rod Bundles at High Temperatures", Proceedings of the U.S. Nuclear Regulatory Commission Nineteenth Water Reactor Safety Information Meeting, NUREG/CP/0119, April 1992.

7. S. Hagen et al., Results of SFD Experiment CORA-13 (OECD International Standard Problem 31), KfK 5054, Forschungszentrum, Karlsruhe, February 1993.

8. F. E. Panisko, D. D. Lanning, N. J. Lombardo, "Lessons Learned from In-Reactor Full-Length, High-Temperature SFD Tests", American Nuclear Society Transactions, 1993 Winter Meeting, San Francisco, November 14-18, 1993.

9. D. D. Lanning, et al., Coolant Boilaway and Damage Progression Program, Data Report - Full-Length High Temperature Experiment 5, PNL-6540, Pacific Northwest Laboratory, April 1988.

10. A. D. Knipe et al., PBF Severe Fuel Damage Scoping Test - Test Results Report, NUREG/CR-4683, EGG-2413, August 1986.

11. S. Hagen, Personal Communication, Forschungszentrum, Karlsruhe, October, 1995.

12. SCDAP/RELAP5 Independent Peer Review, Los Alamos National Laboratory report, LA-12481, January 1993.

13. SCDAP/RELAP5/MOD3.1 Code Manual, MATPRO-A Library of Materials Properties for Light-Water-Reactor Accident Analysis, Volume 4, Revision 1, NUREG/CR-6150, INEL-95/0609 (Formerly EGG-2720), Idaho National Engineering Laboratory, To be Published.

14. V. X. Tung, Hydrodynamic and Thermal Aspects of Two-Phase Flow through Porous Media, PhD Thesis, University of California at Los Angeles, 1988.

15. W. Chu, V. K. Dhir, and J. S. Marshall, "Study of Pressure Drop, Void Fraction, and Relative Permeabilities of Two-Phase Flow through Porous Media", AIChE Symposium Series, Vol 79, No. 255, pp 224-235, 1983.

16. V. X. Tung and V. K. Dhir, "A hydrodynamic Model for Two Phase Flow through Porous Media", International Journal of Multiphase Flow, 14, pp 47-65, 1988.

17. N. K. Tutu, et al.,Debris Bed Quenching under Bottom Flood Conditions (In-Vessel Degraded Core Cooling Phenomenology), NUREG/CR-3850, Brookhaven National Engineering Laboratory, 1984.

18. C. H. Wang and V. K. Dhir, "An Experimental Investigation of Multidimensional Quenching of a Simulated Core Debris Bed", Nuclear Engineering and Design, 110, pp 61-72, 1988.

19. S. M. Jensen, D. W. Akers, B. A. Pregger, Postirradiation Examination Data and Analyses for OECD LOFT Fission Product Experiment LP-FP-2, OECD LOFT-T-3810, Volume 1, December 1989.

20. R. O. Gauntt, R. D. Gasser, "Results of the DF-4 BWR Control Blade-Channel Box Test", Proceedings Eighteenth Water Reactor Safety Information Meeting, NUREG/CP-0114, March, 1991.

21. Z. R. Martinson, et al., PBF Severe Fuel Damage Test 1-1 Test Results Report, NUREG/CR-4684, EGG-2463, October 1986.

22. D. A. Petti, et al. PBF Severe Fuel Damage Test 1-4 Test Results Report,

NUREG/CR-5163, EGG-2542, April 1989.

23. S. Hagen and S. O. Peck, "Temperature Escalation of Zircaloy-Clad Fuel Rods and Bundles under Severe Fuel Damage Conditions", International Meeting on LWR Severe Accident Evaluation, Cambridge, August 28 - September 1, 1983.

24. J. Rempe and C. Allison, "Improved SCDAP/RELAP5 Models for Predicting Heat Transfer from a Molten Pool", ANS Winter Meeting, San Francisco, October 29 - November 2, 1995.

Recent SCDAP/RELAP5 Improvements for BWR Severe Accident Simulations *†

F. P. Griffin

Oak Ridge National Laboratory
Oak Ridge, Tennessee 37831

ABSTRACT

A new model for the SCDAP/RELAP5 severe accident analysis code that represents the control blade and channel box structures in a boiling water reactor (BWR) has been under development since 1991. This model accounts for oxidation, melting, and relocation of these structures, including the effects of material interactions between B_4C, stainless steel, and Zircaloy.

This paper describes improvements that have been made to the BWR control blade/ channel box model during 1994 and 1995. These improvements include new capabilities that represent the relocation of molten material in a more realistic manner and modifications that improve the usability of the code by reducing the frequency of code failures. This paper also describes a SCDAP/RELAP5 assessment calculation for the Browns Ferry Nuclear Plant design based upon a short-term station blackout accident sequence.

1. INTRODUCTION

Work began at Oak Ridge National Laboratory (ORNL) in 1991 to improve the SCDAP/RELAP5 code[1] for boiling water reactor (BWR) applications. SCDAP/RELAP5 is a best estimate analysis tool for light water reactor severe accident applications that has been developed primarily at Idaho National Engineering Laboratory (INEL). INEL is the sole institution responsible for maintaining the official version of SCDAP/RELAP5.

The efforts at ORNL have focussed on the development of a new SCDAP/RELAP5 model that represents the severe accident response of the control blade and channel box structures in a BWR.[2] Sketches of a typical BWR control blade and fuel assembly are shown in Figure 1. The control blade has four wings, each consisting of a stainless steel blade sheath that surrounds a row of small stainless steel absorber tubes

* Research sponsored by the Office of Nuclear Regulatory Research, U.S. Nuclear Regulatory Commission under Interagency Agreement No. 1886-8620-2W with the U.S. Department of Energy under contract DE-AC05-84OR21400 with Lockheed Martin Energy Systems, Inc.

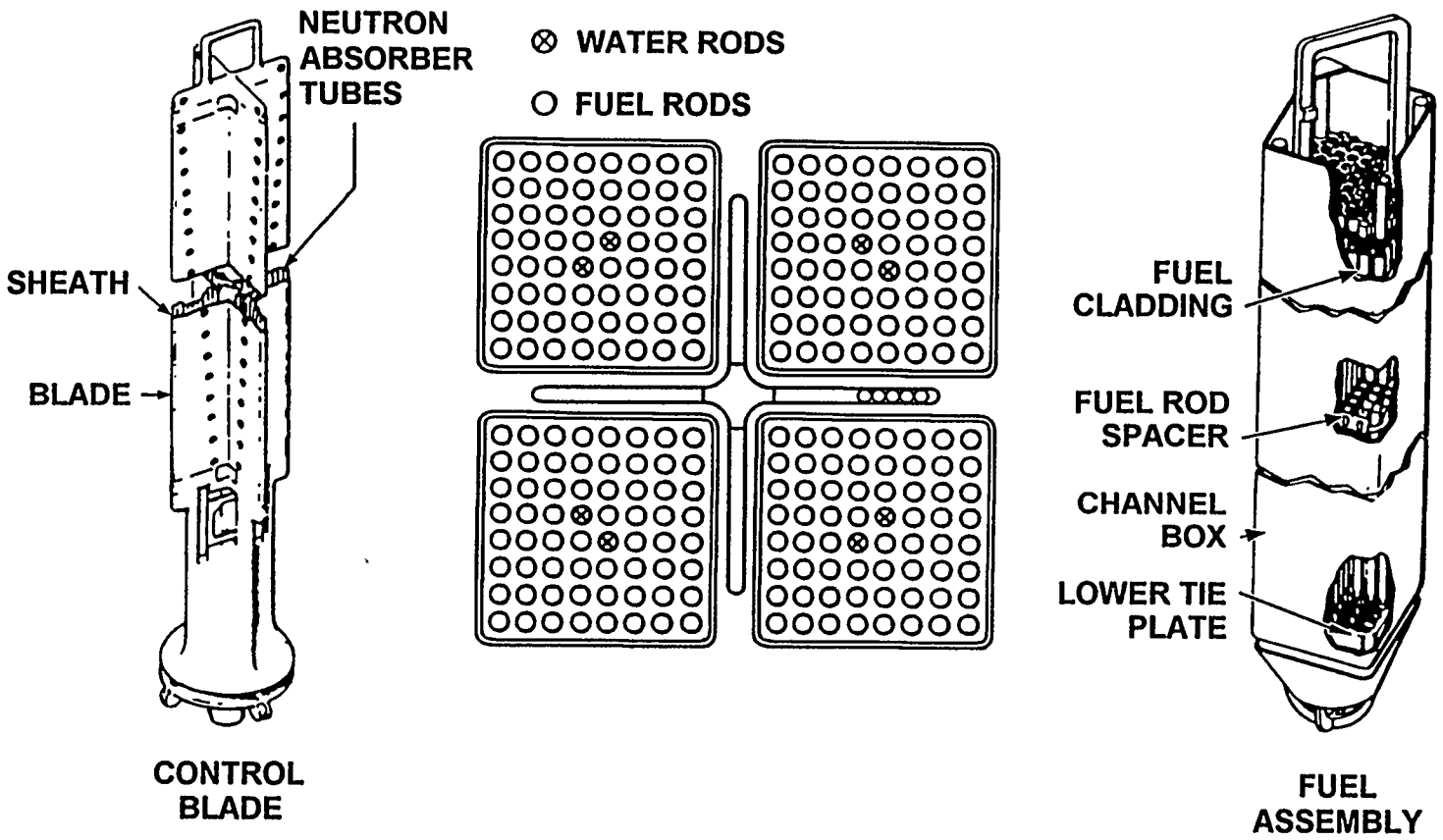

Figure 1. Sketch of typical BWR control blade and fuel assembly.

filled with B_4C powder. The fuel assembly consists of an array of fuel rods surrounded by a Zircaloy channel box. The control blade is located between four fuel assemblies.

The BWR control blade/channel box model was originally developed at ORNL as a result of posttest analyses of the CORA-16 and CORA-17 BWR experiments[3] and accounts for oxidation, melting, and relocation of these structures, including the effects of material interactions. The degradation process begins when the B_4C powder reacts with the stainless steel absorber tubes. This B_4C/stainless steel eutectic liquifies at a temperature of $\sim$1505 K, which is lower than the melting temperature of pure stainless steel. Then, either by failing the stainless steel blade sheath or flowing through the water circulation holes in the sheath (shown in Figure 1), the molten B_4C/stainless steel mixture relocates downward and freezes to form a crust on the surface of the control blade. This crust builds up until a blockage spans the gap between the control blade and the channel box. The Zircaloy channel box reacts with the stainless steel in the blockage and melts at the stainless steel/Zircaloy liquefaction temperature of $\sim$1523 K, which is much lower than the melting temperature of pure Zircaloy.

The basic features of the BWR control blade/channel box model within SCDAP/RELAP5 were described in a previous paper at the 1993 Water Reactor Safety Information Meeting.[4] Subsequently, several new capabilities and improvements have been added to the model and are described in this paper along with an example simulation of a short-term station blackout accident sequence for the Browns Ferry Nuclear Plant design. The improved BWR control blade/channel box model is available from INEL as a part of SCDAP/RELAP5, Mod3.1, Release D.

2. DESCRIPTION OF BWR CONTROL BLADE/CHANNEL BOX MODEL

The control blade/channel box model is based on the nodal configuration shown in Figure 2. The actual control blade configuration of small absorber tubes inside a stainless steel blade sheath is converted into an equivalent slab geometry. At each axial elevation, three radial temperature nodes are used for the control blade while two temperature nodes represent the channel box wall. The surrounding dashed line in Figure 2 represents an adiabatic boundary. Because of thermal symmetry, the three control blade temperature nodes actually represent only half of a control blade divided along the centerline of the row of absorber tubes. The channel box wall is divided into two segments because one segment is adjacent to a control blade while the other is not.

The control blade and channel box interact with two RELAP5 hydraulic volumes: one for the interstitial region and the other for the fuel bundle region. The gap between the blade sheath and the absorber tubes is modeled. This gap communicates with the interstitial coolant volume through a series of holes in the blade sheath (shown in Figure 1). The gap results in two additional surfaces for stainless steel oxidation and also imposes an additional thermal resistance between the blade sheath and the absorber tubes. The portion of the interstitial coolant volume beyond the tip of the control blade provides an important path for molten control blade material to relocate downward onto the core plate.

A finite difference formulation is used to model the thermal responses of the control blade and channel box structures. Energy equations representing conduction and convection heat transfer in the radial direction are solved implicitly to determine new values for the five nodal temperatures at each axial elevation. Axial conduction, relocation/solidification, oxidation, and radiation heat transfer are computed

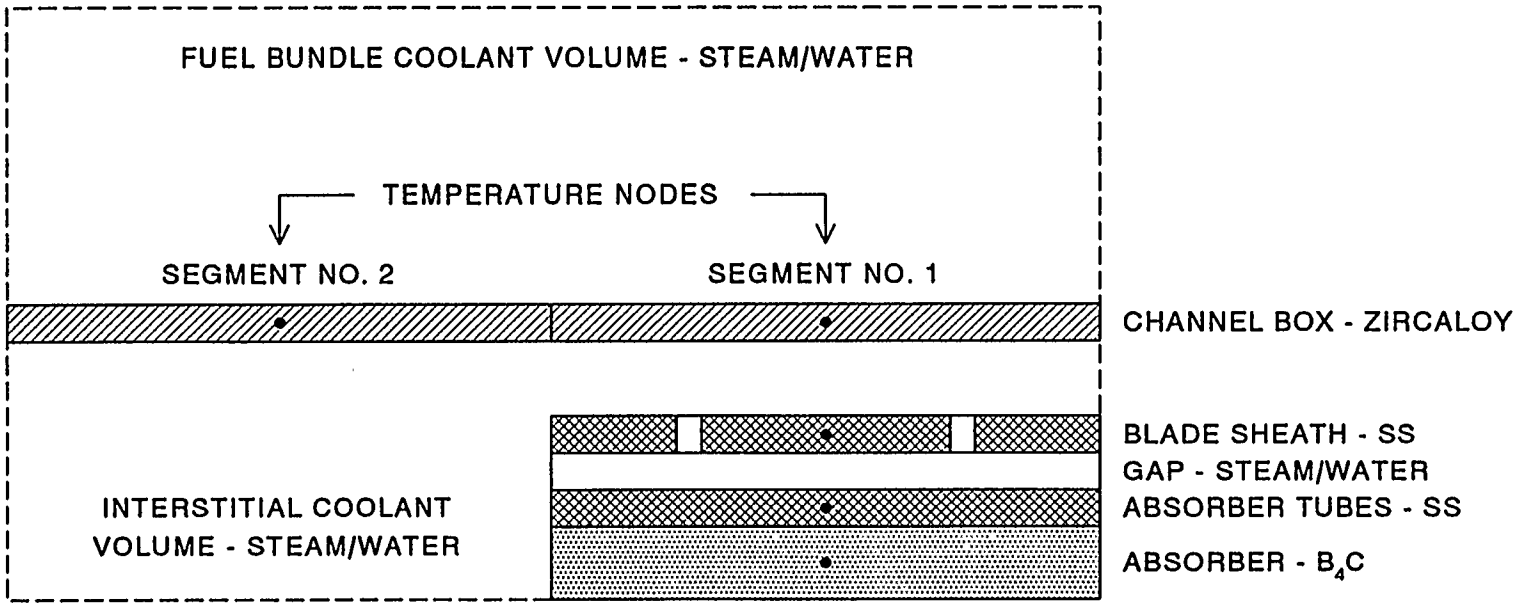

Figure 2. BWR control blade/channel box model with equivalent slab geometry and five temperature nodes at each axial elevation.

explicitly using previous timestep information and are included as constant heat transfer terms in the energy equations.

An approximate solution method is used to account for melting in the energy equations. At the end of each timestep, the new nodal temperatures calculated from the energy equations are compared with their associated melting points. If a nodal temperature is greater than its melting point and the node also contains solid material, then the nodal temperature is adjusted downward to equal its melting point, and the associated sensible heat is used to melt an appropriate amount of the solid material. This temperature adjustment is not made if the node does not contain any solid material (i.e., if only liquid material is present).

Material interactions between B_4C/stainless steel and stainless steel/Zircaloy are represented by using reduced melting temperatures. Eutectic liquefaction temperatures are used in the melting calculations rather than the melting temperatures of the pure materials. The liquefaction temperatures are $\sim$1505 K for B_4C/stainless steel mixtures and $\sim$1523 K for stainless steel/Zircaloy mixtures.

The relocation of molten material is assumed to be controlled by solidification rates. As molten material relocates downward over an underlying solid structure, it solidifies and transfers heat to the underlying structure. In the control blade/channel box model, molten material is allowed to relocate downward until it either solidifies, is diverted horizontally by a blockage, or moves past the bottom of the defined core. The effects of blockages on the relocation of molten material are described in more detail in Section 2.2.

The oxidation of Zircaloy, stainless steel, and B_4C is included in the control blade/channel box model. Based on steam availability and the reaction kinetics, oxidation heat generation rates and hydrogen production rates are calculated for each surface. Oxidation of stainless steel is based on a chemical composition of 74% iron, 18% chromium (which is the major contributor to total reaction energy), and 8% nickel.

Radiation calculations on the fuel bundle side of the channel box are performed in the normal manner by the SCDAP radiation model,[5] with the two segments of the channel box treated as independent surfaces. Radiation calculations on the interstitial side of the channel box are performed internally by the control blade/channel box model. These radiation calculations are activated whenever the local coolant void fraction exceeds a user-specified value.

All hydrodynamic parameters used in the control blade/channel box model are obtained from the RELAP5 data base. These parameters include steam flow rates, coolant properties (pressures, temperatures, void fractions), and convective heat transfer coefficients. Control blade/channel box parameters returned to SCDAP/RELAP5 include hydrogen generation rates, heat transfer rates from the structures to the coolant, and coolant flow area reductions caused by frozen crust formation.

2.1 RECENT MODEL IMPROVEMENTS

Several new capabilities and improvements have been added to the BWR control blade/channel box model during 1994 and 1995. These improvements include: (1) implementation of timestep repetition, (2) modifications that improve execution times for BWR simulations, (3) replacement of hard-wired material property correlations with equivalent correlations from the MATPRO library of material

properties,[6] (4) modifications that allow molten control blade/channel box material to spread radially into the fuel bundle, and (5) modifications that allow molten control blade/channel box material to relocate downward into the lower plenum.

Improvements 1 and 2 have minimal impact on the calculated results for BWR simulations, but they reduce the frequency of water property failures and improve the usability of the code. The timestep repetition modifications (improvement 1) make the control blade/channel box model consistent with logic implemented previously at INEL for the other SCDAP core models and involves saving all necessary variables at the beginning of a timestep so the calculations for the timestep can be repeated if necessary.

The use of MATPRO material properties (improvement 3) makes the code easier to maintain by eliminating redundancy. Improvements 4 and 5 are new capabilities that represent the relocation of molten material during core degradation in a more realistic manner. The relocation modeling is explained in greater detail in Section 2.2.

2.2 RELOCATION LOGIC

During a BWR severe accident, core degradation begins with control blade liquefaction at a temperature of ~1505 K. A molten B_4C/stainless steel mixture relocates downward and solidifies at a lower elevation to form a blockage in the interstitial volume between the control blade and channel box segment No. 1 (see Figure 2). The relocation logic in the control blade/channel box model allows for horizontal movement of molten material when a blockage inhibits downward movement. For a blockage between the control blade and channel box segment No. 1, the horizontal relocation logic proceeds in the following order:

(1) If channel box segment No. 1 has failed, molten control blade material relocates radially through the opening in the channel box wall and down the fuel bundle side of the channel box.
(2) If the interstitial volume beyond the tip of the control blade is open, any remaining molten material relocates laterally from segment No. 1 to segment No. 2.
(3) Any remaining molten material pools up on top of the interstitial blockage.

Molten control blade material that relocates radially through the opening in the channel box wall can freeze to form a second blockage in the fuel bundle volume between channel box segment No. 1 and the first row of fuel rods. When this second blockage exists, molten material relocates radially into the fuel bundle region and down the outer surface of adjacent fuel or simulator rods. The recent model improvements represent this radial spreading into the fuel bundle by transferring the molten material from the control blade/channel box model to the SCDAP fuel or simulator rod models.

Downward-moving molten material that does not solidify before reaching the lowest elevation of the control blade or channel box surfaces relocates below the bottom of the defined core. If a COUPLE finite element mesh[7] is defined by the user to represent lower plenum debris, then the recently added lower plenum relocation logic transfers this molten control blade/channel box material directly into the lower plenum debris bed. (This relocating material does not interact with the structures in the core plate region because SCDAP/RELAP5 does not currently include a model to represent the behavior of the core plate during a severe accident.)

3. ASSESSMENT CALCULATION FOR BROWNS FERRY NUCLEAR PLANT DESIGN

A SCDAP/RELAP5 input deck has been prepared for the Browns Ferry Nuclear Plant design based upon a short-term station blackout (STSB) accident sequence. This STSB simulation was developed by modifying an existing Browns Ferry input deck representing a large-break loss of coolant accident (LOCA) sequence obtained from INEL. The STSB input deck has been used to perform assessment calculations for the purpose of testing the BWR control blade/channel box model improvements described in this paper. A description of the input deck is provided in this section along with some calculated results from the Browns Ferry STSB accident simulation.

A nodalization diagram for the Browns Ferry reactor coolant system is shown in Figure 3. The reactor coolant system is represented from the feedwater inlet to the turbine inlet and includes the reactor pressure vessel, two recirculation loops, the feedwater piping, the control rod drive (CRD) cooling water, and the steam piping. The recirculation loop on the left-hand side of Figure 3 was originally used at INEL to represent the initiating pipe break for a LOCA sequence. For the STSB accident sequence, both recirculation loops remain intact (i.e., the valves between volumes 200 and 998 and volumes 210 and 999 are closed). The Browns Ferry containment is not represented explicitly. Rather, the safety/relief valves (SRVs) discharge into volume 561, which is assumed to remain at a constant pressure of 0.31 MPa (45 psia).

A more detailed nodalization diagram of the lower half of the reactor pressure vessel is shown in Figure 4 with hydraulic volumes represented by open boxes and solid structures represented by shaded boxes. The active core is divided into four radial rings and thirteen axial levels. The center ring of the core (right-hand side of Figure 4) represents ~55% of the fuel assemblies, while the other three rings near the periphery of the core (where the power density is progressively lower) each represent ~15% of the fuel assemblies. The lower 1.07 m (3.5 ft) of the active core is divided into seven axial levels, while the upper 2.74 m (9.0 ft) of the active core is divided into six axial levels.

In each of the four radial rings, there is one set of volumes that represents the coolant flow inside the fuel assemblies (volumes 320, 321, 322, and 323) and another set of volumes that represents the coolant flow outside the fuel assemblies in the interstitial region surrounding the control blades (volumes 370, 324, 325, and 326). The interstitial volumes outside the fuel assemblies are connected by cross-flow junctions that allow coolant to flow horizontally between the center and the periphery of the core. Note that for simplicity, these cross-flow junctions are illustrated in Figure 4 only at axial node 13. Similar cross-flow junctions also exist at axial nodes 1 through 12.

The primary coolant flow through the core (~90% of total) is from the lower plenum (volumes 292, 293, and 294) through the fuel support pieces and lower tie plates (volumes 300, 301, 302, and 303) and into the fuel assemblies. The remaining core coolant flow (~10% of total) is through the interstitial region. Coolant enters the interstitial region by either flowing through holes machined in the lower tie plates, leaking past the core plate, or flowing through the control rod guide tubes (volumes 340 and 350) from the CRD cooling water pumps.

The jet pumps are represented by volumes 260, 265, and 270 (first recirculation loop) and volumes 261, 266, and 271 (second recirculation loop). In a BWR, the upper mixing sections of the jet pumps are connected to the lower diffuser sections by mechanical slip fits for easy removal during maintenance.

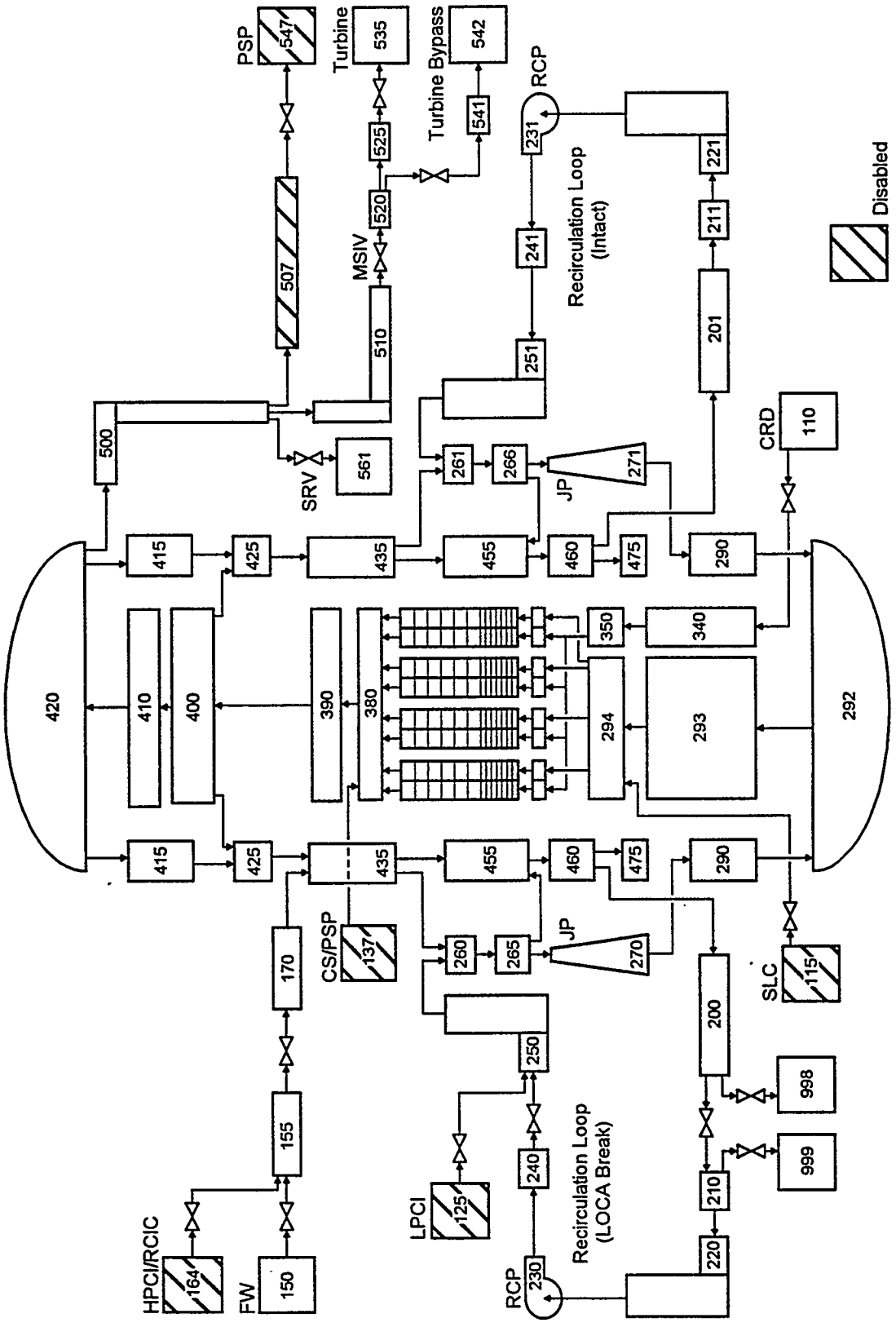

Figure 3. Nodalization diagram of Browns Ferry reactor coolant system.

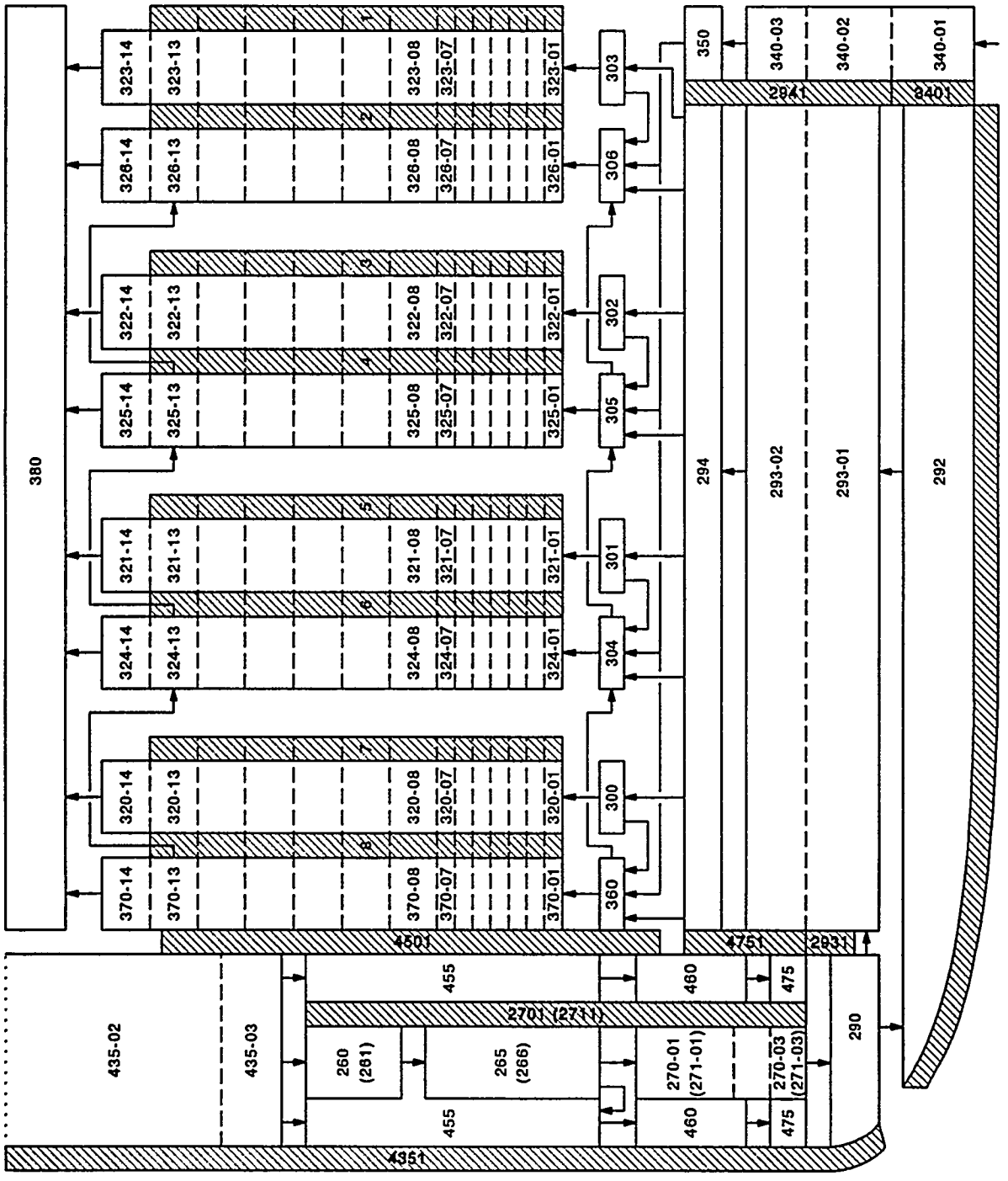

Figure 4. Nodalization diagram of Browns Ferry lower reactor vessel.

The leakage through these slip joints is represented by junctions that connect the jet pumps (bottom of volumes 265 and 266) to the annulus region (volume 455).

The SCDAP components representing the core structures are shown in Figure 4 as shaded boxes with labels 1 through 8. A summary of these SCDAP components is provided in Table 1. All fuel rods and control blade/channel boxes within each core radial ring are represented by single representative SCDAP components. The RELAP5 heat structures representing the pressure vessel wall and the other internal structures are shown in Figure 4 as shaded boxes with 4-digit labels. The lower vessel wall (not labeled in Figure 4) and any lower plenum debris are represented by a COUPLE finite element mesh. There are 18 elements representing the vessel wall and 36 elements (initially filled with water) representing the lower plenum debris volumes.

The radial and axial power profiles used for the Browns Ferry STSB simulation are shown in Figures 5 and 6. Note that the peripheral fuel assemblies produce only one third as much power as the center fuel assemblies. Also note that the peak power in the center fuel assemblies is at a low elevation in the core.

The initial condition for the Browns Ferry STSB simulation is steady-state operation at full reactor power (3293 MWt). The STSB accident sequence is caused by a loss of off-site AC power combined with failure of the emergency diesel generators and is initiated at time zero by: (1) loss of AC power to the recirculation pumps, (2) loss of AC power to the CRD cooling water pumps, (3) initiation of main steam isolation valve (MSIV) closure, (4) initiation of scram, and (5) loss of the turbine-driven feedwater pumps and initiation of feedwater coast-down. Throughout the duration of the STSB accident sequence, all sources of cooling water for the core are unavailable.

After the feedwater trip signal at time zero, the turbine-driven feedwater pumps briefly continue to supply coolant to the vessel during coast-down. In the STSB simulation, the feedwater flow continues at 100% for 11.78 s after the trip signal and then reduces linearly to zero by 35 s after the trip signal. The total

Table 1. Summary of SCDAP components for Browns Ferry simulation

Number	Type	Description
1	Fuel rod	432 fuel assemblies at center of core (ring 1)
2	Control blade/channel box	108 control blades at center of core (ring 1)
3	Fuel rod	104 fuel assemblies (ring 2)
4	Control blade/channel box	26 control blades (ring 2)
5	Fuel rod	128 fuel assemblies (ring 3)
6	Control blade/channel box	32 control blades (ring 3)
7	Fuel rod	100 fuel assemblies at periphery of core (ring 4)
8	Control blade/channel box	19 control blades at periphery of core (ring 4)

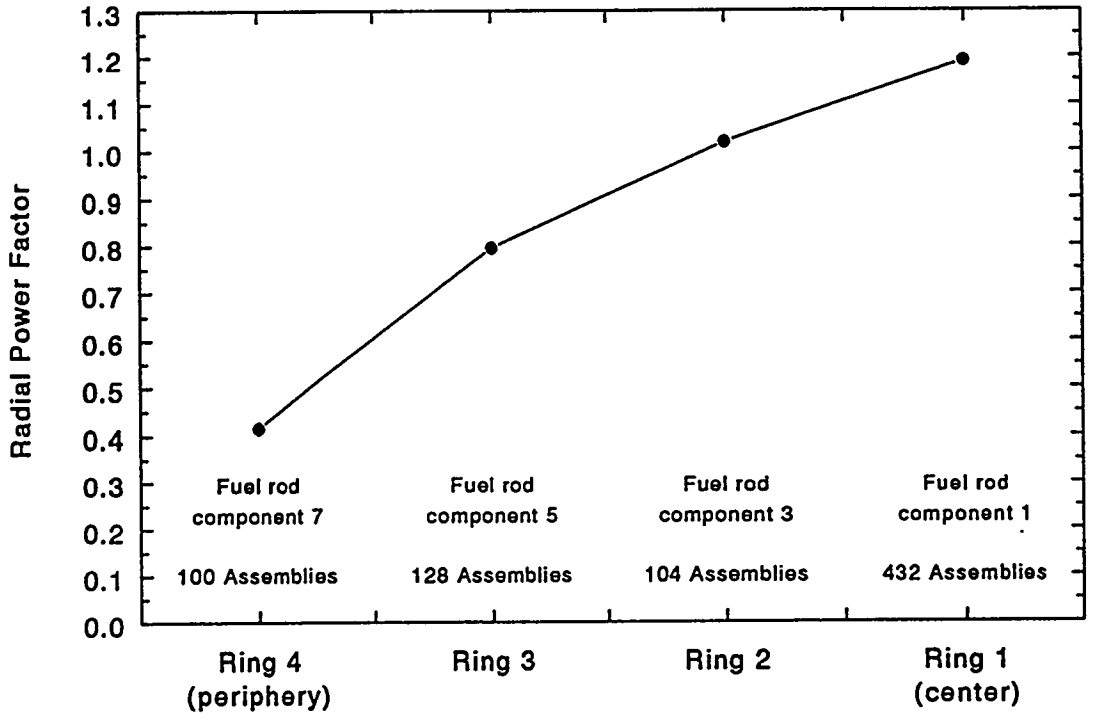

Figure 5. Browns Ferry power profile for 4 radial rings.

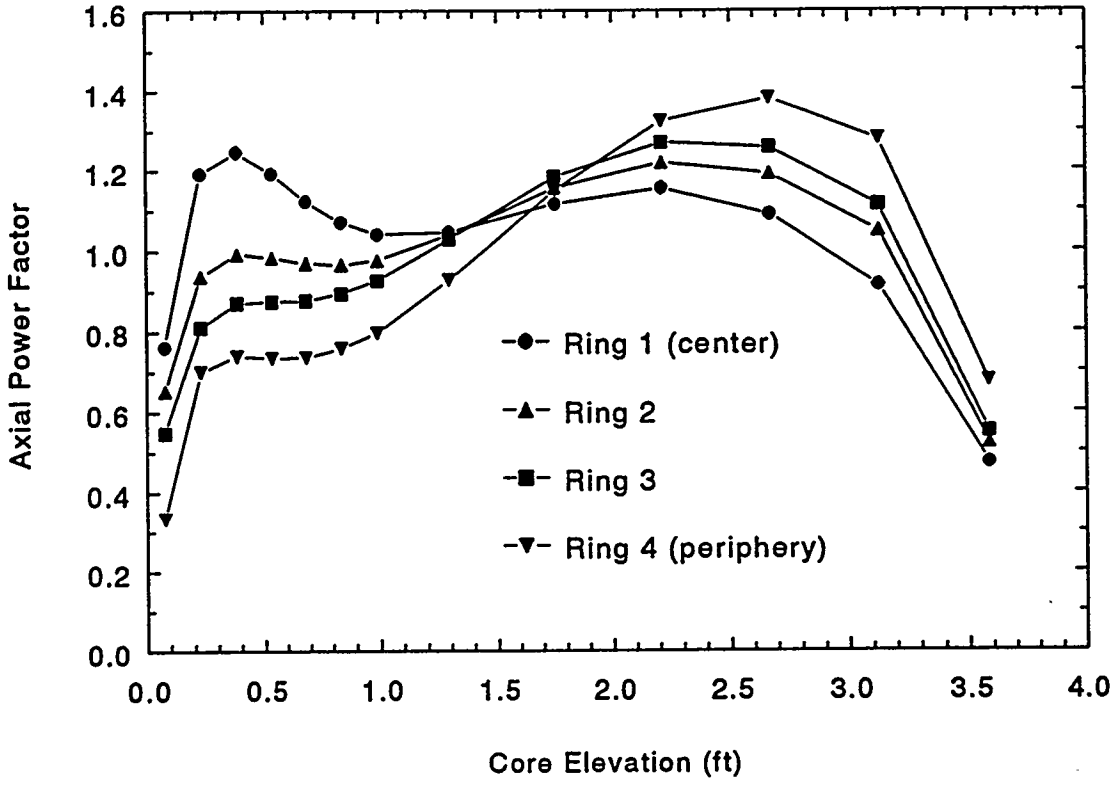

Figure 6. Browns Ferry power profiles for 13 axial nodes.

amount of coolant injected during the feedwater pump coast-down is 39,310 kg (86,660 lbm), which is about 14% of the normal vessel inventory.

Automatic actuation of the SRVs is represented during the initial slow boil-off; manual operation of the SRVs by reactor operators as specified in the Emergency Procedure Guidelines is not represented during this time period. The individual SRVs open and close at different pressures. The first SRV opens when the vessel pressure increases to 7.688 MPa (1115 psia) and remains open until the vessel pressure declines to 6.991 MPa (1014 psia). Other SRVs would also open if the pressure continued to increase.

The calculated response of the vessel pressure is illustrated in Figure 7. The vessel pressure is controlled by the automatic SRV actuations until the Automatic Depressurization System (ADS) is manually initiated as specified in the Emergency Procedure Guidelines, which occurs when the fuel bundle water level in the center radial ring (see Figure 8) reaches one-third of the active fuel height. The vessel depressurizes until it equilibrates with the containment pressure [represented here as a constant 0.31 MPa (45 psia)]. The vessel water inventory flashes during the depressurization, stabilizing in the lower plenum at a level well below the core.

Core degradation occurs under "dry" conditions with very little steam available for oxidation reactions. The calculated hydrogen generation of 210 kg shown in Figure 9 is much less than the theoretical value of ~3000 kg that would be generated by complete oxidation of all Zircaloy from the cladding and channel boxes and all stainless steel from the control blades.

The calculated times of important core degradation events are listed in Table 2. Control blade liquefaction is calculated to begin in core radial ring 1 at 120 min after scram when the control blade temperatures reach 1505 K. This molten control blade material relocates downward and solidifies at

Table 2. Calculated event times for Browns Ferry STSB accident

Description of Event	Time After Scram (min)			
Water level at top of active fuel	59			
ADS initiation, water level at 1/3 active fuel	91			
	Ring 4 (periphery)	Ring 3	Ring 2	Ring 1 (center)
First control blade liquefaction (1505 K)	168	133	125	120
First control blade radial spreading into fuel bundle	260	170	152	131
First fuel cladding relocation (2200 K)	256	166	150	134
Molten ceramic pool (2844 K) slumps into lower plenum		259	259	259
Creep rupture failure of lower vessel wall	300			

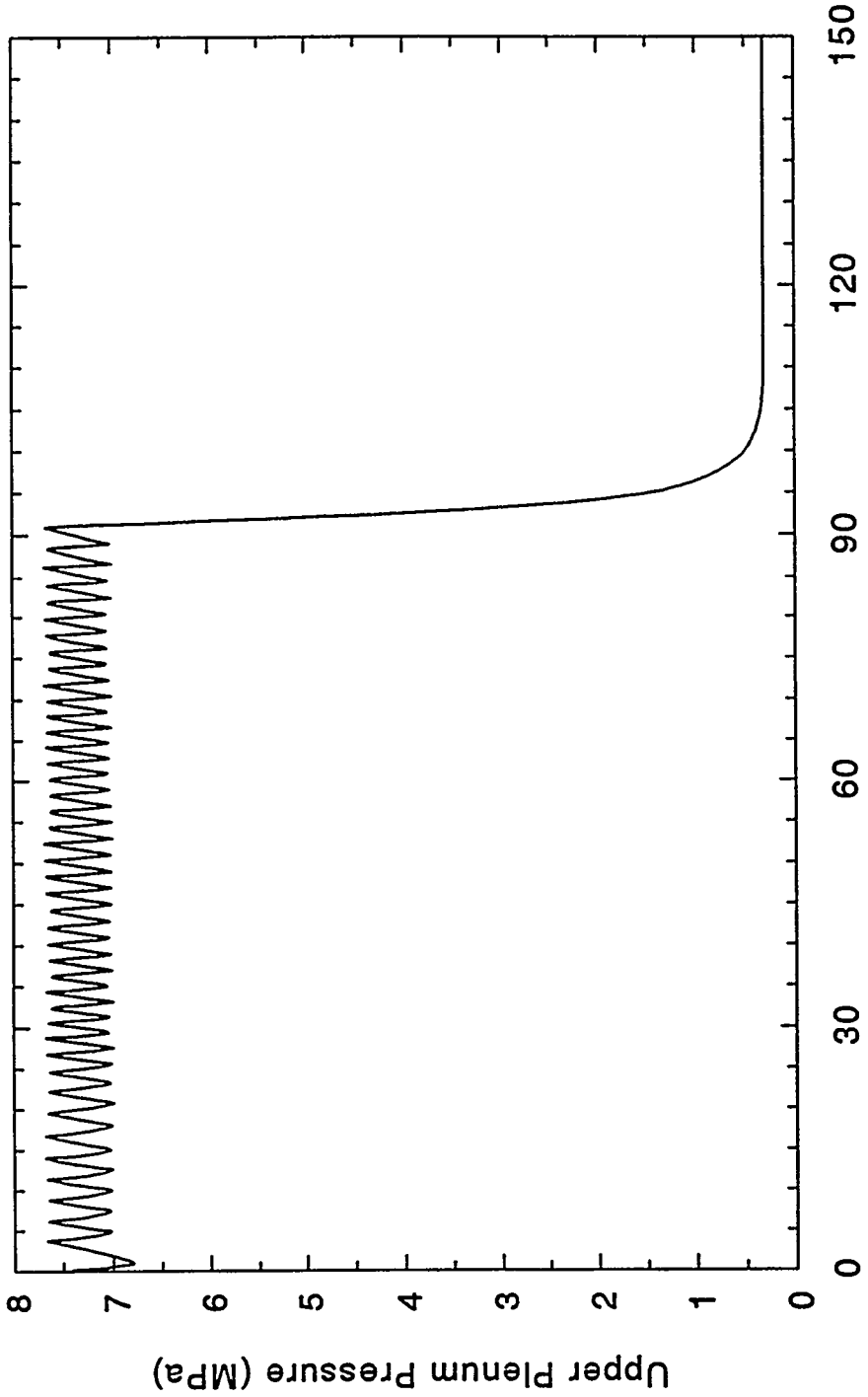

Figure 7. Calculated vessel pressure for Browns Ferry STSB accident.

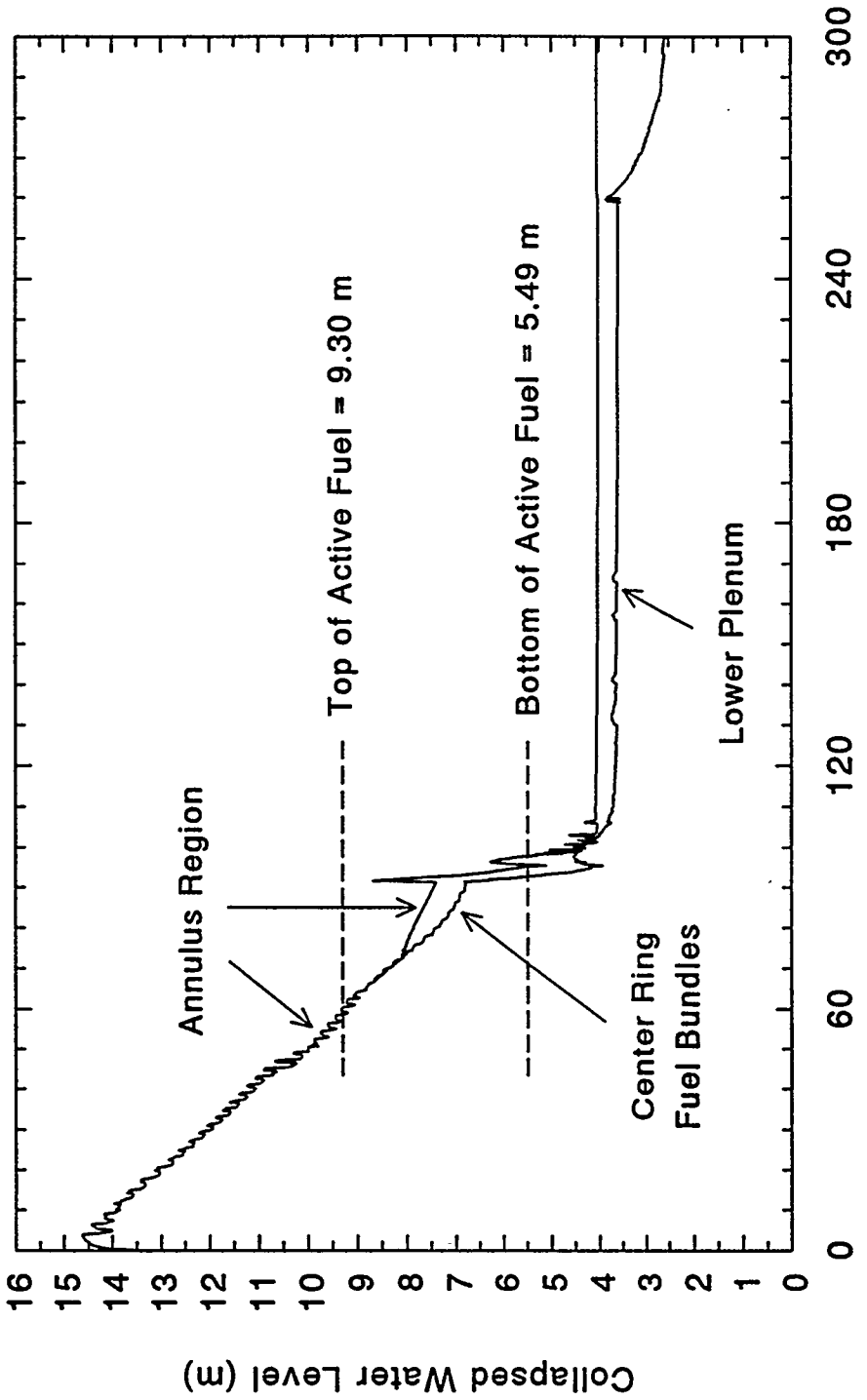

Figure 8. Calculated vessel water levels for Browns Ferry STSB accident.

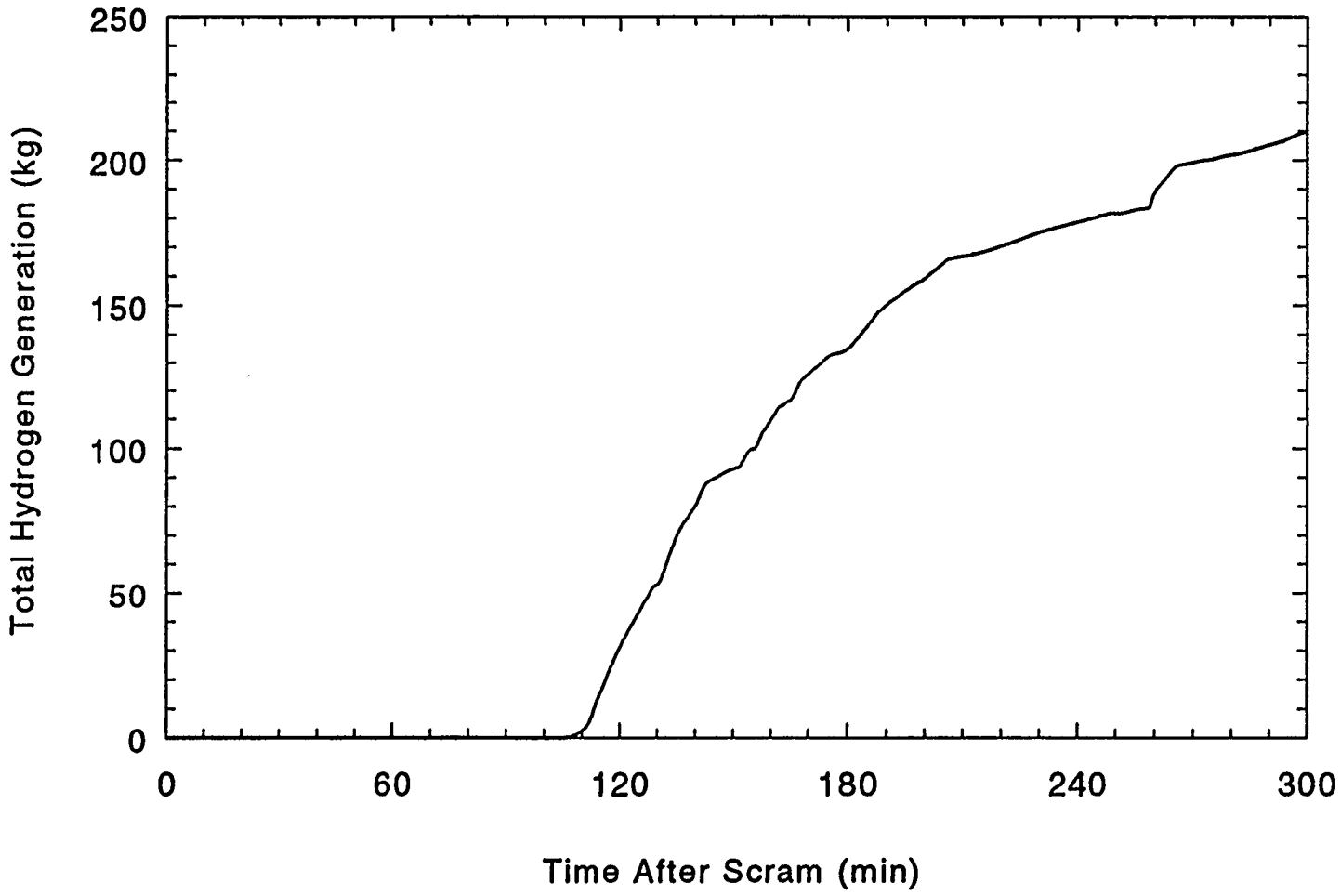

Figure 9. Calculated hydrogen generation for Browns Ferry STSB accident.

lower elevations in the core. At 131 min, extensive blockages have formed around the control blades in core radial ring 1, and molten control blade material is calculated to begin spreading radially into the fuel bundles. Some of the molten control blade material also relocates below the bottom of the core and slumps directly into the lower plenum to form a debris bed (see Figure 10). Rapid quenching of the debris as it falls through the water in the lower plenum is not represented in this calculation, but slow heat transfer from the top surface of the debris bed to the lower plenum water is represented after formation of the debris bed.

The first fuel cladding relocation is calculated to begin in core radial ring 1 at 134 min (see Table 2) when the cladding oxide layer fails at a user-specified temperature of 2200 K. As the core continues to heatup, the fuel rods form a large molten ceramic pool that occupies three of the four core radial rings. At 259 min, this entire molten ceramic pool has reached a temperature of 2844 K and is calculated to slump into the lower plenum (see Figure 10). After this fuel rod debris reaches the lower plenum, the associated decay heat causes the vessel wall temperatures to increase until creep rupture failure of the vessel wall is calculated at 300 min.

4. SUMMARY AND CONCLUSIONS

During the past several years, improvements have been made to the BWR control blade/channel box model in SCDAP/RELAP5. Relocation of molten material is now represented in a more realistic manner by accounting for radial spreading into the fuel bundle and downward movement into the lower plenum. Also, the frequency of execution failures has been reduced by implementing timestep repetition logic for the control blade/channel box model.

SCDAP/RELAP5 assessment calculations have been performed using an input deck that represents a short-term station blackout accident sequence for the Browns Ferry Nuclear plant design. Now that the BWR control blade/channel box model is more mature, these Browns Ferry simulations execute to the time of lower vessel wall failure without water property failures or user intervention to manually reduce the timestep.

Although significant progress has been made to improve SCDAP/RELAP5 for BWR applications, several limitations still exist that will require further development efforts. New or improved models are needed to represent (1) degradation of upper plenum structures (development work is currently in progress), (2) accumulation of debris on and failure of BWR core plates, and (3) quenching of debris as it falls through water in the lower plenum.

5. REFERENCES

1. E. W. Coryell and E. C. Johnsen, editors, *SCDAP/RELAP5/MOD3.1 Code Manual, Volume III: SCDAP/RELAP5 User's Guide and Input Manual*, NUREG/CR-6150, EGG-2720, October 1993.

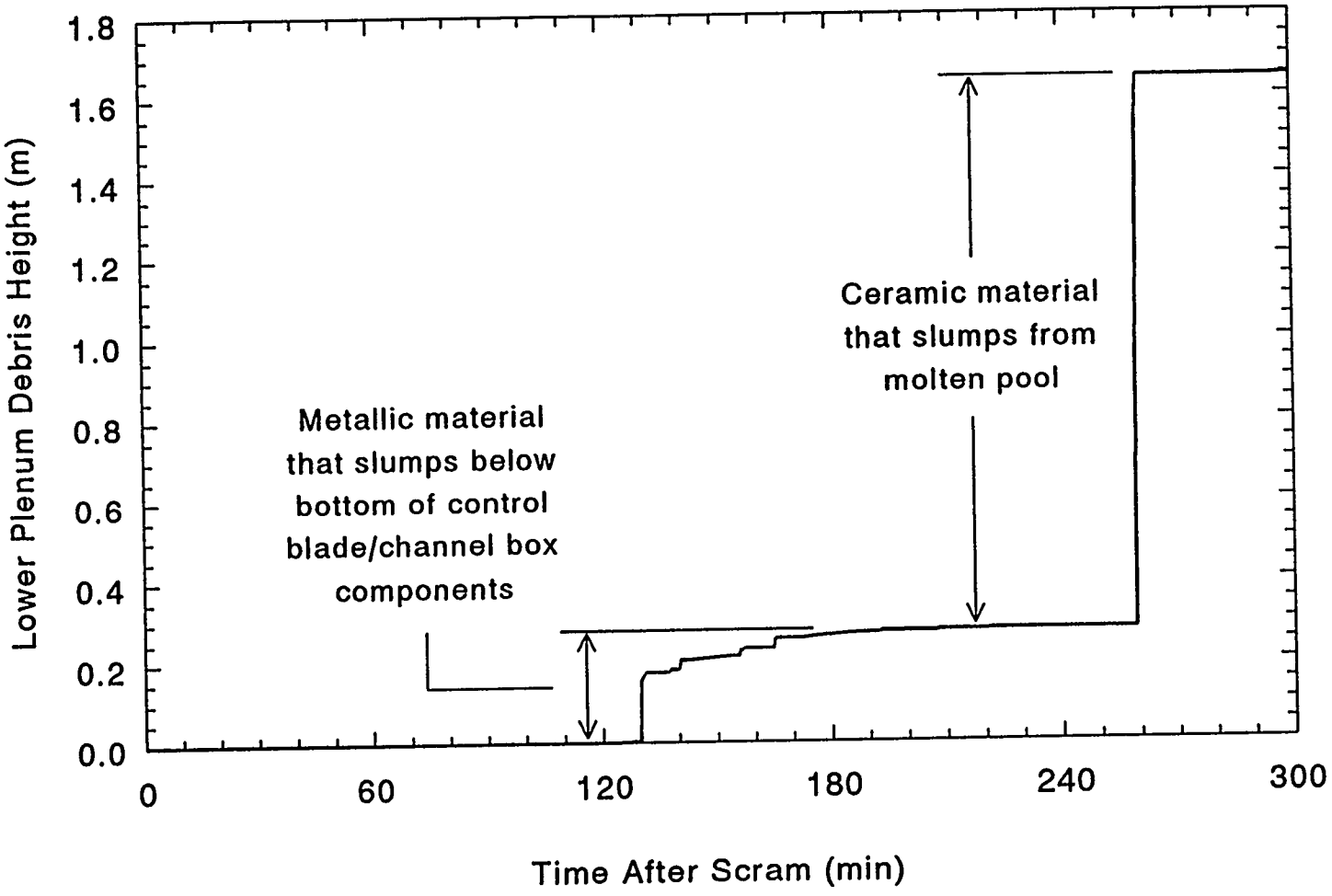

Figure 10. Calculated lower plenum debris height for Browns Ferry STSB accident.

2. F. P. Griffin, *BWR Control Blade/Channel Box Interaction and Melt Relocation Models for SCDAP (Revision 3)*, ORNL/NRC/LTR-92/12/R3, letter report to Dr. Y. Chen, Accident Evaluation Branch, Division of Systems Technology, RES, USNRC, March 31, 1995.

3. L. J. Ott, *Posttest Analyses of the CORA-16 and CORA-17 BWR Experiments*, ORNL/NRC/LTR-92/17, letter report to Dr. A. Behbahani, Accident Evaluation Branch, Division of Systems Technology, RES, USNRC, July 10, 1992.

4. F. P. Griffin, "BWR Control Blade/Channel Box Interaction Models for SCDAP/RELAP5", presented at the Twenty-First Water Reactor Safety Information Meeting, Bethesda, Maryland, October 25-27, 1993.

5. E. W. Coryell, editor, *SCDAP/RELAP5/MOD3.1 Code Manual, Volume I: SCDAP/RELAP5 Interface Theory*, NUREG/CR-6150, EGG-2720, October 1993.

6. D. T. Hagrman, editor, *SCDAP/RELAP5/MOD3.1 Code Manual, Volume IV: MATPRO—A Library of Materials Properties for Light-Water-Reactor Accident Analysis*, NUREG/CR-6150, EGG-2720, November 1993.

7. K. L. Davis, editor, *SCDAP/RELAP5/MOD3.1 Code Manual, Volume II: Damage Progression Model Theory*, NUREG/CR-6150, EGG-2720, October 1993.

Development of an Improved HRA Method: A Technique for Human Error Analysis (ATHEANA)

J.H. Taylor,* W.J. Luckas,* J. Wreathall,+ S.E. Cooper,** D.C. Bley,++

*Brookhaven National Laboratory, Upton, NY
+John Wreathall & Co., Dublin, OH
**Science Applications International Corp., Reston, VA
++Buttonwood Consulting Inc., Oakton, VA

Background

Probabilistic risk assessment (PRA) has become an increasingly important tool in the nuclear power industry, both for the Nuclear Regulatory Commission (NRC) and the operating utilities. The NRC recently published a final policy statement, SECY-95-126, encouraging the use of PRA in regulatory activities. Human reliability analysis (HRA), while a critical element of PRA, has limitations in the analysis of human actions in PRAs that have long been recognized as a constraint when using PRA. In fact, better integration of HRA into the PRA process has long been a NRC issue. Of particular concern, has been the omission of errors of commission - those errors that are associated with inappropriate interventions by operators with operating systems.

To address these concerns, the NRC identified the need to develop an improved HRA method, so that human reliability can be better represented and integrated into PRA modeling and quantification.

Description of the Project

The purpose of the Brookhaven National Laboratory (BNL) project, entitled "Improved HRA Method Based on Operating Experience" is to develop a new method for HRA based on analyzing risk-significant operating experience. This approach will allow a more realistic assessment and representation of the human contribution to plant risk, and thereby increase the utility of PRA. The project's completed, ongoing, and future efforts fall into four phases:

1) Assessment Phase (FY 92/93, documented in NUREG/CR-6093)
2) Analysis and Characterization Phase (FY 93/94, documented in NUREG/CR-6265)
3) Development Phase (FY 95/96, documented in draft report)
4) Implementation Phase (FY96, planned)

Overview of the Results

The Analysis and Characterization Phase (documented in NUREG/CR-6265) developed a multidisciplinary HRA framework with the objective of providing a structured approach for analyzing operating experience and understanding NPP safety, human error, and the underlying factors that affect them. The framework had to be multidisciplinary because the factors affecting human reliability and plant safety are based on many sciences. In the current Development Phase, which is the subject of this paper, the concepts of the framework have matured into a working HRA method, with identified process steps. This working HRA method, albeit in preliminary form, has been expanded by using trial applications concluding in quantification of a human failure event.

The ATHEANA HRA Method

The new HRA method, called ATHEANA (A Technique for Human Error Analysis), improves the ability of PRAs to:

- identify and characterize important human-system interactions and their likely consequences under accident conditions;

- represent the most important severe accident sequences that could occur;
- estimate the frequencies of these sequences and the associated probabilities of human errors; and

- provide recommendations for improving human performance based upon characterizations of the causes of human errors.

In order to achieve these goals in the development of the new HRA method, ATHEANA, it was necessary to establish a new basis for HRA modeling, starting with the development of a better understanding of human performance in serious nuclear power plant accidents and their precursors. ATHEANA is based on a multidisciplinary framework that considers both the human-centered factors (e.g., performance shaping factors such as human-machine interface design, procedures content and format, and training) and the conditions of the plant that give rise to the need for actions and create the operational causes for human-system interactions (e.g., misleading indications, equipment unavailabilities, and other unusual configurations or operational circumstances). The human-centered factors and the influence of plant conditions are not independent of each other; the combined effect of performance shaping factors (PSFs) and plant conditions that create a situation in which human error is likely to occur is an "error-forcing context".

Considerable research was conducted on the various HRA elements of the ATHEANA framework. The representation of human error encompasses both the underlying mechanisms of human error and the consequences of the error mechanism, which is the unsafe action. The error mechanisms are behavioral and cognitive mechanisms causing human errors, that can be triggered by particular plant conditions and PSFs. When applied in the wrong context, error mechanisms can lead to inappropriate actions that can have unsafe consequences that lie within the PRA definition of accident scenarios. "Unsafe actions" are those actions inappropriately taken, or not taken when needed, by plant personnel that result in a degraded plant safety condition. Unsafe action does not necessarily imply that humans are a root cause; people are often set-up by circumstances and conditions to take actions that are unsafe.

In addition to the psychological developments discussed above, analyses of accidents and serious incidents have both confirmed the principles underlying ATHEANA and precipitated the identification and development of these principles. The results of these operational event analyses are formulated in a manner that supports use of ATHEANA. These results are captured in a database which has been developed for this project.

ATHEANA has been developed with the goal of being used in traditional PRA models. In other words, application of ATHEANA will not require major changes to the mechanics of how PRA models are constructed. Furthermore, ATHEANA will be usable by a PRA analyst, using input from experts such as those knowledgeable of plant design and operations, but will not need to rely on having extensive experience in human factors or psychology.

Trial Application of the Concepts

A trial application of ATHEANA was conducted using the following process steps. (It should be noted that the quantification of a HFE based upon the likelihood of EFC's occurring represents a fundamental shift in the conduct of HRA.):

- identification of a human failure event (HFE)
- identification of an unsafe action associated with the HFE
- identification of an error forcing context (EFC) associated with the unsafe action
- estimation of probabilities for each EFC
- quantification of the HFE using the estimated EFC probabilities

For the purposes of the trial application, a PWR small-break LOCA was selected. The specific PRA used in the trial application was the Surry Unit 1 NUREG-1150 PRA. An existing PRA was used so that comparisons could be made between the original PRA and the trial application. As is typical, the sample PRA only modeled human errors of omission. However, to demonstrate the value of ATHEANA, the success of the high pressure injection function was examined and ways in which the operators can fail this function were identified, based upon knowledge gained on the project to date from human factors research and event analyses. As a result, the HFE identified in the trial demonstration was "operators inappropriately terminate HPI". The unsafe action, associated with the HFE, that was selected for the demonstration was described as "Operators turn off operating HPI pumps, given the mistaken belief that the safety injection (SI) termination criteria given in procedures have been satisfied."

Actual plant procedures were used to identify an error forcing context (EFC) that could induce the unsafe action and resulting HFE that were selected for the trial application. The EFC selected was: a stuck open power operated relief valve causing pressurizer level indication to read incorrectly, coupled with PSFs and errors in information processing. A quantification demonstration resulted in an HFE probability of 7.5E-4 and a core damage frequency of 1.5E-5. These calculations demonstrate that HFEs can be significant contributors to plant risk when considered under an appropriate EFC.

Findings

The trial application was a "proof of concept" for ATHEANA; it demonstrated that it is possible to identify and estimate the probabilities of HFEs (and associated EFCs) that have an observable impact on the frequency of core damage, and which are generally not included in current PRAs.

A general process was outlined that addresses the iterative steps of defining HFEs and estimating their probabilities using search schemes.

A knowledge base was developed with the objective of describing the links between unsafe actions and error forcing contexts, and is based on behavioral science theory and analysis of NPP events.

Future Work

There are several activities that are required to complete the development of ATHEANA. The most important of these activities is the development of the ATHEANA application tools. These tools are 1) the implementation guidelines, which is to be a "how to" document, and 2) the frame-of-reference (FOR)

manual, which is a technical basis document. The precursors to these tools presented here have been based on trials of only a few relatively simple example scenarios. The search schemes, in particular, are rudimentary and need to be developed to a more comprehensive level. Hence, to validate the methodology, larger scale demonstrations should be conducted, perhaps including demonstration in a full scale PRA.

In addition to its intended use of providing more comprehensive HFEs and more accurate quantification, other valuable uses of the ATHEANA methodology should be examined, such as root cause analysis and a structured approach to incident analysis/investigation to identify and correct the underlying causes of human error.

Uncertainties in Offsite Consequence Analysis

M. L. Young and F. T. Harper, Sandia National Laboratories
C. H. Lui, U. S. Nuclear Regulatory Commission

ABSTRACT

The development of two new probabilistic accident consequence codes, MACCS and COSYMA, was completed in 1990. These codes estimate the consequences from the accidental releases of radiological material from hypothesized accidents at nuclear installations. In 1991, the U.S. Nuclear Regulatory Commission and the European Commission began co-sponsoring a joint uncertainty analysis of the two codes. The ultimate objective of this joint effort was to systematically develop credible and traceable uncertainty distributions for the respective code input variables using a formal expert judgment elicitation and evaluation process. This paper focuses on the methods used in and results of this on-going joint effort.

Introduction

The U.S. Nuclear Regulatory Commission (NRC) and the European Commission (EC) are co-sponsoring an uncertainty analysis of their respective probabilistic consequence codes, MACCS[1] and COSYMA[2]. Although uncertainty analyses have been performed for the predecessors of MACCS and COSYMA, the distributions for the input variables were largely developed by the code developers rather than the experts involved in the numerous phenomenological areas of a consequence analysis. Moreover, both commissions were aware of the key role of uncertainty in decisions involving prioritization of activities and research, and were interested in initiating a comprehensive assessment of the uncertainty in consequence calculations used for risk assessments and regulatory purposes. Therefore, the objectives of this joint effort are to formulate a state-of-the art approach, and systematically obtain much of the quantitative information necessary to perform uncertainty analyses using these consequence codes.

Uncertainty analyses which have utilized formal expert elicitation techniques to develop distributions for computer code input parameters have been performed in the Level 1 (core damage frequency evaluation) and Level 2 (evaluation of radionuclide transport from the melt to the environment) portions of risk assessments, e.g., NUREG-1150[3]. To ensure the quality of the needed Level 3 uncertainty information, and to facilitate uncertainty propagation in a complete risk assessment, formal expert judgment techniques were selected to develop

distributions for important consequence analysis input parameters where the experimental database does not provide all the necessary information, and the analytical models used for extrapolations are not indisputably correct.

A list of phenomenological areas included in a consequence calculation for which distributions are to be developed jointly is presented in Table 1. The remaining areas, such as protective actions, in a consequence calculation are specific to Europe or the U.S., and joint expert panels will not be held. However, the same approach developed in this joint project will be followed if the commissions decide to convene expert panels in those areas at a later date.

Table 1. Phenomenological Areas in the Consequence Calculation that Require Uncertainty Distributions

Phenomenological Area	Code Input Variable Requiring Uncertainty Distribution
Dispersion	Plume spread parameters*
Deposition	Dry deposition velocity* Wet deposition parameters*
Behavior of deposited material and related doses	Decontamination Resuspension parameters Weathering parameters Shielding factors Penetration factors
Internal Dosimetry	Breathing rate Dose conversion factors
Early health effects	LD_{50} Thresholds
Late health effects	Dose rate effectiveness factors Risk coefficients (cancer)
Food chain	All food chain parameters

* See "Definition of elicitation variables" section of this paper.

Recognizing the magnitude and expense required to complete a full-scale comprehensive consequence uncertainty analysis using formal expert judgment techniques, a trial study was performed to evaluate the feasibility of such a joint effort by initially limiting the scope to the dispersion and deposition code input variables. These two areas were chosen because (1) it has been shown that the dispersion and deposition code input parameters were important with respect to the uncertainties in the different consequence measures[4], (2) the dispersion and deposition modules are the first modules invoked when executing both the MACCS and COSYMA codes, and (3) the EC has sponsored a pilot study in the dispersion and deposition areas, focusing on developing some mathematical tools that were potentially appropriate for use in this comprehensive study.

After successfully demonstrating the joint effort in the dispersion and deposition area, it was decided to continue with other phenomenological areas listed in Table 1: transport of radionuclides through the food chain, behavior of deposited materials and related doses (external dosimetry), early health effects, late health effects, and internal dosimetry. A detailed review of the dispersion and deposition effort was published by the NRC in a three-volume report, NUREG/CR-6244, EUR 15855 EN[5]. This paper briefly describes the completed dispersion and deposition expert elicitation exercise, and the work in progress in those phenomenological areas that is part of this on-going joint project.

Summary of Methods

A state-of-the-art approach was formulated jointly based on two important ground rules: (1) the current code models would not be changed because both the NRC and EC were interested in the uncertainties in the predictions produced by MACCS and COSYMA, respectively, and (2) the experts would only be asked to assess physical quantities which could be hypothetically measured in experiments. Benefits of these ground rules are (1) the codes have already been developed and applied in U.S. and European risk assessments, and (2) eliciting physical quantities avoids ambiguity in variable definitions and, more importantly, the elicited physical quantities are not tied to any particular model and thus have a much wider application.

To ensure the quality of the elicited information, a formal expert judgment elicitation procedure, built on the process developed for and used in the NUREG-1150 study, was followed. Refinements were implemented based on the experience and knowledge gained from several formal expert judgment elicitation exercises performed in the U.S. and Europe since the NUREG-1150 study, such as the pilot dispersion and deposition uncertainty study sponsored by the EC[6], and the waste repository performance assessment in the U.S.[7] The joint methods developed during and implemented in the dispersion and deposition pilot study are summarized in the following sections.

1. Definition of elicitation variables

Elicitation variables are the variables presented to the experts for assessments. For each of the elicitation variables, three percentile values, 5th, 50th, and 95th, from the cumulative distribution functions were requested from each of the experts, with assessments of the absolute upper bound (100th) and lower bound (0th) optional.

When the important code input parameters were not physical variables, it was required to select or formulate physically measurable elicitation variables from which distributions for the corresponding code input parameters could be developed. In the dispersion and deposition modules of the two consequence codes, only the dry deposition code input parameter is a physical variable, the dispersion and wet deposition code input parameters are mathematical constructs found by fitting some simple empirical relations to the experimental data rather than physical variables.

Dispersion elicitation variables

The dispersion model implemented in the MACCS and COSYMA code is the Gaussian plume model (GPM). For a given location, the GPM predicts airborne concentrations of a release as a function of release rate, windspeed, downwind distance, and the plume concentration standard deviations which define plume spread in the horizontal (σ_y) and vertical (σ_z) directions. The important dispersion code input parameters are those that define the spread of the plume. In MACCS and COSYMA, the plume spread parameters are dependent upon downwind distance (x) and are modeled using the power law:

$$\sigma_y = a_y x^{by}$$
$$\sigma_z = a_z x^{bz}$$

Values for a_y, b_y, a_z, b_z are the code input parameters which are defined for each atmospheric stability class, and for which uncertainty distributions are needed. The dispersion elicitation variables from which distributions for the a_y, b_y, a_z, b_z code input parameters were to be developed were defined as follows (for several centerline locations and for several synoptic weather conditions):

a) The normalized concentration measured at a collector located at the centerline (χ_c/Q).
b) The relative concentration at a specified crosswind location y to the centerline concentration (χ_y/χ_c).
c) The relative concentration at a specified vertical location z to the centerline concentration (χ_z/χ_c).
d) The standard deviation associated with the crosswind concentration (s_y) as would be measured by a line of collectors at specified downwind distance from the source.

Deposition elicitation variables

The important deposition parameters are the dry deposition velocity v_d (v_d is defined as the ratio of the rate of deposition of radioactivity to the ground to the air concentration at ground level), and the removal coefficients for wet deposition. The removal coefficients are used in the following way:

$$\Lambda(I) = a_\lambda I^{b\lambda}$$

where I is the rain intensity. The code input parameters for deposition are v_d , a_λ and b_λ. For dry deposition, the input parameter, v_d, is a physical variable which could be directly assessed by the experts. For wet deposition, the input parameters, a_λ and b_λ, are mathematical constructs, and, therefore, required defining a set of elicitation variables from which distributions for these parameters could be derived. The deposition elicitation variables were defined as follows:

a) Distributions on the dry deposition velocity, v_d, for four surface types, six aerosol particle sizes, iodine, and methyl iodide.
b) Distributions for the fraction of material removed by wet deposition for aerosols (four particle sizes), elemental iodine, and methyl iodide.

Furthermore, the terrain for the set of dispersion and deposition questions was defined as flat or gently rolling hills in order to provide information for the majority of the nuclear power plants. Surveys performed in the U.S. and Europe indicate that about 70% of the commercial nuclear power plants are located at sites that can be classified as having uncomplicated terrain and uncomplicated meteorology.

After the project staff formulated the elicitation variables and iterated on a set of elicitation questions, a dry run was carried out using several in-house experts in the dispersion and deposition areas to simulate the real elicitation exercise. Valuable inputs were provided by these in-house experts at the end of the dry run. Insights gained were used to further refine the elicitation questions and improve the elicitation process.

2. Selection of experts

The project staff sought to engage the best experts available in the fields of atmospheric dispersion and deposition. Experience in the NUREG-1150 study and elsewhere has shown that the selection of experts can be subjected to much scrutiny. Therefore, it is necessary to construct a selection procedure that is defensible. The procedure used in this joint effort contains these steps: (1) a large list of experts was compiled from the literature, and by requesting nominations from organizations familiar with the areas of interest; (2) the experts were contacted and curriculum vitae (CV) were requested; and (3) an objective selection board studied the CVs and selected eight experts in the dispersion area and eight experts in

Table 2. Atmospheric Dispersion and Deposition Experts.

Dispersion Experts	Country	Deposition Experts	Country
Pietro Cagnetti	Italy	John Brockmann	U.S.A.
Frank Gifford	U.S.A.	Sheldon Friedlander	U.S.A.
Paul Gudiksen	U.S.A.	John Garland	U.K.
Steve Hanna	U.S.A	Jozef Pacyna	Norway
Jan Kretzschmar	Belgium	Joern Roed	Denmark
Klaus Nester	Germany	Richard Scorer	U.K.
Shankar Rao	U.S.A.	George Sehmel	U.S.A.
Han van Dop	Netherlands	Sean Twomey	U.S.A.

the deposition area according to a set of selection criteria agreed upon before the process. The selection criteria include: reputation in the relevant fields, number and quality of publications, familiarity with the uncertainty concepts, diversity in background, balance of viewpoints, interest in this project, and availability to undertake the task in the timescale prescribed. Two panels of internationally recognized scientists, as listed in Table 2, were formed to participate in the formal expert judgment elicitation process.

3. Preparation of experts for elicitation

The experts were introduced to the purposes of the study, including how their judgments would be used. They were also introduced to background material on our respective consequence codes and the science of probability elicitation. This required the distribution of materials explaining the elements in a consequence analysis, the relation of the questions posed to the parameters in the code models, and the specific initial conditions and assumptions to be used in answering the elicitation questions. Training was conducted to familiarize the experts with the different types of psychological biases in judgment formation. At the end of the training session, practiced exercises were given to the experts so that the project staff could provide feedback to the experts on their performance in assessing probability distributions. The practiced exercises used questions similar to the elicitation questions that had known answers.

All the above preparation work took place in a meeting between the project staff and all experts. During this meeting, the experts were also give a chance to review all the elicitation questions, and discuss the types of uncertainties to be included or excluded from their assessments. It was our goal that all initial and boundary conditions, and elicitation questions were clear and agreeable to the experts at the end of this first meeting.

Following this first meeting, the experts prepared quantitative responses to the elicitation questions, and a written statement explaining their information sources and rationale. The philosophy of the project was to allow the experts to use whatever modeling technique or experimental results they believed were appropriate to assess the given problems. The only constraints placed on the experts by the project were: (1) the initial conditions could only be specified at the same level of detail as our consequence code models, i.e., uncertainty due to lack of detail in the initial conditions needed to be included in the uncertainty distributions provided by the experts; (2) the results had to be usable by the project; and (3) the rationale behind the distributions must be thoroughly documented.

4. Elicitation

All experts were reconvened for a second meeting where individual elicitation sessions were held. At the beginning of this elicitation meeting, the experts delivered presentations explaining how they addressed the issues without giving their quantitative assessments. Following the common session, individual elicitation sessions took place privately with a specialist in probability assessments, and a project specialist in the consequence codes. The elicitation interviews allowed for significant interactions between the elicitation team and the expert in encoding the expert's knowledge into probabilities. Each elicitation session was audio taped for future references.

5. Processing of judgments

The first step in processing the elicited information was the aggregation of the assessments from the individual experts into a single distribution for each elicitation variable. Although many different methods for aggregating expert judgments could be found in the literature, investigating the different weighting schemes was not the objective of this joint effort. A programmatic decision was therefore made to assign all experts equal weight, i.e., all experts on each respective panel were treated as being equally credible. One of the primary reasons that the equal weighting aggregation method was chosen for this study was to ensure the inclusion of different modeling perspectives in the aggregated uncertainty distributions. However, additional information was elicited from the experts that would allow the

application of a performance-based weighting scheme to the elicited dispersion and dry deposition results*.

As previously described, the dry deposition input parameter distributions were elicited directly, and further processing of the aggregated distributions was therefore unnecessary. The dispersion and wet deposition elicitation variables were not code input variables, and it was necessary to process the aggregated dispersion and wet deposition distributions into distributions for the respective code input parameters. A mathematical processing routine has been formulated in the EC pilot study which enabled the project staff to develop distributions for the wet deposition code input parameters from the aggregated elicited distributions. This processing method was also expanded to enable the development of distributions for the dispersion code input parameters from the aggregated elicited χ_c/Q and s_y distributions, and was called the Sigma processing method. Because the Sigma method was based only on the elicited χ_c/Q and s_y data, the distributions developed using this particular method represented the uncertainty in the spread of a Gaussian plume. A second dispersion processing method, called the Chi method, was formulated, and was designed to develop distributions for the dispersion code input parameters from the aggregated distributions over χ_c/Q, χ_y/χ_c, and χ_z/χ_c. Unlike the Sigma method, the Chi method did not require the assumption of a Gaussian dispersion process, and would be capable of capturing the uncertainty in the dispersion process in addition to the spread of the plume.

Results for the Dispersion and Deposition Panels

The dispersion experts were comfortable with the use of the Gaussian dispersion model in MACCS and COSYMA for the conditions within which the models will be applied in uncertainty studies. Although the deposition experts had little problem with the deposition case structure (elicitation questions), they questioned the use of the source depletion model in MACCS and COSYMA, and the omission of the rainout phenomenon in the codes. They provided some constructive and relatively inexpensive solutions to address some of the inadequacies they perceived in the two consequence codes.

At the end of their elicitation sessions, the experts were asked to fill out an evaluation form indicating the difficulties, if any, that were encountered during their involvement with the project, the areas in the project that could be clarified or improved, the positive points about the process, and any other observations that they had. The experts were unanimously favorable toward the project. Most experts indicated they had no problem whatsoever with

---

*A peer review panel of the NUREG-1150 study questioned the use of the equal weighting scheme without the consideration of other methods. Sufficient information was subsequently elicited in the present study to allow the application of alternative weighting schemes to the elicited data.

any aspects of the project, but a few indicated a slight problem with the description of the case structure and had experienced some difficulties in encoding their scientific judgments into probability distributions. The experts were also asked whether the formal expert elicitation approach taken by the project was a reasonable approach for assessing uncertainties in the dispersion and deposition fields. In general, they felt that the use of a formal expert elicitation process was an effective and appropriate method for capturing the uncertainties in their respective fields.

Several dispersion experts relied on the GPM as the central basis for their assessments, but relied on non-Gaussian considerations to develop the requested information on the broader uncertainty distributions. As for the deposition experts, they relied heavily on experimental evidence, and used several analytical models to fill the gaps left by the experimental evidence. The variabilities among responses were greater for the deposition questions than for the dispersion questions.

The individual expert assessments were successfully aggregated for each elicitation variable using the equal weighting method. Figures 1 and 2 provide examples of the individual elicited distributions and the equal weighed aggregated distributions for the crosswind (horizontal) dispersion parameter, and the fraction of elemental iodine removed by rain, respectively.

The project staff was successful in developing distributions for the wet deposition and dispersion code input variables using the Sigma method. To validate these distributions, samples were taken from these derived input distributions, propagated through the MACCS and COSYMA models, and the resulting distributions were compared to the aggregated elicited distributions. It was found that the resulting distributions output by the code models well replicate the aggregated elicited distributions from which they were developed.

Due to the fixed code model constraint, attempts to implement the Chi processing method was only partially successful because some of the aggregated elicited dispersion information was found to be inconsistent with the GPM. Three of the dispersion experts specified off-centerline plume concentrations which were higher than the centerline plume concentration at a given location for the sampling times specified in the case structure. In order to utilize and replicate the elicited information fully, modifications of the current code dispersion model, e.g., a smooth Gaussian profile superimposed with fluctuations, would be necessary. To adhere to the fixed code model ground rule, only those portions of the χ_y/χ_c, and χ_z/χ_c aggregated elicited distributions consistent with the GPM were subsequently used in the Chi method to develop distributions for the dispersion code input parameters. Samples were taken from these derived distributions, propagated through the GPM, and the resulting distributions were found to well replicate those aggregated elicited dispersion distributions consistent with the GPM assumptions.

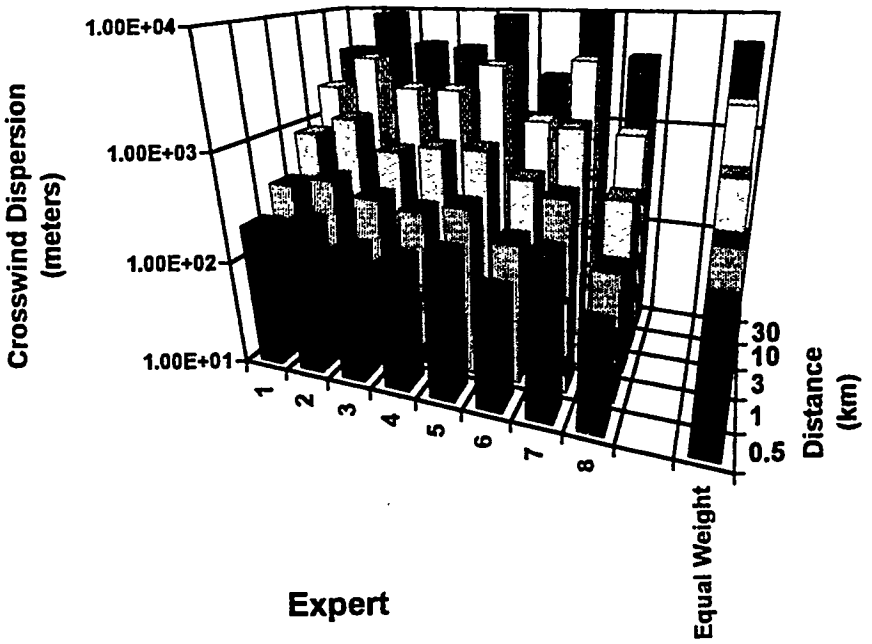

Figure 1.* 50th percentile elicited crosswind dispersion values. Stability class A.

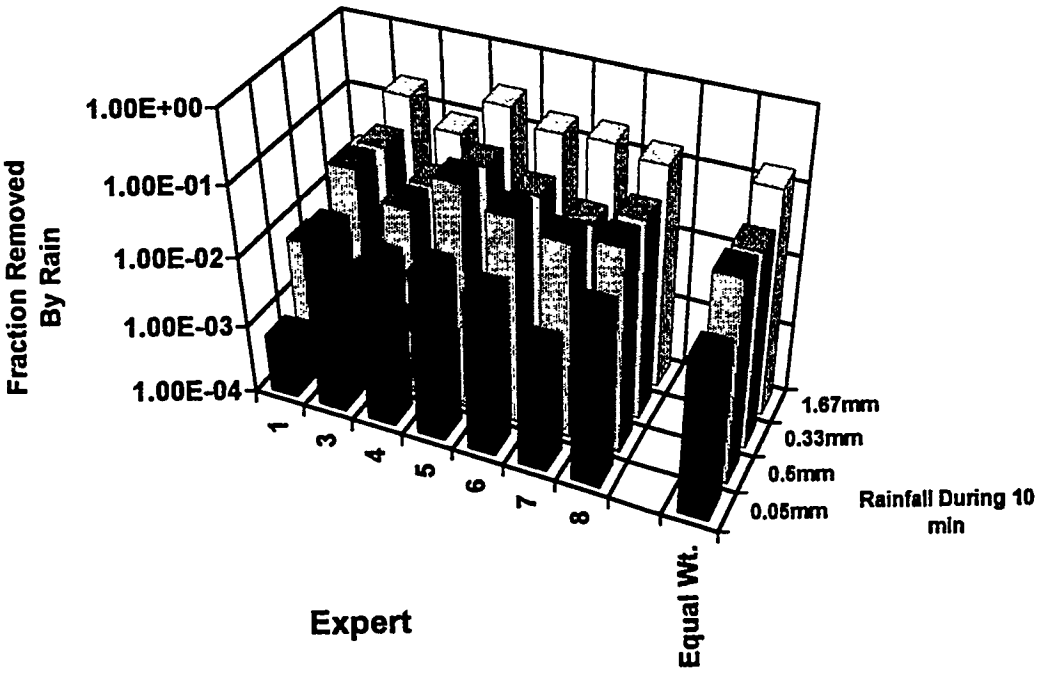

Figure 2.* Elicited and aggregated (equal wt.) 50th percentile fraction of elemental iodine removed by rain during a 10-minute period. Wind velocity unspecified.

* The numbering scheme for the experts used in this figure is not correlated in any way with the order in which the experts are listed in Table 2.

Figures 3 and 4 provide examples of some of the results obtained using the two dispersion processing methods. Both the Chi and Sigma methods were successful in duplicating the portion of the aggregated elicited data consistent with the GPM. However, because the fixed code model ground rule prevented the Chi method being used at its full capability, the simpler Sigma processing method was selected to develop the distributions for the dispersion code input parameters. It is worth noting that the Chi method is a more versatile method, and can be used to develop the dispersion code input parameter distributions from the current set of elicited dispersion information if some more advanced dispersion models are to be implemented in the future versions of these consequence codes.

Conclusions of the Dispersion and Deposition Panels

The aggregated elicited uncertainty distributions represented state-of-the-art knowledge in the areas of atmospheric dispersion and deposition which were assessed by a most qualified group of experts. These distributions were given on physically measurable quantities, and were conditional on the case structures provided to the experts. The experts were not directed to use any particular modeling approach, but were free to use whatever models, data sets, and perspectives that they considered appropriate for the problem. The elicited distributions obtained were developed by the experts from a variety of information sources. The aggregated distributions, therefore, include variations due to different modeling approaches and perspectives.

The aggregated elicited dry deposition distributions captured the uncertainty on the dry deposition velocity of particles of different sizes over different surfaces, while the aggregated elicited wet deposition distributions captured the uncertainty on the fraction of particles removed by rain. The aggregated elicited dispersion distributions captured the uncertainty of the following quantities at several downwind distances: (1) the ratio of the plume centerline concentration relative to the source strength, (2) the standard deviation of the plume width in the crosswind direction, and (3) the ratio of the off-centerline plume concentrations at specified locations in both the vertical and crosswind directions relative to the centerline plume concentration.

Important lessons were learned in processing the elicited dispersion information. Given a fixed model, unless the code input parameters happened to be physical quantities that can be elicited directly, such as in the dry deposition case, an approach such as that adopted in this exercise may result in complicated mathematical treatments in generating code input parameter distributions. Moreover, when the elicited information clearly is incompatible with the assumption of the fixed model, it is not apparent how to rationalize the distributions generated for the model parameters by using only partial information which is compatible to the fixed model. Finally, a carefully designed case structure is crucial to ensure that important information needed to fully characterize all physical processes of interest is obtained from the expert judgment elicitation process.

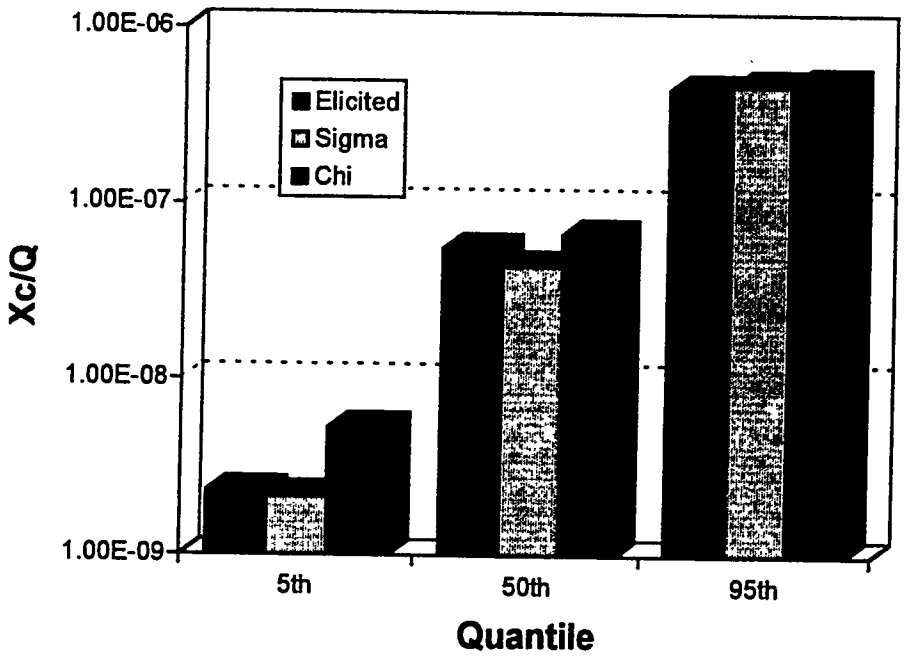

Figure 3. χ_c/Q. Stability Class A. 10 km downwind distance.

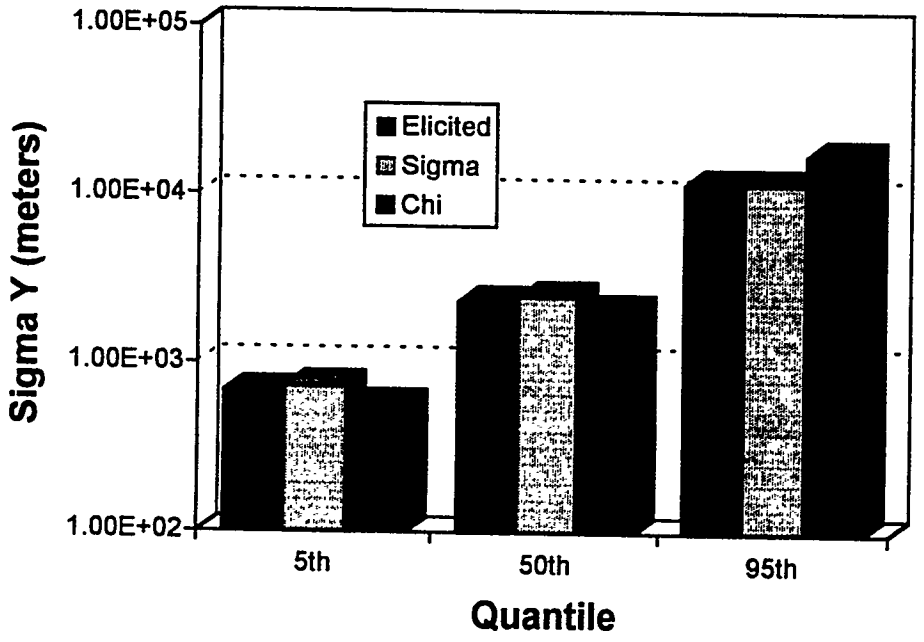

Figure 4. σ_y. Stability Class A. 10 km downwind distance.

Valuable information has been obtained from this exercise, despite the omission of uncertainties due to the non-Gaussian dispersion behavior of plumes. Because the aggregated elicited information is non-model-specific, it can also be fitted by other non-Gaussian analytical models. Thus, the mission of creating a library of atmospheric dispersion and deposition uncertainty distributions which will have many applications outside of the scope of this project has been fulfilled.

In this project, teams from the NRC and EC were able to successfully work together to develop a unified process for the development of uncertainty distributions for the selected consequence code input parameters. Staff with diverse experience and expertise and from different organizations allowed a creative and synergistic interplay of ideas which would not have been possible if they worked in isolation. Furthermore, in this exercise, formal expert judgment elicitation has proven to be a valuable vehicle to synthesize the best available information by a most qualified group. With a thoughtfully designed elicitation approach which addresses issues such as elicitation variable selection, case structure development, probability training, communication between the experts and project staff, and documentation of the results and rationale followed by an appropriate application of the elicited information, formal expert judgment elicitation can play an important role and possibly becomes the only alternative technique to assemble the required information when it is impractical to perform experiments or the available experimental results do not lead to an unambiguous and a non-controversial conclusion.

Status of Work on the Other Panels

The expert elicitation of the food chain transport panel and the deposited material and related doses panel was completed in July 1995. Documentation and processing efforts are currently underway. Joint reports on these two panels are expected to be published in mid-1996. The first expert meeting for the early health effects panel, late health effects panel, and internal dosimetry panel have been held in December 1995, and elicitations are planned for early 1996. Joint reports on the early health effects, late health effects, and internal dosimetry panels are expected to be published in early 1997.

References

1. H.-N. Jow, et. al, "MELCOR Accident Consequence Code System (MACCS)," NUREG/CR-4691, SAND86-1562, Sandia National Laboratories, Albuquerque, N.M., 1990.

2. Kernforschungszentrum Karlsruhe GmbH (FRG) and National Radiological Protection Board (UK), "COSYMA, A New Program Package for Accident Consequence Assessment," Luxembourg, 1990.

3. U. S. Nuclear Regulatory Commission, NUREG-1150, "Severe Accident Risks: An Assessment for Five U. S. Nuclear Power Plants," final summary report, Washington, D.C., 1990.

4. J. C. Helton, J. D. Johnson, M. D. McKay, A. W. Shiver, and J. L. Sprung, "Uncertainty and Sensitivity Analysis of Early Exposure Results with the MACCS Reactor Accident Consequence Model," NUREG/CR-6135, SAND93-2371, Washington, D.C., January 1995.

5. U.S. Nuclear Regulatory Commission and Commission of European Communities, "Probabilistic Accident Consequence Uncertainty Analysis: Dispersion and Deposition Uncertainty Assessment," NUREG/CR-6244, EUR 15855 EN, SAND94-1453, Washington, D.C., January 1995.

6. R. M. Cooke, "Expert Judgment Study on Atmospheric Dispersion and Deposition - Main Report and Annexes," Report of the Faculty of Technical Mathematics and Informatics, no. 91-81, Delft, 1991.

7. K. M. Trauth, R. P. Rechard, and S. C. Hora, "Expert Judgement as Input to Waste Isolation Pilot Plant Performance-Assessment Calculations: Probability Distributions of Significant System Parameters," SAND91-0625, Sandia National Laboratories, Albuquerque, NM, 1993.

ADVANCED ACCIDENT SEQUENCE PRECURSOR ANALYSIS LEVEL 1 MODELS

Martin B. Sattison, Tami A. Thatcher, James K. Knudsen, John A. Schroeder, and Nathan O. Siu

Lockheed Martin Idaho Technologies
Idaho National Engineering Laboratory
P.O. Box 1625
Idaho Falls, Idaho 83415

ABSTRACT

The Idaho National Engineering Laboratory (INEL) has been involved in the development of plant-specific Accident Sequence Precursor (ASP) models for the past two years. Last year 75 individual plant models were developed and delivered to the Nuclear Regulatory Commission (NRC). These models were developed for use with the SAPHIRE suite of PRA computer codes.[1] They contained event tree/linked fault tree Level 1 risk models for the following initiating events: general transient, loss-of-offsite-power (LOOP), steam generator tube rupture (SGTR), small loss-of-coolant-accident (SLOCA), and anticipated transient without scram (ATWS).

Early in 1995 the ASP models were revised based on review comments from the NRC and an independent peer review. These models were released as Revision 1. The Office of Nuclear Regulatory Research (RES) has sponsored several projects at the INEL this fiscal year to further enhance the capabilities of the ASP models. Revision 2 models (JCN W6467) incorporates more detailed plant information into the models concerning plant response to station blackout conditions, information on battery life, and other unique features gleaned from an Office of Nuclear Reactor Regulation (NRR) quick review of the Individual Plant Examination (IPE) submittals. These models are currently being delivered to the NRC as they are completed. A related project, JCN W6355, is a feasibility study and model development of low power/shutdown (LP/SD) and external event extensions to the ASP models. This project will establish criteria for selection of LP/SD and external initiator operational events for analysis within the ASP program. Prototype models for each pertinent initiating event (loss of shutdown cooling, loss of inventory control, fire, flood, seismic, etc.) will be developed. A third project concerns development of enhancements to SAPHIRE. In relation to the ASP program, a new SAPHIRE module, GEM,[2] was developed as a specific user interface for performing ASP evaluations. This module greatly simplifies the analysis process for determining the conditional core damage probability for a given combination of initiating events and equipment failures or degradations.

BACKGROUND

In the summer of 1993, the INEL began construction of 75 plant-specific, train-level, SAPHIRE-based ASP models. These models were based, in part, on the existing ASP models and extensive revisions made by Science Applications International Corporation (SAIC) under subcontract to the Oak Ridge National Laboratory. SAIC's work to convert the ASP models from event tree models with branch point probabilities to linked event trees and fault trees (or Boolean equations) was documented in a report entitled the "Daily Events Evaluation Manual." The Daily Events Evaluation Manual (DEEM)[3] assigned each reactor plant to one of nine plant classes based on the type of responses and equipment requirements necessary to mitigate transients and small losses of coolant accidents. The event trees (for general transients, small loss of coolant accidents, losses of offsite power, and steam generator tube ruptures) were taken from the DEEM with very few changes. The plant-specific fault trees were created using information from Final Safety Analysis Reports (FSARs) and the NRC Source Books.

The first version of the models (Revision 0) was completed in June 1994. These models were intentionally kept simple with the goal of reproducing the current ASP capabilities within a framework possessing a much greater potential for expansion and enhancement. However, some improvements over the previous ASP models were made: 1) ATWS sequences were developed for transients, 2) centrifugal charging pumps were credited, whenever possible, as part of the high pressure injection capability, and 3) venting of the containment for BWRs was modeled. These additions were a step forward, but the greatest benefit of these SAPHIRE-based models was the ability to easily modify the logic to more accurately represent the plant response to an operational event.

While the Revision 0 models were being developed and delivered to NRR, SAIC was subcontracted to perform a review of the lead plant for each of the nine plant classes. Additionally, a BWR plant with a High Pressure Core Spray system was reviewed, making a total of ten plants receiving a peer review.

MODEL IMPROVEMENTS

While the peer reviews were in progress, the Office for Analysis and Evaluation of Operational Data (AEOD) contracted the INEL to investigate the feasibility of making enhancements in several modeling areas. These areas were:

- Uncertainty Analysis. The ASP models have never had the ability to give an uncertainty estimation. It was well-known that a basic parameter uncertainty estimation capability comparable to that of a typical full-scope PRA was necessary and practical. The INEL was also tasked with investigating how to estimate the unique modeling uncertainty associated with simplified ASP models.

- Human Reliability Analysis. The purpose of this task was to make improvements in the current practice for human reliability analysis (HRA) for the ASP program. Specific areas needing attention were the treatment of recovery errors and the assessment of dependency. The goal was to develop a general, easy-to-apply, method which handled actuation, recovery, and dependency through a consistent model of human behavior.

- Common Cause Failure Analysis. The CCF improvements work focused on providing better basic parameter estimates while not increasing the complexity of the models. The current ASP logic models

are straightforward for construction and review purposes and they generate a reasonable number of simple cutsets. Therefore, it was decided that no modifications be made to the current ASP logic structure developed for symmetric redundant systems which is represented by the independent component failure events ANDed together and then ORed with the CCF basic event(s). Since the ASP logic models were to remain unchanged, the focus was placed on the CCF basic events values. Use of the Multiple Greek Letter method was simple for point estimate calculations but was complicated for uncertainty analysis. Therefore, other alternatives were investigated, with conversion to the Alpha method being the final determination. Previously, the CCF basic events included only the global CCF mode of all redundant components that failed a system. Investigation into the impact of not including all the potential CCF terms showed that the CCF contribution was under-estimated by a maximum of about 11 percent.

- Modeling Level of Detail and Scope. There were a number of features missing from the ASP models that may be found in a full-scope PRA, including support system models, testing and maintenance unavailabilities, a wider range of initiating events, external events, containment behavior models, and shutdown/low power models. These enhancements were prioritized and it was decided to develop support system models as part of this work with external events, low power/shutdown risk , and level 2 and 3 risk models being assigned to RES for separate investigation.

Each improvement was demonstrated on several plant models selected from a set of prototype models consisting of Byron, St. Lucie, Peach Bottom, Oconee, and Three Mile Island. These advanced models were delivered to AEOD, proving that such improvements were practical and affordable. Incorporating these enhancements into all 75 SAPHIRE-based ASP models are part of the long-range plans for the ASP program.

REVISION 1 ASP MODELS

The peer review comments were received on all ten Revision 0 ASP models in June 1994. The comments were of two basic types. First, there were comments that pertained to all plants in the class and sometimes to more than one plant class. These comments were carefully reviewed and determinations were made as to which plants these comments were applicable. Furthermore, these comments were prioritized based on the resources available and the effort required to address them. The second type of comment addressed issues pertaining specifically to the plant model being reviewed. Generally these comments were associated with the fault trees, basic events, and documentation of the model. These comments were usually readily addressed.

The peer review comments were the bases for the work scope for developing the Revision 1 ASP models. The general changes, impacting most, if not all of the ASP models included:

- For PWRs, the Revision 0 models assumed that during a LOOP that the power-operated relief valves (PORVs) would be challenged to open with a probability of 1.0. This assumption was retained, but the method of implementation was changed so that the model could be quickly modified to include a probability other than 1.0.

- For PWRs, a basic event modeling the common cause failure of all Auxiliary Feedwater (AFW) System pumps was added. Previously, only common cause failure among the motor-driven AFW pumps was modeled.

- The nonrecovery probabilities for the four initiating events (IE-LOOP, IE-TRANS, IE-SGTR, and IE-SLOCA) were added to the basic event description table. This made it easier for the analyst to model an operational event involving one of these initiators.

- Various descriptions in the documentation were changed to add clarity.

- For BWRs, the post-venting make-up requirements on the LOCA, LOOP, and transient event trees were changed to reflect the following assumption: if a water source was viable before the containment was vented, then it will remain viable after containment venting, unless the source is the suppression pool.

The Revision 1 documentation was reformatted to add clarity, increase detail, enhance readability, and provide greater traceability. The last of the Revision 1 ASP models were delivered to the NRC in June 1995.

REVISION 2 ASP MODELS

The Revision 2 ASP models were started immediately after the completion of the Revision 1 models and are still in progress (completion is expected near the end of the calendar year). This work is sponsored by RES and the work scope is based on comments from the Revision 0 peer review, a compilation of plant configuration information gathered by NRR, and experience from using the previous revisions. The major tasks involved in developing the Revision 2 models include:

- An upgrade of the Emergency AC power modeling to include fault tree models for the major 1E buses and the power supplies to them. This modification eliminated the use of success events to accurately model the combinations of emergency diesel generators allowed in the non-station blackout sequences in the LOOP event tree.

- Incorporation of plant-specific features for each plant based on information collected by NRR in response to the station blackout rule and from reviews of the IPEs. This information provides greater detail in the configuration and operation of emergency AC power systems, systems used to maintain reactor coolant pump seal integrity during station blackout, and other features that improve safety system availability/reliability.

- Modification of the BWR models for the Power Conversion, Main Feedwater, and Condensate event tree top events to provide more detail and to more completely represent the interdependencies among these top events.

ASP MODEL EXTENSION

In the Spring of 1995, RES contracted the INEL to perform a feasibility study to investigate extending the ASP models, giving them the capability of analyzing the risk significance of operational events associated with LP/SD operations, full-power and LP/SD internal flooding, LP/SD fire and earthquakes. Full-power fire and earthquakes were already being evaluated by another project.

This objectives of this project are to 1) determine the types of LP/SD and external events that the extended models should be able to address, 2) establish guidance for the selection of these events for ASP analysis, 3) develop prototype models for each of the identified event types and exercise them with appropriate example problems, and 4) investigate grouping or classification methods to reduce the number of unique models that would be necessary to implement this extension for all 75 ASP models.

Types of LP/SD and External Events

To determine the list of events that the LP/SD and external events models should be able to address, some preliminary research into past operational events was conducted. This produced a comprehensive list of possible event types. Each event type on this list was annotated with a recommendation for implementation. The list was then finalized in a meeting with NRC staff. The final list was limited to the following event types:

- Loss/Degradation of Shutdown Cooling. Events of this type involve a loss or degradation of the decay heat removal function through equipment failures or human error. This event type was determined to be of interest to the NRC and has a high potential for generating accident precursors.

- Loss of Reactor Coolant Inventory Control. Events of this type involve a loss or degradation of reactor coolant system integrity or ability to maintain the required reactor coolant system inventory to prevent voiding and eventual core damage. This event type was evaluated as being of interest to the NRC with a high potential to generate accident precursors.

- Loss of Electrical Power. Events of this type involve a complete or partial loss of AC or DC electrical power, generally leading to a loss or degradation of decay heat removal or inventory control. This event type was evaluated as being of high interest to the NRC with great potential to generate accident precursors.

- Internal Flooding (Full-power and LP/SD). This event type includes actual flooding from water systems within the plant and conditions that impact the ability to mitigate such flooding. These events are of interest to the NRC and have a high potential to generate accident precursors. Flooding events can be categorized as scenarios involving damage caused by (1) rising water levels, (2) water spray (e.g., pipe break, fire suppression system actuation), or (3) water dripping into control or power cabinets.

- LP/SD Seismic Events. Events of this type involve an actual earthquake or degradation of equipment important in mitigating the effects of an earthquake. Events of this type are of interest to the NRC. LP/SD seismic events were not explicitly discussed at the NRC staff interview meeting. However, seismic analysis methods share many characteristics with flooding (an external event) and LP/SD internal events.

- LP/SD Fires. Events of this type involve fires or fire mitigating equipment that can impact decay heat removal or reactor coolant system inventory control. These events are of interest to the NRC.

The following event types were considered, but were not included in this project because they were fairly infrequent, of a low priority, or required further research before they could be properly modeled:

- Inadvertent Reactivity Addition. Events of this type involve reactivity additions that result in inadvertent criticality, requiring reactor scram.

- Overpressurization of the Reactor Coolant System. These events involve a loss of pressure control, and with the reactor coolant system at low temperatures, the potential for exceeding brittle fracture limits does exist.

- Breach of Containment Integrity. Events of this type involve a failure of the containment function in conjunction with one of the other postulated events.

- Spent Fuel Pool Draining/Cooling Failures. Events of this type involve a loss of inventory or cooling in the spent fuel pool, leading to spent fuel pool boiling and fuel damage.

- Direct Fuel Damage. Events of this type involve dropping spent fuel during fuel handling evolutions or dropping heavy lift items on the fuel in the core or spent fuel pool.

Selection Criteria

The event selection process used to determine the most safety significant events reported primarily by licensee event reports (LERs) and other sources has evolved through years of ASP evaluations of full power events and has been expanded to include LP/SD events. The figure-of-merit representing the risk significance of an event in previous ASP evaluations[4] has been the conditional core damage probability (CCDP). Events with a CCDP less than 1.0E-6 (or only slightly above 1.0E-6) are screened from consideration. It is recommended that the CCDP of 1.0E-6 be retained as the screening criterion. This criterion is appropriate for all operational modes (full power, low power and shutdown) and for fuel stored in or out of the vessel. The CCDP is an indication of the risk significance of an individual event and it is a function of the number of and robustness of barriers that prevent fuel damage. A low CCDP indicates that remaining barriers to prevent fuel damage are predicted to have a low probability of failure.

The existing screening process[4] for full power events utilizes a computerized selection process using the Sequence Coding Search System (SCSS) database[5] to select LERs matching specified criteria. This computerized process has evolved over time and has been benchmarked with events that were manually selected. Generally, the process for full power event analysis collects LERs that have the following attributes:

- a LOCA occurred
- a LOOP occurred
- a transient occurred with an entire system failure or multiple system trains were unavailable or at least one train of a safety system was unavailable
- an entire emergency power system was faulted
- other entire safety systems were faulted

It is possible that an event of interest may not be reported in an LER and additional events (that are not necessarily LERs) can be added for consideration. These events include those selected for Augmented Inspection Team (AIT) reporting, Incident Investigation Team (IIT) reporting, the NRC's Performance Indicator Program, or other processes.

The selected events are then reviewed by two independent reviewers to determine if the event should be examined in greater detail. Insights as to the risk significance of the event are used to decide whether the event requires further evaluation. This preliminary determination of the risk significance requires judgment of the random failure probability of remaining systems that function to prevent fuel damage. The systems available during the event need to be known and the success criteria required for systems that can respond to prevent fuel damage must be known. For condition assessment, an understanding of the potential challenges (initiating events) that could occur, and the likelihood of their occurrence must also be known. For events that are similar to those previously analyzed, this manual screening process can be performed readily.

Events that survive the two reviewer screening process require further evaluation to estimate a CCDP. Events that survive the screening process and can be analyzed using the existing models were evaluated and CCDPs were assessed. In the past, any event that could not be treated with the existing ASP probabilistic risk assessment models was categorized as "impractical to analyze".

Modification of the existing screening process to include low power and shutdown (LP/SD) and external events involves the following aspects:

(1) ensure that the computerized selection process selects LP/SD and external events

(2) develop general written guidelines that aid the ASP analysis event selection process

(3) develop coarse screening guidance and procedures to aid screening those events that cannot be screened without a coarse screening evaluation

(4) develop risk insights by exercising LP/SD and external event models to improve and refine the screening criteria in steps 2 and 3.

Specific selection guidance is being developed in the following areas:

(1) Low Power Operations. The selection guidance used for full power operation is conservatively being used for low power operations.

(2) Shutdown Operations. The selection guidance addresses various situations involving loss of shutdown cooling, loss of coolant inventory control, and conditions that could impede proper operator actions.

(3) Full Power External Events. The selection guidance addresses actual occurrences of an external event and various situations where conditions are such that given an external event, the CCDP would likely be greater than 1.0E-6.

(4) Shutdown External Events. The selection guidance for these events is an adaptation of that for shutdown internal events, with the external events viewed as another means of impacting shutdown cooling, inventory control, and operator actions.

Prototype Models

The development of prototype risk models for shutdown and external events at Surry and Sequoyah is in progress. The Surry plant is being modeled for shutdown and external events based on NUREG/CR-6144[6] information. The shutdown model is near completion and work is just underway on the external event models. The Sequoyah model is based on information gleaned from the plant reference materials (FSAR, etc.) and the IPE. Thus, this project is investigating the ease of modeling for plants with previous LP/SD models and those without.

The original Surry LP/SD analysis identified fifteen different plant operating states (POSs), ranging from low power operation and shutdown through midloop operations to plant heatup and startup.
These POSs were placed into six groups based on the accident mitigating features available. The six groups are:

(1) Low Power/Cooldown with Steam Generators
(2) Pressurized RHR Cooldown
(3) Depressurized RHR Cooling with Normal Inventory
(4) Depressurized RHR Cooling with Reduced Inventory
(5) Depressurized RHR Cooling with Refueling Cavity Filled
(6) RCS Heatup

Based on the results of previous shutdown analyses and the operational events of interest in the recent past, it was determined that the prototype models for Surry would address POS groups 2, 3 and 4. These groups are expected to have the greatest potential for events with CCDPs greater than 1.0E-6 and the other POS groups can be evaluated using the existing models.

- POS group 1 can be analyzed using the full-power models with failure to scram excluded from the analysis.

- POS group 5 has a much greater time for recovery of RHR because of the large inventory above the core. The POS group 3 model can be used with adjustments made for the greater recovery time.

- POS group 6 can be analyzed using the POS group 2 model with modifications for the status of steam generator availability.

Additionally, four different time windows were established to characterize the decay heat rate based on time after shutdown.

The shutdown internal event model consists of three event trees: Loss of RHR, Loss of Inventory, and Loss of Offsite Power. The event tree structure was designed to be generic with the plant-specific details being modeled at the fault tree level. The structure is intended to limit the number of event trees required while allowing considerable modeling detail. For each initiating event there is a single event tree, called a root tree, that contains top events to establish the POS group and the time window. The root event tree then transfers to three event trees, each associated with a POS group. The time window information influences the fault tree quantification for the top events in these POS event trees. Figures 1 through 4 are the draft event trees for Loss of RHR. The model allows the user to choose one specific time window and POS group or any combination of time windows and POS groups that apply to the event being evaluated.

The external event modeling work is in the method research phase and there are no results to report at this time.

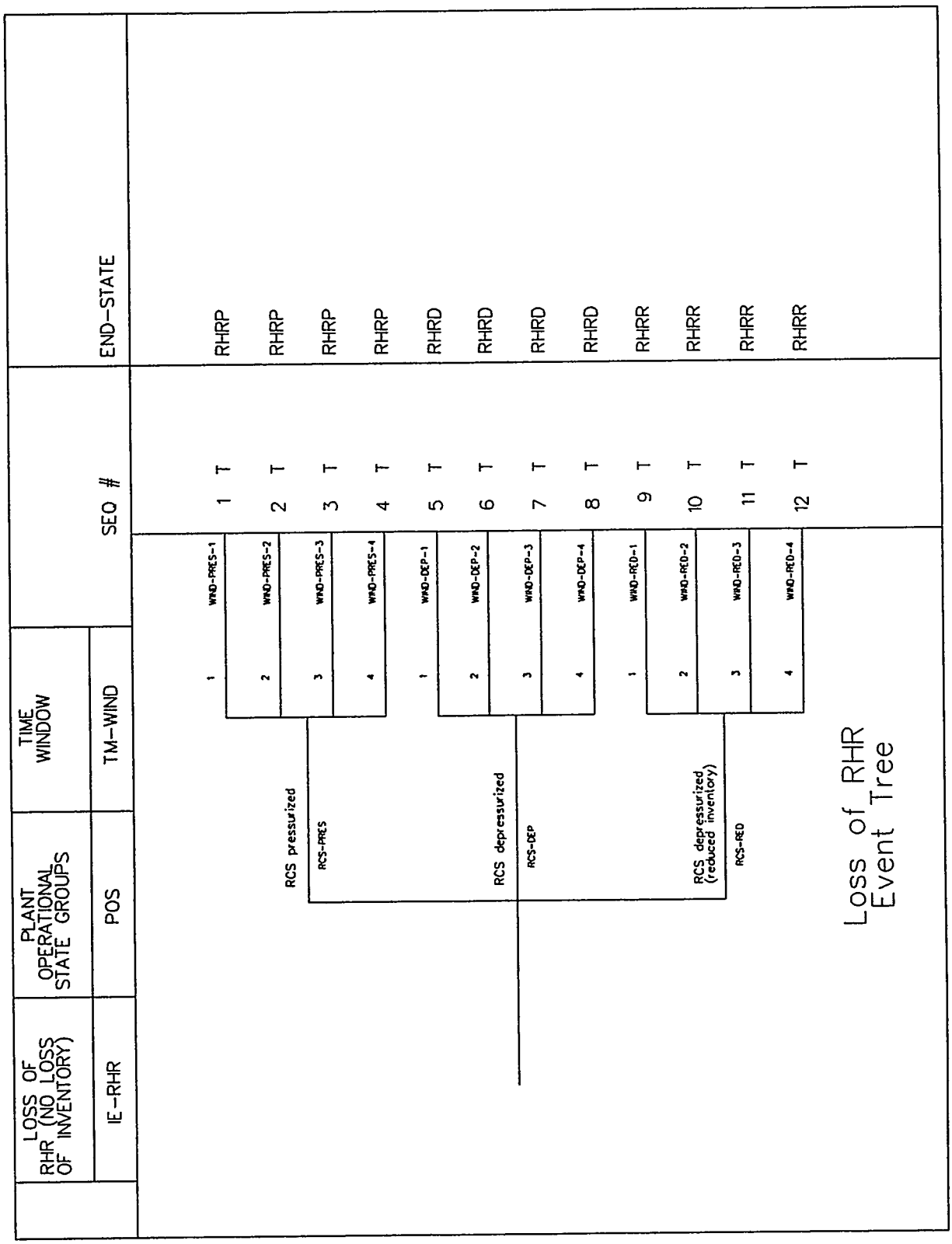

Figure 1. Loss of RHR root event tree.

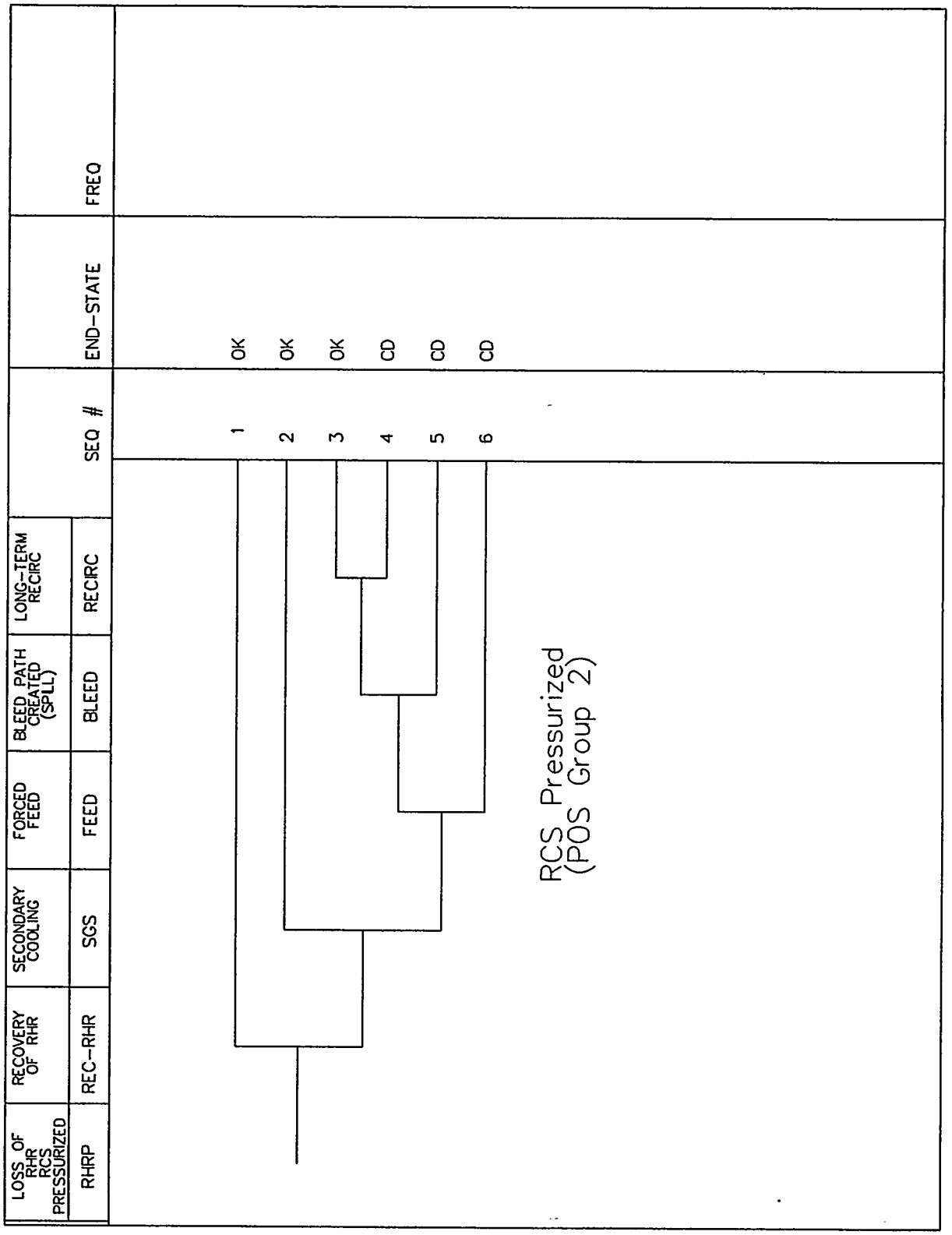

Figure 2. Loss of RHR (RCS pressurized) transfer event tree.

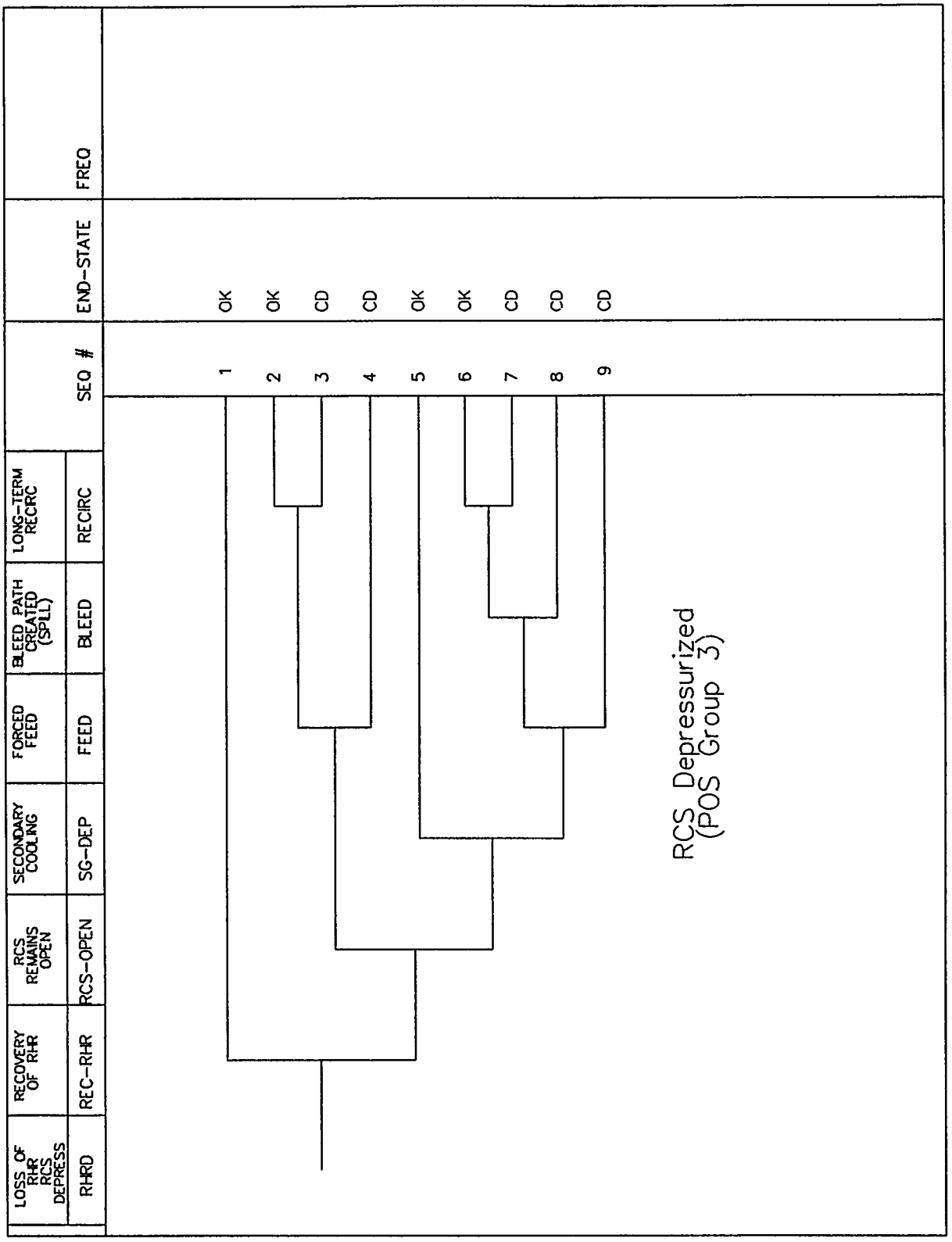

Figure 3. Loss of RHR (RCS depressurized) transfer event tree.

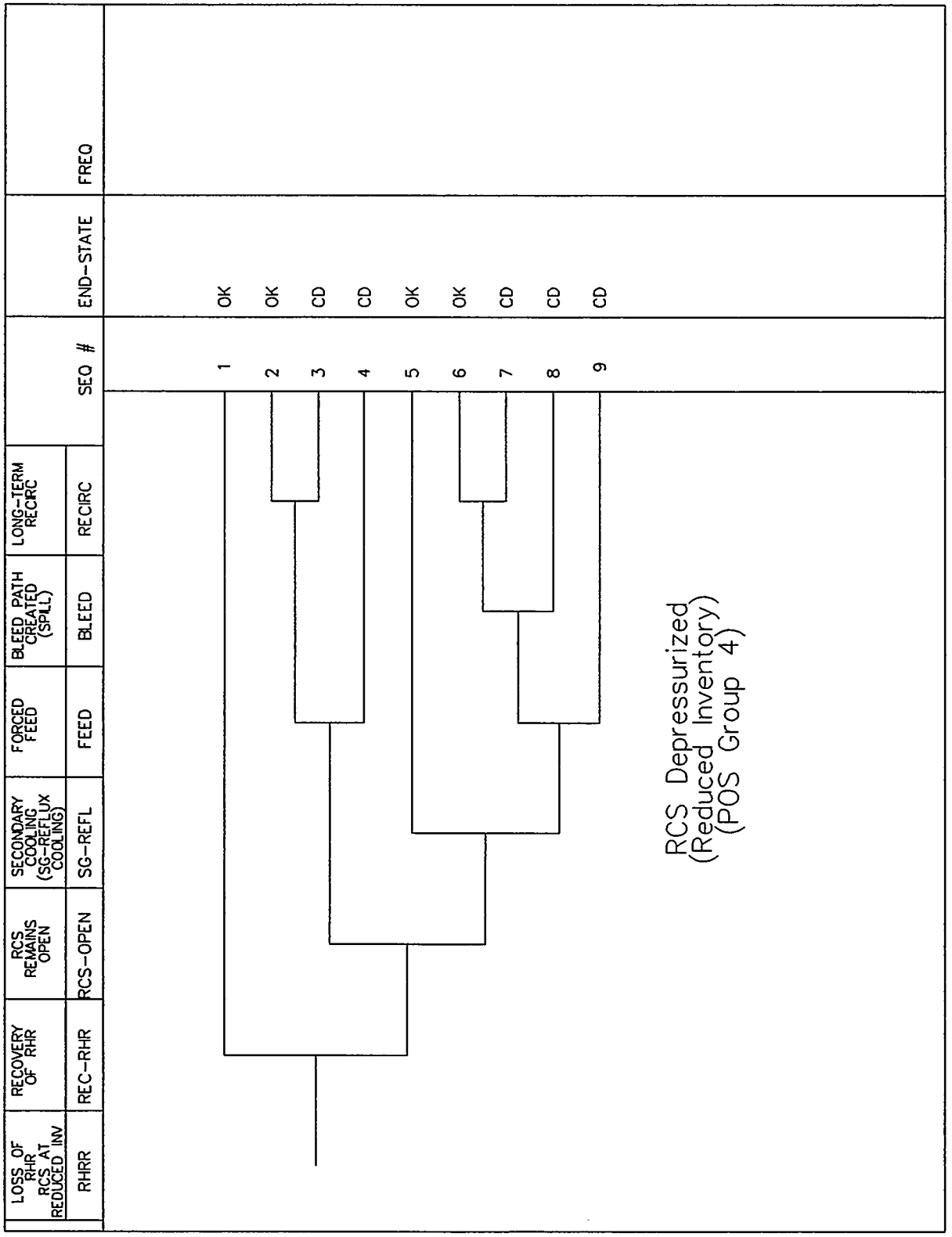

Figure 4. Loss of RHR (RCS at reduced inventory) transfer event tree.

GEM MODULE OF SAPHIRE

The GEM software module has been designed as a highly specialized user interface to the SAPHIRE suite of PRA codes for the evaluation of operational events at commercial nuclear power plants. In particular, GEM implements many aspects of the ASP program analysis methods and can only be used with the ASP program models or other models built to the same specifications. Initiating event assessments and condition assessments are both addressed, each with its own set of unique requirements. The calculation of CCDPs and event importances are automated as much as possible.

ASP Evaluation Definitions and Concepts

The following definitions and concepts are essential to a thorough understanding of the ASP evaluation process and the tools used.

- Precursor. In general, an accident sequence precursor is a sequence of events that successfully prevented core damage, that if additional failures had occurred, would have resulted in core damage. Precursors have been separated into two types. The first type involves the occurrence of an initiating event (analyzed in an initiating event assessment), and the second type involves failures or degradations in mitigating equipment (analyzed in a condition assessment). In the ASP program, a precursor is retained if the likelihood[1] of those additional failures leading to core damage is greater than or equal to 1.0E-6. Occasionally, there are exceptions for events with coincident containment failure or unique influences difficult to analyze. These are reported in the ASP program annual reports but do not necessarily receive the same level of analytical treatment as the more traditional precursors.

- Change Set. A change set is a listing of the risk model basic events that have been designated with a change in probability from the base case. In ASP evaluations, a change set is used to identify the basic events (and initiating events) that must be re-evaluated to represent the events and conditions observed during the reported precursor. GEM assists in creating the proper ASP evaluation change set by automatically identifying basic events that must change once the initiating event or condition duration is specified.

- Conditional Core Damage Frequency (CCDF). The conditional core damage frequency is the hazard rate representing the expected number of core damage events per hour given a set of known failures or plant operating conditions.

- Conditional Core Damage Probability (CCDP). The conditional core damage probability is the likelihood of experiencing a core damage event given a set of known failures or plant operating conditions. When calculated for an operational event, the CCDP is a measure of how close the plant came to core damage during the event. Alternatively, the CCDP can be thought of as the likelihood of

[1] Likelihood is used in this context to indicate either a CCDP or a change in CCDP (i.e., event importance).

failure of the remaining barriers to core damage. The CCDP is calculated by GEM using the following equation:

$$CCDP = 1 - e^{-CCDF * t} \quad (1)$$

This equation assumes that core damage events are a homogeneous Poisson process and that the core damage hazard rate (CCDF) is constant.

- Core Damage Frequency (CDF). The core damage frequency associated with the base case results of an ASP model is comparable to that of a typical PRA except it is expressed on a per hour basis. It is a hazard rate representing the expected number of core damage events per hour.

- Core Damage Probability (CDP). For a condition assessment, the core damage probability is the likelihood of experiencing a core damage event within an exposure time, t, given that all plant and system responses fail at their nominal failure rates. In the past, the ASP program estimated the CDP as

$$CDP = CDF * t \quad (2)$$

This is only an approximation to the actual exponential equation now being used by GEM:

$$CDP = 1 - e^{-CDF * t} \quad (3)$$

- Event Importance. The event importance is a measure of how much greater the core damage probability for the analyzed event was compared to the nominal core damage probability. It is similar to a risk increase difference importance measure (hence, the name "event importance"). The Event Importance is calculated in GEM by

$$I = CCDP - CDP \quad (4)$$

- GEMDATA. GEMDATA is a software package that assists the ASP model developers with the calculation of the various electric power non-recovery probabilities and the reactor coolant pump (RCP) seal loss of coolant accident (LOCA) probability contained in the ASP models.

The unique features of the ASP models that set them apart from the typical PRA model include:

- Initiating event frequencies are expressed on a per hour basis to facilitate condition assessments.

- For the loss of offsite power (LOOP) model, the specific type of LOOP event experienced must be analyzed. The ASP models can address any of four different LOOP events: (1) grid-related, (2) plant-

centered, (3) severe weather, and (4) extremely severe weather. Each type has its own initiating event frequency, probability of non-recovery curve, and probability of reactor coolant pump (RCP) seal failure curve. The base case model uses frequency-weighted average values for the LOOP initiating event frequency, non-recovery values, and RCP seal failure probability.

Initiating Event Assessments

The ASP models contain event trees that model the plant response to a selected set of initiating events. When a precursor to be analyzed involves one of these initiating events, an initiating event assessment is performed. The analyst enters GEM and, after selecting the correct plant model, selects an initiating event assessment and gives it a name. This opens a work space for this particular initiating event assessment.

The analyst next selects the initiating event that occurred from the list provided. GEM will automatically set the selected initiating event's frequency to its pre-assigned short-term non-recovery probability (or 1.0 if recovery is deemed not possible) and will set all other initiating event frequencies to zero. This assumes that the actual precursor involves only the observed initiating event and all other initiators are not applicable. Furthermore, it is assumed that the probability of another initiating event occurring while the first initiating event is still in progress is negligible.

If the initiating event is a LOOP, GEM will display a list of the four different types of LOOP (plant-centered, grid-related, severe weather-related, and extremely severe weather-related) and the analyst must pick one. Each LOOP type has a different short-term non-recovery probability.

Once the initiating event is selected, GEM displays a predefined change set unique to that initiating event. For all initiating events except LOOP, the change set consists only of the entire set of initiating events. The selected initiating event is in the change set because its frequency has been converted to a probability equal to its short-term non-recovery value and the other initiating events are listed because their frequencies have been converted to a probability of zero.

For the LOOP initiating event, the change set again lists all the initiating events, but additionally, the change set includes a predefined list of electric power recovery basic events and the RCP seal LOCA basic event (for PWRs only). These are the basic events that must be changed when going from the nominal LOOP event in the base case model to a specific LOOP type for the event assessment. These basic events are automatically added to the change set and their values are automatically modified to predetermined values based on the plant characteristics, the timing required, and the type of LOOP. These predetermined values are calculated and stored in a data management tool called GEMDATA. The calculational methods and input data used by GEMDATA are directly taken from a code called BLACKOUT[7] previously developed for use in earlier ASP evaluations by SAIC.

The analyst can access any of the basic events listed in the change set if there is a need to make modifications. Other basic events can also be added to the change set list. This would be necessary to model any observed failures or degradations reported for the event being analyzed.

Once the change set list is complete and the desired changes are defined for the basic events, the analyst selects the PROCESS option. GEM automatically generates a basic event data set according to the changes defined in the change set. GEM next determines which system fault trees have been impacted by the changes and identifies the event tree accident sequences that use those fault trees. The logic for those sequences is loaded into memory

and GEM solves the logic for the new minimal cutsets. The minimal cutsets are quantified, the CCDP is calculated and the results are displayed.

Condition Assessments

When a precursor event does not involve the actual occurrence of an initiating event, but does indicate failures or degradation of equipment that would be required to mitigate the consequences of an initiating event, a condition assessment is performed. After entering GEM and selecting the appropriate ASP model, the analyst selects the condition assessment option and gives the assessment a name. This opens up a work space for this particular condition assessment. GEM then prompts the analyst for the duration of the conditions being analyzed. The duration is entered, expressed in hours.

GEM displays a blank change set and provides the ability to add events to the change set to model the observed failures and degradations reported for the event being analyzed.

Once the change set list is complete and the desired changes are defined for the basic events, the analyst selects the PROCESS option. GEM automatically generates a current basic event data set according to the changes defined in the change set. GEM next determines which system fault trees have been impacted by the changes and identifies the event tree accident sequences that use those fault trees. The logic for those sequences is loaded into memory, GEM solves the logic for the new minimal cutsets, and quantifies them. For the sequences that were not impacted by any of the changes, the base case results are copied over into the current case results. The CCDP, CDP, and event importance are calculated and the results are displayed.

FUTURE PLANS

The ASP program is receiving positive attention from the highest levels within the NRC. The trend to enhance the capabilities of the models and improve the analysis techniques will continue. ASP programs are being given priority for funding in these areas. More work will be done to broaden the scope and increase the depth of the models. Uncertainty will be addressed, preparations for extension to Level 2 and 3 are already being planned. Low power and shutdown modeling will continue, eventually covering all 75 ASP models. The same is true for external events modeling. In the near future the models will be to the point that utility involvement will be appropriate and solicited.

Each step takes the program closer to having a full-scope Level 1, 2 and 3 full-power and LP/SD risk model for each operating commercial nuclear power plant in the United States, all with the same scope and level of detail. These models will have a wide range of uses beyond the current ASP program plans as the regulatory environment becomes more risk informed.

REFERENCES

1. Russell, K. D. et al., *Systems Analysis Programs for Hands-on Integrated Reliability Evaluations (SAPHIRE) Version 5.0,* NUREG/CR-6116, July 1994.

2. Russell, K. D. et al., *Systems Analysis Programs for Hands-on Integrated Reliability Evaluations (SAPHIRE) Version 5.0, Graphical Evaluation Module (GEM) Reference Manual,* NUREG/CR-6116, Vol. 6, April 1995.

3. Science Applications International Corporation, *Daily Events Evaluation Manual (Draft),* January 1992.

4. Minarick, J. W. et al., *Precursors to Potential Severe Core Damage Accidents: A Status Report (Series),* NUREG-4674 (Series).

5. Greene, N. M. et al., *Sequence Coding and Search System For Licensee Event Reports, User's Guide,* ORNL/NOAC-231/VI, December 1985.

6. Chu, T. L. et al., *Evaluation of Potential Severe Accidents During Low Power and Shutdown Operations at Surry, Unit 1,* NUREG/CR-6144, Vol. 2, June 1994.

7. Minarick, J. W. et al., *Revised LOOP Recovery and PWR Seal LOCA Models,* ORNL/NRC/LTR-89/11, August 1989.

Advanced Accident Sequence Precursor Analysis Level 2 Models

W. J. Galyean, D. A. Brownson, J. L. Rempe, Idaho National Engineering Laboratory
T. D. Brown, J. J. Gregory, F. T. Harper, Sandia National Laboratories
C. H. Lui, U. S. Nuclear Regulatory Commission

Abstract

The U.S. Nuclear Regulatory Commission Accident Sequence Precursor program pursues the ultimate objective of performing risk significant evaluations on operational events (precursors) occurring in commercial nuclear power plants. To achieve this objective, the Office of Nuclear Regulatory Research is supporting the development of simple probabilistic risk assessment models for all commercial nuclear power plants (NPP) in the U.S. Presently, only simple Level 1 plant models have been developed which estimate core damage frequencies. In order to provide a true risk perspective, the consequences associated with postulated core damage accidents also need to be considered. With the objective of performing risk evaluations in an integrated and consistent manner, a linked event tree approach which propagates the front end results to back end was developed. This approach utilizes simple plant models that analyze the response of the NPP containment structure in the context of a core damage accident, estimate the magnitude and timing of a radioactive release to the environment, and calculate the consequences for a given release. Detailed models and results from previous studies, such as the NUREG-1150 study, are used to quantify these simple models. These simple models are then linked to the existing Level 1 models, and are evaluated using the SAPHIRE code. To demonstrate the approach, prototypic models have been developed for a boiling water reactor, Peach Bottom, and a pressurized water reactor, Zion.

Introduction

The Accident Sequence Precursor (ASP) Program was initiated by the Office of Nuclear Regulatory Research (RES) to provide a structured, probabilistic method of reviewing operational experience to determine and assess both known and unrecognized vulnerabilities that could lead to core damage accidents. The ASP Program is currently implemented by the Office of Analysis and Evaluation of Operational Data (AEOD), and is capable of assessing

internal initiating events during full power operation. In addition, the ASP methodology has been adopted by the Office of Nuclear Reactor Regulation (NRR), and its use has been extended to short-term review of the licensee event notifications under 10 CFR 50.72, inspection findings, and other issues.

As outlined in the ASP Program Plan, ASP program pursues the ultimate objective of performing risk significant evaluations on operational events (precursors) occurring in commercial nuclear power plants (NPPs). To achieve this objective, the RES is supporting the development of simple probabilistic risk assessment (PRA) models for NPPs in the U.S. Presently, only simple Level 1 plant models have been developed which estimate core damage frequencies. However, the plan calls for the capability to append to existing Level 1 outcomes the capability of performing Level 2/3 risk assessments such that the potential consequences and risks could also be assessed. This plan also calls for an examination of the current ASP models such that, when needed, more detailed PRA models can be easily accessed.

As a step towards implementing the ASP Program Plan, RES has placed companion programs at Sandia National Laboratories (SNL) and Idaho National Engineering Laboratory (INEL) with the specific objective to develop ASP Level 2/3 models for U.S. commercial NPPs that are consistent with the existing Level 1 models in the level of detail for direct interface and with the flexibility of linking to more detailed Level 2/3 PRA models when needed. Models for boiling water reactors (BWRs) are being developed at SNL while models for pressurized water reactors (PWRs) are being developed at INEL.

This paper documents the current ASP Level 2/3 model development effort. As done in the Level 1 model development, all NPPs are classified into groups with a single plant being selected from each group as the subject of the initial model development effort. During the plant-group model development, to the extent feasible, information and methods developed and collected in the course of the NUREG-1150 study [NRC, 1990] are utilized. The objectives of the Level 2/3 plant-group model development are to demonstrate: (1) appropriate interfaces between the Level 1 models and the Level 2 models; (2) simplified Level 2 models; (3) source term (ST) estimates; (4) consequence estimates; and (5) integration of the Level 2/3 models into the existing ASP software (i.e., SAPHIRE code suite [Russell et al., 1994]). Each of these issues will be addressed in the following paragraphs.

NPP Plant Groups

Similar to the procedure used in the Level 1 portion of the analysis, the NPPs were organized into plant groups. For the Level 2/3 model development effort, plant groups are based on plant characteristics that can affect the release radioactive material from the damaged core and its transport through the containment. A representative plant is then selected from each group as the subject of the initial model development effort. Initially,

plants have been combined into six PWR plant groups and four BWR plant groups. A PWR plant, Zion, and a BWR plant, Peach Bottom, were the first two plants selected to demonstrate the approach.

Level 1 and Level 2 Model Interface

Since the existing ASP Level 1 event trees simply identify whether or not a particular accident sequence results in core damage, they do not satisfy the informational requirements of the Level 2 analysis. In particular, two modifications have been performed on the Level 1 models to allow the subsequent Level 2 analysis. The first modification was the addition of certain containment systems that are important in the Level 2 analysis. Some Level 2 issues involve consideration of containment systems which are not modeled in the Level 1 event trees. It is important to include containment systems models with the Level 1 event tree in order to account for dependencies, e.g., support systems such as ac power, between the Level 1 systems and the containment systems. This necessitates the use of bridge trees which are event trees that model containment systems and are attached to the end of the Level 1 event trees. As an example, the modified Zion Level 1 event tree for transient is shown in Figure 1. Those accident sequences lead to core damage are now labeled with "bridge" in the "STATE" column. The bridge tree, which is shown in Figure 2, is linked to these sequences.

The second modification was the development of plant damage states. The information from the Level 1 analysis is passed to the Level 2 analysis through the plant damage state (PDS) interface. This interface must describe the plant configuration at core damage, which has resulted from an initiating event and combinations of individual hardware or operator failures. To efficiently transfer information from the Level 1 models to the Level 2 models, accident sequences from the Level 1 analysis are grouped according to characteristics that are relevant to the release of radionuclides from the fuel and core debris and their subsequent transport through the containment. These characteristics define the plant configuration, the availability of mitigation systems, and the timing of the accident at the onset of core damage. These groups of accidents that have similar characteristics are called PDSs. A PDS provides a similar set of initial and boundary conditions for the accident progression analysis; i.e., all the accidents grouped in one PDS should behave similarly for the remainder of the accident progression.

The PDS interface is an important element of the methodology because it, in part, will determine the level of detail that is represented in the Level 2/3 model. Hence, it is important that this interface have the flexibility to handle analyses of various complexity. A vector approach, similar to that used in the NUREG-1150 study, is utilized to define PDSs. In the vector approach, a list of plant characteristics that define the accident at the onset of core damage is identified (i.e., the plant configuration and the status of mitigation systems) and represented as a vector with each position in the vector corresponding to a characteristic.

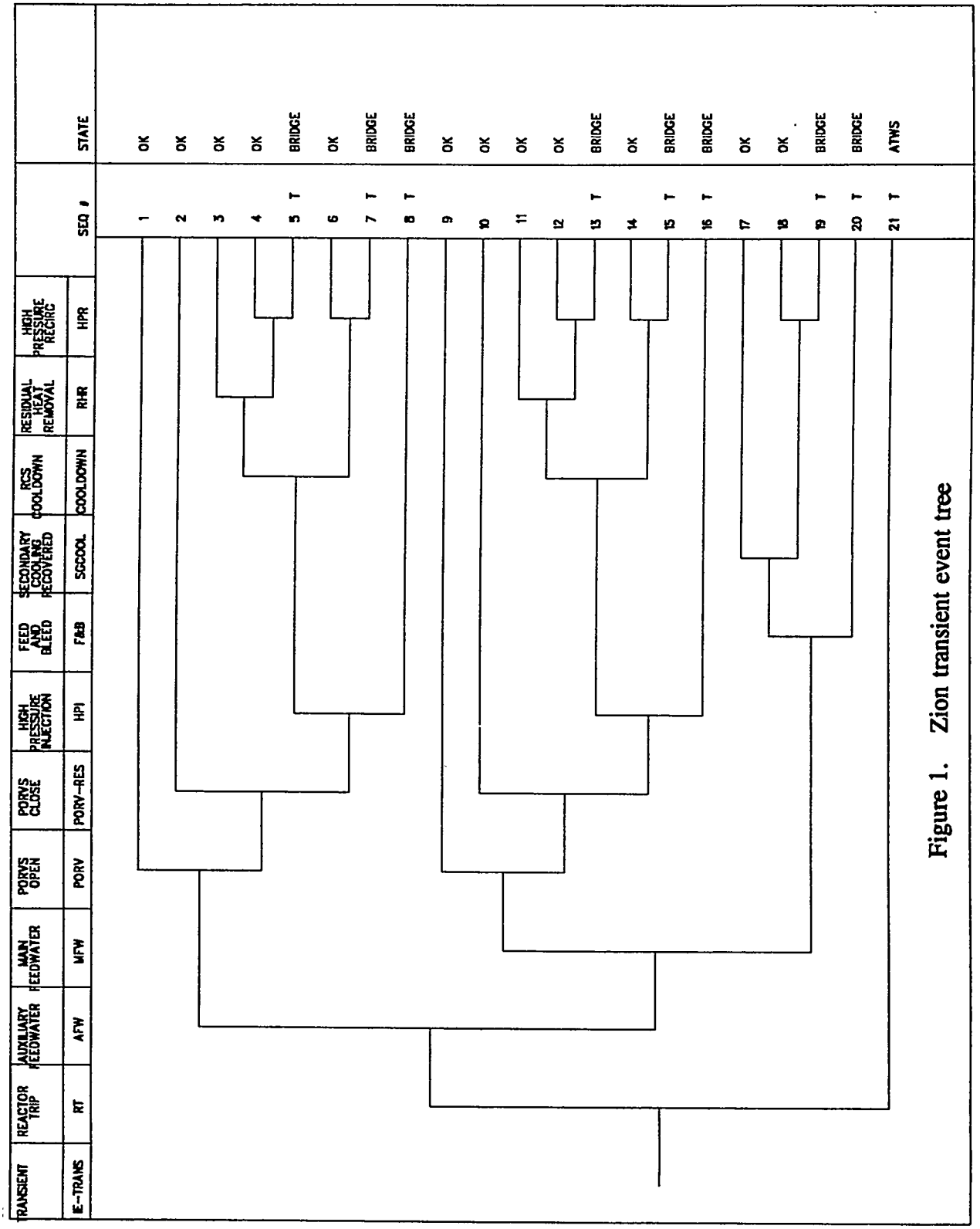

Figure 1. Zion transient event tree

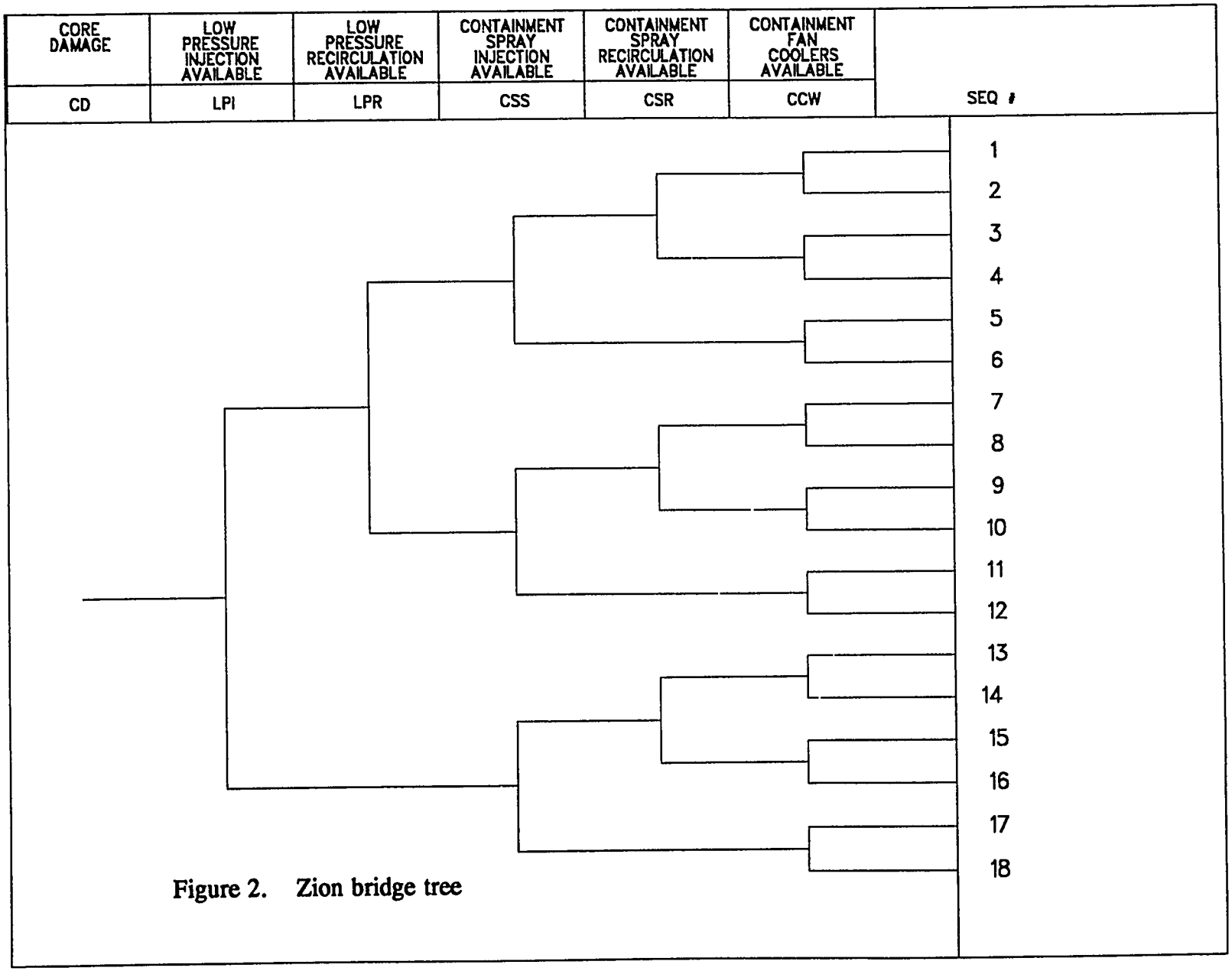

Figure 2. Zion bridge tree

By including more or less characteristics or vector positions, the level of detail in the interface can be adjusted. The SAPHIRE code has been modified to allow PDS vectors to be defined for accidents (represented by either cut sets or accident sequences) using sets of logic rules. These logic rules are applied to each endstate of the bridge tree. Rules, in the form of "IF-THEN" statements, search through the accident sequence logic to determine which character belongs in each vector positions of the PDS identifier. When each position of the vector has been filled with the appropriate character, the PDS vector along with its corresponding frequency, is transferred to the Level 2 portion of the analysis as the initiating event for the next event tree in the process. Table 1 lists the different values used for each of the eight character positions used in the Zion PDS vectors. Table 2 lists the different values used for each of the ten character positions in the Peach Bottom PDS vectors.

Table 1. Zion Plant Damage State Characteristics

---

1. Status of RCS at Onset of Core Damage

T	=	no break (transient)
A	=	large break in the RCS pressure boundary
S_1	=	medium break in the RCS pressure boundary
S_2	=	small break in the RCS pressure boundary
S_3	=	very small break in the RCS pressure boundary
G	=	SGTR
H	=	SGTR with loss of secondary system integrity
V	=	large break in an interfacing system

2. Status of ECCS

B	=	operated in injection and now operating in recirculation
I	=	operated in injection only
R	=	not operating, but recoverable
N	=	not operating, but not recoverable
L	=	LPSI available in both injection and recirculation modes

3. Containment Heat Removal

B	=	operated in injection and now in recirculation
I	=	operated in injection only
R	=	not operating, but recoverable
N	=	never operated, not recoverable

Table 1. (continued)

C	=	available in injection and in recirculation
A	=	available in injection only

4. AC Power

Y	=	available
P	=	partially available
R	=	not available, but recoverable
N	=	not available, not recoverable

5. Contents of RWST

Y	=	injected into containment
R	=	not injected, but could be injected if power recovered
N	=	not injected, cannot be injected in the future

6. Heat Removal from the Steam Generators

X	=	at least one AFWS operating, SGs not depressurized
Y	=	at least one AFWS operating, SGs depressurized
S	=	S-AFWS failed at beginning, E-AFWS recoverable
C	=	S-AFWS operated until battery depletion, E-AFWS recoverable, SGs not depressurized
D	=	S-AFWS operated until battery depletion, E-AFWS recoverable, SGs depressurized
N	=	no AFWS operating, no AFWS recoverable

7. Cooling for RCP Seals

Y	=	operating
R	=	not operating, but recoverable
N	=	not operating, not recoverable

8. Status of Containment Fan Coolers

Y	=	operating
R	=	not operating, but recoverable
N	=	not operating, not recoverable

Table 2. Peach Bottom Plant Damage State Characteristics

1. Status of the Reactor Protection System

A	=	the reactor protection system successfully operated
B	=	the reactor protection system failed but standby liquid control system (SLC) was successful (ATWS)
C	=	both the reactor protection system and the SLC systems failed (ATWS)

2. Status of Electric Power

A	=	onsite power is available
B	=	both onsite and offsite ac and dc power are unavailable
C	=	all ac power unavailable, however, dc power is available

3. Status of Reactor Pressure Vessel Integrity

A	=	RPV intact and no stuck open SRVs
B	=	RPV intact with at least one stuck open SRV
C	=	not used
D	=	S_2 LOCA

4. Status of the Pressure in the Reactor Pressure Vessel

A	=	the RPV is at high pressure and cannot be depressurized due to mechanical or operator failures
B	=	the RPV is at high pressure and cannot be depressurized due high containment pressure
C	=	the RPV is at high pressure and can be depressurized
D	=	the RPV is at low pressure

5. Status of High Pressure Injection Systems

A	=	all systems are failed or unavailable
B	=	the system is recoverable with the recovery of electric power
C	=	at least one system is available

Table 2 (continued)

6. Status of Low Pressure Injection Systems (LPCS/LPCI)

A	=	all low pressure injection systems are failed
B	=	LPCI or LPCS is recoverable with the recovery of ac power
C	=	LPCS of LPCI is available
D	=	HPSW is available

7. Status of Containment Heat Removal

A	=	RHR has failed
R	=	RHR is recoverable with recovery of ac power
N	=	RHR is working

8. Status of Containment Venting

A	=	the containment vent system is failed
B	=	the containment vent system is recoverable with the recovery of electric power
C	=	the containment was vented
D	=	the containment vent system is available but has not been used

9. Status of Containment Integrity

A	=	nominal leakage
B	=	pre-existing leakage in the drywell
C	=	pre-existing leakage in the drywell head
D	=	pre-existing leakage in the wetwell
E	=	pre-existing rupture in the drywell
F	=	pre-existing rupture in the drywell head
G	=	pre-existing rupture in the wetwell

10. Timing for Onset to Core Damage

A	=	core damage occurs in the short-term
B	=	core damage occurs in the long-term

The ASP PDSs group together Level 1 accident sequences. A number of factors contributed to the decision to base the PDSs on accident sequence logic instead of individual cut sets. First and foremost, the accident sequence logic provide a sufficient amount of information to develop an interface for the Level 2 analysis that is consistent with the level of detail used in the Level 1 analysis. A number of additional factors supported the use of accident sequences:

- While a single Level 2 model will be used to represent a plant group, PDSs need to be developed for each plant within the group. When many plants are involved it is desirable to use the same logic to form PDSs for each plant. For a set of plants in a plant group, the event trees and, hence, the accident sequences, tend to be very similar whereas at the fault tree level there tend to be more differences. Developing PDSs based on accident sequences rather than cut sets reduces the need to create special rules for assigning accident sequences to a PDS for each plant.

- It is desirable to minimize the effect that changes to the Level 1 model will have on the definition of the PDSs and hence, the Level 2 model. It is anticipated that future modifications to the Level 1 models are more likely to affect the fault trees than the event trees. If the PDSs were based on cut sets, each time a fault tree is modified the logic used to assign cut sets to PDSs would have to be reviewed and possibly modified. By basing the PDSs on accident sequences the changes that will have to be made to the PDSs due to changes to the Level 1 model will be minimized.

- It is desirable to have the PDS interface transparent and scrutable. The methods by which rules are developed to assign sequences to PDSs is less complicated and easier to review than when cut sets are assigned to PDSs.

Combined, the Level 1 event trees and the bridge trees provide sufficient information to create PDSs that are at a level of detail that is consistent with the Level 1 ASP analysis. The PDSs create a flexible interface between the Level 1 and Level 2 analyses and define the initial and boundary conditions for the accident progression analysis.

Level 2 Model

The ASP Level 2 model starts with the PDS vector, and models the progression of the severe accident with respect to containment performance, and predicts the magnitude and timing of the resultant radioactive release to the environment. The model consists of an event tree that is a simplified, graphical version of the accident progression event trees (APET) originally developed as part of the NUREG-1150 program. This Level 2 event tree (referred to as either an APET or a containment event tree) is used to define a set of source term vectors (developed in a similar manner as the PDS vectors) that characterize the magnitude and timing of any radioactive material released from the containment as a result of a core damage

accident.

Source terms for each source term vector are estimated using simplified codes that rely on input from more detailed codes, such a RELAP/SCADAP and MELCOR, and other information sources. Since hundreds of source term vectors may be generated from the ASP model, the source terms are combined into a more manageable number using an partitioning algorithm [Iman et al., 1990] that is similar to that developed for the NUREG-1150 study. In this approach, source term vectors are combined into source term groups (STGs) based on their potential to cause early and latent health effects. A representative source term is then selected for each STG.

Since the source term vectors can be defined a priori based on the definition of the ASP APET, both the source term calculation and the partitioning of source terms into source term groups can be performed outside or "offline" from the normal ASP analysis process. By performing the source term calculations offline, the ASP analysis is not burdened by repeating calculations that only need to be performed once. Hence, in the Level 2 model used in an ASP analysis, source terms are never explicitly estimated and displayed. Instead, the ASP APET is used to define the source term vectors which are then combined into source term groups using logic rules that replicate the source term groups defined using the partitioning algorithm. These groups then form the interface between the Level 2 and the Level 3 model. The ASP APET and the source term model are described in the two sections that follow.

Accident Progression Model

The Level 2 models developed for the ASP program are greatly simplified versions of the NUREG-1150 APETs. Basically, the events deemed the most relevant to the identification of a source term vector are extracted from the detailed APETs and organized into a graphical event tree which becomes the ASP APET. Events considered include consideration of vessel failure, the status of containment integrity, and source term mitigation features such a containment sprays and pools. In most cases, the split fractions for the ASP APET are generated by evaluating the detailed APET using the ASP PDSs as input and then rolling up the detail APET (using the EVNTRE code [Griesmeyer et al., 1989]) to the corresponding intermediate level. In some cases, logic models are developed and included in the ASP APET in the form of fault trees which support a particular top event appearing on the ASP APET. As an example, the ASP Level 2 event trees (including the transfer trees) for the Zion plant model are shown in Figures 3, 4, 5 and 6. Table 3 contains the description of the top events for the Zion Level 2 event trees.

Source Term Model

Two different approaches for estimating source terms are being investigated in this study. The first approach relies on the parametric algorithms, collectively called XSOR [Jow et al.,

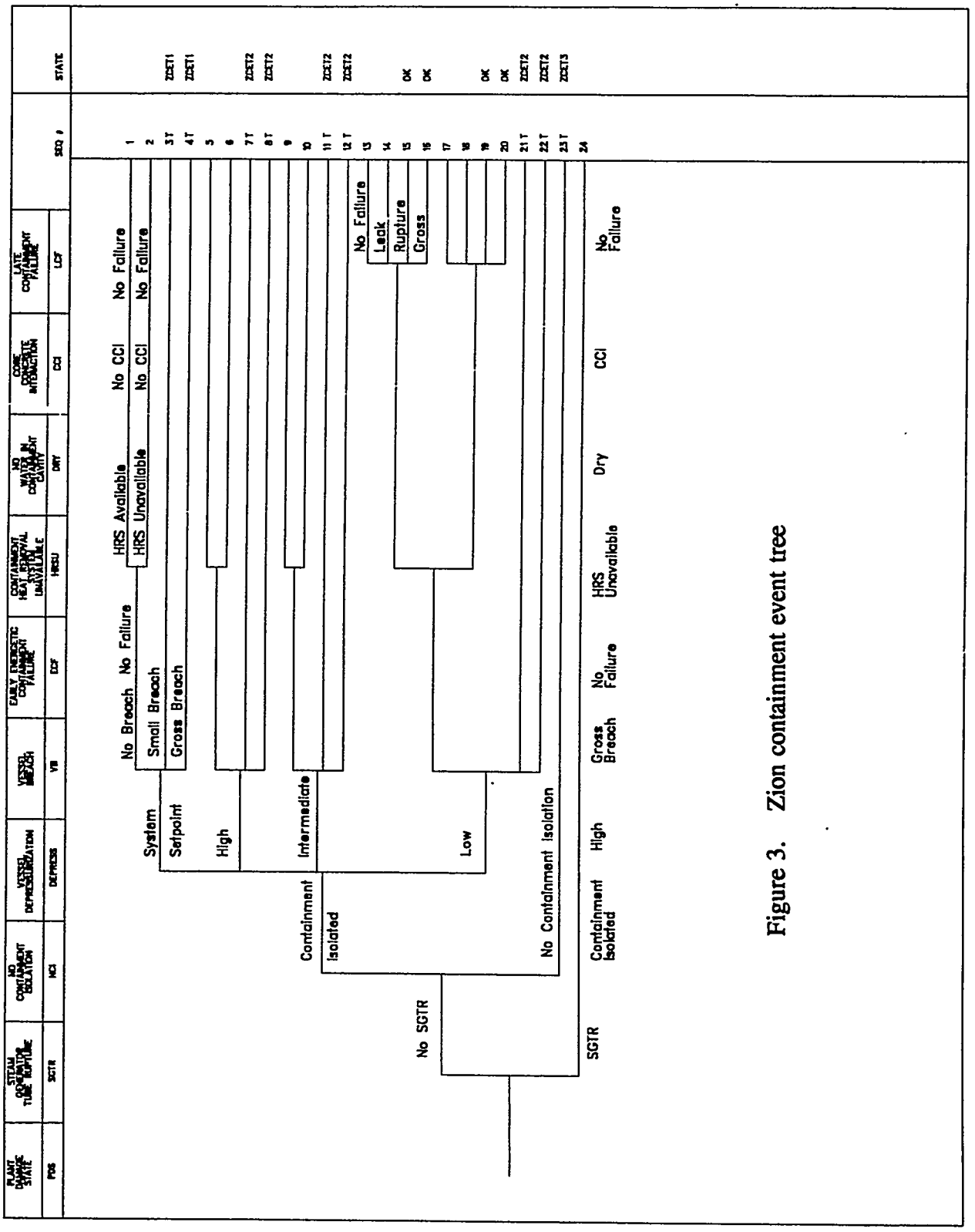

Figure 3. Zion containment event tree

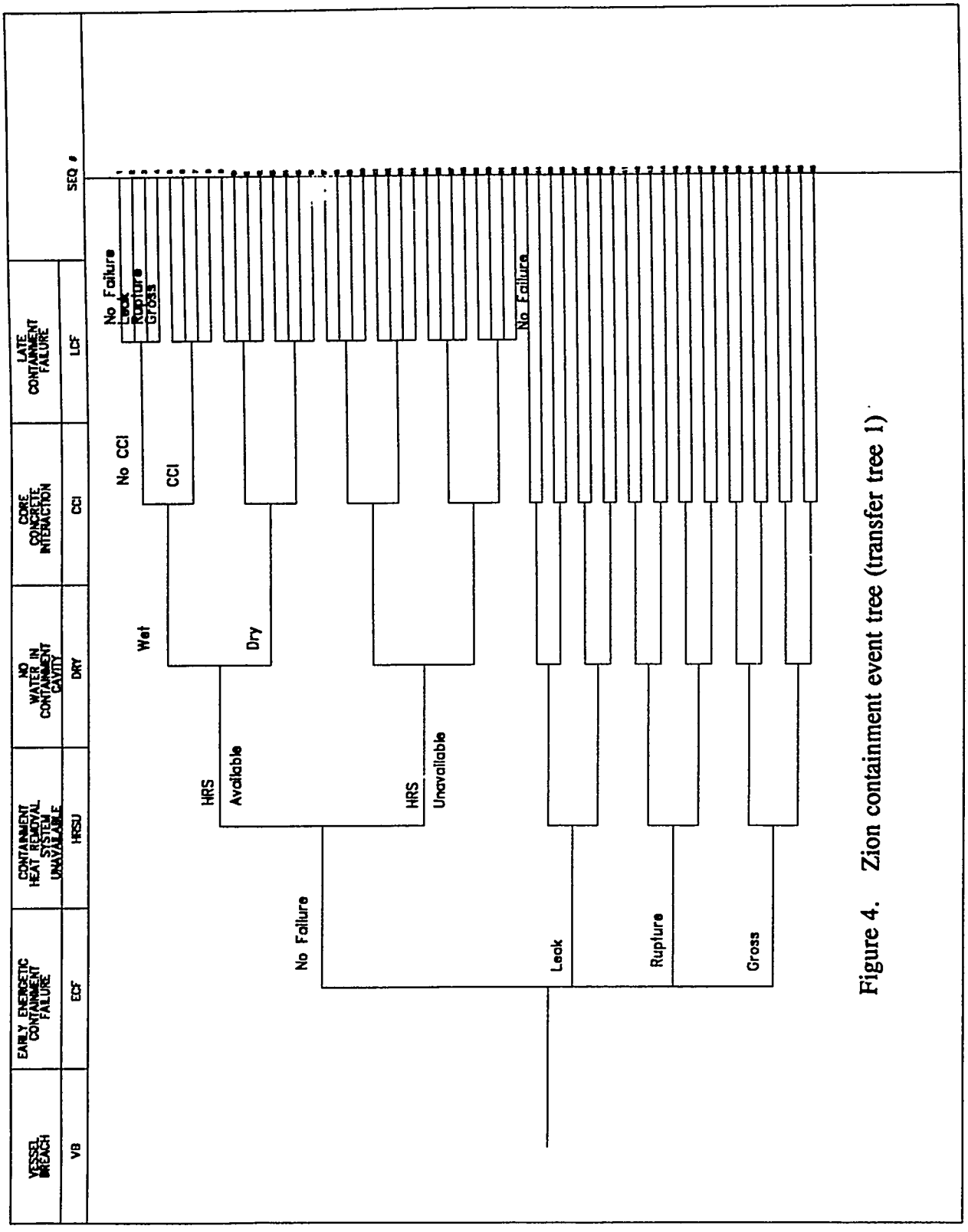

Figure 4. Zion containment event tree (transfer tree 1)

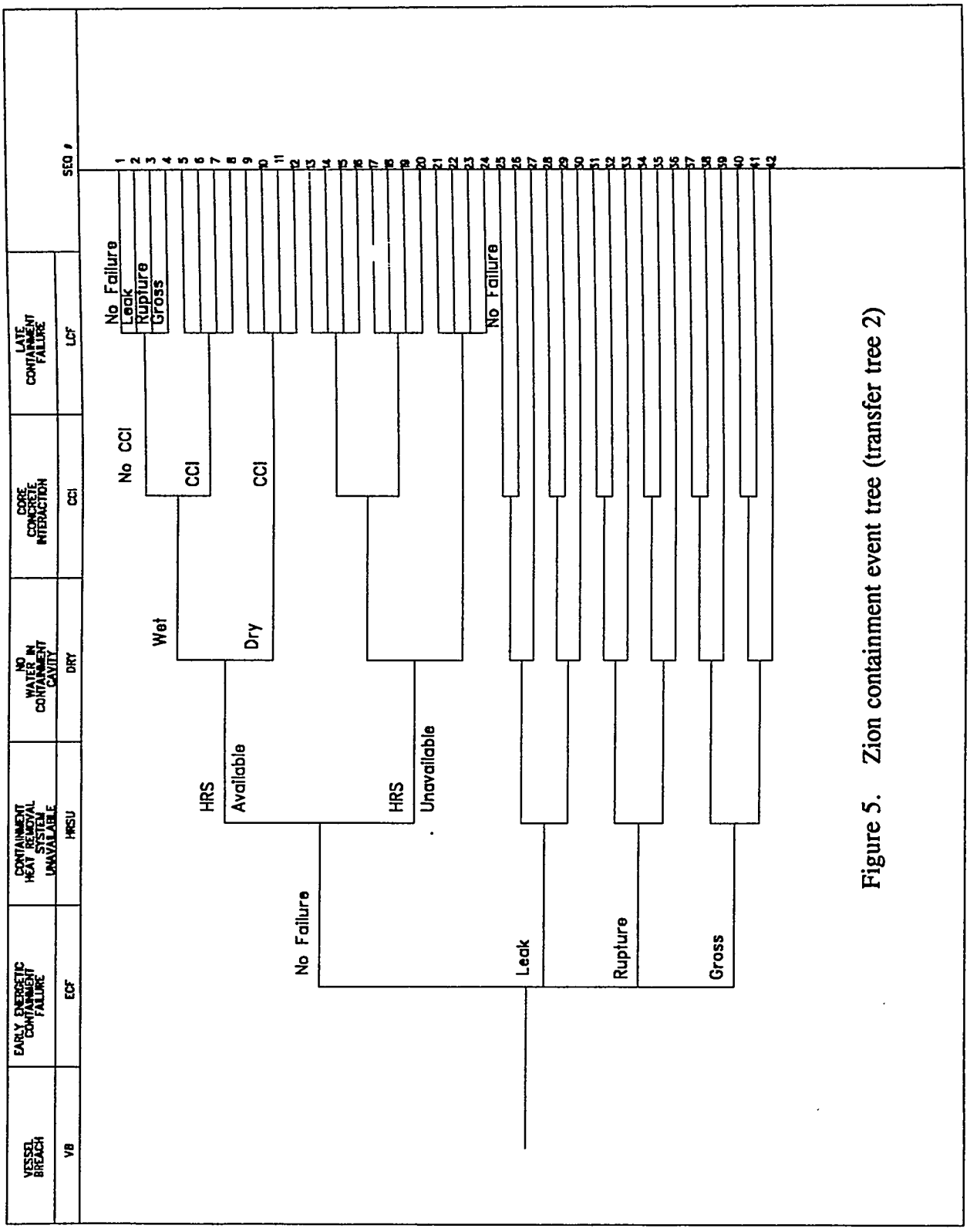

Figure 5. Zion containment event tree (transfer tree 2)

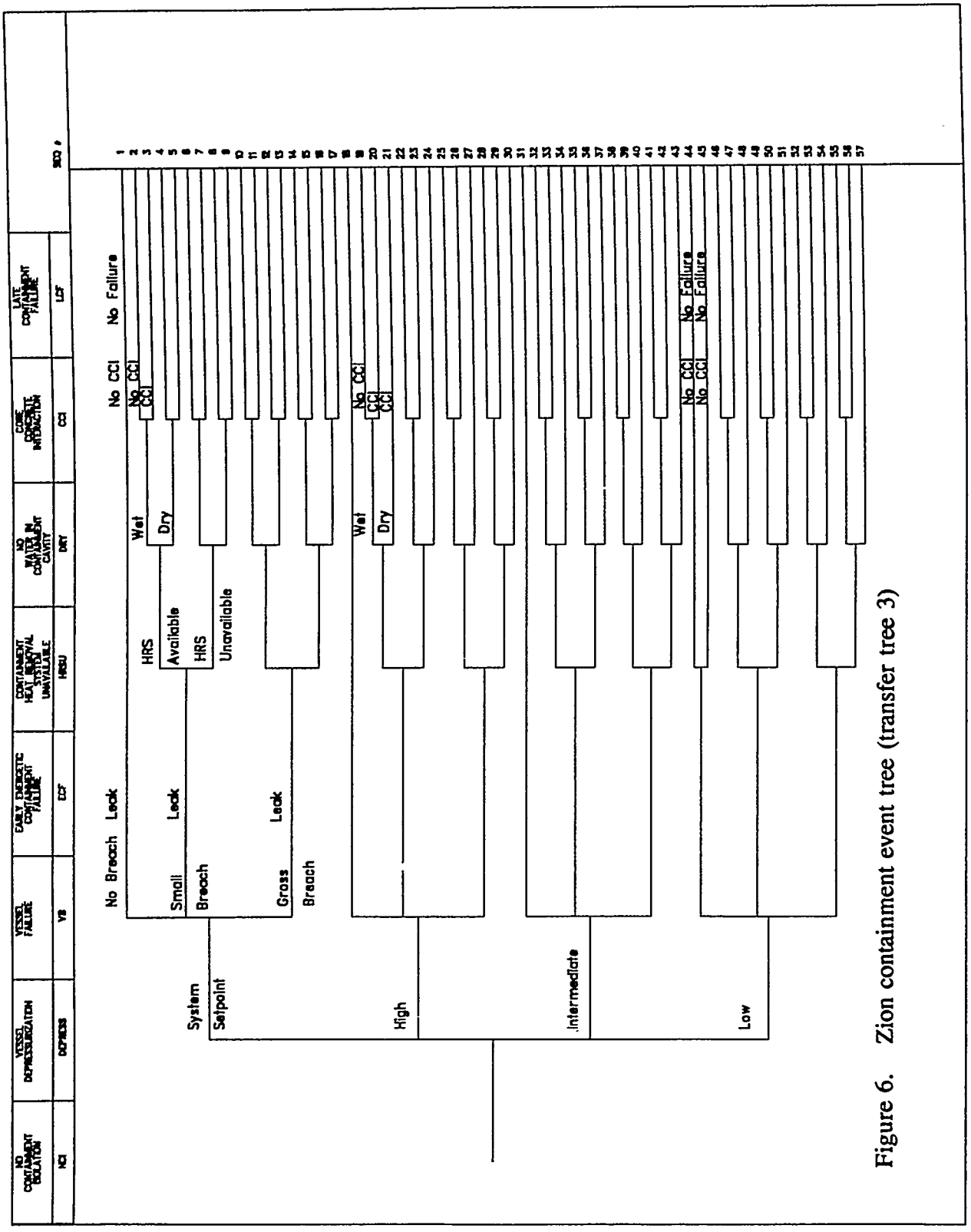

Figure 6. Zion containment event tree (transfer tree 3)

Table 3. Zion Containment Event Tree Top Events

1. PDS (plant damage state)

   The initiating event for the ASP Level 2 analysis.

2. SGTR (steam generator tube rupture)

   Success of this top event indicates that no SGTR occurred or the steam generator isolated upon SGTR.

3. CONT-ISOL (containment isolation)

   Success of this top event indicates that the containment is isolated.

4. DEPRESS (RCS pressure at vessel breach)

   Branch 1 indicates low RCS pressure (less than 200 psi)
   Branch 2 indicates intermediate pressure (between 200 and 600 psi)
   Branch 3 indicates high RCS pressure (between 600 and 2000 psi)
   Branch 4 indicates safety relief valve set point pressure (greater than 2000 psi)

5. VESS-FAIL (vessel failure mode)

   Branch 1 indicates no vessel failure
   Branch 2 indicates a small vessel failure area ($\leq$ 0.4 m^2)
   Branch 3 indicates a large vessel failure area ($>$ 0.4 m^2)

6. EARLY-CF (early containment failure mode)

   Branch 1 indicates no early containment failure
   Branch 2 indicates a small containment leak (nominal size of $\sim$ 0.009 m^2)
   Branch 3 indicates a containment rupture of medium size (nominal size of $\sim$ 0.7 m^2)
   Branch 4 indicates a catastrophic containment failure of substantial size with extensive damage to the containment structure

Table 3. (continued)

7. CONT-HRS (containment heat removal system)

   Success of this top event indicates that the containment heat removal system is available.

8. CONT-H2O (presence of water in vessel cavity)

   Success of this top event indicates that water is present in the vessel cavity.

9. CCI (core concrete interaction)

   Success of this top event indicates that core concrete interaction does not occur.

10. LATE-CF (late containment failure mode)

    Branch 1 indicates no late containment failure
    Branch 2 indicates a small containment leak (nominal size of $\sim$ 0.009 m^2)
    Branch 3 indicates a containment rupture of medium size (nominal size of $\sim$ 0.7 m^2)
    Branch 4 indicates a catastrophic containment failure of substantial size with extensive damage to the containment structure

---

1993], developed for the NUREG-1150 study . Some modifications and simplifications were made when applying the NUREG-1150 algorithms for the source term calculations most notably in the representation of the timing of the accident. Whereas uncertainty distributions were included in the source term analysis for NUREG-1150, only the mean values of the NUREG-1150 distributions were used for the ASP base analysis, so that each source term vector would produce a single source term.

The development of Level 2/3 models for plants not included in the NUREG-1150 study required the development of a new code, the Parametric Source Term (PST) code. The PST code is a framework of equations based on activity transport between volumes in the release pathway from the core, through the vessel, through the containment, and to the environment.

In simple terms, the equations consider various losses (deposition, decay, exit flows,etc.) and source terms (inlet flows, resuspension, daughter products, core-concrete interactions, oxidation, etc.) for each volume. Exact solutions to differential equations are obtained to estimate activity transport in each volume for each time interval. Hence, PST is fast running because it allows fairly large time intervals to be selected. PST currently performs point estimate calculations. However, it has been developed so that source term uncertainty distributions may be estimated using Monte Carlo technique with importance sampling or Latin Hypercube techniques to quantify PST input parameter distributions. The primary differences between XSOR parametric codes and the PST code are that the PST modeling framework: 1) ensures conservation of activity as it is transported across various volumes in its release pathway; 2) allows a limited amount of consideration on the time-dependent behavior of input parameter uncertainty distributions; 3) allows more direct application of recent state-of-the-art severe accident analysis code results for input quantification (and thus reduces the dependence of expert opinion); and 4) increases modeling flexibility because linkage between volumes is specified by user input.

Level 3 Model

The ASP Level 3 model is represented by a "consequence event tree"; an example tree is shown in Figure 7. The initiating event for the Level 3 tree is a source term group defined by the Level 2 model. The consequence event tree includes two sets of consequence results. The first set corresponds to a modeling approach that adopts the protective measures used in the NUREG-1150 study whereas the second set assumes that no protective measures are implemented. The two sets of protective measure assumptions are distinguished by the top event CSQNPM. The second top event in the tree represents the six consequence measures calculated for the ASP analysis (while this top event, CSQMEAS, has seven outcomes, the first event is never used as indicated by the "@" sign). The six consequence measures used in this study include: 1) effective whole body dose equivalent, 0-25 mi.; 2) effective whole body dose equivalent, 0-50 mi.; 3) thyroid dose, 0-25 mi.; 4) thyroid dose, 0-50 mi.; 5) individual early fatality probability, 0-1 mi.; and 6) individual latent cancer fatality probability, 0-10 mi. The unique feature of this tree is that consequences instead of probabilities are used to quantify the top event CSQMEAS. Hence, the result for each sequence is not a frequency but risk (i.e., frequency of the sequence multiplied by the consequence of the sequence).

The consequence analysis was performed offline in a manner similar to the source term analysis. Consequences were estimated for each STG defined in the Level 2 analysis using MACCS Version 1.5.11.1 [Chanin et al., 1990; Jow et al., 1990; Rollstin et al., 1990; Chanin et al., 1993], NRC's current state-of-the-art offsite consequence analysis code for use in probabilistic risk assessments. The consequences were estimated for the offsite population using the following assumptions:

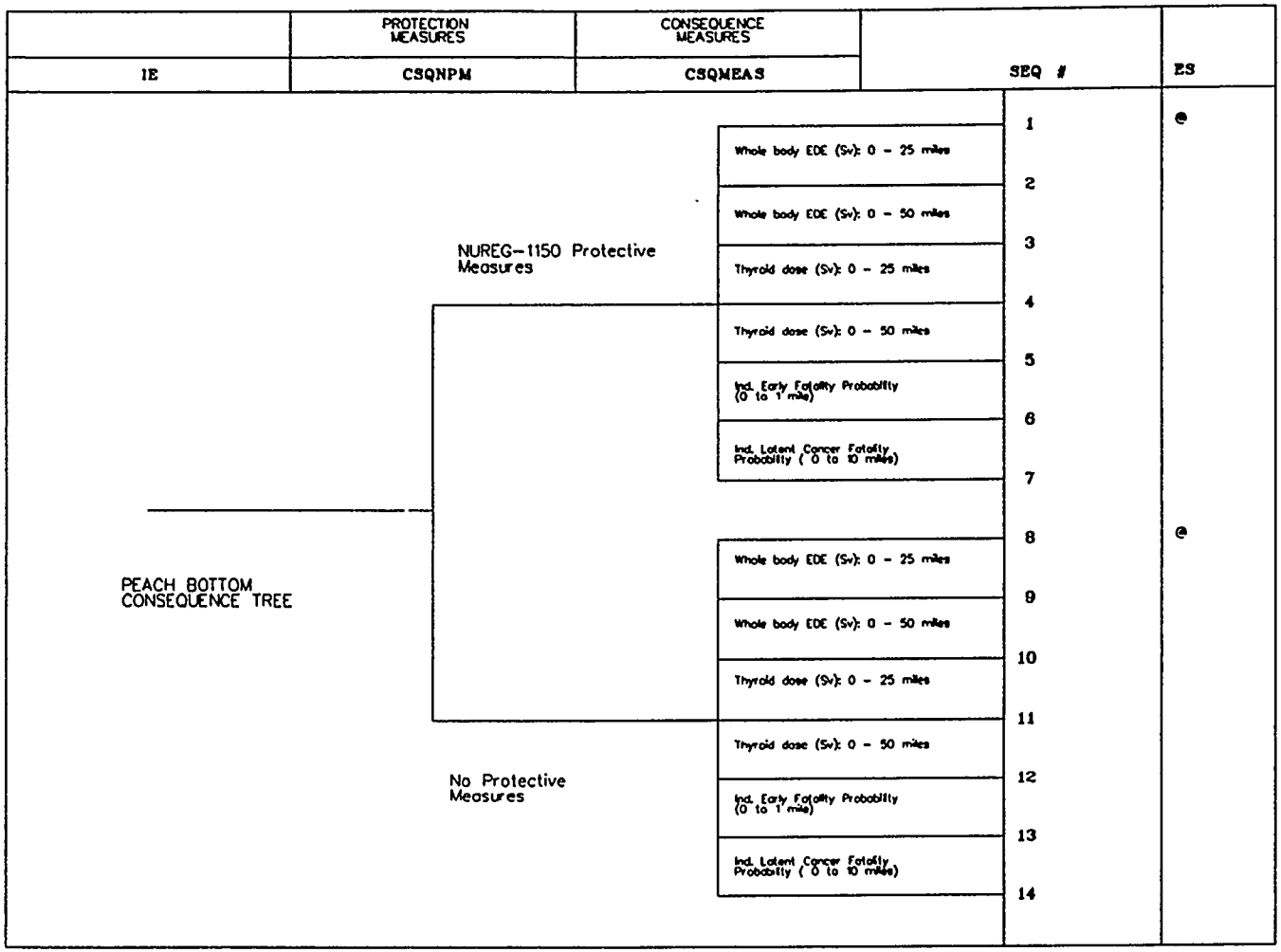

Figure 7. Consequence event tree

- Meteorology was based on an "eightieth percentile site" as evaluated by Brookhaven National Laboratory staff for use in prior studies [Hanson et al., 1994].

- The exclusion area used was 1/2 mile, and the emergency preparedness zone (EPZ) used was 10 miles.

- The population density used was 340 persons/mi^2.

- All exposure pathways except ingestion were included.

The results from the calculations were then used to quantify the top event CSQMEAS in the Level 3 tree.

Risk Integration

The ASP Level 1, Level 2, and Level 3 models are evaluated in an integrated manner to yield risk results using the SAPHIRE code suite. The integration process is depicted in Figure 8. The Level 1 core damage sequences generated by evaluating the Level 1 event and fault trees, and expanded through the use of the bridge trees, are partitioned into PDS (i.e., each bridge tree endstate is assigned a PDS vector). The PDS (and associated frequencies) then become the initiating events for the Level 2 analysis. The Level 2 sequences generated by evaluating the ASP APETs are used to define source term vectors (i.e., each APET endstate is assigned a source term vector); these vectors are then partitioned into STGs. The STGs and associated frequencies, then become the initiating events in the Level 3 analysis. The Level 3 sequences are generated by evaluating the consequence event tree and partitioning into one of two sets of consequence measures, corresponding to the two emergency response scenarios. Combining the consequence measures with the frequencies of the STGs, then produces risk estimates in terms of the consequence measure of interest, such as early fatalities per reactor-year.

Presently, each step of the calculational process is executed manually using IRRAS. Although no external file manipulations or inputs are needed (all calculations from Level 1 sequence frequencies to final risk estimates are performed in, and using IRRAS), the process requires approximately 15 individual steps. Long-term plans call for automating the process using the GEM module in SAPHIRE. The ideas here is to develop a macro such that the entire process of going from Level 1 accident sequences to risk can be performed with a single SAPHIRE command.

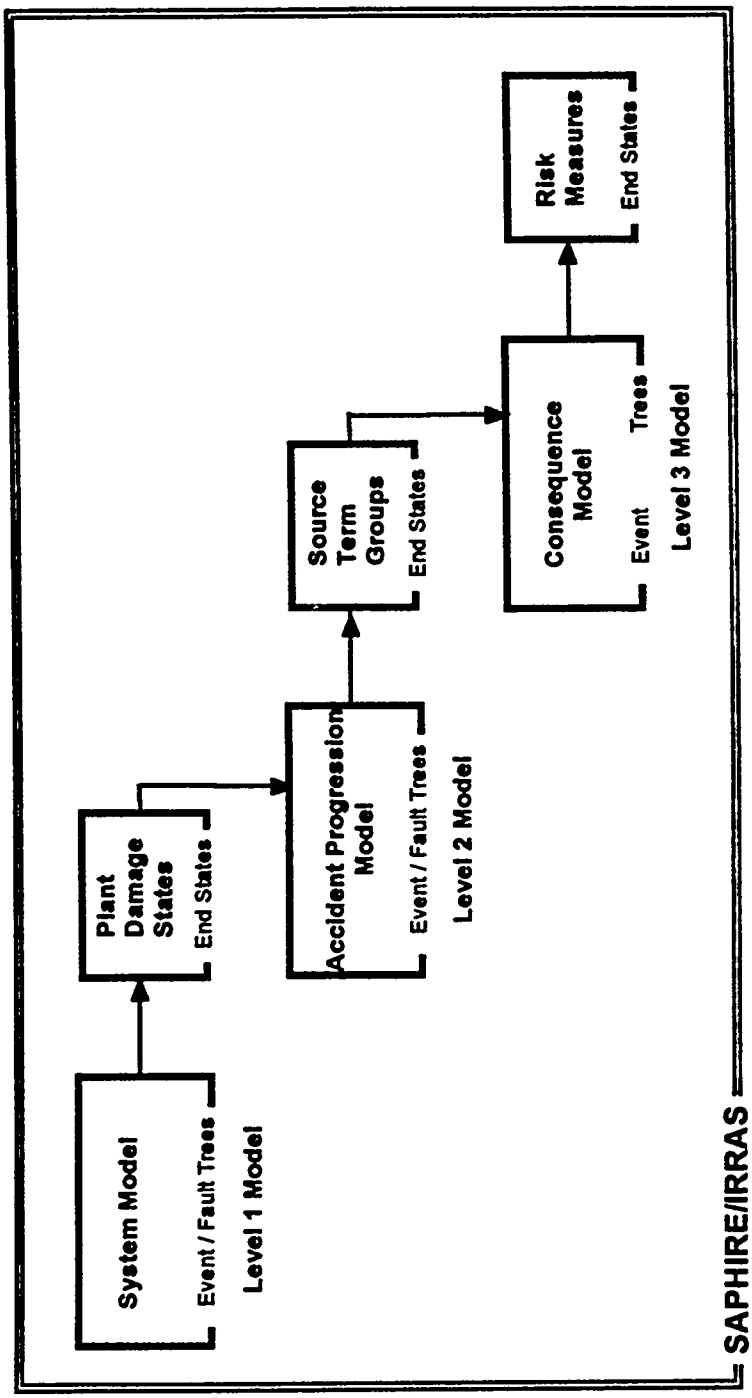

Figure 8. Schematic of the integrated ASP risk model

Summary

A methodology has been developed for appending to the ASP Level 1 analysis the capability to estimate consequences and risk for operational events (precursors) occurring in commercial nuclear power plants. To estimate consequences and risk, a linked event tree approach is utilized where event trees are used to model the Level 1, Level 2 and Level 3 portions of the analysis. Whereas the endstates from the Level 1 tree represent the frequency of core damage for an operation event, the endstates from the Level 3 tree represent its risk. Through carefully constructed interfaces, these event trees are automatically linked together and evaluated in a integrated fashion using the SAPHIRE code suite. To reduce the computational time requirements for a typical ASP analysis, source terms and consequences are evaluated offline, and coded into the SAPHIRE database for ASP analysis. It is the results from these evaluations that are summarized in the consequence tree. Embedded in this methodology is the flexibility to link Level 2/3 models of various levels of detail to the Level 1 models. Through this approach, it is now possible to estimate both the frequency and the risk associated with operational events. To demonstrate this methodology, prototypic models have been developed for a BWR and a PWR plant. All plant-group models are being developed, and are expected to be completed in early 1996. Subsequent to the completion of the Level 2/3 plant-group models, the adequacy of these models will be examined based on plant information and experimental data which have become available after the NUREG-1150 study, such as the IPE program. It is expected that these plant-group models will be further refined to account for the important characteristics that differentiate the NPPs.

References

[Chanin et al., 1990] D. I. Chanin et al., "MELCOR Accident Analysis Consequence Code System," NUREG/CR-4691, SAND86-1562, Sandia National Laboratories, Vol 1, February 1990.

[Chanin et al., 1993] D. Chanin, et al., "MACCS Version 1.5.11.1: A Maintenance Release of the Code," NUREG/CR-6059, SAND92-2146, Sandia National Laboratories, October 1993.

[Griesmeyer et al., 1989] J. M. Griesmeyer et al., "A Reference Manual for the Event Progression Analysis code (EVNTRE)," NUREG/CR-5174, SAND88-1607, Sandia National Laboratories, September 1989.

[Hanson et al., 1994] A. L. Hanson et al., "Calculations in Support of a Potential definition of a Large Release," NUREG/CR-6094, BNL-NUREG-52387, Brookhaven National Laboratory, May 1994.

[Iman et al., 1990] R. L. Iman et al., "PARTITION: A Program for Defining the

Source Term/Consequence Interface in the NUREG-1150 Probabilistic Risk Assessments," NUREG/CR-5262, SAND88-2940, Sandia National Laboratories, May 1990.

[Jow et al., 1990] H-N Jow et al., "MELCOR Accident Analysis Consequence Code System," NUREG/CR-4691, SAND86-1562, Sandia National Laboratories, Vol 2, February 1990.

[Jow et al., 1993] H-N Jow et al., "XSOR Code User's Manual," NUREG/CR-5360, SAND89-0943, Sandia National Laboratories, November 1993.

[NRC, 1990] U.S. Nuclear Regulatory Commission, "Severe Accident Risks: An Assessment for Five U. S. Nuclear Power Plants," NUREG-1150, Vols. 1-3, December 1990-January 1991.

[Rollstin et al., 1990] J. A. Rollstin et al., "MELCOR Accident Analysis Consequence Code System," NUREG/CR-4691, SAND86-1562, Sandia National Laboratories, Vol 3, February 1990.

[Russell et al., 1994] K. D. Russell et al., "Systems Analysis Programs for Hands-on Integrated Reliability Evaluations (SAPHIRE) Version 5.0," NUREG/CR-6116, EGG-2716, Vol. 1-10 Idaho National Engineering Laboratory, July 1994.

NEW DEVELOPMENTS IN THE SAPHIRE COMPUTER CODES*

Kenneth D. Russell, S. Ted Wood, and Kellie J. Kvarfordt
Lockheed Martin Idaho Technologies
Idaho National Engineering Laboratory
P.O. Box 1625
Idaho Falls, Idaho 83415

SUMMARY

The Systems Analysis Programs for Hands-on Integrated Reliability Evaluations (SAPHIRE) refers to a suite of computer programs that were developed to create and analyze a probabilistic risk assessment (PRA) of a nuclear power plant. The programs in this suite include: Models and Results Data Base (MAR-D) software, Integrated Reliability and Risk Analysis System (IRRAS) software, Systems Analysis and Risk Assessment (SARA) software, Fault tree, Event tree, and Piping and instrumentation diagram (FEP) graphical editor, and the Graphical Evaluation Module (GEM) software. Each of these programs performs a specific function in taking a PRA from the conceptual state all the way to publication.

Many recent enhancements to this suite of codes have been made. This presentation will provide an overview of these features and capabilities. The presentation will include a discussion of the new GEM module. This module greatly reduces and simplifies the work necessary to use the SAPHIRE code in event assessment applications. An overview of the features provided in the new Windows version will also be provided. This version is a full Windows 32-bit implementation and offers many new and exciting features. [A separate computer demonstration was held to allow interested participants to get a preview of these features.] The new capabilities that have been added since version 5.0 will be covered. Some of these major new features include the ability to store an unlimited number of basic events, gates, systems, sequences, etc.; the addition of improved reporting capabilities to allow the user to generate and "scroll" through custom reports; the addition of multi-variable importance measures; and the simplification of the user interface. Although originally designed as a PRA Level 1 suite of codes, capabilities have recently been added to SAPHIRE to allow the user to apply the code in Level 2 analyses. These features will be discussed in detail during the presentation.

The modifications and capabilities added to this version of SAPHIRE significantly extend the code in many important areas. Together, these extensions represent a major step forward in PC-based risk analysis tools. This presentation provides a current up-to-date status of these important PRA analysis tools.

---

*. Work supported by the U.S. Nuclear Regulatory Commission, Office of Nuclear Regulatory Research, under DOE Idaho Operations Office Contract DE-AC07-76ID01570.

INTRODUCTION

The U. S. Nuclear Regulatory Commission has developed a powerful suite of personal computer programs for the performance of probabilistic risk assessments (PRAs). This suite of programs, known as the Systems Analysis Programs for Hands-on Integrated Reliability Evaluations (SAPHIRE), allows an analyst to perform many of the functions necessary to create, quantify, and evaluate the risk associated with a facility or process being analyzed. These programs include software to define the data base structure, to create, analyze, and quantify the data, and to display results and perform sensitivity analyses. The programs in this suite include: Models And Results Data Base (MAR-D) software, Integrated Reliability and Risk Analysis System (IRRAS) software, SystemsAnalysis and Risk Assessment (SARA) software, Fault tree, Event tree, and P&ID (FEP) graphical editor software, and the Graphical Evaluation Module (GEM). Version 5.0 is documented in NUREG/CR-6116. Each of these programs performs a specific function in taking a PRA from the conceptual state all the way to publication.

Throughout the development of these software packages, various versions of each program were released. Because the programs functioned as an integrated package, and much confusion resulted from unknown compatibility of packages with different version numbers, it was determined in 1992 to combine these separate software package under one umbrella known as SAPHIRE. The first version of this integrated system was released in 1992 and was identified as SAPHIRE 4.0. This version of SAPHIRE and the following version 5.0 have proven to be a very powerful set of tools for the performance of risk assessments. Developmental work continues on the SAPHIRE system and a new version will be released soon. This paper will provide an overview of the new features contained in the next release of the SAPHIRE code. This overview will present a description of the general changes and a description of the more specific changes by functional area.

GENERAL FEATURES

The new version of SAPHIRE has many enhancements and changes. One of the most significant changes in this version of SAPHIRE is the removal of the limit on the number of basic events, gates, systems, event trees, etc in the data base. The user can now store up to 1 million of each of the data types in SAPHIRE. Previous to this, the user was limited to 10,000 of each type of data. This limit was determined to be insufficient for certain types of PRAs, so the limit was increased. The limiting factor is now essentially the amount of disk space and the speed of the processor used to analyze the data.

In conjunction with this change to the limits, the number of characters allowed in the basic event, gate, system, etc. names was also increased to 24-characters from the 16 previously allowed. It was determined that increasing this size beyond 24 characters would hinder the effective display of the data in reports and on the screen, hence, the 24 character choice. This allows the user to store more information in the names, but does not get so large as to replace the function of the description. This also allows the user to have more character positions to use when partitioning the sequence cut sets into end states.

The basic event data entry has been changed to provide more error checking and prevent the user from entering invalid or inconsistent data. The calculation and uncertainty type is used to check the information entered by the user. If the data is invalid then the user is prevented from leaving the field until correct data is entered. If the data is inconsistent, then the user is given a warning message, but allowed to leave the field or optionally choose a better value. These features provide much better data integrity and help the user to understand the result of basic event data entry choices.

The uncertainty analysis software has been changed in SAPHIRE to allow the user to generate up to 90,000 samples. This feature allows more flexibility in cases where large samples can make a difference in the results. The uncertainty analysis routines have also been modified to fix inconsistencies and speed up the processing.

Change-Set Enhancements

Many screens have been changed to simplify the user interface and allow easier access to the features in SAPHIRE. One of the areas that has changed more than others is the generate changes and change set area. Recall that a change set is used to modify base case basic event probability values. First, the changes sets have been divided into two groups. These two groups are change sets and flag sets. Flag sets are used in sequence generation only and do not show up on the generate menu. Flag sets are added and defined in the modify data base area or dynamically from event tree rules. Change sets are defined in the generate area. Change and flag sets can now be marked as "read only". This prevents a user from inadvertently changing or deleting a predefined change or flag set.

When a user added a 'probability" change in previous versions, a menu showing all events in the family was displayed. The events with individual probability changes showed up as an entry with a letter "P" or "p" beside their names. If the user wanted to know the events in the change set, they would have to generate a report, since searching down through the list of all events was too difficult. This is changed in the new version of SAPHIRE. The "single" change set option now only displays the events that are in the change set. This menu is shown in Figure 1. The user gets the list of events in the family when they are adding a new event to the current list in the change set. This method is much simpler and the user can see at a glance those events modified by a change set. The ability to automatically generate default flag sets for an accident sequence has been added to SAPHIRE and will be discussed further in the Event Tree Rules Enhancements section of this paper.

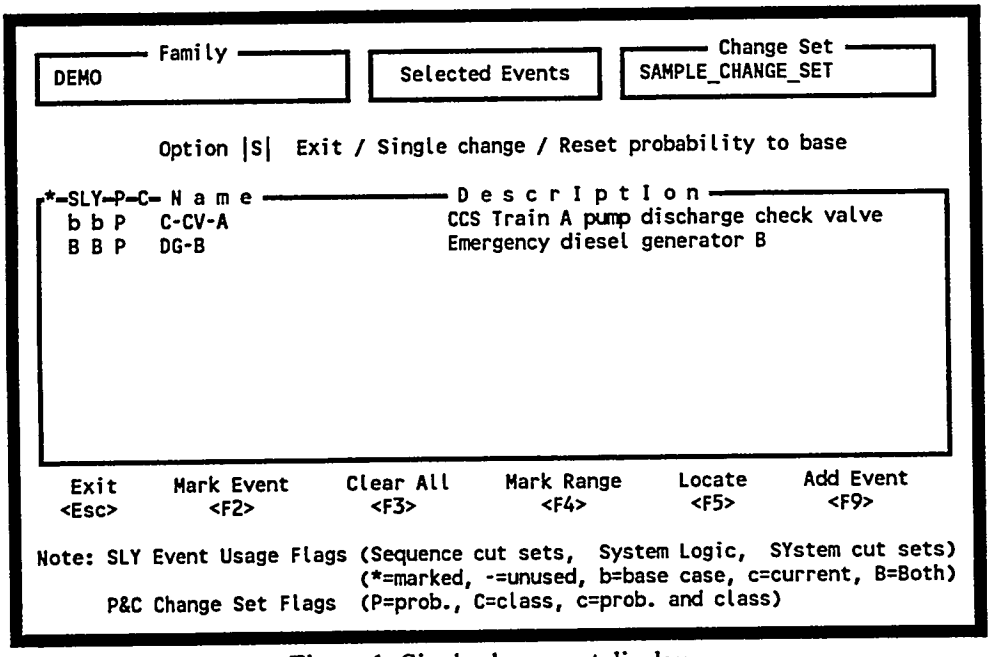

Figure 1. Single change set display.

User Defined Reports

A new feature added to this version of SAPHIRE is the custom report feature. This feature allow the users to define and store their own custom reports of information in the SAPHIRE data base. The user is presented with a "Custom" option in all the report areas. This option allows the user to edit or define a custom report. A sample custom basic event report editing screen is shown in Figure 2. The user can add

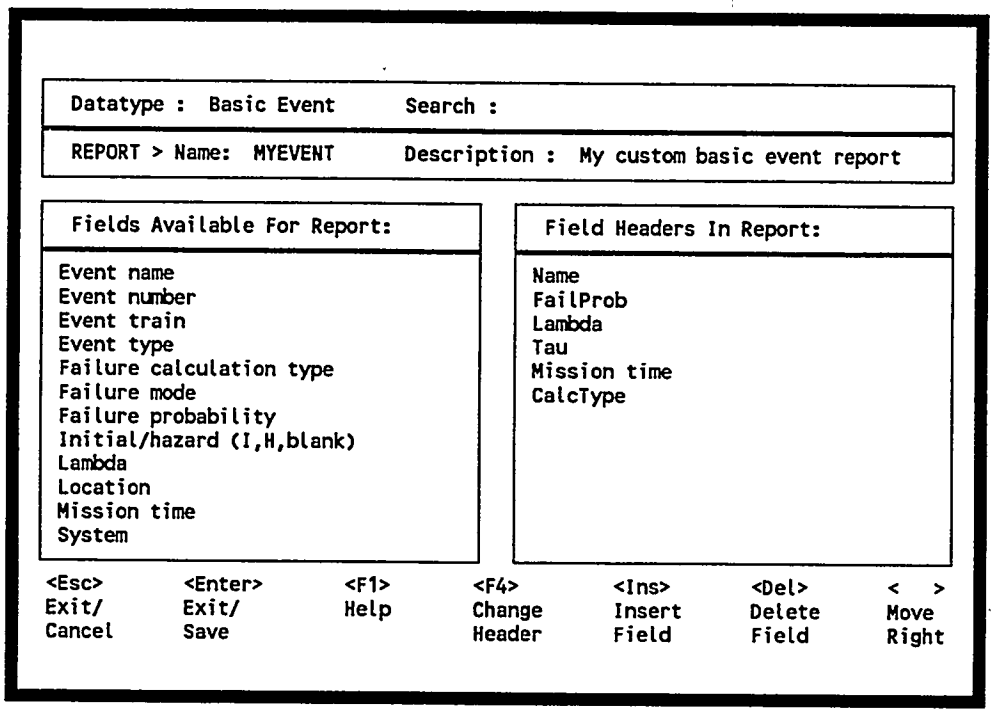

Figure 2. Sample custom report editing.

or remove fields in the data base to the custom report. Once the report is defined, the user can generate the report. The menu showing the available custom reports is shown in Figure 3. The report is then available for review through a powerful report viewer. This viewer allows the user to scroll up down, left, or right, viewing the information in the report. If desired, the user can send the report to a printer or to a file for later printing. Once a report is defined, it is stored with the data base until the user deletes it. This allows the user to build a library of often used reports.

Multi-Variable Importance Measures

The multi-variable importance option allows the user to calculate importance measures on a group

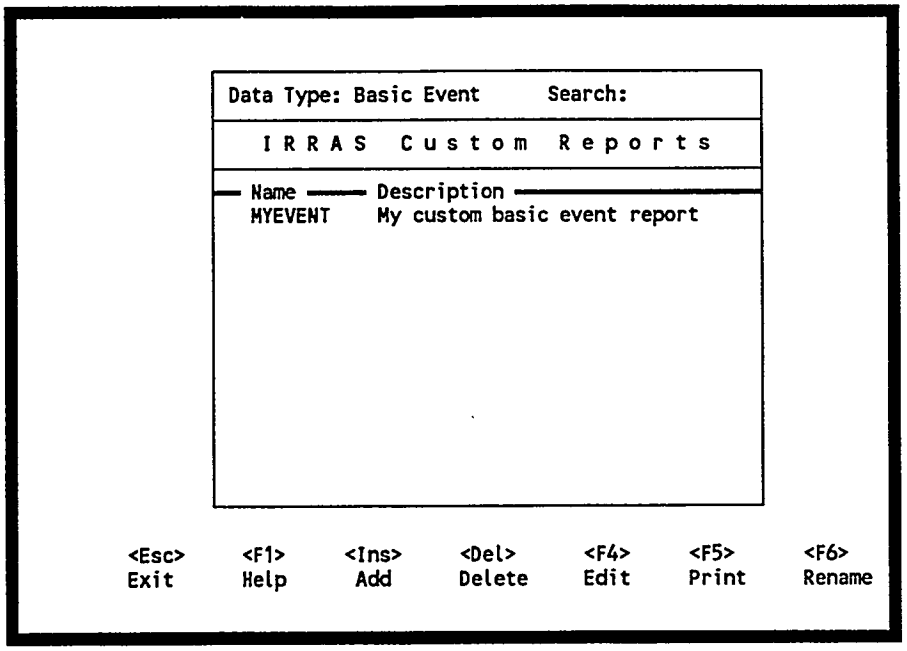

Figure 3. Custom report menu.

of basic events as if they were one event. If this option is selected, the user is presented with a list of all the basic events in the data base. From this list, the user selects a group of events that are to be treated as one event in the importance measures calculations. This selection list is shown in Figure 4. SAPHIRE then computes the importance measures specified by the user and treats all occurrences of the selected events as

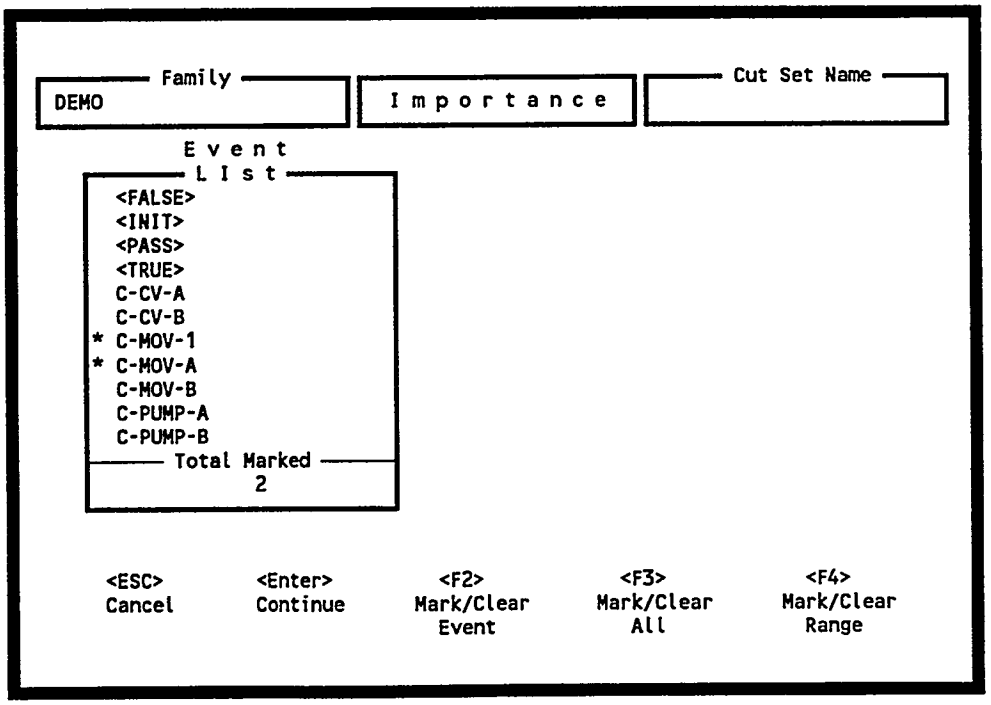

Figure 4. Multi-variable event select menu.

one event. The importance measures are then displayed showing the various contributions of each basic event. The multi-variable importance measure display is shown in Figure 5. The multi-variable importance measure is shown as a combined event with the label "Multi-Variable". This feature can be used to determine the importance of a group of events to a system, sequence, group of sequences, or to the family.

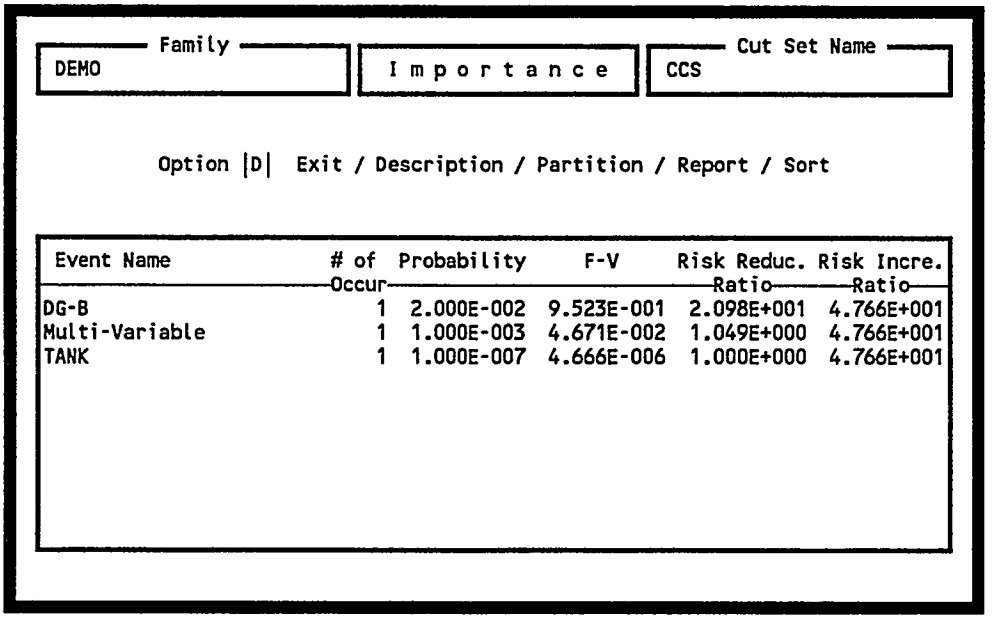

Figure 5. Multi-variable importance display.

Improved Cut Set Generation

The cut set generation algorithm in SAPHIRE continues to be improved in many ways. The performance of the fault tree solution algorithm has been improved by the incorporation of a hash technique to store and identify gates as the fault tree is loaded. The time it previously took to load and merge a fault tree from the data base has been reduced to an insignificant number as compared to the fault tree solution phase. The size restriction on the number of gates allowed in a fault tree has also been removed by this change.

The "N/M" gate type specification has been modified to allow the user to define a 2 digit number for each part of the gate. Hence, it is possible for the user to define a gate type of "10/99". In practice, the user should be aware of the potentially numerous cut sets resulting from large n/m gate definitions. In conjunction with the increase in n/m gate definition sizes, the software has been modified to expand the n/m gates during the cut set generation phase of the processing rather than during the fault tree loading phase. This allows n/m gates to be considered in independent subtree analysis and reduces the time it takes to solve trees with n/m gates by a significant amount.

The fault tree algorithm has also been modified to detect more inconsistencies in the user logic

definition. Previously, the user could define two gates differently in transfer trees and the code would not detect these differences. This version of SAPHIRE will detect these difference and force the user to resolve the inconsistency, resulting in fewer errors.

Support for Level 2 Analyses

The SAPHIRE code has been enhanced with new features to allow the user to perform many of the functions necessary to extend the application of the code to Level 2 analyses. Some of these enhancements will be discussed in this section. Previously, SAPHIRE allowed the user to generate the accident sequence cut sets. These cut sets could then be assigned to plant damage states using the end state partitioning capabilities. Once assigned to end states, these cut sets could be "Gathered" into end states or plant damage states. At this point the user would manually extract the values obtained for the end states and transfer them to a Level 2 analysis code. SAPHIRE can now take the end state results and transfer them automatically to a Level 2 event tree as the initiating event.

This is done by defining a basic event for each end state and assigning the basic event the new calculation type "E". This calculation type finds an end state in the data base with the same name as the basic event and uses the min cut upper bound of that end state as the probability value for the basic event. This event should also be set as an initiating event, since the next step is to create a level 2 event tree that uses the end state as the initiating event. The level 2 event tree can then be developed and sequences generated for it. These new sequences can then be partitioned into release categories using the same end state partitioning capabilities. The new release category end states can then be processed similar to the plant damage states and passed to a consequence event tree to further catagorize and quantify the output. Of course, this process can be repeated as often as necessary to attain the desired results.

The process described above is simple; however, if many end state are involved, then the work required to generate all the end state events and event trees could be quite time consuming. As a result, SAPHIRE has features built in to automate this process. Using a command in the partitioning editor, the user can tell SAPHIRE to automatically generate the basic event, the end state, the event tree. These data items will all have the same name and the user can transfer from the automatically generated event tree to the desired Level 2 event tree. This feature also allows the analyst to use the same Level 2 event tree to handle multiple plant damage states. With the features described here, the SAPHIRE code can be applied to Level 2 analyses in a very simple way using concepts already familiar to the analyst.

In addition to these direct improvements to support Level 2 analyses, several changes have been made to SAPHIRE to allow the Level 2 analyst more flexibility in the event tree and partition rules. For instance, the event tree rules have been changed to allow the analyst to branch on character positions within the event tree name. Since the Level 2 event tree initiating event name is the same as the Level 1 plant damage state name, the analyst can use the initiating event name character testing feature to check on conditions in Level 1 before branching in the Level 2 event tree. A more detailed discussion of these features will be given in the event tree and partition rule improvement sections of this paper.

Event Tree Rule Improvements

The event tree linkage rules have been enhanced in SAPHIRE to provide more flexibility and power. The event tree rules are used to determine the top substitutions to be made for a particular sequence. These

rules are quite powerful and easy to use. In the new version of SAPHIRE, the rules have been enhanced to allow the analyst to test on the characters in the initiating event name. The user can indicate the entire initiating event name or use wild card characters to indicate "don't care" character positions. This feature was provided to support the needs of Level 2 analyses, however, it can be used for Level 1 work also.

Another feature added to the event tree rules is the ability to set the end state and default flag set for a sequence . The user can do this by testing the various conditions of interest, then assigning the end state or flag set according to this condition. A sample example of this feature is as follows:

```
if (condition) then
   Top = EndState(name);
   Top = Flag(name);
endif;
```

The user must specify the "Top" where the substitution for the end state or flag set will be tested. If the user desires to have the condition tested for every sequence then "Top" can be replaced with the base event tree name. SAPHIRE only tests the condition when checking for a replacement for a top event in the event tree. In this case, the top does not really get replaced. The end state or flag set is assigned the value associated with the name in parenthesis. The user must have defined the information in the flag set name prior to generating the sequence logic that uses this flag set. This feature is useful for assigning the default flag set for a sequence if the user has a "known" limited list of possible flag sets that are to be used. If the list is not limited, or the combination of events in the flag set are not obtainable prior to sequence logic generation, then another new feature in SAPHIRE can be used.

This new feature allows the user to dynamically define the information in a flag set, create the flag set, and assign the flag set to a sequence. To access this feature, the analyst must use the True, False, and Ignore keywords. An example of the use of these keywords is as follows:

```
if (condition) then
   Top = True(Event1, Event2, ...);
   Top = False(Event1, Event2, ...);
   Top = Ignore(Event1, Event2, ...);
endif;
```

Again, the user must specify the "Top" where the substitution condition is to be tested, then include the list of events that are to be set to either True, False, or Ignore, given a true condition. If the user desires to have the condition tested for every sequence then "Top" can be replaced with the base event tree name. The user can specify multiple occurrences of the keywords given different conditions. SAPHIRE will keep track of all the various settings of events in the rules for a sequence. Before the sequence is created, SAPHIRE will check to see if a dynamically generated flag set containing the specified list of event settings already exists. If it does, then SAPHIRE uses the previously generated flag set. If one does not exist with the required event settings, then SAPHIRE creates one and assigns it to the default flag set for the sequence. When SAPHIRE generates the cut sets for the sequence, it will first set the events in the default flag set for this sequence to their indicated values then solve the sequence. This allows the analyst to maintain a single version of a system top and prune it according to the event tree logic rather than maintain multiple versions of the same system top.

Another feature included in the event tree rule editor is the ability to test on substituted system tops

in the logic for a sequence. The user can enter a condition like the following:

```
if system(name) then
  |some top substitutions
endif;
```

The condition test will check to see if a system with the given name appears in the current sequence logic. If it does, then the condition is true; otherwise, it is false.

Finally, SAPHIRE has been modified to remove the case sensitivity in the rule editor and compiler. Previously, some keywords were lowercase and names were uppercase. This resulted in a lot of typing errors and confusion. As a result, a changes was made to ignore the case of the rules entered in SAPHIRE. The case is maintained the way the user inputs it, but it is all converted to uppercase for compiling.

End State Partition Improvements

The end state partition option allows the user to assign end states to accident sequence cut sets on a cut set by cut set basis. The user inputs rules that can test on various conditions in the cut set to determine the end state to assign to the cut set. In the new version of SAPHIRE, the user can test on the characters in the name of the initiating event. This test can be on the entire name or on part of the name. Comparing on part of the name is accomplished using "wild cards". This feature is used primarily in the Level 2 analysis to allow the user to check the conditions present in the Level 1 analysis for this cut set before assigning a Level 2 end state name or character attribute. The initiating event name used in the Level 2 event tree is the end state created in Level 1.

Another new feature provided in the end state partitioning is the ability to set all cut sets in a sequence to a specified end state. Normally, each cut set in a sequence is checked to determine the end state to assign. If the user is not checking on events in the cut set, and desires that all cut sets in a sequence be assigned the same end state, then this feature can be used. An example using this feature is as follows:

```
If (condition) then
  GlobalPartition = "End-State-Name";
endif;
```

When SAPHIRE processes the "GlobalPartition" keyword during the assignment of an end state, it sets a flag that causes all the cut sets in the current sequence to be assigned to the end state generated for the first cut set. This significantly reduces the time required to process large numbers of cut sets and compare the rule conditions.

The last new feature added to the end state partitioning module is to support the Level 2 users. To properly understand the application of this feature the user must be aware of the way SAPHIRE implements Level 2 analysis. Typically, at the end of a Level 1 analysis, the accident sequence cut sets are partitioned into plant damage states. These plant damage states are then gathered into end states and quantified. SAPHIRE allows this end state result to be further processed by using it as the initiating event for a Level 2 event tree. In order to do this, the user must create a basic event with the same name as the end state and having a calculation type of "E". This causes SAPHIRE to use the min cut upper bound for the end state as the value for the end state basic event. A Level 2 event tree must then be created with this basic event as the

initiating event. Since many of the end states are typically processed using the same Level 2 event tree, a single event tree is usually created and each end state event tree is transferred to this base event tree. If the user has a large number of Level 1 plant damage states, then the process of creating all these intermediate event trees could be time consuming. This is where the new feature comes in. The user can specify in the end state partitioning rules for the Level 1 event tree, that the process described above be automatically executed for the user. This is done by using the following option:

```
If(condition) then
  Transfer = Event Tree Name;
endif;
```

The keyword "Transfer" causes SAPHIRE to automatically create the basic event, the end state, and the event tree. The event tree has the end state basic event as its initiating event and transfers to the specified event tree. This feature significantly reduces the time required to link the Level 1 results to the Level 2 analyses. This same process can be used to link the Level 2 results to another event tree for further processing.

Windows Version

This release of SAPHIRE will include a Windows version of the software. The main menu of the Windows version is shown in Figure 6. This version is a true 32-bit Graphical User Interface (GUI)

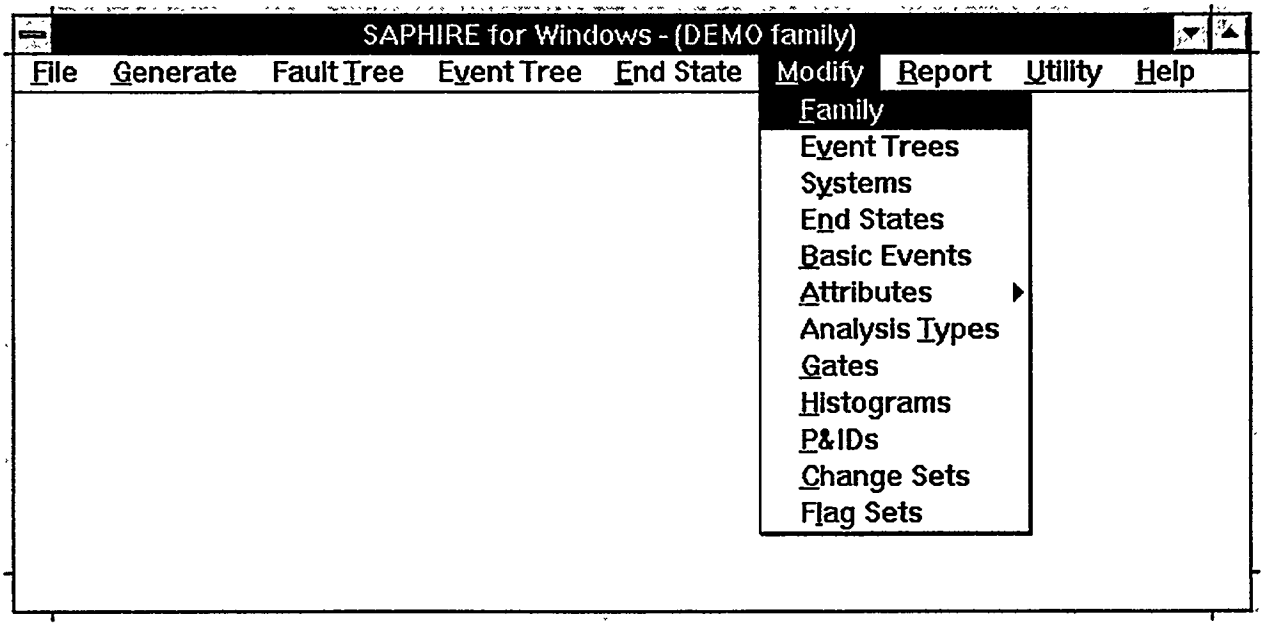

Figure 6. SAPHIRE Windows main menu.

implementation of the SAPHIRE system. It is Win32s compatible and will run under Windows 3.1, Windows 95, and Windows NT. Since the software uses a 32-bit architecture, it performs best under Windows 95 or Windows NT. Windows NT is the recommended operating system. The initial release will be similar to the DOS 32-bit version as far as menus and general features are concerned. The system cut set generation menu is displayed in Figure 7. This display demonstrates the similarity of the Windows version of SAPHIRE to the DOS version. As enhancements are made, changes will occur that streamline and optimize the interface for Windows. The design decisions that were made to allow the software to run on the 640k memory limits

of DOS will be reviewed, and a more intuitive interface developed.

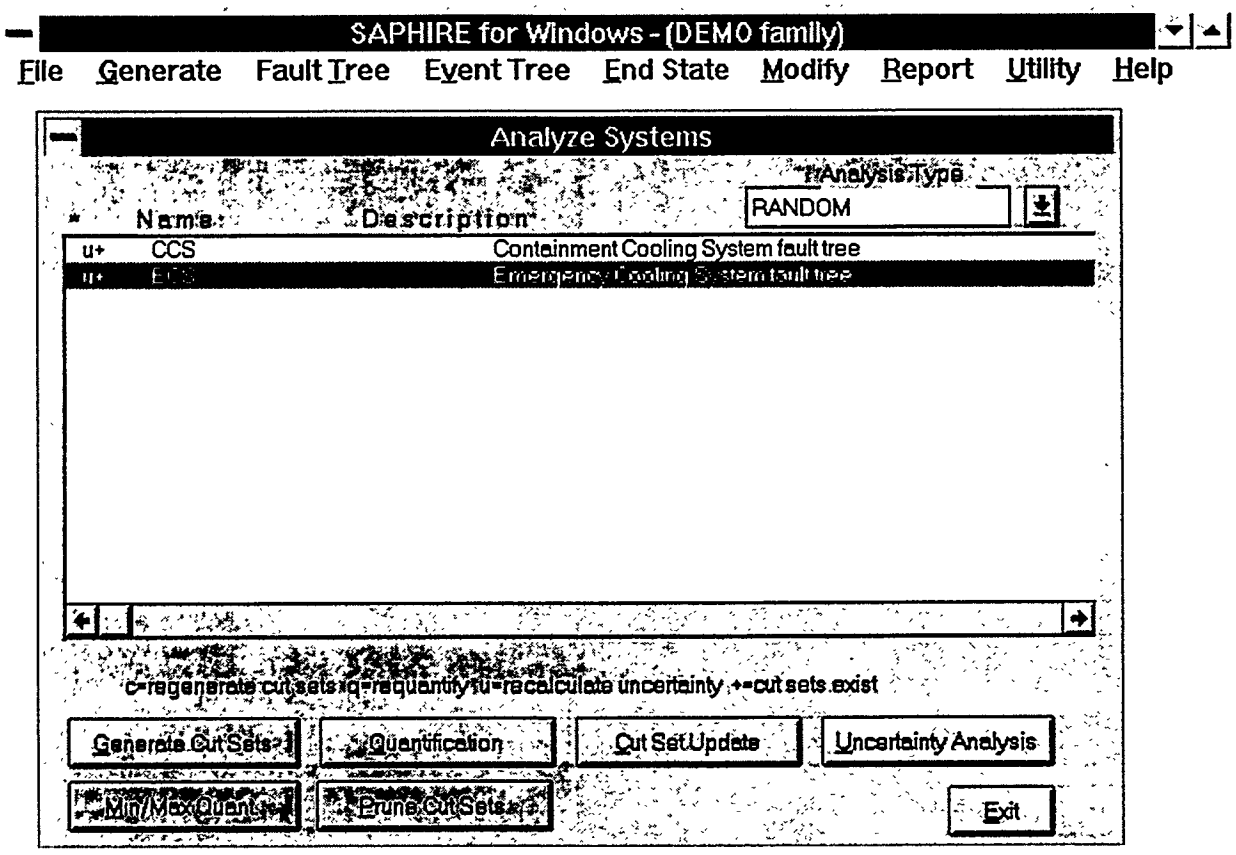

Figure 7. System Cut set generation menu.

The three graphical editors have also been converted to Windows and are included in this release. These three editors are shown in Figure 8, Figure 9, and Figure 10. The primary advantage of the Windows version of these editors is the ability to target any screen resolution and support any Windows-supported printer output devices. After the initial version, changes will be made to more completely integrate the editors with the relational data base. Previous versions of the software have required the graphical editors to be separate from the cut set generation and data base entry and modification routines. This is no longer required under Windows; hence, the software can be changed to allow the analyst to click on a basic event or gate in the graphical editors and edit the data base information associated with that entity. The user will also be able to invoke the cut set generation and display options from the graphical editors.

The underlying software for both the DOS and Windows versions are identical, hence, both versions will benefit from the extensive testing that has been performed on the SAPHIRE system and have 100% data base compatibility. The user can run a process using the DOS version and switch to the Windows version with no change to the data base.

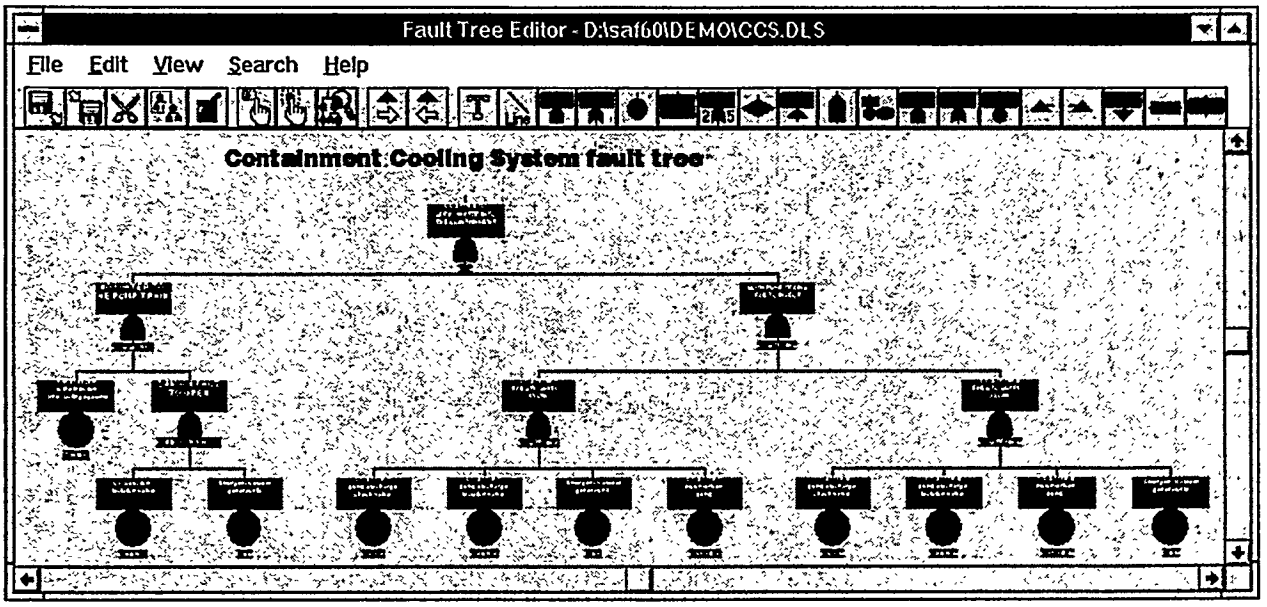

Figure 8. Fault tree editor.

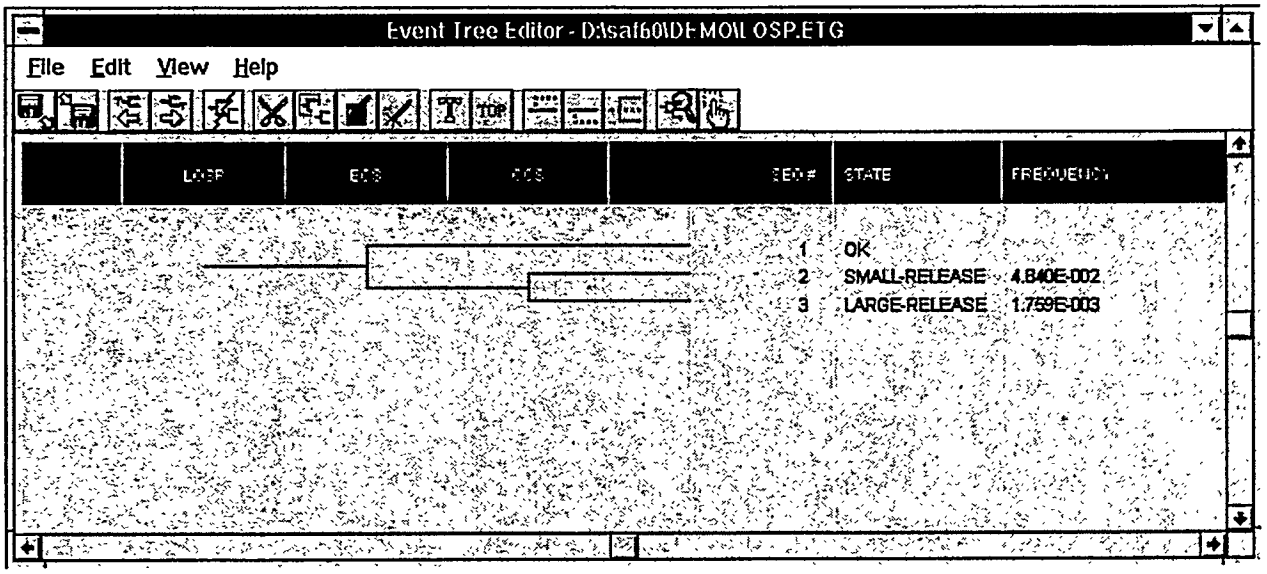

Figure 9. Event tree editor.

The software is all 32-bit native windows code. This allows running applications that require large amounts of memory, since the entire 32 bit address space of the processor can be accessed. The code is also 15-20% faster than the 32-bit DOS version due to the elimination of the need to switch between real and protected processor modes to transfer information between disk and memory under DOS. This speed

enhancement is in addition to that gained by improving the algorithms.

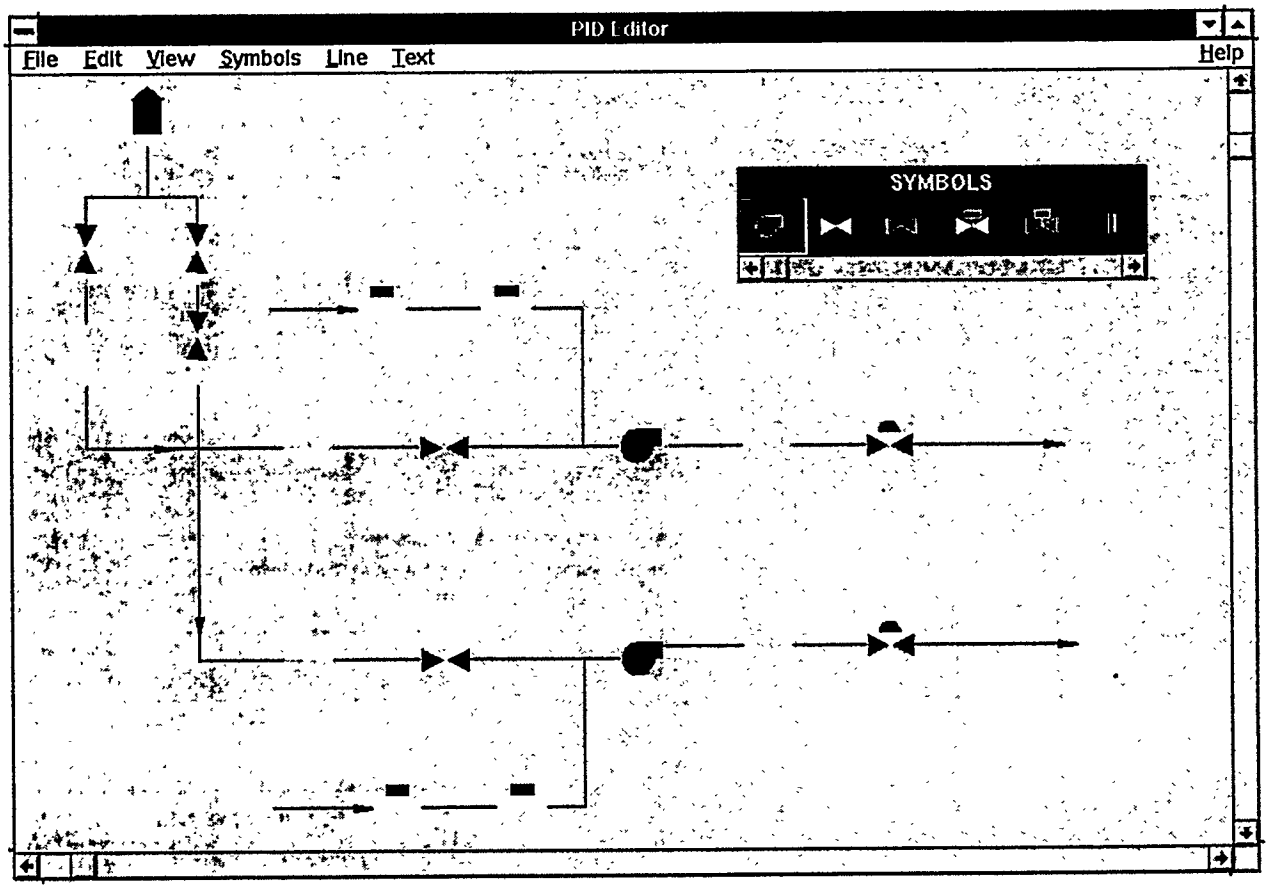

Figure 10. P&ID editor.

Graphical Evaluation Module

This release of SAPHIRE includes an application-specific module for performing Accident Sequence Precursor (ASP) and event assessment analyses. This module takes advantage of the underlying capabilities of SAPHIRE while automating many of the functions the user would have to perform to do an ASP analysis. This new module is called the Graphical Evaluation Module (GEM) and is a special application tool designed for evaluation of operational occurrences using the ASP program methods. This module has recently been documented as Vloume 6 of NUREG/CR-6116. The main GEM menu is shown in Figure 11. GEM provides the capability for an analyst to quickly and easily perform conditional core damage probability (CCDP) calculations. The analyst can then use the CCDP calculations to determine if the occurrence of an initiating event or a condition adversely impacts safety. It uses models and data developed in SAPHIRE specially for the ASP program. GEM requires more data than that normally provided in SAPHIRE to perform all the automated functions properly. The GEM module will operate on standard SAPHIRE data bases; however, some of the features built into the code for automatically detecting certain conditions and setting events to the appropriate value for this condition would not be available. Except for this feature, all functions available in GEM would be available to the non-ASP user.

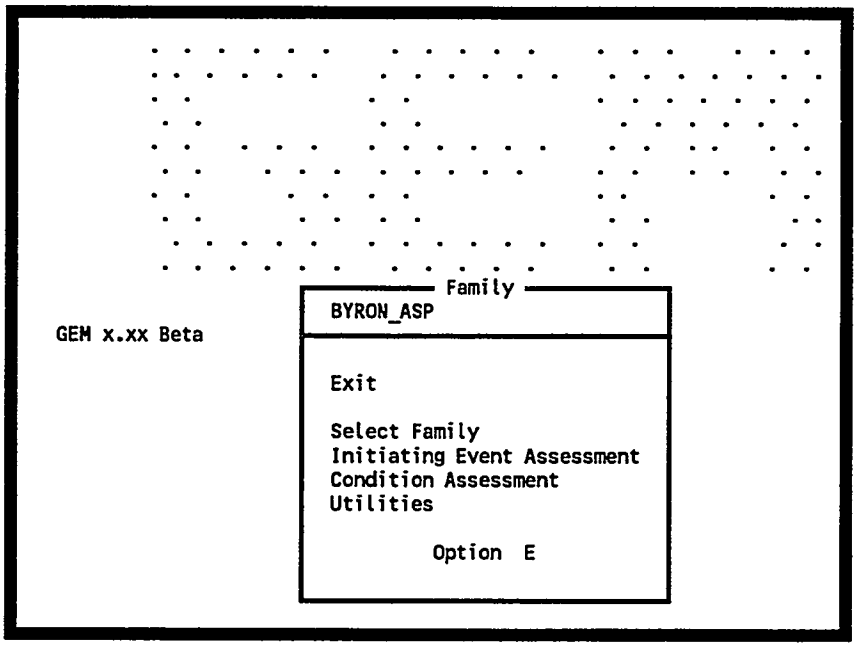

Figure 11. GEM main menu.

GEM simplifies the operational event analysis process and automates the construction of current-value input to the analysis software. You can modify the events in the models without changing the base-case values. GEM processes these events with IRRAS modules and algorithms. GEM automatically applies new recovery action failure probabilities depending on which initiating event you are analyzing. For conditions not involving an initiating event, GEM calculates a conditional core damage probability (CCDP) based on the modified basic event probabilities and the duration of the condition. The results pertaining to the CCDP are documented in various customized reports generated by the program.

Initiating Event Assessments

ASP models contain event trees that model the plant response to a selected set of initiating events. When a precursor to be analyzed involves one of these initiating events, an initiating event assessment is performed. The analyst enters GEM and after selecting the desired plant model, selects an initiating event assessment and gives it a name. This opens a work space for this particular initiating event assessment.

The analyst next selects the initiating event that occurred from the list provided. GEM will automatically set the selected initiating event's frequency to its pre-assigned, short-term, non-recovery probability (or 1.0 if recovery is deemed not possible) and will set all other initiating event frequencies to zero. This assumes that the actual precursor involves only the observed initiating event and all other initiators are not applicable. Furthermore, it is assumed that the probability of another initiating event occurring while the first initiating event is still in progress is small.

If the initiating event is a Loss Of Offsite Power (LOOP), GEM will display a list of the four different types of LOOP (plant-centered, grid-related, severe weather-related, and extremely severe weather-related) and the analyst must pick one. Each LOOP type has a different short-term, non-recovery probability.

Once the initiating event is selected, GEM displays a predefined change set unique to that initiating event. For all initiating events except LOOP, the change set consists only of the entire set of initiating events. The selected initiating event is in the change set because its frequency has been converted to a probability equal to its short-term, non-recovery value and the other initiating events are listed because their frequencies have been converted to a probability of zero.

For the LOOP initiating event, the change set again lists all the initiating events, but additionally, the change set includes a predefined list of electric power recovery basic events and the RCP seal LOCA basic event (for PWRs only). These are the basic events that must be changed when going from the nominal LOOP event in the base case model to a specific LOOP type for the event assessment. These basic events are automatically added to the change set and their values are automatically modified to predetermined values based on the plant characteristics, the timing required, and the type of LOOP.

The analyst can access any of the basic events listed in the change set if a need exists to make modifications. Other basic events can also be added to the change set list. This would be necessary to model any observed failures or degradations reported for the event being analyzed.

Once the change set list is complete and the desired changes are defined for the basic events, the analyst selects the PROCESS option. GEM automatically generates a current basic event data set according to the changes defined in the change set. GEM next determines which system fault trees have been impacted by the changes and identifies the event tree accident sequences that use those fault trees. The logic for those sequences are loaded into memory and GEM solves the logic for the new minimal cut sets. The minimal cut sets are quantified, the CCDP is calculated and the results are displayed. With the exception of the CCDP calculation, GEM processes the accident sequences in exactly the same manner as IRRAS. The result display for initiating event assessment is shown in Figure 12.

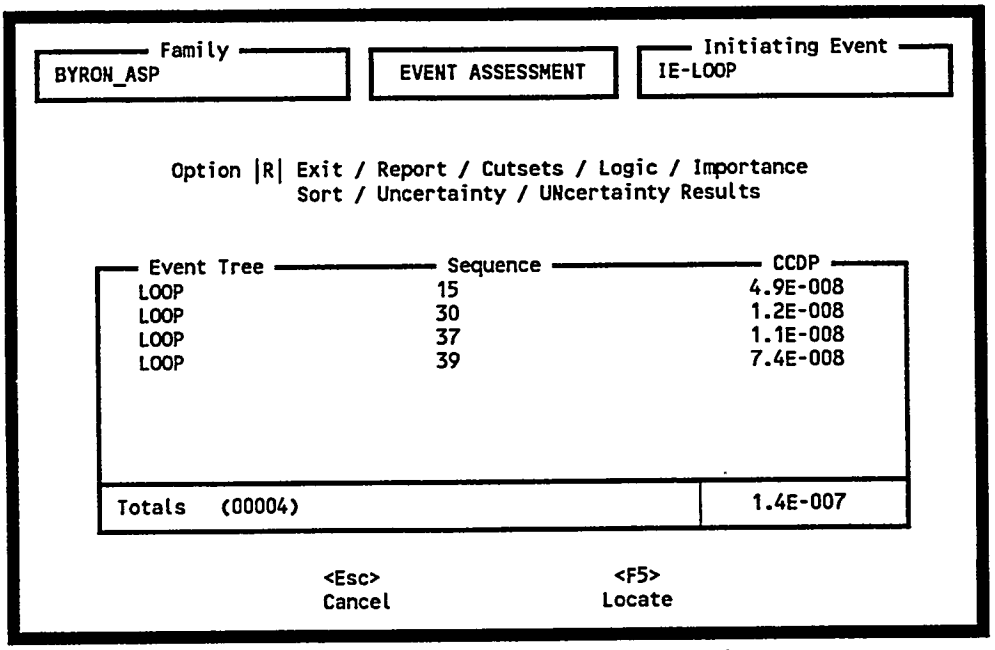

Figure 12. Initiating event assessment results.

Condition Assessments

When a precursor event does not involve the actual occurrence of an initiating event, but does indicate maintenance, failures, or degradation of equipment that would be required to mitigate the consequences of an initiating event, a condition assessment is performed. After entering GEM and selecting the desired ASP plant model, the analyst selects the condition assessment option and gives the assessment a name. This opens up a work space for this particular condition assessment. GEM then prompts the analyst for the duration of the conditions being analyzed. The duration is entered, expressed in hours.

GEM displays a blank change set and provides the ability to add events to the change set to model the observed failures and degradations reported for the event being analyzed.

Once the change set list is complete and the desired changes are defined for the basic events, the analyst selects the PROCESS option. GEM automatically generates a current basic event data set according to the changes defined in the change set. GEM next determines which system fault trees have been impacted by the changes and identifies the event tree accident sequences that use those fault trees. The logic for those sequences are loaded into memory, GEM solves the logic for the new minimal cut sets, and quantifies them. For the sequences that were not impacted by any of the changes, the base case results are copied over into the current case results. If you attempt to look at the current case cut sets for one of these sequences you will get the message, "No cut sets to process." The CCDP is calculated and the results are displayed. With the exception of the CCDP calculation, GEM processes the accident sequences in exactly the same manner as IRRAS.

The GEM module is a significant enhancement to the SAPHIRE package that encapsulates and minimizes the complexity of interacting with a full PRA using codes designed for the PRA analyst. This is done by focusing on the needs of a specific group of users and designing the interface to meet these specific needs. As a result, the code is easier to user and less error prone. The result display for a condition assessment is shown in Figure 13.

Family: BYRON_ASP

CONDITION ASSESSMENT

Option |R| Exit / Report / Cutsets / Logic / Importance
Duration / Sort / Uncertainty / UNcertainty Results

Event Duration (hours): 2.000E+001

Event Tree	Sequence	CCDP	CDP	Importance
LOOP	05	4.0E-006	8.8E-009	4.0E-006
LOOP	07	+0.0E+000	3.5E-011	-3.5E-011
LOOP	08	3.4E-006	1.4E-009	3.4E-006
LOOP	10	8.9E-007	1.9E-009	8.9E-007
LOOP	11	7.5E-007	3.2E-010	7.5E-007
LOOP	14	7.0E-006	1.9E-010	7.0E-006
LOOP	15	3.0E-005	2.2E-009	3.0E-005
LOOP	18	8.0E-007	2.1E-011	8.0E-007
Totals (00046)		1.3E-004	1.6E-007	1.3E-004

<Esc>Cancel <F5>Locate

Figure 13. Condition assessment results display.

Multiple Execution Capability

With the increased use of multi-tasking operating systems like Windows, it became desirable for the user of SAPHIRE to be able to open multiple data bases at the same time. Previous DOS-based versions of SAPHIRE did not consider this situation. If the user tried to execute a second copy of SAPHIRE, the data base would be flagged as needing rebuilding and errors would occur. As a result of this, SAPHIRE has been modified to allow the user to open multiple data bases at the same time. The user must change to subdirectory where the data base files reside and execute SAPHIRE from there. This is typically done by typing "..\I386" instead of the typical "I386". This assumes that the user is opening a data base off the installation directory where the I386.BAT file is located. SAPHIRE also checks before opening a data base and if the data base is currently being used by another copy of SAPHIRE, then an error message to this effect is displayed and the program terminates. This prevents the data base from being corrupted. This feature allows the user to simultaneously review the results of two different data bases at the same time, or to check the values in one SAPHIRE data base against another.

Cut Set Recovery

In version 5.0, the ability to apply rule-based cut set recovery was implemented. This version enhances the original version by adding the capability for the user to perform many cut set editing commands in the recovery rules. For instance, the user can add new cut sets, copy existing cut sets, or delete events from cut sets. The original implementation of the cut set recovery analysis only allowed the user to add a recovery event to an existing cut set. This powerful new feature provides the user with the ability to do much more extensive editing of the cut sets than was previously possible. An example of the new commands is as follows:

```
If (condition) then
   CopyRoot;                  | Copies the root cut set creating a new current cut set
   AddEvent = Event name;     | Adds the event to the current cut set
   DeleteEvent = Event name;  | Deletes the specified event from the current cut set
   NewCutset;                 | Creates a new empty current cut set
   DeleteRoot;                | Deletes the root cut set
   CopyCutset;                | Copies the current cut set and makes a new current cut set
endif;
```

Automated Data Base Upgrade

With the many changes to the data base for new version of SAPHIRE, it would be a substantial task for the user to convert the data from older versions. This task is made easier, however, by an automated version detection and upgrade facility build into the new version of SAPHIRE. This facility checks the selected data base to determine its version number. If the version number is not the same as the current operating version of the software, then the user is prompted to determine if an upgrade to the new version is desired. If the user chooses to continue, then SAPHIRE automatically converts all existing data to be compatible with the software. All new fields not already present in a data record are given default values and all other values are convert to the new format. This conversion may take a few minutes to complete, after which the data will be available for immediate access. This process effectively eliminates version upgrade problems for the user. Once converted, however, the user will be unable to use the new data with previous

versions of the software. One down side of the increase in the number of events, gates, systems, etc. that the user can store in a data base is that the size of a data base has essentially doubled. This means that the disk space required to store a data base will be twice that previously required in previous versions. The benefit gained by having unlimited storage of data base data was deemed to be worth the increased space requirements.

CONCLUSIONS

The new version of SAPHIRE continues to provide an integrated set of tools for the PRA analyst. This version promises to be even more powerful and easier to user than pervious versions. It eliminates many of the problem size restrictions in previous versions while improving the performance. The addition of many new features and the enhancement support for Level 2 analyses allows SAPHIRE to extend its capabilities into many important areas for risk assessments. The addition of the Windows version SAPHIRE keeps it current with the state-of-the-art in computer technology and operating systems. These changes help SAPHIRE continue to lead the way in user friendly, integrated, risk assessment software.

CORE DAMAGE FREQUENCY PERSPECTIVES FOR BWR 3/4 AND WESTINGHOUSE 4-LOOP PLANTS BASED ON IPE RESULTS

Susan Dingman[1], Jeff LaChance[2], Allen Camp[1], Mary Drouin[3]

[1] Sandia National Laboratories
[2] Science Applications International, Corporation
[3] U.S. Nuclear Regulatory Commission

This paper discusses the core damage frequency (CDF) insights gained by analyzing the results of the Individual Plant Examinations (IPEs) for two groups of plants: boiling water reactor (BWR) 3/4 plants with Reactor Core Isolation Cooling systems, and Westinghouse 4-loop plants. Wide variability was observed for the plant CDFs and for the CDFs of the contributing accident classes. On average, transients with loss of injection, station blackout sequences, and transients with loss of decay heat removal are important contributors for the BWR 3/4 plants, while transients, station blackout sequences, and loss-of-coolant accidents are important for the Westinghouse 4-loop plants. The key factors that contribute to the variability in the results are discussed. The results are often driven by plant-specific design and operational characteristics, but differences in modeling approaches are also important for some accident classes.

The U.S. Nuclear Regulatory Commission (NRC) issued Generic Letter 88-20 in November 1988 requesting that all licensees perform an Individual Plant Examination (IPE) to identify any plant-specific vulnerabilities to severe accidents, and to report the results to the Commission. The scope of the IPE effort includes examination of internal events, including those initiated by internal flooding, occurring at full power. A memorandum from the Executive Director of Operations to the Office of Nuclear Regulatory Research in NRC on May 12, 1993 recommended that the NRC document the significant safety insights resulting from this program and show how the safety of reactors has been improved by the IPE initiative.

The IPE Insights Program was initiated to document significant safety insights, based on the IPEs, for the different reactor and containment types and plant designs. The major insights to be gained through this program include:

- How has the IPE program impacted reactor safety?
  - How many of the plants have identified vulnerabilities or other safety issues, and what safety enhancements have been made as a result?
  - How have the improvements impacted the safety of plants?
  - Are there any "generic" improvements that have significantly affected the plant core damage frequencies (CDFs) and containment performance, or are the plant improvements plant specific?

- What is driving the CDF and containment performance?
  - What are the important design and operational features that affect the CDF and containment performance?
  - How important is the role of the plant operators?
  - How much influence do the IPE methodology and assumptions have on the results?

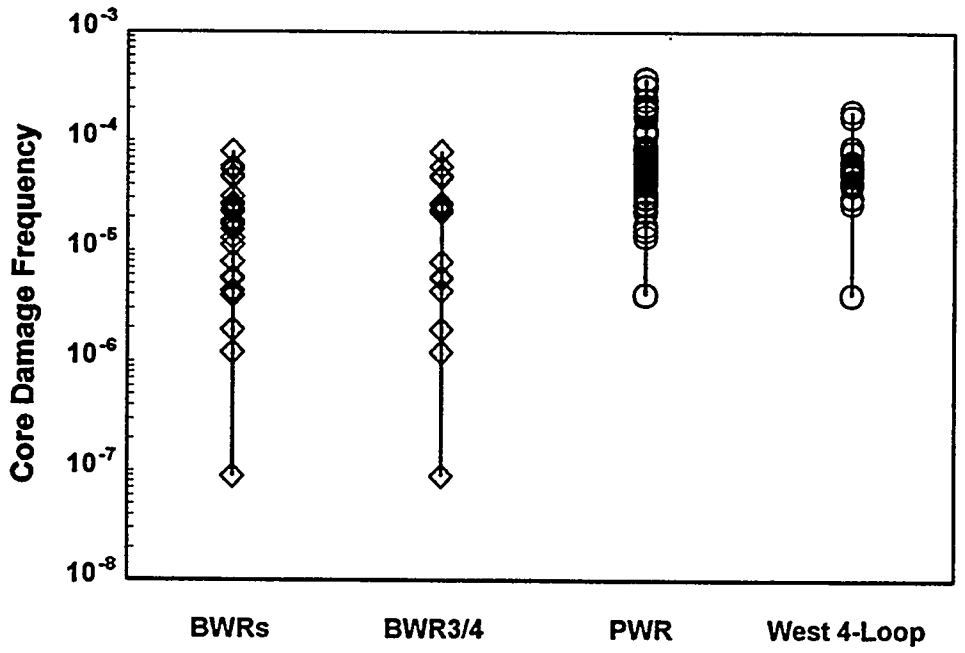

Figure 1. CDFs Reported in IPEs for Various Plant Groups

To gain these insights, the IPEs were examined to determine what the collective IPE results imply about the safety of U.S. nuclear power plants. Variations and commonalities among plant results were studied to determine which factors were most influential on the results (CDF and containment performance). In addition, the improvements that have been made at the plants, and the impact of these improvements on the plant CDF and containment performance were examined. This paper will focus on the insights regarding CDF results; other papers at this meeting discuss the impact of plant improvements and insights regarding containment performance.

This paper presents insights from the IPEs regarding CDF results for two plant groups: boiling water reactors (BWRs) 3 and 4 with Reactor Core Isolation Cooling (RCIC) systems[1] and Westinghouse 4-loop plants. The plant CDFs reported in the IPE submittals for the individual plants in these two plant groups are shown in Figure 1 along with the plant CDFs for the entire BWR group and the entire pressurized water reactor (PWR) group. On average, the BWR CDFs fall below the PWR CDFs, but there is some overlap between the two plant groups. There is a wide spread in the reported CDFs for both the BWR 3/4 and Westinghouse 4-loop plant groups. In fact, the range for these two groups spans nearly the full range for the BWR and PWR plants collectively. Both plant groups contain a single low outlier plant with a CDF about an order of magnitude below the CDF for the plant with the next highest CDF. The reasons for the variability in CDFs among the plants are discussed in the following two sections.

[1] Some BWR 3 plants have isolation condensers instead of RCIC; they are not considered in this plant group.

BWR 3/4 Perspectives

Twenty-one units (15 IPE submittals) make up the BWR 3/4 group of plants with RCIC. All of the units are housed in Mark I containments except for Limerick 1 and 2 and Susquehanna 1 and 2, which are in Mark II containments.

Figure 2 shows the contribution to plant CDF from the following accident classes: station blackout (SBO), anticipated transient without scram (ATWS), transients with loss of injection (T), transients with failure of decay heat removal (DHR), loss-of-coolant accidents (LOCA), and internal floods (FLD). The importance of specific accident classes to CDF varied significantly from plant to plant; however, the following accident classes were important for many of these plants:

- Station blackout - the loss of all offsite and onsite AC power, and
- Transients with loss of coolant injection.

In general terms, these accident classes are important contributors to CDF since they involve initiating events and/or subsequent system failures that defeat the redundancy in systems available to mitigate potential accidents. Lesser contributions were identified for the group on average from accident classes involving transients with loss of decay heat removal, ATWS, LOCAs, and internal floods. However, some IPEs did report important contributions from these accident classes. Although interfacing systems LOCAs are potentially important risk contributors since the containment is bypassed, none of the plants reported significant CDFs or radionuclide releases from interfacing system LOCAs since this accident class involves low frequency initiating events. The variation in the reported IPE results is attributed to many factors including plant-specific design features, modeling assumptions, and variation in data (including the probability of operator errors). These factors are discussed below for each accident class.

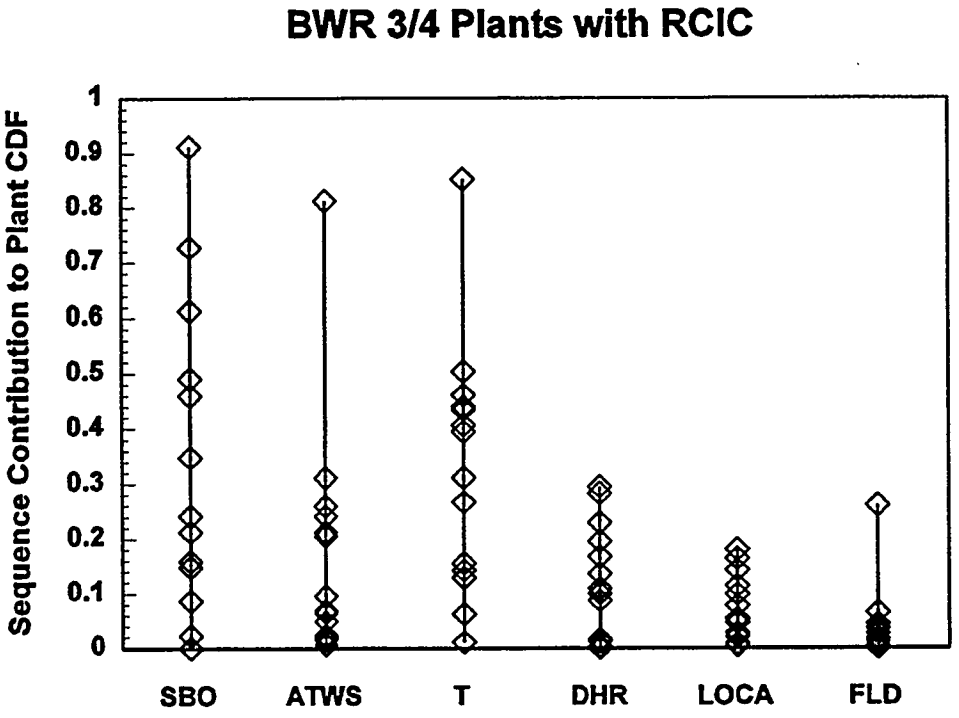

Figure 2. Accident Class CDFs for BWR 3/4 Plants with RCIC

Station blackout accidents are important contributors to CDF for most of the plants in this group. Station blackout accidents involve an initial loss of offsite power followed by failure of the emergency onsite AC power sources. The failure of AC power sources results in failure of multiple mitigating systems, leaving only steam-driven systems such as RCIC and the High Pressure Coolant Injection (HPCI) system available for coolant injection.

Generally, plant design and operational features had a larger impact on the station blackout CDF than did modeling characteristics, but no single factor dominated. Usually, combinations of contributors were important, and those combinations varied from plant to plant. With that in mind, the most influential plant features and modeling characteristics are identified and discussed below.

- Number of emergency AC power sources - The number of emergency diesel generators (usually from two to four per unit) directly affects the reliability of the emergency AC power system. Generally, the higher the number of emergency diesel generators, the lower the station blackout contribution. However, plant-specific features or modeling assumptions (such as the diesel generator cooling water system alignment at Hope Creek) can reduce the diesel generator reliability or, alternatively, increase the reliability (such as occurred in the Susquehanna IPE due to the elimination of common cause failures). The availability of additional and diverse AC power sources (such as the gas turbine generator at Fermi 2) or a separate offsite power source in addition to the normal grid connection (such as exists at Pilgrim and Vermont Yankee) reduced the station blackout contributions at those units.

- Battery depletion time - When AC power is lost, the only injection systems available are turbine driven systems (HPCI and RCIC) or, for some plants, diesel-driven firewater. Battery power is needed to provide control for HPCI and RCIC, or to maintain the automatic depressurization system (ADS) valves open so that the low-pressure firewater system can be used. Thus, when the batteries are depleted, all cooling is lost and core damage follows. Battery depletion times range from 2 hours at Brunswick 1 and 2 to 14 hours for Pilgrim, with the longer times reflecting plants making extensive use of load shedding. The contribution from station blackout accidents is generally lower for units with longer battery depletion times since the probability of recovering AC power and AC-powered mitigating systems increases with time. In fact, units with battery depletion times greater than 4 hours had significantly lower station blackout CDFs than plants with 4-hour or shorter battery depletion times.

- Use of diesel-driven firewater - Some units use diesel-driven firewater systems as a diverse means of supplying coolant injection when HPCI and RCIC have failed. The vessel must be depressurized and maintained at low pressure in order for firewater to be used. Further, this nonstandard use of the firewater system requires that piping connections and power to certain valves be available, along with appropriate procedures. The ability and the time required to inject coolant water using the firewater system thus varies from unit to unit. The station blackout contribution for units with firewater injection capability generally was dominated by sequences with early failure of RCIC and HPCI and with insufficient time available to align firewater for injection.

Transients with loss of coolant injection are important contributors to the CDF for most plants in this group. This accident class is dominated by sequences involving loss of the relatively few high-pressure coolant injection systems (typically feedwater, HPCI, and RCIC), and failure to depressurize the vessel so that the multiple low-pressure coolant injection systems can be used. Transients with loss of high-pressure injection, successful vessel depressurization, and failure of low-pressure injection systems are of

lesser importance because of the significant redundancy in low-pressure injection systems. The most common transient initiating events are those that fail feedwater such as loss of offsite power, loss of feedwater, and main steam isolation valve (MSIV) closure. Loss of DC buses are also important initiating events at some plants because DC power is needed to provide control for HPCI and RCIC, and to maintain the ADS valves open so that the vessel can be depressurized.

For this group of accidents, there are two issues that are critical to the CDF. One issue involves plant-specific design characteristics while the other issue involves plant operating procedures and training along with modeling assumptions.

- Availability of alternate high-pressure injection systems - The availability of high-pressure injection systems in addition to feedwater, RCIC, and HPCI reduces the contribution of this class of accident. Several licensees (Brunswick, Cooper, and Susquehanna) used plant-specific calculations to show that the Control Rod Drive (CRD) hydraulic system in the enhanced flow mode can provide sufficient coolant injection immediately after a reactor scram to maintain core cooling. The Quad Cities IPE credited a unique safe shutdown injection system which helped reduce the importance of all loss of injection and loss of DHR sequences. Several units with motor-driven feedwater pumps (Monticello, Fermi, and Vermont Yankee) also calculated lower contributions since, unlike steam-driven feedwater pumps, these pumps can continue to operate during a transient with main steam isolation valve closure.

- Operator failure to depressurize - During the past few years, operating procedures have changed to direct the operators to inhibit ADS for most transients. If high-pressure injection then fails, the operators must recognize this condition and manually depressurize the reactor vessel to allow use of low-pressure systems. Operator error probabilities for failure to manually depressurize the vessel varied widely in the IPEs and significantly impacted the results. Whether this wide variability in the human error probabilities is due to plant-specific factors such as training or procedures or is due to some other factors is not clear.

Transients with loss of DHR are important for many of the BWR 3/4 plants. Loss of DHR transient sequences involve accidents where coolant injection succeeds, but containment heat removal fails. In this situation the suppression pool heats up, leading to containment pressurization, and if the containment is not vented, it will eventually fail. Coolant injection eventually fails, either as a result of a hot suppression pool, or the adverse conditions created in containment or the reactor building when the containment is vented or fails. These adverse conditions include loss of net positive suction head in the suppression pool or steam in the reactor building.

The key factors affecting the CDF from loss of DHR sequences involve plant-specific design and operating conditions as well as the assumptions made in the IPEs. The modeling issues are important to the results and represent an important area of uncertainty. The key factors are identified and discussed below:

- Ability of emergency core cooling system (ECCS) pumps to continue operating under severe containment conditions - ECCS pumps can fail for a variety of reasons during these accidents. Net positive suction head (NPSH) requirements may not be met if the containment fails or is vented. The pumps may fail due to high suppression pool temperature or due to steam in the reactor building. The IPEs vary significantly in their assessments of pump operation under these conditions. Some of these differences are due to actual variations in pump design or venting procedures; however, significant uncertainty remains in this area.

- Availability of alternate injection sources - Many of these plants have injection sources available that are located outside the containment and reactor building, and thus are not subject to the potential harsh environments noted above. Examples of such systems are CRD and condensate. Plants with such systems have lower CDFs, and these differences are based on actual plant design differences as opposed to modeling assumptions.

- Treatment of venting - Most of the Mark I containments are now equipped with hardened vents to prevent containment failure and harsh environments in the reactor building. Use of these vents can reduce the CDF for this accident class. However, all plants did not model these vents in their IPEs, and some IPEs accounted for loss of NPSH upon venting. Therefore, there are significant differences from plant to plant based on their treatment of venting and its effects.

ATWS sequences are significant contributors for some plants in the BWR 3/4 group. ATWS sequences involve a transient, followed by failure to shutdown the nuclear chain reaction by inserting the control rods. Power generation continues at levels far in excess of normal decay heat. An ATWS sequence can be mitigated by boron injection using the Standby Liquid Control (SLC) system, control of coolant injection, and heat removal.

The ATWS results were impacted more by modeling assumptions than by plant-specific design features. The key factors varied from plant to plant and are identified and discussed below:

- Failure of boron injection - The SLC system provides boron injection that can shut down the nuclear reaction. An important failure mode of the SLC reported in the IPEs was the failure to initiate the system. The probabilities for operator failure to initiate SLC vary by orders of magnitude among the IPEs. Some of these variations are due to different assumptions about timing, but uncertainties remain. Monticello and Fitzpatrick also credited alternate means of injecting boron using systems such as the CRD system. Generally plants with low operator error probabilities for initiating SLC and with alternate means of injecting boron had lower ATWS contributions from loss of SLC sequences.

- Power reduction using level control - Some licensees (e.g., Hatch 1 and 2) assumed that if boron injection failed, controlling the water level in the core would reduce power to within the turbine bypass capacity of the plant and allow for alternate means of placing the plant in cold shutdown. However, most licensees assumed that level control could only be successful in conjunction with the use of SLC. The ATWS contribution from loss of boron injection sequences was reduced for licensees that credited level control by itself as a means of reducing core power to a stable level.

- Operator failure to inhibit ADS and control coolant injection - If the operator fails to take action to manually inhibit ADS, the HPCI will be lost and low-pressure systems will inject at a high flow rate that is not easily controlled, possibly leading to boron flushing and to a large power surge that repressurizes the system and causes low-pressure injection to cease. Repeated cycles of pressurization may eventually lead to failure of either the reactor coolant system boundary or the low-pressure injection system. In the IPEs the probabilities for operator failure to inhibit ADS vary by several orders of magnitude. This action could be the object of further study, as the reasons for the wide variation are not obvious from the submittals. Some licensees, including Pilgrim and Brunswick, assumed that failure to inhibit ADS would not lead to core damage if the operator controlled low-pressure coolant injection flow. These plants generally had lower ATWS contributions from sequences involving failure to inhibit ADS.

LOCAs are not dominant contributors to most BWR 3/4 plants. Because LOCAs are low-frequency events and since BWR 3/4 plants have a variety of diverse injection sources to mitigate a LOCA, LOCAs are not usually important to either the core damage frequency or risk for these plants. The amount of credit given for alternate injection systems was the major parameter accounting for the variability in the LOCA results. For example, Susquehanna reported a low contribution from small-break LOCAs partially due to the credit given for enhanced CRD flow for mitigating this size LOCA. Other plants such as Fitzpatrick credited limited-volume systems such as condensate for partially mitigating a large LOCA. Most licensees assumed that vessel depressurization was needed for medium LOCAs (including stuck-open relief valves) in those cases where HPCI failed. This assumption contributed to medium LOCAs being the dominant LOCA core damage contributor at several plants.

Internal flooding is not important for most BWR 3/4 plants. Internal flooding events involve rupture of water lines or operator errors that result in a release of water that can directly fail required mitigating systems (e.g., through loss of cooling) and/or fail other mitigating systems due to submergence or spraying of required components. The most important factor in determining the importance of flooding is the plant layout. Separation of mitigating system components and compartmentalization reduces the impact of internal flood initiators. Internal flooding events were not dominant at most plants because no internal flood initiator was identified (due to the above factors) that would completely fail all systems required to mitigate a flood-induced transient without additional random failures. For a few plants, important internal flooding sequences were identified, generally involving service water system breaks that impacted equipment through both loss of cooling and through flood impacts on other mitigating systems.

Westinghouse 4-Loop Perspectives

Thirty-two plant units (20 IPE submittals) make up the Westinghouse 4-loop plant group. Twenty-two of the plant units are in large dry containments, one is in a subatmospheric containment, and nine are in ice-condenser containments.

Figure 3 shows the contribution to plant CDF from the following accident classes: station blackout, anticipated transient without scram , transients, loss of coolant accidents, internal floods, interfacing systems LOCAs (ISLOCAs), and steam generator tube ruptures (SGTR). The importance of specific accident classes to CDF varied significantly from plant to plant; however, the following accident classes were important for many of these plants:

- Transients,
- LOCAs, and
- Station blackout - the loss of all offsite and onsite AC power.

In general terms, transients are important contributors to CDF because they involve relatively high initiating event frequencies coupled with system failures that defeat the redundancy in systems available to mitigate potential accidents. LOCAs are more important for these PWR plants than for BWR plants because there are fewer systems available in the PWRs to provide low-pressure coolant injection. Station blackout accidents are relatively important for the Westinghouse 4-loop plants because they leave few systems available to prevent core damage. A few plants identified internal flooding accidents as being important, generally reflecting plant-specific weaknesses. With the exception of a single outlier plant in each category, none of the plants found ATWS or steam generator tube rupture sequences to be important contributors, and none of the plants reported significant CDFs from interfacing system LOCAs. These accidents are normally low contributors because of the low frequency of the initiating event. Although steam generator tube rupture and interfacing system LOCAs were generally found to be low contributors to CDF, they can be important risk contributors since they bypass containment. The variation in the reported IPE results is attributed to many factors including plant-specific design features, modeling

assumptions, and variation in data (including the probability of operator errors). These factors are discussed below for each accident class.

Transients are important contributors to CDF for nearly all of the Westinghouse 4-loop plants. This accident class involves events that cause the reactor to trip, followed by failure to bring the reactor to safe shutdown [either failure to remove decay heat or failure to replace reactor coolant inventory following an accident-induced LOCA, normally a reactor coolant pump (RCP) seal LOCA]. Transients represent a broad category, covering both general initiators (such as reactor trip or loss of main feedwater) as well as support-system initiators (such as loss of service water or AC/DC bus).

The specific failures leading to core damage for transients were found to be quite plant-specific. However, there are some key factors affecting the CDF from transients that are common among many of the submittals. These key factors involve plant-specific design and operating conditions as well as the assumptions made in the IPEs. The modeling issues are important to the results and represent an important area of uncertainty. The key factors are identified and discussed below:

- Service water and component cooling water dependencies - At most of the plants, there is a relatively high dependence of other plant systems on component cooling water and/or service water. Thus, loss of either of these support systems is important to the overall transient CDF. For example, the dominant transient sequence at D. C. Cook is loss of component cooling water, leading to an RCP seal LOCA that cannot be mitigated. The configurations vary considerably among the plants, however, and plants with the ability to use alternate cooling configurations when the primary cooling system is lost generally have lower transient CDFs.

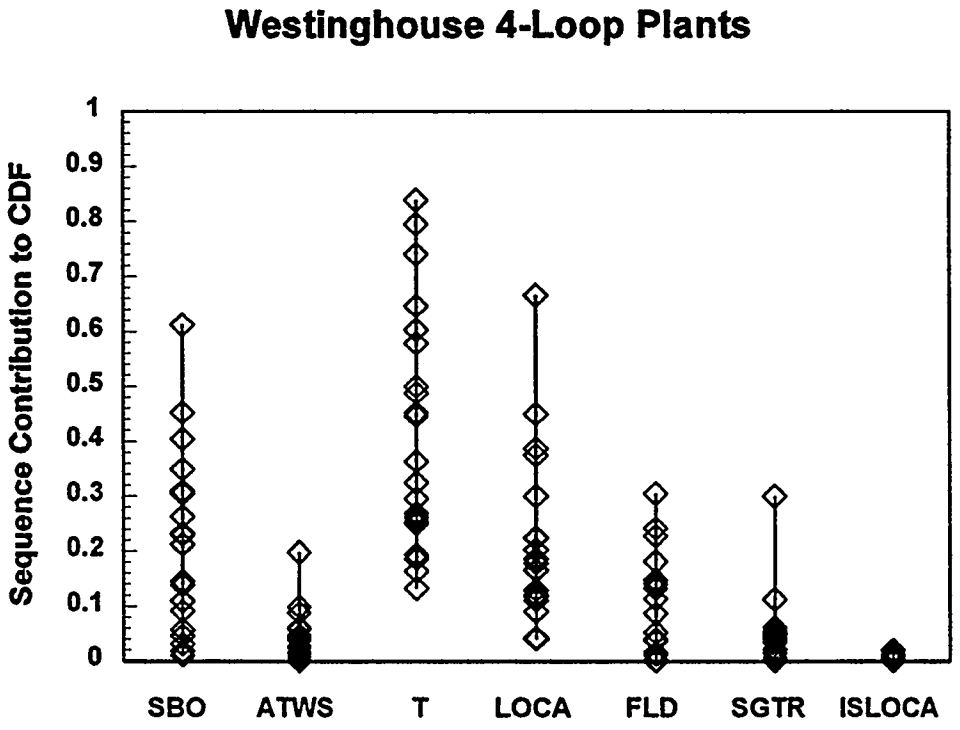

Figure 3. Accident Class CDFs for Westinghouse 4-Loop Plants

- Susceptibility to RCP seal LOCAs - For some of the plants, the importance of RCP seal LOCAs is reduced because of plant design characteristics that reduce the threat from RCP seal LOCAs. These include the use of the newer seals that are less susceptible to leakage than the older design (e.g., Braidwood, Byron, Vogtle had small RCP LOCA contributions because of using the newer seals), availability of backup systems to cool the seals when the normal configuration fails (e.g., the safe shutdown facility at Catawba and McGuire can provide RCP seal cooling), and use of different support systems for cooling the RCP seals than for providing injection (so that loss of a single system does not lead to an unmitigable LOCA). The modeling of RCP seal LOCAs varied considerably among the IPEs, with some using low probabilities of leakage and low leak rates while others used much higher values for both parameters. This variability in design and modeling had a significant impact on the results.

- Ability to cross-tie - The ability to cross-tie between systems or between units was more important for the PWRs than the BWRs because there are fewer systems available in the PWRs to provide core cooling. The ability to cross-tie somewhat compensates for this reduced redundancy. However, many plants with capability to cross-tie did not credit this in the IPE submittals.

LOCAs are important contributors to CDF for many of the plants in this group. The most common LOCA contributors are small LOCAs, but some plants are instead dominated by large or medium LOCAs. The small LOCAs are generally the larger contributors to CDF because they have a higher frequency. The dominant contributor to core damage involves failure of injection systems after the borated water storage tank is depleted and the injection pumps switch to the recirculation mode (in which water is drawn from the containment sump). Recirculation involves realigning systems, and typically involves more components than required for the injection mode, and this complexity leads to a higher failure probability.

Generally, plant design and operational features had a larger impact on the LOCA CDF than did modeling characteristics. Overall, the most influential factors are those discussed below.

- Switchover to recirculation - Most of the plants require some manual actions to initiate recirculation because high-pressure recirculation draws suction from low-pressure systems during recirculation at most plants. However, at many of the plants, the switchover of the low-pressure systems from the refueling water storage tank to the containment sump is automatic, which simplifies the actions required by the operators, and thus increases the probability of successfully completing the action. At Haddam Neck, for example, the switchover is manual, and this plant has the highest LOCA CDF for the Westinghouse 4-loop plants. For ice-condenser plants especially, the lower containment design pressure results in earlier actuation of containment sprays, so there is less time to perform the switchover. Therefore, the degree of automation is particularly important for ice-condenser plants.

- Size of refueling water storage tank - Some plants have large refueling water storage tanks so that the switchover to recirculation (and the associated complications discussed above) is either not necessary or is significantly delayed, which gives the operators more time to complete the necessary actions for the switchover to recirculation. Larger refueling water storage tanks were found to have an important effect on the LOCA CDF. For example, the two plants with the lowest LOCA CDFs, Braidwood and Byron, have relatively large refueling water storage tanks, and do not require switchover to recirculation for small LOCAs.

- Alternate actions to mitigate a LOCA - Some plants credited alternate actions such as depressurizing the reactor coolant system using the steam generator relief valves when high-pressure injection fails during a LOCA or refilling the refueling water storage tank if recirculation

fails. The ability of these strategies to succeed is plant specific, but the strategies were found to be important for those submittals that credited the actions.

Station blackout accidents are important contributors to CDF for many of the Westinghouse 4-loop plants. Station blackout accidents involve an initial loss of offsite power followed by failure of the emergency onsite AC power sources. The failure of AC power sources results in failure of all injection systems and failure of motor-driven auxiliary feedwater (AFW). This leaves only turbine-driven AFW available for cooling the core and no systems available to provide injection to make up the loss through any RCP seal LOCAs that develop during the transient.

Generally, plant design and operational features have a larger impact on the station blackout CDF than do modeling characteristics, but no single factor dominates. Usually, combinations of contributors are important, and those combinations vary from plant to plant. Overall, the most influential factors are those discussed below.

- Modeling of RCP seal LOCAs and seal design - Because seal cooling is lost during a station blackout, RCP seal LOCAs are important for many of the Westinghouse 4-loop plants. As noted in the discussion of transients above, RCP seal LOCA modeling varies among the submittals, and has a significant impact on the results. Also important is whether the plants have replaced the RCP seals with the newer, temperature-resistant design. Vogtle, for example, has installed the new seals, and because of this has a relatively low contribution from station blackout accidents that involve RCP seal LOCAs (although station blackout accidents without seal LOCAs are relatively high for this plant).

- Number of emergency AC power sources - The number of emergency diesel generators (usually two or three per unit) directly affects the reliability of the emergency AC power system. Further, a few plants have a diverse AC power source, such as a gas turbine generator or an independent safe shutdown facility, and are less susceptible to common cause failures of diesel generators. Plant-specific operating history can also be important, and for example, drives Vogtle to have the highest station blackout CDF for this plant group.

- Battery depletion time - Although some plants have indicated that they have the capability to manually control AFW when DC power is lost, most plants need battery power to provide control for AFW. Thus, for most plants, when the batteries are depleted, all cooling is lost and core damage follows. Battery depletion times range from 1 to 12 hours for this group, with the longer times reflecting plants making extensive use of load shedding.

Internal flooding is important for some of the Westinghouse 4-loop plants. Internal flooding events involve rupture of water lines that result in a release of water that can directly fail required mitigating systems and/or fail other mitigating systems due to submergence or spraying of required components. The effects of internal flooding are highly plant specific, depending on the layout of equipment within the plant and the relative isolation of rooms. Because of this diversity of design and layout, each plant has different vulnerabilities to flooding and generic conclusions regarding flooding cannot be drawn. The plants with the largest flood contributions typically were dominated by floods that affected support systems such as electric power and service water, which have plant-specific designs.

ATWS is not a dominant contributor for most Westinghouse 4-loop plants. ATWS sequences involve a transient, followed by failure to shutdown the nuclear chain reaction by inserting the control rods. Power generation continues at levels far in excess of normal decay heat. An ATWS sequence can be mitigated by pressure control and heat removal. Because of the low frequency of failure to scram, ATWS is a relatively low contributor (less than 10% of CDF) for nearly all the plants in this group. The single plant

with a significant ATWS contribution, Indian Point 3, operates with the power-operated relief valve (PORV) block valves closed, which reduces the relief capacity of the primary system during the early phase of an ATWS.

Steam generator tube rupture is not a dominant contributor to CDF for most Westinghouse 4-loop plants. Steam generator tube rupture sequences involve leakage from the primary to the secondary through a ruptured steam generator tube, followed by either failure to mitigate the leak or failure to establish long-term core heat removal. Steam generator tube rupture accidents are a minor contributor to plant CDF at most Westinghouse 4-loop plants because of the low frequency of the rupture occurring. However, the contribution to risk is more significant at many plants because the releases bypass containment.

Although nearly always minor, the contribution to CDF from steam generator tube rupture is primarily driven by assumptions made in the IPEs. Steam generator tube rupture accidents require considerable involvement from operators, and modeling of operator errors as well as alternate strategies varies widely among the IPEs. Although this is an area containing large uncertainties, it does not have a large impact on the overall plant CDF.

Summary

The objective of the IPE Insights Program is to document the significant safety insights, based on the IPEs for different reactor and containment types and plant designs. That objective is being achieved by examining the IPE CDF and containment performance results for individual plants in various groups and searching for commonalities and differences. For the BWR 3/4 and Westinghouse 4-loop Plants, transients, station blackout, and LOCAs (for PWRs) tend to dominate, but individual plant results vary considerably, reflecting both differences in plant design and operational characteristics, and differences in IPE modeling.

SEVERE ACCIDENT PROGRESSION PERSPECTIVES FOR MARK I CONTAINMENTS BASED ON THE IPE RESULTS*

C. C. Lin
J. R. Lehner
W. T. Pratt
Brookhaven National Laboratory
Upton, NY 11973

M. Drouin
U.S. Nuclear Regulatory Commission
N. Bethesda, MD 20852

ABSTRACT

Based on the level 2 analyses in the IPE submittals accident progression perspectives were obtained for all containment types. These perspectives consisted of insights related to the containment failure modes, the releases associated with those failure modes, and the factors responsible for the results reported. To illustrate the types of perspectives acquired regarding severe accident progression, insights obtained for Mark I containments are discussed here.

Mark I containments have relatively high strength but small volumes and rely on pressure suppression pools to condense steam released from the reactor coolant system during an accident. In these containments those accidents that cause structural failure of the drywell shortly after the core debris melts through the reactor vessel were found to be dominant contributors to risk. The importance of individual containment failure mechanisms depended on plant-specific features and in some cases on modeling assumptions; however, the following mechanisms were found important for many Mark I containments: (1) Drywell shell melt-through caused by direct contact with the core debris (i.e., liner melt-through), and (2) Drywell failure caused by rapid pressure (and temperature) pulses at the time of reactor vessel melt-through

Drywell failure caused by gradual pressure (and temperature) buildup due to gases and steam released during core/concrete interactions is important in some IPEs. In other IPEs venting was found to be an important contributor. However, accidents that bypass containment (such as interfacing systems LOCA) or involve containment isolation failure were not important contributors to the CDF in any of the IPEs for Mark I plants. These accidents are also not important to risk (even though they can involve large fission product release) because their frequencies of occurrence are so much lower than the frequencies of early structural failure caused by other accidents that dominate the CDF.

*Work performed under the auspices of the U.S. Nuclear Regulatory Commission.

BACKGROUND

NRC issued Generic Letter 88-20 in November 1988 requesting that all licensees perform an Individual Plant Examination (IPE) to identify any plant-specific vulnerabilities to severe accidents, and to report the results to the Commission. There are four general purposes of the IPE program for the licensees, as stated in the Generic Letter:

1. Develop an appreciation of severe accident behavior;

2. Understand the most likely severe accident sequences that could occur at the plant;

3. Gain a more quantitative understanding of the overall probabilities of core damage and fission product releases; and

4. If necessary, reduce the overall probabilities of core damage and fission product releases by modifying, where appropriate, hardware and procedures that would help prevent or mitigate severe accidents.

The Executive Director of Operations to the Office of Nuclear Regulatory Research in NRC recommended on May 12, 1993 that NRC should publish a document highlighting the significant safety insights resulting from this program and showing how the safety of reactors has been improved by the IPE initiative. The IPE Insights Program was initiated to document such safety insights. Significant insights and improvements identified from the IPE submittals are captured and are documented in a soon-to-be-published NUREG report.

The major insights to be gained through the IPE Insights program include:

- How has the IPE program affected reactor safety?

- What is driving the CDF and containment performance?
  - What are the important design and operational features that affect the CDF and containment performance?
  - How important is the role of the plant operators?
  - How much influence do the IPE methodology and assumptions have on the results?

APPROACH

To accomplish these objective, the IPEs were examined by NRC Research, with the assistance of Brookhaven National Laboratory (BNL) and Sandia National Laboratory (SNL), to determine what the collective IPE results imply about the safety of U.S. nuclear power plants. SNL concentrated on obtaining insights based on the level 1 results reported in the IPEs, while BNL focussed on the level 2 results reported. Variations and commonalities among plant results were studied to determine which factors were most influential on the results. In addition, the improvements that have been made at the plants, and the impact of these improvements were examined.

The approach used by BNL for the level 2 insights consisted of: (1) comparing results of IPE submittals for plants with similar containments to obtain average values and ranges of failure probabilities, (2) identifying the major contributors to containment failure and fission product release cited in the IPEs for particular containment types, (3) comparing the IPE results to those found in previous PRA studies such as NUREG-1150, (4) establishing the reasons for the variation in the results, and (4) identifying the modifications and changes made by the licensees in response to their IPE findings.

The examination of the level 2 results documented in the IPEs indicated that there was significant variability in performance results among containments of similar type for every containment group. This variability could be traced back to differences in individual features among containments of the same type, but also to differences in assumptions made in the IPE analyses. These differences in assumptions included what phenomena were considered, how containment loads were developed, how containment capability was assessed, and the operator actions credited.

The rest of this paper illustrates the perspectives and insights gained from the examination of the level 2 analyses in the IPE submittals by summarizing the perspectives obtained for one group of containments, i.e. the BWR Mark I type.

BWR Mark I Perspectives

Twenty-four BWR units (17 IPE submittals) are housed in Mark I containments. All of the plants in the BWR 2/3 group and most of the plants in the BWR 3/4 group have Mark I containments. These containments have relatively high strength but small volumes and rely on pressure suppression pools to condense steam released from the reactor coolant system during an accident.

Those accidents that cause structural failure of the drywell shortly after the core debris melts through the reactor vessel were found to be dominant contributors to risk. The importance of individual containment failure mechanisms depended on plant-specific features and in some cases on modeling assumptions; however, the following mechanisms were found important for many Mark I containments.

- Drywell shell melt-through caused by direct contact with the core debris (i.e., liner melt-through)
- Drywell failure caused by rapid pressure (and temperature) pulses at the time of reactor vessel melt-through

In general terms, these failure mechanisms are important to risk because of the relatively short time available for radioactivity decay, natural deposition processes, and for accident response actions. In addition, drywell failure means fission products released from the damaged core bypass the suppression pool (significant retention can occur if aerosol fission products pass through a suppression pool). The relatively short time to fission product release and the magnitude of the release means these failure mechanisms are important to all risk measures (i.e., acute and latent health effects including land contamination). These failure mechanisms can also occur for any accident class that involves release of a significant amount of core debris from the reactor vessel. A few plants identified other failure mechanisms as being important. Drywell failure caused by gradual pressure (and temperature) buildup due to gases and steam released during core/concrete interactions is important in some IPEs. In other IPEs venting was found to be an important contributor. However, accidents that bypass containment (such as interfacing systems LOCA) or involve containment isolation failure were not important contributors to the CDF in any of the IPEs for Mark I plants. These accidents are also not important to risk (even though they can involve large fission product release) because their frequencies of occurrence are so much lower than the frequencies of early structural failure caused by other accidents that dominate the CDF. Each failure mechanism is discussed in more detail below.

Liner melt-through was found to be the most important contributor to early containment failure for Mark I containments. This failure mechanism occurs frequently in Mark I containments, because for most Mark I containments, the reactor pedestal and the drywell floor are at the same level and openings exist between the pedestal region and the floor; this design allows the core debris to flow across the drywell floor and fail the steel drywell shell either by direct melt-through or via creep rupture.

The capability to flood the drywell floor, the design configuration of the drywell, and assumptions regarding core debris dispersal on the drywell floor determine, on a plant-specific basis, whether liner melt-through is a significant containment failure mechanism. The most important plant features and modeling characteristics are discussed below.

- Drywell floor flooding - The presence of a water pool on the drywell floor was found to mitigate liner melt-through in all of the submittals. The benefit of water on the drywell floor prior to vessel failure as a mitigating mechanism for liner melt-through is significant and should be highlighted in future accident management plans of utilities with Mark I containments.

- Containment design configuration - The design of the drywell sump and drywell floor can prevent liner melt-through in some Mark I containments. For example, containment sumps in the Monticello plant are large enough to contain the molten core material and thus prevent it from reaching the containment boundary. In the Oyster Creek drywell, a concrete curb prevents or limits the core debris from reaching the containment shell. Also, the Brunswick containment is unique among Mark I designs because it is of concrete rather than steel construction. Thus, even if the molten core debris reaches the Brunswick containment, it would be difficult to thermally degrade such a thick concrete structure.

- Core debris characteristics - The amount of core debris released to the drywell and the fluidity of the core debris assumed in the IPEs determined whether or not liner melt-through occurred. Liner melt-through was found to be an important risk contributor if a large amount of core debris at high temperature was assumed to be released to the drywell. Under these circumstances, the core debris can flow across the floor and melt-through the shell. Liner melt-through was not important to risk if smaller quantities of core debris at lower temperatures (less able to flow across the floor) were assumed to be released into the drywell. As different modeling assumptions can produce such significantly different results (i.e., containment failure vs. no failure) any actions taken by the utilities to mitigate this failure mechanism should reflect this uncertainty. Therefore, as water can effectively mitigate liner melt-through, it is prudent to eliminate the uncertainty regarding containment failure caused by this failure mechanism by ensuring a flooded drywell floor.

A number of utilities were proactive and identified minor hardware modifications and changes in procedures to ensure a flooded drywell floor prior to reactor vessel melt-through. The availability of alternate water sources to the drywell spray header, such as water from a diesel driven fire pump during a station black-out, was shown to significantly reduce the likelihood of early failure in the Browns Ferry IPE. Another example is the Monticello plant where connections are available which enable the operators to use RHR service water for containment spray. The Nine Mile Point 1 submittal mentions the potential benefit of supplying the drywell sprays from external sources such as the containment spray raw water pumps. Peach Bottom has the capability of supplying the sprays with water from an external pond or the Emergency Cooling Tower. Several IPEs, such as Duane Arnold and Monticello, also discussed the possibility of relaxing the restrictions on drywell spray initiation in the current EOPs, thus providing greater assurance that there would be water on the drywell floor.

High pressure and temperature loads at the time the core debris melts through the reactor vessel is a significant contributor to early containment failure for Mark I containments. This failure mechanism occurs in Mark I containments because of their relatively small volumes. High pressures and temperatures occur in containment when the RCS depressurizes as the core debris melts through the reactor vessel. Hydrogen (from clad oxidation) and steam are the driving force for pressurization. If the pressure pulse exceeds the ultimate pressure capability of the containment, then failure will occur at the weakest location either in the wetwell or the drywell.

The RCS pressure at vessel melt-through, the containment failure location, and modeling assumptions regarding the rate of RCS depressurization and amount of core debris dispersed determined whether this failure mechanism

is a significant contributor to early containment failure for individual Mark I containments. The most important accident characteristics, design features and modeling assumptions are discussed below.

- RCS pressure at time of vessel melt-through - Containment failure via this mechanism is prevented if the RCS is depressurized before the core debris melts through the reactor vessel. The importance of this failure mechanism to risk therefore depends on the importance of accident classes in which the RCS is at high pressure (such as transient events with failure of the ADS). Enhancing the depressurization capability of the RCS was explored by a number of utilities but adverse effects were identified which need to be carefully considered.

- Containment failure location - The containment failure location can significantly influence the importance of this failure mechanism to risk. If failure occurs in the wetwell, then significant retention of the aerosol fission products occurs in the suppression pool making this failure mechanism less risk significant. Conversely, if failure occurs in the drywell, then the fission products are released without the benefit of pool scrubbing and the risk is much higher.

- RCS depressurization characteristics - The rate of RCS depressurization, steam generation, and characteristics of core debris dispersal determine the risk significance of the failure mechanism. If rapid depressurization is assumed (caused by a large opening in the reactor vessel) then high pressure pulses can occur that have a high likelihood of containment failure. In addition, if a large amount of high temperature core debris is assumed to be released and dispersed into the containment atmosphere then it can directly heat it and containment failure is very likely to occur. Containment failure does not occur if lower depressurization rates combined with less core debris dispersal are assumed. Again, different modeling assumptions give very different results and these uncertainties need to be factored into any strategy designed to prevent or mitigate this failure mechanism.

Ways of preventing or mitigating the pressure (and temperature) loads at vessel melt-through are enhanced RCS depressurization capability, containment venting and spray operation. Of these possible actions, RCS depressurization is potentially the most effective. Containment vents of sufficient capacity to mitigate pressure loads at the time of vessel melt-through (with the RCS at high pressure) do not exist in most Mark I containments and would not be practical to install, and spray operation cannot effectively mitigate all pressure loads associated with RCS depressurization during severe accidents.

A number of utilities explored controlled depressurization of the RCS prior to melt-through of the reactor vessel as a mitigation strategy for rapid over pressure failure of Mark I containments. Enhancement of the emergency depressurization capability was also an issue raised as part of the NRC's containment performance improvements (CPI) program. Although some utilities recognized the benefit of this strategy a number of potential adverse effects were also noted. For example, if low pressure injection systems are not available, then depressurization causes loss of coolant inventory which can significantly reduce the time to fuel damage and vessel melt-through. This in turn reduces the time available for other recovery actions. Given the uncertainty associated with pressure loads and the potential adverse effects some utilities recommended further study prior to implementing this strategy.

High pressure and temperature loads caused by core/concrete interactions are a significant contributor to late containment failure for Mark I containments. Gradual pressurization at high temperatures caused by noncondensible gases and steam released from the drywell floor during core/concrete interactions can fail Mark I containments several hours after vessel melt-through. This failure mechanism occurs because of the relatively small volume of Mark I containments. Failure can occur either in the wetwell or in the drywell. Generally, this failure mechanism is less risk significant than the two early failure mechanisms discussed above because of the longer time available for radioactive decay, natural deposition processes and for accident response. However,

even for late failures, if the failure location is in the drywell then, significant fission product release can still occur making this failure mechanism important to longer term risk measures (i.e., latent health effects and land contamination).

The significance of this failure mechanism to late containment failure is determined by whether or not the drywell is flooded, the design configuration of the drywell, the availability of sprays or venting, and modeling assumptions regarding the quantity and temperature of core debris dispersed across the drywell floor. The most important accident characteristics, design features and modeling assumptions are discussed below.

- Drywell floor flooded - A flooded drywell floor helps the drywell spray and containment heat removal (CHR) systems to control pressurization and prevent structural failure of the containment. Water can cool the core debris and limit concrete erosion (and hence limit gas generation) so that steam is the main driving force for containment pressurization. The drywell spray and CHR systems are designed to condense steam and remove heat from containment and therefore can control the containment pressure under these circumstances.

- Drywell floor not flooded - If the drywell floor is not flooded (and liner melt-through does not occur) venting may be needed to prevent over pressure failure of the containment. Without water, the hot core debris can cause significant concrete erosion (and hence significant gas release). The heat from this core/concrete interaction can raise the temperature of the drywell to a range where the structural capacity of the steel containment shell is significantly reduced. The quantity of gases released from this interaction also depends on the type of concrete used. For example, limestone concrete releases significantly more gases than basalt concrete. The drywell spray and CHR systems cannot control the pressure in containment if the driving force for pressurization is non condensible gases. Under these circumstance, the only way to control pressure is to relieve gases via venting (preferably from the wetwell in order to benefit from pool scrubbing).

- Containment design configuration - The design of the drywell and pedestal region can limit contact between the water and core debris in some Mark I containments. For example, large sumps in the pedestal region produce deep pools of molten core debris, which are difficult to cool with water. Forming a coolable debris bed is particularly difficult if the water is added after the core debris is in the sumps. Therefore, in some IPEs, core/concrete interactions continued even after water was added to the drywell.

- Core debris characteristics - In the absence of water, the amount of core debris released to the drywell and its temperature determined the extent of core/concrete interactions. If a large amount of core debris at high temperature was assumed released from the reactor vessel then extensive concrete erosion was predicted in the IPEs. Under these circumstances, even if water was added to the core debris , core/concrete interactions were predicted to continue for some Mark I designs. Conversely, if smaller quantities of core debris at lower temperatures were assumed, then much less concrete erosion occurred even without water. Clearly, different modeling assumptions give different results which were considered by utilities when developing strategies to mitigate these failure mechanisms.

Most utilities used a combination of strategies to mitigate gradual pressure build-up caused by core/concrete interactions. The drywell floor flooding strategies designed to prevent liner melt-through if successful will also limit long-term core/concrete interactions and hence limit noncondensible gas generation. If these early flooding strategies were not successful, then most utilities explored other ways of flooding the drywell floor. For instance, the Monticello IPE submittal noted that debris cooling with an alternate injection source, such as fire water, limits the temperature rise in containment and extends the time to containment failure by over-pressurization. In all the IPEs containment sprays were found to be of great benefit for preventing or mitigating late containment failure.

In addition to the advantages mentioned earlier, the cooling provided by the containment sprays will retard the revaporization of fission products deposited on containment surfaces. Sprays can also scrub fission products existing in the containment atmosphere and provide a water source for covering ongoing core/concrete interactions. High temperature effects were also addressed in other ways in some IPEs. Nine Mile Point 1 considered raising the preload on the drywell head bolts as a way of increasing the probability of maintaining containment integrity at elevated temperatures. Finally all utilities have the capability to prevent late structural failure by venting.

Containment venting is an important way of preventing and mitigating core damage in Mark I containments. Venting was used extensively in the IPEs to reduce releases and thus risk, and it was also an important element of the CPI program. Containment venting was used to prevent core damage in accidents involving loss of containment heat removal. It was also used to prevent late structural failure for those accidents in which the core melts through the reactor vessel. However, a few utilities stated in their IPEs that their analyses indicated that the installation of a hardened vent did not significantly impact risk and therefore was only of marginal benefit. In one case the utility stated that they would not install a hardened vent.

In response to the recommendations in Generic Letter 89-16, most utilities with Mark I containments committed to install a hardened wetwell vent system (in some cases a hardened vent was already in place). A hardened vent leading from the wetwell to outside the containment building provides an independent means for containment pressure relief and heat removal while maintaining a habitable environment in the reactor building. The utilities used these venting systems to prevent core damage for some accidents involving loss of containment heat removal. Under these circumstances venting is "clean" because it occurs prior to core damage and involves minimal release of radioactivity.

Venting, after core damage has occurred, as a way of preventing structure failure of the containment was considered to be a last resort by most utilities because it can involve significant fission product release. The advantage of venting from the wetwell (benefit of pool scrubbing) was emphasized in most IPE strategies. The pressure at which venting should be started was also examined in detail by several utilities. The impact of high temperatures on the structural capability of the drywell was also noted. For example, the NMP Unit 1 IPE reported that at 400°F the containment could fail at pressures below the current venting pressure in the EOPs. Further analysis was recommended that could refine the vent actuation pressure.

Containment venting is important to risk in some Mark I containments. If venting occurs shortly after core meltdown and the flow path is directly from the drywell or from the RCS to the environment, then the suppression pool will be bypassed. Under these circumstances, venting would cause a significant release of fission products to the environment. In this context a number of utilities expressed concern about the current BWR Owners Group guidelines for containment flooding (filling the containment solid with water to a level equal with the top of fuel in the RPV) and the venting necessary to carry it out. Since drywell (i.e. unscrubbed) venting is needed to relieve the pressure buildup resulting from the compression of the gas space during containment flooding, there is the potential of an early release of significant magnitude associated with the flooding strategy. A number of utilities speculated that other actions, or even no action, was preferable to carrying out the containment flooding strategy.

Accidents that bypass containment are not important to risk for Mark I containments. If the pressure boundary between the high pressure RCS and a low pressure auxiliary system fails (called an interfacing systems LOCA) then a LOCA outside containment can occur. If water cannot be supplied to the reactor, core damage will occur and a direct path can exists to the environment. Therefore, these accidents can lead to a large early release of fission products. However, interfacing systems LOCA are not risk significant for BWR Mark I containments because of their relatively low frequency compared with the frequency of accidents that dominate the CDF and which can lead to early structural failure. The IPEs reported interfacing systems LOCA frequencies that are about

an order of magnitude lower in BWR plants than in PWRs. The lower BWR frequency are in part due to the lower RCS pressures in BWR plants compared with PWRs.

Although interfacing systems LOCA are not important to risk one submittal (the Nine Mile Point Unit 1 IPE) did identify a unique way of bypassing containment. In that IPE, failure of the emergency condenser tubes due to high temperature creep rupture was identified as leading to containment bypass. In a degraded core accident failure between the primary and secondary side of the emergency (or isolation) condenser provides a pathway for release similar to a steam generator tube rupture in PWRs. This failure mode was found to have a relatively low frequency (compared with the frequency of early structural failure) at Nine Mile Point, Unit 1, and was therefore not important to risk. Isolation condensers are found in one other BWR 2 plant and two early BWR 3 plants and presumably this bypass accident is also applicable to these plants. It is therefore necessary to determine that this failure mechanism is also a low risk (low frequency compared with the frequency of early structural failure) event in these other plants.

Accidents that involve failure to isolate containment are not important to risk for Mark I containments. Isolation failures can be preexisting or occur at the time of the initiating event. If the isolation failure is large (i.e., exceeds X volume percent per day) and if core melt occurs, then fission product release can also be large. In addition, because the containment is open at the time of core damage, the offsite site consequences can be significant. These events are not risk significant in BWR Mark I plants because of their relatively low frequencies. Preexisting isolation failures in Mark I plants can be precluded because the containment atmosphere is inerted with nitrogen. Therefore, any loss of containment atmosphere due to preexisting leaks can be easily detected. In addition, failure to isolate containment on demand was found to be a relatively low frequency event compared with the frequencies of other accidents that can cause early structural failure of the containment.

ATWS sequences were risk significant in a number of IPEs for plants with Mark I containments. These sequences belong to an accident class in which containment heat removal and containment venting are inadequate. In ATWS events the energy deposited to the containment can overwhelm the normal containment heat removal mechanisms as well as the available vent paths, leading to early core damage and containment failure. The inability to remove heat from the containment causes containment failure to occur before core damage. The containment failure in turn can lead to the loss of emergency core cooling systems (due to a loss of net positive suction head for pumps drawing from the suppression pool, for instance) with resulting core damage and vessel failure. Depending on the accident progression, core damage could occur first, but containment failure follows quickly. These accidents are risk significant since core damage, vessel failure and containment failure can occur within a short time interval, thus producing conditions for significant release to the environment. However, many IPE submittals indicated that, by proper RPV level control and by opening the maximum number of vent paths, many ATWS scenarios could be controlled. The significance of ATWS events in the different IPEs depended on some plant specific features, such as the ability of pumps to work with saturated water, as well as on assumptions regarding power level, point in the fuel cycle, and rapidity of operator response.

Accidents with successful reactor scram but loss of containment heat removal were found to be relatively unimportant to risk in all the IPEs. The ability to vent the containment was a major factor in reducing the importance of this class of accident. Also, the interval between loss of containment heat removal and containment failure is relatively long in these sequences, allowing time for emergency measures on and off site.

Figure 1 shows the conditional probability for the various Mark I containment failure modes.

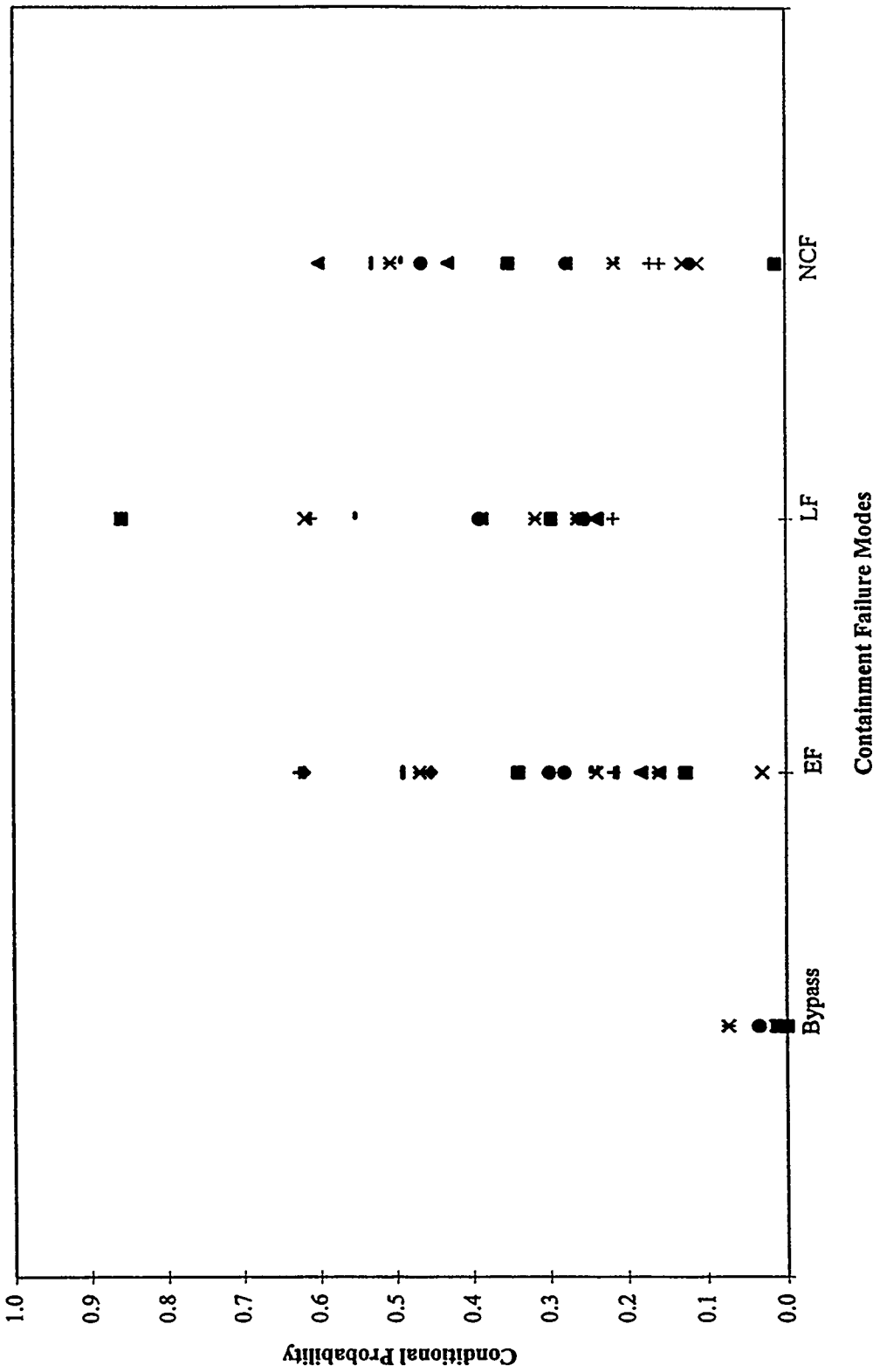

Figure 1 Conditional Containment Failure Probabilities for BWR Mark I Containment

PERSPECTIVES ON PLANT VULNERABILITIES & OTHER PLANT AND CONTAINMENT IMPROVEMENTS

Jeffrey LaChance[1], Alan Kolaczkowski[1], Julie Kahn[1]
Richard Clark[2], John Lane[2]

[1]Science Applications International Corporation
[2]U.S. Nuclear Regulatory Commission

The primary goal of the Individual Plant Examination (IPE) Program was for licensees to identify plant-unique vulnerabilities and actions to address these vulnerabilities. A review of these vulnerabilities and plant improvements that were identified in the IPEs was performed as part of the IPE Insights Program sponsored by the U.S. Nuclear Regulatory Commission (NRC). The main purpose of this effort was to characterize the identified vulnerabilities and the impact of suggested plant improvements.

No specific definition for "vulnerability" was provided in NRC Generic Letter 88-20[1] or in the subsequent NRC IPE submittal guidance documented in NUREG-1335[2]. Thus licensees were left to use their own definitions. Only 20% of the plants explicitly stated that they had vulnerabilities. However, most licensees identified other plant improvements to address issues not explicitly classified as vulnerabilities, but pertaining to areas in which overall plant safety could potentially be increased.

The various definitions of "vulnerability" used by the licensees, explicitly identified vulnerabilities, proposed plant improvements to address these vulnerabilities, and other plant improvements are summarized and discussed.

Plant Vulnerabilities

One of the reporting guidelines presented in the IPE submittal guidance document, NUREG-1335, is that each IPE present "a list of any vulnerabilities identified by the review process, a concise discussion of the criteria used by the utility to define vulnerabilities, and the fundamental causes of each vulnerability." As discussed below, most of the licensees clearly identified their criteria for identifying vulnerabilities. However, only 20% of the licensees *clearly stated they had vulnerabilities* and identified potential improvements in equipment, procedures, or training programs to address these vulnerabilities.

Vulnerability Definitions

The guidance in NUREG-1335 pertaining to the identification of vulnerabilities leaves the licensees to use their own definitions of the term "vulnerability." The definitions for vulnerability used in many of the IPE submittals were based on one of two sets of quantitative criteria: (1) the criteria provided in the NUMARC Severe Accident Issue Closure Guidelines Document 91-04[3], and (2) NRC's Safety Goal Policy Statement defining a core damage frequency objective of 1E-4/ry and a large release objective of 1E-6/ry. A third criteria utilized in some IPE submittals was based on using importance measures or the results of sensitivity studies to determine which

components or systems were the most vital to the plant. Several variations and combinations of these criteria were identified in the submittals and are discussed below. No specific definition of vulnerability could be identified for approximately 29% of the plants. However, for a significant number of these plants, some sort of criteria was utilized to identify areas for improving the plant safety. The criteria used to identify vulnerabilities, as well as to identify other areas warranting plant improvements, are discussed in subsequent paragraphs.

The most commonly applied quantitative criteria for identifying plant vulnerabilities are contained in the NUMARC guidelines. Twenty-three percent of the plants reported using some variation of the NUMARC guidelines for identifying what they explicitly called vulnerabilities. The NUMARC guidelines constitute a graded review process to identify areas warranting additional scrutiny. Accident sequences are grouped into functional groupings suggested by the guidelines, and the quantitative results are compared against four criteria levels consisting of values for core damage frequencies (CDFs) or with percent contribution values to the total plant CDF that decrease at each level. A parallel set of criteria levels exist in the NUMARC guidelines for specifically addressing containment bypass accident sequences. Some licensees defined a vulnerability as a functional sequence exceeding 1E-4/ry CDF or contributing greater than 50% to the total plant CDF; i.e., the top evaluation criteria level in the NUMARC guidelines. Additionally, some licensees defined a containment bypass vulnerability as any such functional sequence of this type with a CDF greater than the NUMARC top criteria of 1E-5/ry or contributing greater than 20% to the total CDF. Some licensees, when using the NUMARC guidelines, identified vulnerabilities associated with sequences meeting any of the graded NUMARC criteria (not just the top criteria). In many of these cases, resolution of a vulnerability meeting the lower tier NUMARC criteria is addressed simply by incorporating the issue into future accident management strategies. Other licensees modified the NUMARC top criteria definition of vulnerability slightly. When this was done, the modification was usually that the percent contribution forms of the criteria were not used on the basis that a large percentage of a small absolute frequency should not be used to identify a vulnerability. Yet other licensees used the NUMARC guidelines in combination with additional criteria for identifying vulnerabilities. For example, some licensees added a Level 2 criteria related to the frequency of a source term bin exceeding 1E-5/ry. One plant, Waterford, explicitly added criteria related to single failures, common cause failures, support system failures, and operator errors that had a significant impact on the core damage frequency in their vulnerability screening. The vulnerability screening criteria for WNP-2 also required the total CDF be within the NRC safety goal of 1E-4/ry and included a search for sequences that are outliers when compared to similar plants due to a plant specific feature.

The core damage frequency and large release objectives from the NRC Safety Goal Policy Statement were used by 22% of the licensees to define "vulnerability." These approaches are nearly equivalent to some of the NUMARC criteria in that they focus on just the absolute frequencies for CDF (but in this case the total plant CDF instead of an accident grouping frequency) and a large significant release. Any sequences contributing significantly to exceeding either or both criteria were examined by licensees to determine which design or operational aspects caused such a vulnerability, and resolutions were investigated to lessen the potential for such a vulnerability. Some plants chose to use modified safety goal frequencies in their definitions (e.g. 5E-4/ry for CDF and 5E-5/ry for an early release frequency). One plant (Oyster Creek) applied the criteria at the systemic sequence level instead of for the total plant CDF. Another plant (Palisades) changed the large release criteria from 1E-6/ry to 10% of the plant CDF. Some licensees that used the NRC Safety Goals in their vulnerability screening also used additional criteria. The most common criteria was a comparison to similar plants for the purpose of identifying any new or unusual core damage or containment failure mechanisms specific to their plant. Others also included a criteria that required that any systems, components, or operator actions that significantly impact the core damage frequency be listed as vulnerabilities. One plant (Davis-Besse) considered that a vulnerability might exist if the frequency of core damage is sensitive to a highly uncertain aspect of the plant response but indicated that further evaluation to reduce the uncertainty would be a more appropriate response than a change to the plant. Finally, several plants added Level 2

vulnerability criteria that addressed the performance of containment mitigating systems and the containment itself during severe accidents.

For 26% of the plants, the percent contribution to CDF was used as the base criteria for screening vulnerabilities. Some plants also included the percent contribution to containment failure in their vulnerability screening. The licensees usually relied on the relative contribution of systemic sequences, plant damage states, containment failure modes, and release categories to identify the important contributors to the plant risk. These important contributors were equated to areas where vulnerabilities may exist. Importance measures and sensitivity studies were also generally utilized to identify the fundamental causes or plant features contributing to these potential vulnerabilities. Generally, quantitative thresholds, as exist in the NUMARC guidelines, were not established for screening vulnerabilities based on the percent contribution to CDF or containment failure. Instead, the licensees applied qualitative thresholds using terms such as "significant" or "disproportionately high." Some licensees indicated that a plant feature would only be considered a vulnerability if it was a proportionately higher contributor or outlier when compared to similar plants. Thus, a 50% contributor to CDF might not be a vulnerability if it has a similar contribution at similar plants. One licensee (Turkey Point 3/4) indicated that vulnerabilities would only be considered for issues where they had the highest confidence in the results of their IPE.

For the remaining 29% of the plants, no vulnerability screening criteria could be explicitly identified. However, all of these plants used their IPE results to help identify other plant improvements. Fifteen percent used the NUMARC criteria to help identify areas for plant improvements, but did not explicitly state that the NUMARC criteria were being used to identify vulnerabilities. Fourteen percent appeared to use the percent contribution to CDF and sensitivity studies to help identify and evaluate the impact of other plant improvements.

Identified Vulnerabilities and Associated Plant Improvements

Using the various definitions of vulnerability discussed above, about 20% of the plants explicitly identified vulnerabilities in their IPE submittals. The vulnerabilities for Boiling Water Reactors (BWRs), which are discussed first in this section, exhibited no commonality based on plant type or initiator, nor did the vulnerabilities focus on a particular plant design aspect (e.g., support systems). Pressurized Water Reactor (PWR) vulnerabilities are discussed next. The same vulnerability issues, pertaining to particular plant design aspects, were identified for several PWR plants. Other PWR vulnerabilities tended to be plant-unique.

Only four BWR plants (11% of all BWRs) identified vulnerabilities. Millstone 1 identified both hardware and operational/procedure issues as vulnerabilities. These involved failure of the water supplies to the isolation condensers, failure of the operator to initiate the isolation condensers in time to prevent safety relief valves from lifting and subsequently sticking open and requiring coolant makeup, failure of the operator to restore or maintain the reactor vessel level in some accident scenarios, and drywell steel liner melt-through (a generic Mark I containment issue). The only resolution to the vulnerabilities identified in the IPE involved procurement of a portable diesel pump and corresponding procedural changes for it's use in supplying water to the isolation condenser. Fitzpatrick identified a vulnerability in the plant electrical configuration that results in loss of three Residual Heat Removal (RHR) loops (either directly or through the RHR service water system) when either one of two 4.16 kV buses is lost. Fitzpatrick was considering procedure modifications and training for using firewater as a backup to RHR service water and installation of a cross-tie between RHR service water trains. Hope Creek identified a ventilation system vulnerability that would result in loss of essential electrical switchgear. During the IPE analysis process, the utility developed a recovery procedure to address this vulnerability by aligning alternate means of cooling. Credit for this recovery procedure was taken in the final IPE results. Susquehanna identified several vulnerabilities in various areas some of which could be considered generic to most BWRs. The first involved the need for manual actions to bypass the High

Pressure Coolant Injection (HPCI) pump suction transfer and to bypass the high exhaust pressure trips for the HPCI and Reactor Core Isolation Cooling (RCIC) systems. To address this vulnerability, consideration was being given to revising the control strategy for HPCI suction transfer; in addition, the HPCI/RCIC backpressure trip setpoints were raised. Another vulnerability identified at Susquehanna related to the need for manual flow control to avoid severe power excursions upon failure of HPCI and condensate during an anticipated transient without scram (ATWS) scenario. Revision of the control logic to allow immediate operator control of injection from the Low Pressure Coolant Injection (LPCI) and Core Spray (CS) systems is being reviewed; also, a bypass switch on the isolation valve permissives for both systems was installed. Yet another identified vulnerability at Susquehanna involves a potential waterhammer when the Condensate Transfer System keepfull function is lost after a loss of offsite power or station blackout; a potential resolution under review is to provide an alternate, independent power supply for the condensate transfer pumps.

Among the 17 PWRs (23% of all PWRs) that identified vulnerabilities, identification of the same vulnerability issues was evident among some of these plants. For instance, concerns related to loss of coolant accidents (LOCAs) caused by failure of reactor coolant pump seals, particularly when induced by loss of seal cooling, were identified by Calvert Cliffs, Turkey Point, Fort Calhoun, D.C. Cook, Summer, and Beaver Valley. In these cases, resolution of the issue involved implementation or consideration of alternate cooling capabilities, inclusion in severe accident management guidelines, or consideration of new pump seal materials. Loss of critical switchgear ventilation equipment concerns were raised as vulnerabilities at Calvert Cliffs and Beaver Valley with implementation or consideration of alternate cooling capabilities as the resolution. Auxiliary Feedwater System turbine-driven pump reliability issues were identified at Calvert Cliffs, Summer, Millstone 3, and Kewaunee with corresponding equipment modifications or enhanced operator training identified to resolve these issues. Surry, Kewaunee, and Salem identified significant internal flooding issues as vulnerabilities. These flooding issues were addressed by incorporation of a number of procedural and hardware improvements. Interfacing system LOCA issues were identified at Salem, Kewaunee, Millstone 3, and Beaver Valley with corresponding procedure improvements made or under consideration to address improved valve testing or LOCA identification and isolation. The need to enhance depressurization guidance for the operators during steam generator tube ruptures was identified at Beaver Valley and Calvert Cliffs. Switchover from the injection phase to the recirculation phase of coolant injection was identified as a vulnerability at Summer, Haddam Neck, and Millstone 3. Procedural improvements to give operators more time to perform the switchover and improved operator training were being considered.

The other vulnerabilities among the PWRs tended to be plant-unique and involved such things as inadequate surveillance of specific valves, effects of losses of specific electrical buses, compressed air system failures, battery depletion and the inability to cross-tie buses during loss of power conditions, among other examples. Two IPEs also identified external event related vulnerabilities. Millstone 3 identified a seismic-induced station blackout scenario that is dominated by diesel generator oil cooler anchor bolt failure (subsequently replaced) and Turkey Point was considering revising the procedure for preparing the plant to weather a hurricane.

In summary, 20% of the plants identified vulnerabilities, including 11% of the BWRs and 23% of the PWRs. The identified vulnerabilities at the BWRs showed no commonality but for at least one plant, the identified vulnerabilities could be generic to many BWRs. For the PWR plants, there were some common vulnerabilities identified that focused on particular design aspects. It should be noted that while only a fraction of the submittals actually identified vulnerabilities using their respective definitions, nearly all the plants went on to identify other areas warranting investigation for additional improvements. These other improvements are discussed in the subsequent sections.

Other Plant Improvements

As previously discussed, the major goal of the IPE process was to identify any unique plant vulnerabilities and make any improvements necessary to address these vulnerabilities. It is clear from the submittals, however, that most licensees went beyond this limited intent and identified other improvements (over 500 were identified by the plants) worthy of consideration or implementation, even though no specifically associated vulnerabilities were identified.

Recognizing this fact, a logical question to ask is "what are these other improvements and what are the impacts of the changes that have been implemented or the potential impacts of those improvements being considered for implementation?" To answer this question, the IPE submittals were reviewed to identify and categorize plant improvements explicitly mentioned in the submittals. Based on the submittal documentation, the plant improvements were categorized, to the extent possible, as to two types of information: (1) whether the improvements were already credited in the submittal and implemented, and so are already reflected in the results and insights previously summarized in this paper, and (2) whether the improvement is operational, maintenance-related, or involves design changes. Additionally, the reduction in core damage frequency estimated by the licensee as a result of implementing the improvement was also noted, if available.

The potentially generic (versus plant-unique) nature of the improvements means that they have implications and potential significance for all the plants. For instance, some improvements may be worthy of industry-wide consideration; others may be important to a select group of plants, etc. Hence, as part of the improvement assessments discussed later, the extent to which similar improvements were identified at numerous plants was also identified.

The following discussions summarize the other plant improvements documented in the IPE submittals. In many cases, a few years have past since the submittal date. Hence, some of the planned improvements or those under evaluation may have been implemented (or dropped from consideration) as of the date of this paper.

Assessment of Other Plant Improvements In BWRs

Nearly all the BWR plants made or are evaluating changes to improve AC reliability, improve DC reliability and add to battery operable life under an extended blackout, as well as address other system weaknesses. While the area of improvement was the same, the specific improvements varied considerably. This suggests that there is no *one* specific fix that is right for all plants to lessen the core damage potential due to loss of power. For instance, AC system changes took the form of added or replaced diesel generators, redundant offsite power capabilities and improved recovery potential, and better proceduralized bus cross-tie capabilities. Unique to the BWR 5s and 6s in this area, but not explicitly identified for every BWR 5 or 6, were identified improvements to add flexibility in the use of the High Pressure Core Spray (HPCS) Division III diesel for operating Division I and II loads. A few plants identified specific diesel cooling improvements. One plant identified a service water valve change while a few others indicated that the use of firewater as a backup to diesel cooling was planned or being evaluated. All of these changes were clearly attempting to lessen the potential for AC power loss and so were generally preventive in nature. Likewise, DC system improvements took many different forms and included alternate battery charging capabilities, battery upgrades, additional load shedding, and improving cross-tie capabilities. These changes generally addressed the ability to

maintain at least one train of DC power during loss of AC conditions, which is necessary to operate AC-independent systems and to power instrumentation/indications for providing plant status information to the operator.

Other changes were identified in the IPE submittals which also lessen the vulnerability to station blackout but reduce the core damage potential from other types of accidents as well. Generally, these all provide more reliable core cooling and/or improve the successful use of the AC-independent core cooling systems during prolonged operation. For instance, various isolation condenser improvements were identified for most of the earlier BWR designs. These improvements included better valve reliability, adding procedural guidance for isolation condenser use during an extended blackout, and providing prolonged firewater capability for the shell-side of the isolation condenser during a long station blackout condition. Note that the focus of these improvements was on the cooling system common to all early vintage BWRs that is independent of AC power for operation.

Similarly, improvement considerations were indicated at some plants to ensure better overall reliability and availability of the AC-independent coolant injection systems in the BWR 3s and 4s (HPCI and RCIC). For example, some plants indicated improvements to ensure that these systems were, indeed, AC-independent (e.g., changing a RCIC room exhaust fan from AC-powered to DC-powered). Yet other plants were evaluating further procedural guidance regarding emergency depressurization so that the operator will be less likely to inadvertently lose HPCI and RCIC due to low primary system pressure. A few plants were evaluating improvements so that the operators would be better prepared to replenish the Condensate Storage Tank (CST), the preferred source of water for HPCI and RCIC, if necessary. Some plants also identified improvements regarding the ability to use firewater as a backup to HPCI and RCIC for core injection. All of these improvements address more reliable coolant injection capability and as such, provide better prevention of core damage for a variety of accident classes. While these types of changes were identified in a number of the BWR 3 and 4 design submittals, many were under evaluation and so the extent that these improvements have been implemented can not be determined by simply examining the IPE submittals.

The BWR 5 and 6 designs also identified improvements targeted at the one AC-independent core cooling system in their design; RCIC. In at least two cases, implementation of a bypass of the RCIC high steam tunnel trips was identified as a useful change.

While not prevalent, ventilation improvements were indicated in some IPE submittals. This suggests that the sensitivity to the potential effects of loss of ventilation to rooms containing electrical switchgear, DC system equipment, and core cooling pump systems may be different among plants and is thus more of a plant-specific issue.

Only a few submittals specifically identified improvements for dealing with loss of RHR or ATWS-type scenarios. These involved ensuring the use of the CST for coolant injection pump suction whenever the suppression pool temperature is very high (to avoid loss of pump net positive suction head), automatic inhibiting of the Automatic Depressurization System (ADS) during an ATWS, and the use of an alternate boron injection capability. Such changes clearly are targeting different issues related to either loss of RHR or ATWS accidents. Procedural guidance to use the CST for pump suction improves the long-term operability of coolant injection systems even when the suppression pool temperature is above pump design basis limits. Automatically inhibiting ADS during an ATWS reduces the potential for failing to perform this action when the operator is attempting to respond to a variety of fast-acting symptoms during this class of accident. Use of an alternate boron injection capability is an attempt to further

increase the probability of successful boron injection when it is required. These changes are also preventive in nature in that they are designed to reduce the potential for core damage.

As can be observed from the descriptions provided above, most BWR improvements can be classified as procedure/operation changes (approximately 40%), design/hardware changes (approximately 50%), or both. Few improvements appeared to be maintenance-related changes. Typically, the design or procedural changes indicated an element of revised training in order to properly implement the actual change. Approximately 50% of the BWR improvements were implemented, with about 20% implemented and credited in the IPEs, but many were planned or were under evaluation It should be noted that some of the identified improvements (18% of all the identified BWR improvements and 38% of the ones actually implemented) may have been initiated by other requirements (primarily the station blackout rule) while the remainder was initiated due to the IPE process.

Quantitative values for specific improvements were generally not explicitly reported in the BWR IPE submittals but for some implemented (and IPE credited) changes, specific estimates of reductions in CDFs were provided. Installation of a hardened vent brought about widely varying reductions in CDFs at five plants, ranging from "minor" to 15%. At River Bend, the addition of a portable diesel generator backup for station batteries, together with certain firewater modifications, accomplished an 87% decrease in CDF. AC power improvements that were quantitatively analyzed include adding a gas turbine generator (37% reduction in CDF) and establishing alternate offsite power sources at two different plants (17% and 50% reductions). Aligning a portable diesel generator to supply battery chargers during a station blackout was calculated to reduce the CDF at one plant by 31%. The use of firewater as a vessel injection source was also identified as a possible plant improvement and was evaluated at one plant to reduce the CDF by 13%. A change in the ADS logic to automatically inhibit depressurization during an ATWS was found to reduce the CDF at one plant by 23%. As for maintenance improvements, the addition of a procedure to test the HPCS suction line to the suppression pool was reported at one plant to reduce the CDF by 13%. Operational improvements at BWRs that were quantitatively evaluated included aligning LPCI or CS pumps to the CST (80% reduction in the CDF), load shedding on DC buses during a station blackout (13%), and removal of the ADS inhibit requirement during non-ATWS scenarios (19%). An exceptional CDF reduction of two orders of magnitude was calculated at Hope Creek, due to implementation of a switchgear ventilation recovery procedure. These quantitative impacts clearly indicate the extent to which safety has been improved by making improvements to the plants in response to the IPE requirements.

Assessment of Other Plant Improvements In PWRs

Station blackout and related power issues were addressed by improvements in all types of PWRs; i.e. all vendor plants. The AC system-related improvements took many forms indicating that no *one* single fix was the best for all PWRs. These improvements included the addition or replacement of diesels with emphasis on the addition of swing diesels among units. Many PWRs also highlighted the addition or upgrading of gas turbines to their plants, and cited improved cross-tie capabilities and bus loading changes. There also appeared to be an emphasis on AC equipment room cooling improvements. These included such changes as the addition of temperature alarms, more redundancy in the ventilation systems, and procedural improvements for dealing with loss of ventilation. These improvements generally focused on lessening the chance of a total loss of AC power and so were preventive in nature. Many of the PWR IPEs also cited DC system improvements as beneficial to their plants. These improvements took the form of

DC bus load shedding, battery upgrades, alternate battery charging features, and improved DC bus cross-tie capabilities. Higher DC system reliability and prolonged battery life provide a better ability to cope with a loss of AC power condition by providing power to continue to operate the AC-independent steam-driven Auxiliary Feedwater System (AFWS) pump train and by providing power to instrumentation and indications of plant status to the operator.

A prevalent PWR improvement area involved reactor coolant pump seal LOCAs and related loss of seal cooling issues. These were addressed by identified improvements in the B&W and Westinghouse plants; but notably were *not* identified among the CE plants. The reason for this, based solely on the submittals, is uncertain. These identified improvements typically dealt with alternate seal flow capability, sometimes even under loss of power conditions. The addition of high temperature seals was notably documented in a number of Westinghouse IPE submittals. Hence, dealing with this potential source of primary coolant loss during station blackout as well as during other loss of seal cooling scenarios was generally of importance to PWR plants.

AFWS improvements were identified for many PWRs and most commonly for the Westinghouse plants. These typically included additional backup water supplies such as the firewater system and redundant pump cooling capability. Other reliability and diversity improvements were identified in a few of the plants, including the ability to operate AFWS manually even under loss of DC power. These improvements address the ability to use the one AC-independent core cooling system in PWRs even during loss of DC power, thereby increasing the chances of preventing core damage due to loss of secondary cooling.

Other examples of PWR improvements include procedural and some design improvements for many of the PWRs, particularly the Westinghouse plants, to deal with internal flooding. Specific improvements varied, indicating the plant-specific nature of dealing with flooding issues. Across all the PWRs, there was a scattering of identified changes to deal with steam generator tube ruptures, interfacing system LOCAs, and other miscellaneous system weaknesses. In particular, better procedural guidance for dealing with steam generator tube ruptures and improved testing and valve status checking were cited for lessening the potential for interfacing system LOCAs.

As can be observed from the descriptions above, most PWR improvements can be classified as procedure/operation changes (approximately 50%), design/hardware changes (about 40%), or both. Few improvements appeared to be maintenance-related changes. Typically, the design or procedural changes indicated an element of revised training in order to properly implement the actual change. Forty-five percent of the PWR improvements were identified as implemented, with 30% implemented and credited in the IPEs, but many were planned or were under evaluation Most of the improvements were identified as a result of the IPE process with only a small percentage (12% of all planned or actually implemented improvements) associated with other requirements (primarily the station blackout rule).

Quantitative values for specific improvements were generally not explicitly reported in the PWR IPE submittals but for some implemented (and IPE credited) changes, specific estimates of reductions in CDFs were provided. The addition of one or more diesel generators at five different plants brought about calculated CDF reductions ranging from 21% to 43%. The addition of two gas turbine generators at two different plants resulted in calculated CDF reductions of 43% and 51%. Reactor coolant pump seal cooling improvements at three plants were calculated to reduce CDF by between 14% and 59%. The addition of high temperature seal materials for the reactor coolant pumps was calculated to reduce the CDF by between 2% and 20% by several plants. The addition of an AFWS pump was

identified as potential plant improvements by two plants that resulted in CDF reductions of 7% and 24%. Operational improvements at PWRs included refilling the Reactor Water Storage Tank (83% reduction in the CDF), procedural changes to arrange for alternate cooling sources for charging pumps (25% reduction), and modify an emergency procedure to align the city water supply to the AFWS pumps upon failure of the CST supply (32% reduction). Maintenance improvements included staggering safety injection system pump testing (3% reduction in CDF) and revised maintenance practices on switchgear room ventilation system chillers (11% reduction). Even considering typical uncertainties of PRA results, reductions of this magnitude represent quantitatively important reductions in the potential for plant damage. The largest such reductions were not in any one single area; but instead involved improvements in the areas of internal flooding, loss of ventilation to AFWS, and reactor coolant pump seal cooling for particular plants.

Summary

Using various definitions for "vulnerability," about 20% of the licensees explicitly identified vulnerabilities in the IPE submittals. Note that, while only a fraction of the submittals actually identified vulnerabilities, nearly all of the plants went on to identify other areas warranting investigation for potential improvements. The IPE program served as a catalyst for further improving the overall safety of nuclear power plants, as a result of numerous other improvements either implemented, planned, or under evaluation. This additional product of the IPE Program is a very important element in measuring the success of the IPE program. Meaningful and cost-effective equipment and procedural changes to the plants have been a benefit to the overall safety of the industry and may not have occurred without implementation of the IPE process, with its inherent, systematic analysis of plant safety.

The licensees of 11% of the BWRs explicitly stated that their plants had vulnerabilities. Although no common vulnerabilities were identified, some of the vulnerabilities could be considered generic to many BWRs. These vulnerabilities involved HPCI suction transfer, HPCI and RCIC high turbine exhaust pressure trips, low pressure injection system valve permissives and control logic, and potential waterhammer issues following a loss of offsite power.

Among the 23% of PWRs that identified vulnerabilities, certain vulnerability issues were common among more than one plant. These included concerns related to reactor coolant pump seal LOCAs, AFWS turbine-driven pump reliability issues, interfacing system LOCA issues, internal flooding issues, switchover from the coolant injection phase to the coolant recirculation phase, loss of critical switchgear ventilation equipment, and the need to enhance operator guidance for depressurization during steam generator tube ruptures. Other vulnerabilities among the PWRs tended to be plant-unique, involving such things as inadequate surveillance of specific valves, losses of specific electrical buses, compressed air system failures, battery depletion, and the inability to cross-tie buses during loss-of-power conditions, among others, some of which were quite unique.

As for other plant improvements not specifically associated with explicitly identified plant vulnerabilities, many were generic in nature with the most often-cited plant improvements for BWRs involving station blackout and the PWR improvements tending to address both loss of power and loss of reactor coolant pump seal cooling. Both types of plants often identified changes aimed at improving core cooling or injection reliability, particularly for those systems or portions thereof that can operate during loss of AC power. PWRs notably more often identified improvements to

address internal flooding and interfacing system LOCAs, than did the BWRs. Other less-cited and plant-specific improvements were identified to address a number of other accident class issues at individual plants. Most improvements tended to be procedural or hardware-oriented (as opposed to maintenance-related) and a few appear to have quantifiably significant effects on the CDF for particular plants. Based on the number and variety of other plant improvements implemented, planned, or under evaluation at the time of the submittals, it is apparent that the level of awareness of the potential for severe accidents has increased at many of the nuclear utilities. The extent and specificity of the improvements shows an understanding of plant design and operational characteristics where specific improvements may be warranted.

References

[1]"Individual Plant Examination for Severe Accident Vulnerabilities," Generic Letter 88-20, U.S. Nuclear Regulatory Commission, Washington, DC, November 23, 1988.

[2]"Individual Plant Examination: Submittal Guidance," NUREG-1335, U.S. Nuclear Regulatory Commission, Washington, DC, August, 1989.

[3]"Severe Accident Issue Closure Guidelines," NUMARC 91-04, January 1992.

[4]"Safety Goals for the Operations of Nuclear Power Plants: Policy Statement," Title 10 CFR, Federal Register, August 4, 1988.

IPE RESULTS AS COMPARED WITH NUREG-1150*

W.T. Pratt
John Lehner
Brookhaven National Laboratory
Upton, NY 11973

A. Camp
Sandia National Laboratory
Albuqurque, NM 87185

E. Chow
U.S. Nuclear Regulatory Commission
Rockville, MD 20852

ABSTRACT

In 1990, the NRC published NUREG-1150 which assessed the risks for five U.S. nuclear power plants. This paper provides a comparison of the results and perspectives obtained from the NUREG-1150 study to those obtained form the Individual Plant Examination (IPE) program. Specifically, results and perspectives on core damage frequency and containment performance are compared.

BACKGROUND

In 1990 the NRC published NUREG-1150 (Ref. 1), which assessed the risks for five U.S. nuclear power plants:

- Unit 1 of Surry Power Station, a Westinghouse-designed three-loop reactor in a subatmospheric containment building; [also evaluated in WASH-1400 (Ref. 2)]
- Unit 1 of the Zion Nuclear Plant, a Westinghouse-designed three-loop reactor in a large, dry containment;
- Unit 1 of the Sequoyah Nuclear Power Plant, a Westinghouse-designed four-loop reactor in an ice condenser containment building;

*This work was performed under the auspices of the U.S. Nuclear Regulatory Commission.

- Unit 2 of the Peach Bottom Atomic Power Station, a General Electric-designed BWR-4 reactor in a Mark I containment building (also evaluated in WASH-1400);

- Unit 1 of the Grand Gulf Nuclear Station, a General Electric-designed BWR-6 reactor in a Mark III containment building.

While the NUREG-1150 plants represent a spectrum of designs, they do not cover all vendors and do not represent a large enough sample to be considered representative of the industry.

On August 8, 1985, the Nuclear Regulatory Commission (NRC) issued a Policy Statement on Severe Accidents regarding Future Designs and Existing Plants (50 FR 32138) that introduced the Commission's plan to address severe accident issues for existing commercial nuclear power plants. In this Policy Statement, the Commission addressed its plan to formulate an approach for a systematic safety examination of existing plants to study particular accident vulnerabilities and desirable cost-effective changes to ensure that there is no undue risk to public health and safety. To implement this plan, NRC issued Generic Letter 88-20 (Ref. 3) in November 1988 requesting that all licensees perform an Individual Plant Examination (IPE) to identify any plant-specific vulnerabilities to severe accidents, and to report the results to the Commission. Most licensees performed a level 1 and 2 PRA in response to the generic letter and reported core damage frequency (CDF) and accident progression results to the Commission. In this paper, the CDF and accident progression results reported in NUREG-1150 are compared with IPE results for comparable reactor and containment designs. The perspectives obtained from NUREG-1150 and the IPEs are also compared.

Core Damage Frequency Results

Figure 1 shows the NUREG-1150 CDF results compared to the IPE results. In the NUREG-1150 analyses, an uncertainty distribution was calculated for each of the five plants. For those five plants, the lower and upper extremities of the bars in Figure 1 represent the 5th and 95th percentiles of the distributions, with the mean value of each distribution also shown. More detailed descriptions of the shapes of the distributions can be found in NUREG-1150. As can be seen in Figure 1, the NUREG-1150 CDF results fall within the range of the IPE CDF results.

Figure 1 shows that the range between the 5th and 95th percentiles covers from one to two orders of magnitude for the five NUREG-1150 plants. When comparing the NUREG-1150 results to the IPE results, the reader should remember that the IPE results reflect a mix of means and point estimates. Uncertainty distributions are not shown here for the IPEs, as they are not available in many cases. However, when uncertainties have been provided, their range is consistent with the NUREG-1150 distributions. The uncertainty ranges do make it clear that undue weight should not be put on small differences among the results. Based upon Figure 1, the overall NUREG-1150 and IPE results are reasonably consistent.

Figure 2 shows the results broken down for PWRs and BWRs. The average CDFs for Surry, Sequoyah, and Zion fall within the range of PWR IPE values. Note that two values are presented for Zion in NUREG-1150, with the second, lower value reflecting some plant changes as of October 1990. Likewise, the Peach Bottom and Grand

Gulf average CDFs fall within the range of BWR IPE values. Figure 3 further shows the NUREG-1150 results compared to particular IPE plant groupings. In each case the differences are within the range expected, given that there are many plant-specific design differences and PRA modeling differences.

Both NUREG-1150 and the IPEs have shown that the relative contributions of accident sequences to the CDF are plant specific. Therefore the accident sequence which dominates in one plant may not be dominant in another. However, Figures 4 and 5 show that the mix of contributors is consistent with the results found in NUREG-1150. That is, for the PWRs, station blackout, transients and loss-of-coolant-accidents (LOCAs) tend to be important contributors, while for the BWRs, station blackout and transients tend to be the most important, with lesser contributions from anticipated transients without scram (ATWS) and LOCAs. Internal flooding was examined only for the Surry and Peach Bottom plants in NUREG-1150 and was not found to be important. Internal flooding is a significant contributor for a few of the IPEs. At a more detailed level, the specific failures leading to core damage sequences are plant-specific and cannot be easily compared between NUREG-1150 and the IPEs.

Accident Progression Results

After evaluating the accident sequences leading to core damage and calculating the CDF, both the NUREG-1150 and IPE programs evaluated the ability of the containments to prevent the release of radioactivity. The five containment types included in the NUREG-1150 study are compared with IPE results for similar containment designs. The only exception is the IPE results for BWRs with Mark II containments. This containment design was not included in NUREG-1150 and therefore could not be compared with the IPE results for Mark II containments.

Figures 6 and 7 show the probability of early containment failure conditional on core damage obtained in NUREG-1150 compared to the IPE results. These probabilities include events that cause structural failure of containment and also isolation failure. Accidents that cause containment bypass (such as interfacing systems LOCA and steam generator tube rupture) are not included in these figures. However, the frequency of these events is combined with the frequency of early containment failure for the results presented in Figures 8 and 9.

In the NUREG-1150 analyses, uncertainty distributions were calculated for the containment failure and bypass estimates. Therefore, for the five NUREG-1150 plants the 5th and 95th percentiles and the means of the distribution are shown in the figures. As can be seen in the figures, the NUREG-1150 results (mean values) fall within the range of the IPE results for each containment type. However, the ranges between the 5th and 95th percentiles for some of the NUREG-1150 results are quite wide (from two to three orders of magnitude) and span the IPE results.

Figures 6 and 7 provide a comparison of the NUREG-1150 results for the conditional probability of an early failure for each containment type evaluated in NUREG-1150 with those calculated in the IPEs. NUREG-1150 found that the conditional probability of early failure is significantly lower for PWRs with large volume and subatmospheric containments than for PWRs and BWRs with pressure suppression containments. This trend is not as apparent in the IPE results. The conditional probability of early failure for large volume containments in the IPEs varies from 0.002 to 0.33 with an average value of 0.05 and for subatmospheric containments from

0.004 to 0.25 with an average of 0.1. These results can be compared with the conditional probabilities of early containment failure for ice condenser containments, which vary from 0.005 to 0.05 with an average value of 0.01, and for BWR containments, which vary from about 0.01 to 0.63 with an average of 0.26.

The IPE results do indicate that BWR containments generally have higher conditional probabilities for early failure than for PWR plants but there is significant variability in the results. For example, there are several IPEs with Mark I containments that have extremely low early failure probabilities. These low probabilities are in some cases caused by modeling assumptions (neglecting liner melt-through) or by plant specific features (sumps or curbs that physically prevent liner melt-through). Conversely there are PWRs with large dry containments that have relatively high early failure probabilities. These higher probabilities are also caused by modeling assumptions (e.g., containment failure pressure) and by plant specific features (e.g., the sump and recirculation piping in the Palisades plant) not found in other large dry containment designs. The greater variation in the IPE results was expected because a much larger number of plants were analyzed using a wider range of modeling assumption than in the NUREG-1150 study.

Figures 8 and 9 provide a comparison of the NUREG-1150 and IPE results for the frequency (per reactor year) of a severe accident with early containment failure or bypass. The NUREG-1150 results show that on the basis of absolute frequency, early containment failure or bypass for the BWR designs analyzed are similar (the means are within 1E-6/ry to 6E-6/ry) to that of the PWRs. The reason for this result is that the core damage frequencies were found to be lower for the BWRs than for the PWRs studied in NUREG-1150. Therefore, although the conditional probabilities of early failure were higher for BWRs this was compensated for by the lower CDF. The average IPE frequencies are similar to the NUREG-1150 values but individual plant results vary significantly. The frequency of early failure and bypass for the PWR IPEs varied from about 7E-8/ry to 6E-5/ry with an average of 9E-6/ry and BWR IPEs varied from about 3E-7/ry to 3E-5/ry with an average of 6E-6/ry.

In general the events that contribute to the IPE frequencies in Figures 8 and 9 are similar to those that contributed in the NUREG-1150 study. For example, direct containment heating is an important failure mode for PWRs with large dry and subatmospheric containments, hydrogen combustion is important for PWR ice condensers and BWR Mark III containments, and liner melt-through is important for BWR Mark I containments. In addition, accidents that bypass containment are significant contributors to the frequencies shown in Figure 8 for some PWR plants. However, both studies have shown that the relative contributions of the various containment failure modes vary between plants and depend on plant specific features and modeling assumptions.

Core Damage Frequency Perspectives

NUREG-1150 provided general perspectives for BWRs and PWRs based on the five plants included in that study. The perspectives derived from NUREG-1150 are compared with those obtained from the IPE results below. The approach adopted is to summarize a NUREG-1150 perspective and then determine whether or not the IPE results support those findings.

NUREG-1150 Perspective: BWRs tend to have lower CDFs than PWRs

BWRs tend to have internal event core damage frequency distributions that are lower than those of PWRs, although this finding is less pronounced for the IPEs. Figure 2 shows that there is overlap between the PWR and BWR CDFs in the IPEs. There are several reasons why the BWR CDFs tend to be lower than the PWR CDFs. The LOCA sequences, often significant in the PWR core damage frequencies, are usually minor contributors in the case of the BWRs. This is not surprising, since most BWRs have many more systems than PWRs for injecting water directly into the reactor coolant system to provide makeup. Further, BWRs can more easily depressurize to use low pressure systems. PWRs have highly reliable emergency core cooling (ECC) systems, but with less redundancy and diversity than BWRs. PWRs generally have one high-pressure and one low-pressure ECC system (both multitrain), plus a set of accumulators. For many types of transient events, BWRs also tend to have more systems that can provide decay heat removal than PWRs. For transient events that lead to loss of water inventory due to stuck-open relief valves or primary system leakage, BWRs have numerous systems to provide makeup. PWRs usually have somewhat higher station blackout frequencies, because, unlike BWRs, if AC power is lost they have no systems to inject directly into the reactor coolant system to provide makeup in the case of system leakage from stuck-open relief valves or seal leaks.

NUREG-1150 Perspective: Support systems are crucial to the CDF

For both BWRs and PWRs, the reliability of the support systems is quite important in determining the CDF. These systems include electric power, service water, instrument air, HVAC, and other systems that support the frontline emergency core cooling systems. Because the design of these support systems varies considerably among plants, caution must be exercised when making statements about generic classes of plants, such as PWR versus BWR. Both types of plants have sufficient redundancy and diversity so as to make multiple independent failures unlikely. Support system failures introduce dependencies among the systems and thus can become dominant for both types of plants. For example, the interdependencies introduced by the support systems can override the higher redundancy of the BWR ECCS. Several of the perspectives below result from support system vulnerabilities.

NUREG-1150 Perspective: Operator recovery actions significantly reduce the CDFs

Recovery actions range from simple actions such as manually opening a valve to complex actions such as providing injection from nonsafety systems. The NUREG-1150 PRAs and the IPEs have taken extensive credit for operator recovery actions. Improvements in emergency operating procedures over the past several years are responsible for increased reliability of the operators and identification of additional actions that they can take. The move to symptom-based procedures during the 1980s has been a very positive step. While there is considerable variability among the plants concerning the effectiveness of particular recovery actions, the overall impact is positive.

NUREG-1150 Perspective: Properly designed crossties between systems can substantially decrease the core damage frequency

Many plants can crosstie at least a few important systems. Crossties allow failures within systems to be circumvented. The crossties can be fairly simple connections among parallel trains of a system or complex connections among different units of a multiunit site. Crossties typically involve systems such as electric power, auxiliary feedwater, service water, and various water storage tanks. These crossties have lowered the CDF at many plants. Since there is a potential for incorrect cross connecting, proper administrative control is very important.

NUREG-1150 Perspective: Station blackout is important at both PWRs and BWRs

Station blackout events are usually important at both PWRs and BWRs. On average, station blackout accidents contribute a higher percentage of the core damage frequency for the BWRs. However, when viewed on an absolute scale, station blackout tends to have a higher frequency at the PWRs than at the BWRs. To some extent this is due to design differences between BWRs and PWRs leading to different susceptibilities. For example, in station blackout accidents, Westinghouse PWRs are potentially vulnerable to reactor coolant pump seal LOCAs following loss of seal cooling, leading to loss of inventory with no method for providing makeup. BWRs, on the other hand, have at least one injection system that does not require ac power. While important, it would be incorrect to imply that the differences noted above are the only considerations that drive the variations in the core damage frequency. Probably more important is the electric power system design at each plant, which is largely independent of the plant type.

NUREG-1150 Perspective: Containment venting can reduce CDF at BWRs

Unlike most PWRs, the response of containment is often a key in determining the core damage frequency for BWRs. For example, in Mark I containments, there are a number of ways in which containment conditions can affect coolant injection systems. High pressure in containment can lead to closure of primary system relief valves, thus failing low pressure injection systems, and can also lead to failure of steam-driven high-pressure injection systems due to high turbine exhaust back pressure. High suppression pool temperatures can also lead to the failure of systems that are recirculating water from the suppression pool to the reactor coolant system. If the containment ultimately fails, certain systems can fail because of the loss of net positive suction head in the suppression pool, and also the reactor building is subjected to a harsh steam environment that can lead to failure of equipment located there. Venting the containment can reduce or eliminate many of the above concerns. NUREG-1150 examined the effect of containment venting on the core damage frequency at Peach Bottom which has a Mark I containment. Assuming the containment venting system was not available, the point estimate of the core damage frequency increased by a factor 2.6. Many of the BWR IPEs have taken credit for containment venting.

NUREG-1150 Perspective: Loss of service water or component cooling water can be dominant at PWRs

For the NUREG-1150 Zion analysis and many of the PWR IPEs, it was assessed that component cooling water is needed for operation of the charging and high-pressure safety injection pumps. Loss of component cooling water (or loss of service water, which will also render component cooling water inoperative) will result in loss of these high-pressure systems. This can further lead to loss of cooling to reactor coolant pump seals, resulting in leakage from the reactor coolant system without the capability to inject high-pressure makeup into the primary system. Thus, loss of component cooling water or service water can both cause a small LOCA and disable the systems needed to mitigate it. Seal leakage tends to be more of an issue for Westinghouse plants, although the problem is not confined solely to those plants. New seals, which are already being implemented at some plants will considerably reduce the likelihood of significant leakage.

NUREG-1150 Perspective: Feed and bleed cooling is an important safety strategy at many PWRs

Feed and bleed cooling substantially reduces the CDF at many PWRs. It represents an alternative method for decay heat removal in transients involving a total loss of feedwater. Successful feed and bleed cooling requires either opening at least one PORV or, at some plants, using high pressure pumps that can lift the safety relief valves. Therefore, it is important to keep power-operated relief valves unblocked at many PWRs. At some plants, chronic problems with PORV leakage leads to operation with the associated block valves closed. Opening these block valves requires operator action and is prevented by loss of power or hardware failures in certain scenarios. This reduces the availability of decay heat removal via feed and bleed cooling.

NUREG-1150 Perspective: Switchover to recirculation is important to LOCA CDFs at PWRs

There is substantial variation among the PWR LOCA CDFs. A significant part of this variation is driven by plant-specific aspects of the switchover to recirculation in the later stages of a LOCA. For example, NUREG-1150 found higher LOCA CDFs for Sequoyah than the other plants due to three factors: (1) a low containment spray setpoint that resulted in early spray actuation for small LOCAs (the sprays take suction from the refueling water storage tank which is also supplying makeup to the reactor coolant system), (2) a relatively small refueling water storage tank, and (3) manual switchover to recirculation. Other PWRs with some or all of these features tend to have the highest LOCA CDFs.

Accident Progression Perspectives

A similar approach is adopted in this section. First the NUREG-1150 perspective is summarized and then it is determined whether or not the IPE results support the finding.

NUREG-1150 Perspective: Large dry and subatmospheric containments are highly likely to maintain integrity during a severe accident

The NUREG-1150 results for the Zion and Surry Plants indicate that large dry and subatmospheric containment designs appear to be quite robust in their ability to contain severe accident loads. This study shows a high

likelihood of maintaining integrity throughout the early phases of severe accidents in which the potential for large release of radionuclides is greatest. The predicted likelihood of early containment failure in the Zion (large volume containment) plant and the Surry (subatmospheric containment) plant in NUREG-1150 are quite small (mean value of about 0.01). The principal mechanisms leading to these failures are loads resulting from high-pressure melt ejection in accident sequences with high reactor coolant system (RCS) pressures (at time of vessel breach) and in-vessel steam explosions in sequences with low RCS pressure at vessel breach. The uncertainties in describing the magnitude of severe accident loads at vessel breach for pressurized scenarios and the likelihood of depressurization prior to lower head failure are large, however. The principal reason that the probability of early containment failure from loads at vessel breach is so small in the NUREG-1150 Surry and Zion analyses is that the reactor coolant system is not likely to be at high pressure when vessel meltthrough occurs. Some of the mechanisms that were found to be effective in depressurizing the vessel are hot leg or surge line failure at elevated temperature, failure of a reactor coolant pump seal, or a stuck-open relief valve.

Generally, the IPE results for large dry and subatmospheric containments indicate probabilities of early containment failure that are higher than those calculated in NUREG-1150. The IPE average early failure probabilities are 0.05 for large dry containments and 0.1 for subatmospheric containments with some individual plant results above 0.3. The higher probabilities of early containment failure for the IPEs are caused in some cases by plant specific features and in other cases by modeling assumptions. For example, the highest early failure probability (0.33) in Figure 6 is for the Palisades plant and it reflects a containment failure mode that is unique to Palisades. The postulated failure mode assumes that molten core debris from the reactor cavity flows into the sump and subsequently into recirculation piping. The debris is assumed to meltthrough the pipe wall and enter the Auxiliary Building. This failure mode was not identified in other PWRs with large volume or subatmospheric containment.

NUREG-1150 Perspective: The likelihood of early containment failure is higher for ice condenser designs than for large dry and subatmospheric designs

The NUREG-1150 results for the Sequoyah plant indicate that the likelihood of early failure during a severe accident for the Sequoyah plant is higher (0.065) than for the large dry and subatmospheric designs, but is less than for the BWRs analyzed. Early failure is primarily associated with loads introduced at the time of vessel breach. Containment rupture from high overpressure loads at the time of vessel breach is likely to result in significant damage to the containment wall and subsequent bypass of the ice bed. The IPE results indicate that in general ice condenser containments have lower probabilities for early failure than large dry and subatmospheric designs. The average of the IPE early failure probabilities is 0.02 for ice condenser containments compared with 0.05 for large dry and 0.1 for subatmospheric designs. Although the differences in the average values for the various designs are less than a factor of five the IPE results for ice condenser containments are lower than might have been expected based on NUREG-1150. All of the failures modes (direct containment heating, hydrogen combustion, in-vessel steam explosions and direct contract of the core debris with the container wall) found important in the NUREG-1150 Sequoyah analysis were considered in the IPEs but judged to have lower probabilities. In some cases these lower probabilities were derived from modeling assumptions in other cases accident sequence and plant specific features (flooded cavity, ice remaining, etc.) were used to justify the results.

NUREG-1150 Perspective: There is a substantial likelihood for early failure in BWR Mark I containments as a result of direct attack of the drywell shell by molten core debris

This failure mode was found to be the dominant failure mechanism in the NUREG-1150 Peach Bottom (Mark I containment) study. However, at the time Generic Letter 88.20 (Ref. 3) was issued there was considerable uncertainty regarding the likelihood of failure of the drywell as a result of this mechanism. The utilities were therefore given the option of not addressing it in their IPEs. However, most utilities did include consideration of liner meltthrough. For those utilities that did consider this failure mechanism, a significant potential was found for early drywell failure (as shown in Figure .7). In those submittals that did not consider liner meltthrough, the potential for early containment failure was generally found to be quite low. In some IPEs, this failure mechanism was eliminated because of plant specific features (such as large sumps or the presence of curbs).

NUREG-1150 Perspective: Venting can eliminate some sequences that would otherwise result in gradual overpressure failure of Mark I containments

The principal benefit of wetwell venting indicated by the NUREG-1150 Peach Bottom study is in the reduction of the core damage frequency. In many BWR IPEs the CDF was also reduced by taking credit for containment venting. Although the NUREG-1150 study found that venting is not effective in eliminating some early drywell failure mechanisms, venting could eliminate other sequences that would otherwise have resulted in gradual overpressure failure of the containment. Therefore, venting was found to lower the likelihood of late containment failure in NUREG-1150. In general, most IPE results for Mark I containments also include late containment venting as a way of preventing late containment failure. However, in at least one submittal early drywell venting is a predominant venting mode. In these plants early drywell venting accompanies a containment flooding procedure.

NUREG-1150 Perspective: Hydrogen deflagration is the principal mechanism for early containment failure in BWR Mark III containments

In NUREG-1150 the Grand Gulf containment was predicted to fail at or before vessel breach in a substantial fraction (0.4) of severe accident sequences. Hydrogen deflagration was found to be the principal mechanism for early containment failure in NUREG-1150. The IPE results indicate that energetic events at the time of vessel breach including hydrogen combustion are the principal causes of early containment failure. However, the conditional probabilities of early failure in the IPEs were less (0.005-0.25) than the NUREG-1150 value (0.4). The IPEs also found energetic events at the time the core debris penetrates the reactor vessel as important contributors to the probabilities of early failure. However, these events were again judged to have lower probabilities in the IPEs than in NUREG-1150. The differences seem to be largely driven by modeling assumptions (magnitude of pressure loading, failure pressure of containment, etc.) and by the high reliability associated with the hydrogen ignition systems in the IPEs.

NUREG-1150 Perspective: Venting was not found effective in preventing containment failure for accident scenarios involving core damage in Mark III containments

In the NUREG-1150 Grand Gulf study accidents involving station blackout (SBO) were found to dominate the core damage frequency. Containment venting was considered unlikely for SBO accidents and therefore it was not found to be particularly effective at Grand Gulf. However, in the Grand Gulf IPE venting of the primary system using the Main Steam Isolation Valves (MSIVs) was a significant contributor to the probability of loss of early containment integrity. In other IPEs venting was also found to be a significant contributor to loss of containment integrity but late in an accident sequence.

NUREG-1150 Perspective: If core damage is arrested invessel, the likelihood of containment failure is small for all containment types

The potential was found in NUREG-1150 for the arrest of core degradation within the reactor vessel as the result of recovery procedures (such as in the TMI-2 accident) in a significant fraction of core damage scenarios. The likelihood of containment failure is very small in these scenarios. The potential for arrest of in-vessel core degradation was not considered for all of the IPE submittals. However, for those IPEs that did consider this effect the impact on the accident progression results was significant. The IPE results also indicate that if the core is retained in the reactor vessel then the likelihood of containment failure is very small.

NUREG-1150 Perspective: Containment bypass events represent a large fraction of high consequence accidents for PWR containments

NUREG-1150 results indicate that containment bypass sequences (severe accidents initiated by steam generator tube ruptures, tube ruptures induced by hot circulating gases, or interfacing systems LOCAs) represent a substantial fraction of high consequence accidents. The absolute frequency of these types of failure were however found to be small (about 5E-6/ry) in NUREG-1150. The IPE results also found that these types of events have a relatively low frequency (the average of the PWR IPE result is very similar to the NUREG-1150 values). Bypass events were also found to be significant contributors to the frequency of early containment failure and bypass in the IPE submittals. In fact, some of the highest frequencies (1E-5/ry) in Figure 8 are dominated by bypass accident frequencies.

SUMMARY

Results and perspectives reported in NUREG-1150 for five nuclear power plants have been compared with the IPE results and perspectives for similar reactor and containment designs. The results and perspectives obtained from the two studies are generally similar. However, there are a number of notable differences. These differences are caused in some cases by plant specific features and in others by modeling assumptions.

REFERENCES

1. U.S. Nuclear Regulatory Commission (USNRC), "Severe Accident Risks: An Assessment for Five U.S. Nuclear Power Plants," NUREG-1150, December 1990.

2. USNRC, "Reactor Safety Study - An Assessment of Accident Risks in U.S. Commercial Nuclear Power Plants," WASH-1400 (NUREG-75/014), October 1975.

3. USNRC, "IPE for Severe Accident Vulnerabilities," Generic Letter No. 88-20, 1989.

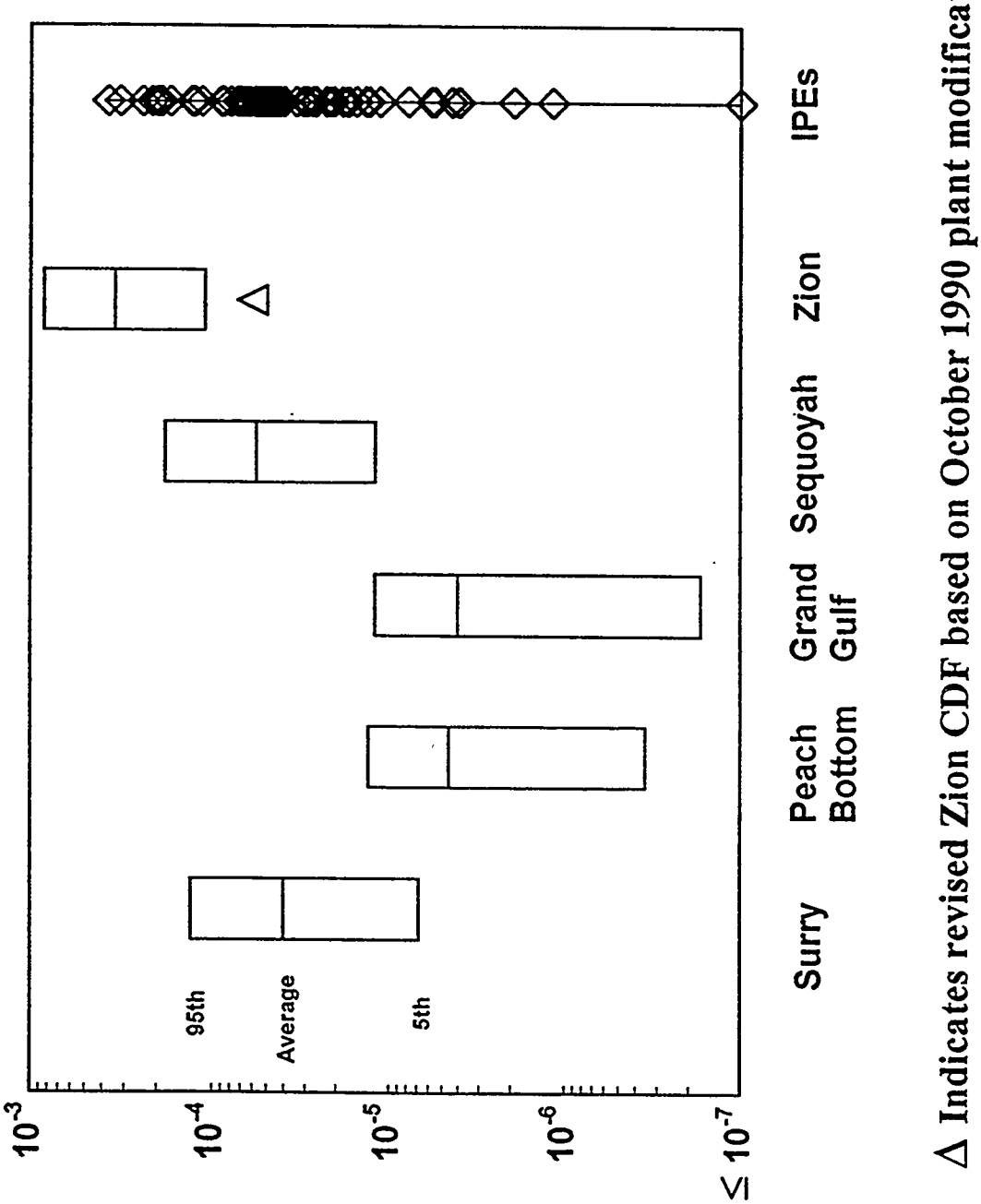

Figure 1 Comparison of NUREG-1150 and IPE CDFs

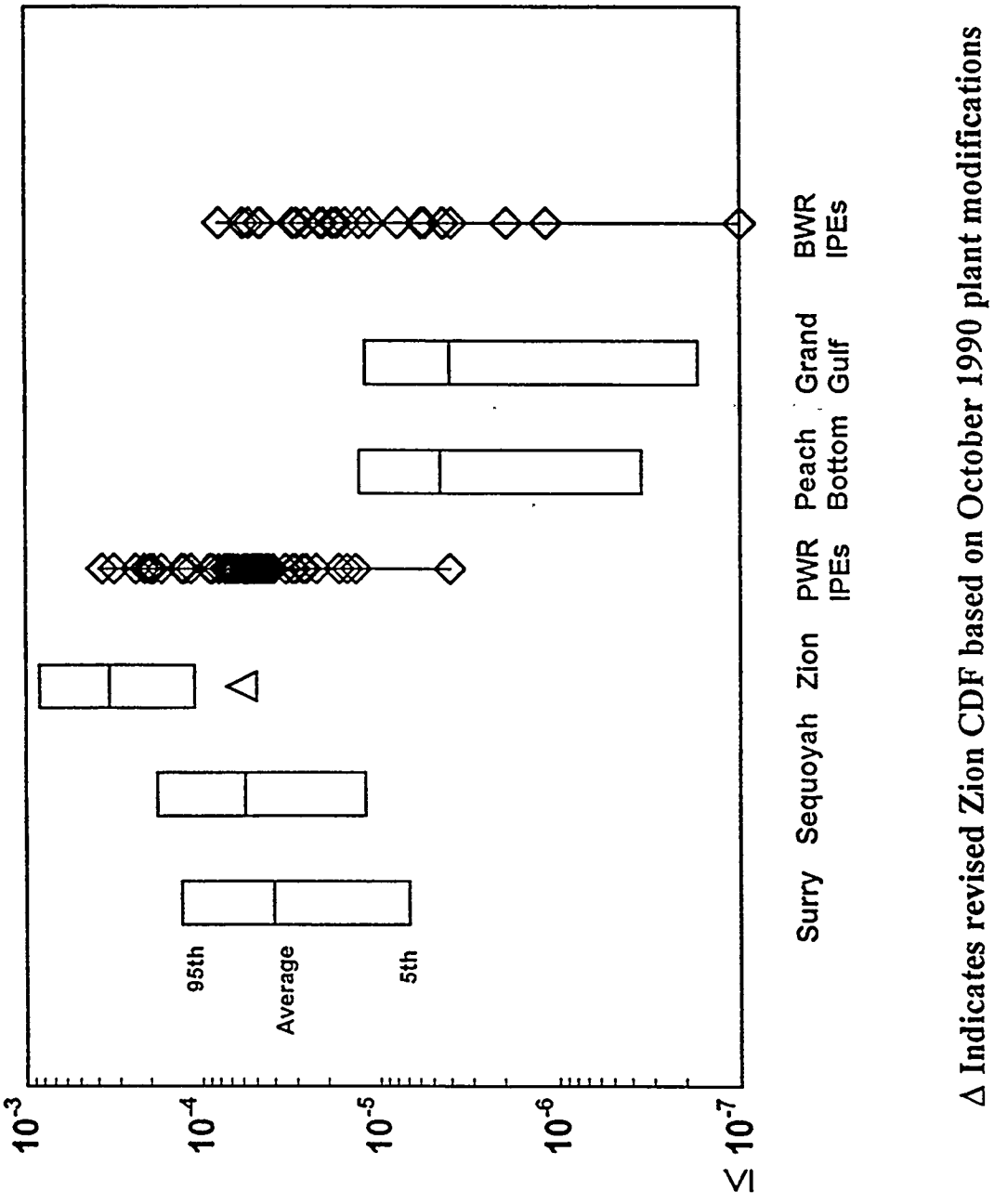

Figure 2 Comparison of NUREG-1150 and IPE CDFs for PWRs and BWRs

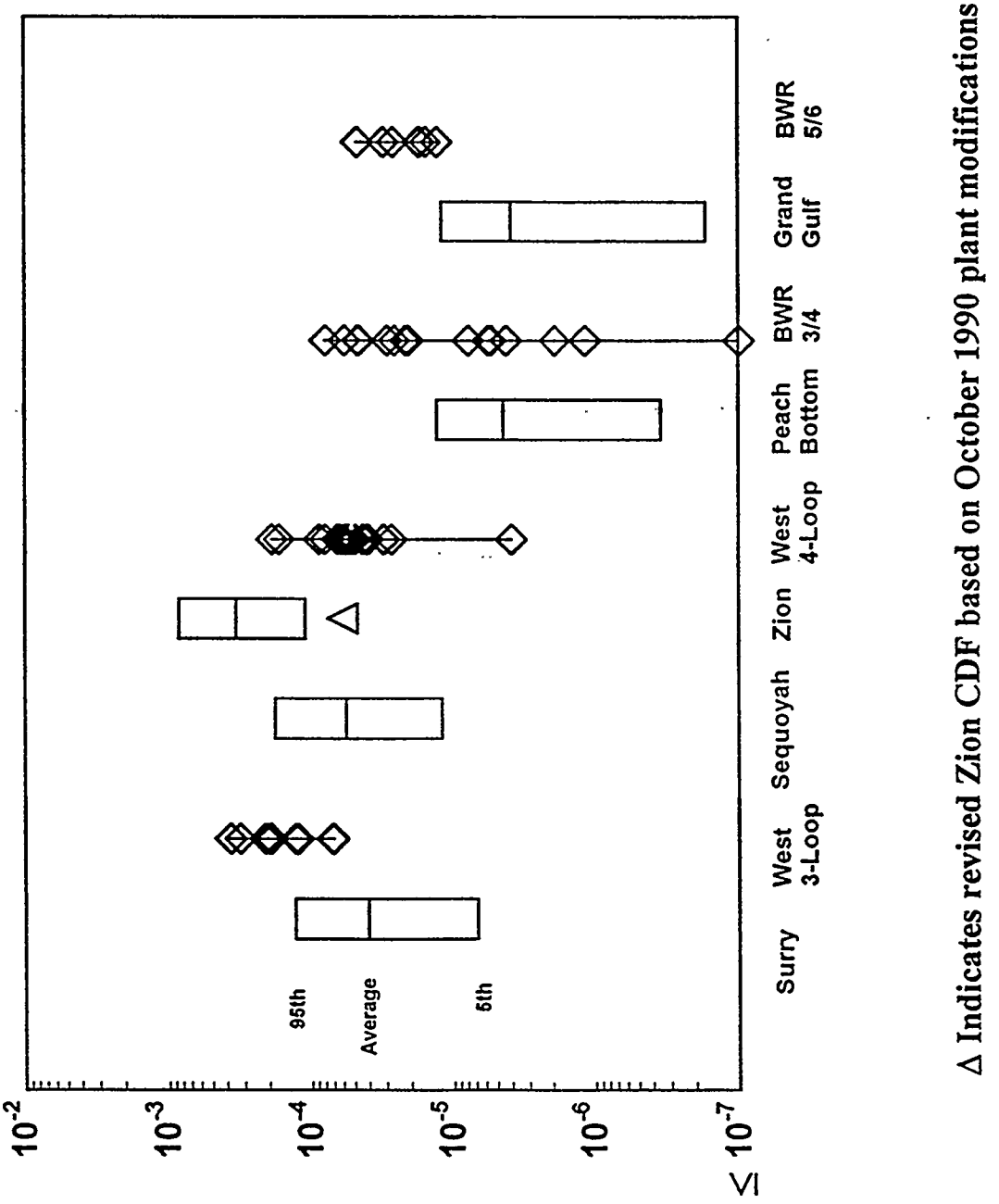

Figure 3 Comparison of NUREG-1150 and IPE CDFs for Selected Plant Types

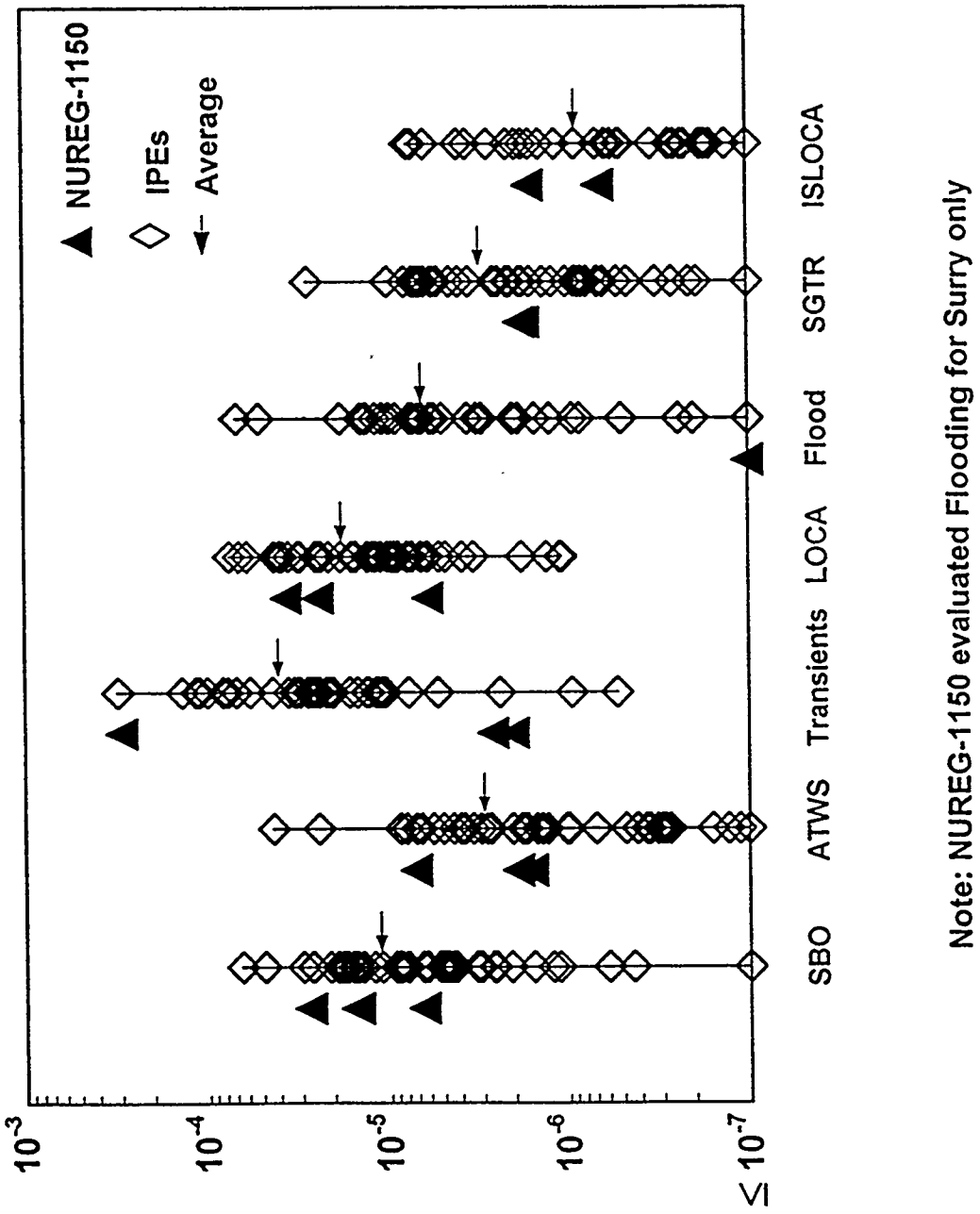

Figure 4 Comparison of NUREG-1150 and IPE PWR Dominant Contributors

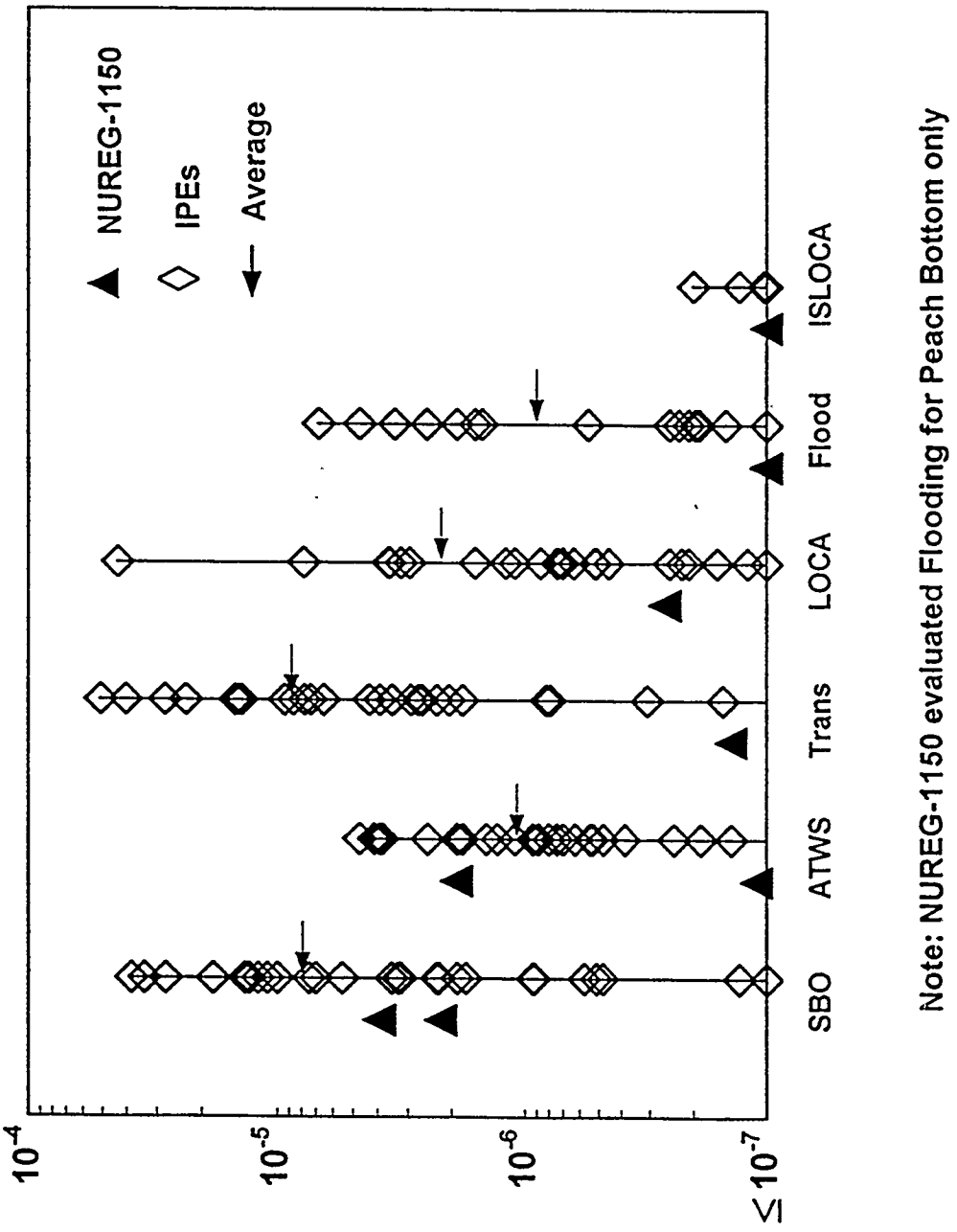

Figure 5 Comparison of NUREG-1150 and IPE BWR Dominant Contributors

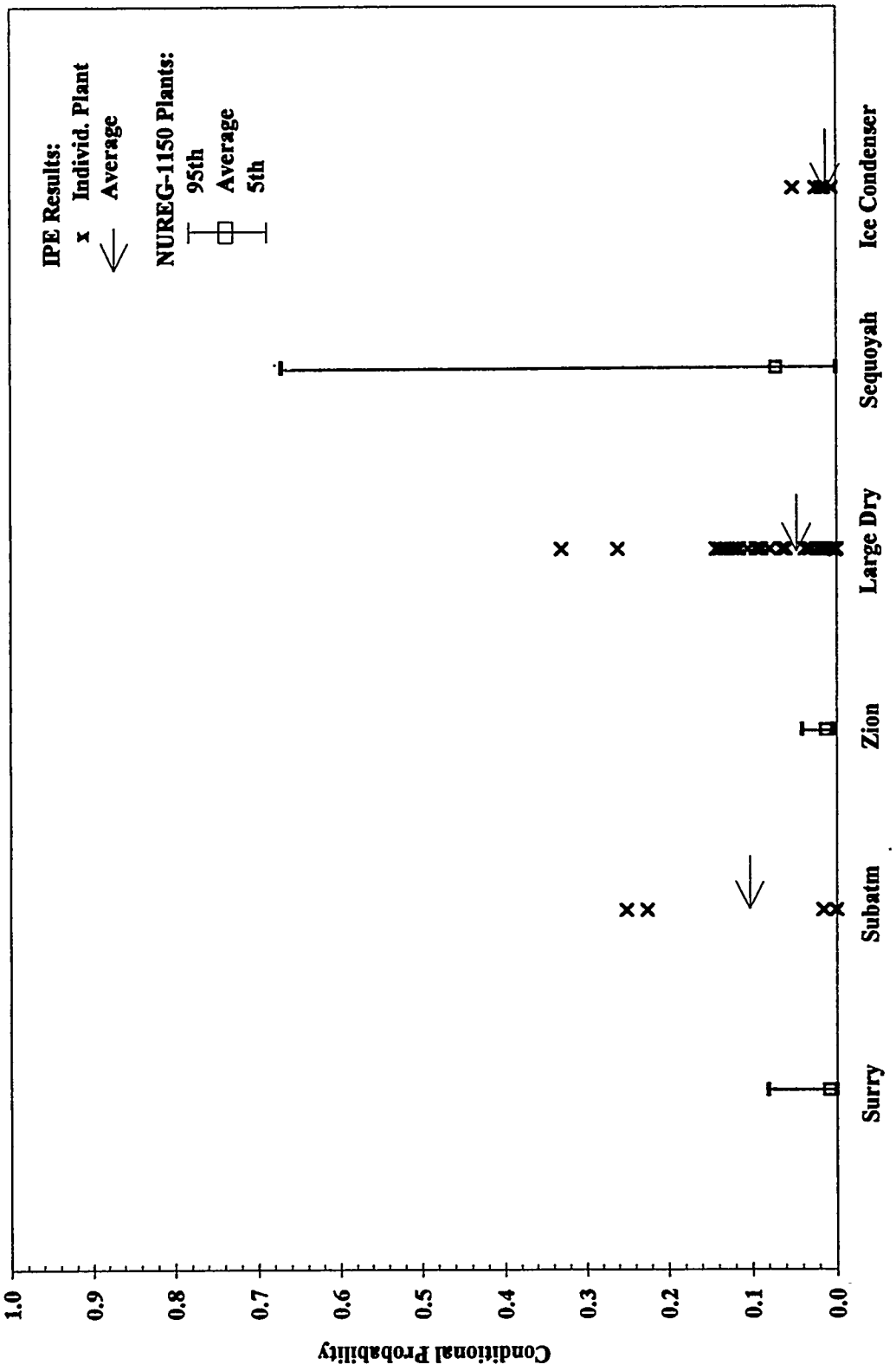

Figure 6 Comparison of NUREG-1150 and IPE Conditional Probabilities for Early Containment Failure for PWR Plants

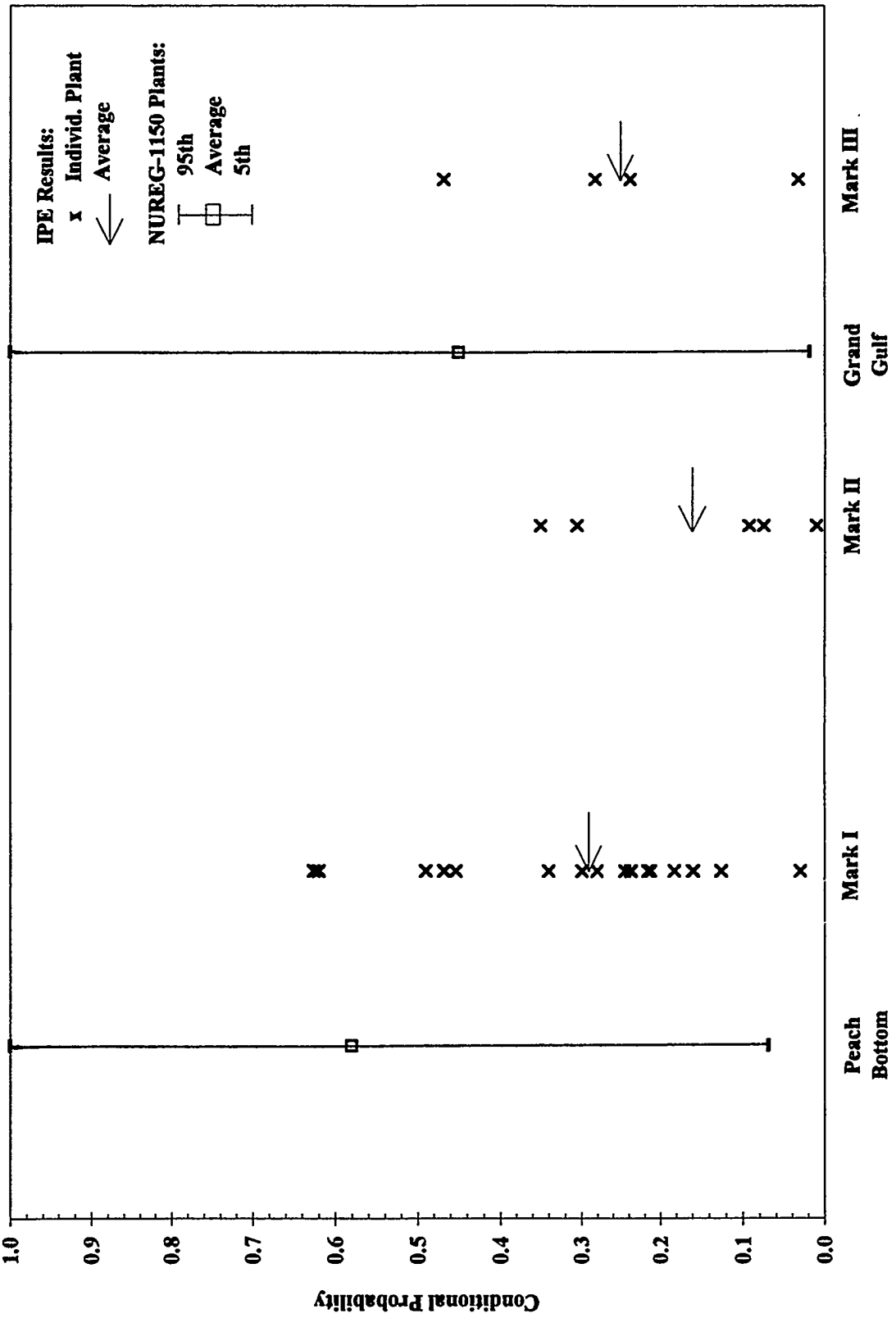

Figure 7 Comparison of NUREG-1150 and IPE Conditional Probabilities for Early Containment Failure for BWR Plants

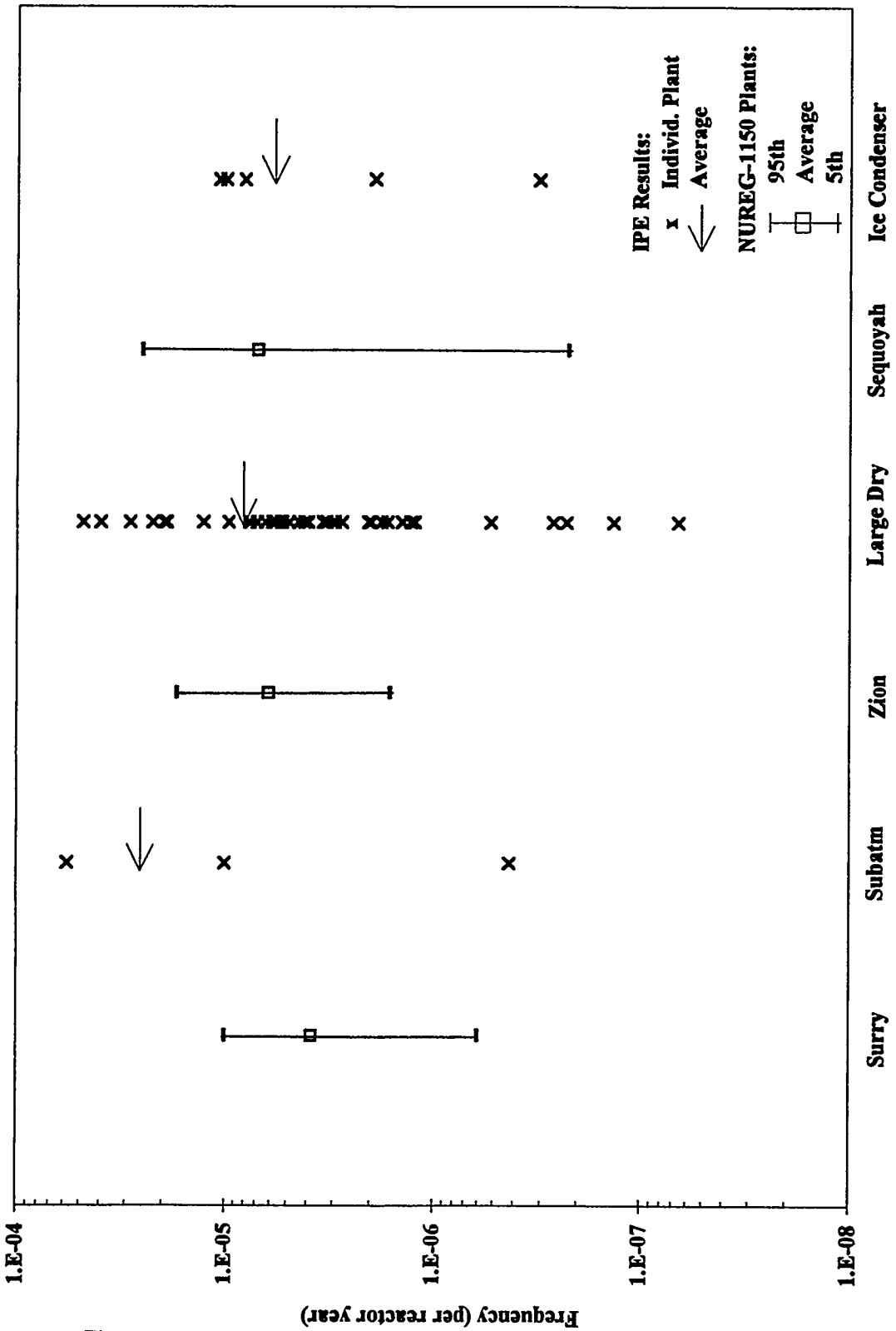

Figure 8 Comparison of NUREG-1150 and IPE Frequencies (per reactor year) of Early Containment Failure or Bypass for PWR Plants

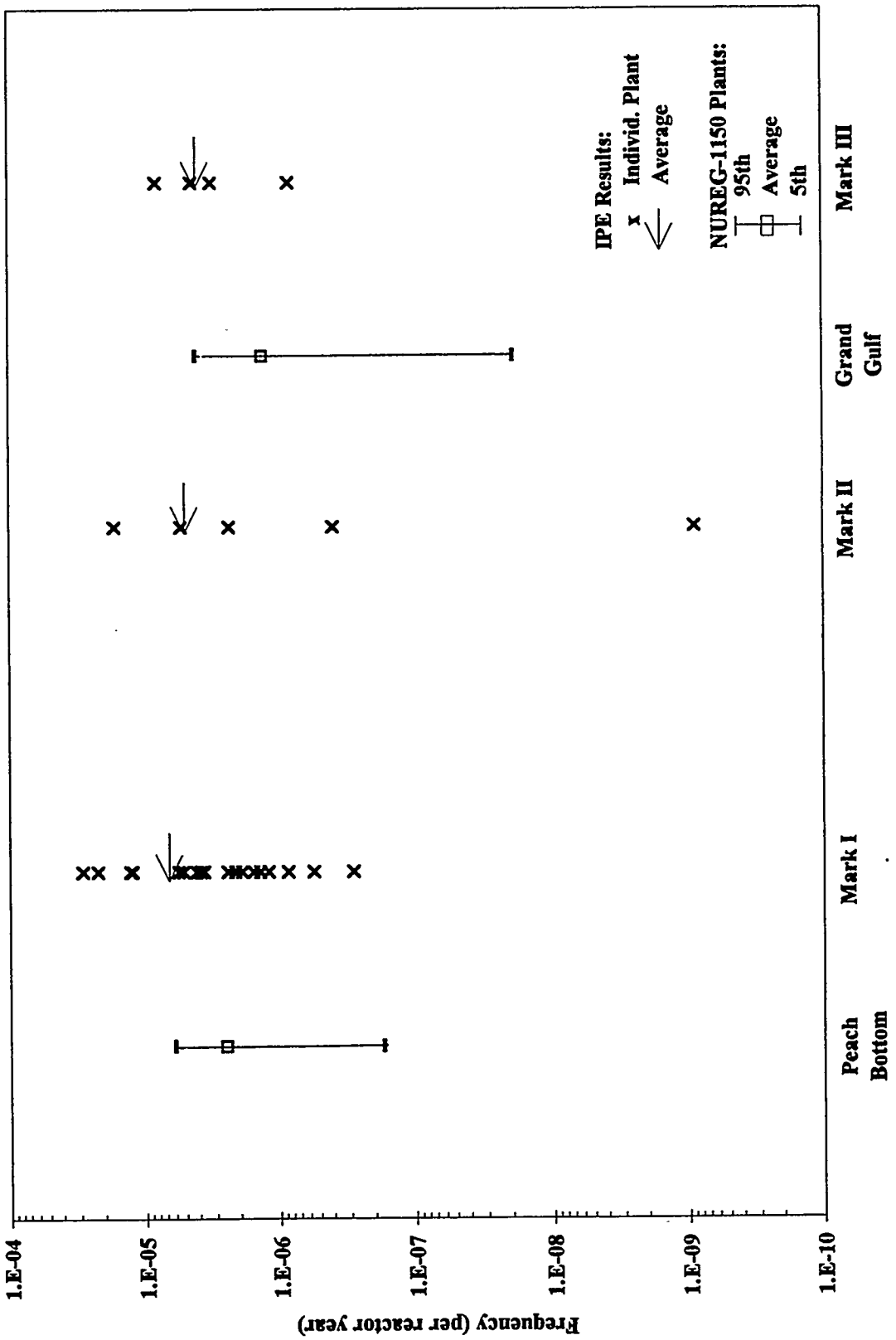

Figure 9 Comparison of NUREG-1150 and IPE Frequencies (per reactor year) of Early Containment Failure of Bypass for BWR Plants

IPE DATA BASE: PLANT DESIGN, CORE DAMAGE FREQUENCY AND CONTAINMENT PERFORMANCE INFORMATION*

J. Lehner
C. C. Lin
W. T. Pratt
Brookhaven National Laboratory
Upton, NY 11973

T. Su
L. Danziger
U.S. Nuclear Regulatory Commission
Rockville, MD 20852

ABSTRACT

A data base, called the IPE Data Base has been developed that stores data obtained from the Individual Plant Examinations (IPEs) which licensees of nuclear power plants have conducted in response to the Nuclear Regulatory Commission's (NRC) Generic Letter GL88-20. The IPE Data Base is a collection of linked files which store information about plant design, core damage frequency, and containment performance in a uniform, structured way. The information contained in the various files is based on data contained in the IPE submittals.

The information extracted from the submittals and entered into the IPE Data Base can be manipulated so that queries regarding individual or groups of plants can be answered using the IPE Data Base. The IPE Data Base supports detailed inquiries into the characteristics of individual plants or classes of plants.

Substantial progress has been made on the IPE Data Base over the last two years and it is largely complete. The recent focus of the work on the IPE Data Base has been the development of a user friendly version which is menu driven and allows the user to ask queries of varying complexity easily, and without the need to become familiar with particular data base formats or conventions such as those of dBase IV or Microsoft Access. The user can obtain the information he or she is interested in by quickly moving through a series of on-screen menus and "clicking" on the appropriate choices. In this way even a first time user can benefit from the large amount of information stored in the IPE Data Base without the need of a learning period.

*Work performed under the auspices of the U.S. Nuclear Regulatory Commission.

BACKGROUND

As previously reported [1] a data base, called the IPE Data Base, has been developed that stores data obtained from the Individual Plant Examinations (IPEs) which licensees of nuclear power plants have conducted in response to the Nuclear Regulatory Commission's (NRC) Generic Letter GL88-20 [2]. The IPE Data Base is a collection of linked files which store information about plant design, core damage frequency (CDF), and containment performance in a uniform, structured way. The information contained in the various files is based on data contained in the IPE submittals.

The information extracted from the submittals and entered into the IPE Data Base can be manipulated so that queries regarding individual or groups of plants can be answered using the IPE Data Base.

There are two sections of the IPE IPE Data Base, corresponding to the Level 1 analysis in the IPE submittals and the Level 2 analysis.

The titles of the Level 1 files, indicating the focus of the information contained in each, are the following: General Plant Information, Front-Line Systems, Support Systems, Dependency Table, Core Damage Prevention Strategies, Mission Success Paths, and the Accident Sequence Table. The link between these files is a basic list of BWR and PWR systems, in terms of which:

(a) the design of any BWR or PWR can be described with reasonable fidelity (General Plant Information, Front-Line Systems, Support Systems, Dependency Table),

(b) plant-specific dominant accident sequences can be described accurately (Accident Sequence Table), and

(c) the success paths assumed in the IPE (i.e., its mission success criteria) can be tabulated (Core Damage Prevention Strategies, Mission Success Paths).

The Level 1 portion of the IPE Data Base is connected to the Level 2 portion through the Plant Damage States. The Level 2 files in the IPE Data Base are the following: Plant Damage State Definitions, C-matrix, (containment performance), Source Terms, and Level 2 Analysis Parameters, (source term characteristics).

Another data file, containing high level information on CDF contributors, was added to the above structure and coupled to the rest of the IPE Data Base files. This additional file contains summary information found in each IPE submittal regarding initiating event frequencies and the total contribution to core damage from each initiating event. Because of the way information was reported in the submittals, the previously existing accident sequence files of the IPE Data Base contain only partial results regarding the contribution to core damage from various initiators. The summary information file remedies this situation.

The IPE Data Base supports detailed inquiries into the characteristics of individual plants or classes of plants. In particular, one can compare the core damage frequency and containment performance of BWRs and PWRs as a function of their design features, based on information which is contained in the IPE submittals.

The IPE Data Base is designed to provide helpful information for general questions like: What features does each submittal take credit for? How does this factor into the core damage frequency and/or containment performance of the plant? If two plants in basically the same class have markedly different CDF and/or containment performance, what is responsible for this? If a class of plants seems to share a particular contributor to core damage, what design features are responsible for this?

Substantial progress has been made on the IPE Data Base over the last two years and it is largely complete. Entries into the IPE Data Base from the IPE internal events examination have been finished with all IPEs entered.

FOCUS OF CURRENT DEVELOPMENT

The recent focus of the work on the IPE Data Base has been the development of a user friendly version which is menu driven and allows the user to ask queries of varying complexity easily, and without the need to become familiar with particular data base formats or conventions such as those of dBase IV or Microsoft Access. The user can obtain the information he or she is interested in by quickly moving through a series of on-screen menus and "clicking" on the appropriate choices. In this way even a first time user can benefit from the large amount of information stored in the IPE Data Base without the need of a learning period.

The development of this user friendly version is currently (October 1995) incomplete and will undoubtedly undergo substantial changes before being released next year. However, the following discussion and the accompanying figures show the direction of the development and indicate the ease with which a user will be able to manipulate the IPE Data Base. At the same time, what follows also serves to illustrate the kind of information available in the database and provides examples of some very simple queries.

One of the first menus a user will see will provide a choice of which IPE Data Base files to manipulate as well as choice of which plants to enquire about. Figure 1 shows the current scheme where the General Plant Information File has been chosen and some of the possible selection criteria are shown, i.e. plant name, vendor, reactor type, or containment type. Combinations of these criteria can be used and additional criteria are being added. Figure 2 shows the result of selecting a single plant by name. Figure 3 shows the result of selecting all BWRs with Mark I containments. Note that in the latter case the screen indicates that what is shown is the first of 18 records and the other records can be accessed by "clicking" on the "First," "Previous," "Next," or "Last" buttons. Subsequent development will allow viewing more than one record at a time.

Figure 4 shows a simple query regarding the information on core damage frequency. The left side of the screen shows that the query asks for all Westinghouse four loop plants with a CDF greater than 1.E-5. The right side of the screen indicates there are 20 such plants, with the fifth record shown, i.e. Comanche Peak 1&2. Again viewing more than one record per screen will be available in the future.

Figure 5 indicates the kind of information available in the Accident Sequence File of the IPE Data Base. A single plant, St. Lucie 1, has been selected and the screen indicates that the IPE submittal for this plant provided information on 109 accident sequences, with the fourth sequence shown on the screen. The screen shows the designation given this sequence in the IPE submittal, the plant damage state (PDS) it was assigned to, the initiator (S3: a small-small LOCA), and the CDF of the sequence along with the total plant CDF. The screen also indicates that high pressure recirculation (HPR) and another system, designated AR1 in the generic IPE Data Base nomenclature, have failed and led to core damage in this sequence. The "Notes" field on the right side of the screen provides additional information. To determine what system corresponds to AR1 in this plant the user can go to the Front Line Systems File and see, as indicated in Figure 6, that AR1 for St. Lucie refers to the Shutdown Cooling System.

If the user wants to see the success strategies used in the St. Lucie IPE for the S3 initiator, the Success Strategy File for this plant indicates, as shown in Figure 7, that there are four strategies with the first one indicated on the screen (Record 1 of 4). This strategy relies on high pressure injection (HPI), high pressure recirculation (HPR), secondary side heat removal (SSMU), and containment heat removal (CPSR). A look at the other strategies, such as feed and bleed for instance, would show that they all require HPR, and this correlates with the fact that HPR failure leads to core damage for this initiator, as indicated in the accident sequence shown in Figure 5.

Figures 8 and 9 illustrate part of the information on containment performance stored in the IPE Data Base. Figure 8 shows that for the Release Class designated B4-R in the St. Lucie Submittal fission product release fractions are provided for noble gases, iodine, cesium, and tellurium. Figure 9 indicates the properties associated with this release class in terms of a number of parameter designators. Currently the user would have to refer to an IPE Database dictionary to decipher these designators, but they will be replaced with readily understandable phrases in the near future.

SUMMARY AND CONCLUSION

In its present form, the IPE Data Base serves as a tool to store, examine and compare the enormous amount of information contained in the body of IPEs, and can enhance the future use of this information for various applications.

A user friendly version of the IPE Data Base is continuing to be developed. The above discussion indicates the general direction of this development but the final product will contain many additional features and will be optimized in terms of search parameters and screen appearance.

Besides completion of the user friendly database version, remaining work on the IPE Data Base involves updating the information contained in it, based on responses received from the licensees to requests for information generated during the NRC's review of the individual submittals. In addition, information from the external events examination part of the IPE process, the IPEEE, may eventually be incorporated into the IPE Data Base.

REFERENCES

1. J. R. Lehner and R. Youngblood, "IPE Database Structure and Insights," *Proceedings of the 21st Water Reactor Safety Information Meeting*, October 25-27, 1993.

2. D. M. Crutchfield, "Individual Plant Examination for Severe Accident Vulnerabilities," *U.S. Nuclear Regulatory Commission Generic Letter 88-20, GL 88-20*, November 23, 1988.

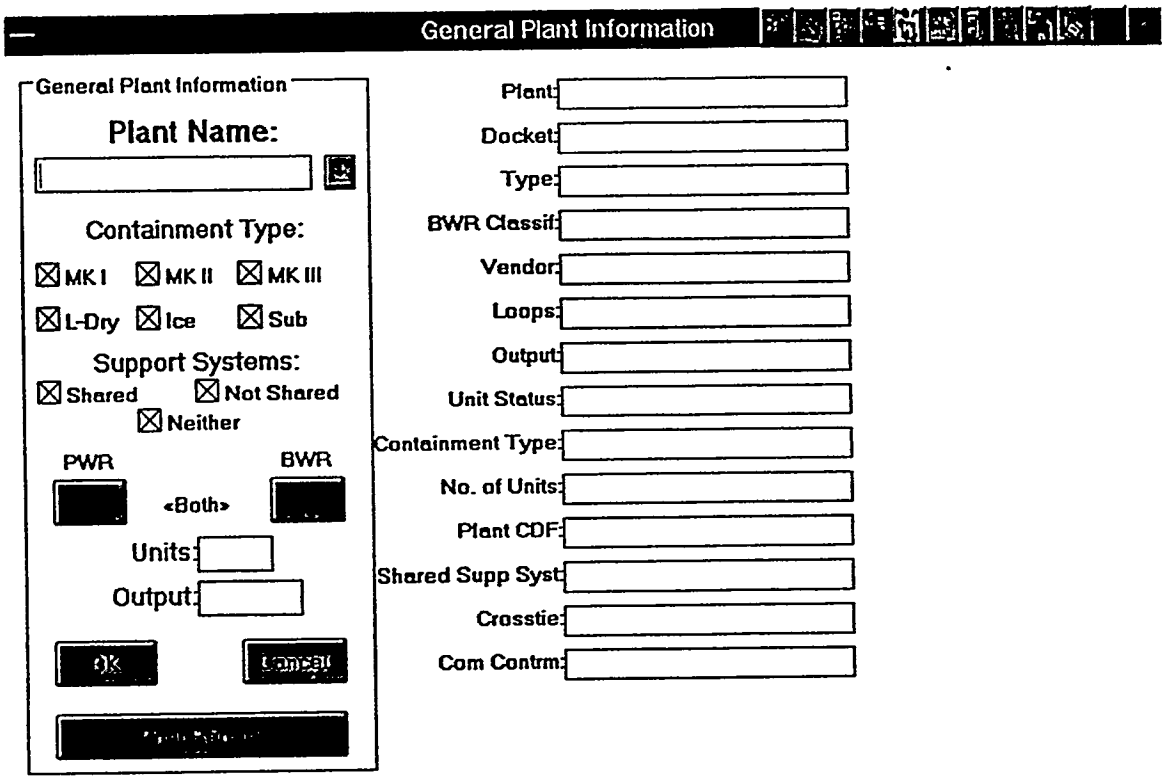

Figure 1 General Plant Information Screen

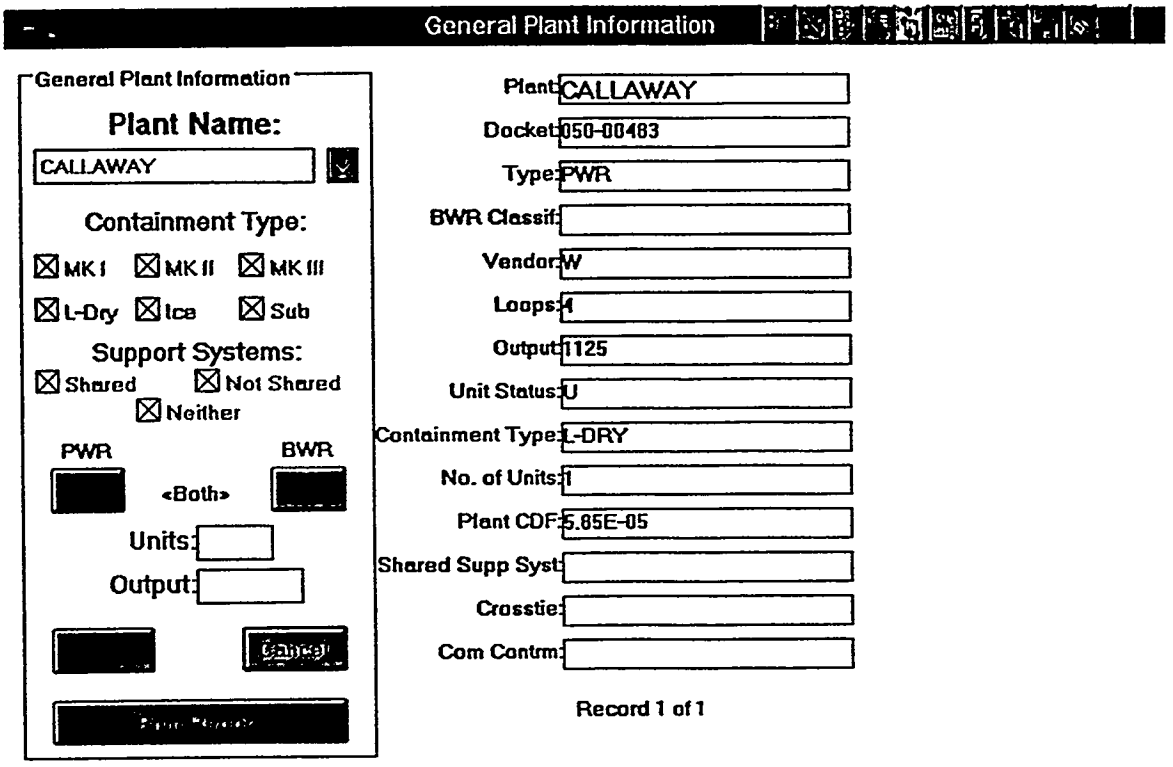

Figure 2 General Plant Information Screen with Single Plant Selected

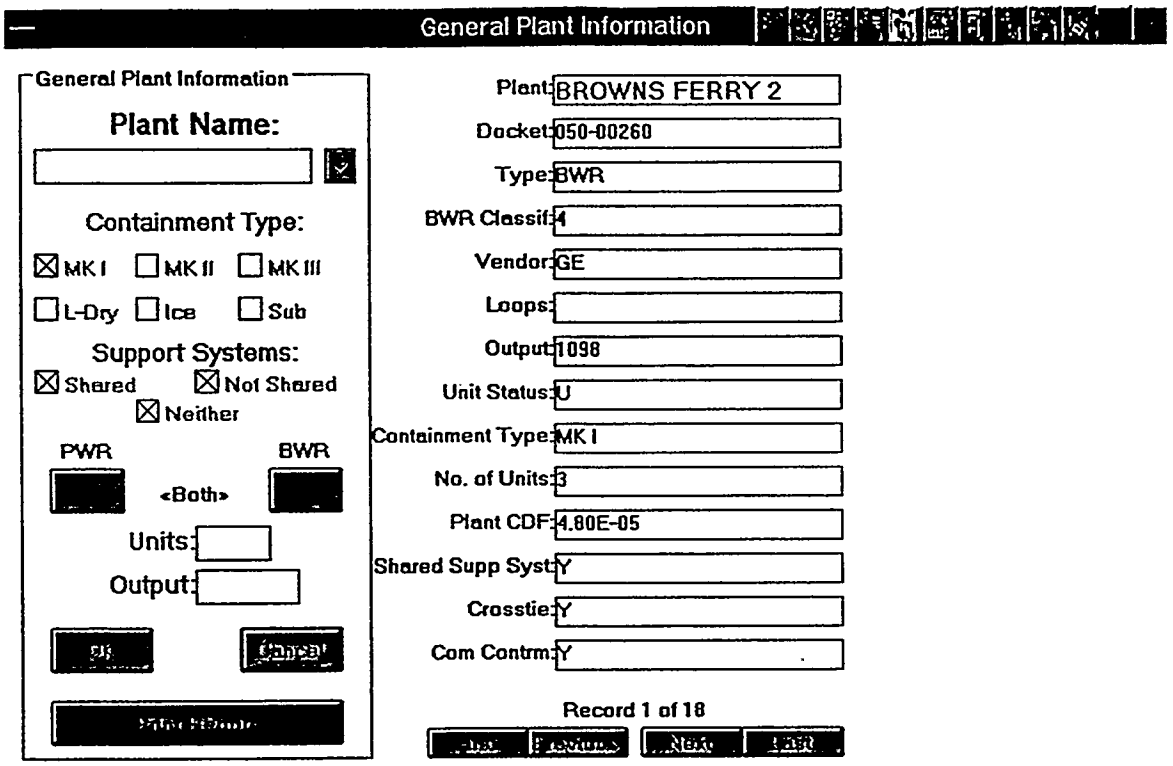

Figure 3 General Plant Information Screen with all Mark I Plants Selected

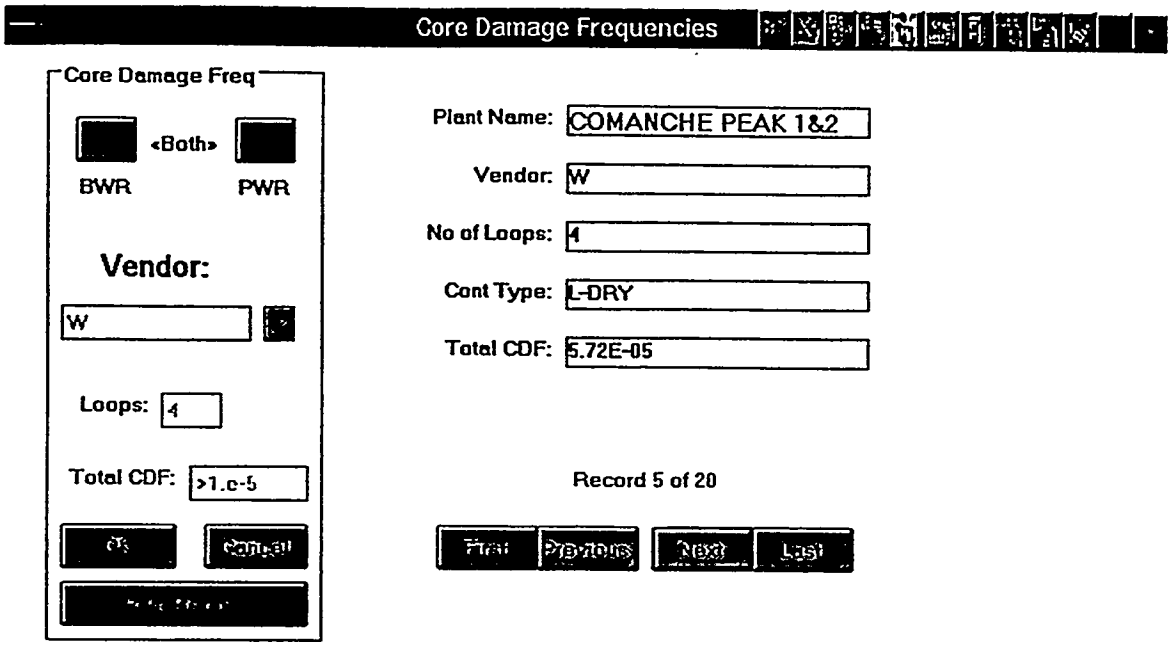

Figure 4 Example of Core Damage Frequency Query Screen

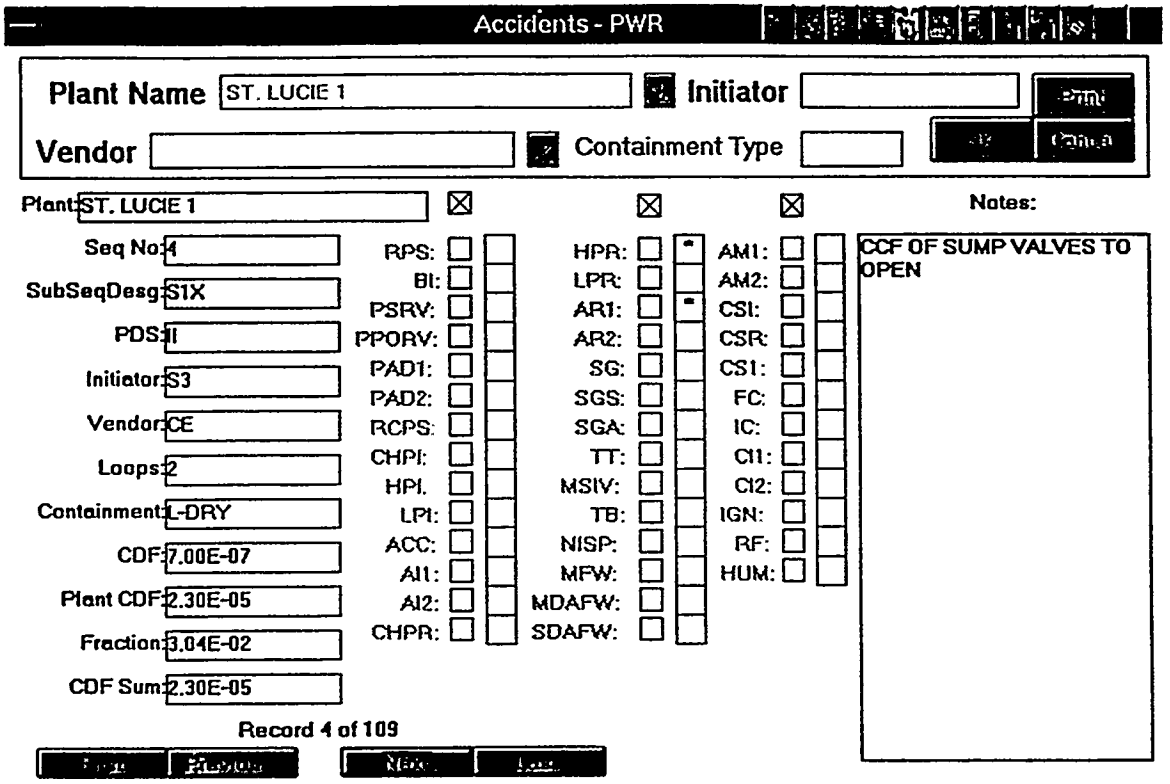

Figure 5 Example of Accident Sequence Screen

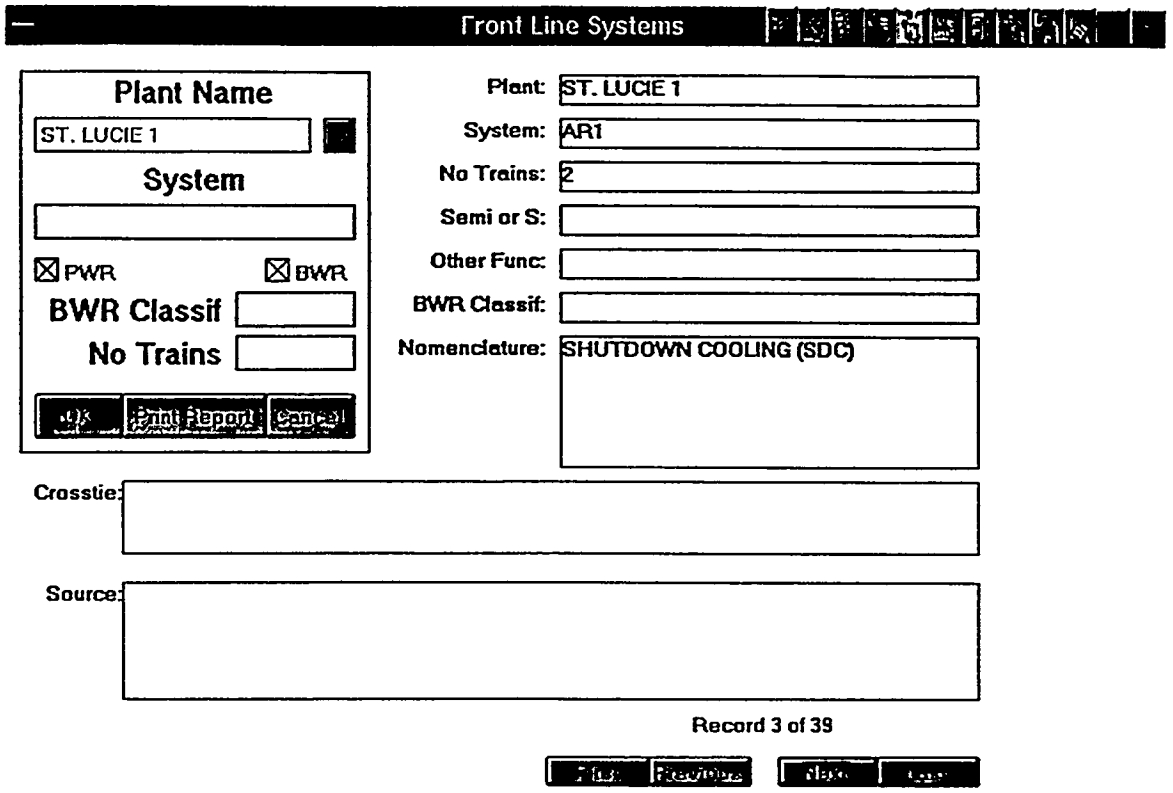

Figure 6 Example of Front-Line Systems Screen

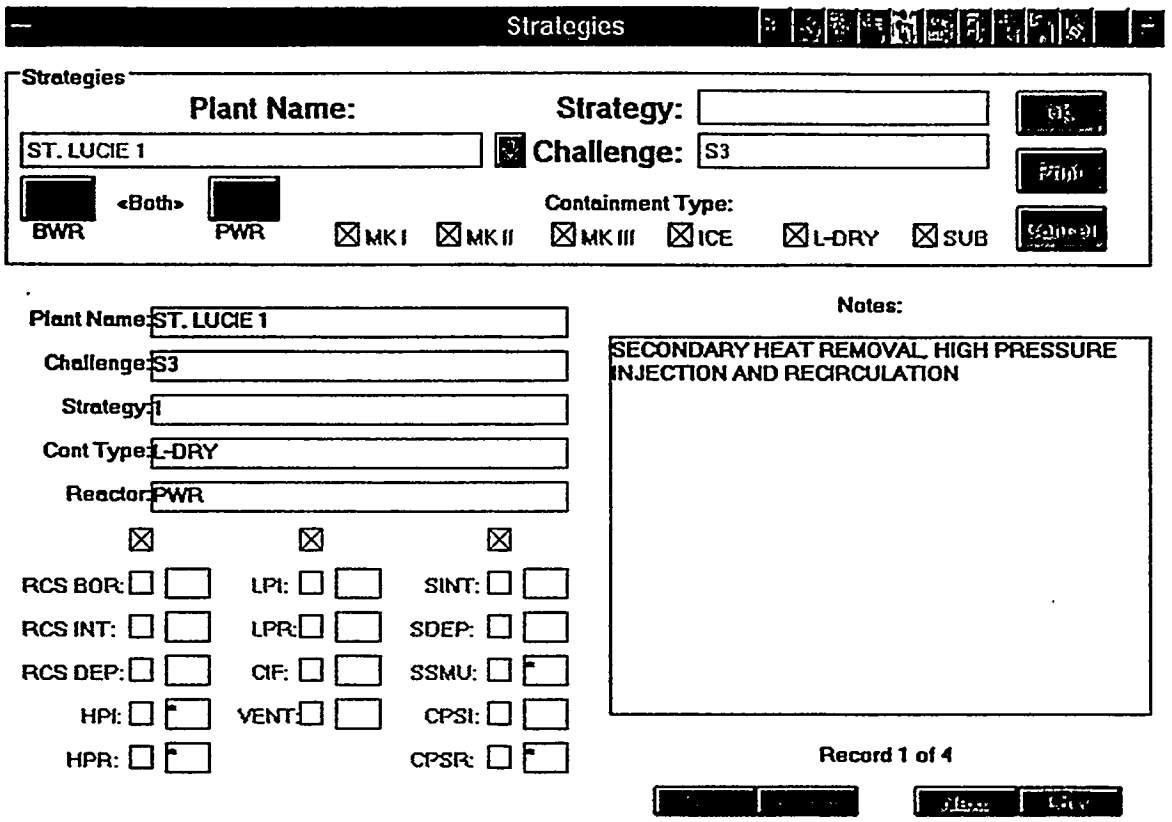

Figure 7 Example of Success Strategy Screen

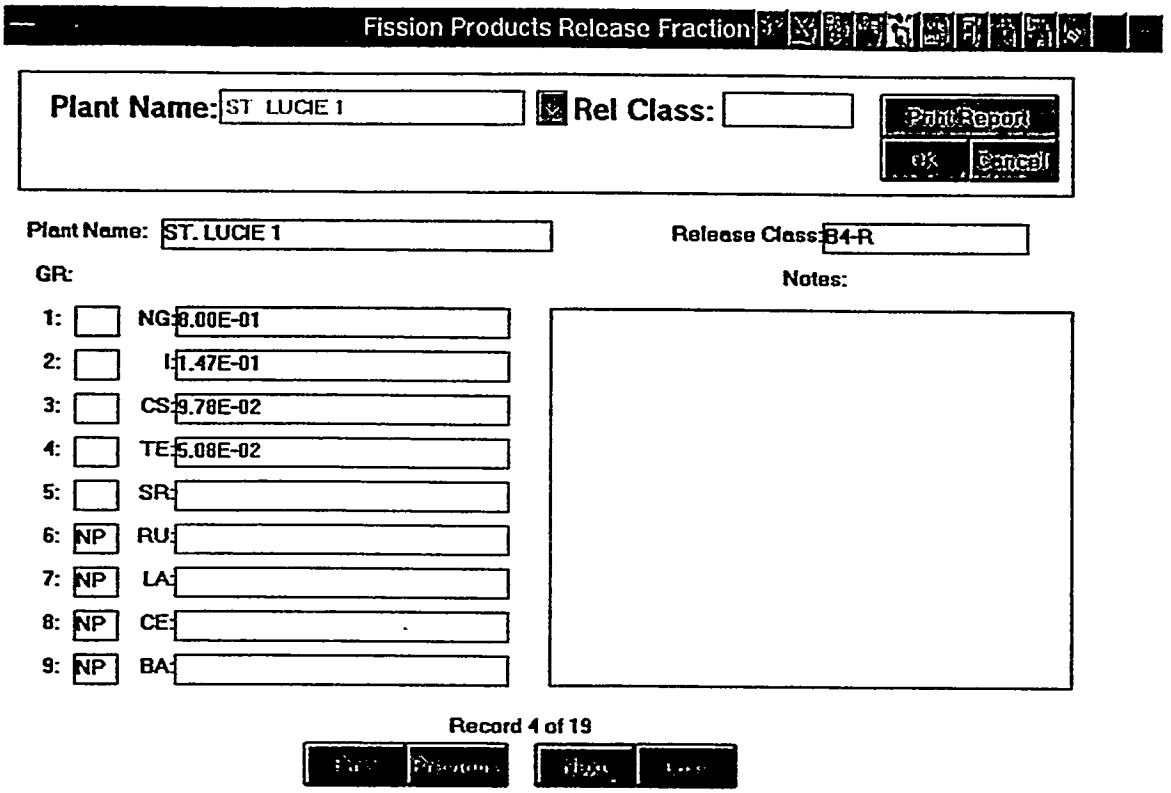

Figure 8 Example of Fission Product Release Fraction Screen

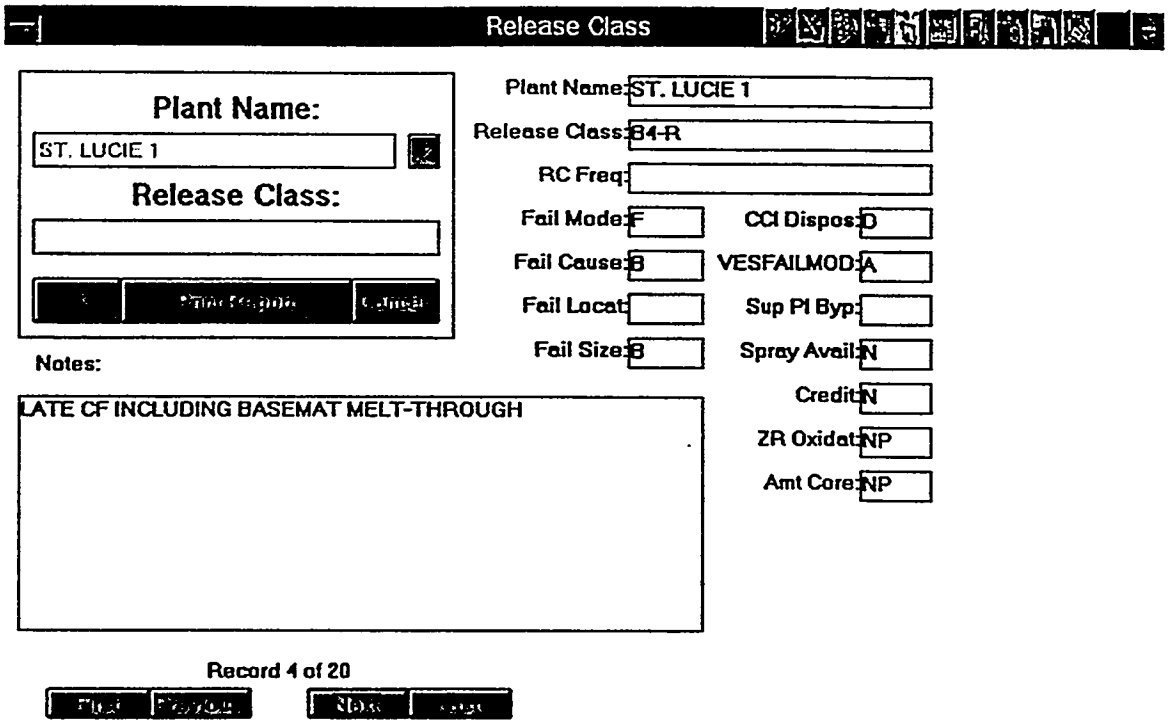

Figure 9 Example of Release Class Parameter Screen

NRC FORM 335 (2-89) NRCM 1102, 3201, 3202

U.S. NUCLEAR REGULATORY COMMISSION

BIBLIOGRAPHIC DATA SHEET

(See instructions on the reverse)

1. REPORT NUMBER (Assigned by NRC, Add Vol., Supp., Rev., and Addendum Numbers, if any.)

NUREG/CP-0149
Vol. 2

2. TITLE AND SUBTITLE

Proceedings of the Twenty-Third Water Reactor Safety Information Meeting

Human Factors Reaearch, Advanced I&C Hardware & Software, Severe Accident Research, Probabilistic Risk Assessment Topics, Individual Plant Examination

3. DATE REPORT PUBLISHED

MONTH	YEAR
March	1996

4. FIN OR GRANT NUMBER

A3988

5. AUTHOR(S)

Compiled by Susan Monteleone, BNL

6. TYPE OF REPORT

Conference Proceedings

7. PERIOD COVERED *(Inclusive Dates)*

October 23-25, 1995

8. PERFORMING ORGANIZATION – NAME AND ADDRESS *(If NRC, provide Division, Office or Region, U.S. Nuclear Regulatory Commission, and mailing address; if contractor, provide name and mailing address.)*

Office of Nuclear Regulatory Research
U.S. Nuclear Regulatory Commission
Washington, DC 20555-0001

9. SPONSORING ORGANIZATION – NAME AND ADDRESS *(If NRC, type "Same as above"; if contractor, provide NRC Division, Office or Region, U.S. Nuclear Regulatory Commission, and mailing address.)*

Same as Item 8 above.

10. SUPPLEMENTARY NOTES C. Bonsby, NRC Project Manager
Proceedings prepared by Brookhaven National Laboratory

11. ABSTRACT *(200 words or less)*

This three-volume report contains papers presented at the Twenty-Third Water Reactor Safety Information Meeting held at the Bethesda Marriott Hotel, Bethesda, Maryland, October 23-25, 1995. The papers are printed in the order of their presentation in each session and describe progress and results of programs in nuclear safety research conducted in this country and abroad. Foreign participation in the meeting included papers presented by researchers from France, Italy, Japan, Norway, Russia, Sweden, and Switzerland. The titles of the papers and the names of the authors have been updated and may differ from those that appeared in the final program of the meeting.

12. KEY WORDS/DESCRIPTORS *(List words or phrases that will assist researchers in locating the report.)*

BWR type reactors-reactor safety, international organizations-meetings, PWR type reactors-reactor safety, water cooled reactors-proceedings, Human Factors, Reactor Control Systems, Reactor Instrumentation, Probabilistic Estimation, Risk Assessment

13. AVAILABILITY STATEMENT

Unlimited

14. SECURITY CLASSIFICATION

(This Page) Unclassified

(This Report) Unclassified

15. NUMBER OF PAGES

16. PRICE

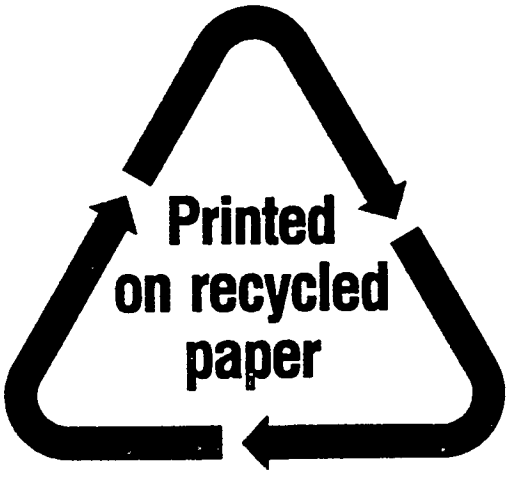

Federal Recycling Program